Czech Technical University in Prague

Faculty of Mechanical Engineering

Department of Automobiles, Internal Combustion Engines and Railway Vehicles

Ph.D. Thesis

2018 Zdeněk Žák

A 1-D Unsteady Model of a Twin Scroll Radial Centripetal Turbine for Turbocharging Optimization

A Ph.D. Thesis

Submitted to the Faculty of Mechanical Engineering, Department of Automobiles, Internal Combustion Engines and Railway Vehicles of Czech Technical University in Prague

by

Zdeněk Žák

in fulfilment of the requirements for the degree of

Doctor of Philosophy

Supervisor:
prof. Ing. Jan Macek, DrSc.

Supervisor specialist:
doc. Ing. Oldřich Vítek, Ph.D.

Study Programme:
Mechanical Engineering

Field of Study:
Machines and Equipment for Transportation

2018

Annotation

The thesis describes the development of methodology, which utilizes the map-less approach in simulation of a radial centripetal turbine with twin scroll. The steady flow turbine maps are not utilized during the entire process. The twin scroll turbine, which operates under unsteady conditions on engine, achieves different level of the impeller admission.

For validation and calibration of the turbine performance under arbitrary level of the impeller admission, a specific turbocharger test bed with separated sections upstream of a turbine was developed. The test bed enables to achieve arbitrary level of the impeller admission via throttling in sections or closure of one section. A selected twin entry turbine was measured under steady flow conditions on the mentioned test bed with open loop. The required number of turbine working points in case of map-less approach is relatively low in comparison with the classical steady flow maps, which are generated for each level of the impeller admission. The turbine was measured at full, partial and extreme partial admission with closed section. The steady flow experimental data were evaluated by the developed software.

An unsteady full 1-D model of a turbine with twin scroll was developed in GT-SUITE simulation environment. The model of the whole turbine with scrolls, mixing of flows at nozzle ring upstream of the impeller, turbine wheel, leakages and outlet pipe has to be calibrated under steady flow in compliance with the data measured on the turbocharger test bed. The fully calibrated twin scroll turbine model is then prepared for the unsteady simulation with the internal combustion engine model.

A turbocharged six cylinder diesel engine equipped with the twin scroll turbine was properly measured at steady states and transients. The goal of the measurement was to obtain data for verification of the turbine model behaviour under highly pulsating flow conditions.

The model of the experimental internal combustion engine was developed and properly calibrated by experimental data. The engine steady states and also transient operation conditions were simulated by means of the engine model with full 1-D turbine. The simulation results were compared with experiments.

The comprehensive methodology utilizing the map-less approach was validated and verified by the engine simulation with full 1-D turbine model under real conditions, measured on the turbocharged internal combustion engine. The results were also compared with the classical map based approach.

Anotace

Disertační práce popisuje vývoj metodiky, která nevyužívá stacionární mapy turbíny pro simulace radiální dostředivé turbíny se dvouvstupovou skříní. Stacionární mapy turbíny nejsou v celém procesu použity. Dvouvstupová turbína, která pracuje za nestacionárních podmínek na motoru, dosahuje různé úrovně ostřiku oběžného kola turbíny.

Pro validaci a kalibraci turbíny při libovolné úrovni ostřiku oběžného kola, byl vyvinut specifický testovací stav turbodmychadel s oddělenými sekcemi před turbínou. Testovací stav umožňuje dosáhnout libovolné úrovně ostřiku oběžného kola pomocí škrcení v sekcích nebo zavřením jedné sekce. Vybraná dvouvstupová turbína byla měřena za stacionárních podmínek na zmíněném testovacím stavu s otevřenou smyčkou. Požadovaný počet pracovních bodů turbíny je v případě přístupu nevyžadujícího mapy relativně nízký v porovnání s klasickými stacionárními mapami, které jsou generovány pro každou úroveň ostřiku oběžného kola. Turbína byla měřena při plném, parciálním a extrémním parciálním ostřiku se zavřenou sekcí. Stacionární experimentální data byla vyhodnocena vyvinutým programem.

Nestacionární plně 1-D model turbíny se dvěma sekcemi byl vyvinut v simulačním prostředí GT-SUITE. Model celé turbíny se spirálami, míšením proudů v rozváděcím ústrojí před oběžným kolem, rotorem turbíny, netěsnostmi a výstupní trubkou musí být kalibrován za stacionárních podmínek v souladu s daty naměřenými na testovacím stavu turbodmychadel. Plně kalibrovaný model turbíny se dvouvstupovou skříní je poté připraven pro nestacionární simulace s modelem spalovacího motoru.

Přeplňovaný šestiválcový vznětový motor vybavený dvouvstupovou turbínou byl podrobně testován v ustálených stavech a přechodových režimech. Cílem měření bylo získání dat pro ověření chování modelu turbíny za silně pulzačních podmínek.

Model experimentálního spalovacího motoru byl vyvinut a patřičně kalibrován dle experimentálních dat. Stacionární stavy a také přechodové režimy motoru byly simulovány pomocí modelu motoru s plně 1-D modelem turbíny. Výsledky simulací byly porovnány s experimenty.

Ucelená metodika využívající přístupu bez stacionárních map turbíny byla validována a ověřena simulacemi spalovacího motoru s plně 1-D modelem turbíny za skutečných podmínek, změřených na přeplňovaném spalovacím motoru. Výsledky byly také porovnány s klasickým přístupem založeným na mapách.

Prohlášení o autorství

Nemám závažný důvod proti užití tohoto školního díla ve smyslu § 60 Zákona č. 121/2000 Sb., o právu autorském, o právech souvisejících s právem autorským a o změně některých zákonů (autorský zákon).

V Praze dne ....

Zdeněk Žák

Acknowledgements

V prvé řadě děkuji školiteli panu prof. Ing. Janu Mackovi, DrSc. Tato práce by nemohla nikdy vzniknout bez jeho cílené podpory a podmínek, které vytvořil. Předkládaná práce navazuje na jeho mnohaleté úsilí a čerpá z jeho znalostí a zkušeností.

Dále děkuji panu doc. Ing. Oldřichu Vítkovi, Ph.D. Na jeho dlouholetou práci navazuje simulační část této disertace.

Velké poděkování patří pánům prof. Ing. Michalu Takátsovi, CSc. a Ing. Miloslavu Emrichovi, Ph.D. za bezvadnou přípravu brzdového stanoviště a provedení zkoušek na experimentálním spalovacím motoru.

Dále děkuji pánům Bc. Tomáši Vlčkovi, Břetislavu Bezouškovi a Jiřímu Černému za přípravu motoru a brzdového stanoviště.

Panu Ing. Petru Hatschbachovi, CSc. děkuji za spolupráci při měření vlastností kanálů hlavy válců a při vývoji měřicí tratě pro turbodmychadla.

Panu Ing. Ondřeji Gotfrýdovi, Ph.D. děkuji za zprovoznění palivového čerpadla v návaznosti na otevřenou řídicí jednotku experimentálního motoru. Děkuji panu Ing. Jiřímu Vávrovi, Ph.D. za pomoc při přípravě motoru a cenné rady v oblasti experimentů.

Děkuji za spolupráci pánům Ing. Ondřeji Bolehovskému, Ing. Antonínu Mikulcovi, Ing. Jiřímu Pakostovi, Ph.D., Ing. Jiřímu Hvězdovi, Ph.D. a paní Mgr. Sylvě Ondrejičkové, Th.D.

Panu Pavlu Marschovi děkuji za kooperaci při dodávkách polotovarů a výrobě měřicích přípravků.

V neposlední řadě patří velké poděkování pánům ze společnosti ČZ a.s. divize Turbo, kteří se podíleli na vývoji měřicí tratě a realizaci zkoušek na testovacím stavu turbodmychadel. Děkuji pánům Ing. Jiřímu Pinkasovi, Ing. Oldřichu Havelkovi, Ondřeji Matějkovi, Václavu Mačlovi, Ing. Liboru Machovi a dalším.

Je pravděpodobné, že jsem na někoho zapomenul a omlouvám se za to.

Děkuji všem svým blízkým za podporu a pochopení.

The work was strongly supported by the financial donation of Dr. Thomas Morel, founder and president of Gamma Technologies, Inc. The support was essential for experimental research and it is gratefully appreciated.

This work was also supported by:

Technological Agency, Czech Republic, programme Centres of Competence, project #TE01020020 Josef Božek Competence Centre for Automotive Industry.

This research has been realized using the support of The Ministry of Education, Youth and Sports program NPU I (LO), project LO1311:'Development of Centre of Vehicles for Sustainable Mobility'.

EU Regional Development Fund in OP R&D for Innovations (OP VaVpI) and Ministry of Education, Czech Republic, project #CZ.1.05/2.1.00/03.0125 Acquisition of Technology for Centre of Vehicles for Sustainable Mobility.

Zvoníček's Foundation, Czech Republic, project - Development of a 1-D Model of a Radial Turbocharger Turbine Supported by the Financial Donation of Dr. Thomas Morel

Zvoníček's Foundation, Czech Republic, project - Experimental Investigation of Twin Scroll Turbocharger Turbine Performance Supported by the Financial Donation of Dr. Thomas Morel

All the support is gratefully acknowledged.

Table of Contents

Contents

List of Figures

List of Tables

Symbols and Abbreviations

Symbols

A	[m^2]	cross-sectional area
$A_0 - A_n$		coefficients in regression formulas
A_s	[m^2]	heat transfer surface area
A_{t_ref}	[m^2]	reference area of a turbine
acc	[m.s-2]	acceleration
b	[m]	width
B	[m]	cylinder bore
BMEP	[bar]	brake mean effective pressure
BSFC	[g/(kW.h)]	brake specific fuel consumption
BSR	[1]	blade speed ratio
c	[m.s-1]	velocity (or absolute velocity)
c_{2_r}	[m.s-1]	radial component of absolute velocity c 2 (impeller inlet)
c_{2_t}	[m.s-1]	tangential component of absolute velocity c 2 (impeller inlet)
c_{3_t}	[m.s-1]	tangential component of absolute velocity c 3 (impeller outlet)
C		coefficient
$C_0 - C_n$		coefficients in regression formulas
C_D	[1]	discharge coefficient
C_{D_ζ}	[1]	discharge coefficient upstream of rotating channel
C_f	[1]	friction coefficient
c_p	[J/(kg.K)]	specific heat
C_p	[1]	pressure loss coefficient

c_s	[m.s-1]	fictitious isentropic velocity
C_s	[1]	swirl coefficient
CD	[1]	discharge coefficient
D	[m]	diameter
dx	[m]	discretization length
e	[J.kg-1]	internal energy plus kinetic energy per unit mass
$E_0 - E_n$		coefficients in regression formulas
h	[J.kg-1]	specific enthalpy
h	[W.m-2.K-1]	heat transfer coefficient
H	[J]	enthalpy
K		coefficient
$K_1 - K_4$		coefficients in regression formula
K_{wind}	[1]	coefficient of windage losses
K_{zeta}	[1]	correction of impeller incidence loss
L	[m]	length
level	[1]	level of impeller admission
m	[kg]	mass
$\dot{m}$	[kg.s-1]	mass flow rate
mu	[1]	discharge coefficient
p	[bar]	pressure
P	[W]	power
P_{turb}	[W]	internal turbine power
PR	[1]	pressure ratio
$\dot{Q}$	[W]	heat transfer rate
r	[J/(kg.K)]	gas constant
R	[J/(kg.K)]	gas constant

Re	[1]	Reynolds number
RPM	[RPM]	revolutions per minute, speed
s	[J/(kg.K)]	specific entropy
t	[s]	time
T	[K]	temperature
T_{swirl}	[N.m]	swirl torque
tip_{speed}	[m.s-1]	tip speed of wheel
Tq	[N.m]	torque
u	[m.s-1]	velocity (or circumferential velocity)
V	[m^3]	volume
w	[m.s-1]	velocity (or relative velocity)
w_{2_N}	[m.s-1]	relative velocity at nozzle outlet
$w_{2\_r\_c}$	[m.s-1]	relative radial velocity at compressor wheel outlet
$\bar{}$		average of quantity

Greek Letters

α_2	[rad]	nozzle exit angle
β	[1]	coefficient of restitution
β_{2_N}	[rad]	angle between velocities w 2_N and w 2_I
β_3	[rad]	impeller exit angle
$\Delta\alpha_2$	[rad]	deviation of nozzle exit angle
Δ		difference
Δ	[1]	overall error delta
ΔP	[1]	error of turbine power
ΔPR_A	[1]	error of pressure ratio A
ΔPR_B	[1]	error of pressure ratio B

ζ	[1]	kinetic energy loss coefficient
η	[1]	efficiency
κ	[1]	specific heat ratio
μ	[1]	discharge coefficient
μ	[Pa.s]	dynamic viscosity
ν	[m^2/s]	kinematic viscosity
ρ	[kg.m-3]	density
ψ	[1]	flow function

Subscripts and Superscripts

0	stagnation state
2	inlet of turbine impeller
2_c	at compressor wheel outlet
2_I	at impeller inlet
2_N	nozzle outlet
2_N_A	at outlet of turbine section A (upstream of flow mixing)
2_r_c	radial, compressor outlet
3	outlet of turbine impeller
A	quantity valid for turbine section A
AB	overall quantity of a twin scroll turbine
adi	adiabatic
ave	average
B	quantity valid for turbine section B
bear	bearings
c	compressor
case	casing
comp	compressor

corr	corrected
crit	critical
down	downstream
E	transfer to environment
Euler	based on Euler turbine theorem
fluid	fluid
I	impeller
imp	impeller
IN	inlet
inlet	quantity at inlet
inlet_tot	total quantity at inlet
ise	isentropic
large	large (diameter)
leak	leakage
loss	loss
m	measured
max	maximum
mech	mechanical
N	nozzle (nozzle ring)
nozzle	nozzle
oil	oil
out	quantity at outlet
OUT	quantity at outlet
overall	overall quantity
r	radial
R	reference

red	reduced
ref	reference
rel	relative
REQ	required
s	isentropic
sep	separation of flow
shaft	turbocharger shaft
small	small (diameter)
static	static
t	total quantity
t	tangential
t_s	total - static
t_t	total - total
tot	total quantity
total	total quantity
turb	turbine
up	upstream
wall	wall
wind	windage

Abbreviations

BMEP	brake mean effective pressure
BSFC	brake specific fuel consumption
BSR	blade speed ratio
CAD	computer aided design
CFD	computational fluid dynamics

DAQ	data acquisition
EGR	exhaust gas recirculation
PID	proportional integral derivative
TPA	three pressure analysis
TVD	total variation diminishing
VTG	variable turbine geometry (VGT, VNT)
WG	waste gate

1. Introduction

The continual need for the increasing efficiency of all energy conversion processes is very strong not only in the automotive industry. The powertrain of a vehicle has to be efficient as high as possible and ecological during the entire lifecycle on the other hand. To find the optimum compromise is more and more demanding, because many of the requirements are contradictory.

The trends of downsizing, downspeeding and hybridization of vehicle powertrain units are obvious. The focus on prevailing real driving conditions and natural unsteady character of internal combustion engine operation is an actual challenging task. The behaviour of the turbocharged reciprocating internal combustion engine during transients is a crucial factor for vehicle dynamic, formation of emissions and fuel economy. The interactions between internal combustion engine and turbocharger, when the turbine operates under unsteady pulsating flow conditions, significantly influence the overall engine efficiency due to the continually increasing boost pressure level.

Development of the vehicle is comprehensive technical problem. The goal is to find the optimal compromise. It is not acceptable to develop any part separately without the relation to another part in the network.

During the development of the turbocharged internal combustion engine, it is necessary to develop specific turbocharger concurrently, because only the overall efficiency (i.e. fuel economy) matters. Comprehensive simulation analyses at the early stage of the development are important more than ever. The development of simulation technics, which are able to describe the unsteady phenomena inside the reciprocating internal combustion engine and the turbocharger using the physical background, is the right way how to improve the predictive capability of the models and the overall development process of the powertrain unit. It must be stressed that experimental and simulation research has to be in synergy and the dialog between engineers is fundamental.

The multi entry axial turbines are used for turbocharging of large bore internal combustion engines in stationary and marine applications. Twin entry radial centripetal turbocharger turbines are used in the automotive industry. The twin scroll design is beneficial in conjunction with the engine with firing interval between cylinders around 120 degrees of a crank angle (240 degrees in exhaust manifold branches), i.e. six cylinder engines. The advantages consist in the higher efficiency of a turbine and better engine response during the transients due to better utilization of exhaust gas energy. The twin entry turbines are also used for the four cylinder engines to improve the engine behaviour during transients. The firing interval between cylinders in mentioned case is 180 degrees, thus out of optimum and the high pulsating flow upstream of a turbine cannot be utilized as effective as in the case of six cylinder engine.

The thesis deals with the twin scroll centripetal radial turbine and map-less approach in detail. The experimental research on the steady flow turbocharger test bed is the basis for the development of the turbine model with physical

background. The predictive capability of the calibrated twin scroll turbine model is then verified through the simulation of the whole turbocharged compression ignition engine. The simulation results are properly compared with data measured on the experimental six cylinder engine.

2. State of the Art

Turbocharging is a fundamental topic of the automotive industry as briefly described in the introduction. The continual improvement of experimental and simulation methodologies is crucial in the development process of the high efficient and ecological turbocharged internal combustion engines. The state of the art of the turbocharger measurement and modelling is summarized in following parts.

2.1 Turbocharger Measurement

Standard turbocharger maps are measured on the steady flow hot gas stands with open loop. A compressor is characterized by the map with constant speed lines and appropriate isentropic efficiencies of each operating points (*Figure 1*). The pressure ratio is typically defined between total states upstream and downstream of the compressor. The mass flow rate via machine is usually corrected to a reference state, which has to be known (3). The GT-SUITE environment [4] enables to correct mass flow rate through more sophisticated relation (4) with reference specific heat ratio and gas constant. The turbocharger speeds have to be corrected by means of the same technique (1) and (2).

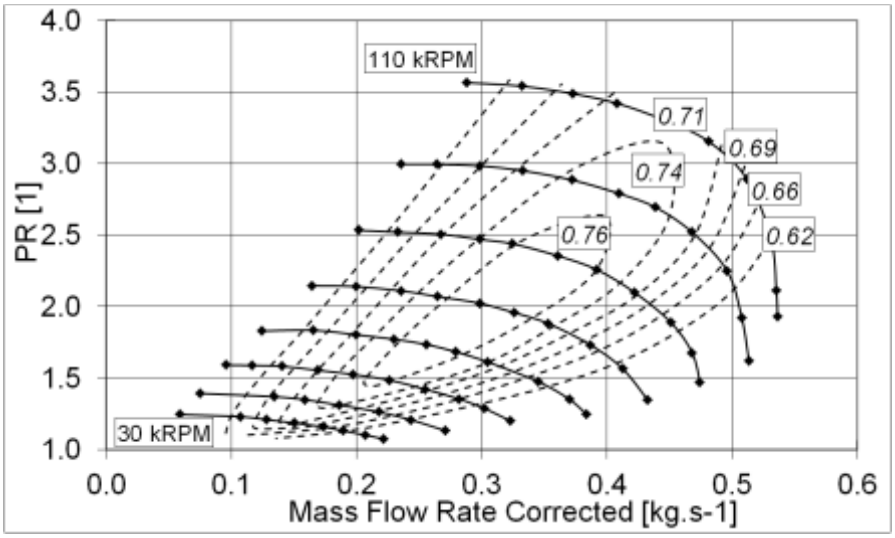

Figure 1 Example of compressor map - constant speed lines and areas with constant isentropic efficiency of a compressor; PR total-total

$$RPM_{corr} = \frac{RPM}{\sqrt{\frac{T_{inlet\_tot}}{T_{ref}}}} \quad (1)$$

$$RPM_{corr} = RPM \sqrt{\frac{\kappa_{ref}}{\kappa_{inlet}} \frac{R_{ref}}{R_{inlet}} \frac{T_{ref}}{T_{inlet\_tot}}} \tag{2}$$

$$\dot{m}_{corr} = \dot{m} \frac{p_{ref}}{p_{inlet\_tot}} \sqrt{\frac{T_{inlet\_tot}}{T_{ref}}} \tag{3}$$

$$\dot{m}_{corr} = \dot{m} \frac{p_{ref}}{p_{inlet\_tot}} \sqrt{\frac{\kappa_{ref}}{\kappa_{inlet}} \frac{R_{inlet}}{R_{ref}} \frac{T_{inlet\_tot}}{T_{ref}}} \tag{4}$$

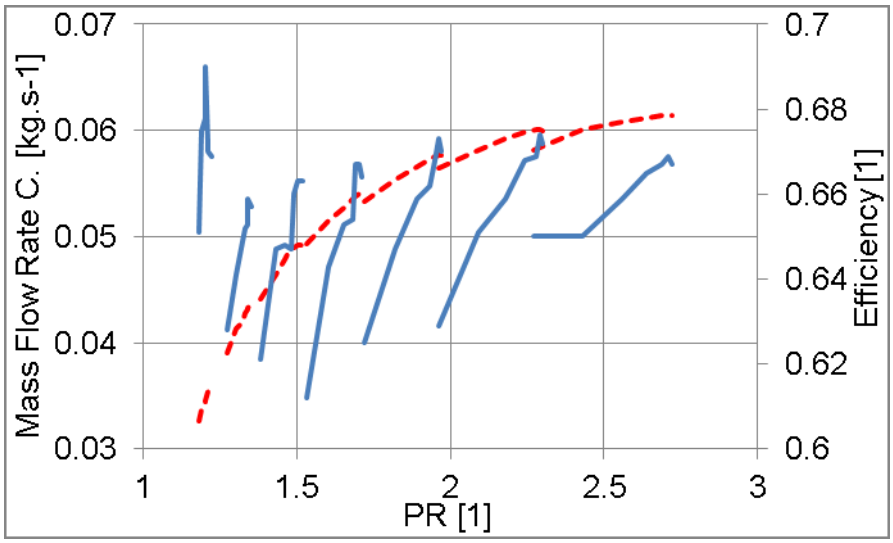

Figure 2 Example of turbine map (raw experimental data) - corrected mass flow rate via turbine (red dashed line) and isentropic efficiency (blue); PR total-static

The turbine speed and mass flow rate are corrected in the same manner as a compressor - *Figure 2*. The relations (1) - (4) stated above are valid for a turbine too. The reference pressure and temperature have to be listed with the map. When the correction equation in the extended form is used, the reference specific heat ratio and gas constant have to be known too of course. The reference state is commonly different from the compressor one.

Many turbocharger manufacturers provide turbine maps in SAE format with reduced values. The knowledge of the reference specific heat ratio and gas constant is required only in the case of extended equations [4], see (5) - (8).

The main problem of the most frequent experimental method mentioned above is the narrow range of turbine load, which is represented by the BSR (blade speed

ratio). The range of turbocharger speed seems to be relatively wide, but the range of turbine BSR is narrow with operating points close to optimum. The reasons are that the turbine is working with one compressor and the temperature of exhaust gases upstream of the turbine is constant. The measurement of the turbine in wide range of BSR is generally demanding and very expensive, as will be discussed in the part dealing with the experimental research. The impact of heat transfer from a turbine on the compressor parameters is presented in e.g. [33].

$$RPM_{red} = \frac{RPM}{\sqrt{T_{inlet\_tot}}} \tag{5}$$

$$RPM_{red} = \frac{RPM}{\sqrt{T_{inlet\_tot}}} \sqrt{\frac{\kappa_{ref}}{\kappa_{inlet}} \frac{R_{ref}}{R_{inlet}}} \tag{6}$$

$$\dot{m}_{red} = \dot{m} \frac{\sqrt{T_{inlet\_tot}}}{p_{inlet\_tot}} \tag{7}$$

$$\dot{m}_{red} = \dot{m} \frac{\sqrt{T_{inlet\_tot}}}{p_{inlet\_tot}} \sqrt{\frac{\kappa_{ref}}{\kappa_{inlet}} \frac{R_{inlet}}{R_{ref}}} \tag{8}$$

The standard measurement of turbochargers with twin entry turbine is the same as with the single volute. The inlet volutes upstream of the turbine are connected into one branch downstream of the combustion chamber. The turbocharger test bed remains without any changes. When the design of turbine volutes is symmetrical, the mass flow rates via sections are identical, thus the admission of the impeller is equal. The unequal admission occurs, when the housing with asymmetrical volutes is utilized, due to different flow areas (*Figure 3*). The level of an impeller admission establishes naturally without the influence of the operating staff. The turbine maps are provided in identical form as single scroll machine without the information about the conditions in each volute.

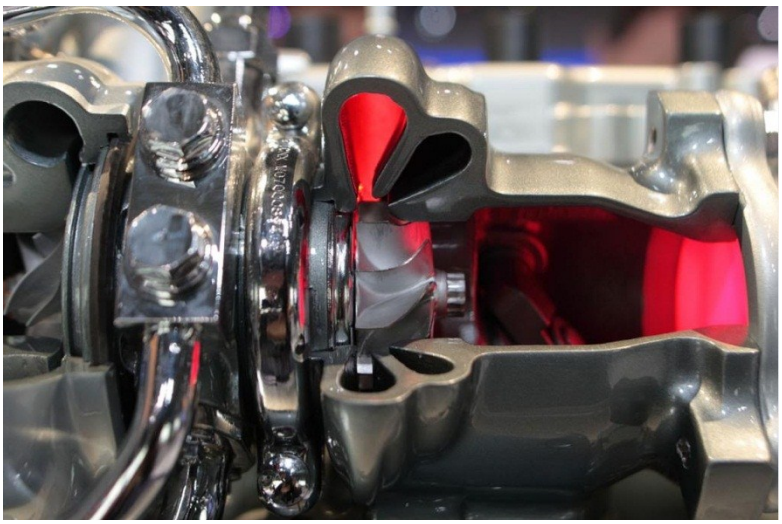

Figure 3 Twin entry radial centripetal turbine with asymmetrical scrolls for automotive applications (Mitsubishi Heavy Industries Technical Review)

Many researchers conclude that the availability of the twin entry turbine steady flow maps under full admission only is not sufficient. The typical operating modes of multi entry turbines are under high pulsating flow with unequal or partial admission of the turbine impeller, i.e. the regimes very different to the steady flow with full admission which are measured on the turbocharger test bed.

The full admission of the wheel occurs when the states in sections are almost equal and the design of volutes is symmetrical. The unequal admission means that the flows in sections are different independently on the layout of the scrolls. Some authors refer the technical term partial admission to the state when the mass flow rate in one section drops to zero, which is the extreme level of partial admission. The unequal and partial admission (of various levels) will be used in the current text as synonyms.

The aim of the work [6] was to experimentally analyse the swallowing capacity of a turbine under different levels of partial admission. It was necessary to measure on the specific turbocharger test bed with separated exhaust branches upstream of a turbine with the possibility to influence the pressures and mass flow rates in each section independently. The feasibility of changing the temperatures in sections is not so important, but may be useful.

The goal of FVV project Extended Turbine mapping [25] was an extensive measurement of twin entry turbines under unequal (partial) admission of the impeller to obtain steady flow maps of that work areas. The first evolution of the test bed was equipped with the single combustion chamber and flow was divided into separated branches, *Figure 4*. The next generation was fitted by two independent combustion chambers - *Figure 5.* The feasibility to independently and easily control pressures, mass flow rates and temperatures in sections is the benefit of the second generation.

The set of steady flow maps is then used in the arbitrary simulation code to represent the turbine behaviour under different level of partial admission. The obtained data has to be extrapolated out of the measured range and used in simulation. Interpolation is essential part of the 0-D map based approach. The

main problem of the described work consists in very demanding experimental research with huge amount of working points. All inadequacies of the 0-D quasi steady modelling occur, i.e. the description of turbine behaviour under unsteady high pulsating flow.

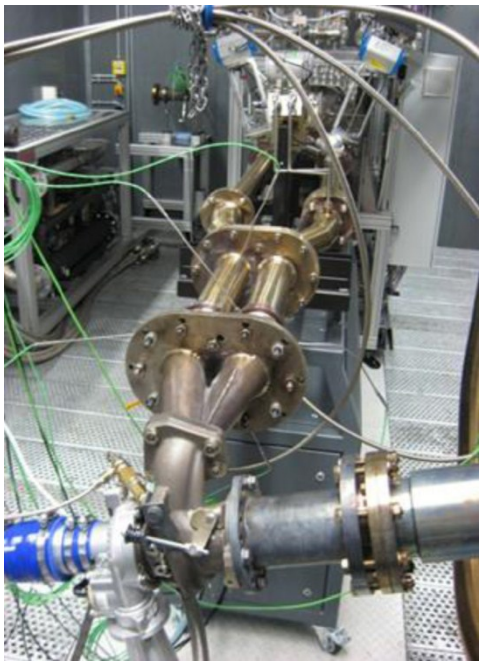

Figure 4 Hot gas stand with single burner, modified for twin entry turbine measurement [25]

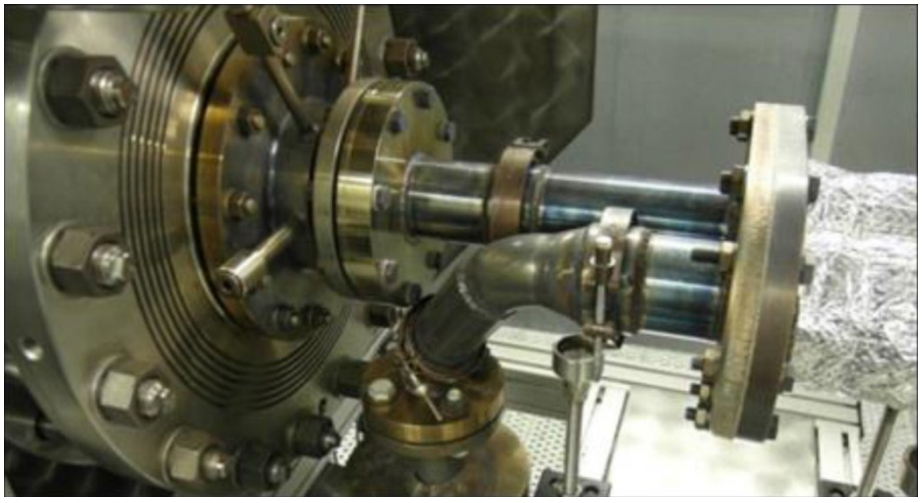

Figure 5 Double burner concept for twin entry measurement [25]

The results of the measurement on the test bed with two combustion chambers are also discussed in [31]. The described research is very time consuming and expensive by virtue of the needful wide ranges of pressure ratios, BSR, levels of admission to obtain sufficient data for the creation of steady flow maps.

Similar research was presented in [28]. The aim was to identify the features of a turbine with asymmetric scrolls under equal, unequal and partial admission. The standard steady flow maps describing the influence of sections on the overall parameters are discussed.

2.2 Modelling of a Turbocharger

A simple method how to represent the turbine is to model a nozzle with the assumption of isentropic compressible flow. The mass flow rate is calculated using the pressure ratio. The next step is to simulate two nozzles in series. The model could be improved by the intermediate volume between nozzles to approximate the turbine swallowing capacity by the volume filling and emptying under pulsating flow.

The most frequent manner how to simulate the turbocharger turbine in engine simulation codes is to utilize the steady flow maps of corrected or reduced mass flow rate and isentropic efficiency of a turbine as a function of the pressure ratio. The steady flow maps are often extrapolated out of the measured range and interpolated to provide the turbine efficiency and instantaneous mass flow rate via machine. The mentioned quasi steady 0-D map based approach is a standard for 1-D/0-D simulation codes.

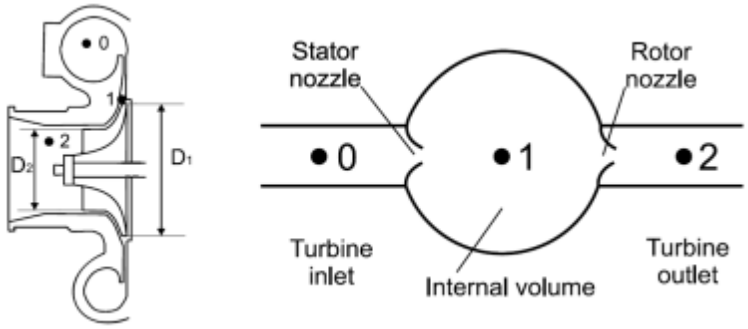

Figure 6 Turbine modelled by two ideal nozzles and embedded volume [7]

The turbine in *Figure 6* is modelled by two ideal nozzles with pressure drop across the stator and rotor. The embedded volume simulates the mass accumulation of the machine. The steady flow maps of a turbine are an essential input of the described algebraic model. The results of the model after the calibration can be used in arbitrary engine simulation code, where the turbine is solved as a boundary condition [7].

The 0-D map based fast model of the twin entry turbine was developed to support the development and calibration of the combustion engine control strategies in [26]. The control oriented fast model predicts the turbine performance under different admission conditions via interpolation and extrapolation of the measured steady flow maps.

The meanline model of a single entry turbine with variable geometry described in [5] is able to predict the turbine steady state performance. The model of nozzle-less and nozzled single scroll turbine is used primarily for the measured maps extension. The meanline model contribution for estimation of radial turbine maps is also discussed in [21].

The semi empirical meanline steady flow 0-D model presented and applied in [15], [16] and [18] simulates the expansion process, velocities and flow directions. The turbine geometry (wheel dimensions, housing geometry and inlet and outlet blade angles), pressure ratio, rotational speed and inlet temperature are required. An

empirical model for the calculation of loss coefficients is also included. The meanline model, calibrated by the measured steady flow performance maps, is able to derive steady flow maps that are consequently used in the engine simulation.

The meanline model of a twin scroll turbine has been presented in [29]. Total pressures and total temperatures are rated in each volute. The design of scrolls may be symmetric or asymmetric. Static pressures of sections are supposed equal in the splitter. The uniform flow to the impeller is simulated by the continuity, energy and momentum conservation laws. The basement of the model is the set of 1-D flow and thermodynamic equations. The losses are simulated by the several empirical models. Contribution of the model consists in the generation of steady flow maps especially when the full turbine geometry is not available.

The narrow range and often pure quality of steady flow maps provided by turbocharger manufacturers, call for the research and development of the tools for the data evaluation and extrapolation out of the measured range.

The turbine maps are often extrapolated to zero blade speed ratio (BSR) and zero efficiency, and to maximum BSR by linear extrapolation without physical background.

The model described in [8] and [20] utilizes the nozzle equation for interpolation and extrapolation of the mass flow rate via turbine. The efficiency is calculated using the definition of total-static isentropic efficiency and velocity triangles.

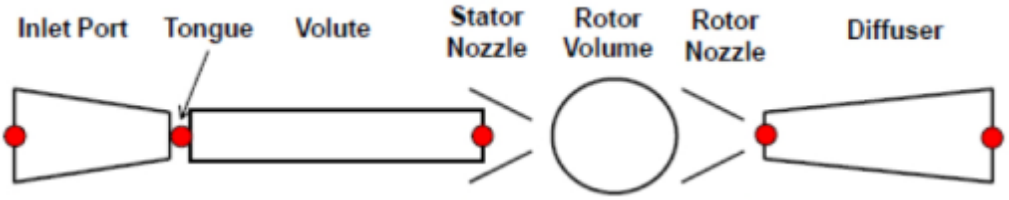

Figure 7 Scheme of a turbine model in a 1-D gas dynamic code [24]

The radial turbine model ([24] and *Figure 7*) is used for the simulation of a pulsating flow. The model built-up from 1-D pipes and two nozzles with the intermediate volume is calibrated by the standard steady flow maps.

Several models are presented in papers [13], [22] and [23]. The draft of the steady flow 1-D model described by standard continuity, energy and momentum equations is in *Figure 8*. The equations are discretized in finite differences and integrated in the iterative way. The steady 1-D model is used to obtain extended turbine maps based on the classical measurements on the turbocharger test bed under steady flow.

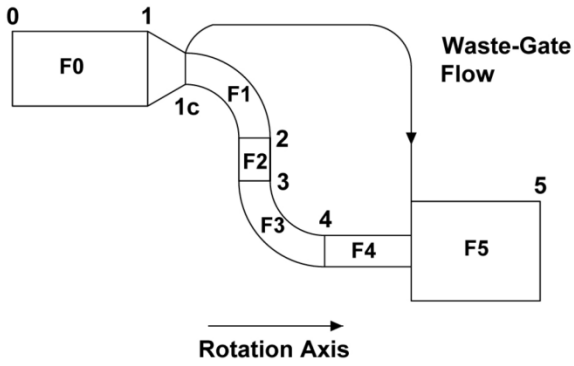

Figure 8 Sketch of waste gate turbine 1-D model (inlet pipe, volute, wheel and outlet pipe) [13]

The results are also utilized to derive the map of turbine wheel only. The pressure ratio across the impeller is calculated. The mass flow rate via wheel is reduced by the total pressure and temperature at wheel inlet. The described "wheel map" is then used in the turbine model compound of 1-D pipes in GT-SUITE environment. The turbine impeller is represented by the object with "wheel map" - the standard 0-D map based approach in GT-SUITE. The mentioned 1-D pipes should represent the unsteady behaviour of volute, impeller duct and outlet duct - *Figure 9*.

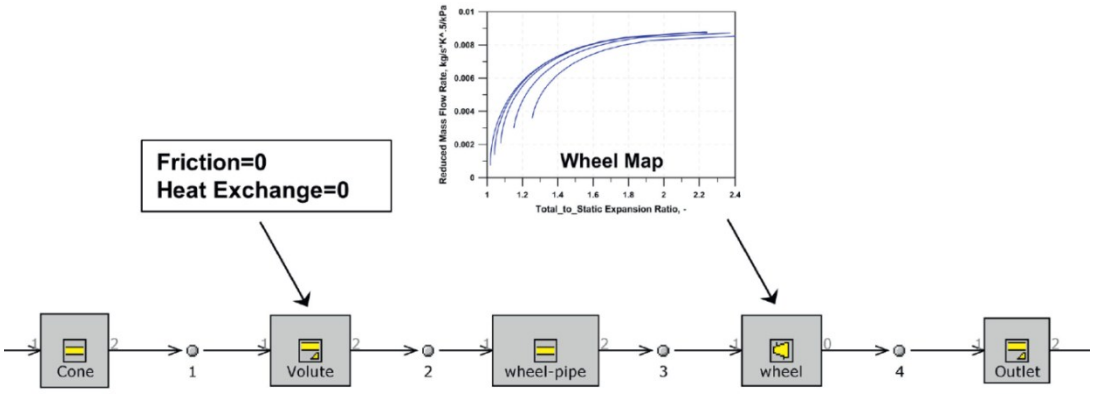

Figure 9 Combination of 0-D approach with "wheel map" and 1-D pipes to simulate the volute and ducts of an impeller and turbine outlet [13]

The further model (*Figure 10*) utilizes the extended turbine map based on results of the 1-D steady model with the virtual 1-D unsteady pipe at the turbine inlet.

Both approaches combine the 1-D unsteady pipes and classical 0-D steady state turbine maps. It is the easiest way how to simulate the volume of the turbine. It must be stressed that both models in GT-SUITE do not describe the unsteady flow of a turbine correctly. It is not a description of the physical phenomena inside a turbine.

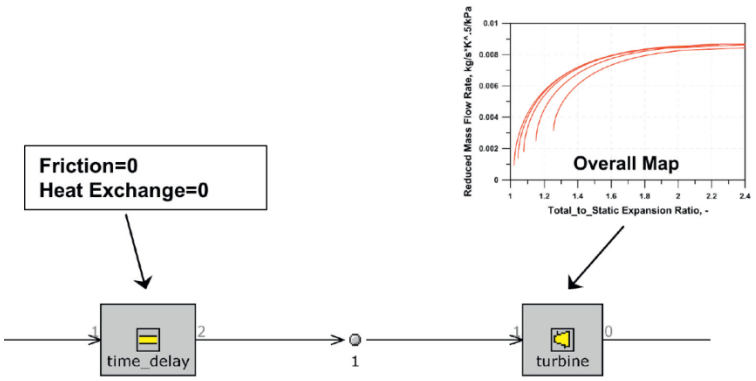

Figure 10 Model with steady flow map and virtual unsteady 1-D pipe upstream of a turbine 0-D object [13]

The same simple way how to attempt to model the turbine unsteady performance is described in [30]. The classical quasi steady approach with the turbine maps is the basis of the model. The length and volume of the turbine volute are simulated by the 1-D unsteady pipe upstream of the turbine object.

The combination of quasi stationary 0-D turbine object with 1-D pipes to simulate the volume of a turbine is also presented in [19]. The turbine maps measured under steady non-pulsating flow have been extrapolated via 3-D CFD simulation of the specific turbine.

The paper [32] shows the results of FVV research project Extended Turbine mapping. The experimental research was provided on the open loop hot gas stand with two combustion chambers. This type of the test bed allows control mass flow rates, pressures and temperatures in each scroll section entirely independently.

The steady flow maps measured under equal admission of an impeller are used and the swallowing capacity of each section is specified by the user as a fraction of the overall capacity in the simulation code. The models in GT-SUITE consist of two wholly separated turbines or the turbine inlets are connected via orifice to allow the cross flow between exhaust branches - *Figure 11*. The parameters of the connection orifice upstream of a turbine should be calibrated.

In a further model, the cross flow turbine with specific maps is determined to calculate the mass flow rate between individual turbines in dependence on the scroll pressure ratio, *Figure 12.* It must be stated that the function of the cross flow turbine is the same as the calibrated orifice between branches upstream of the turbine in *Figure 11*. The principal problem of the exhaust pipes connection upstream of the turbine object is that the location is not correct. The mixing of flows occurs inside a turbine at different pressures.

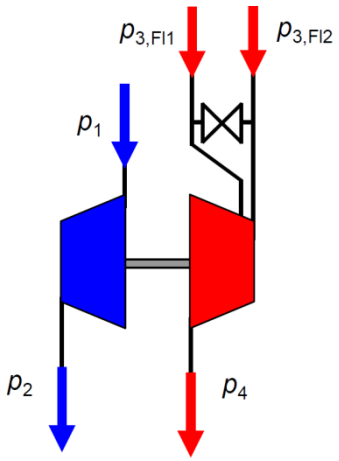

Figure 11 Simple twin scroll turbine model with two individual turbines connected by orifice to simulate the cross flow [32]

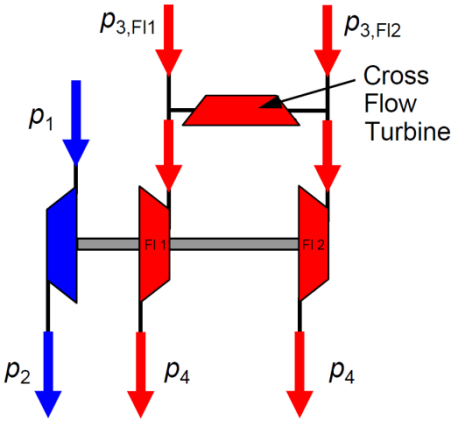

Figure 12 Analogical model with third "cross flow turbine", each turbine with individual steady flow map [32]

The improvement of the modelling multi entry turbine by means of the connection orifice (*Figure 13*) is recommended by Gamma Technologies [4]. There is probably no other method of improvement when the turbine is simulated by steady flow maps. The results of the solution are discussed in [17].

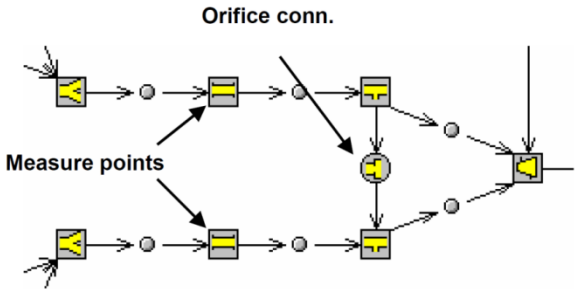

Figure 13 Exhaust manifold with connection orifice between branches upstream of a twin entry turbine [17]

The algebraic model of a twin scroll turbine is presented in paper [27]. The results provided as a co-simulation with software PROMO for combustion engine modelling are discussed.

The study of the twin entry turbine geometry effects on prediction of parameters under pulsating flow is shown in [9]. The tool is a 1-D compressible flow solver. The governing Euler equations are solved by the two step Lax-Wendroff scheme combined with the total variation diminishing (TVD). Five 1-D models with different geometry (combined and separated volutes) were developed and tested under full admission pulsating flow. The model of two inlet cross sections with junction tongue is included.

The current model is able to solve full admission of the impeller only. The model is unable to calculate the reverse flow in the turbine section. The mass flow rates are calculated, but the model is not able to solve the turbine power and efficiency.

The same second-order accurate compressible flow solver has been used in the study [12]. The turbine behaviour under pulsating flow is compared with unsteady experimental data and the results of the meanline model.

The integration of the meanline turbine model and the 1-D gas dynamic code is described in [10]. The 1-D turbine model is able to predict the unsteady swallowing capacity and the instantaneous turbine power is calculated by the meanline model. The solved unsteady flow via the volute of a single entry turbine is an input to meanline model.

The 1-D model is solving the Euler equations by second order finite difference method with Lax-Wendroff scheme combined with TVD limiter. Four rotor inlet points around the volute are modelled.

The meanline model calculates the instantaneous turbine power by solving the velocity triangles at inlet and exit of the impeller and taking into account the flow losses across the turbine.

The mentioned model was not tested in conjunction with the model of the internal combustion engine and does not include the mixing of flows in the case of the twin entry turbine.

The development of another 1-D radial turbine model is demonstrated in [11]. The quasi steady 0-D model of the rotor as a constant rothalpy element was developed. The accumulation and wave effects are located in the turbine volute. The model is compound from 1-D elements discretized by the finite volumes and solved through Godunov scheme. The model is calibrated by the results of 3-D CFD simulation under steady and pulsating flow. The mentioned model of a radial turbine is not able to solve the reverse flow in stator and rotor.

The results of the in-house code solving the governing equations for the volute, nozzle and impeller are discussed in [14]. The predictions of the unsteady turbine performance are based on the Euler equations with source terms. The source terms are determined from the measured steady flow maps of a turbine. The impeller is assumed adiabatic with 1-D flow along the central line, represented by two control volumes - for the axial and radial section, see *Figure 14*. The

computational grid points are in *Figure 15*. The model was not tested in combustion engine simulation.

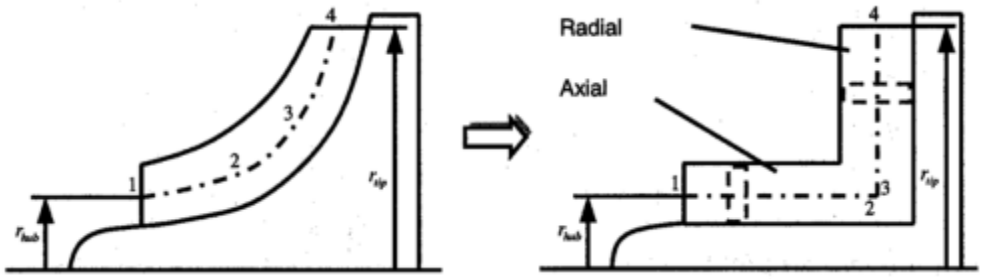

Figure 14 Simplified 1-D geometry of an impeller

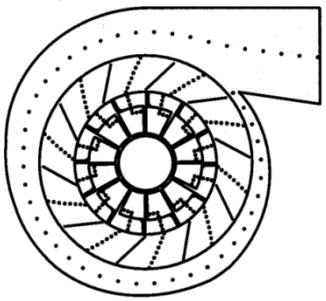

Figure 15 Distribution of computational grid points in absolute and relative frames

The 1-D model of a radial centripetal turbine with compressible flow in the rotating channel is in detail described in [37]. The model is able to generalize and extrapolate experimental results out of the measured ranges. The resulting steady flow turbine maps are suitable during the turbocharger matching procedure.

The unsteady flow model of a single scroll radial centripetal turbine using the 1-D approach developed in the GT-SUITE environment is demonstrated in [34] and [36]. The unsteady central streamline model uses the GT-SUITE solver. The turbine is compound from the discreet components such as 1-D pipes with variable areas, source terms, modules for momentum mixing and splitting and orifices with variable discharge coefficients. The mentioned model is able to cooperate with any model in GT-SUITE directly. The results obtained using 0-D map based and full 1-D approaches are discussed in [34].

The submitted thesis describes the methodology based on the map-less approach. The classical steady flow maps of a turbine are not utilized during the entire process of the turbine model development. The methodology utilizing the map-less approach requires the measurement of the twin scroll turbine under different level of the impeller admission on the specific turbocharger test bed with separated sections. The measured experimental data has to be evaluated for the purposes of turbine model calibration process. The appropriate full 1-D model of a radial centripetal turbine with twin scroll has to be developed.

It has to be stressed properly that the present simulation research builds on the work mainly of prof. Ing. Jan Macek, DrSc. and doc. Ing. Oldřich Vítek, Ph.D.

published in [37], [36], [34] and [35]. The main features and experience from the previous 1-D turbine models will be employed.

2.3 GT-SUITE 1-D Solver

Today, the development of 1-D unsteady flow solver is almost finished, so it is convenient to utilize existing validated solvers. The GT-SUITE Lax-Wendroff flow solver with staggered grid at pipe connections, used for simulations, is described in [4]. The governing equations are the conservation of mass (9), energy (10) and (11) and momentum (12), see [4].

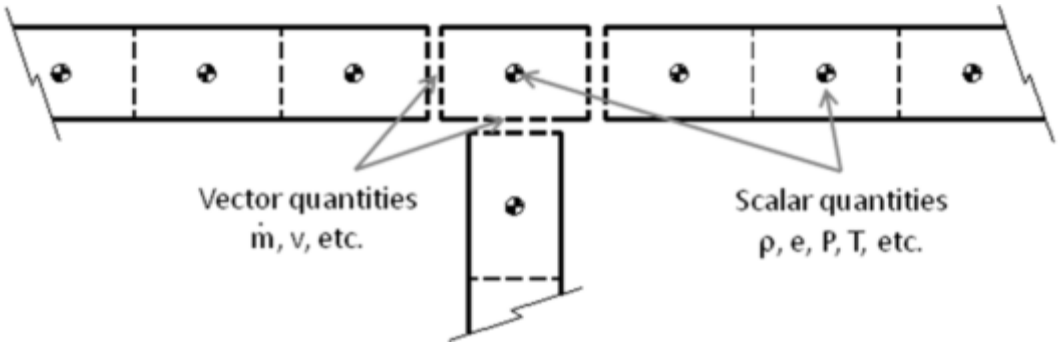

Figure 16 Schematic of staggered grid approach: vector quantities calculated at boundaries, scalars calculated at centroid [4]

$$\frac{dm}{dt} = \sum_{boundaries} \dot{m} \tag{9}$$

$$\frac{d(me)}{dt} = -p\frac{dV}{dt} + \sum_{boundaries} (\dot{m}H) - hA_s\left(T_{fluid} - T_{wall}\right) \tag{10}$$

$$\frac{d(\rho HV)}{dt} = \sum_{boundaries} (\dot{m}H) + V\frac{dp}{dt} - hA_s\left(T_{fluid} - T_{wall}\right) \tag{11}$$

$$\frac{d(\rho u A)}{dt} = \\ = \frac{dpA + \sum_{boundaries}(\dot{m}u) - 4C_f \frac{\rho u|u|}{2} \frac{dxA}{D} - C_p \left(\frac{1}{2}\rho u|u|\right) A}{dx} \tag{12}$$

The equations are calculated in one dimension only. There are explicit and implicit time integration methods. The mass flow rate, density and internal energy are primary solved variables in the case of the explicit method. The primary solution of the implicit method consists in the mass flow rate, pressure and total enthalpy.

The explicit method is determined for highly unsteady flow with pressure pulsations in engine air flows and fuel injection systems. The right hand side of the governing equations stated above is calculated via the values from the previous time step. The values at the new time step are solved by integration of the primary variables derivative over the time step.

The implicit method is useful for simulation with the large time steps, where the high frequency phenomena are not important. The implicit method calculates the values of all finite volumes simultaneously in an iterative way via the non-linear system of algebraic equations.

The model is discretized into finite volumes. The pipe is divided into one or more volumes and the flowsplit is described by a single volume. The finite volumes are connected via boundaries. The vector variables such as mass flux, velocity, mass fraction fluxes, etc. are calculated for each boundary. The scalar variables (pressure, temperature, density, internal energy, enthalpy, species concentration, etc.) are assumed to be uniform over each volume as drawn in *Figure 16.* The description of the solver is stated in [4].

3. Goals of the Research

The main goal of the thesis is to develop comprehensive methodology, based on the map-less approach, which enables to describe the performance of the radial centripetal turbine with twin scroll under steady and unsteady conditions by the full 1-D model.

The first goal is to develop the specific turbocharger test bed, which is capable to measure the performance of the twin entry turbocharger turbine under steady flow with the different level of the impeller admission. It is also necessary to create the software for evaluation of the directly measured physical quantities.

The second goal is to develop the modular unsteady 1-D model of a radial centripetal turbine with twin scroll in available 1-D simulation software. The model must be able to describe the phenomena inside a turbine, mixing of flows upstream of the impeller, arbitrary level of impeller admission and interactions between the reciprocating internal combustion engine and the turbocharger.

The third goal is to validate and verify the mentioned methodology by the simulation of the internal combustion engine with the unsteady 1-D model of a twin scroll turbine at steady states and transients. The simulation results have to be compared with experimental data measured on the experimental diesel engine.

4. Experiments - Turbocharger

The goal of the chapter is to describe the development of the specific turbocharger test bed, which is capable to measure the performance of a twin entry turbocharger turbine under steady flow with the different level of the impeller admission and the testing procedure of a turbocharger equipped with the twin entry volute.

The turbocharger energy balance and definition of the overall parameters of the turbine with twin scroll are presented in detail. Evaluation of experimental data and obtained results are properly discussed.

4.1 Test Bed Development

The first aim of the project was the development of the specific turbocharger test bed, which would allow the measurement of the turbochargers equipped with a twin entry turbine. The standard approach, when the turbine is measured under full equal admission of the impeller like the single scroll turbine, is useless for the description of the interactions between divided sections of the twin entry turbine.

It is necessary to separate the turbine sections on the test bed and to control the flow parameters upstream of the turbine. Then it is possible to study the influence of different conditions upstream of sections and their changes on the turbine performance and overall parameters.

The project began in cooperation with ČZ a.s. Turbo division in Strakonice, Czech Republic. The state of the art testing laboratory of the turbochargers with single combustion chamber has been selected as the basement of the intended research activities.

The required capabilities of the test bed were: throttling in sections to achieve different levels of the turbine wheel admission, closing sections, measurement of mass flow rates in separated sections including the back flow, all relevant pressures and temperatures and testing all sizes of turbochargers with twin scroll from the ČZ a.s. production.

At the beginning of the test bed development, several models of virtual test bed were created and properly tested in the GT-SUITE environment [SW 1]. The virtual open loop turbocharger test bed with a model of the combustion chamber and necessary PID controllers is a very useful tool not only during the development of new testing device but also before any real measurement. The detailed description of the model is presented in the simulation part of the thesis.

The main dimensions of the test bed were predicted using the mentioned virtual model. After selection of the turbine for testing purposes, the turbine operating ranges were calculated. There is no problem to unload the turbine (i.e. to achieve high blade speed ratios - BSR) when it is driven by cold air only.

There are three ways how to overload the turbine (i.e. to achieve low BSR): 1) increase the enthalpy upstream of a turbine, 2) load the turbine by the compressor with large wheel, 3) load the compressor in closed air circuit by higher density of air at inlet, which is complicated due to needed air cooling and additional load of a turbocharger thrust bearing. The first is problematic due to limited temperatures at combustion chamber outlet and turbine inlet and the second by virtue of the compatibility of compressor and bearing housings. The combination of both approaches (i.e. high temperature turbine upstream and the compressor with larger wheel) has been used for overloading the tested turbine.

The mass flow rates in separated sections are measured and evaluated indirectly through the pressure difference on the orifice with defined diameter. The whole system was properly simulated in GT-SUITE environment.

The full range of conditions in sections during the measurement was calculated. The measuring sections with orifices are designed in compliance with the ČSN EN ISO 5167:2003 standard. The assembly drawings were drawn by the staff of ČZ a.s.

Ing. Petr Hatschbach, CSc. created a computer program based on the mentioned ISO standard, which is capable to calculate a suitable diameter of the orifice for the entered range of mass flow rates. The corresponding pressure difference on the orifice is also calculated. The relevant ranges of mass flow rates and temperatures were predicted via the model of the open loop test bed for twin entry turbines created in GT-SUITE.

The testing possibilities of the developed test stand are shown in *Figure 17.* The twin entry turbine may be measured under full admission of the impeller. It is possible to achieve arbitrary level of partial admission via throttling in sections. The extreme level of partial admission is attainable through the enclosure of a section. The measurement of the back flow in section, if occurs, is also feasible.

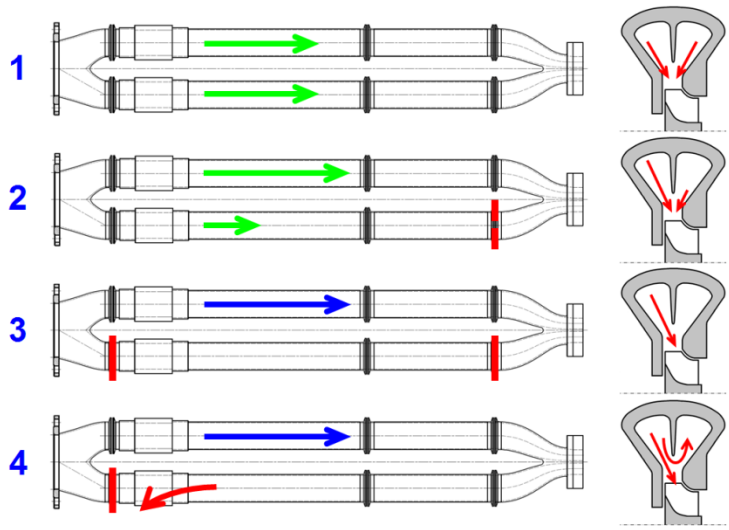

Figure 17 Test bed measurement capability: 1) uniform (full - equal) admission; 2) partial (unequal) admission (throttling in one section); 3) partial admission with closed section; 4) backflow

The operation parameters of the test stand are in *Table 1.* The tested turbine could be driven by cold air, exhaust gases (burning of natural gas) or mixture of cold air and exhaust gases. The maximum mass flow rate via the stand and maximum temperature downstream of the combustion chamber are strictly limited. The limitation of the mass flow rate complicates the measurement of a compressor map when the turbine is driven by the cold air only. The high turbocharger speeds, i.e. higher pressure ratios of a compressor are not accessible.

Table 1 Parameters of the open loop turbocharger test bed

Operation mode	air / exhaust gases / mixture
Fuel	natural gas
Maximum mass flow rate	0.5 kg.s-1
Maximum burner outlet temperature	1273 K

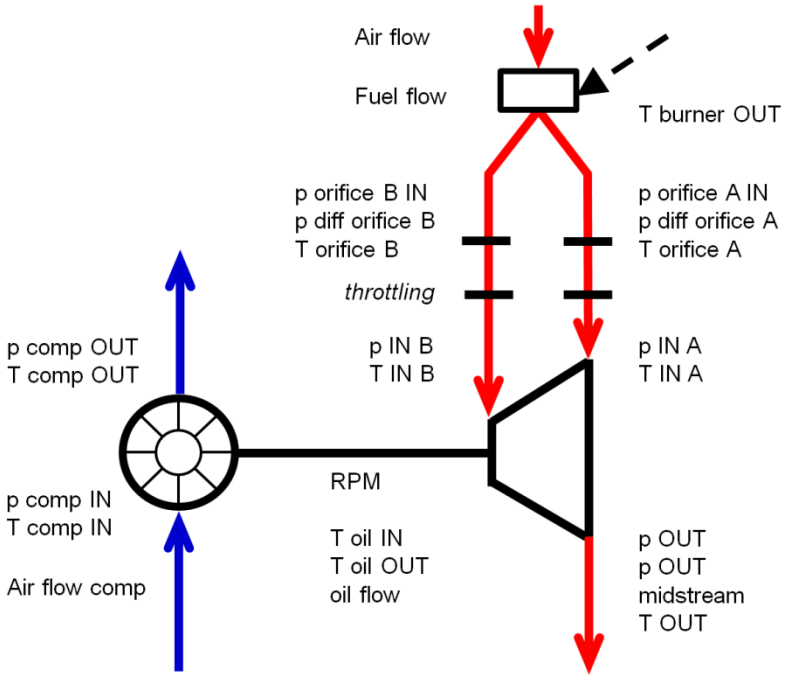

Figure 18 Measurement chain of the developed turbocharger test bed with open loop for twin scroll turbines

The measurement chain of the built testing device is presented in *Figure 18.* All measured physical values are also stated in *Table 2.* All mentioned values are needful for evaluation of the measured machines performance under arbitrary steady flow conditions. The standard data acquisition system (DAQ) has been used not only for the data recording but also for control of the open loop turbocharger stand.

Table 2 Overview of measured physical values on turbocharger test bed

Compressor	mass flow rate	p inlet	T inlet
		p outlet	T outlet
	speed		
Burner	air mass flow rate		T outlet
	fuel mass flow rate		
Section A		p orifice IN	
		p difference	T downstream
Section B		p orifice IN	
		p difference	T downstream
Turbine		p inlet A	T inlet A
		p inlet B	T inlet B
		p outlet	T outlet
		p outlet midstream	
Oil	mass flow rate		T inlet
			T outlet
Ambient		p ambient	T ambient

The Micro-Epsilon sensor for counting the compressor revolutions is in *Figure 19.* Every blade of the compressor wheel generates a pulse and the controller calculates the speed pursuant to number of blades and number of pulses in time.

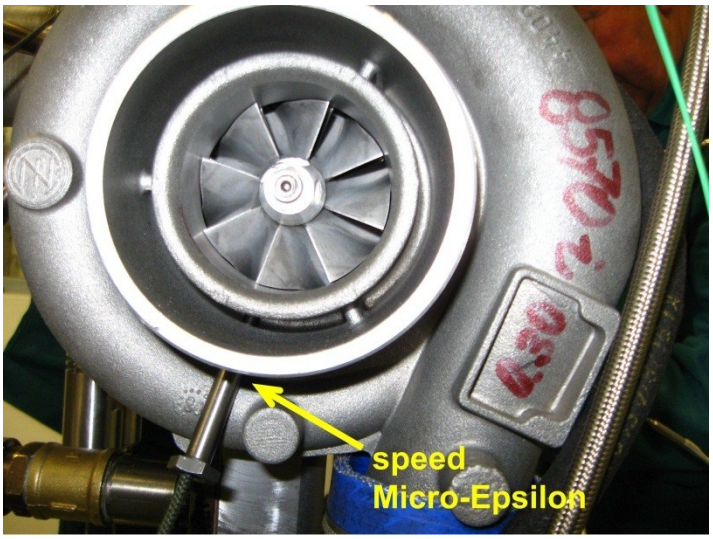

Figure 19 Detail of compressor with Micro-Epsilon sensor for measurement of turbocharger speed

The test cell overview before measurement is shown in *Figure 20*. The parts for sensing of the oil temperatures at turbocharger inlet and outlet were designed specially for the tested type of a turbocharger (*Figure 21*). It is important to measure the oil temperatures close to bearings housing, to reach an acceptable level of measurement accuracy.

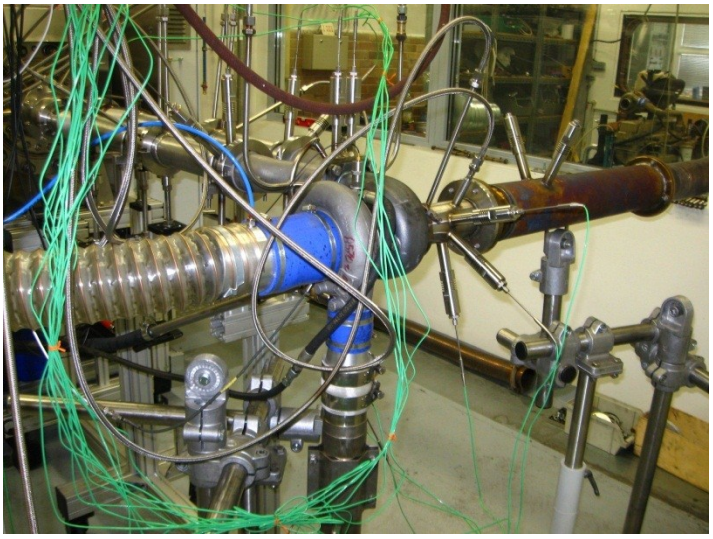

Figure 20 View of the prepared test bed from the compressor side

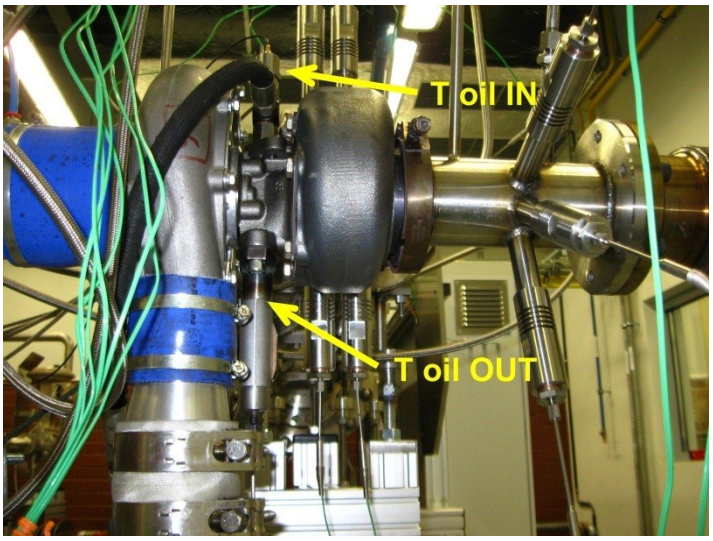

Figure 21 Measurement of inlet and outlet oil temperatures

The mass flow rate (air, exhaust gases or mixture) via the single combustion chamber is divided into separated sections downstream of a burner. The layout of equipment with pipe compensators in sections is shown in *Figure 22*.

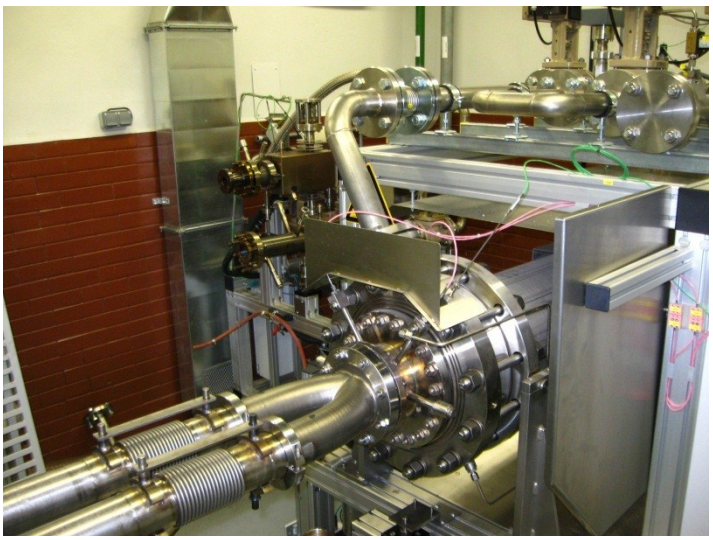

Figure 22 Division of flow into sections downstream of a combustion chamber

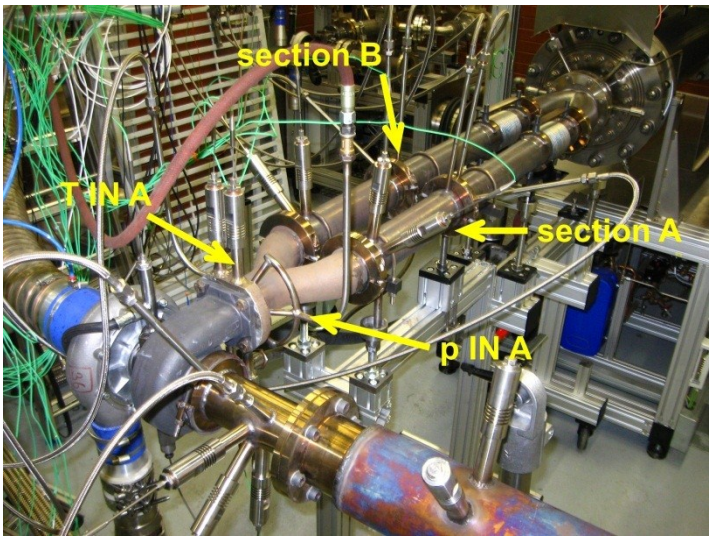

Figure 23 Twin scroll turbocharger test bed overview; separated sections A, B; measuring points of pressure and temperature turbine upstream (analogical for section B)

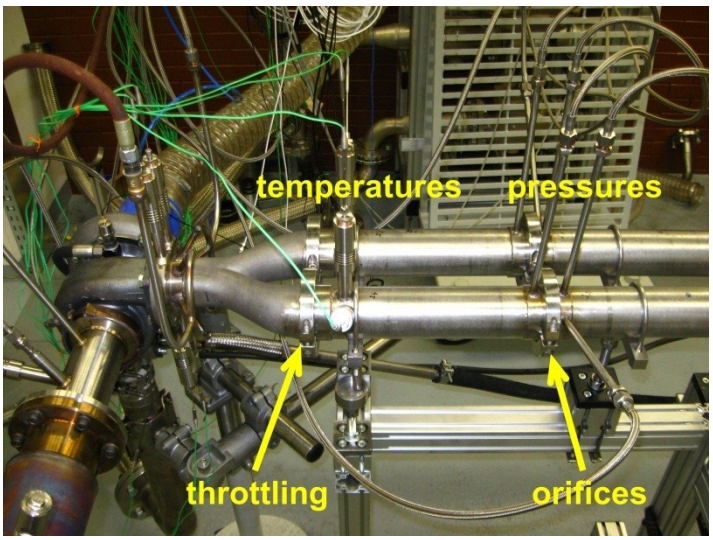

Figure 24 Location of orifices for measuring of mass flow rates in sections (static pressures, pressure differences, temperatures downstream of orifices); location of throttling in both sections if required

Throttling, which is necessary for reaching of required level of the impeller wheel partial admission, is feasible in both separated sections upstream of the turbine (*Figure 24*). The extreme level of partial admission is accessible via the closure of one section. The mentioned feature of the test bed may be useful during the testing of a turbine with symmetric design of twin scroll and essential for the measurement of a turbine with asymmetric sections.

The measurement location of pressure difference across the orifices, downstream temperatures and values upstream of a turbine is highlighted in *Figure 23* and *Figure 24*.

For the simulation purposes such as 3-D CFD, may be useful information about the influence of the tangential velocity downstream of the turbine. The layout of the measurement chain downstream of the turbine was suited to mentioned scopes. The pipe downstream of the turbine has been fitted with the usual static pressure take-offs and also with the probe which is able to sense the static pressure midstream of flow at turbine outlet. See *Figure 25* and *Figure 26.*

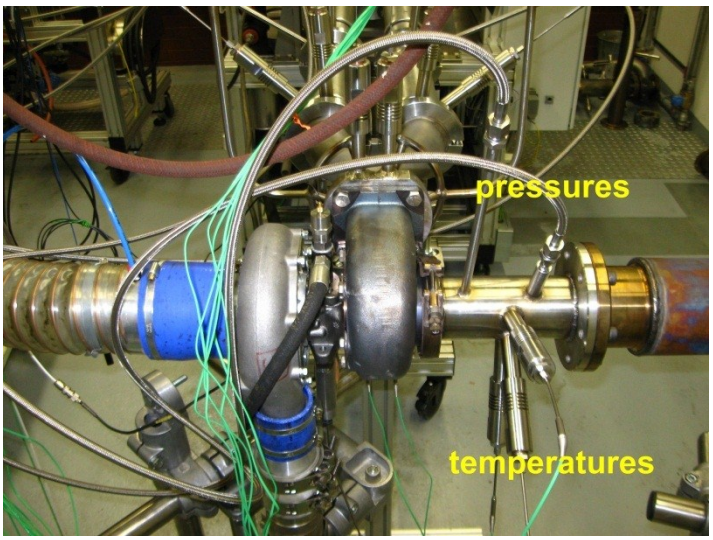

Figure 25 Measurement of temperature, static pressure and midstream pressure turbine downstream

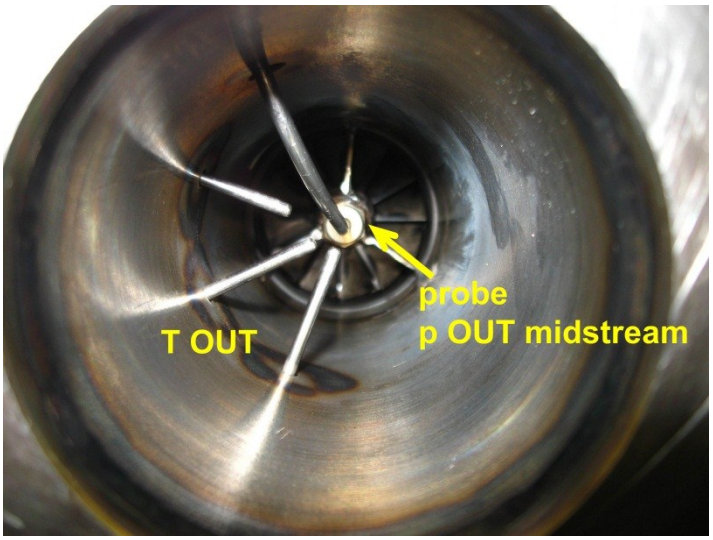

Figure 26 Turbine outlet temperature (three thermocouples); probe for the measurement of midstream static pressure

4.2 Description of Turbocharger Testing

The aim of the measurement on the turbocharger test bed under steady flow is to obtain comprehensive experimental data, essential for calibration process of the turbine 1-D model.

The map-less approach requires several levels of turbine load (BSR), pressure ratio and impeller admission. It is necessary to measure extreme cases, i.e. full admission and partial admission of an impeller when one turbine section is closed. Three levels of impeller admission were measured in our case - full, partial (throttling in one section) and partial with closed section.

This is one of great advantage of the map-less approach, because relatively low number of measured operating points under steady flow is sufficient for the description of the twin scroll turbine behaviour. The range of experimental data is also sufficient for the calibration process of the twin scroll turbine 1-D model, which has a physical background. The properly calibrated comprehensive 1-D model also enables reasonable extrapolation, which is so useful at the early stage of the development process.

The map-less approach does not mean that it is not possible to create classical steady flow turbine maps. The fundamental fact is that turbine maps are useless during the whole process from experiments on the turbocharger test bed, data evaluation and full 1-D twin scroll turbine calibration to complex unsteady simulation of the turbocharged internal combustion engine. The advantage of the map-less approach consists in the possibility to derive steady flow turbine maps at any phase of the process, thus right after the measurement or to use tailored regression formulas for turbine efficiency and discharge coefficient. Very interesting and beneficial is the feasibility to use the fully calibrated 1-D turbine model as a generator of steady flow maps, which are still very important for simple fast running or real-time models. All possibilities will be presented in simulation part of the work.

The map based approach for twin scroll turbine is very different. It is necessary to cover whole range of the turbine working area. The special turbine map has to be measured for each particular level of impeller admission with changing pressure and blade speed ratios. It is essential to measure much more working points in comparison with the map-less approach, what is demanding and very expensive. The extrapolation of measured steady flow maps, without proper simulation tool based on physics, is problematic. The generated maps are also valid only for the tested turbine and further utilization of maps is limited especially for virtual prototypes.

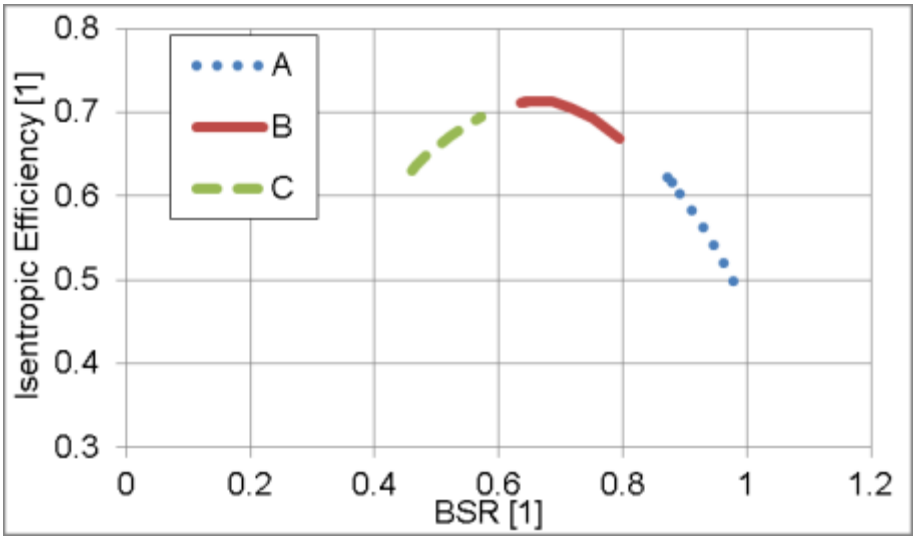

Figure 27 Turbine efficiency vs. blade speed ratio (BSR); A) turbine unloaded (turbine driven by cold air) - blue dotted line; B) turbine driven by exhaust gases T = 873 K - red line; C) turbine overloaded, coupled with larger compressor wheel, driven by exhaust gases T = 1073 K - green dashed line

At the beginning of the project, thus before the real measurement, it was necessary to properly simulate all planned experiments. The simulation on the virtual open loop test bed for turbochargers with twin scroll turbine is the best way how to specify the conditions of real-world experiments. The virtual twin entry turbine was created for the mentioned purposes. The parameters (mass flow rate, efficiency) were close to supposed real turbine later selected for real experiments.

For the evaluation of the turbine parameters, it is crucial to measure turbine behaviour in a wide range of load. The turbine load is described by the blade speed ratio - BSR. The situation is briefly presented in *Figure 27*.

The turbine, driven by cold air only, is unloaded and able to achieve high blade speed ratios. With the temperature of exhaust gases about 900 K upstream of the turbine, the turbine is able to run with isentropic efficiency close to optimum. The left branch of the turbine characteristic is very important working area, where the turbine is overloaded, thus the blade speed ratio and isentropic efficiency decrease.

The results of the simulation study showed that the selected turbine type combined with the standard (appropriate) compressor wheel is unable to reach sufficiently low BSR only by the increase of exhaust gases temperature upstream of the turbine. The temperature upstream of the turbine is limited due to material of the impeller and the temperature downstream of the combustion chamber is strictly limited too (*Table 1*).

The compressor with larger wheel and casing compatible with the housing of bearings was found for the described purposes. The combination of the compressor with larger wheel and relatively high temperature upstream of the turbine about 1100 K seemed to be sufficient for our research.

The further step was the determination of the required level of partial admission of the turbine wheel. The standard testing consists in the measurement under equal admission of the impeller and the situation is the same as the testing of the single scroll machine. Many cases with the different level of partial (unequal) admission were simulated on the virtual test bed in GT-SUITE. The testing with embedded throttling sheet metal in section and with the section closure was specified based on the simulation results.

The measurement of the compressor maps (of both compressors with standard and larger wheel) was the integral part of the experimental research. The goal was to evaluate the influence of the heat transfer from the turbine on the apparent compressor power and efficiency.

The knowledge of the compressor power is essential, because the turbine power cannot be determined from the enthalpy head on the side of the turbine as described in the chapter 4.4. Map less approach was applied also to compressor power using direct measurement of compressor power. It was based on specific enthalpy (temperature) difference with negligible heat transfer from a turbine (turbine driven by cold air) and measurement of a mass flow rate via compressor.

It was needful to measure the compressor maps when the turbine was driven by exhaust gases and by cold air only. The measurements under cold conditions are

demanding and the evaluation of the whole compressor map is impossible because of the limited air mass flow rate via the test bed. Used turbocharger test bed is primarily specified for long-term cyclic testing, so the maximum admissible mass flow rate is relatively low (0.5 kg.s-1).

The measurements were specified by the conditions in the section A upstream of the turbine. The flow parameters in section A were also used for the control of the test bed via the online data acquisition. The pressure and temperature in control section A were held constant during each test. The load of the turbine was changed by means of the different mass flow rate via compressor. The compressor map is quite narrow bounded by two extremes - compressor surging and choking. The first was operating point close to compressor surging, the second was the point at maximum attainable mass flow rate via the compressor and then several points between these extremes. This type of turbine measurement is demanding due to narrow working range of a turbine with a compressor utilized as a load. The usage of further compressor is requisite for the extension of the operating region.

This is a typical feature of the measurement on a turbocharger test bed with open loop. The experiments on the turbine loaded by the appropriate dynamometer or brake would be preferable, but much more expensive too.

The measurement of the mass flow rate via turbine with the blocked impeller (*Figure 28*), i.e. with the blade speed ratio BSR = 0 (isentropic efficiency = 0), was also included in the prepared detailed schedule of the experiments.

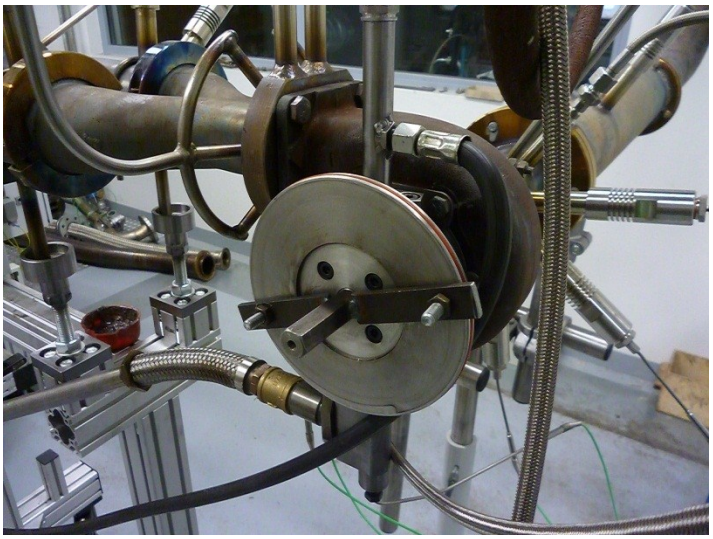

Figure 28 Measurement with blocked turbine wheel, BSR = 0

4.3 Overall Parameters of Twin Entry Turbine

For the description of the twin scroll turbine features, it is needful to define parameters for model validation, thus comparison of measured and simulated results. The map less approach needs mass flow rates in individual scroll sections and total turbine power at given turbine speed only, nothing else. For comparison and analysis purposes, it is possible to define conventional turbine parameters, as

discharge coefficient or isentropic efficiency. The issue is in definition of ideal averaged state for those standard but not necessary parameters.

The definitions in equations below are used during the measured data evaluation and also valid in all models. The generally accepted definitions of the multi entry turbine parameters are not established and differ significantly.

The actual mass flow rate and power are essential physical quantities for the description of turbine performance. The established definitions of other values have to be taken into account during the results analysis, but are not needed during simulation. In the current work, the overall values of the twin scroll turbine are averaged by the actual isentropic power of each section. Averaging of mass flow rate in sections may be also useful in some specific cases and results are similar to power weighted.

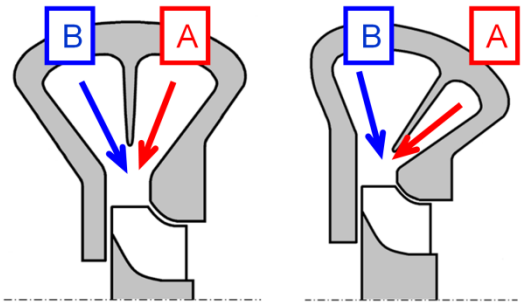

Figure 29 Sketches of twin entry turbine housings, symmetric design of sections (left), asymmetric design (right)

The map-less approach, selected for the current research, is based on the description of the turbine performance under arbitrary level of load and impeller admission by overall parameters, not by the database of the measured steady flow maps. The physical model of a turbine as a whole machine is the integral part of the internal combustion engine cycle simulation.

It is necessary to define the overall parameters of a twin entry turbine with different design under any conditions in sections (*Figure 29*). The overall twin entry turbine parameters are weighted in accordance with the isentropic power of each section as stated in (13), (14) and (15). The only exception is the definition of the discharge coefficient as noted below.

$$P_{ise\_AB} = P_{ise\_A} + P_{ise\_B} \tag{13}$$

$$(\dot{m}_A + \dot{m}_B)\Delta h_{ise\_AB} = \dot{m}_A \Delta h_{ise\_A} + \dot{m}_B \Delta h_{ise\_B} \tag{14}$$

$$(\dot{m}_A + \dot{m}_B)\frac{c_{s\_AB}^2}{2} = \dot{m}_A\frac{c_{s\_A}^2}{2} + \dot{m}_B\frac{c_{s\_B}^2}{2} \tag{15}$$

The definition of the fictitious isentropic velocity (16) is derived from the balance of isentropic powers (13).

$$\frac{c_{s\_AB}^2}{2} = \frac{1}{(\dot{m}_A + \dot{m}_B)}\left(\dot{m}_A\bar{c}_{p\_A}T_{IN\_A\_tot}\left[1 - PR_A^{\frac{1-\bar{\kappa}_A}{\bar{\kappa}_A}}\right] + \right.$$
$$\left. + \dot{m}_B\bar{c}_{p\_B}T_{IN\_B\_tot}\left[1 - PR_B^{\frac{1-\bar{\kappa}_B}{\bar{\kappa}_B}}\right]\right) \tag{16}$$

The level of partial admission of an impeller is defined as a fraction of the isentropic power in appropriate section to the total isentropic power (17). The admission level of the section B is analogical to relation for section A in (17).

$$level_A = \frac{\dot{m}_A\frac{c_{s\_A}^2}{2}}{\dot{m}_A\frac{c_{s\_A}^2}{2} + \dot{m}_B\frac{c_{s\_B}^2}{2}} \tag{17}$$

The twin scroll turbine pressure ratio (total - static) is calculated via the equation (18). The related estimation of the total pressure turbine upstream (20) is derived from the simple relation of the pressure ratio in (19). The relevant total pressure upstream of a turbine is used in the relation of the discharge coefficient (23).

$$PR_{AB\_t\_s} = \left[1 - \frac{\dot{m}_A\frac{c_{s\_A}^2}{2} + \dot{m}_B\frac{c_{s\_B}^2}{2}}{(\dot{m}_A + \dot{m}_B)\bar{c_p}T_{IN\_AB\_tot}}\right]^{\frac{\bar{\kappa}}{1-\bar{\kappa}}} \tag{18}$$

$$PR_{AB} = \frac{p_{IN\_AB\_tot}}{p_{OUT}} \tag{19}$$

$$p_{IN\_AB\_tot} = PR_{AB}\, p_{OUT} \tag{20}$$

The determination of the turbine wheel tip speed (21) is used for the calculation of the overall turbine blade speed ratio via the equation (22).

$$tip_{speed} = u_2 = \frac{\pi D_{ref} 10^{-3} RPM}{60} \tag{21}$$

$$BSR_{AB} = \frac{u_2}{c_{s\_AB}} = \frac{\pi D_{ref} 10^{-3} RPM}{60\, c_{s\_AB}} \tag{22}$$

The overall discharge coefficient of a twin entry turbine is the only exception, because it is defined as a fraction of the mass flow rates sum to the reference mass flow rate via machine (23).

$$\mu_{AB} = \frac{\dot{m}_A + \dot{m}_B}{\dot{m}_{ref}} = \frac{\dot{m}_A + \dot{m}_B}{A_{t\_ref} \frac{p_{IN\_AB\_t}}{\sqrt{r_{IN\_AB\_t}\, T_{IN\_AB\_t}}} \sqrt{\psi_{AB}}} \tag{23}$$

The turbine discharge coefficient is a relative value proportional to reference mass flow rate, but the base value has to be stated. The arbitrary reference area A t_ref is the key. For our purposes, the size of reference area is specified from the experiment with the blocked turbine wheel at PR = 2.2 (approximately) and zero blade speed ratio. The discharge coefficient of the mentioned operating point is selected to μ AB = 1, A t_ref is then rated and held constant for all experiments and simulation.

The flow function ψ AB evaluation depends on the actual pressure ratio compared to the critical value, (24) and (25). If the actual turbine pressure ratio is higher than the critical value, the flow function must be calculated in compliance with the equation (26), else the valid relation is (27).

$$PR_{AB} \geq PR_{AB\_crit} \quad \Rightarrow \psi_{AB\_max} \tag{24}$$

$$PR_{AB\_crit} = \left(\frac{2}{\kappa_{IN\_AB\_tot} + 1}\right)^{\frac{\kappa_{IN\_AB\_tot}}{1-\kappa_{IN\_AB\_tot}}} \tag{25}$$

$$\psi_{AB\_max} = \kappa_{IN\_AB\_tot}\left(\frac{2}{\kappa_{IN\_AB\_tot} + 1}\right)^{\frac{\kappa_{IN\_AB\_tot}+1}{\kappa_{IN\_AB\_tot}-1}} \tag{26}$$

$$\psi_{AB} = \frac{2\kappa_{IN\_AB\_tot}}{\kappa_{IN\_AB\_tot} - 1}\left(PR_{AB}^{\frac{-2}{\kappa_{IN\_AB\_tot}}} - PR_{AB}^{\frac{-\kappa_{IN\_AB\_tot}-1}{\kappa_{IN\_AB\_tot}}}\right) \tag{27}$$

The specific heat ratio κ IN_AB_total belongs to the total temperature IN_AB.

The classical steady flow maps in corrected or reduced format could be obtained from the results of experiments, if required for any map based model. The knowledge of the overall parameters stated in relations above is needed to calculate the reduced turbocharger speeds (28) and the reduced mass flow rate via turbine (29).

$$RPM_{red\_AB} = \frac{RPM}{\sqrt{T_{IN\_AB\_tot}}}\left(\frac{\kappa_{ref}}{\kappa_{IN\_AB\_tot}}\,\frac{r_{ref}}{r_{IN\_AB\_tot}}\right)^{0.5} \tag{28}$$

The specific heat ratio and gas constant IN_AB_total appertain to the total inlet temperature AB. The reference conditions, different for air and exhaust gases in general, have to be listed with generated steady flow maps.

$$\dot{m}_{red\_AB} = \frac{(\dot{m}_A + \dot{m}_B)\sqrt{T_{IN\_AB\_tot}}}{p_{IN\_AB\_tot}}\left(\frac{\kappa_{ref}}{\kappa_{IN\_AB\_tot}}\,\frac{r_{IN\_AB\_tot}}{r_{ref}}\right)^{0.5} \tag{29}$$

4.4 Turbocharger Energy Balance

Simplified energy balance of a turbocharger is briefly described in the chapter. Determination of correct compressor and turbine power is fundamental for evaluation of the measured data as will be discussed in the following chapter. The turbocharger with main energy fluxes is presented in *Figure 30*.

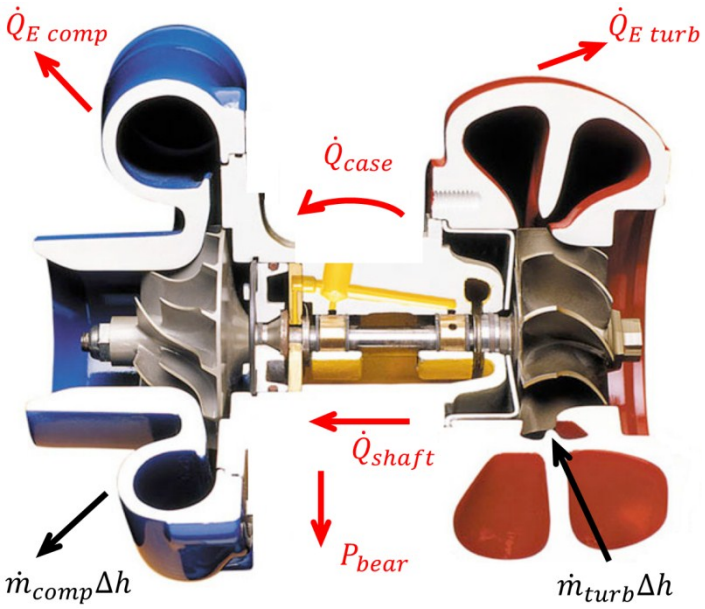

Figure 30 Simplified energy balance of a turbocharger with relevant energy fluxes

The turbine power cannot be evaluated from the balance of enthalpies introduced in (30). The turbine measurement with hot gas is influenced by the heat transfer in turbocharger components. A turbine does not work under adiabatic conditions. The values $\dot{Q}_{Ecomp}$ and $\dot{Q}_{Eturb}$ are negligible at low load, when turbine is driven by cold air, with mean temperature during expansion close to compressor mean temperature in the best case. Then, $\dot{Q}_{case}$, which is the most significant, and $\dot{Q}_{shaft}$ are almost zero. The heat fluxes may by neglected at higher load, as shown in [33].

$$P_{comp_{adi}} + P_{bear} + \dot{Q}_{Ecomp} + \dot{Q}_{shaft} + \dot{Q}_{case} + \dot{Q}_{Eturb} = \\ = \dot{m}_{turb}\left(h_{turb\_IN\_tot} - h_{turb\_OUT\_tot}\right) \tag{30}$$

The correct turbine power is defined in the equation (31). The sum of correct compressor power and pure power losses in bearings is essential for correct turbine power evaluation in any case. The aim is to identify from experimental results the pure losses in bearings and the compressor power close to adiabatic conditions without the influence of heat transfer from turbine side.

$$P_{turb} - P_{wind} = P_{comp\_adi} + P_{bear} \tag{31}$$

The isentropic efficiency of a turbine is calculated as a quotient of turbine power to total-static isentropic power (32). The flow mixing upstream of the impeller is the irreversible process. This fact has to be taken into consideration at valuation of all isentropic values stated at the turbine side. The relevance of turbine isentropic efficiency will be discussed in simulation parts.

$$\eta_{turb\_ise} = \frac{P_{turb} - P_{wind}}{P_{ise\_AB\_t\_s}} = \frac{P_{comp\_adi} + P_{bear}}{P_{ise\_AB\_t\_s}} \tag{32}$$

The overall turbine efficiency (33) is obtained as a product of isentropic turbine efficiency (32) and mechanical efficiency of a turbocharger (34).

$$\eta_{turb\_overall} = \frac{P_{comp\_adi}}{P_{ise\_AB\_t\_s}} \tag{33}$$

$$\eta_{mech} = \frac{P_{comp\_adi}}{P_{comp\_adi} + P_{bear}} \tag{34}$$

4.5 Measured Data Evaluation

The chapter deals with the problem, how to obtain valid compressor power (close to adiabatic conditions), pure power losses in turbocharger bearings and correct turbine power from experiments, thus the principal data for simulation models and their calibration. Described methodology is utilized in the appropriate software for processing of measured experimental data [SW 2].

The temperatures measured in steady flow by the thermocouples on the turbocharger test bed are between the values of the static and total temperatures (35), [42]. The fact of the partial flow deceleration is respected by the coefficient of restitution beta = 0.87 in (36).

$$T < T_m < T_{tot} \tag{35}$$

$$T_m = T + \beta(T_{tot} - T) = T + \beta\frac{c^2}{2c_p} = T + \beta\frac{1}{2c_p}\left(\frac{\dot{m}\, r\, T}{A\, p}\right)^2 \tag{36}$$

The derived relations for calculation of static and total temperatures are introduced in (37) and (38).

$$T = \frac{-1 + \left(1 + 4\beta \frac{1}{2c_p}\left(\frac{\dot{m}\, r}{A\, p}\right)^2 T_m\right)^{0.5}}{2\beta \frac{1}{2c_p}\left(\frac{\dot{m}\, r}{A\, p}\right)^2} \tag{37}$$

$$T_{tot} = \frac{1}{\beta}(T_m - T + \beta T) \tag{38}$$

The power losses in bearings cannot be evaluated from the measured oil enthalpy head (39), because the sensed temperatures are influenced by heat flux from the turbine driven by hot exhaust gases. The pure power losses in bearings have to be known for the proper energy balance of the turbocharger as described in chapter 4.4.

$$\dot{m}_{oil}\left(h_{OUT\_oil} - h_{IN\_oil}\right) = P_{bear} + \dot{Q}_{shaft} \tag{39}$$

The evaluation method of the correct power losses in bearing consists in usage of the regression model, used and verified in the previous work [56].

The built-up regression formula (40) for evaluation of power losses in bearings was used in the first step on power losses calculated from measured oil temperatures and mass flow rate (39). The regression formula was applied only on the results of hot tests (turbine driven by hot exhaust gases). The aim of the first step is to find suitable regression coefficients. The comparison of measured power losses and results of regression is presented in *Figure 31.* Low power losses from experiments are caused by very low temperature difference between oil inlet and outlet, low bearings load or measurement during turbocharger warm-up. The regression (with coefficients stated from hot tests) was applied to all measured points. Level of power losses prediction by the regression is acceptable including the points at low temperature at the turbine.

$$\begin{aligned} P_{Oil} = {} & A_0 + A_1 T_{ave\_tot\_IN\_AB;OUT} + A_2 T^2_{ave\_tot\_IN\_AB;OUT} + \\ & + A_3 RPM + A_4 RPM^2 + A_5 RPM^3 + A_6 p_{IN\_AB} + A_7 p_{OUT} + \\ & + A_8 p_{comp\_IN} + A_9 p_{comp\_OUT} \end{aligned} \tag{40}$$

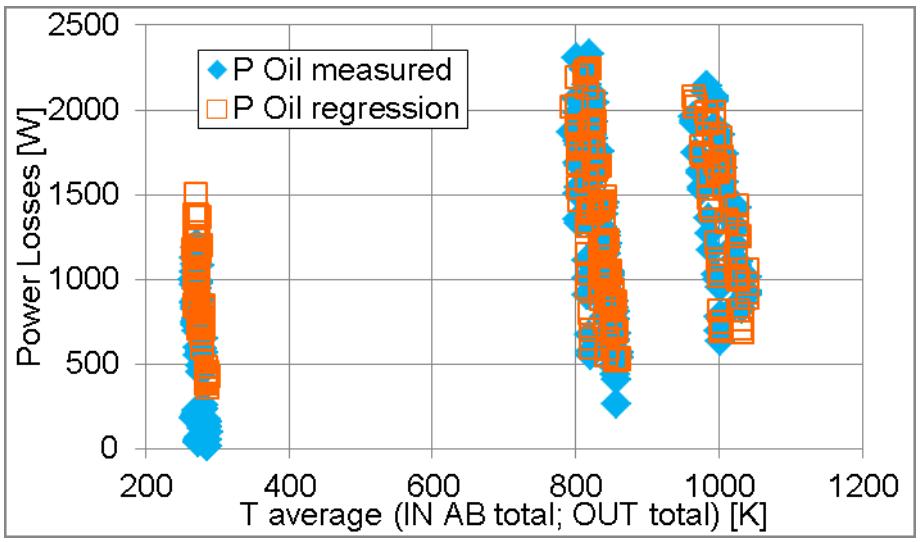

Figure 31 Power losses in bearings (measurement of oil mass flow rate and temperatures) - blue; results of regression model - orange squares; horizontal axis - average of total temperatures at turbine inlet sections A, B and turbine outlet

In the valid regression formula (41) for the pure power losses in bearings, the coefficients stated from hot tests are applied and average total temperature across the turbine is replaced by average oil temperature.

Measurement of low oil temperature difference during the cold tests, when the turbine is driven by cold air, is very problematic and resulting power losses in bearings are unreasonably low. Relevance of pure power losses in bearings is higher, when the regression coefficients are stated from hot measurements only.

$$P_{bear} = A_0 + A_1 T_{ave\_oil\_IN;OUT} + A_2 T^2_{ave\_oil\_IN;OUT} + \\ + A_3 RPM + A_4 RPM^2 + A_5 RPM^3 + A_6 p_{IN\_AB} + A_7 p_{OUT} + \\ + A_8 p_{comp\_IN} + A_9 p_{comp\_OUT} \quad (41)$$

The pure power losses in bearings compared to the experimental results are shown in *Figure 32*. The heat flux via turbocharger shaft calculated using the equation (39) is also illustrated.

Power losses in bearings (the influence of heat transfer from turbine side to oil is excluded) calculated via (41) seem to be reasonable. The regression predicts acceptable losses under all working condition.

The described method is relatively simple and not absolutely correct. The losses in bearings are not so high compared to compressor power, but the influence on final turbine results is not neglectable.

Level of measurement accuracy may increase with higher oil mass flow rate through turbocharger, higher oil temperature and longer time of each test on the steady flow test bed.

It would be also useful for the future improvement to create a simulation model of the turbocharger bearings to improve the predictive capability and level of accuracy. Modelling of bearings is currently out of thesis scope.

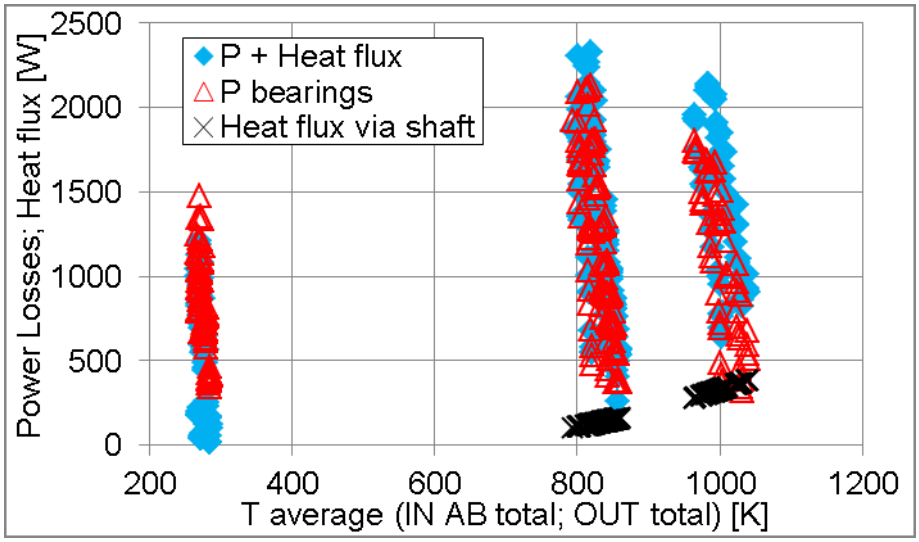

Figure 32 Power losses in bearings (measurement influenced by the heat transfer from turbine side) - blue; pure power losses in bearings - red triangles; heat flux via turbocharger shaft - black; horizontal axis - average of total temperatures at turbine inlet sections A, B and turbine outlet

The pure power losses in bearings are known, so the second unavoidable term in relation (31) of turbine power has to be evaluated. Power of the measured compressor is determined from the mass flow rate and enthalpy head through the relations (42) and (43). The heat flux from the turbine to compressor housing increases compressor outlet temperature so that it affects the enthalpy difference - (42) and (43).

$$P_{comp} = \dot{m}_{comp} \Delta h_{comp\_t\_t} \tag{42}$$

$$\Delta h_{comp\_t\_t} = \overline{c}_p \left(T_{comp\_OUT\_tot} - T_{comp\_IN\_tot} \right) \tag{43}$$

$$\Delta h_{comp\_IN\_t;OUT\_ise\_t} = \overline{c}_p \left(T_{comp\_OUT\_ise\_t} - T_{comp\_IN\_tot} \right) \tag{44}$$

The isentropic efficiency of the compressor (total - total states) is defined (45) as a fraction of the enthalpy differences (44) and (43).

$$\eta_{comp\_ise\_t\_t} = \frac{\Delta h_{comp\_IN\_t;OUT\_ise\_t}}{\Delta h_{comp\_t\_t}} \quad (45)$$

For the evaluation of turbine power from experimental data, it is essential to know the actual compressor power under any conditions. The regression formula (46) based on the Euler theorem for compressors [33], was used for determination of compressor power.

$$P_{comp\_adi} = \dot{m}_{comp} \left(K_1 u_{2\_c}^2 + K_2 w_{2\_r\_c} u_{2\_c} + K_3 w_{2\_r\_c}^4 + K_4 \frac{u_{2\_c}^4}{w_{2\_r\_c}^2} \right) \quad (46)$$

The needed relative radial velocity at compressor wheel outlet (48) is derived from measured mass flow rate via compressor (47). Main dimensions of standard and larger compressor wheel (outlet diameter D 2_c and width b 2_c) are known. The circumferential velocity is calculated simply by the formula (49).

$$\dot{m}_{comp} = A\rho w = \pi D_{2\_c} b_{2\_c} \rho_{2\_c} w_{2\_r\_c} \quad (47)$$

$$w_{2\_r\_c} = \frac{\dot{m}_{comp}}{\pi D_{2\_c} b_{2\_c} \rho_{2\_c}} \quad (48)$$

$$u_{2\_c} = \frac{\pi D_{2\_c} RPM}{60} \quad (49)$$

The valid isentropic efficiency of the compressor is estimated as a quotient of isentropic power and compressor power without impact of the heat transfer from the turbine (close to adiabatic conditions) (50).

$$\eta_{comp\_adi\_ise\_t\_t} = \frac{\dot{m}_{comp}\, \Delta h_{comp\_IN\_t;OUT\_ise\_t}}{P_{comp\_adi}} \quad (50)$$

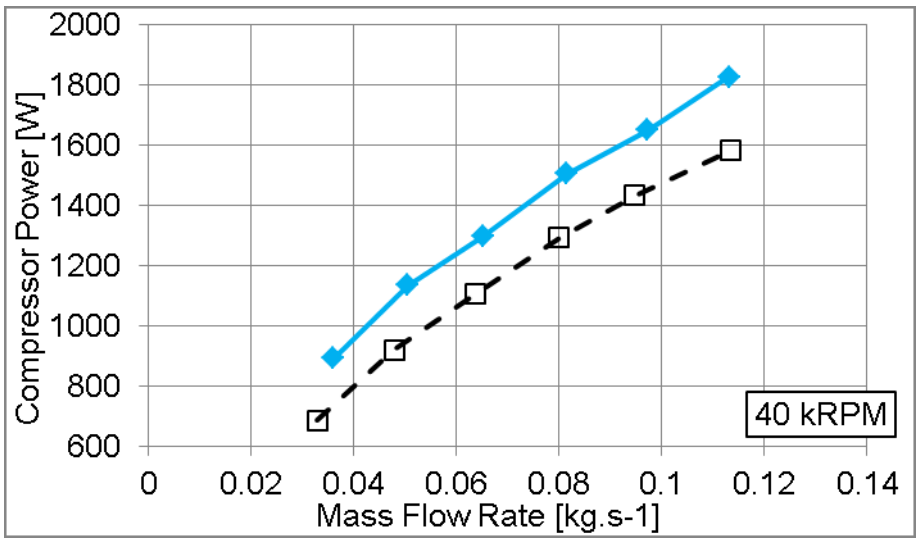

Figure 33 Compressor power evaluated from measured temperature difference (standard compressor wheel); turbine driven by exhaust gases (blue); turbine driven by cold air (black dashed line); turbocharger speed 40 kRPM

The compressor power with standard wheel, the appropriate type of compressor to the tested turbine, evaluated from measured temperature difference and mass flow rate under cold and standard conditions is compared in the pictures. The expression, cold conditions means that the turbocharger turbine is driven by cold air. The standard temperature of exhaust gases upstream of the turbine is about 900 K - standard conditions. Compressor power should not depend on temperature at turbine. At higher temperature at turbine, compressor power is influenced by the heat transfer from the turbine side and the compressor power evaluated from temperatures at compressor inlet/outlet is not correct. The biggest differences are visible at low speeds, where the influence of heat transfer from the turbine on measured values downstream of the compressor is highest - *Figure 33*. The heat transfer impact from the turbine driven by hot exhaust gases decreases with increasing turbocharger speed - *Figure 34* and *Figure 35*.

The coefficients used in the regression formula (46) for estimation of compressor power under any conditions in dependence on compressor speed are plotted in *Figure 36*. The coefficient courses are valid for compressor type with the standard wheel.

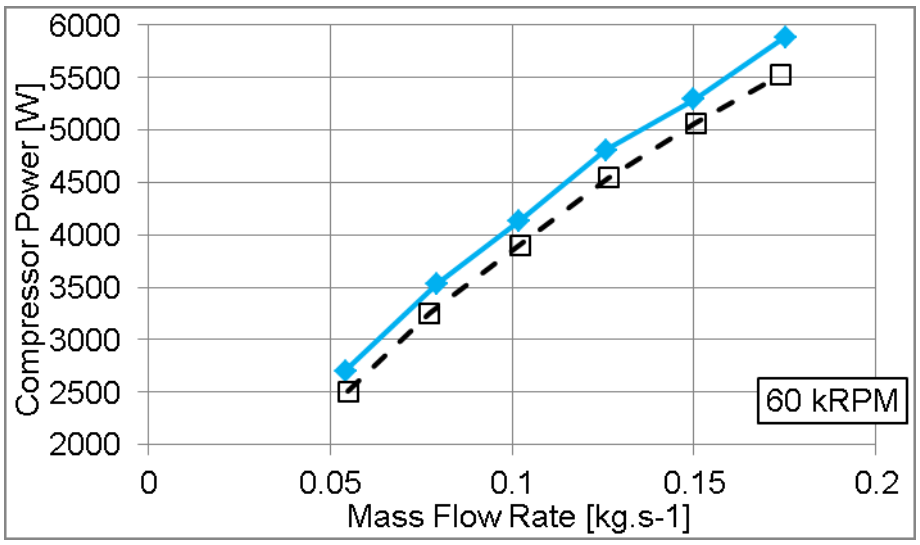

Figure 34 Compressor power evaluated from measured temperature difference (standard compressor wheel); turbine driven by exhaust gases (blue); turbine driven by cold air (black dashed line); turbocharger speed 60 kRPM

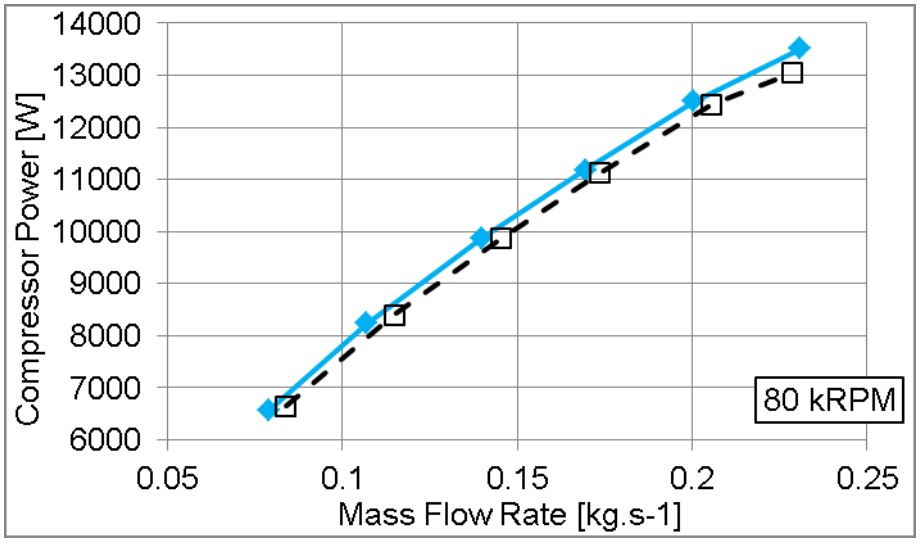

Figure 35 Compressor power evaluated from measured temperature difference (standard compressor wheel); turbine driven by exhaust gases (blue); turbine driven by cold air (black dashed line); turbocharger speed 80 kRPM

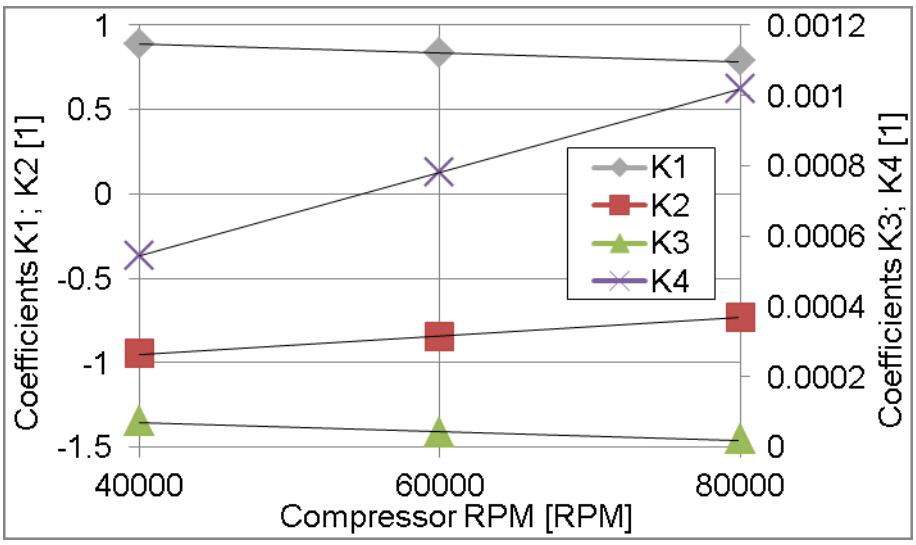

Figure 36 Courses of regression coefficients K1 - K4 used in formula for calculation of compressor power (standard compressor wheel)

The examples of results for the standard compressor are presented in following pictures. The efficiency of the compressor measured under cold conditions compared with results of the regression formula based on the Euler theorem is visible in *Figure 37*. The sufficient level of accuracy of the applied regression model is obvious from *Figure 37* and *Figure 38*.

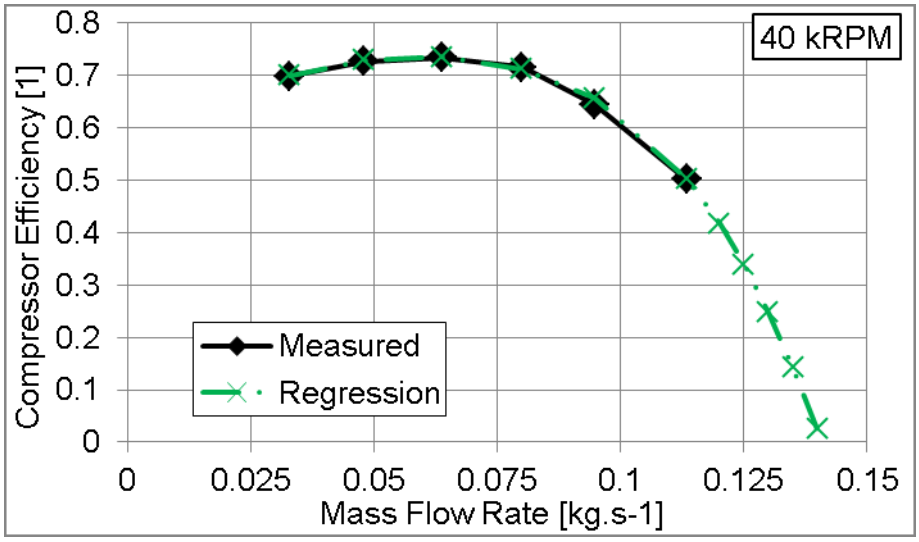

Figure 37 Comparison of measured compressor efficiency (turbine driven by cold air) with results of regression formula; standard compressor wheel; turbocharger speed 40 kRPM

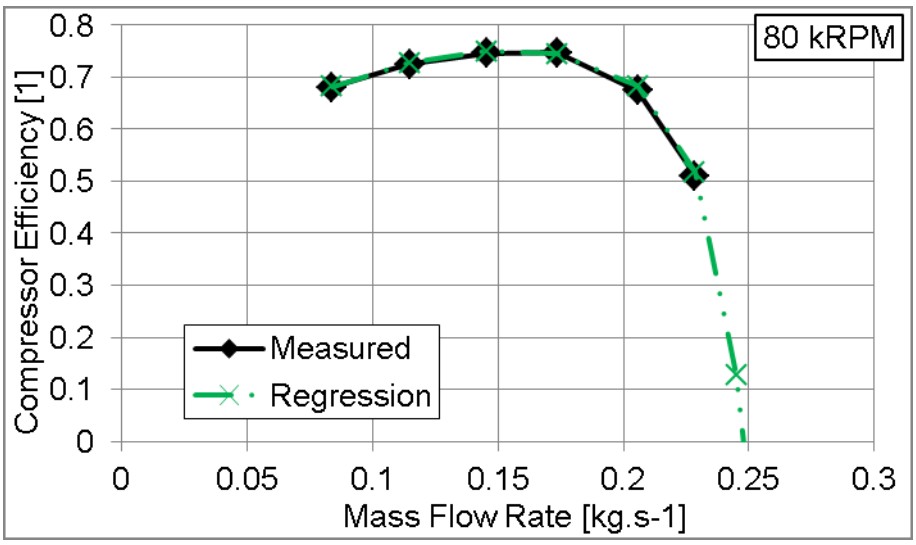

Figure 38 Comparison of measured compressor efficiency (turbine driven by cold air) with results of regression formula; standard compressor wheel; turbocharger speed 80 kRPM

The important results are presented in *Figure 39* and *Figure 40*. The efficiency of the standard compressor measured with high temperature upstream of the turbine, thus the state compressor downstream influenced by heat transfer from the turbine, is significantly lower compared with the efficiency of the adiabatic machine estimated via the regression formula. The differences decrease with the increasing compressor speed, which is in agreement with experimental results described above.

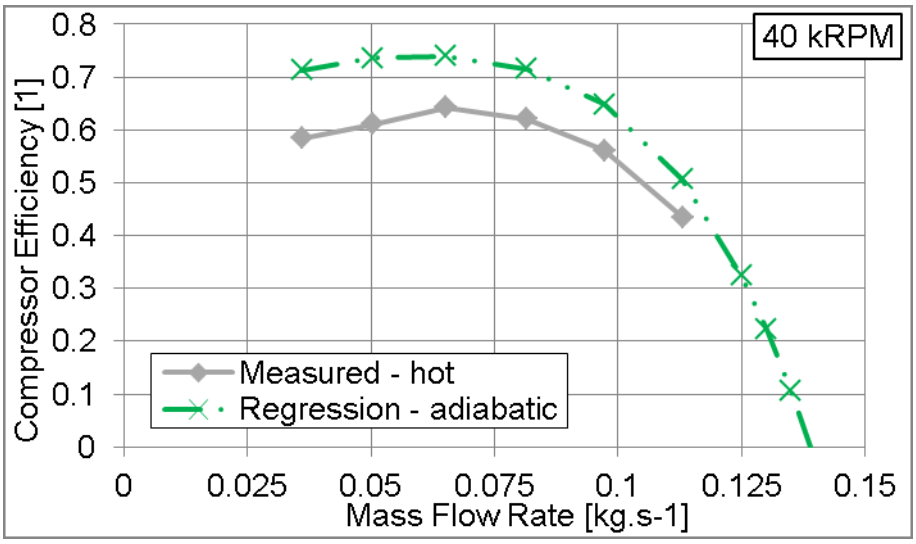

Figure 39 Comparison of measured compressor efficiency (turbine driven by exhaust gases) and efficiency of the adiabatic machine based on regression formula; standard compressor wheel; turbocharger speed 40 kRPM

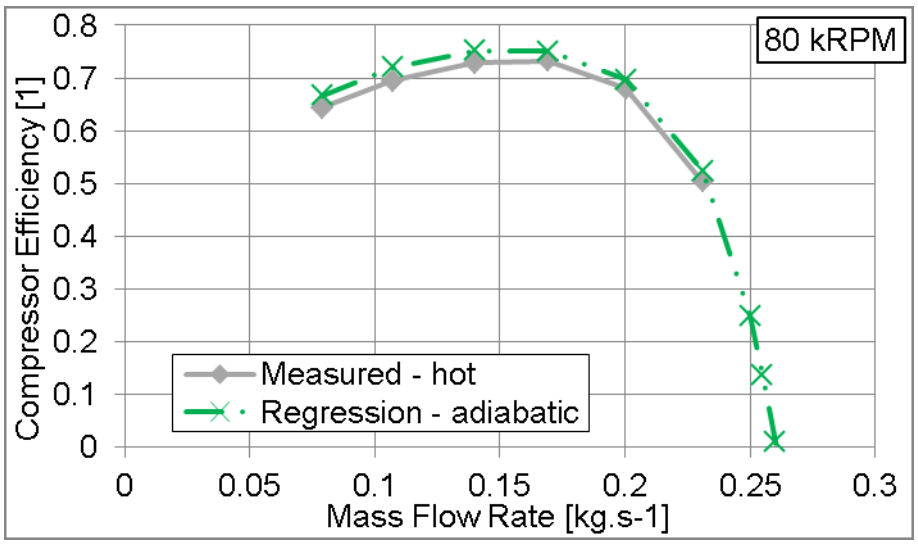

Figure 40 Comparison of measured compressor efficiency (turbine driven by exhaust gases) and efficiency of the adiabatic machine based on regression formula; standard compressor wheel; turbocharger speed 80 kRPM

The evaluated map (with areas of constant efficiency) of the adiabatic compressor with standard wheel is in *Figure 41*. The map of the adiabatic compressor with larger wheel, used for turbine loading, is plotted in *Figure 42*. The difference between compressors is obvious from comparison of the corrected mass flow rates. The results of experiments and regression model tailored to the compressor with the larger wheel are introduced in Appendix 1.

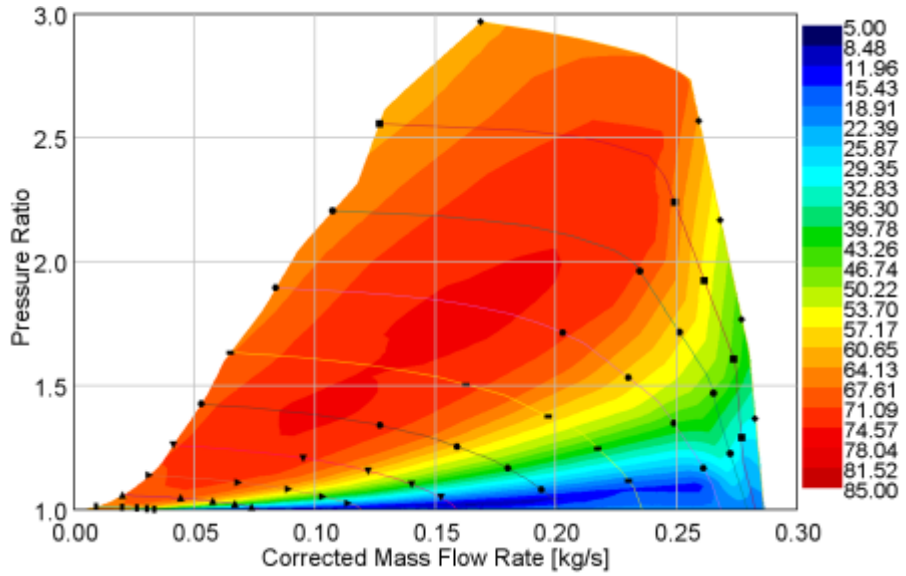

Figure 41 Map of the adiabatic compressor (standard wheel), plotted contours of constant efficiency

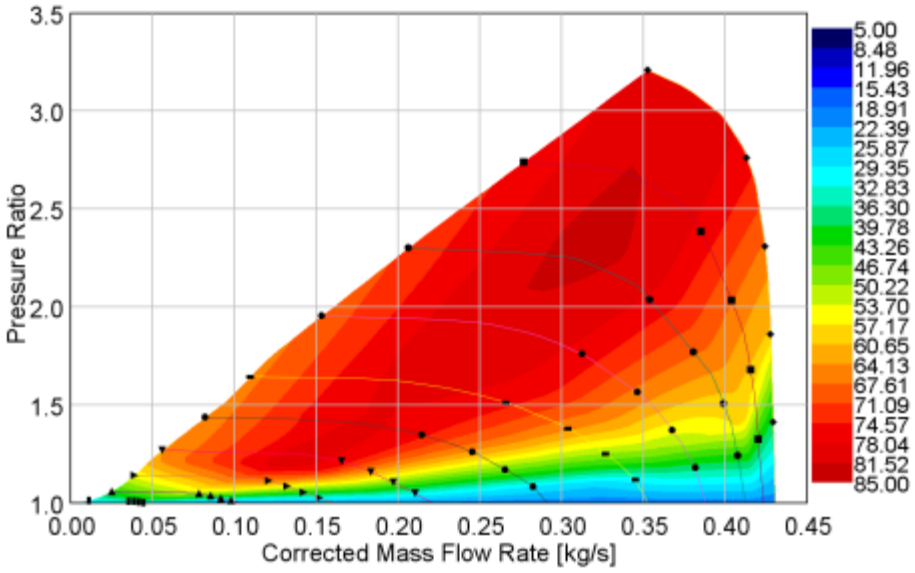

Figure 42 Map of the adiabatic compressor (compressor with larger wheel), plotted contours of constant efficiency

The turbine power, as a sum of the pure power losses in bearings and the power of adiabatic compressor is estimated, so we have to continue with the evaluation of data measured on the steady flow test bed.

The mass flow rates in sections are evaluated from static pressures upstream of orifices, pressure differences, downstream temperatures and orifice dimensions using the standard ČSN EN ISO 5167:2003 in iterative way.

The total and static temperatures upstream of a twin entry turbine are estimated using equations (51) and (52).

$$\dot{m}_A \overline{c}_{p\_A}\left(T_{IN\_A\_tot} - T_{ref}\right) + \dot{m}_B \overline{c}_{p\_B}\left(T_{IN\_B\_tot} - T_{ref}\right) = \\ = (\dot{m}_A + \dot{m}_B)\overline{c}_{p\_AB}\left(T_{IN\_AB\_tot} - T_{ref}\right) \tag{51}$$

$$\dot{m}_A \overline{c}_{p\_A}\left(T_{IN\_A} - T_{ref}\right) + \dot{m}_B \overline{c}_{p\_B}\left(T_{IN\_B} - T_{ref}\right) = \\ = \left(\dot{m}_A \overline{c}_{p\_A} + \dot{m}_B \overline{c}_{p\_B}\right)\left(T_{IN\_AB} - T_{ref}\right) \tag{52}$$

The isentropic power of a turbine defined between total states could be calculated via the analogical formulas (53) and (54).

$$P_{ise\_AB\_t\_t} = \\ = \dot{m}_A \overline{c}_{p\_A}\left(T_{IN\_A\_tot} - T_{ref}\right) + \dot{m}_B \overline{c}_{p\_B}\left(T_{IN\_B\_tot} - T_{ref}\right) + \\ -(\dot{m}_A + \dot{m}_B)\overline{c}_p\left(T_{OUT\_ise\_AB\_tot} - T_{ref}\right) \tag{53}$$

$$P_{ise\_AB\_t\_t} = (\dot{m}_A + \dot{m}_B)\overline{c}_{p\_AB}\left(T_{IN\_AB\_tot} - T_{ref}\right) + \\ -(\dot{m}_A + \dot{m}_B)\overline{c}_p\left(T_{OUT\_ise\_AB\_tot} - T_{ref}\right) \tag{54}$$

The isentropic power of a twin entry turbine (total - static), needed for estimation of isentropic or overall turbine efficiency, is determined via following formulas (55) or (56).

$$P_{ise\_AB\_t\_s} = \\ = \dot{m}_A \overline{c}_{p\_A}\left(T_{IN\_A\_tot} - T_{ref}\right) + \dot{m}_B \overline{c}_{p\_B}\left(T_{IN\_B\_tot} - T_{ref}\right) + \\ -(\dot{m}_A + \dot{m}_B)\overline{c}_p\left(T_{OUT\_ise\_AB} - T_{ref}\right) \tag{55}$$

$$P_{ise\_AB\_t\_s} = (\dot{m}_A + \dot{m}_B)\overline{c}_{p\_AB}\left(T_{IN\_AB\_tot} - T_{ref}\right) + \\ -(\dot{m}_A + \dot{m}_B)\overline{c}_p\left(T_{OUT\_ise\_AB} - T_{ref}\right) \tag{56}$$

The requisite static temperature at turbine outlet after isentropic expansion is calculated using the relations (57) and (58).

$$T_{OUT\_ise\_AB} = T_{IN\_AB}\left(\frac{p_{OUT\_ise\_AB}}{p_{IN\_AB}}\right)^{\frac{\overline{\kappa}-1}{\overline{\kappa}}} = T_{IN\_AB}\left(\frac{p_{OUT}}{p_{IN\_AB}}\right)^{\frac{\overline{\kappa}-1}{\overline{\kappa}}} \tag{57}$$

$$p_{OUT\_ise\_AB} = p_{OUT} \tag{58}$$

The total temperature at turbine outlet is specified by the equations (59) or (60).

$$T_{OUT\_ise\_AB\_tot} = T_{OUT\_ise\_AB}\left(\frac{p_{OUT\_ise\_AB}}{p_{OUT\_ise\_AB\_tot}}\right)^{\frac{1-\kappa_{OUT\_ise\_AB}}{\kappa_{OUT\_ise\_AB}}} =$$

$$= T_{OUT\_ise\_AB}\left(\frac{p_{OUT}}{p_{OUT\_tot}}\right)^{\frac{1-\kappa_{OUT\_ise\_AB}}{\kappa_{OUT\_ise\_AB}}} \tag{59}$$

$$T_{OUT\_ise\_AB\_tot} = T_{IN\_AB\_tot}\left(\frac{p_{OUT\_ise\_AB\_tot}}{p_{IN\_AB\_tot}}\right)^{\frac{\overline{\kappa}-1}{\overline{\kappa}}} =$$

$$= T_{IN\_AB\_tot}\left(\frac{p_{OUT\_tot}}{p_{IN\_AB\_tot}}\right)^{\frac{\overline{\kappa}-1}{\overline{\kappa}}} \tag{60}$$

The total temperature upstream of a turbine could be obtained by the relation (61).

$$T_{IN\_AB\_tot} = T_{IN\_AB}\left(\frac{p_{IN\_AB}}{p_{IN\_AB\_tot}}\right)^{\frac{1-\kappa_{IN\_AB}}{\kappa_{IN\_AB}}} \tag{61}$$

The static pressure turbine upstream is estimated via (62). The total pressure turbine upstream is known from the overall pressure ratio (18) and outlet static pressure (20).

$$p_{IN\_AB} = p_{IN\_AB\_tot}\left(\frac{T_{IN\_AB\_tot}}{T_{IN\_AB}}\right)^{\frac{\kappa_{IN\_AB}}{1-\kappa_{IN\_AB}}} \tag{62}$$

The average overall specific heat ratio is described in (63). The analogical approach to averaging has been used for the gas constant (64) and specific heat (65).

$$\kappa_{IN\_AB} = \frac{c_{p\_IN\_A}\dot{m}_A + c_{p\_IN\_B}\dot{m}_B}{\left(c_{p\_IN\_A} - r_{IN\_A}\right)\dot{m}_A + \left(c_{p\_IN\_B} - r_{IN\_B}\right)\dot{m}_B} \tag{63}$$

$$r_{IN\_AB} = \frac{\dot{m}_A r_{IN\_A} + \dot{m}_B r_{IN\_B}}{\dot{m}_A + \dot{m}_B} \tag{64}$$

$$c_{p\_IN\_AB} = \frac{\kappa_{IN\_AB}\, r_{IN\_AB}}{\kappa_{IN\_AB} - 1} \tag{65}$$

Some physical quantities estimated for the single section of a turbine are used for calculation of the twin entry turbine overall parameters stated above. It is also convenient to evaluate parameters of each single section. The following relations, written for the section A, are also valid for the second section of course. It is easy to determine the pressure ratio (total - static) of a single section (66).

$$PR_{A\_t\_s} = \frac{p_{IN\_A\_tot}}{p_{OUT}} \tag{66}$$

The flow function ψ A depends on the actual pressure ratio compared to the critical pressure ratio (67) and (68).

$$PR_{A\_crit} = \left(\frac{2}{\kappa_{IN\_A\_tot} + 1}\right)^{\frac{\kappa_{IN\_A\_tot}}{1-\kappa_{IN\_A\_tot}}} \tag{67}$$

$$PR_A \geq PR_{A\_crit} \quad \Rightarrow \psi_{A\_max} \tag{68}$$

Depending on results of (68), the flow function may be determined by the relations (70) or (69). The specific heat ratio κ IN_A_total corresponds to the total temperature at turbine inlet A.

$$\psi_{A\_max} = \kappa_{IN\_A\_tot}\left(\frac{2}{\kappa_{IN\_A\_tot} + 1}\right)^{\frac{\kappa_{IN\_A\_tot}+1}{\kappa_{IN\_A\_tot}-1}} \tag{69}$$

$$\psi_A = \frac{2\kappa_{IN\_A\_tot}}{\kappa_{IN\_A\_tot} - 1}\left(PR_A^{\frac{-2}{\kappa_{IN\_A\_tot}}} - PR_A^{\frac{-\kappa_{IN\_A\_tot}-1}{\kappa_{IN\_A\_tot}}} \right) \tag{70}$$

The discharge coefficient of the single section is estimated as a fraction of the mass flow rate via section to the reference mass flow rate (71). The reference area A t_ref is the same as introduced in chapter 4.3.

$$\mu_A = \frac{\dot{m}_A}{\dot{m}_{ref}} = \frac{\dot{m}_A}{A_{t\_ref}\frac{p_{IN\_A\_t}}{\sqrt{r_{IN\_A\_t}T_{IN\_A\_t}}}\sqrt{\psi_A}} \tag{71}$$

The important input for calculation of the overall twin entry turbine parameters is the fictitious isentropic velocity of each isolated section (72).

$$c_{s\_A} = \left[2\overline{c}_{p\_A} T_{IN\_A\_tot}\left(1 - PR_A^{\frac{1-\overline{\kappa}_A}{\overline{\kappa}_A}} \right) \right]^{0.5} \tag{72}$$

The static temperature after isentropic expansion could be specified from (73).

$$T_{OUT\_ise\_A} = T_{IN\_A}\left(\frac{p_{OUT}}{p_{IN\_A}} \right)^{\frac{\overline{\kappa}_{IN\_A}-1}{\overline{\kappa}_{IN\_A}}} \tag{73}$$

The equation of total temperature after isentropic expansion follows (74).

$$\begin{aligned} T_{OUT\_ise\_A\_tot} &= T_{OUT\_ise\_A}\left(\frac{p_{OUT}}{p_{OUT\_tot}} \right)^{\frac{1-\kappa_{OUT\_ise}}{\kappa_{OUT\_ise}}} = \\ &= T_{IN\_A\_tot}\left(\frac{p_{OUT\_tot}}{p_{IN\_A\_tot}} \right)^{\frac{\overline{\kappa}-1}{\overline{\kappa}}} \end{aligned} \tag{74}$$

The blade speed ratio is described by the formula (75).

$$BSR_A = \frac{\pi D_{ref} RPM}{60\ c_{s\_A}} \tag{75}$$

The isentropic power of the single section (total - total) is calculated via (76). Similar relation between total and static states is in (77).

$$P_{ise\_A\_t\_t} = \\ = \dot{m}_A \overline{c}_{p\_A}\left(T_{IN\_A\_tot} - T_{ref}\right) - \dot{m}_A \overline{c}_p\left(T_{OUT\_ise\_A\_tot} - T_{ref}\right) \tag{76}$$

$$P_{ise\_A\_t\_s} = \\ = \dot{m}_A \overline{c}_{p\_A}\left(T_{IN\_A\_tot} - T_{ref}\right) - \dot{m}_A \overline{c}_p\left(T_{OUT\_ise\_A} - T_{ref}\right) \tag{77}$$

The steady flow maps, for example in the reduced form, may be derived if required using the following relations of reduced speed (78) and reduced mass flow rate via single section (79). The specific heat ratio and gas constant IN_A_total appertain to the total temperature at the inlet of particular section. The reference conditions have to be introduced and delivered with the generated steady flow maps.

$$RPM_{red\_A} = \frac{RPM}{\sqrt{T_{IN\_A\_tot}}} \left(\frac{\kappa_{ref}}{\kappa_{IN\_A\_tot}} \frac{r_{ref}}{r_{IN\_A\_tot}} \right)^{0.5} \tag{78}$$

$$\dot{m}_{red\_A} = \frac{\dot{m}_A \sqrt{T_{IN\_A\_tot}}}{p_{IN\_A\_tot}} \left(\frac{\kappa_{ref}}{\kappa_{IN\_A\_tot}} \frac{r_{IN\_A\_tot}}{r_{ref}} \right)^{0.5} \tag{79}$$

The 1-D turbine model, described in detail in the chapter 6, uses loss coefficients, which are generally dependent on Reynolds number. Additional correction to gas kinematic viscosity is necessary, when a turbine is operating far from standard conditions (e.g., using cold air for driving it), if assuming that loss parameters are corrected to standard temperature.

At the beginning, the turbine isentropic efficiency (80) has to be corrected to windage losses (81). The windage losses automatically take into account low Reynolds number impact with speed dependent value only, i.e., they automatically increase their relative significance for high BSR.

$$\eta_{turb\_ise} = \frac{P_{comp\_adi} + P_{bear}}{P_{ise\_AB\_t\_s}} = \frac{P_{turb} - P_{wind}}{P_{ise\_AB\_t\_s}} \quad (80)$$

The windage losses, discussed also in chapter 6.3, depend on Reynolds number (82), circumferential velocity and density at nozzle outlet. The value of windage losses is the subject of turbine 1-D model calibration, see chapter 6.4 for details. The values depend directly on calibration coefficient K wind.

$$P_{wind} = \frac{K_{wind}\rho_{2\_N}\left(D_{imp\_IN}10^{-3}\right)^2 u_2^3}{Re_{2\_N}^{0.2}} \quad (81)$$

$$Re_{2\_N} = \frac{D_{imp\_IN}10^{-3}u_2}{\frac{\mu_{2\_N}}{\rho_{2\_N}}} \quad (82)$$

The windage losses were calculated via the 1-D turbine model at different temperatures. The reference temperatures at turbine inlet equalled to measured values on the steady flow test bed. The required temperature upstream of a turbine, for correction of turbine isentropic efficiency, was 900 K. The turbine isentropic efficiency was then corrected according to relation (83).

$$\eta_{turb\_ise} = \frac{P_{comp\_adi} + P_{bear} + P_{wind\_ref} - P_{wind\_REQ}}{P_{ise\_AB\_t\_s}} \quad (83)$$

The resultant isentropic efficiency from (83), corrected to windage losses, was consequently corrected in a term of equation (86).

Utilized correction is similar to Ainley and Mathieson correlation in [1]. The basic feature of the correction is that the exponent on temperature is derived from corrected Reynolds number in (84).

$$Re^{0.2} \sim \frac{(uL)^{0.2}}{\nu^{0.2}} \sim \frac{1}{\nu^{0.2}} \sim \left(T^{\frac{3}{2}}\right)^{0.2} \sim T^{0.3} \quad (84)$$

The coefficient used for turbine isentropic efficiency correction is derived in (85). The reference efficiency is the efficiency already corrected to windage losses as stated above.

$$\eta_{turb\_ise} = 1 - K\, T_{IN\_AB\_REQ}^{0.3}$$
$$K = \frac{1 - \eta_{turb\_ise\_ref}}{T_{IN\_AB\_ref}^{0.3}} \tag{85}$$

Valid isentropic efficiency of a turbine is calculated via equation (86). The reference values equal to measured values. The required temperature turbine upstream, for correction purposes, was 900 K.

$$\eta_{turb\_ise} = 1 - \frac{1 - \eta_{turb\_ise\_ref}}{T_{IN\_AB\_ref}^{0.3}} T_{IN\_AB\_REQ}^{0.3} \tag{86}$$

Turbine discharge coefficient was corrected in the same way as efficiency in (86).

$$\dot{m} = c_s \sqrt{\frac{\eta_{turb\_ise}}{\eta_{turb\_ise\_ref}}} A \frac{p_2}{r T_{2\_ise}} \frac{T_{2\_ise}}{T_2} \left(\frac{T_2}{T_{2\_ise}} \right)_{ref} \tag{87}$$

The correction coefficient (90) for discharge coefficient is derived from the equation (87). Requisite quotient of relevant temperatures (88) is stated in (89).

$$T_2 = T_1 - \eta_{turb\_ise} \left(T_1 - T_{2\_ise} \right)$$
$$T_2 = T_1 \left\{ 1 - \eta_{turb\_ise} \left[1 - \left(\frac{1}{PR_{AB}} \right)^{\frac{\kappa_{IN\_AB\_tot} - 1}{\kappa_{IN\_AB\_tot}}} \right] \right\} \tag{88}$$

$$\frac{T_{2\_ise}}{T_2} = \frac{1 - \eta_{turb\_ise} \left[1 - \left(\frac{1}{PR_{AB}} \right)^{\frac{\kappa_{IN\_AB\_tot} - 1}{\kappa_{IN\_AB\_tot}}} \right]}{PR_{AB}^{\frac{\kappa_{IN\_AB\_tot} - 1}{\kappa_{IN\_AB\_tot}}}} \tag{89}$$

$$C = \sqrt{\frac{\eta_{turb\_ise}}{\eta_{turb\_ise\_ref}}} \frac{1 - \eta_{turb\_ise}\left[1 - \left(\frac{1}{PR_{AB}}\right)^{\frac{\kappa_{IN\_AB\_tot}-1}{\kappa_{IN\_AB\_tot}}}\right]}{1 - \eta_{turb\_ise\_ref}\left[1 - \left(\frac{1}{PR_{AB}}\right)^{\frac{\kappa_{IN\_AB\_tot}-1}{\kappa_{IN\_AB\_tot}}}\right]} \tag{90}$$

Valid discharge coefficient of the turbine is calculated using relation (91). The reference values in (90) and (91) are known from experiments.

$$\mu_{AB} = \mu_{AB\_ref}\, C \tag{91}$$

The comparison of measured data and results after correction for full admission and pressure ratio approximately 1.3 is presented in *Figure 43* and *Figure 44*. The tendency of efficiency decrease with higher blade speed ratio corresponds with assumption and tested type of the radial turbine. Decrease of discharge coefficient is proportional to corrected isentropic efficiency.

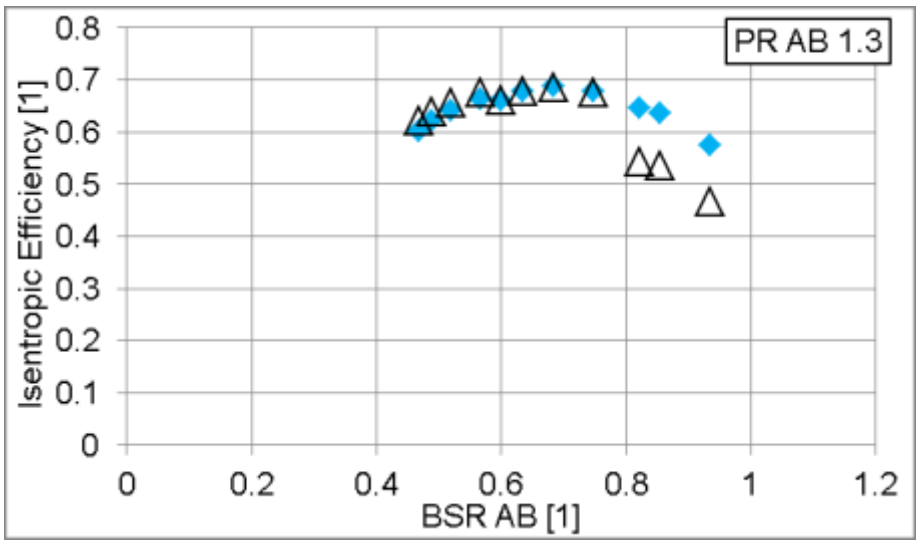

Figure 43 Turbine isentropic efficiency, overall pressure ratio PR AB = 1.3, full admission of a turbine wheel; experimental data without correction (blue); corrected data (black triangles)

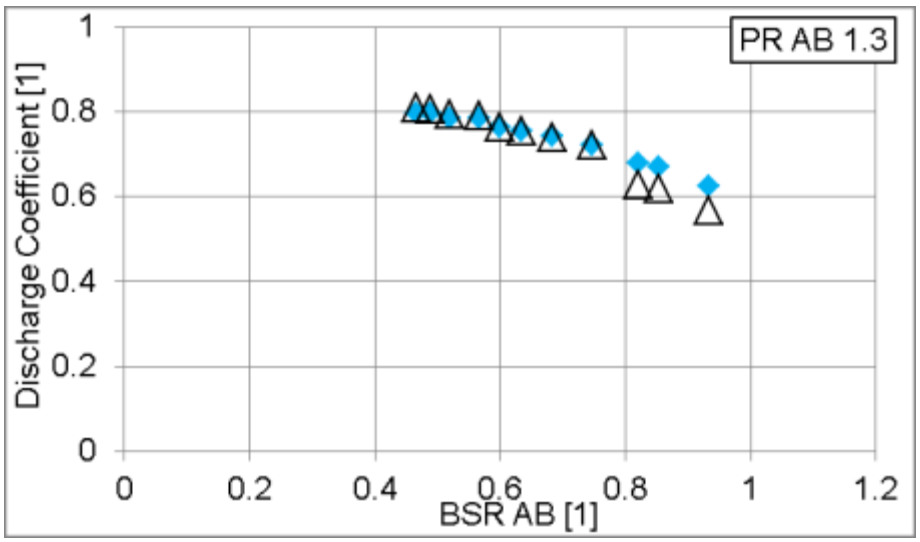

Figure 44 Discharge coefficient of a turbine, overall pressure ratio PR AB = 1.3, full admission of a turbine wheel; experimental data without correction (blue); corrected data (black triangles)

Resulting isentropic turbine efficiency and appropriate discharge coefficient at higher pressure ratio after correction are in *Figure 45* and *Figure 46*.

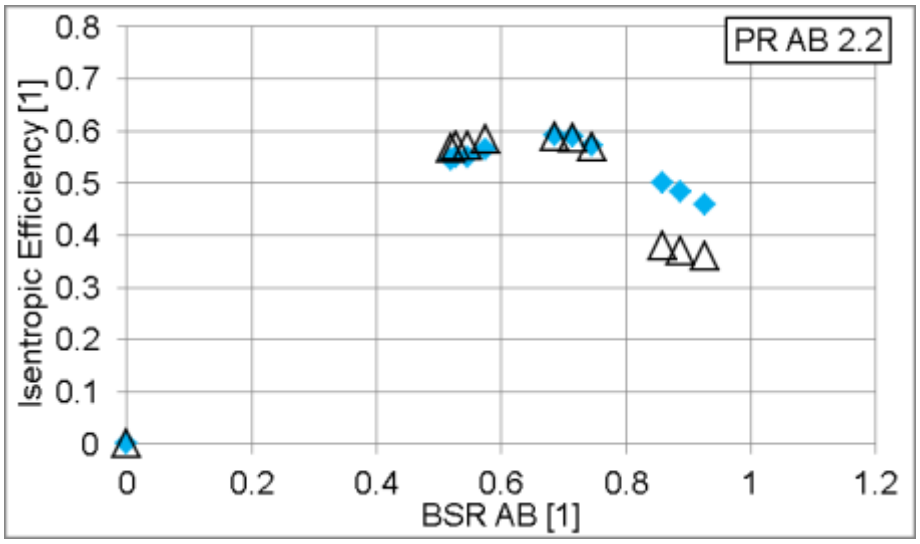

Figure 45 Turbine isentropic efficiency, overall pressure ratio PR AB = 2.2, full admission of a turbine wheel; (zero point measured at BSR = 0); experimental data without correction (blue); corrected data (black triangles)

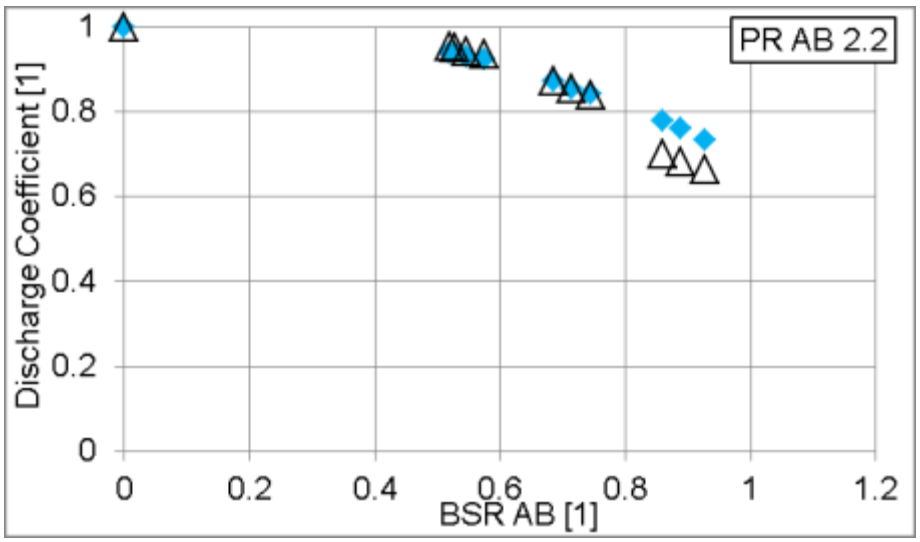

Figure 46 Discharge coefficient of a turbine, overall pressure ratio PR AB = 2.2, full admission of a turbine wheel; (zero point measured at BSR = 0); experimental data without correction (blue); corrected data (black triangles)

4.6 Results

The experiments on the steady flow turbocharger test bed with open loop were carried out at first attempt. Some measurements in specific areas are not perfect. The experimental work on the turbocharger test bed may be improved in future research.

The summary of all evaluated experiments is presented in *Figure 47*. The courses of turbine isentropic efficiency under different level of turbine wheel admission in dependence on total mass flow rate via machine show the main features of the measured twin entry turbine. The tested twin entry turbine reaches comparable level of optimum isentropic efficiency under partial admission with the level A approximately 0.87 as in the case with the equal admission of the impeller. The turbine under extreme level of admission, with closed section, achieves lower maximum isentropic efficiency compared to previous cases.

The summary experimental results in *Figure 47* and *Figure 48* show the influence of the tested twin entry turbine design on the isentropic efficiency under different conditions in sections.

The preliminary design of the turbine scroll, sections flow areas and their fraction and impeller main dimension may be the contribution and advantage of the developed turbine model based on the physical approach as discussed in simulation part of the thesis.

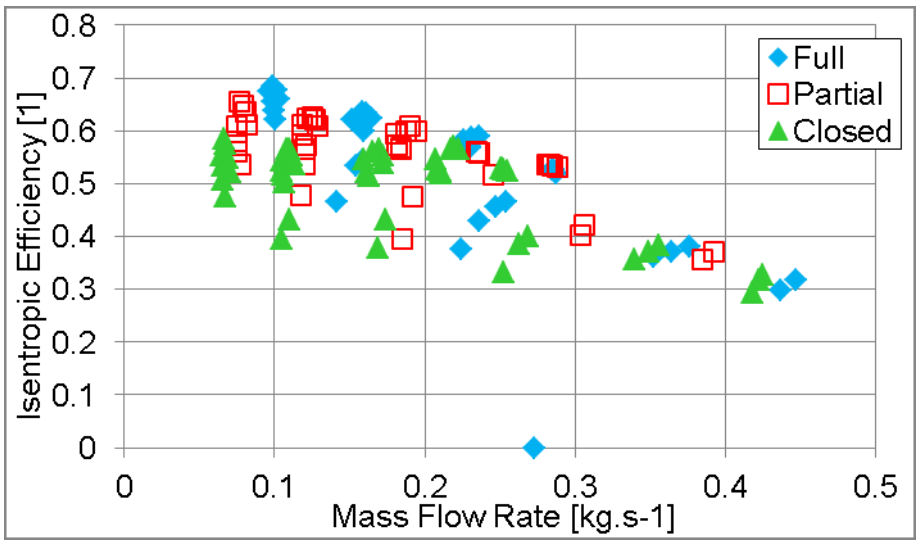

Figure 47 Turbine isentropic efficiency under full admission of an impeller (blue); partial admission with throttling in one section (red squares) - level A = 0.87; closed section (green triangles)

The impact of different conditions in turbine sections on the isentropic efficiency in dependence on the blade speed ratio, thus turbine load, is presented in *Figure 48*.

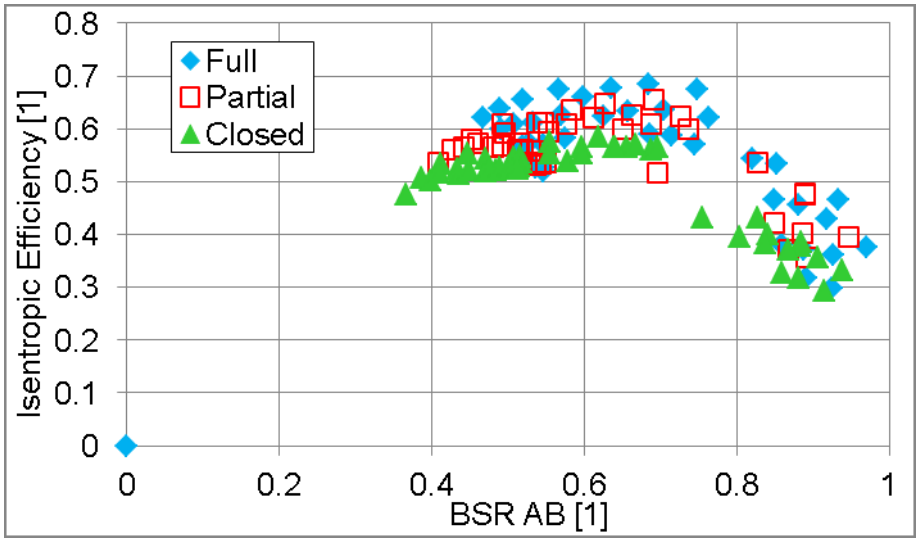

Figure 48 Turbine isentropic efficiency vs. blade speed ratio (BSR); full admission (blue); partial admission level A = 0.87 (red squares); one turbine section closed (green triangles)

The courses of turbine isentropic efficiency at low overall pressure ratio in dependence on the blade speed ratio are in *Figure 49*. The turbine behaviour under different steady flow conditions in sections is consistent with presumptions. The turbine isentropic efficiency is highest under equal admission of the impeller and lowest in the extreme case of the partial admission with closed section. The corresponding courses of discharge coefficient are in *Figure 50*.

The overall pressure ratio of evaluated results is approximately but not accurately constant. The constant pressure level was kept in the governing turbine section A during experiments on the turbocharger test bed. It would be convenient in the

future research to calculate the overall turbine pressure ratio online via data acquisition, use the overall pressure ratio as a governing value and keep it constant for the set of measurements. The courses of turbine isentropic efficiency would be smoother in dependence on blade speed ratio. It is clearly visible in *Figure 49* that courses are not entirely smooth due to slightly different pressure ratio. In any case, the correction of losses in dependence on Reynolds number, suitable for unseparated boundary layer in a blade cascade, is not well valid for closed partition of a nozzle ring.

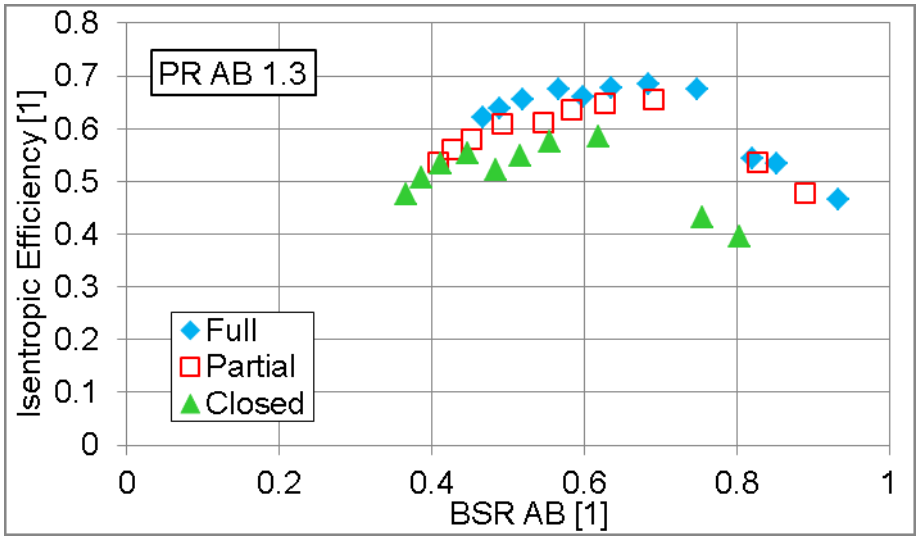

Figure 49 Comparison of turbine isentropic efficiency courses - overall pressure ratio PR AB = 1.3; full admission - blue; partial admission level A = 0.87 - red squares; closed section - green triangles

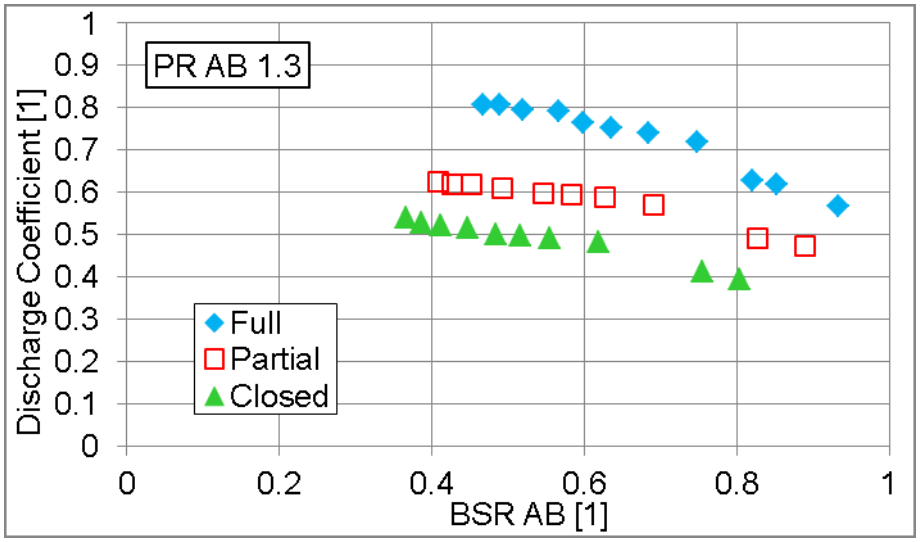

Figure 50 Discharge coefficient of a turbine - overall pressure ratio PR AB = 1.3; full admission - blue; partial admission level A = 0.87 - red squares; closed section - green triangles

The influence of increasing total mass flow rate via machine on turbine efficiency is obvious with increasing overall pressure ratio - *Figure 51*. The turbine isentropic efficiency under full and partial admission (level A approximately 0.87) are comparable at all blade speed ratios. The efficiency under extreme level of wheel

admission with closed section is comparable with values under full and partial admission at high blade speed ratios.

The reason is probably in impeller inlet and exit losses. Closed partition reduces impeller inlet angle at fixed nozzle exit angle (vaneless nozzle ring) due to momentum exchange between used and closed partitions. The effect of better inlet angle compensates kinetic energy loss due to mixing. Lower mass flow rate with closed partition and fixed pressure ratio cause the impeller exit being relatively large and the impeller exit influence on impeller pressure ratio is smaller than for full admission. In the case of full admission, the density at impeller exit is reduced more significantly. Those qualitative results may be found in the central streamline model.

The power losses in bearings are not so significant, so the isentropic efficiency of turbine decreases. The losses in bearings are not negligible, because they change the resulting courses of turbine parameters. The bearing losses are comparable under various level of the impeller admission.

The turbine efficiency is influenced by the geometry of inlet sections and impeller. At high pressure ratios, the impeller exducer is overloaded by expanded gas of high mass flow rate and low density. The outlet kinetic energy loss increases. The turbine under partial admission at the same overall pressure ratio may reach higher isentropic efficiency, because the mass flow rate in the high loaded section is reduced by reaching sonic limit. The impact of momentum loss at the twin scroll outlet may be compensated by better efficiency of the exducer.

The phenomenon is visible in *Figure 51* and *Figure 47*. Altogether, the results show that the proposed correction of losses for Reynolds number is possible but not fully satisfactory if boundary layer tends to be separated for more viscous, high temperature flow. Correcting factor dependent on angle of incidence or on basic incidence angle loss can be used in the future.

If assessing the importance of high BSR points, the small elaborated isentropic enthalpy head at fixed turbine speed should not be forgotten. It means that the weight of high BSR points may be reduced, since they are not too significant for the overall prediction accuracy.

The obtained values of turbine isentropic efficiency under different conditions in sections, i.e. different levels of partial admission and pressure ratios, compared at the same total mass flow rate via turbine would show different results, of course.

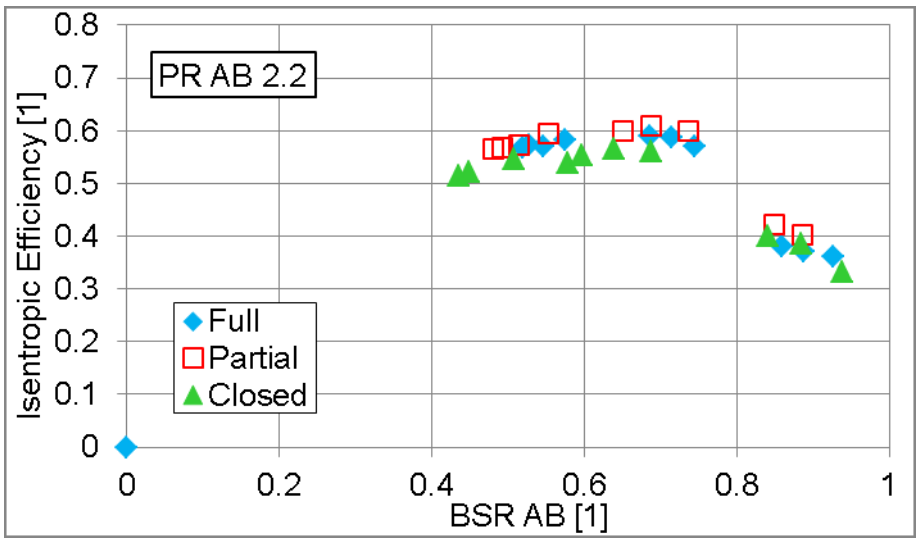

Figure 51 Comparison of turbine isentropic efficiency courses - overall pressure ratio PR AB = 2.2; full admission - blue (zero point measured at BSR = 0); partial admission level A = 0.87 - red squares; closed section - green triangles

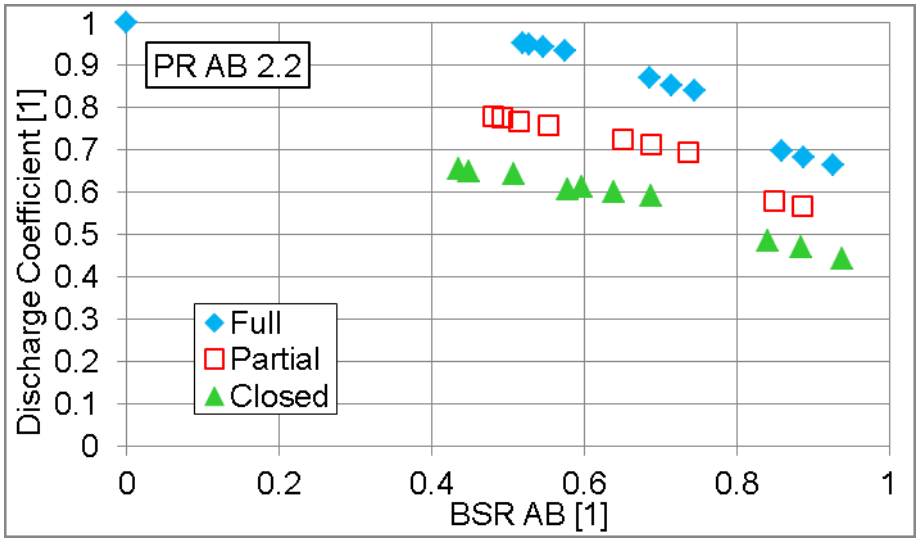

Figure 52 Discharge coefficient of a turbine - overall pressure ratio PR AB = 2.2; full admission - blue (zero point measured at BSR = 0); partial admission level A = 0.87 - red squares; closed section - green triangles

The measured zero point, i.e. the operating point with the blocked turbine wheel, is also shown in *Figure 51* and *Figure 52*. At the blocked impeller, the blade speed ratio and efficiency are zero, of course. The zero point contribution consists in measurement of mass flow rate without the influence of centrifugal force. It is useful for estimation of the discharge coefficient (see A t_ref above) and also for the regression model of a turbine if required.

The total review of evaluated experimental results obtained from the steady flow test bed is stated in Appendix 2. The results of research carried out on the turbocharger test bed were also presented in [48] and [49].

The software for the evaluation of all experimental data measured on the developed open loop steady flow test bed for a twin entry turbine was developed during the research [SW 2].

5. Experiments - Internal Combustion Engine

The current chapter introduces experiments on the internal combustion engine. The goal of the experimental research on the turbocharged internal combustion engine is to describe the synergy between the engine and turbocharger under real conditions. The measured unsteady data are fundamental for evaluation of predictive capability of the developed simulation models, especially the full 1-D twin scroll turbine model. Data from steady state measurements are important for the proper calibration of the internal combustion engine model.

Transient load response was measured due to its relevance for vehicle engines, but due to limited feasibility of engine dynamometer control only at constant engine speed.

The transients are generally the most demanding operating modes of the simulation models. The stability and capability of the full 1-D twin scroll turbine model to describe rapidly changing values are crucial. The verification of the predictive capability of the developed 1-D twin scroll radial centripetal turbine model under highly unsteady real conditions, which are typical for the turbocharged internal combustion engine, is the most important part of the thesis.

It has to be stressed at the beginning of the chapter that the measurement chain and obtained experimental data come from the close cooperation with prof. Ing. Michal Takáts, CSc. and Ing. Miloslav Emrich, Ph.D. All the work and support during the project is gratefully appreciated.

5.1 Description of the Experimental Engine

The experimental internal combustion engine is equipped with the same type of turbocharger with twin scroll turbine and standard compressor wheel as measured on the steady flow turbocharger test bed. The turbocharger used for turbocharging of the experimental engine is another part than used for steady flow experiments. The type of the turbocharger (turbine wheel, compressor wheel, housings etc.) is the same, but the pieces are different due to manufacturing tolerances.

The main parameters of the internal combustion engine are stated in *Table 3*. The engine with six cylinders in line is suitable for utilization of the twin scroll turbine advantages by virtue of the optimal firing interval between cylinders. The multi entry turbine design is suitable for the internal combustion engines with number of cylinders equal to the multiples of three.

The selected experimental diesel engine is designed for agricultural tractors. The volume of the intake plenum is small. The engine is equipped with asymmetric exhaust manifold with two separated branches of different length. The first exhaust branch connects the cylinders 1 - 2 - 3 into the turbine section B. The turbine section A connects the cylinder 4 - 5 - 6. The branches are very short, thus the volume of the exhaust manifold is low. The engine layout with pulsation exhaust

system and firing interval 240 degrees between cylinders in each exhaust branch is suitable for our research, because we are interested in the turbine behaviour under unsteady high pulsating flow.

The engine load, maximum brake mean effective pressure about 13 bar, and the level of turbocharging are not so high compared to contemporary similar diesel engines for agriculture, but for our specific purposes, when the internal combustion engine is a source of exhaust gases for a turbocharger, are engine parameters suitable. Moreover, the six cylinder engine with low volume pulse exhaust manifold with separated branches is essential for the research on interactions between the internal combustion engine and turbine equipped with twin scroll.

Table 3 Parameters of the experimental internal combustion engine John Deere

Label	John Deere 6068 Diesel
Type	compression ignition
Fuel	diesel oil
Cylinders	6 in-line
Bore [mm]	106.426
Stroke [mm]	127
Displacement [dm3]	6.779
Valves (IN/EX)	1 / 1
Firing order	1 - 5 - 3 - 6 - 2 - 4
Fuel injection pump	Bosch VP44 (injection timing and rate control)
ECU	open source (NI CompactRIO platform)
Turbocharger	CZ K27 Twin scroll

Figure 53 Piston and connecting rod of the experimental engine, example of geometrical data used in the simulation

All available geometrical data, important for the simulation, were collected after engine disassembly at the beginning of the project. The example of parts is shown in *Figure 53*.

5.2 Measurement on a Flowbench

The cylinder head of the experimental engine was tested on a flowbench in cooperation with Ing. Petr Hatschbach, CSc. The aim was to identify the discharge and swirl coefficients of intake ports and discharge coefficients of exhaust ports (*Figure 54*).

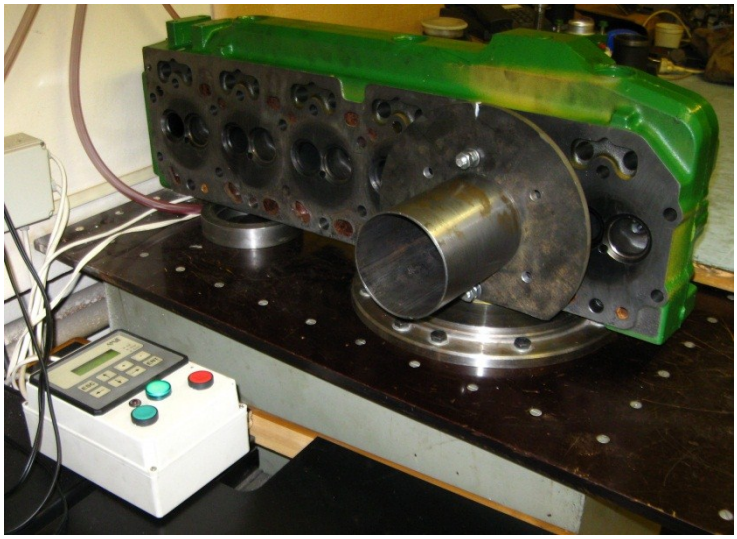

Figure 54 Cylinder head on a flowbench

The discharge coefficients are calculated using the following relations. The pressure ratio across the measuring section is estimated from (92).

$$PR = \frac{p_{OUT}}{p_{IN\_total}} \tag{92}$$

The isentropic density at the throat, valid for the subsonic flow is stated in (93).

$$\rho_{ise} = \rho_0 \, (PR)^{\frac{1}{\kappa}} \tag{93}$$

The corresponding isentropic velocity at the throat under subsonic flow is calculated through the relation (94).

$$w_{ise} = \sqrt{r \, T_0 \, \frac{2 \, \kappa}{\kappa - 1} \left[1 - (PR)^{\frac{\kappa - 1}{\kappa}} \right]} \tag{94}$$

The critical or choked flow occurs when the pressure ratio is less than or equal to the result of fraction in (95).

$$PR \leq \left(\frac{2}{\kappa + 1}\right)^{\frac{\kappa}{\kappa-1}} \tag{95}$$

The isentropic density at the throat for critical or choked flow is determined via (96).

$$\rho_{ise} = \rho_0 \left(\frac{2}{\kappa + 1}\right)^{\frac{1}{\kappa-1}} \tag{96}$$

The appropriate isentropic velocity under critical or choked flow is calculated via formula (97).

$$w_{ise} = \sqrt{\kappa\, r\, T_0\, \frac{2}{\kappa + 1}} \tag{97}$$

The resultant discharge coefficient of a valve is then estimated through relation (98).

$$C_D = \frac{\dot{m}}{A_R\, \rho_{ise}\, w_{ise}} \tag{98}$$

The swirl coefficient of the intake port is defined by the formula (99). The definition is consistent with the relation used in GT-SUITE software [4]. The definitions of swirl coefficient in literature are various. See [3] and [41] for example. The utilized formula has to be stated with estimated numbers.

$$C_S = \frac{2\, T_{swirl}}{\dot{m}\, w_{ise}\, B}$$
$$|C_S| \leq 1 \tag{99}$$

The effects of intake ports swirl coefficients on combustion and in-cylinder heat transfer may be simulated by the relevant models in arbitrary simulation environment.

The measured values of intake port discharge coefficients are shown in *Figure 55* and swirl coefficients in *Figure 56*.

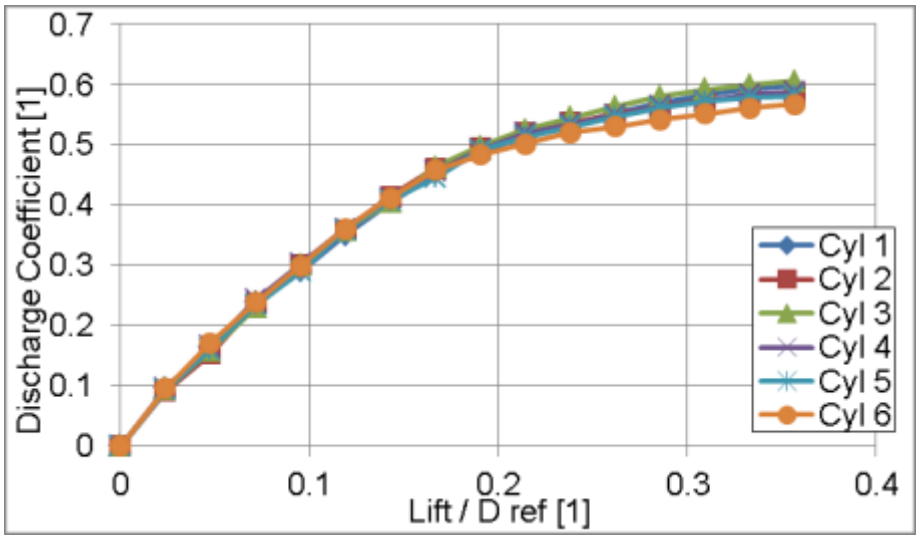

Figure 55 Discharge coefficient of intake valves vs. reference array (valve lift / reference valve diameter)

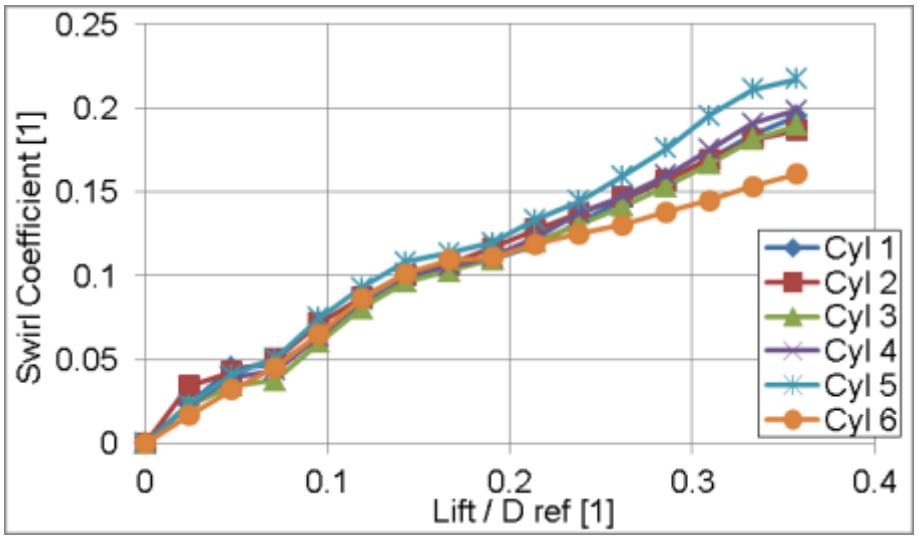

Figure 56 Swirl coefficient of intake ports vs. reference array (valve lift / reference valve diameter)

The discharge coefficients of exhaust ports are presented in *Figure 57*.

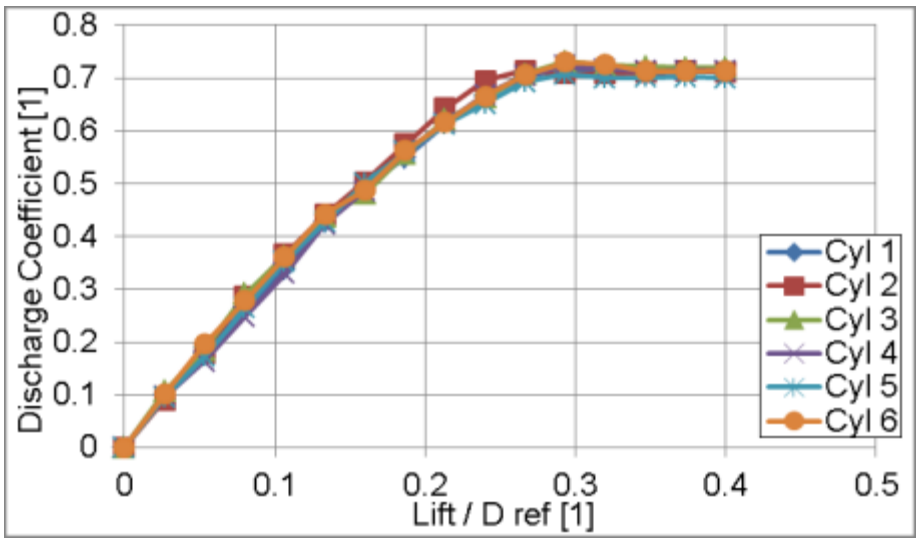

Figure 57 Discharge coefficient of exhaust valves vs. reference array (valve lift / reference valve diameter)

The valve timing and valve lift measured on the experimental engine by Ing. Jiří Vávra, Ph.D. and Ing. Miloslav Emrich, Ph.D. are shown in *Figure 58*.

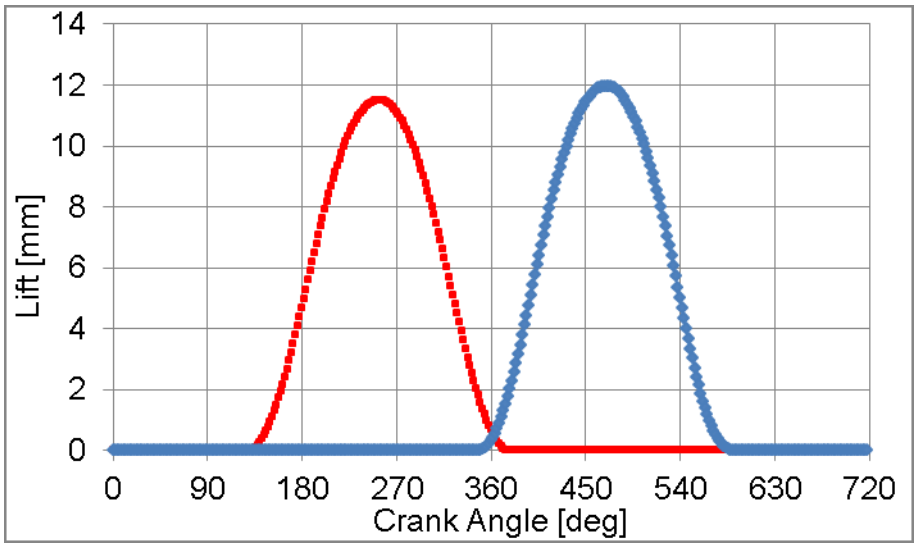

Figure 58 Valve lifts measured on the experimental engine, exhaust valve (red), intake valve (blue)

Data introduced in the chapter are utilized as inputs for the model of experimental combustion engine created in the GT-SUITE environment.

5.3 Measurement Chain

The goal was to build up a proper measurement chain for testing the interactions between the reciprocating internal combustion engine and twin entry turbine under pulsating unsteady flow. The same type of turbocharger used for turbocharging of the experimental engine was measured on the steady flow test bed. The experimental data, measured under real conditions on the turbocharged engine,

are essential for validation and verification of the relevant turbine unsteady 1-D model, calibrated using data obtained on the steady flow turbocharger test bed.

The equipment of the engine test cell is briefly listed in *Table 4*. The active dynamometer used for experiments is equipped with the constant speed control. As an active dynamometer, it also enables to drive the tested internal combustion engine.

Table 4 Engine test cell equipment

Dynamometer	VUES - AC, 440 kW, 1800 N.m, 7500 RPM
Air flow meter	ABB Sensyflow
Dynamic fuel meter	AVL
Opacimeter	AVL
Analysers	Horiba, ABB
Lambda meter	Motec
Pressure sensors	Kulite, AVL
Data acquisition - DAQ	NI CompactDAQ platform open source DAQ SW

The measurement chain, presented in *Figure 59*, was developed with the focus on the unsteady behaviour of the engine and turbocharger, thus the pressure indication at proper locations is inserted. The engine is equipped with the pressure indication at the intake port inlet, in the cylinder and at the outlet of the exhaust port. The measurement of those three unsteady pressures is required for the three pressure analysis discussed in the simulation part. The pressures at the inlets of turbine sections and at the turbine outlet are indicated too. The measured values are stated in *Table 5.*

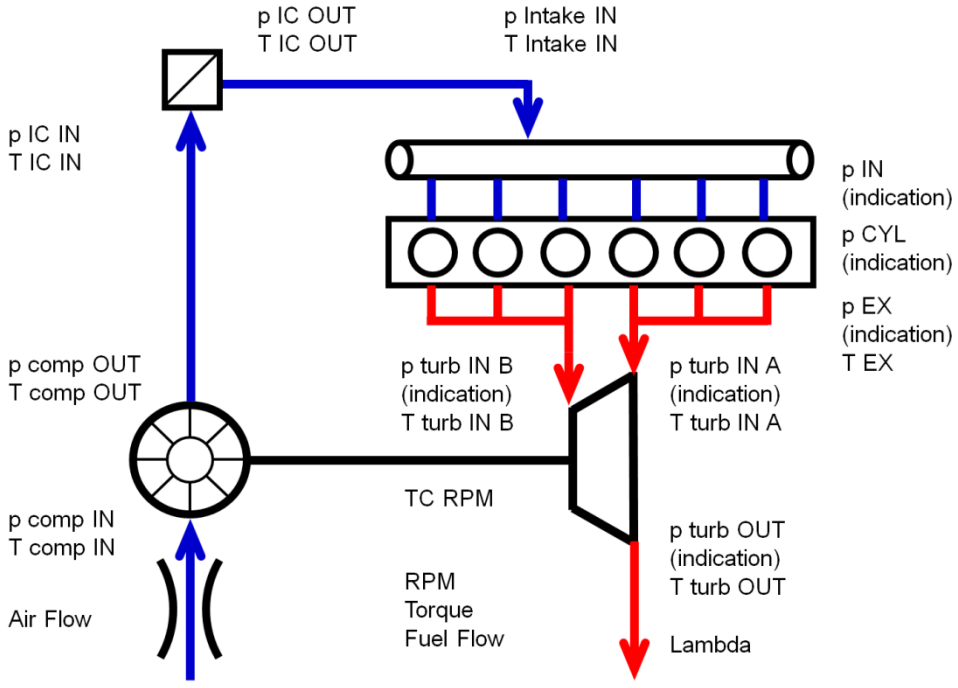

Figure 59 Measurement chain of the experimental internal combustion engine

Table 5 Overview of measured physical values on engine test cell

Fast DAQ		p intake indication (cyl 6)	
		p cyl indication (cyl 6)	
		p exhaust indication (cyl 6)	
		p turbine IN A indication	
		p turbine IN B indication	
		p turbine OUT indication	
	turbocharger speed		
Slow DAQ		p comp IN	T comp IN
		p comp OUT	T comp OUT
		p intercooler IN	T IC IN
		p intercooler OUT	T IC OUT
		p plenum IN	T plenum IN
			T EX (cyl 6)
		p turbine IN A	T turbine IN A
		p turbine IN B	T turbine IN B
		p turbine OUT	T turbine OUT
	engine speed		
	brake torque		
	air mass flow rate		
	fuel mass flow rate		
	lambda		
Ambient		p ambient	T ambient

Many additional values were sensed for the safe running of the tested engine and dynamometer.

The overview of prepared experimental engine in the test cell is presented in *Figure 60*. The compressor of the turbocharger is fitted with the Micro-Epsilon sensor for the turbocharger speed sensing - *Figure 61*.

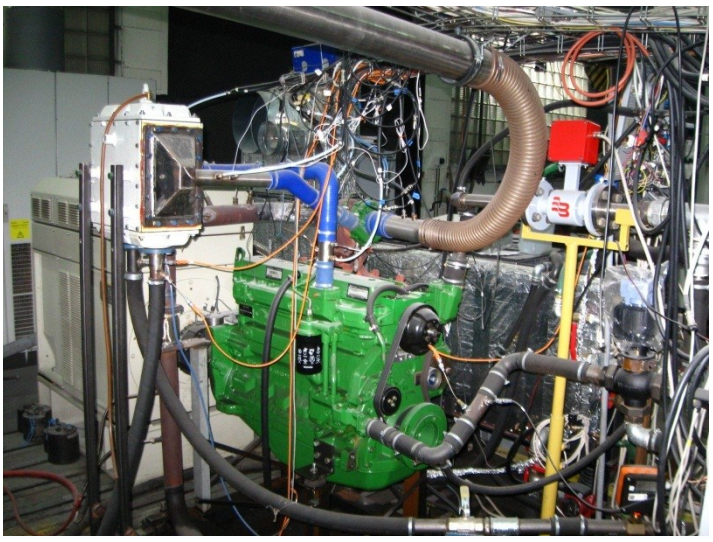

Figure 60 View of the engine test cell with the experimental engine

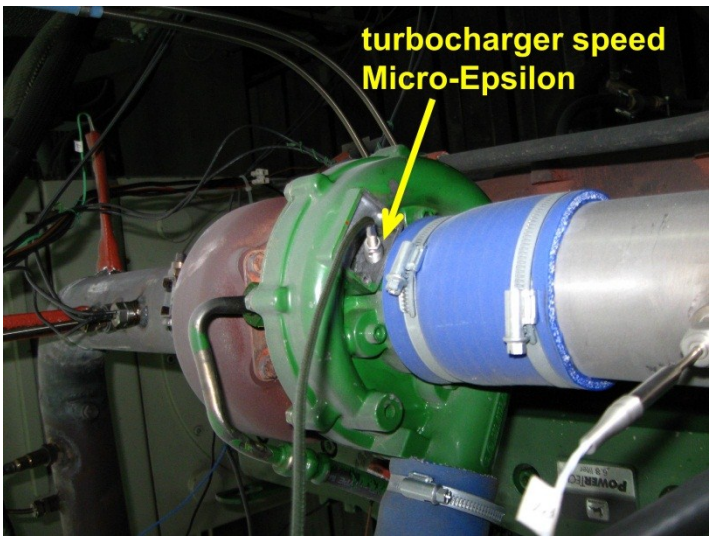

Figure 61 Compressor with Micro-Epsilon sensor for measurement of turbocharger speed

The pressure indication required for three pressure analysis is shown in *Figure 62* and *Figure 63*.

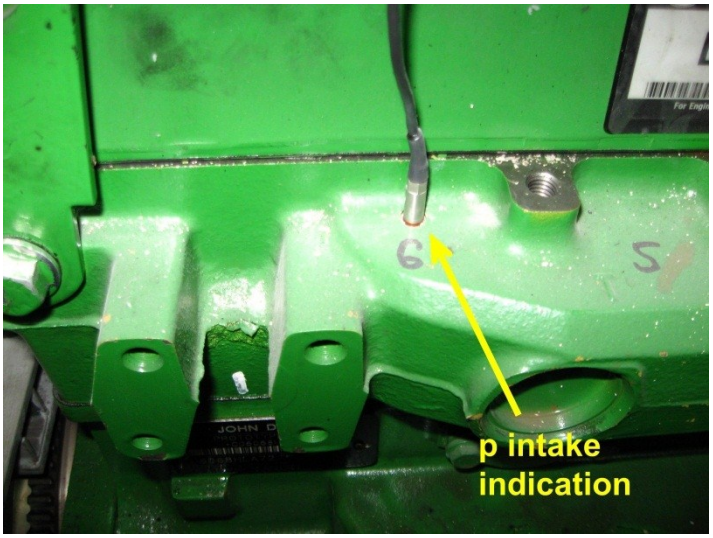

Figure 62 Sensor for indication of pressure (inlet of intake port) required for TPA (three pressure analysis)

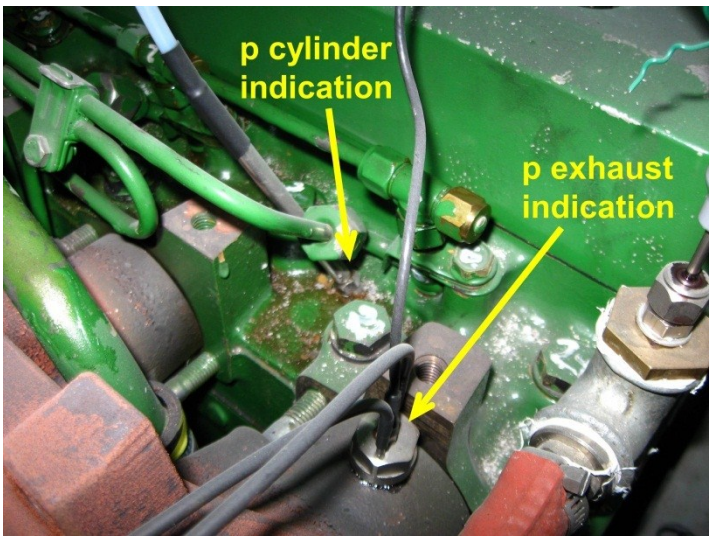

Figure 63 Adapter with sensor for in-cylinder pressure indication, indication of pressure at exhaust port outlet

The location of pressure sensors upstream of the turbine section are highlighted in *Figure 64.* The thermocouples for sensing of temperatures in turbine sections inlets are visible in *Figure 65*.

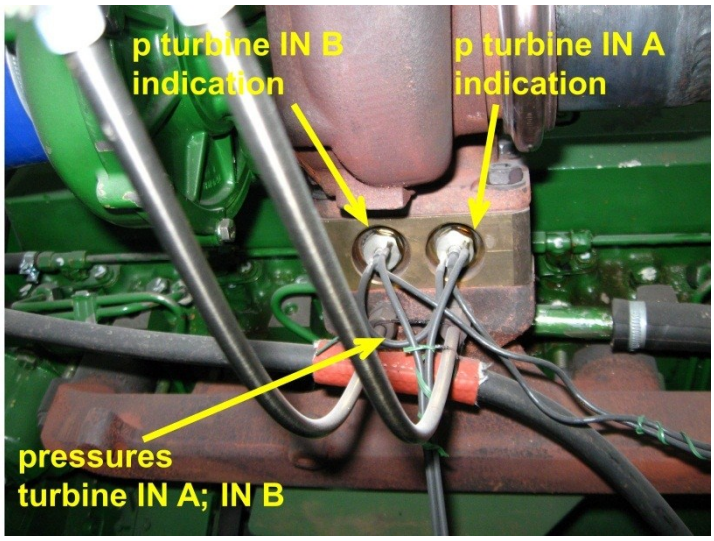

Figure 64 Location of sensors for pressure indication in sections turbine upstream, auxiliary measurement of static pressures in turbine sections

Figure 65 Measurement of temperatures in sections upstream of a turbine

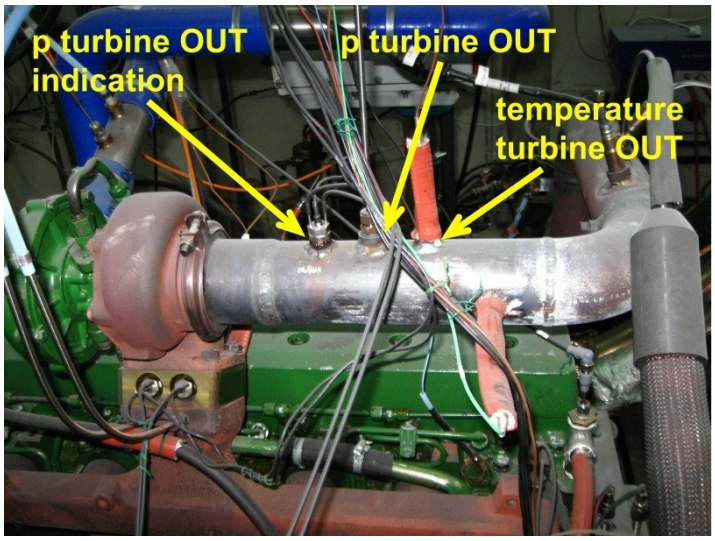

Figure 66 Location of pressure sensors and thermocouples turbine downstream

The points of pressures and temperatures measurement are highlighted in *Figure 66*.

5.4 Evaluation of Results

The evaluated integral parameters of the measured internal combustion engine are presented in following pictures. The brake torque and brake mean effective pressure of all measured operating points are in *Figure 67* and *Figure 68*.

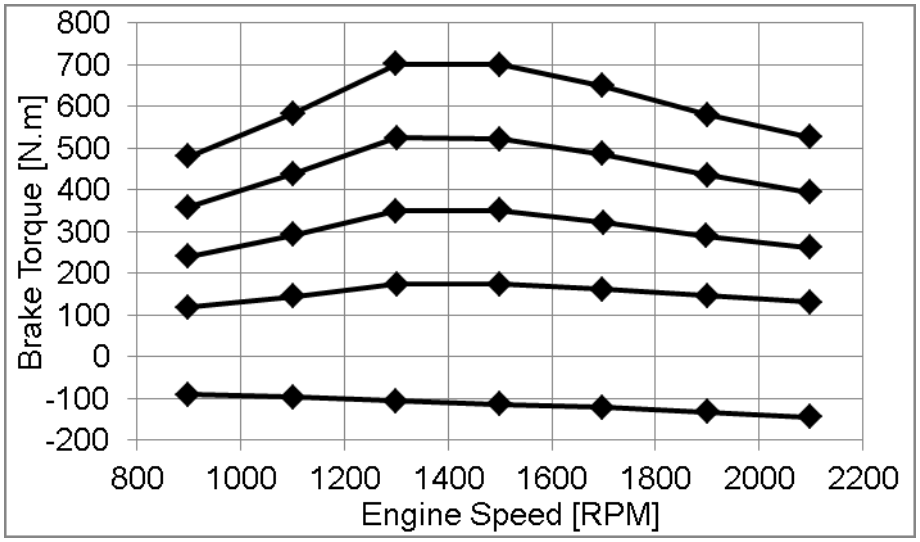

Figure 67 Brake torque of measured engine operating points

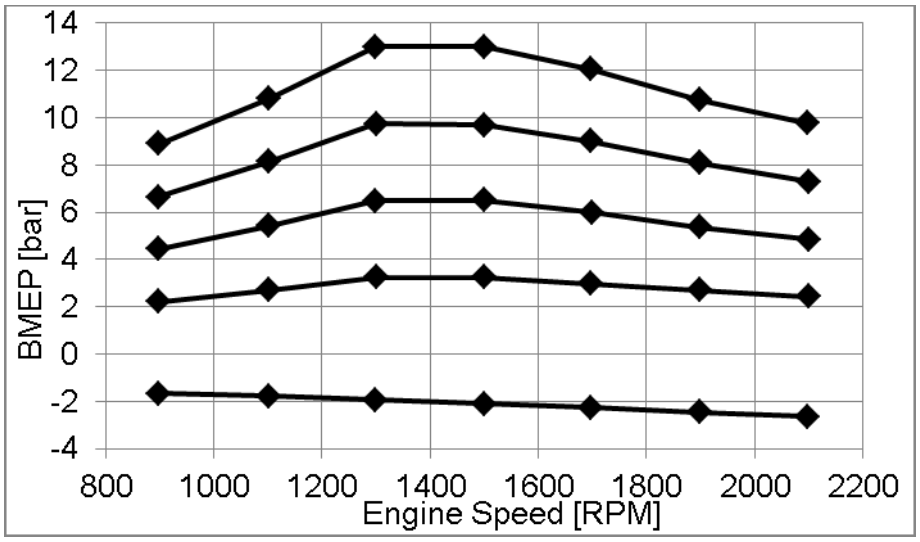

Figure 68 Brake mean effective pressure of the experimental engine

The complete engine characteristic with areas of constant brake specific fuel consumption is shown in *Figure 69*.

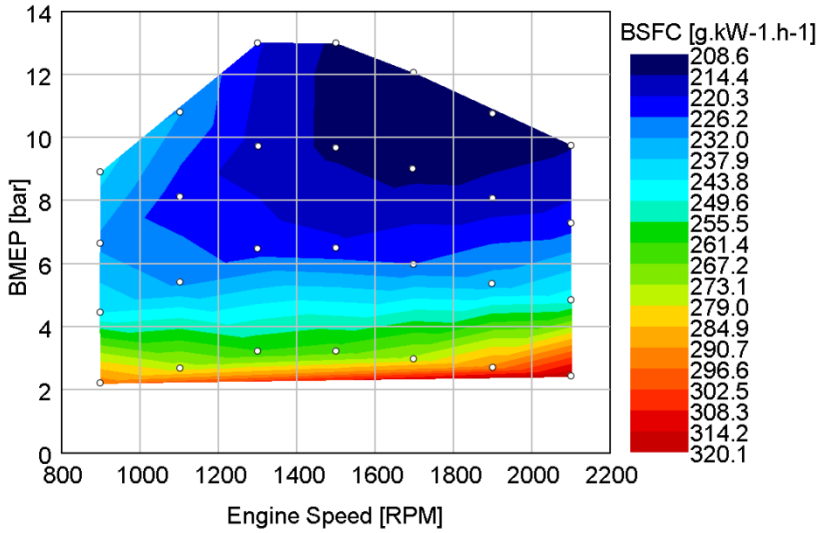

Figure 69 Complete characteristic of the tested engine, contour plot of measured constant brake specific fuel consumption

Each steady state point measured on the engine test bed is summarized in collection of data from slow and fast data acquisition. Raw experimental data was processed for the utilization during the calibration processes of developed models in GT-SUITE. The indicated pressures at the intake port, in the cylinder and at the exhaust port outlet are used in the basic model of a single cylinder engine, derived from the developed model of the six cylinder diesel engine, during the three pressure analyses, which are unavoidable for the calibration process of the cylinder model. All measured physical values listed in *Table 5* were utilized for the calibration of appropriate parts of the six cylinder engine model. Details are presented in the simulation part of the thesis.

Engine transients were the integral part of experimental research on the engine test bed. The dynamometer is equipped with the control of engine speed. The transients were defined by the fuel mass flow rate in time at constant engine speed. The engine brake torque, after the step change of injected fuel amount, increased from the initial level to approximately maximum brake torque at specified speed. The course of fuel mass flow rate change was limited by the original control unit of the fuel injection pump.

All experimental results are compared with the simulation results in simulation chapters below. The results were also presented in [51].

6. Simulation - Twin Entry Turbine

It has to be stressed properly that the simulation research of a radial turbine builds on the previous work mainly of prof. Ing. Jan Macek, DrSc. and doc. Ing Oldřich Vítek, Ph.D. published in [37], [36], [34] and [38]. The newly developed 1-D model of a twin scroll radial centripetal turbine presented in the thesis utilizes the main features and huge experience from the previous 1-D model of a turbine with the single scroll. The experiences from the development of several boosting systems [58] and pressure wave supercharger [55], [57] and [59] are employed in the research work.

The developed unsteady full 1-D model of a twin scroll turbine, described in detail in the chapter, was properly calibrated under steady flow. The calibration process of the model consists in the effort of finding proper combination of defined calibration coefficients, when the differences between simulation results and experiments are lowest. The calibrated 1-D turbine model was connected to the developed model of the experimental six cylinder diesel engine for verification of the turbine model capability under unsteady highly pulsating flow.

The comparison of the full 1-D turbine model behaviour during transients at the constant engine speed with the experimental data was the last loading test.

The models of the twin scroll turbine, six cylinder compression ignition engine, derived single cylinder engine and several turbocharger test beds are completely developed in GT-SUITE environment (chapter 2.3). The advantage of the commercial available simulation software consists in the connectivity of all models in the environment. The accessibility of developed models for researchers and customers is easy, because the GT-SUITE is well-known and popular simulation software.

6.1 Modelling of the Test Beds

Several models of the turbocharger test bed were created during the development of the unsteady turbine model. The behaviour of the turbocharger models have to be simulated properly under steady flow. The model of the turbocharger test bed with the closed loop is a suitable tool for the turbine - compressor matching. The virtual steady flow test stand is fitted with the model of the combustion chamber.

The burner running is controlled via the PID controllers with different regulation strategies, e.g. constant turbocharger speed, turbine pressure ratio, compressor pressure ratio or temperature upstream of a turbine. The combustion of an arbitrary fuel is available in the GT-SUITE model.

The steady flow test bed with the closed loop is useful for the turbine - compressor matching and verification of basic steady flow maps, but unusable for more detailed simulation.

The model of the steady flow turbocharger test bed with open loop is the proper tool for comprehensive turbocharger modelling. The model may be equipped with the combustion chamber, which is unavoidable for simulation of exhaust gases flow. It is also useful, when the real hot gas stand is simulated. In the case of stand with open loop, the inlet and outlet conditions at the turbine (or combustion chamber) and compressor side have to be actuated. This type of actuation in simulation is quite demanding.

The real turbocharger test bed, described in chapter 4.1, is equipped with the sophisticated control system, which is able to find the specific working point of a turbocharger defined by the operator automatically and repeatedly. The repeatability of measurements should be better in comparison with the older turbocharger test bed without automatic control and acquisition system.

The problems occurring in simulation are identical to problems in reality. It is needful to control the temperature upstream of the turbine in a broad range to achieve the required blade speed ratios. The turbine has to be combined with various compressors to extend the turbine load by virtue of increased mass flow rate via compressor.

During the development of the test stand with separated sections intended for measurement of twin entry turbines, several models of the test bed with and without the burner were created. The virtual test bed is the proper tool at the early stage of the development. The various arrangements were simulated and the acceptable solution was found. The measuring sections with orifices for the estimation of mass flow rates in separated sections are consistent with the standard ČSN EN ISO 5167:2003. The level of unequal partial admission was predicted via throttling in the turbine section. All required turbine operating points were properly simulated and a detailed schedule of experimental work was prepared.

The model of a turbine dynamometer is a robust simulation solution. The turbine is running at constant speed and conditions upstream of the turbine are controlled in accordance with the requirements. It is easy to reach arbitrary working point under steady flow.

The models of virtual turbocharger test stands are collected in a software library [SW 1]. The simulation tools and results were published in [53], [48] and [49].

6.2 Twin Entry Turbine Model Fundamentals

The last evolution of the unsteady full 1-D model of a centripetal radial turbine with the twin scroll is presented in the chapter. The model completely developed in the GT-SUITE simulation environment is fully modular, relatively easy to rebuild and ready for recalibration. It enables to adapt the current model to required specific design of a turbine - *Figure 70*. The model fully includes the twin volute with symmetrical and asymmetrical design, the scrolls are thus generally asymmetrical in the model. When one section of a scroll is closed, the model behaves like a single scroll turbine automatically. The operating mode with closed section, as an extreme level of the impeller admission, was also measured on the turbocharger

test bed. The scrolls are drawn in *Figure 71*. It is possible to simulate vaneless or bladed nozzle ring. The radial turbine presented in the thesis is equipped with a parallel symmetrical twin scroll and vaneless nozzle ring. The current model is adiabatic but ready for very specific purposes of non-adiabatic conditions in relation to turbocharger energy balance with required heat fluxes.

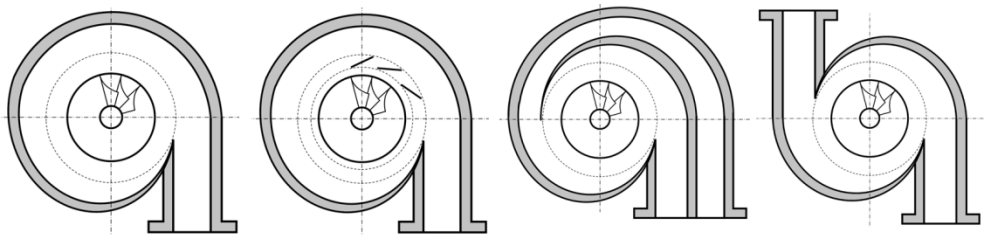

Figure 70 Turbine housings (from left), single or twin scroll with parallel sections with vaneless nozzle ring; with bladed nozzle ring; circumferentially divided twin entry (double volute); two separated inlets

The turbine type with variable turbine geometry (VTG, VGT or VNT) was successfully tested and presented in [56]. Model may be extended by the waste gate (WG), exhaust gas recirculation valves (EGR) or outlet turbine diffuser. These components will be tested in the future.

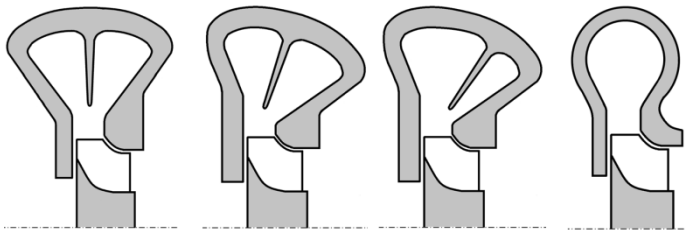

Figure 71 Symmetric and asymmetric design of sections; single scroll

The 1-D model is fully unsteady, so it enables to describe fast changing values inside the whole turbine. The turbine model is ready to cooperate with any model in GT-SUITE. Every physical quantities and turbine parameters are computed online directly in the model.

The model predicts backflows in sections. The developed specific turbocharger test bed for twin scroll turbines is ready for measurement of backflows in sections, but the specific experiments will be carry out in the future.

The turbine geometry required for the 1-D model is summarized in *Table 6.* Inlet diameter of scroll section (circular cross section) has equivalent area as inlet port of a real turbine with non-circular shape. The length of each section scroll is required. Only half of the length is used in the model, then one section begins to interact with the other. The turbine wheel is described by main dimensions such as inlet diameter and width, outlet large and small diameter. The estimation of the impeller centre line length, i.e. the centre-line of flow inside a channel, may be problematic little bit. It is the estimation from CAD model of a wheel in our case. The impeller in radial direction is modelled as single rotating channel with appropriate equivalent diameter (circular cross section). The rotating channel represents all channels of the real turbine wheel and its area is equivalent to

overall inlet area of the impeller. The inlet area is reduced by the impeller vanes area at inlet, so the mentioned area or number of vanes is required. The equivalent diameter of a single rotating channel may be entered directly into the model. The last are dimensions of the turbine outlet pipe. The reference area of a turbine A t_ref is also needful for computation of the proper discharge coefficient. The reference area of a turbine, derived from the measurement with blocked turbine wheel at the pressure ratio about 2.2, is a constant value for all computations.

Table 6 Required geometrical data of modelled turbine

inlet diameter of scroll section A
inlet diameter of scroll section B
length of scroll A
length of scroll B
impeller diameter (inlet)
impeller width (inlet)
impeller diameter (outlet) - large
impeller diameter (outlet) - small
impeller centre line length
impeller vanes area (inlet)
number of impeller vanes
equivalent diameter of single rotating channel
outlet pipe diameter
outlet pipe length

The sketch of an impeller with main dimensions is in *Figure 72*. The averaged impeller outlet diameter is calculated using the (100). The outlet averaged diameter, based on real geometry of an impeller, is relevant for all values at turbine outlet.

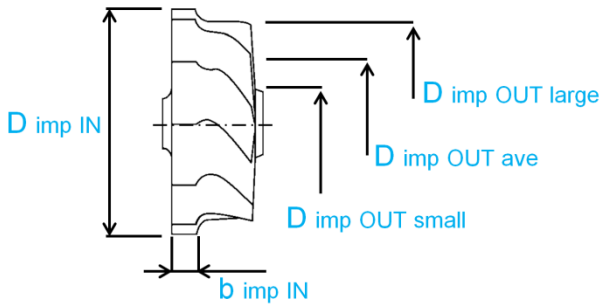

Figure 72 Main dimensions of an impeller

$$D_{imp\_OUT\_ave} = \left(\frac{D_{imp\_OUT\_large}^2 + D_{imp\_OUT\_small}^2}{2} \right)^{0.5} \quad (100)$$

It would be helpful to perform the sensitivity analysis of all required geometrical data on the results of fully calibrated turbine model in the future. The knowledge of the influence of each dimension on the predictive capability of the turbine model

would be valuable for the virtual prototypes, when dimensions are not available. There is also possibility that some data are insignificant for overall results and estimation is sufficient. This would help in situation, when the complete set of information about the particular turbine is not available.

When the geometry is completely entered into the model, all necessary experiments are evaluated and prepared for the comparison with simulation results, the turbine 1-D model is ready for the beginning of the calibration procedure. The parameters required for the calibration process of the twin entry turbine 1-D model are stated in *Table 7*.

Table 7 Calibration coefficients of the twin scroll turbine model

Alpha 2	[rad]	nozzle exit angle
Delta Alpha 2	[rad]	deviation of nozzle exit angle
Beta 3	[rad]	impeller exit angle
K sep	[1]	flow separation coefficient
K zeta	[1]	correction of impeller incidence loss
K wind	[1]	coefficient of windage losses
mu Leakage Static	[1]	discharge coefficient of static leakages
mu Leakage Rotating	[1]	discharge coefficient of rotating leakages
p Loss Coefficient Impeller	[1]	pressure loss coefficient in impeller pipe
CD A	[1]	discharge coefficient at section A outlet
CD B	[1]	discharge coefficient at section B outlet
p Loss Coefficient Nozzle A	[1]	pressure loss coefficient in section A
p Loss Coefficient Nozzle B	[1]	pressure loss coefficient in section B

Alpha 2 - nozzle exit angle
The coefficient directly influences the dimension at the outlet of the vaneless nozzle ring. It is the principal coefficient with dominant effect on overall turbine model results.

Delta Alpha 2 - deviation of nozzle exit angle
Coefficient represents deviation between mass and momentum averaged exit angles. Delta alpha does not influence the outlet diameter of nozzle ring, but directly influences the velocity c 2_t, which is involved in the Euler turbine theorem as described below.

Beta 3 - impeller exit angle
It influences the dimension at the turbine wheel outlet. It is also fundamental coefficient with dominant effect on results like alpha 2.

K sep - flow separation coefficient
The diameter at impeller outlet, thus the effective flow cross section, is reduced by the flow separation coefficient. The coefficient K sep also reduces the diameter of the pipe at turbine outlet. The coefficient represents natural reduction of impeller outlet diameter due to separated flow independently of impeller exit angle beta 3.

K zeta - correction of impeller incidence loss
Coefficient corrects the additional incidence loss to impeller.

K wind - coefficient of windage losses
Tuning coefficient stated in the formula for calculation of turbine windage losses.

mu Leakage Static - discharge coefficient of static leakages
Discharge coefficient of static leakage orifice, which controls the mass flow rate via this leakage, i.e. the portion of mass flow rate through turbine and of course the ratio of mass flow rates between static and rotating leakages.

mu Leakage Rotating - discharge coefficient of rotating leakages
Discharge coefficient of rotating leakage orifice, which controls the mass flow rate via this leakage, i.e. the portion of mass flow rate through the turbine and of course the ratio of mass flow rates between static and rotating leakages.

p Loss Coefficient Impeller - pressure loss coefficient in impeller pipe
The coefficient controls the pressure losses in pipes which model the turbine wheel.

CD A - discharge coefficient at the section A outlet (upstream of flow mixing)
The value is inserted directly into the orifice template in the turbine model. The orifice takes place between the section A outlet and the flowsplit template that is responsible for the mixing of flows.

CD B - discharge coefficient at the section B outlet (upstream of flow mixing)
The value is inserted directly into the orifice template in the turbine model. The orifice takes place between the section B outlet and the flowsplit template that is responsible for the mixing of flows.

p Loss Coefficient Nozzle A - pressure loss coefficient in section A
Coefficient influences pressure losses in pipe that represents the scroll section A.

p Loss Coefficient Nozzle B - pressure loss coefficient in section B
Coefficient influences pressure losses in pipe that represents the scroll section B.

6.3 Model Structure

The full 1-D map-less approach is based on the physical description of phenomena inside the turbine scroll, mixing of flows from separated sections, impeller and turbine outlet. Instead of map based model with no spatial dimension, the real turbine is decomposed to pipes (including rotating pipes with external acceleration and pipes with changing cross section area) and pipe connection modules with defined discharge coefficients, dependent in general on turbine parameters. The unsteady mass flow rate is an automatic result. The unsteady turbine power is evaluated from signals of mass flow rate, speed and flow velocity inside a pipe using Euler turbine theorem. In the following part, the structure of the twin scroll turbine 1-D model with main parts will be described in detail. The description respects the natural flow direction inside the turbine from inlet sections to outlet pipe.

The velocity triangles utilized in the turbine model are displayed in *Figure 73*. The following equations refer to velocities drawn in *Figure 73* and *Figure 74*.

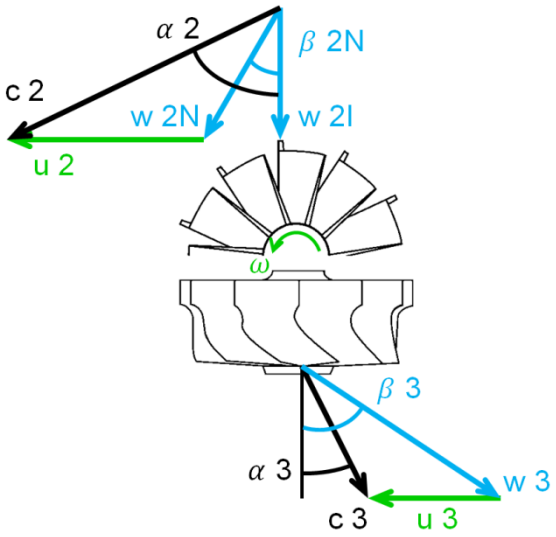

Figure 73 Velocity triangles, u 2 - circumferential velocity (impeller inlet), w 2N - relative velocity at nozzle outlet, w 2I - relative velocity at impeller inlet, c 2 - absolute velocity (impeller inlet), u 3 - circumferential velocity (impeller outlet), w 3 - relative velocity at impeller outlet, c 3 - absolute velocity (impeller outlet)

Figure 74 Velocity triangles, impeller inlet (left), c 2 - absolute velocity, t - tangential, r - radial; impeller outlet (right),c 3 - absolute velocity, t - tangential, a - axial

The simplified scheme of the turbine model developed in GT-SUITE is drawn in *Figure 75*. Layout of the entire model is in Appendix 7. Parallel sections A and B are connected in the zone of flow mixing modelled using the flowsplit template in function of flow joint. The flowsplit is the general name of the universal template of flow splitting or joining. The calibration of the flow joint is prerequisite. It consists in the finding of proper angles between inlet ports and the volume of the part. The diameters of inlet and outlet ports are controlled via actual dimension of vaneless nozzle ring in accordance of calibrated values. The mixing of flows occurs at the right place and correct pressures impeller upstream. The calibrated discharge coefficients also take place in the orifices between section outlets and flow joint.

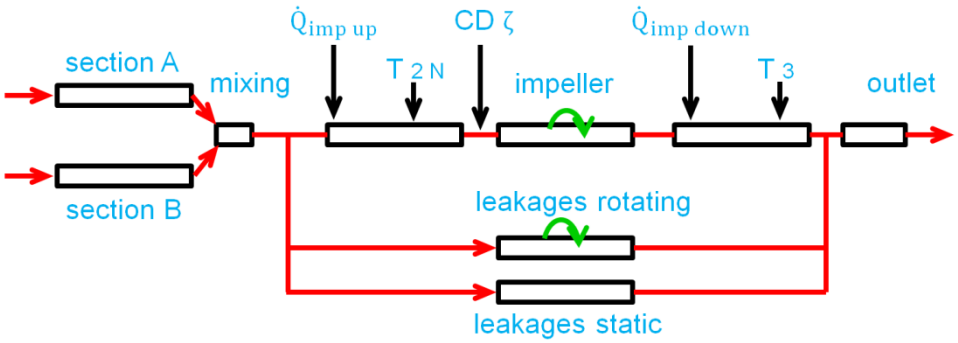

Figure 75 Simplified scheme of a 1-D radial centripetal turbine with twin scroll

The efficiency of the nozzle A (101), i.e. efficiency of enthalpy to kinetic energy transformation, describes only the pipe of the scroll section A ahead of flow mixing zone. The velocity c 2_N_A and pressure p 2_N_A are values at the pipe outlet. The relation for section B is analogical.

$$\eta_{N\_A} = \frac{\frac{c_{2\_N\_A}^2}{2}}{c_p T_{IN\_A\_tot}\left[1 - \left(\frac{p_{2\_N\_A}}{p_{IN\_A\_tot}}\right)^{\frac{\kappa-1}{\kappa}}\right]} \tag{101}$$

The flow after mixing continues via the vaneless nozzle ring. The nozzle outlet diameter (102), upstream of first transformation from stator to rotor, is given by the actual angle alpha 2, thus one of fundamental calibration coefficient.

$$D_{nozzle\_OUT} = \left(4 D_{imp\_IN} b_{imp\_IN} cos(\alpha_2)\right)^{0.5} \tag{102}$$

The portion of overall mass flow rate is separated in the zone of nozzle ring and flows through the parallel circuit of leakages. The leakages are divided into static and rotating. The rotating leakage is exposed to the same acceleration as the rotating channel representing the radial part of the turbine wheel is. The portion of mass flow rate via the static and rotating leakages is the subject of calibration.

After the flow left the nozzle ring, the total state transformation from stator to rotor takes place. The transformation from static coordinates to rotating coordinate system between the nozzle and rotating channel is described below. For orientation between relevant stagnation and relative states, the corresponding h-s diagram of a radial centripetal turbine is drawn in *Figure 76*.

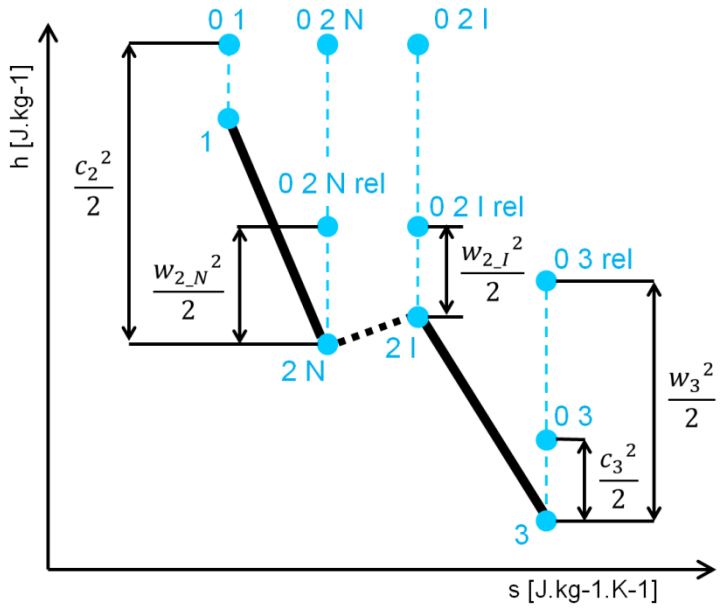

Figure 76 h-s diagram of radial centripetal turbine

$$u_2 = \frac{\pi D_{imp\_IN} 10^{-3} RPM}{60} \tag{103}$$

The relative velocity at the nozzle outlet w 2_N (104) is calculated from the tangential and radial components of absolute velocity c 2 and circumferential velocity u 2. The circumferential velocity u 2 at the impeller inlet is stated in (103).

$$w_{2\_N} = \left[\left(c_{2\_t} - u_2\right)^2 + c_{2\_r}^2\right]^{0.5} \tag{104}$$

The tangential (105) and radial (106) components of absolute velocity c 2 are influenced by the deviation of nozzle exit angle delta alpha 2. Velocity c 2_t is involved in the Euler turbine theorem, so it directly influences basic turbine torque.

$$c_{2\_t} = c_2 sin(\alpha_2 + \Delta\alpha_2) \tag{105}$$

$$c_{2\_r} = c_2 cos(\alpha_2 + \Delta\alpha_2) \tag{106}$$

Then it is necessary to establish relative stagnation state at vaneless nozzle outlet p 0_2_N_rel (107) using the relative velocity w 2_N and known values in appropriate pipe, which simulates the nozzle outlet. The relative stagnation state p 0_2_I_rel calculation (108) is based on the values sensed from the rotating

channel inlet. The rotating channel pipe represents the radial part of the turbine wheel in the model.

$$p_{0\_2\_N\_rel} = \left(p_{2\_N}10^5 + 0.5\rho_{2\_N}w_{2\_N}^2\right)10^{-5} \quad (107)$$

$$p_{0\_2\_I\_rel} = \left(p_{2\_I}10^5 + 0.5\rho_{2\_I}w_{2\_I}^2\right)10^{-5} \quad (108)$$

The relative stagnation temperature at the nozzle outlet T 0_2_N_rel can be determined by static temperature T 2_N and relative velocity w 2_N in equation (109). The relative stagnation temperature T 0_2_I_rel (110) at the impeller inlet is established in the similar way by static temperature T 2_I and relative velocity at the rotating channel inlet w 2_I. The relative stagnation temperatures at the nozzle outlet and impeller inlet should be equal.

$$T_{0\_2\_N\_rel} = T_{2\_N} + \frac{w_{2\_N}^2}{2c_p} \quad (109)$$

$$T_{0\_2\_I\_rel} = T_{2\_I} + \frac{w_{2\_I}^2}{2c_p} \quad (110)$$

The fictitious heat flux at beginning of the transformation zone, based on the stagnation temperature T 0_2_N at nozzle outlet, relative stagnation temperature T 0_2_N_rel and mass flow rate via the turbine decreased by the mass flow rate through leakages, is specified by the relation (111). The fictitious heat supply or removal for achievement of the required state impeller upstream is performed in the model by heat input rate variable in specific transformation pipe.

$$\dot{Q}_{imp\_up} = (\dot{m}_A + \dot{m}_B - \dot{m}_{leak})c_p\left(T_{0\_2\_N} - T_{0\_2\_N\_rel}\right) \quad (111)$$

The correction of actual static temperature to the temperature T 2_N from the nozzle outlet takes place downstream of the heat supply or removal in the transformation pipe. The required static temperature is imposed to the flow by the variable imposed fluid temperature of the specific orifice template. The temperature of flow is overwritten by the required value.

The overall effect of forced heat supply/removal and imposed static temperature T 2_N to fluid is that during the transformation from the stator to rotor upstream of the

impeller the heat is always removed from the flow. The result of the transformation from static coordinates to rotating coordinate system should be the equality of the static pressures at the nozzle outlet p 2_N and impeller inlet p 2_I and corresponding static temperatures T 2_N and T 2_I. This is the end of the first transformation in the turbine model and flow is ready to enter the rotating channel, which simulates the first part of the turbine wheel.

The main part of the impeller incidence loss is included implicitly, because the rotating channel cross section respects the real direction of flow, which is mainly radial. The correction of the impeller incidence loss is carried out using the calibrated discharge coefficient upstream of a turbine wheel.

The incidence loss corrected by the calibration coefficient K zeta is calculated using the equations (112) and (113), taking into account that the loss of cross section sudden change is respected by the orifice module automatically. The derived discharge coefficient, entered to the orifice upstream of the rotating channel, is introduced in (114).

$$\zeta_{imp} = \left(tan\left(\beta_{2\_N}\right) + K_{zeta}\right)^2 \tag{112}$$

$$\zeta = \zeta_{imp} - \tan^2\left(\beta_{2\_N}\right) \tag{113}$$

$$C_{D\_\zeta} = \sqrt{\frac{1}{1+\zeta}} \tag{114}$$

The impeller is simulated by two pipes. The first one, in radial direction, is the rotating channel exposed to acceleration. The second is the outlet part of the impeller in axial direction. The impeller expansion efficiency is established by relation (115).

$$\eta_{imp} = \frac{\frac{w_3^2}{2} + \frac{u_2^2}{2} - \frac{u_3^2}{2}}{c_p T_{0\_2\_I\_rel}\left[1 - \left(\frac{p_3}{p_{0\_2\_I\_rel}}\right)^{\frac{\kappa-1}{\kappa}}\right]} \tag{115}$$

The pipe that simulates the rotating channel is exposed to the acceleration, which depends on actual turbine wheel speed. The acceleration at rotating channel inlet is calculated via relation (116).

$$acc_{imp\_IN} = -D_{imp\_IN}10^{-3}0.5\left(\frac{2\pi RPM}{60}\right)^2 \quad (116)$$

The corresponding acceleration at the outlet of the rotating channel is specified by equation (117). The introduced accelerations are also valid for the rotating leakage in the parallel flow circuit of leakages. The pipe of rotating leakage is thus exposed to the same acceleration at the inlet and outlet as the rotating channel. The proper values are imposed to the pipes via the body force acceleration variable.

$$acc_{imp\_OUT} = -D_{imp\_OUT\_ave}10^{-3}0.5\left(\frac{2\pi RPM}{60}\right)^2 \quad (117)$$

The relevant impeller outlet diameter that is governed by the fundamental calibration coefficient beta 3 is determined by (118). The natural reduction of impeller outlet diameter due to separated flow is represented by independent flow separation coefficient. The diameter of a pipe at turbine outlet is also reduced by the K sep coefficient.

The relevant impeller outlet surface area, given by the impeller exit angle beta 3, is reason for the coefficient beta 3 great effect on the turbine model overall results.

$$D_{imp\_OUT} = K_{sep}\left[\left(D^2_{imp\_OUT\_large} - D^2_{imp\_OUT\_small}\right)cos(\beta_3)\right]^{0.5} \quad (118)$$

The transformation from rotating coordinate system to static coordinates of stator begins at impeller outlet. The circumferential velocity at the impeller outlet is established using the relation (119).

$$u_3 = \frac{\pi D_{imp\_OUT\_ave}10^{-3}RPM}{60} \quad (119)$$

The relative stagnation temperature T 0_3_rel at the impeller outlet, see h-s diagram in *Figure 76*, established from the static temperature T 3 and relative velocity w 3 at impeller outlet is described by (120).

$$T_{0\_3\_rel} = T_3 + \frac{w_3^2}{2c_p} \quad (120)$$

The stagnation temperature at the impeller outlet T 0_3 (121) is given by the static temperature T 3 and absolute velocity c 3 at impeller outlet.

$$T_{0\_3} = T_3 + \frac{c_3^2}{2c_p} \tag{121}$$

The fictitious heat flux impeller downstream is based on the computed values of relative stagnation temperature T 0_3_rel, stagnation temperature T 0_3 and mass flow rate via turbine without the mass flow rate of leakages (122). The fictitious heat supply or removal is imposed to transformation pipe by heat input rate variable.

$$\dot{Q}_{imp\_down} = (\dot{m}_A + \dot{m}_B - \dot{m}_{leak}) c_p \left(T_{0\_3\_rel} - T_{0\_3}\right) \tag{122}$$

The static temperature downstream of the heat supply/removal is overwritten by the required static temperature T 3, thus the temperature upstream of the transformation zone, in the specific orifice template. Along the transformation procedure from the impeller to the turbine outlet the heat is always removed from the fluid. This is the consequence of the overall effect of heat supply or removal and imposed static temperature. After the finalization of second transformation, the mass flow rate from the parallel circuit of leakages joins the main turbine mass flow rate. The model is terminated by the outlet pipe.

It has to be stressed that all stated equations are calculated directly in the GT-SUITE model and completely prepared for unsteady operation of a twin entry turbine.

The basic torque is calculated using the Euler turbine theorem (123). The physical robustness of the Euler turbine theorem consists in the dependence of torque on the tangential components of absolute velocities at the impeller inlet c 2_t and outlet c 3_t and appropriate mass flow rates. The velocity c 2_t (105) depends on calibration coefficients alpha 2 and delta alpha 2.

$$\begin{aligned} Tq_{Euler} &= \\ &= \dot{m}_{2\_N} 0.5 D_{imp\_IN} 10^{-3} c_{2\_t} - \dot{m}_3 0.5 D_{imp\_OUT\_ave} 10^{-3} c_{3\_t} \end{aligned} \tag{123}$$

The consequent power is established by relation (124) using the actual turbine speed.

$$P_{Euler} = Tq_{Euler}\frac{2\pi RPM}{60} \tag{124}$$

The relevant turbine power (125), in 1-D model, results from the basic power, based on the Euler turbine theorem, reduced by windage losses - P wind. The balance of power (31) is described in chapter 4.4.

$$\begin{aligned} P_{turb} - P_{wind} &= P_{comp\_adi} + P_{bear} \\ P_{Euler} - P_{wind} &= P_{comp\_adi} + P_{bear} \end{aligned} \tag{125}$$

The windage losses are calibrated under steady flow via the calibration coefficient K wind in equation (126). The corresponding Reynolds number is estimated from (127).

$$P_{wind} = \frac{K_{wind}\rho_{2\_N}\left(D_{imp\_IN}10^{-3}\right)^2 u_2^3}{Re_{2\_N}^{0.2}} \tag{126}$$

$$Re_{2\_N} = \frac{D_{imp\_IN}10^{-3}u_2}{\frac{\mu_{2\_N}}{\rho_{2\_N}}} \tag{127}$$

The power on turbocharger shaft (128), directly utilized by the compressor, is the power from Euler theorem reduced by windage losses - P wind and power losses in bearings - P bear. The pure power losses in bearings are known from the tailored regression formula based on experimental results. Details are in the chapter 4.5. The regression formula is a part of the turbine 1-D model, so the valid power losses in bearings are known under any conditions, both steady and unsteady. The mechanical efficiency of the turbocharger shaft model naturally equals to 1, because all power losses are included in relation (128). The assessment of mechanical efficiency is fully under control of the turbine model. The model of the turbocharger shaft comprises the moment of inertia of all rotating parts (turbine wheel, shaft and compressor wheel).

$$P_{shaft} = P_{comp\_adi} = P_{Euler} - P_{wind} - P_{bear} \tag{128}$$

The turbine isentropic efficiency is in the 1-D model defined as a quotient of the actual turbine power and isentropic power (129). The isentropic efficiency, based on the mentioned relation (129), is valid only under steady flow conditions. The turbine performance under unsteady conditions is the part of the current research with the highest priority. At unsteady turbine operation, the isentropic turbine efficiency is not relevant due to the mass accumulation inside the different part of the model. The accumulation of mass during unsteady operation is natural behaviour of the model and also of the real turbine, so the efficiency calculated from isentropic enthalpy head cannot be used, because the isentropic enthalpy differences cannot be simply integrated. The efficiency is biased and unusable for the evaluation of unsteady results.

From the general point of view, the relevant physical quantities that describe the performance of the turbocharged internal combustion engine are brake values such as brake torque and brake specific fuel consumption, so only the brake efficiency of the whole engine is important and decisive. The partial efficiency of the turbine or turbocharger is irrelevant.

$$\eta_{turb\_ise} = \frac{P_{Euler} - P_{wind}}{P_{ise\_AB\_t\_s}} \tag{129}$$

The evaluation of turbocharger mechanical efficiency implemented in the turbine model is based on quotient of power on shaft and turbine power (130).

$$\eta_{mech} = \frac{P_{shaft}}{P_{Euler} - P_{wind}} = \frac{P_{Euler} - P_{wind} - P_{bear}}{P_{Euler} - P_{wind}} \tag{130}$$

The turbine overall efficiency (131) is also valid only under steady flow conditions like the isentropic efficiency above. The overall turbine efficiency is biased during the unsteady turbine operation because of the natural mass accumulation in different parts of the 1-D turbine model and impossibility to integrate partial isentropic enthalpy heads.

$$\eta_{turb\_overall} = \frac{P_{shaft}}{P_{ise\_AB\_t\_s}} = \frac{P_{Euler} - P_{wind} - P_{bear}}{P_{ise\_AB\_t\_s}} \tag{131}$$

All equations, concerning twin scroll turbine, defined in chapters 4.3, 4.4, 4.5 and 4.6 are also calculated in the unsteady full 1-D turbine model. The regression formulas of pure bearing losses are included.

6.4 Calibration Procedure under Steady Flow

The real twin scroll radial turbine, in compliance with map-less philosophy, is represented by several experimental results. The parameters were measured at different pressure ratio, relatively broad range of blade speed ratio and under different levels of the impeller admission. No classical steady flow map is required during the entire process. The set of experimental data presented in the chapter 4.6 should be sufficient for the calibration procedure of the developed twin scroll turbine 1-D model with robust physical background. The steady flow calibration procedure of the 1-D model covers all measured working points of the tested turbine.

The definition of isentropic states, in the case of a turbine with twin scroll where the mixing of flows takes place, is problematic, because the mixing of flows is an irreversible process. The relevance of physical quantities, with any isentropic quantity in the definition, is discussed in the chapter below. The crucial physical values describing the turbine performance are mass flow rate and corresponding turbine power.

The goal of the calibration procedure of the 1-D turbine model was to find the best model setup under steady flow via the combination of calibration coefficients, where the differences between simulation and experimental results are lowest.

A simple virtual steady flow turbine test bed, with features of the ideal turbine dynamometer, was used for the purposes of the steady flow calibration procedure. The forced mass flow rates and temperatures from experiments were specified for each turbine section in the model. The turbine speed was also at the same value as at the correspondent measurement. The simulation results were compared with the experimental data at the same conditions at the turbine inlet and outlet.

Calibration procedure conditions:

1-D turbine model inputs:
- forced mass flow rate and temperature upstream of section A
- forced mass flow rate and temperature upstream of section B
- pressure and temperature downstream of a turbine
- turbine speed

Calibration coefficients:
Alpha 2 - nozzle exit angle
Delta Alpha 2 - deviation of nozzle exit angle
Beta 3 - impeller exit angle
K sep - flow separation coefficient
K zeta - correction of impeller incidence loss
K wind - coefficient of windage losses
mu Leakage Static - discharge coefficient of static leakages
mu Leakage Rotating - discharge coefficient of rotating leakages
p Loss Coefficient Impeller - pressure loss coefficient in impeller pipe
CD A - discharge coefficient at section A outlet (upstream of flow mixing)
CD B - discharge coefficient at section B outlet (upstream of flow mixing)
p Loss Coefficient Nozzle A - pressure loss coefficient in section A
p Loss Coefficient Nozzle B - pressure loss coefficient in section B

Goals of optimization:
- pressure ratio of section A (66)
- pressure ratio of section B
- turbine power defined by (125)

Criteria of optimization:
- minimum overall error Delta (132)

$$\Delta = \frac{1}{3}\left[abs\left(\frac{PR_{A\_sim}}{PR_{A\_exp}} - 1\right) + abs\left(\frac{PR_{B\_sim}}{PR_{B\_exp}} - 1\right) + \right.$$
$$\left. + abs\left(\frac{\{P_{Euler} - P_{wind}\}_{sim}}{\{P_{turb} - P_{wind}\}_{exp}} - 1\right)\right] \quad (132)$$

AND concurrently
- error of pressure ratio A, error of pressure ratio B or error of turbine power may not exceed specified maximum value (133)

$$\Delta PR_A = abs\left(\frac{PR_{A\_sim}}{PR_{A\_exp}} - 1\right) \leq \Delta PR_{A\_MAX}$$
$$\Delta PR_B = abs\left(\frac{PR_{B\_sim}}{PR_{B\_exp}} - 1\right) \leq \Delta PR_{B\_MAX} \quad (133)$$
$$\Delta P = abs\left(\frac{\{P_{Euler} - P_{wind}\}_{sim}}{\{P_{turb} - P_{wind}\}_{exp}} - 1\right) \leq \Delta P_{MAX}$$

In the case of extreme partial admission of an impeller, when the section B is closed, the error of pressure ratio B is irrelevant of course, so only the pressure ratio of turbine section A and turbine power are taken into account during the calibration procedure.

The aim of steady flow calibration was to find the proper combination of all calibration coefficients. Three parameters were taken into account during the results evaluation. The simulated and measured pressure ratio of section A, pressure ratio of section B and turbine power under steady flow were compared.

The optimization procedure began like the classical design of experiments with all combinations of calibration coefficients - full factorial. The range of each coefficient was broad and the size of the iteration step was also relatively large. After each iteration and results evaluation, the range of each coefficient was narrower and size of the step smaller in promising areas with the best results from previous iteration, in accordance with the principle of the gradient method. The goal was to find the combination of calibration coefficients, where the differences of selected

three criteria, as written above, between simulation results and experiments were lowest. After the steady flow calibration, the fully calibrated model of a twin entry turbine is ready for the on-engine simulation.

The further improvement of the calibration procedure may consist in the development of the independent automatic optimization routine based on some specific tool such as DASY [45] or commercial available software modeFRONTIER verified in e.g. [56] or [36]. The special simulation tools are able, after the learning phase, to evaluate results and decide on the further progress independently. DASY and modeFRONTIER can utilize the genetic algorithm for optimization. The whole calibration procedure of the 1-D turbine in conjunction with some optimization tool is the key.

6.5 Results

The results of the calibrated twin scroll turbine model under steady flow at the virtual test bed are presented in following pictures and also in Appendix 3. The previous results of different single or twin scroll turbine models were published in [51], [52], [46] and [53].

The measurement at the steady flow turbocharger test bed was carried out at first attempt. Many problems were solved before the real experimental work by the proper simulation work with virtual prototypes, but final experimental results are not entirely perfect. This fact is important for the evaluation of calibrated model results. The measurement procedure should be improved in the future step by step. The calibration process may be simplified by the almost automatic procedure with a proper optimization tool.

The courses of the calibration coefficients, as results of the steady flow calibration procedure, are stated below. The resultant calibration coefficients depend on the overall pressure ratio of a turbine and the level of admission. The measured pressure ratios of turbine sections A and B are changing with the turbine blade speed ratio, because the experiments were defined by the constant pressure in governing section A, so the experiments were carried out with changing overall pressure ratio of a turbine. For a given level of an impeller admission, the calibration coefficients change with turbine pressure ratio, which is visible in the following pictures. The calibration coefficients are changing with working conditions and concurrently with changing overall pressure ratio, so the values of coefficients at approximate constant level of turbine pressure ratio differ.

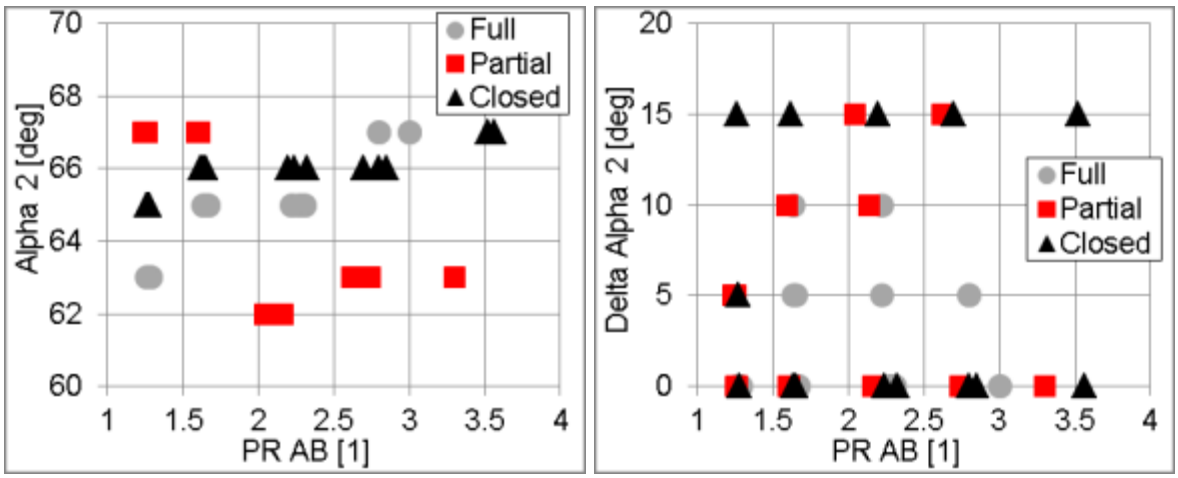

Figure 77 Calibration coefficients, Alpha 2 - nozzle exit angle (left), Delta Alpha 2 - deviation of nozzle exit angle (right); full admission of an impeller (gray circle), partial admission level A = 0.87 (red square), one section closed (black triangle)

The dominant influence on the overall turbine parameters have only two calibration parameters, nozzle exit angle alpha 2 (*Figure 77*) and impeller exit angle beta 3 in *Figure 78*. The coefficients directly affect the cross section areas of essential parts in the turbine model.

Delta alpha 2, which represents deviation between mass and momentum averaged angles, influences the first term in the Euler turbine theorem via the velocity c 2_t. Increasing values of delta alpha 2 cause higher turbine power, so the higher values are necessary under cold conditions at high blade speed ratio, where the turbine power is not sufficient. It has to be stressed that higher values of delta alpha 2 are used only at high blade speed ratios under cold conditions, as it is clearly visible in following pictures with calibration coefficients plotted versus blade speed ratio. Despite of high values of delta alpha 2, the turbine power is not sufficient under cold conditions.

Flow separation coefficient K sep represents reduction of impeller outlet diameter due to separated flow. K sep does not depend on the impeller exit angle.

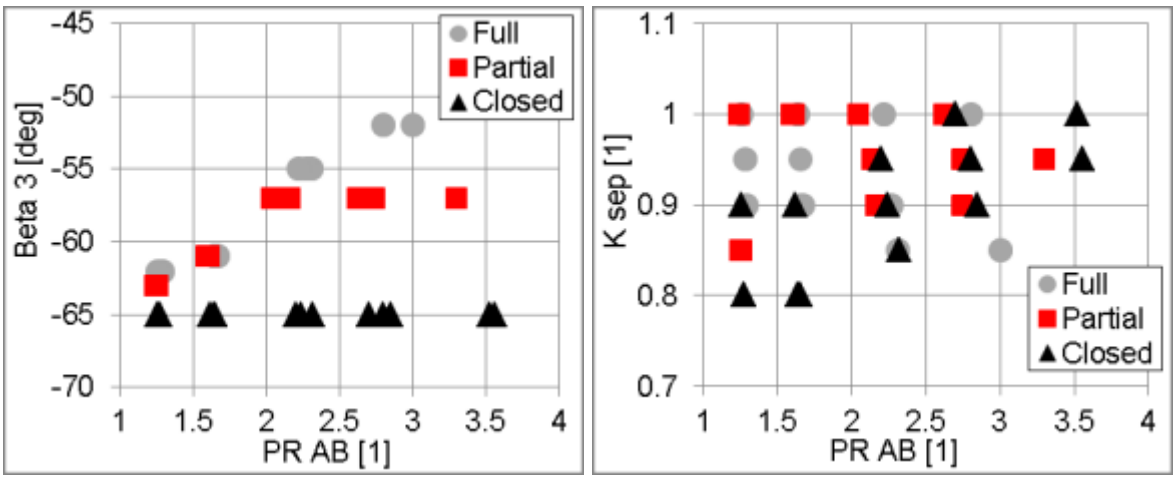

Figure 78 Calibration coefficients, Beta 3 - impeller exit angle (left), K sep - flow separation coefficient (right); full admission of an impeller (gray circle), partial admission level A = 0.87 (red square), one section closed (black triangle)

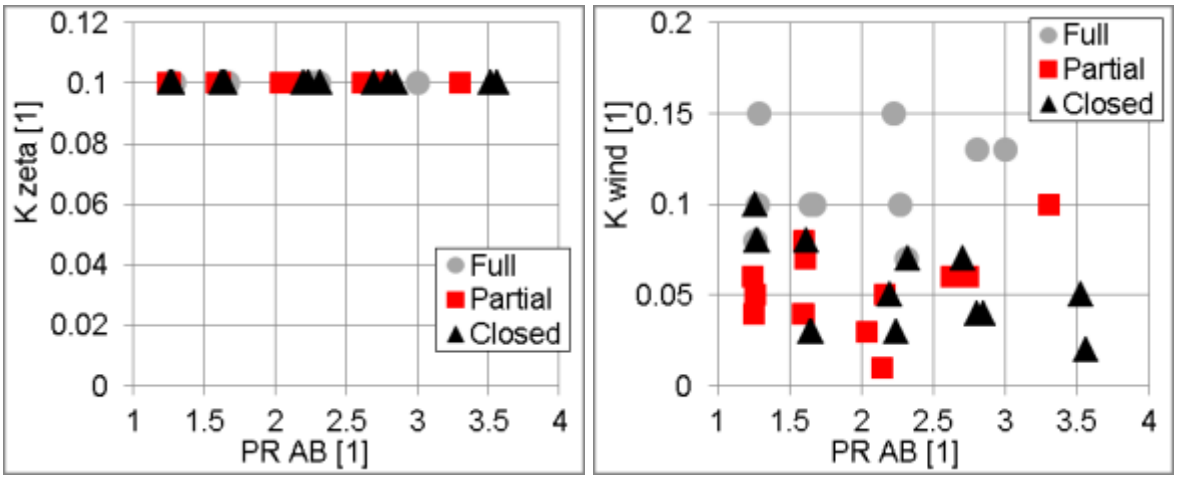

Figure 79 Calibration coefficients, K zeta - correction of impeller incidence loss (left), K wind - coefficient of windage losses (right); full admission of an impeller (gray circle), partial admission level A = 0.87 (red square), one section closed (black triangle)

The correction of the impeller incidence loss is carried out using the discharge coefficient upstream of a turbine wheel via calibration coefficient K zeta (*Figure 79*). The turbine power is reduced by windage losses via the K wind coefficient.

The discharge coefficients of static and rotating leakages, which straightly control the mass flow rates via leakages, are in *Figure 80*. Only the overall mass flow rate via leakages is important for the 1-D model results. The distribution of mass flow rate between static and rotating leakages seems to be insignificant. Discharge coefficients were the same and changed together during the calibration procedure.

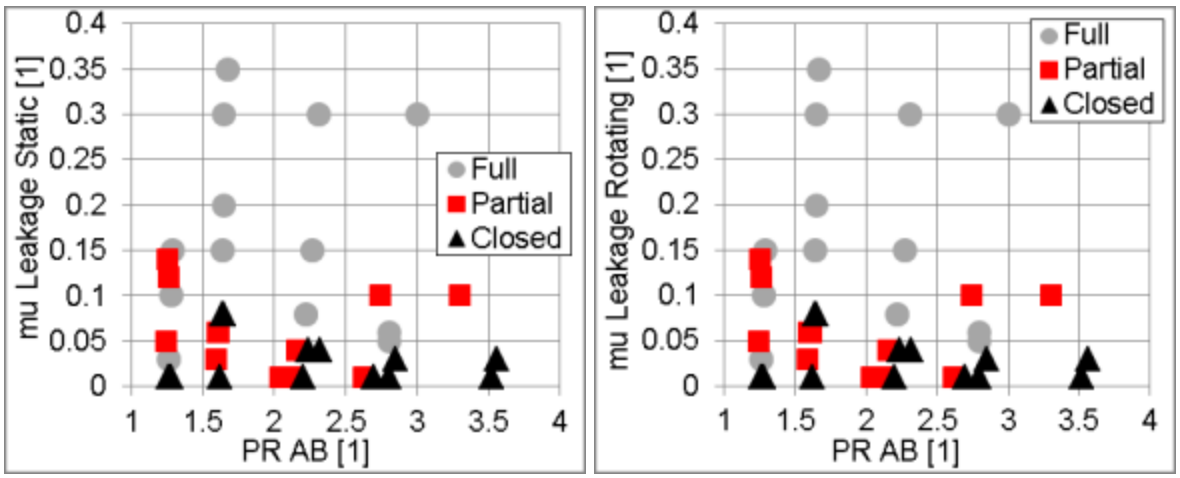

Figure 80 Calibration coefficients, mu Leakage Static - discharge coefficient of static leakages (left), mu Leakage Rotating - discharge coefficient of rotating leakages (right); full admission of an impeller (gray circle), partial admission level A = 0.87 (red square), one section closed (black triangle)

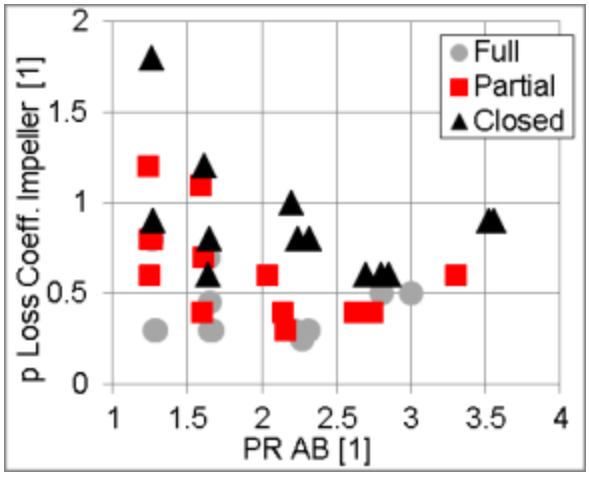

Figure 81 Calibration coefficient, pressure loss coefficient in impeller pipe; full admission of an impeller (gray circle), partial admission level A = 0.87 (red square), one section closed (black triangle)

The values of the pressure loss coefficient in impeller, which controls the pressure losses in pipes of the impeller wheel, are plotted in *Figure 81*.

The discharge coefficients CD A and CD B (*Figure 82*) at the turbine section outlets, upstream of flow mixing, depend on the overall pressure ratio of a turbine and mass flow rate level in each turbine section. The pressure loss coefficients in sections A and B are stated in *Figure 83*. As obvious from figures, the discharge coefficient at section outlet combined with the pressure loss coefficient are important for the achievement of the required state in particular turbine section under partial admission of an impeller with the proportion between mass flow rates 80:20 or 20:80.

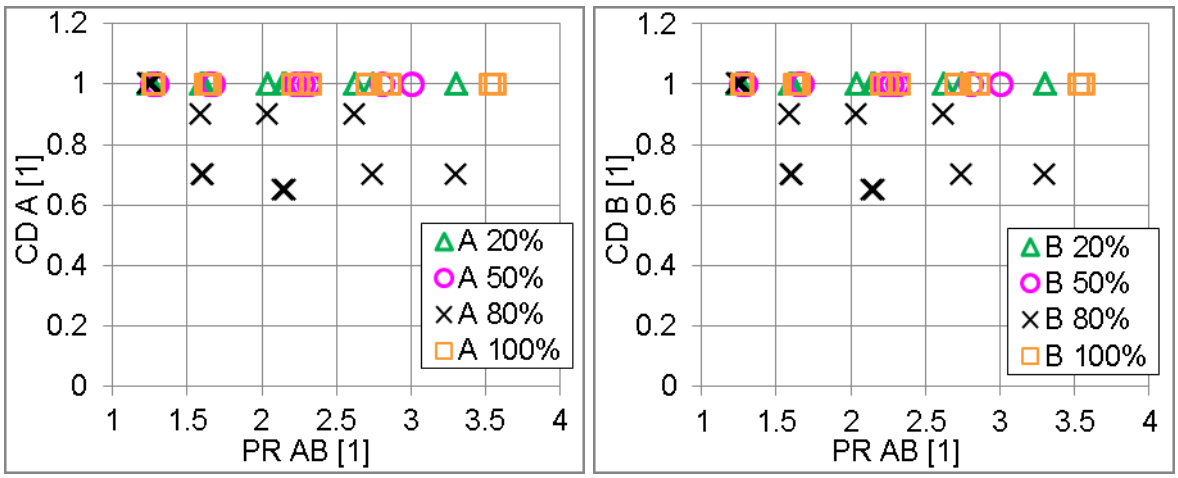

Figure 82 Calibration coefficients, CD A - discharge coefficient at section A outlet {upstream of flow mixing} (left) and CD B - discharge coefficient at section B outlet {upstream of flow mixing} (right) according to mass flow rate level in each section

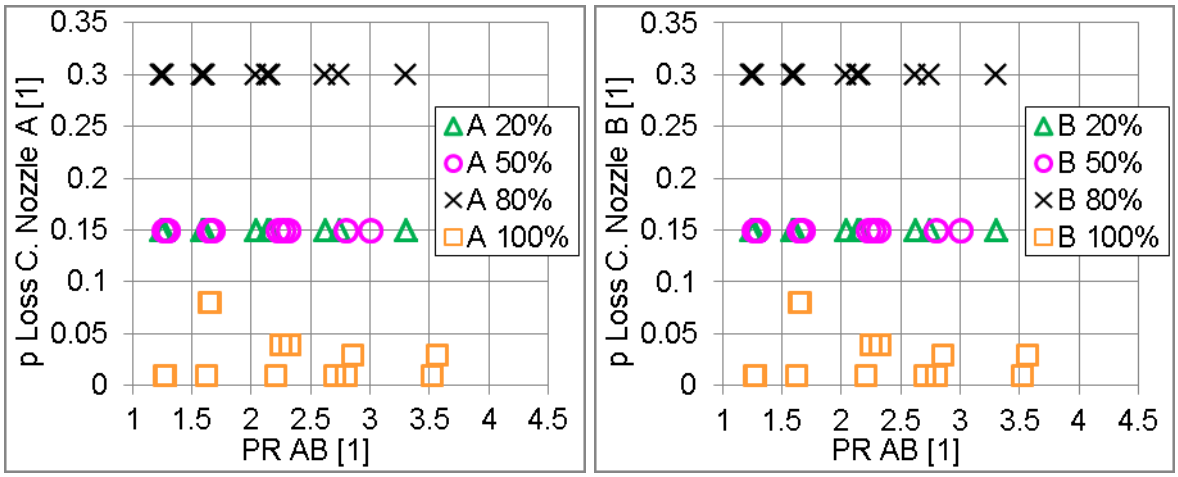

Figure 83 Calibration coefficients, pressure loss coefficient in section A (left) and pressure loss coefficient in section B (right) according to mass flow rate level in each section

In the following pictures, the experimental and simulated results under steady flow, full impeller admission at overall pressure ratio approximately 2.2, are compared and plotted versus turbine speed and also overall blade speed ratio. The pictures with results plotted versus overall blade speed ratio are more practical.

The forced mass flow rate and corresponding temperature in each section were specified at the exactly same values as during the experiments. The mass flow rates in turbine sections versus turbine speed are in *Figure 84* and versus blade speed ratio in *Figure 85.* The temperatures of the introduced working points in simulation and experiments are the same (*Figure 86* and *Figure 87*).

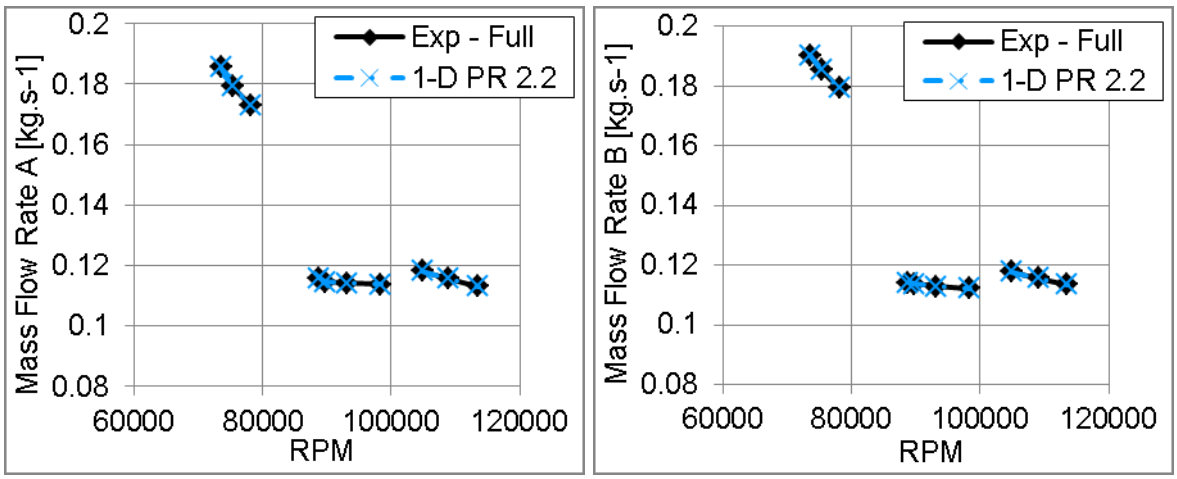

Figure 84 Mass flow rates in sections A and B vs. RPM (approximate pressure ratio level PR AB = 2.2), full admission of an impeller; experiments (black); simulation 1-D turbine (blue crosses)

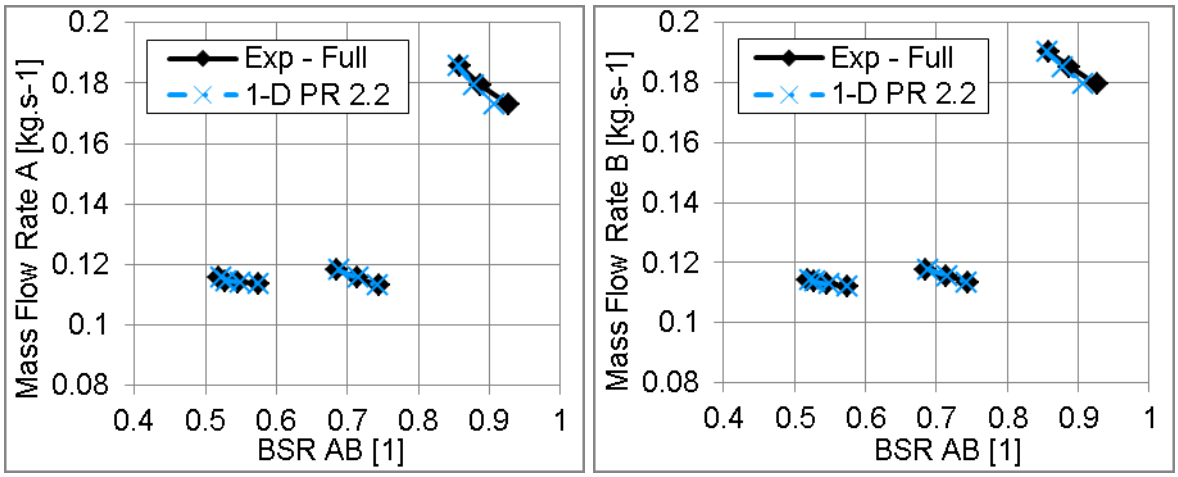

Figure 85 Mass flow rates in sections A and B vs. BSR (approximate pressure ratio level PR AB = 2.2), full admission of an impeller; experiments (black); simulation 1-D turbine (blue crosses)

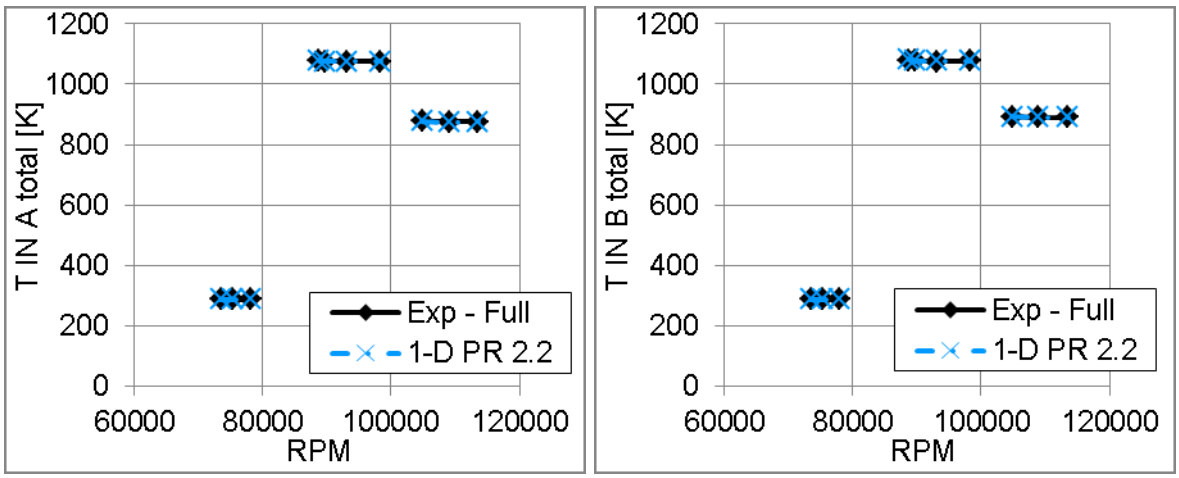

Figure 86 Total temperatures in sections upstream of a turbine vs. RPM (approximate pressure ratio level PR AB = 2.2), full admission of an impeller; experiments (black); simulation 1-D turbine (blue crosses)

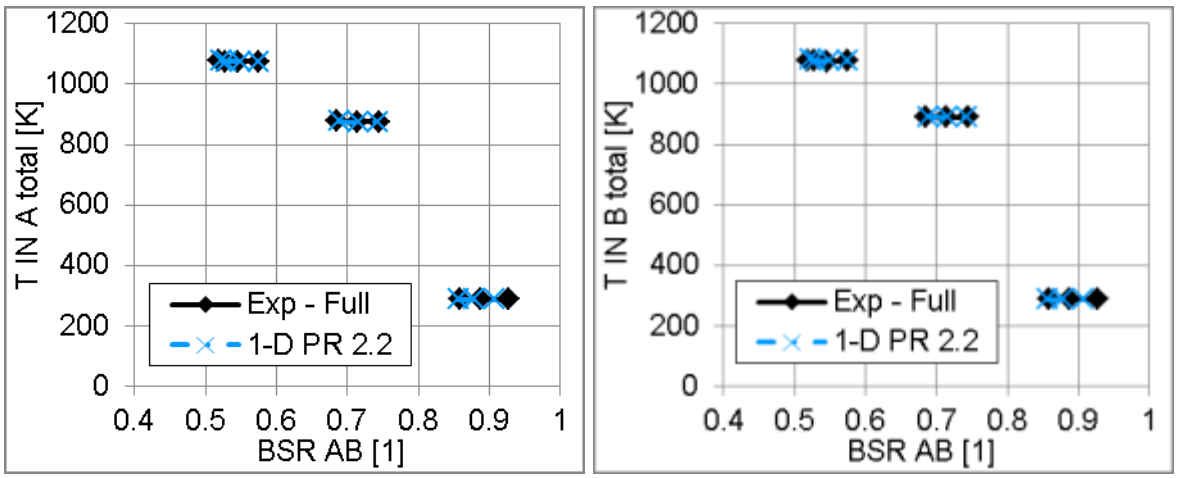

Figure 87 Total temperatures in sections upstream of a turbine vs. BSR (approximate pressure ratio level PR AB = 2.2), full admission of an impeller; experiments (black); simulation 1-D turbine (blue crosses)

The visible differences (here at high blade speed ratios) are absolutely correct, caused by the biased values of the overall blade speed ratio AB, which is defined by (22). The fictitious isentropic velocity cs AB (16) is the component of the blade speed ratio definition. The isentropic velocity cs AB depends on the pressure ratio of turbine sections A and B.

When the differences between measured and simulated pressure ratios of turbine sections occur, the overall blade speed ratio computed by the simulation has to be different from the experimental value. The comparison of all experimental or simulated values in dependence on turbine speed is always correct. The comparison of values plotted versus overall blade speed ratio is also always valid, but the biased value of blade speed ratio due to different pressure ratios has to be kept in mind.

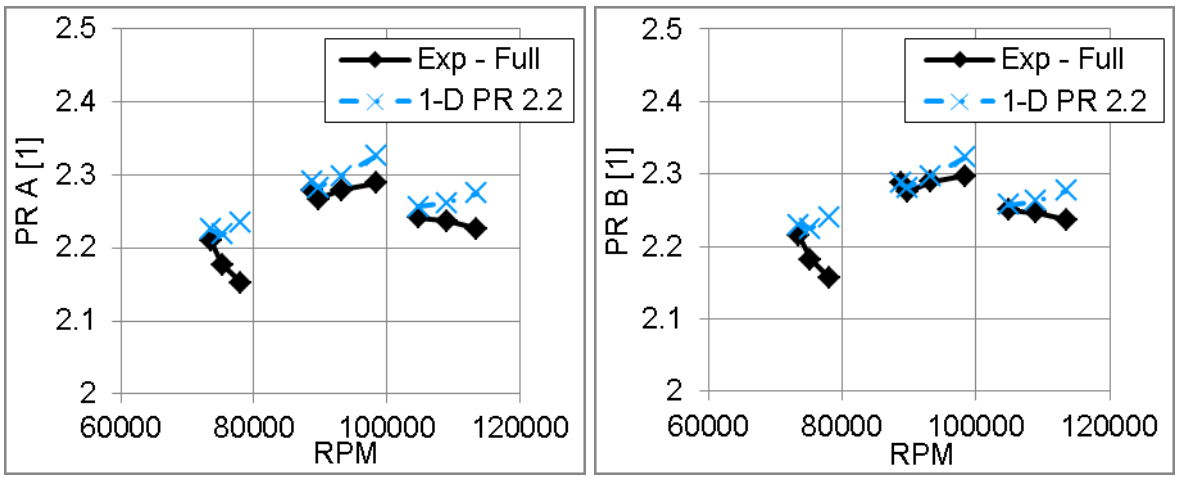

Figure 88 Pressure ratio A (left) and B (right) vs. RPM (approximate pressure ratio level PR AB = 2.2), full admission of an impeller; experiments (black); simulation 1-D turbine (blue crosses)

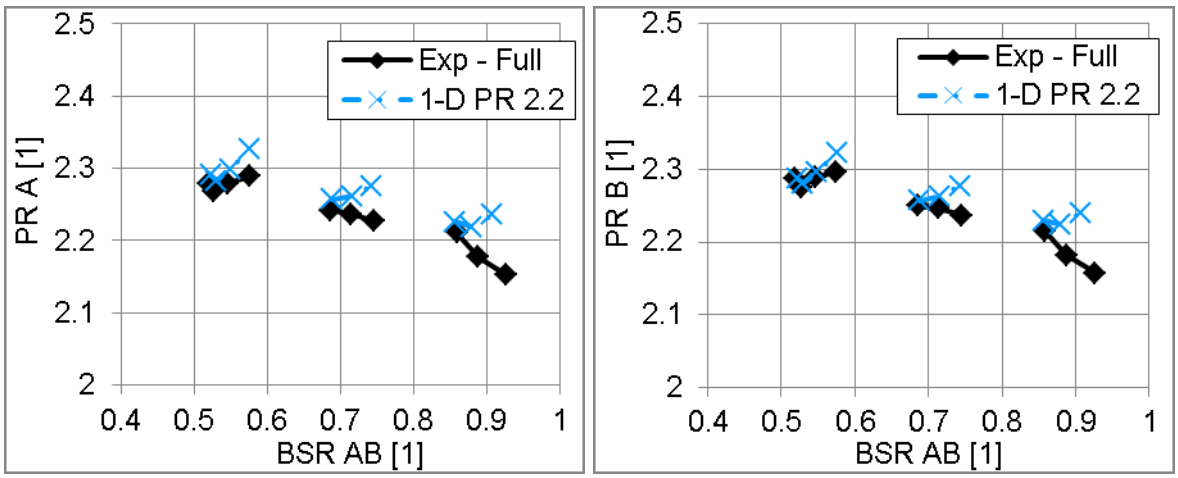

Figure 89 Pressure ratio A (left) and B (right) vs. BSR (approximate pressure ratio level PR AB = 2.2), full admission of an impeller; experiments (black); simulation 1-D turbine (blue crosses)

The comparison of the experimental and simulated pressure ratios of turbine sections is presented in *Figure 88* and *Figure 89*. Decreasing pressure ratios with changing conditions during the experiments are obvious in *Figure 89*. The calibration coefficients stated in figures above and below depend on the overall pressure ratio of a turbine and level of impeller admission. The calibration coefficients plotted versus blade speed ratio show the changing values of coefficients with decreasing pressure ratios, thus the overall pressure ratio of a turbine. Mentioned figures, presented below, may help to understand the behaviour of the 1-D turbine model and to explain, what setup of the model is necessary to achieve required values with relatively low errors.

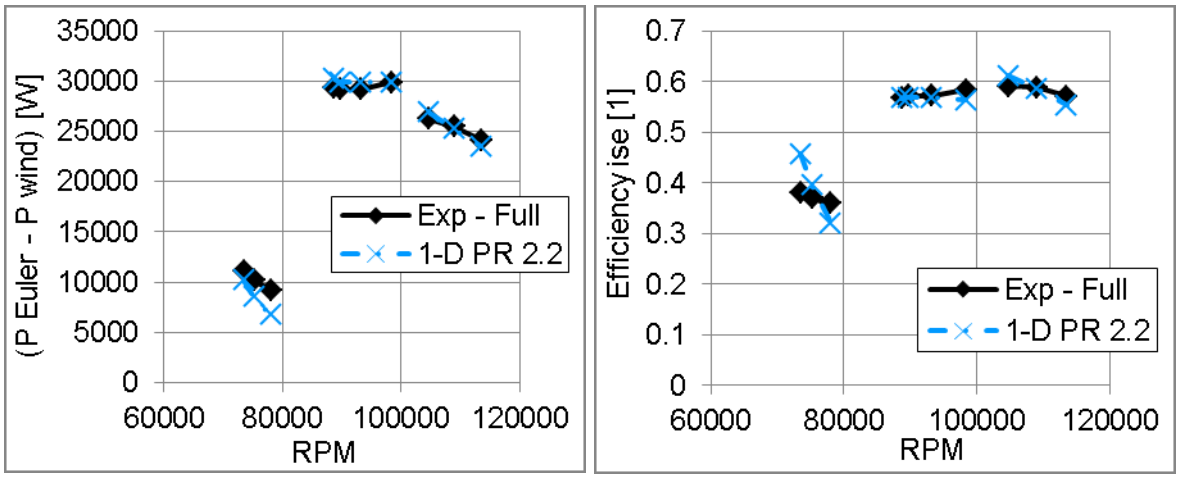

Figure 90 Turbine power (left) and isentropic efficiency (right) vs. RPM (approximate pressure ratio level PR AB = 2.2), full admission of an impeller; experiments (black); simulation 1-D turbine (blue crosses)

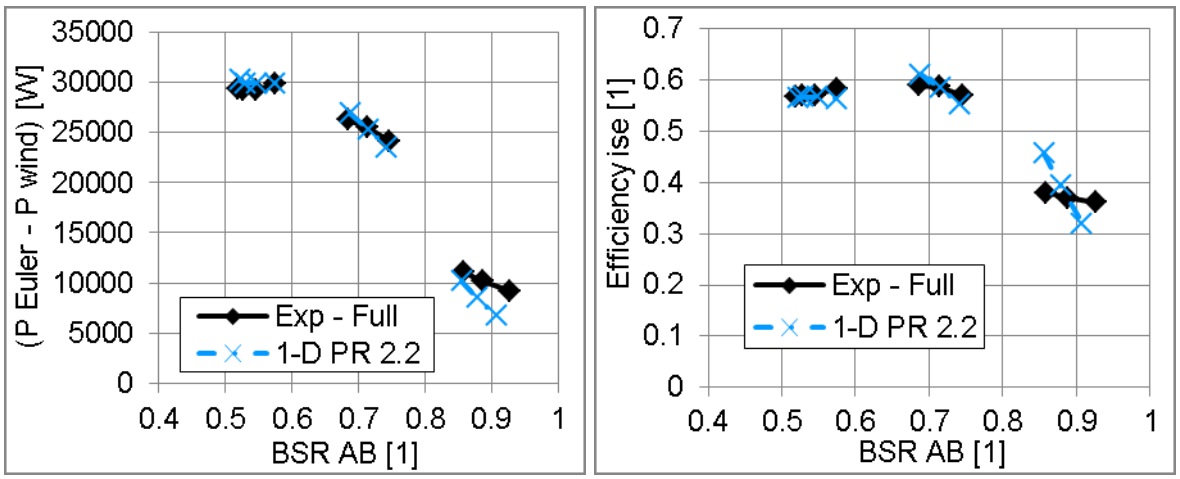

Figure 91 Turbine power (left) and isentropic efficiency (right) vs. BSR (approximate pressure ratio level PR AB = 2.2), full admission of an impeller; experiments (black); simulation 1-D turbine (blue crosses)

The turbine power and isentropic efficiency are stated in *Figure 90* and *Figure 91*. Simulated turbine power at high blade speed ratios is lower than power evaluated from experiments and concurrently the pressure ratios (*Figure 89*) are higher than measured. It is not possible to achieve required turbine power and pressure ratios A, B under cold conditions using any combination of calibration coefficients in the turbine model. The important fact is that the power of a turbine under cold conditions at high blade speed ratios is relatively low and not so important for the simulation in conjunction with the internal combustion engine, which is the main goal of the work.

The isentropic efficiency of a turbine (129) is relevant in the case of full admission of the impeller. The errors of turbine efficiency under cold conditions (*Figure 91*) are also higher than in the case, when the turbine is driven by hot exhaust gases. The relevance of the isentropic efficiency under partial admission and extreme partial admission with closed section is limited due to irreversible process of flow mixing.

The efficiencies of enthalpy to kinetic energy transformation in sections A and B are in *Figure 92*. The impeller expansion efficiency predicted by the model is in *Figure 93*.

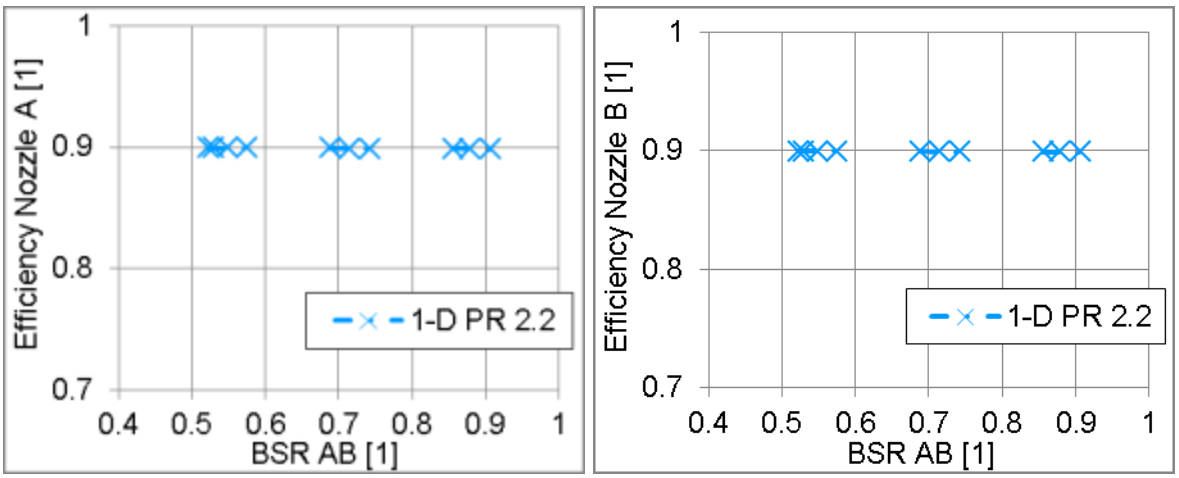

Figure 92 Efficiency of a nozzle - section A (left) and section B (right) vs. BSR (approximate pressure ratio level PR AB = 2.2), full admission of an impeller; experiments (black); simulation 1-D turbine (blue crosses)

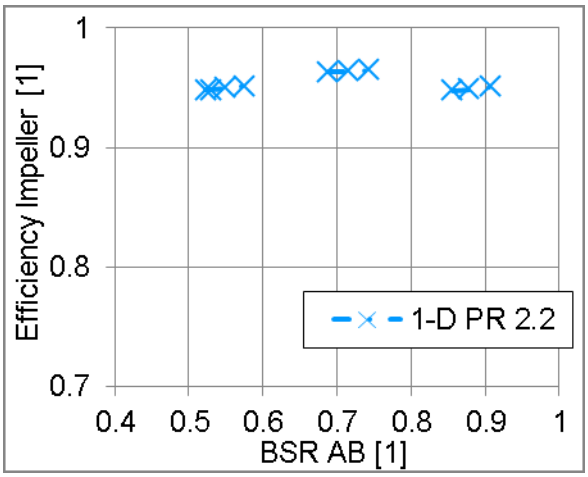

Figure 93 Efficiency of an impeller vs. BSR (approximate pressure ratio level PR AB = 2.2), full admission of an impeller; experiments (black); simulation 1-D turbine (blue crosses)

The courses of corresponding calibration coefficients at approximate pressure ratio level 2.2, plotted versus blade speed ratio, are well-arranged, because it is directly visible how coefficients are changing with changing operating conditions.

The nozzle exit angles alpha 2 (*Figure 94*) are held constant for the set of operating points under given level of admission and approximately constant level of overall pressure ratio. Deviation of nozzle exit angle delta alpha 2, which influences turbine power via velocity c 2_t, is increasing at high blade speed ratio, thus under cold conditions, because higher values increase turbine power.

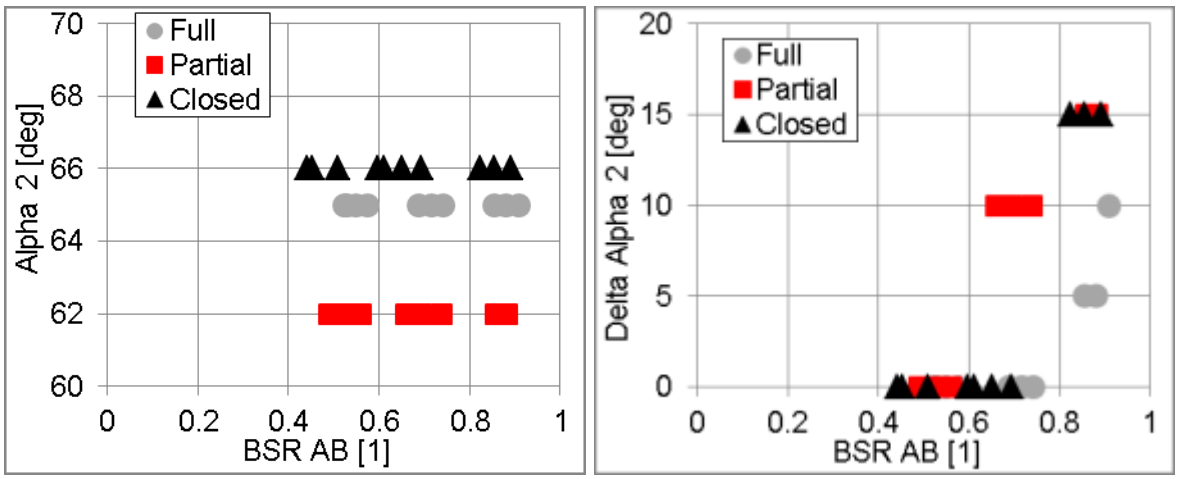

Figure 94 Calibration coefficients plotted vs. blade speed ratio BSR AB (approximate pressure ratio level PR AB = 2.2), Alpha 2 - nozzle exit angle (left), Delta Alpha 2 - deviation of nozzle exit angle (right); full admission of an impeller (gray circle), partial admission level A = 0.87 (red square), one section closed (black triangle)

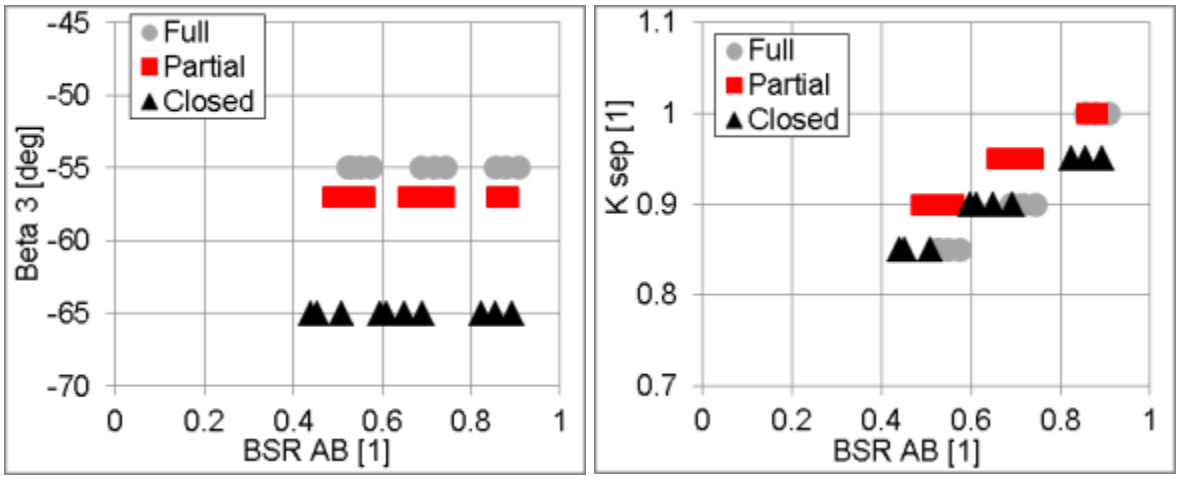

Figure 95 Calibration coefficients plotted vs. blade speed ratio BSR AB (approximate pressure ratio level PR AB = 2.2), Beta 3 - impeller exit angle (left), K sep - flow separation coefficient (right); full admission of an impeller (gray circle), partial admission level A = 0.87 (red square), one section closed (black triangle)

The impeller exit angles beta 3 (*Figure 95*) are held at constant level, for given admission and pressure conditions, as coefficient alpha 2 above. The influence of the separated flow at impeller outlet is represented by the K sep coefficient independently of the impeller exit angle.

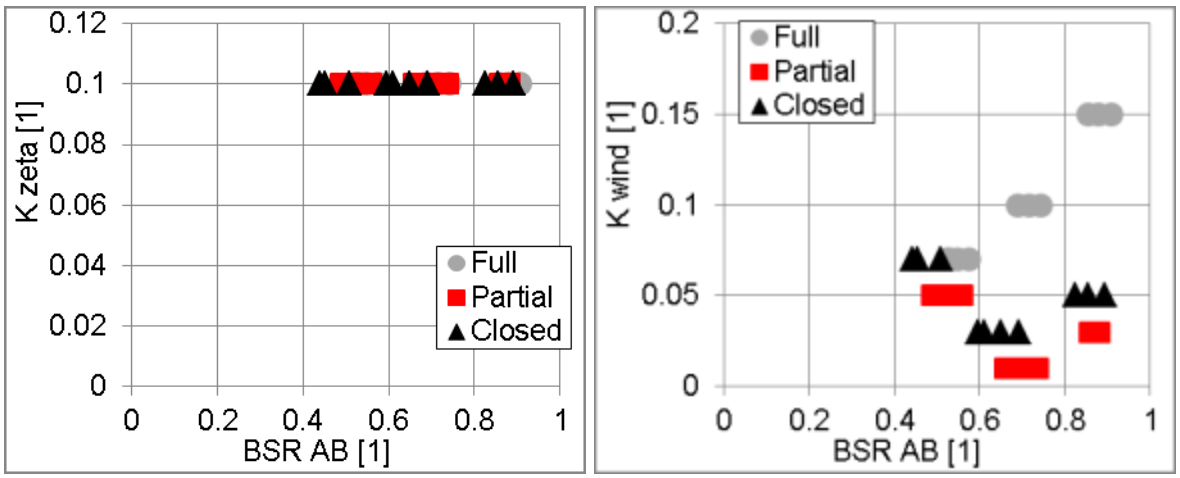

Figure 96 Calibration coefficients plotted vs. blade speed ratio BSR AB (approximate pressure ratio level PR AB = 2.2), K zeta - correction of impeller incidence loss (left), K wind - coefficient of windage losses (right); full admission of an impeller (gray circle), partial admission level A = 0.87 (red square), one section closed (black triangle)

The traces of impeller incidence loss correction and windage losses coefficient are in *Figure 96*. The discharge coefficients of static and rotating leakages, changed together during calibration, are shown in *Figure 97*. Pressure loss coefficient in impeller pipe is plotted in *Figure 98*.

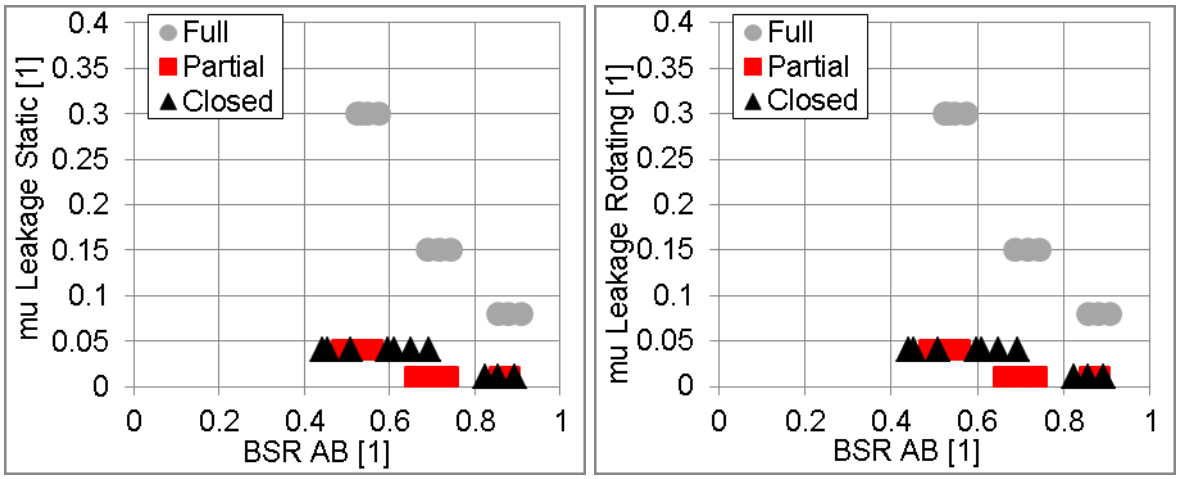

Figure 97 Calibration coefficients plotted vs. blade speed ratio BSR AB (approximate pressure ratio level PR AB = 2.2), mu Leakage Static - discharge coefficient of static leakages (left), mu Leakage Rotating - discharge coefficient of rotating leakages (right); full admission of an impeller (gray circle), partial admission level A = 0.87 (red square), one section closed (black triangle)

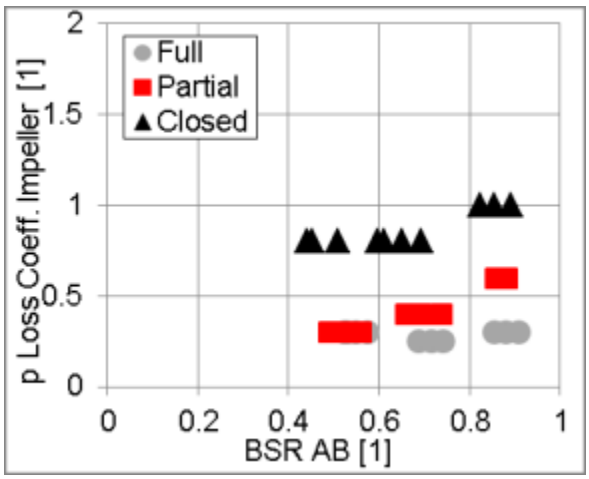

Figure 98 Calibration coefficient plotted vs. blade speed ratio BSR AB (approximate pressure ratio level PR AB = 2.2), pressure loss coefficient in impeller pipe; full admission of an impeller (gray circle), partial admission level A = 0.87 (red square), one section closed (black triangle

The discharge coefficients CD A and CD B (*Figure 99*) at outlet of turbine sections, upstream of flow mixing, are varying only in the case of impeller partial admission with approximately 80% of overall mass flow rate in dominant section. The correction is necessary for reaching required differences between turbine sections.

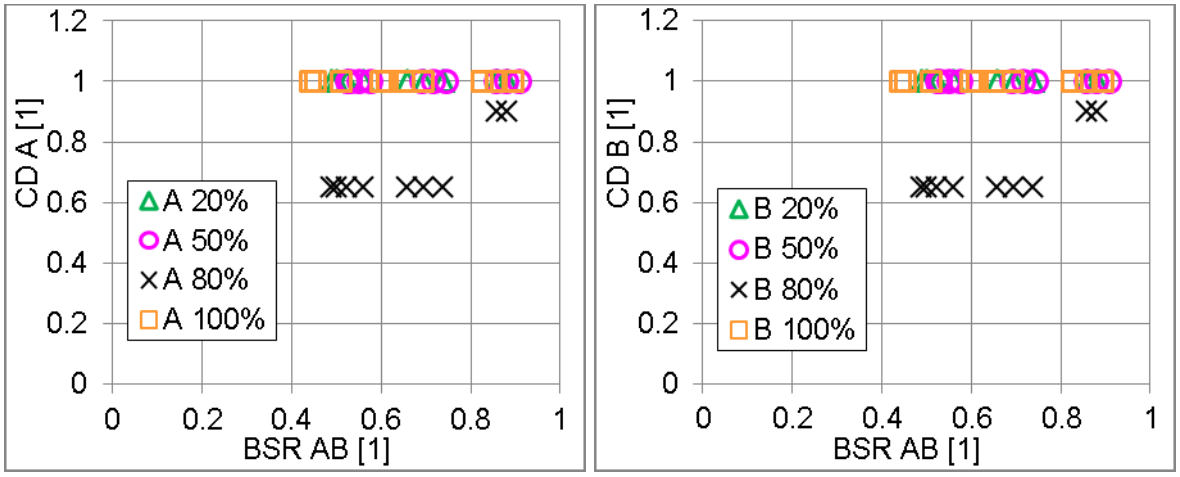

Figure 99 Calibration coefficients plotted vs. blade speed ratio BSR AB (approximate pressure ratio level PR AB = 2.2), CD A - discharge coefficient at section A outlet {upstream of flow mixing} (left) and CD B - discharge coefficient at section B outlet {upstream of flow mixing} (right) according to mass flow rate level in each section

As mentioned above, it is not easy, in the full 1-D turbine model, to reach requisite pressure differences between sections of a turbine under partial admission with significant difference of mass flow rates. The combination of discharge coefficient at section outlet and pressure loss coefficient in section was chosen for mentioned purposes in the current turbine model. The pressure loss coefficients in the sections in dependence on the mass flow rate are stated in *Figure 100*.

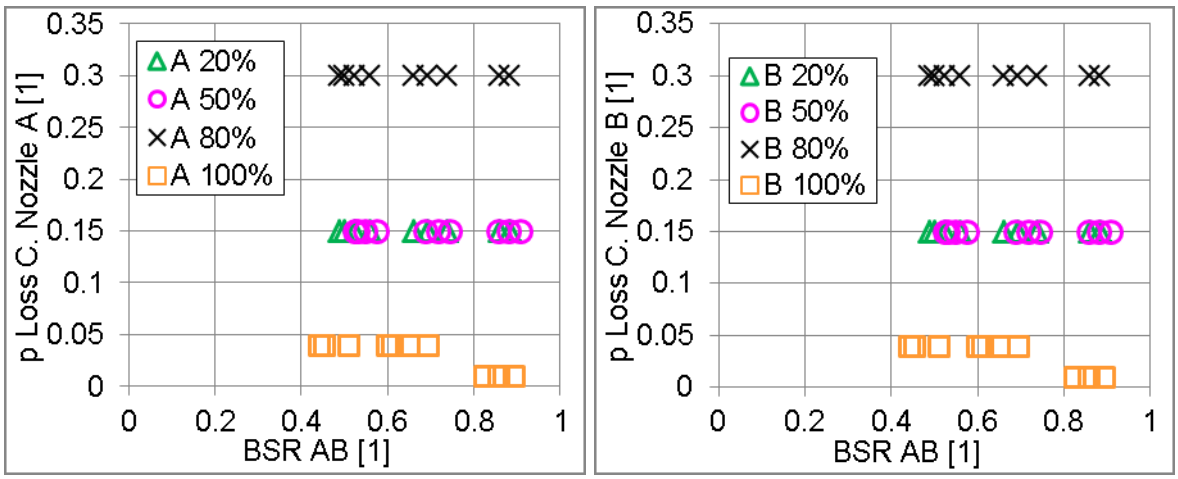

Figure 100 Calibration coefficients plotted vs. blade speed ratio BSR AB (approximate pressure ratio level PR AB = 2.2), pressure loss coefficient in section A (left) and pressure loss coefficient in section B (right) according to mass flow rate level in each section

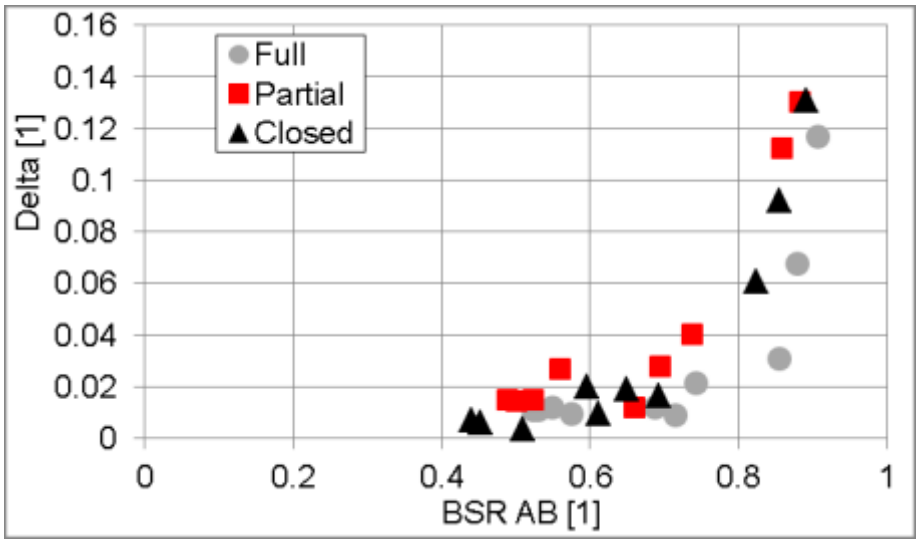

Figure 101 Overall error - Delta plotted vs. blade speed ratio BSR AB (approximate pressure ratio level PR AB = 2.2); full admission of an impeller (gray circle), partial admission level A = 0.87 (red square), one section closed (black triangle)

As clearly visible from the overall error Delta in dependence on the blade speed ratio (*Figure 101*), the error increases with blade speed ratio. The results with overall error higher than four percent are from simulation with low temperatures upstream of a turbine.

The problem consists in the level of accuracy of the experiments under cold conditions, when the turbine was driven by the cold air only. The problematic level of accuracy is confirmed by the simulation results of the turbine 1-D model. The model with low temperatures upstream of a turbine is not able to achieve required pressure ratio levels in turbine sections and concurrently to generate sufficient power. The simulation results are compromise of both contradictory requirements. The achieved overall errors under cold conditions are relatively high, but the turbine power is low. Also the working points at high blade speed ratios are not so

important from the on-engine simulation point of view. The problems of turbine measurement under cold conditions were observed before in [56].

The overall errors at high temperatures upstream of a turbine, at lower blade speed ratios and ratios close to optimum, are acceptable in all operating points from steady flow calibration. The overall errors increase at low temperatures, thus high blade speed ratios. The trend is obvious in all cases. It has to be stressed again that working points under cold conditions are not so important for the turbine model utilization for internal combustion engine simulation.

The overall errors defined by relation (132) at approximate pressure ratio level 1.3 and 1.6 are presented in *Figure 102* and *Figure 103*. All working points in mentioned figures with error higher than four percent were simulated under cold conditions.

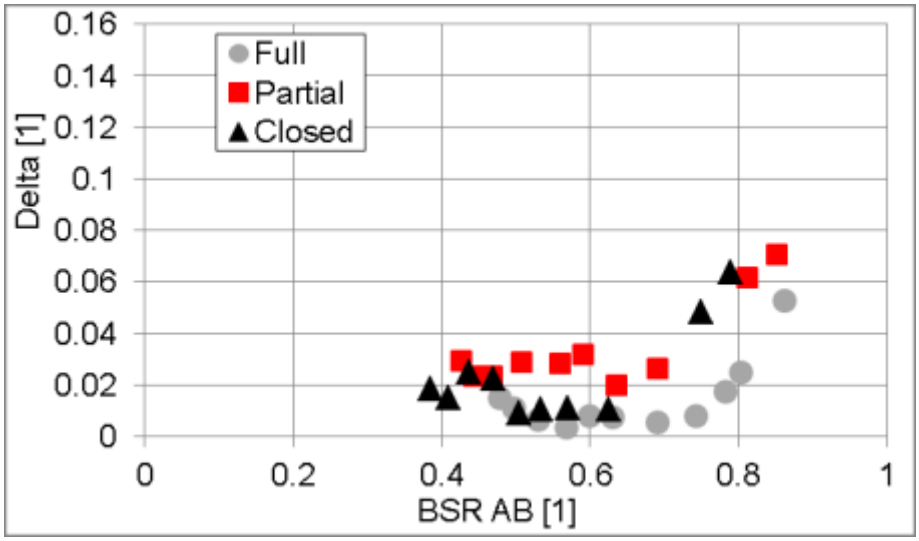

Figure 102 Overall error - Delta plotted vs. blade speed ratio BSR AB (approximate pressure ratio level PR AB = 1.3); full admission of an impeller (gray circle), partial admission level A = 0.87 (red square), one section closed (black triangle)

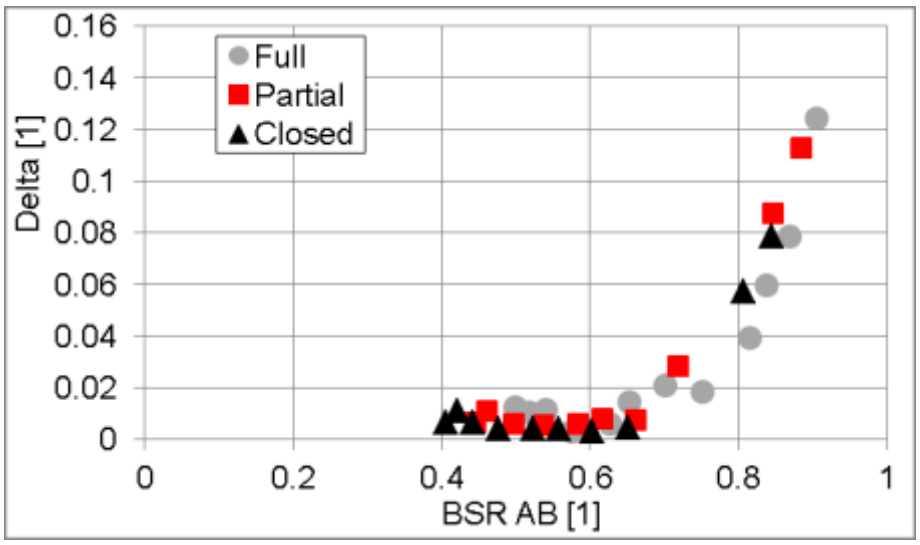

Figure 103 Overall error - Delta plotted vs. blade speed ratio BSR AB (approximate pressure ratio level PR AB = 1.6); full admission of an impeller (gray circle), partial admission level A = 0.87 (red square), one section closed (black triangle)

The overall errors at approximate pressure ratio level 2.7 (*Figure 104*) and 3.3 (*Figure 105*) are stated below. The results with error higher than approximately five percent are from simulation with low temperatures upstream of a turbine (points at high blade speed ratios).

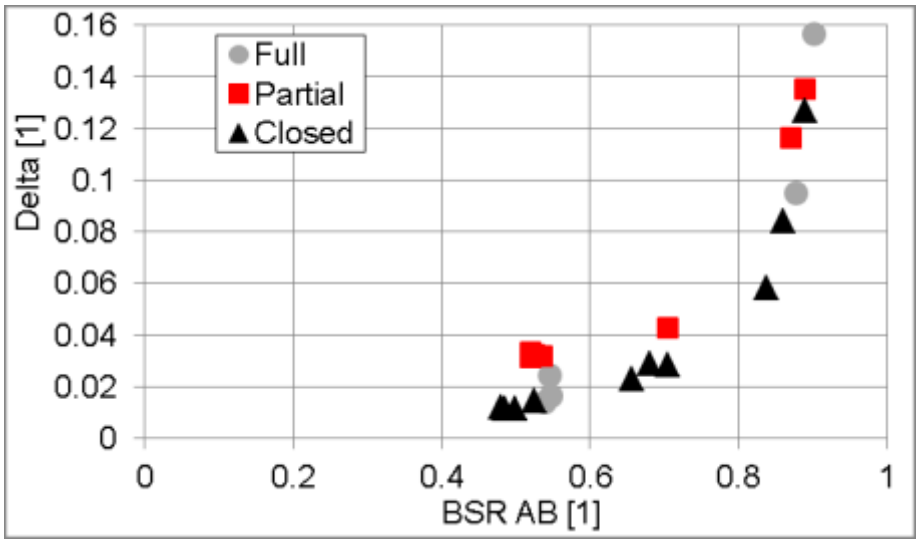

Figure 104 Overall error - Delta plotted vs. blade speed ratio BSR AB (approximate pressure ratio level PR AB = 2.7); full admission of an impeller (gray circle), partial admission level A = 0.87 (red square), one section closed (black triangle)

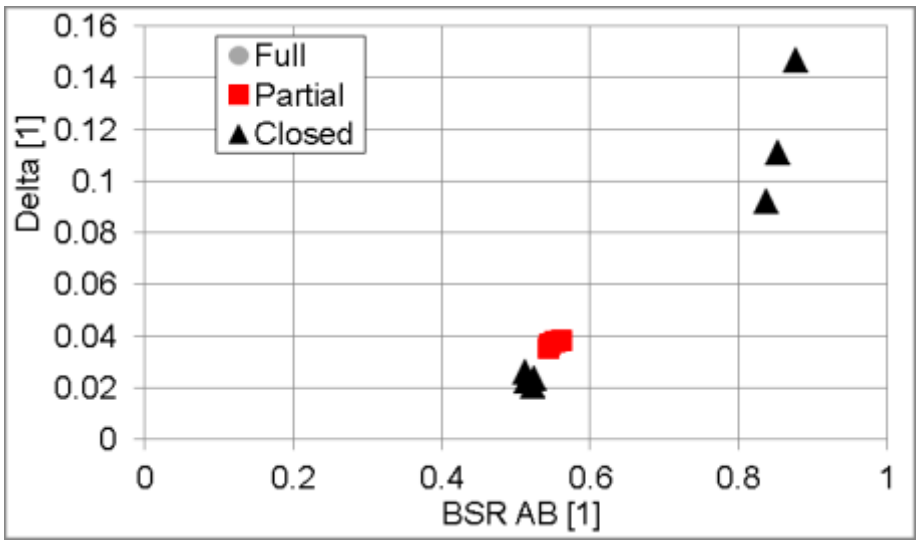

Figure 105 Overall error - Delta plotted vs. blade speed ratio BSR AB (approximate pressure ratio level PR AB = 3.3); full admission of an impeller (gray circle), partial admission level A = 0.87 (red square), one section closed (black triangle)

There is a real possibility for the future improvement of the steady flow calibration procedure that less important calibration coefficients may remain at the compromise constant level in dependence on the impeller admission and pressure ratio. The differences between experiments and simulation results would be probably higher at least at some areas, but the calibration of the model by lower number of calibration coefficients would be extremely beneficial due to simplification. The shortening of the model preparation process (modification or remodelling, dimension setup and nearly automatic steady flow calibration procedure) would also increase the turbine 1-D model utilization in practice. The described premise should be proved or refuted in the future research.

The robustness and predictive capability of the calibrated model under real unsteady conditions during on-engine simulation are presented in following parts. The unsteady simulation in conjunction with the internal combustion engine and transients of a turbocharged engine are the most interesting areas of this research. The correct physical tendencies of the simulation model, at the expense of greater local errors, are essential for the purposes of virtual prototypes. The design recommendation and further research direction are valuable.

The steady flow results summary of the calibrated 1-D turbine model equipped with the twin scroll is in Appendix 3. Fully calibrated unsteady 1-D model of a radial centripetal turbine with the twin scroll [SW 3], developed in GT-SUITE, is a part of the software library.

7. Simulation - Internal Combustion Engine

The simulation results of the whole turbocharged internal combustion engine, compared with the experimental data, are discussed in the sequent chapters. The engine steady states are complemented by the transient operation at constant engine speed. The description of the simulation models used for the verification of the twin entry turbine 1-D model features under unsteady flow is also introduced.

7.1 Model for TPA

The measurement chain of the experimental engine is described in chapter 5.3. The processing of the raw measured data is the essential and demanding part of the simulation work.

The goals of the simulation work are to analyse consistency of the experimental data measured on the real internal combustion engine, including sensitivity studies, obtain appropriate burn rate profiles and convection multiplier used in the cylinder heat transfer model.

The single cylinder engine model for three pressure analysis was derived from the comprehensive model of the experimental six cylinder diesel engine described below.

The model for three pressure analysis consists of the intake and exhaust ports, valves and the cylinder model in the analytical mode. The pressure arrays indicated in the cylinder, intake and exhaust ports, fuel mass flow rate and average temperatures at intake and exhaust ports are the main input data.

The results of three pressure analyses of each engine operating point are consequently utilized in the model of the whole internal combustion engine.

7.2 Simulation of the Six Cylinder Diesel Engine

In the following part, a six cylinder diesel engine model connected with the unsteady full 1-D model of a twin entry radial centripetal turbine is described in detail. The experience from [60] and [54] was employed. The unsteady 1-D model of the twin entry turbine is fully calibrated under steady flow conditions. The goal of the on-engine simulations is the verification of the turbine model behaviour under real conditions of the highly pulsating flow. Engine steady states and transients are investigated. The transient conditions are the most demanding tests of the turbine 1-D model stability and capability. Obtained integral and unsteady simulation results are compared with the experimental data from the engine test bed.

The arrangement of the internal combustion engine model developed in the GT-SUITE is identical to the experimental engine in the test cell.

The measurement chain is extensive and well prepared, so the quantity and accuracy level of the experimental data are sufficient. The detailed processing of measured data is unavoidable at the beginning of the calibration process.

All available engine geometry, material properties, weights of parts and moments of inertia are implemented into the created internal combustion engine model. The friction mean effective pressures are entered into the model directly.

The internal combustion engine model is described below from the air inlet to outlet. The model of the compressor is represented by the map of an adiabatic compressor with the standard wheel evaluated from the measurement on the steady flow turbocharger test bed.

The mechanical efficiency of the turbocharger shaft equals to one in the case of the simulation with the 1-D turbine. The shaft moment of inertia covers all rotating parts of the turbocharger, thus the compressor wheel, shaft and turbine wheel. The connection among the 1-D turbine model, turbocharger shaft and consequently compressor wheel is modelled using the specific template (torque) in GT-SUITE. The actual shaft torque calculated by the 1-D turbine model is sent to the turbocharger shaft directly. The unsteady turbocharger speed is estimated from the power balance on shaft. The actual speed is sensed from the turbocharger shaft and sent to the turbine 1-D model.

The situation is different in the 0-D simulation with the turbine model based on classical steady flow maps. The maps are determined from the isentropic quantities. The turbocharger shaft cannot be simulated as an ideal shaft. The unsteady mechanical efficiency of the shaft is calculated using the tailored regression formula of pure power losses in bearings. The model is similar to the corresponding part of the 1-D turbine model.

The intercooler downstream of the compressor, modelled as a bank of tubes, has the same dimension and volume as the real one in the test cell. The intercooler efficiency, upstream and downstream temperatures and pressure loss were properly calibrated. The intake plenum is modelled by pipes and flowsplits. The main dimensions copy the real engine.

The main dimensions of the cylinder head, ports (intake and exhaust) including the discharge coefficients and intake and exhaust valves are entered into the model. The valve lifts and timing, measured on the engine, were verified by the sensitivity analysis during the model calibration process.

The measured fuel mass flow rate is applied in the model directly. The fuel mass flow rate may be controlled via PID controller with various strategies, e.g. required level of brake mean effective pressure or air-fuel ratio (lambda).

The engine cylinders are modelled independently, so the trapped air mass, burned mass at cycle start, air-fuel ratio, efficiencies etc. may be different in each cylinder.

The detailed cylinder wall temperature solver based on the finite element model is used for the estimation of cylinder structure temperatures. The cylinder liner, piston and cylinder head with valves and valve guides are included in the structure. The material properties and dimensions of piston, cylinder wall, water jackets and

valves from the real engine are applied. The finite element model was calibrated in relation to the cylinder heat transfer model.

The in-cylinder heat transfer, discussed in [39], is simulated using the standard Woschni GT template [4]. The Woschni GT model is based on the improved Woschni's standard correlation [43], [44] and [3]. It is feasible to tune the convection and radiation multiplier. The radiation multiplier usually equals to one for diesel engines, so the only way how to influence the heat transfer rate is the convection multiplier. There is also a feasibility to utilize the developed user model of in-cylinder heat transfer. The user model created in Fortran allows to use any correlation formula and to change any of calibration coefficient used in the corresponding formula [47] and [50].

The combustion burn rate profiles, obtained by the three pressure analyses of each steady state point, are used in the cylinder model.

The exhaust runner is modelled by pipes and flowsplits in the same manner as the intake plenum. The dimensions are identical with the real part. The exhaust runner is asymmetric because of the engine mounting in tractor. The branch upstream of the turbine section A is slightly longer. The exhaust runner downstream, are simple pipes, used for indication sensors during measurement.

The internal combustion engine model is then connected with the unsteady full 1-D twin entry turbine model. It is also possible to utilize the standard 0-D turbine model with the classical steady flow map. The exhaust branches upstream of the twin entry 0-D model may be connected via orifice. The connection between branches improves the results of 0-D twin entry turbine model as discussed below.

The exhaust manifold downstream of the turbine is similar to the real one at the engine test cell. The turbine waste gate control is prepared in the model as well, but the turbocharger used in the project has no regulation.

The model of the experimental engine was properly calibrated using the measured data. The physical quantities such as brake torque, brake specific fuel consumption and overall brake efficiency of the engine are relevant from the on-engine simulation point of view. The partial efficiencies, e.g. turbine isentropic efficiency which is influenced by the natural mass accumulation inside the turbine, are unimportant for our purposes.

The models of the experimental six cylinder compression ignition engine John Deere 6068 and a derived single cylinder engine model for three pressure analysis (TPA) in GT-SUITE are a part of the software library [SW 4].

7.3 Results

The simulation results of the turbocharged internal combustion engine with the full 1-D twin entry turbine model are presented in the following section. The resultant integral parameters of the simulation are compared with relevant experimental data.

The internal combustion engine model was properly calibrated using the available data (geometry, material properties, moments of inertia etc.) and measured physical quantities. The 1-D model of the twin scroll turbine was calibrated under steady flow conditions using the data measured on the turbocharger test bed.

It has to be stressed again that the internal combustion engine was equipped with the same type of the turbocharger, which was tested on the turbocharger test bed, but two pieces of the turbocharger were used during the work. The first turbocharger was utilized for turbocharging of the internal combustion engine and the second was tested on the steady flow turbocharger test bed.

The reasons are obvious. It was necessary to perform experimental work concurrently. The experiments at demanding conditions, especially on the turbocharger test bed, are also relatively risky and destruction of the machine can easily happen.

In case of only one turbocharger, the repetition of all performed measurements before the destruction is likewise unrealistic because of time and financial expenses. The verification of the turbocharger from the engine on the same turbocharger test bed was not carried out for the same reasons.

For the on-engine simulation, the connected full 1-D turbine model calibrated under steady flow, was utilized without any modification or recalibration.

The general physical quantities measured on the engine test bed are compared with simulation in sequent pictures. For the internal combustion engine valuation as a whole machine, the important parameters are the brake mean effective pressure (*Figure 106*) and brake specific fuel consumption (*Figure 107*). The experimental and simulated values are fully comparable.

The engine was used as a source of highly pulsating flow of exhaust gases. The unsteady conditions upstream and downstream of the turbine are important from the turbine model point of view.

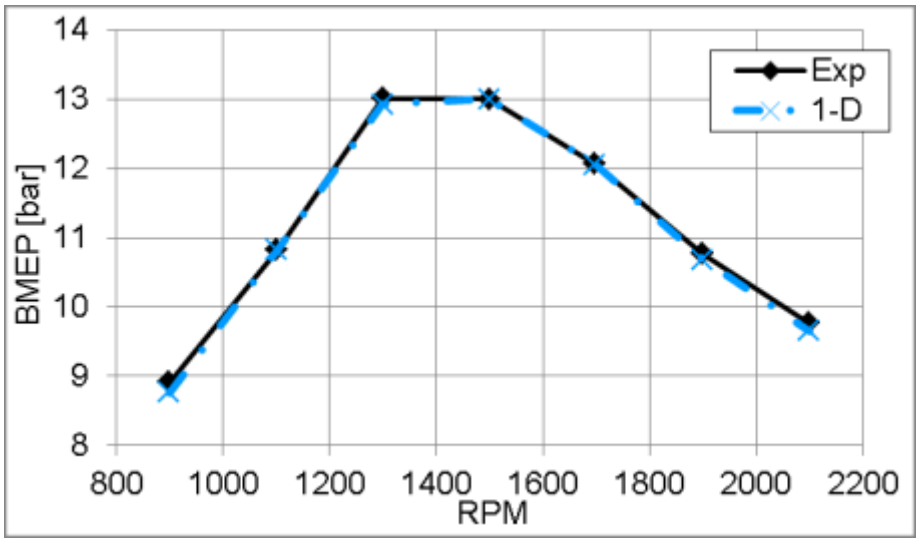

Figure 106 Brake mean effective pressure, experiment (black solid line), simulation with full 1-D unsteady turbine (blue dashed and dotted line)

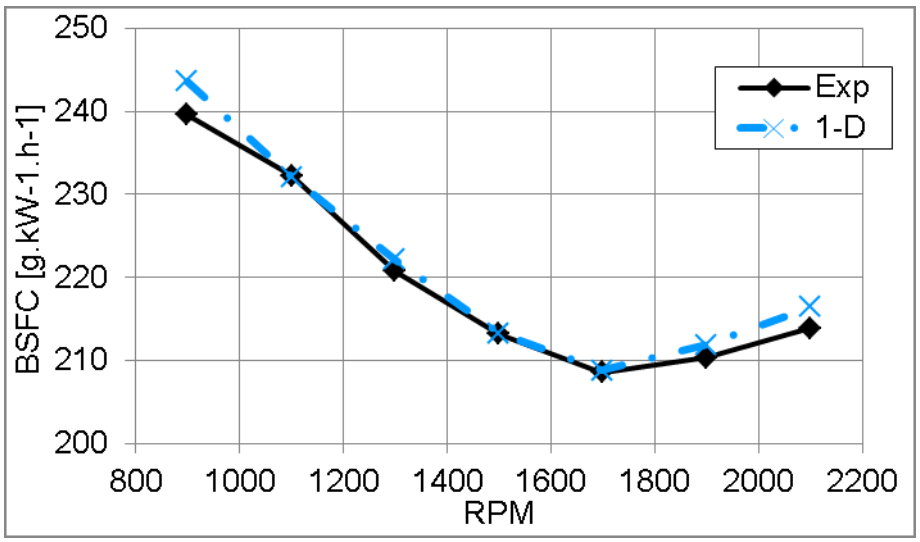

Figure 107 Brake specific fuel consumption, experiment (black solid line), simulation with full 1-D unsteady turbine (blue dashed and dotted line)

The air mass flow rate through the engine predicted by the model is higher than measured data (*Figure 108*). The reason may consist in the manufacturing tolerances of tested turbochargers. The castings of turbine housing are not uniform and variances among pieces are common. Mentioned possibility is relatively probable, because measured and simulated turbocharger speeds (*Figure 112*) are fully comparable.

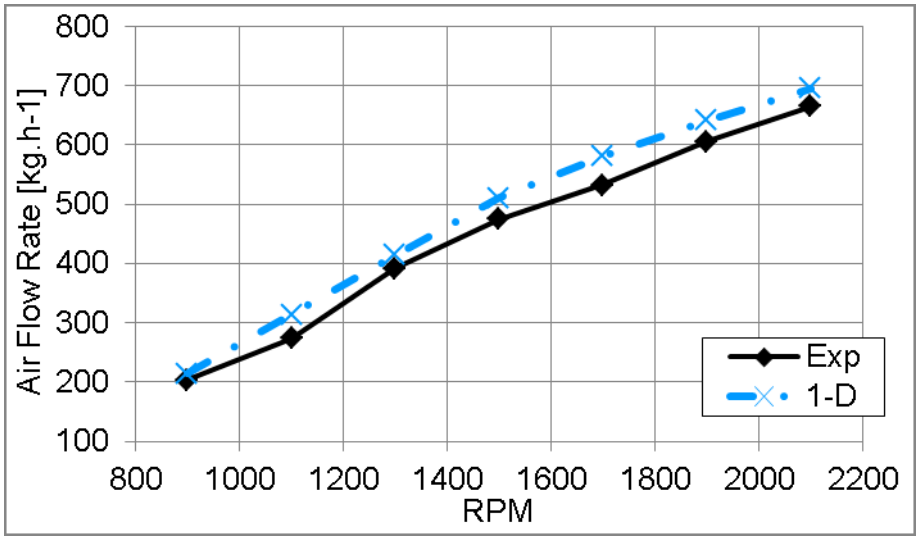

Figure 108 Air mass flow rate, experiment (black solid line), simulation with full 1-D unsteady turbine (blue dashed and dotted line)

The fuel mass flow rates in *Figure 109* are naturally identical, because the measured values are imposed into the engine model directly. It is convenient to remark that no measured physical quantity is accurate. The calculated lambda in *Figure 110* is consistent with the simulated air and fuel mass flow rates. The differences between maximum pressures in the cylinder performed by the simulation and indicated values (*Figure 111*) are not significant.

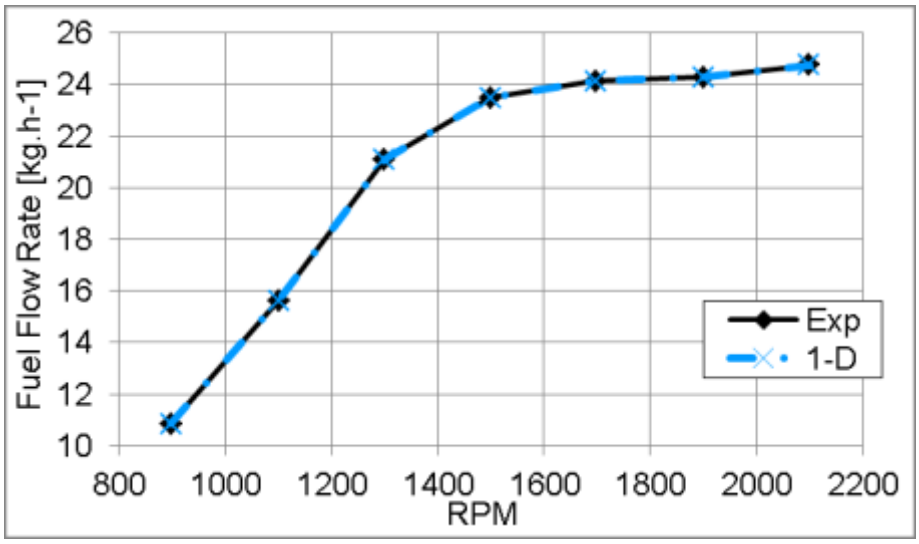

Figure 109 Fuel mass flow rate, experiment (black solid line), simulation with full 1-D unsteady turbine (blue dashed and dotted line)

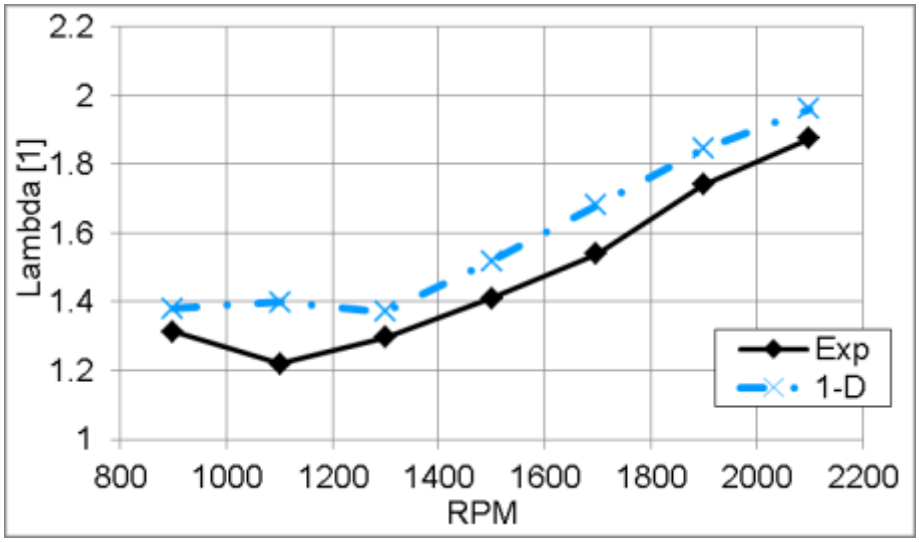

Figure 110 Lambda, experiment (black solid line), simulation with full 1-D unsteady turbine (blue dashed and dotted line)

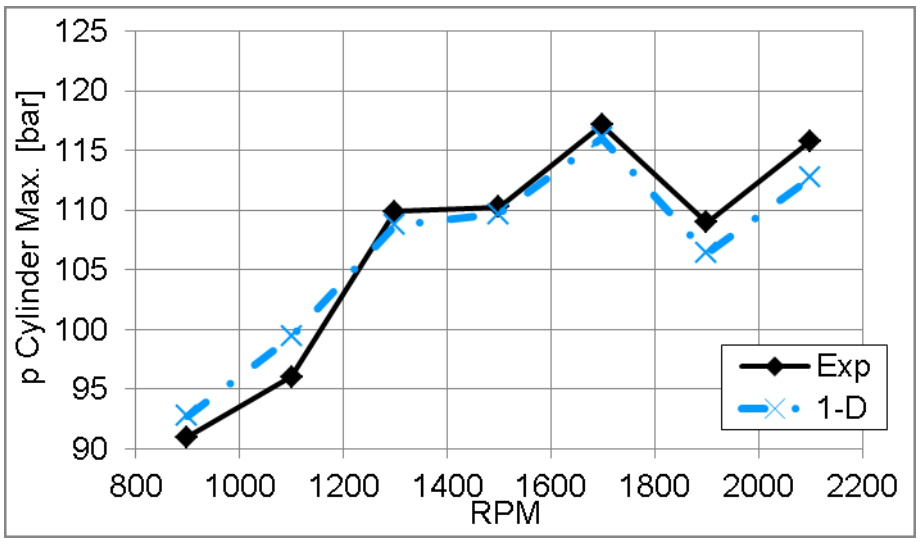

Figure 111 Maximum pressure in cylinder, experiment (black solid line), simulation with full 1-D unsteady turbine (blue dashed and dotted line)

The compliance of experimental and simulated values of turbocharger speed (*Figure 112*), related pressure downstream of the compressor (*Figure 113*) and pressure in the intake plenum (*Figure 114*) is sufficient. The temperatures in the intake plenum are also comparable (*Figure 115*).

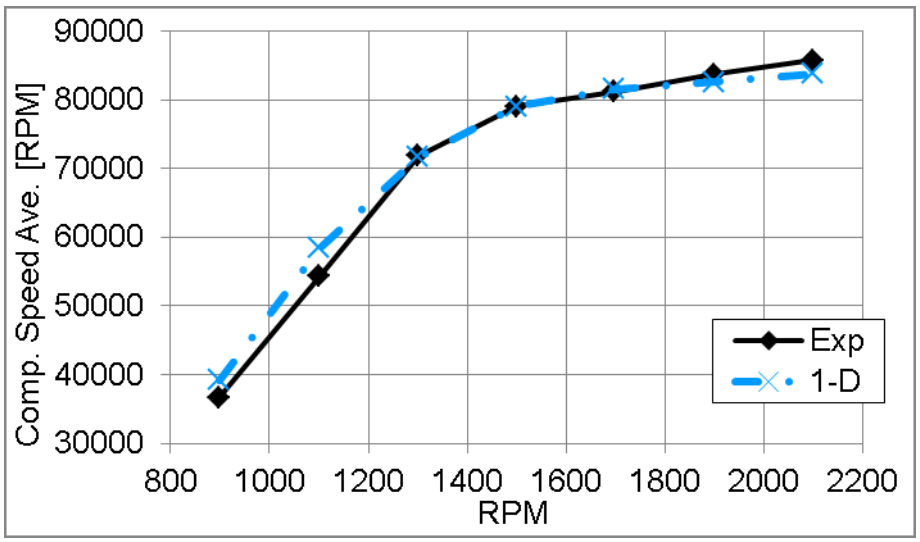

Figure 112 Compressor speed, experiment (black solid line), simulation with full 1-D unsteady turbine (blue dashed and dotted line)

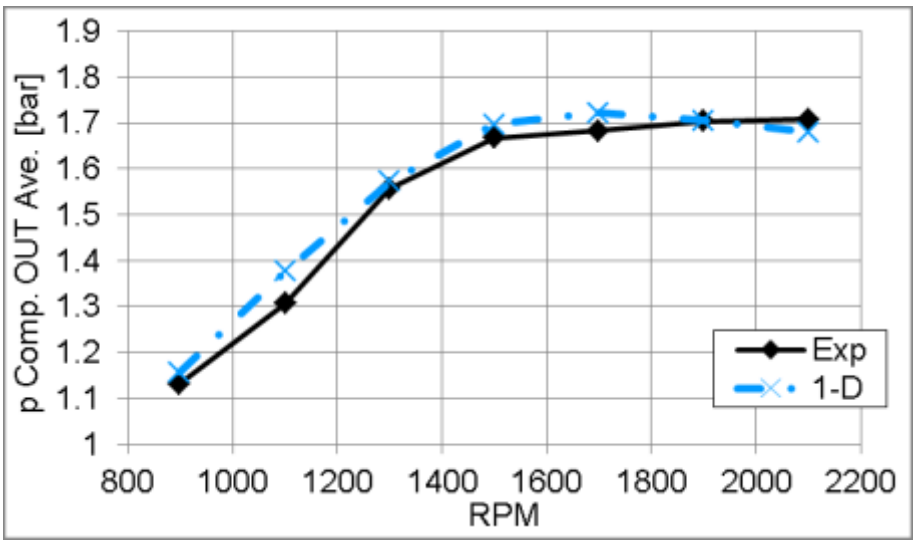

Figure 113 Pressure downstream of a compressor, experiment (black solid line), simulation with full 1-D unsteady turbine (blue dashed and dotted line)

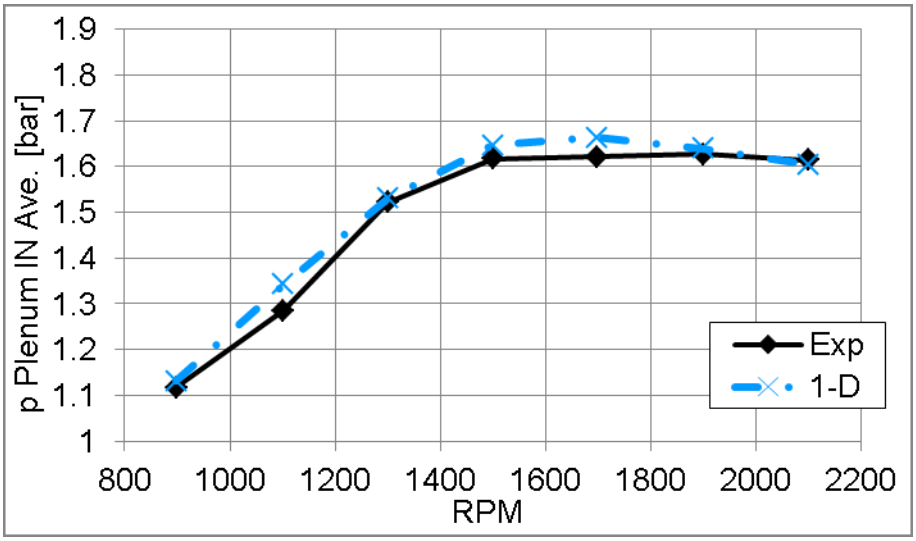

Figure 114 Pressure in intake plenum, experiment (black solid line), simulation with full 1-D unsteady turbine (blue dashed and dotted line)

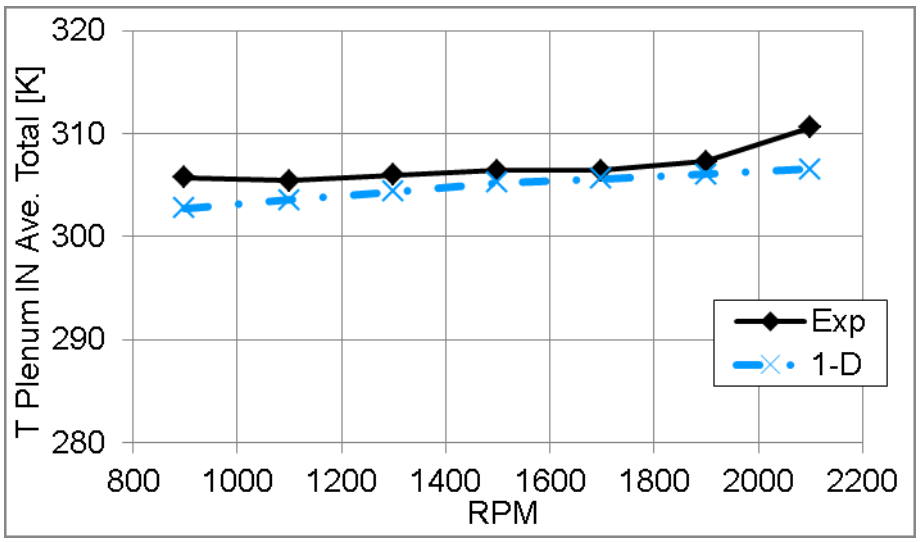

Figure 115 Total temperature in intake plenum, experiment (black solid line), simulation with full 1-D unsteady turbine (blue dashed and dotted line)

The probable differences between two pieces of turbocharger used for experimental work, one piece tested on the steady flow test bed and second for the turbocharging of the experimental engine, may be visible in the comparison of measured and simulated pressures at the turbine. The crucial fact is that two pieces of a turbocharger cannot be wholly identical.

The important conditions upstream and downstream of the turbine are stated below. The pressures indicated at inlets of the turbine section A (*Figure 116*) and section B (*Figure 118*) are not absolutely identical due to asymmetrical branches of the exhaust runner. The differences are small. The exhaust branches are asymmetrical in the simulation model as well, but the pressures predicted by the 1-D turbine model are almost the same. The accordance with the indicated values is however relatively good.

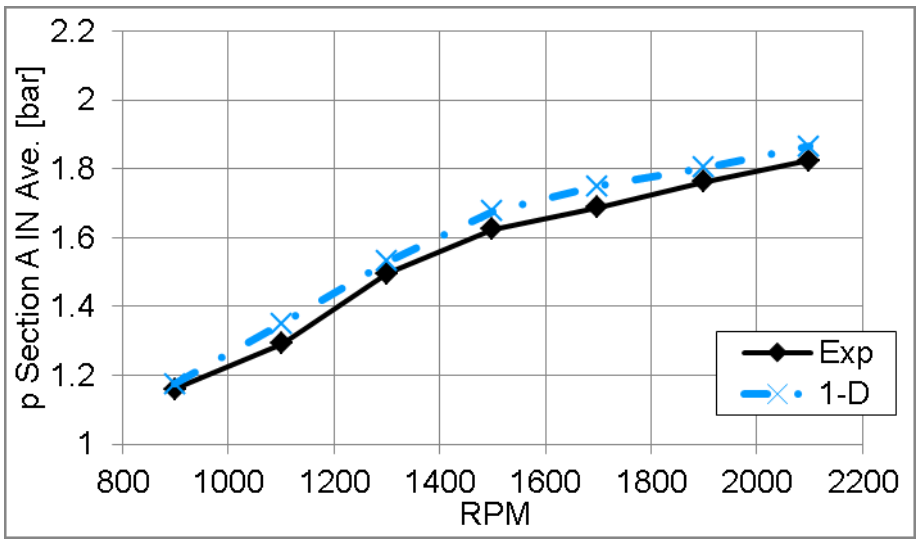

Figure 116 Pressure at inlet of turbine section A, experiment (black solid line), simulation with full 1-D unsteady turbine (blue dashed and dotted line)

It has to be stressed that the sections of a turbine are modelled as fully symmetrical and interchangeable in the current 1-D turbine model, but it is not wholly correct, because the section A is closer to the turbine outlet and conditions in sections, which are geometrically almost identical (manufacturing tolerances), have to be different. The experiments under partial admission of an impeller with throttling in one section were also carried out only for one section with major mass flow rate. This is a proposal for the future research. It would be convenient to test the partial admission subsequently with throttling in both sections of a turbine.

The current fully calibrated 1-D model of a turbine has the tendency to represent the turbine sections as equal (*Figure 116* and *Figure 118*).

The relevance of measured engine temperatures is the lowest from the entire measurement chain. The thermocouples at inlets of turbine sections are exposed to exhaust gases three times per engine cycle. The temperature relevance increases with time duration of each steady state measurement.

The temperatures at inlets of turbine sections in *Figure 117* and *Figure 119* predicted by the model are satisfactory compromise.

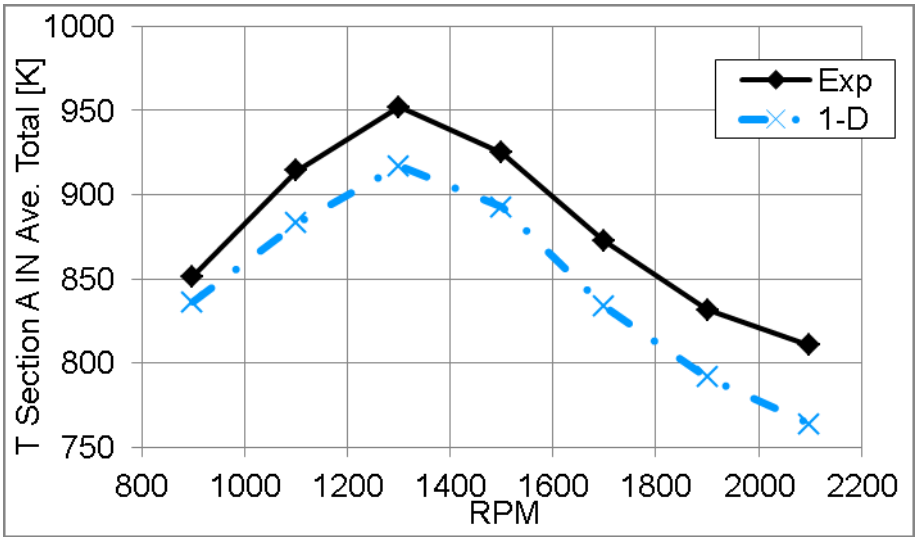

Figure 117 Total temperature at inlet of turbine section A, experiment (black solid line), simulation with full 1-D unsteady turbine (blue dashed and dotted line)

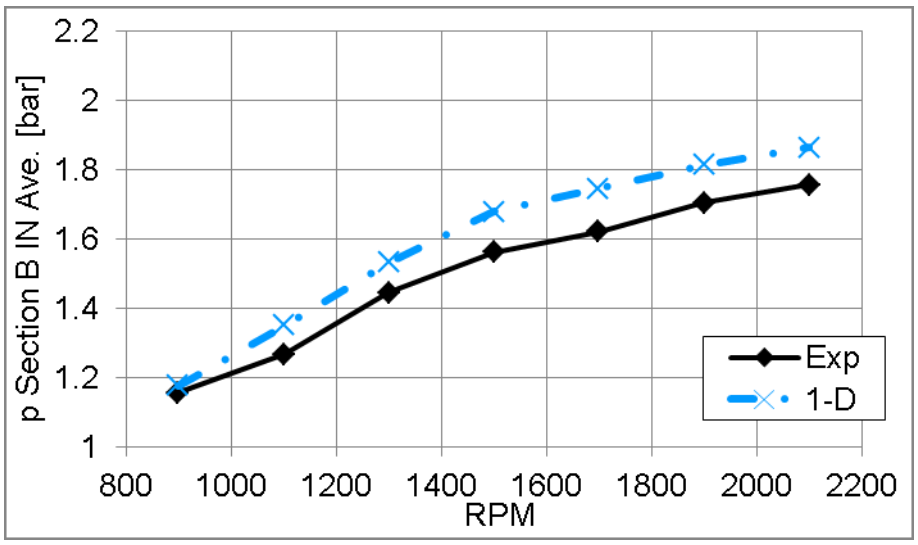

Figure 118 Pressure at inlet of turbine section B, experiment (black solid line), simulation with full 1-D unsteady turbine (blue dashed and dotted line)

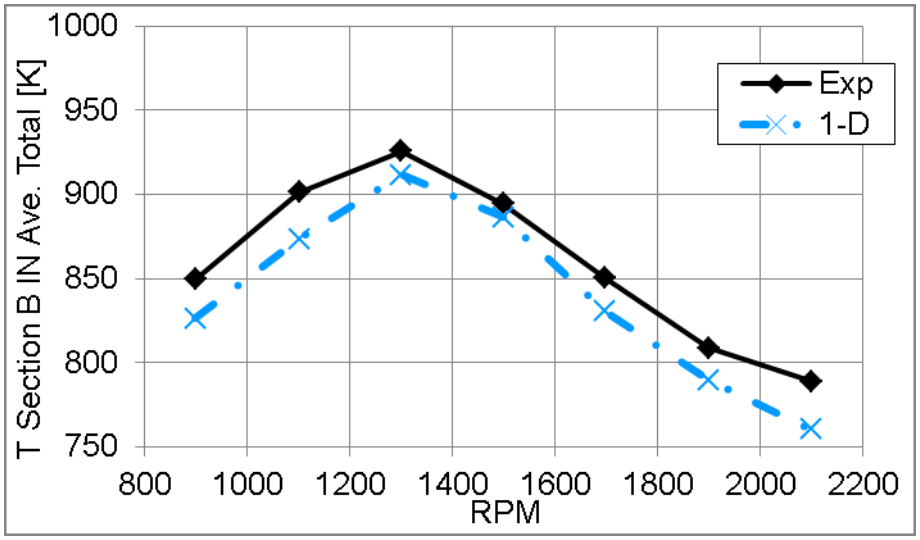

Figure 119 Total temperature at inlet of turbine section B, experiment (black solid line), simulation with full 1-D unsteady turbine (blue dashed and dotted line)

The exhaust manifold structure downstream of the turbine is made of several pipes with different diameter and embedded high volume container with unknown dimensions. Modelling of that structure especially in 1-D is not trivial. The exhaust manifold model, built-up from pipes with constant dimensions, utilizes only one constant friction multiplier for the pressure loss achievement. The comparison of simulation and experiment is shown in *Figure 120.*

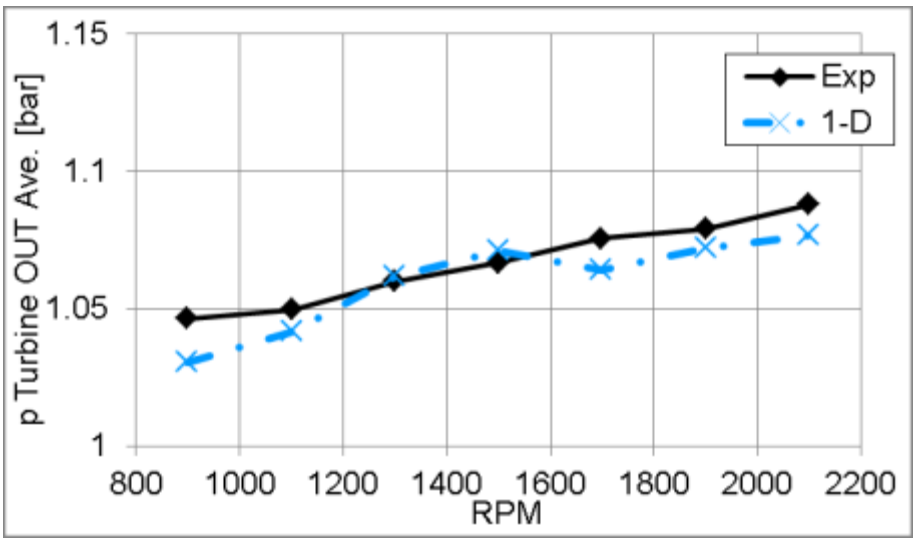

Figure 120 Pressure turbine downstream, experiment (black solid line), simulation with full 1-D unsteady turbine (blue dashed and dotted line)

The trend of temperature turbine downstream (*Figure 121*) is similar to temperatures upstream of a turbine.

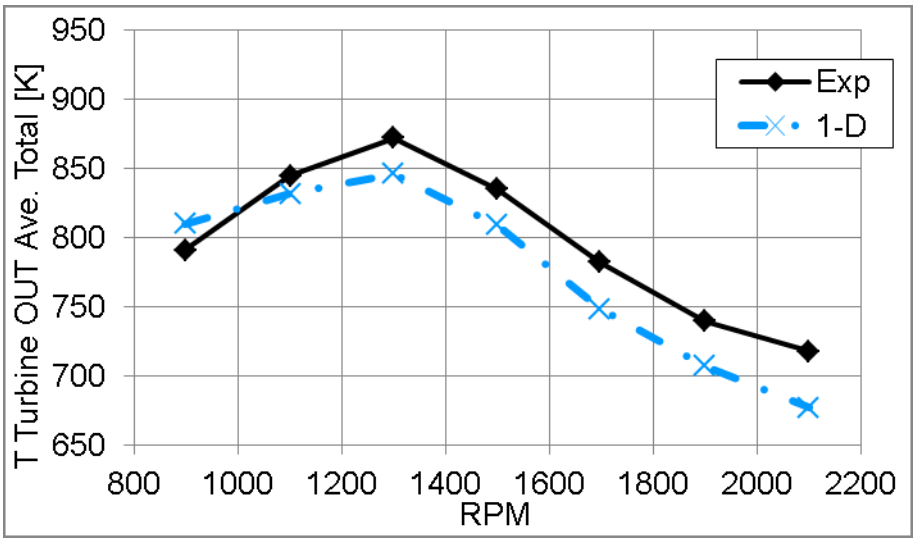

Figure 121 Total temperature turbine downstream, experiment (black solid line), simulation with full 1-D unsteady turbine (blue dashed and dotted line)

The shown integral data from simulations of the turbocharged internal combustion engine with the unsteady full 1-D model of the twin scroll turbine confirms the predictive capability of the turbine model under real conditions of highly pulsating flow. The level of results compared with experiments is relatively high at all working points. The performance of the turbine 1-D model under highly unsteady conditions is very important for the model utilization in practice.

The main goal of the thesis is to introduce the map-less approach in case of the twin scroll turbine modelling. The model with physical background should be stronger and more reliable in predictions out of its calibration range. This situation is typical at the beginning of the development, when experiments are not available.

The current conditions are different from the stage of virtual prototypes, because the models are calibrated in accordance with the experiments. The results of map-less approach and classical map based approach are introduced below.

It has to be stressed that the confrontation of 1-D (map-less) and 0-D (map based) approaches is not the aim. The discussion of results shows alternatives.

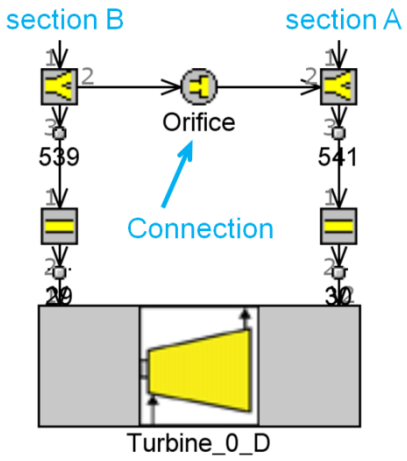

Figure 122 0-D turbine model (map based approach) with connection between branches used for 0-D simulation

The scheme of the 0-D turbine template, which represents a turbine by the classical steady flow map, with the connected exhaust branches upstream of the turbine is drawn in *Figure 122.* The turbine map used for the 0-D simulation is in *Figure 265* described by the isentropic efficiency and discharge coefficient (Appendix 4). The map is based on the results of the 1-D twin scroll turbine model with the full admission of the impeller at the virtual steady flow turbine test bed, so it takes advantage of the fully calibrated 1-D model. The map is then represented by the simulation software. The results under partial admissions of the impeller were not taken into account. The turbine sections in 0-D model have equivalent influence (50:50), so the look-up values from the turbine map are multiplied by the fraction 0.5 and imposed to the appropriate turbine section.

There are many ways how to generate the turbine maps for engine simulation. The data measured on the turbocharger test bed may be utilized directly or after the evaluation and extrapolation by feasible tool. It is also possible to utilize the results of calibrated or uncalibrated higher level models like 1-D or 3-D. The standard interpretation of the steady flow turbine map in simulation software is influenceable by the user via fitting of efficiency and discharge coefficient.

The turbine may be represented by specific regression formulas of isentropic efficiency and discharge coefficient in combination with blank turbine map. The advantage of the tailored regressions and blank map is the full control of turbine parameters. The turbine isentropic efficiency and mass flow rate, from discharge coefficient, are determined using actual pressure and blade speed ratios. The great advantage of this approach consists in the full control of the turbine parameters by the user. There is no interpretation and fitting of delivered steady flow turbine map by simulation software, because there is no map supplied. The user only is fully responsible for the utilized regression equations, thus for the steady flow map of a specific turbine. The briefly described approach was applied in GT-SUITE

simulation tool using the classical 0-D turbine template several times with success as shown for example in [53]. The similar regression relations were used in [56]. This is probably one of the best methods how to describe the turbine performance using map-based 0-D approach.

The diameter of connection orifice between exhaust branches upstream of the turbine has to be calibrated. The usage of the orifice should improve the twin entry turbine behaviour under partial admission. There are two problems. The location of the cross connection between exhaust branches is incorrect. The real mixing of flows occurs inside the turbine at the nozzle ring at appropriate pressures. The second problem is that experiments have to be available for the orifice diameter estimation. The results of engine simulation without the connection of exhaust branches, presented below, are not sufficient.

The comparison of simulation results and experiments is in sequent pictures. The best results of engine simulation with the 0-D turbine are shown. The steady flow turbine map, based on the results of the full 1-D turbine model, was used. The diameter of the connection orifice between exhaust branches was optimized and the best compromise is the diameter 20 mm.

The air mass flow rate via engine is in *Figure 123.* The simulation results with the 1-D and 0-D turbine are almost the same.

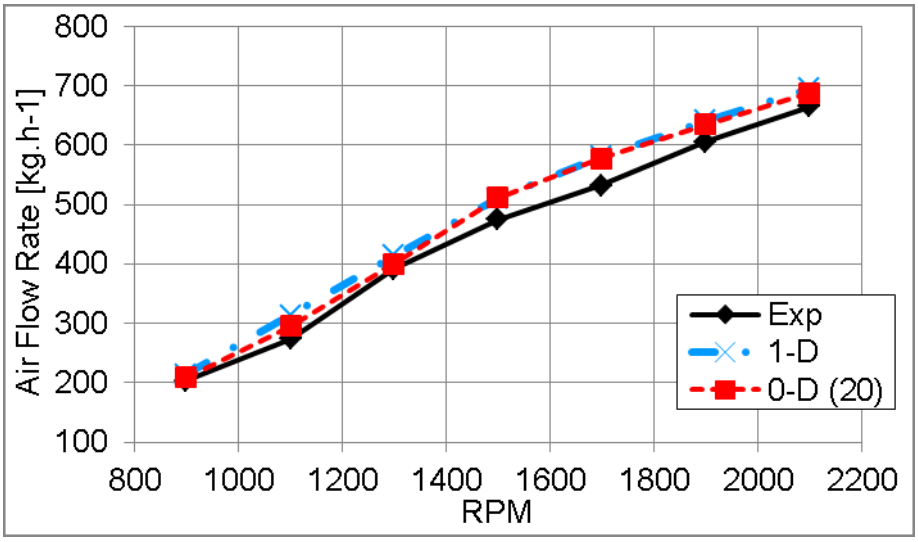

Figure 123 Air mass flow rate, experiment (black solid line), simulation with full 1-D unsteady turbine (blue dashed and dotted line), simulation with 0-D turbine map - sections connected via orifice D = 20 mm (red dashed line)

The simulated pressures downstream of the compressor in *Figure 124* and turbocharger speed in *Figure 125* are also similar.

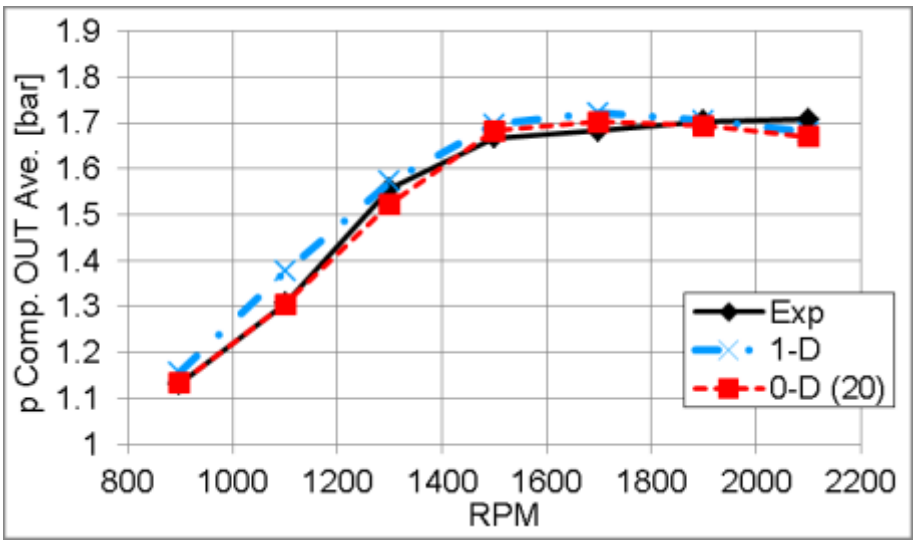

Figure 124 Pressure downstream of a compressor, experiment (black solid line), simulation with full 1-D unsteady turbine (blue dashed and dotted line), simulation with 0-D turbine map - sections connected via orifice D = 20 mm (red dashed line)

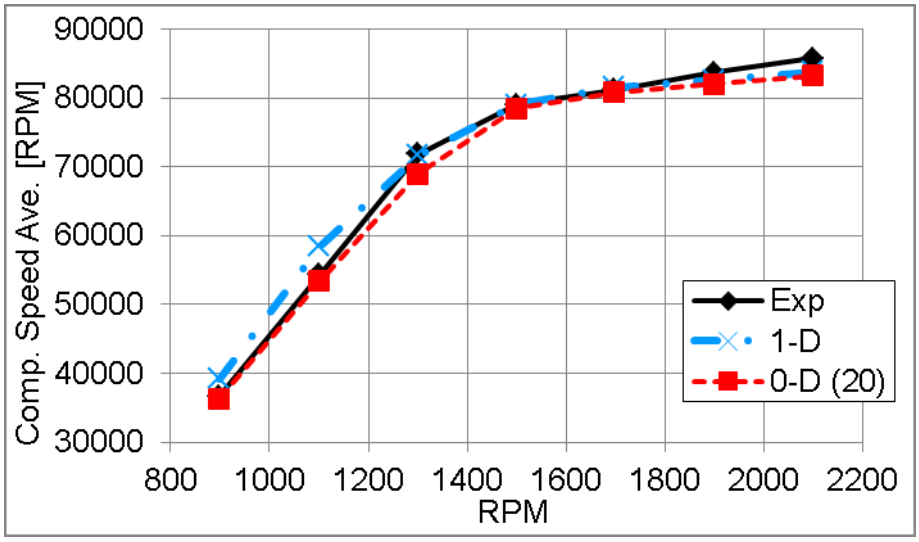

Figure 125 Compressor speed, experiment (black solid line), simulation with full 1-D unsteady turbine (blue dashed and dotted line), simulation with 0-D turbine map - sections connected via orifice D = 20 mm (red dashed line)

The slight difference is visible in *Figure 126*, where are compared the pressures at the turbine section inlet.

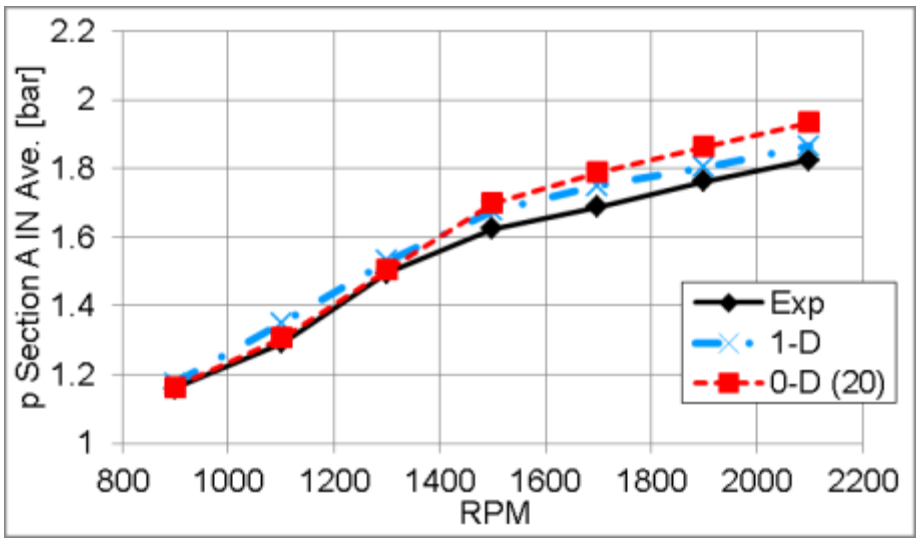

Figure 126 Pressure at inlet of turbine section A, experiment (black solid line), simulation with full 1-D unsteady turbine (blue dashed and dotted line), simulation with 0-D turbine map - sections connected via orifice D = 20 mm (red dashed line)

Further results are in Appendix 4. The differences between results of full 1-D and 0-D turbine modelling are accented in case of a four cylinder internal combustion engine equipped with the twin scroll turbine, thus under highly unsteady conditions. The results with a four cylinder engine were presented in [52] and [51]. The conditions during the extreme engine transient operation are unfavourable for the 0-D approach.

The influence of the connection between exhaust branches on the results of engine simulation utilizing the 0-D turbine model is discussed in sequent part. The simulations without the connection upstream of the turbine and with orifice diameters 10 mm and 20 mm were performed. The cross-sectional area of the orifice with the diameter 10 mm is equal to approximately 7% of one turbine section cross-sectional area at the inlet. In the case of the orifice diameter 20 mm, the fraction is approximately 27%.

The examples of results are in *Figure 127* and *Figure 128.* The air mass flow rate through the engine (*Figure 127*) is overestimated at all points, when the exhaust branches upstream of the turbine are not connected. It is clearly visible that the connection upstream of the turbine 0-D model improves the simulation results. The results with the connection orifice are comparable with 1-D results and of course with experimental data.

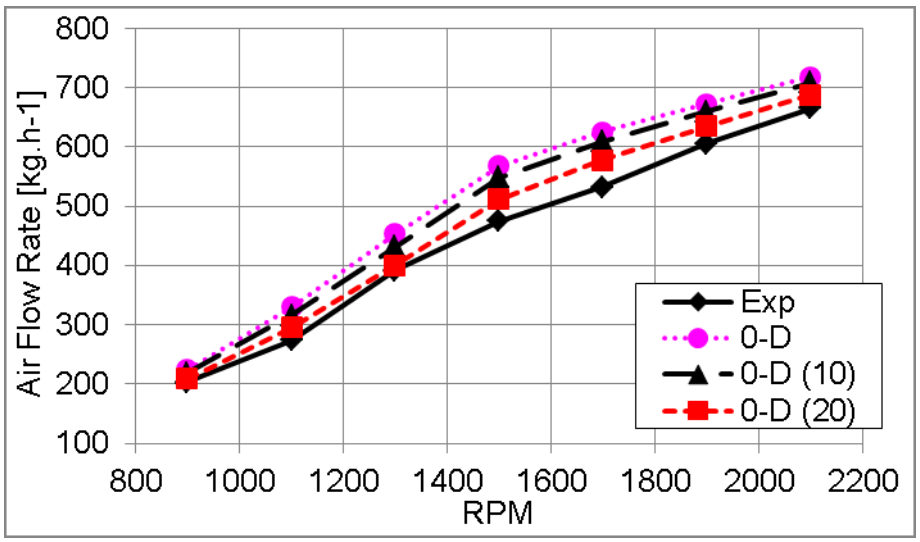

Figure 127 Air mass flow rate, experiment (black solid line), simulation with 0-D turbine map - sections without connection (purple dotted line), simulation with 0-D turbine map - sections connected via orifice D = 10 mm (black dashed line), simulation with 0-D turbine map - sections connected via orifice D = 20 mm (red dashed line)

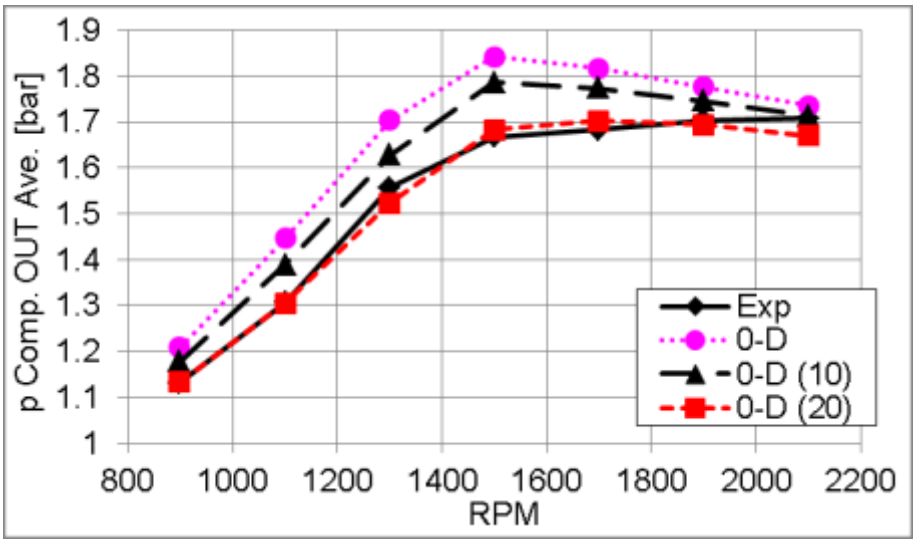

Figure 128 Pressure downstream of a compressor, experiment (black solid line), simulation with 0-D turbine map - sections without connection (purple dotted line), simulation with 0-D turbine map - sections connected via orifice D = 10 mm (black dashed line), simulation with 0-D turbine map - sections connected via orifice D = 20 mm (red dashed line)

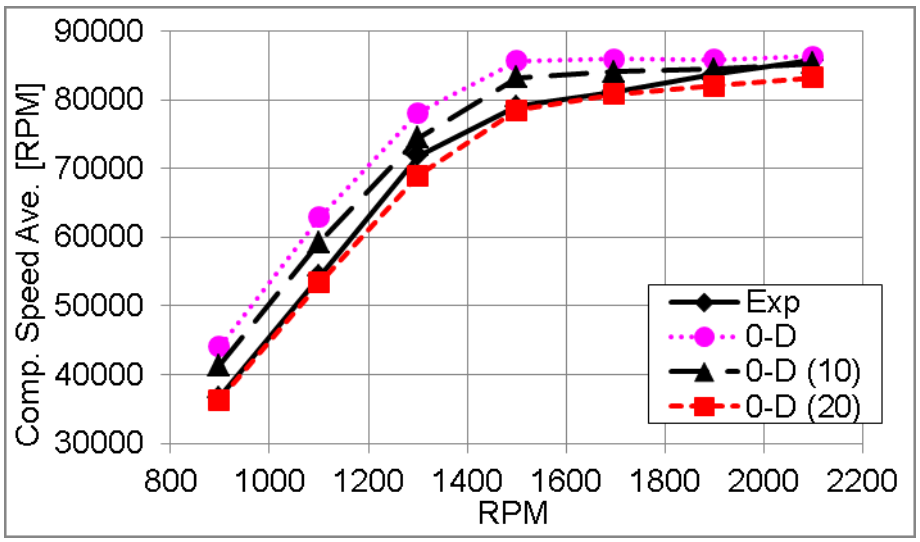

Figure 129 Compressor speed, experiment (black solid line), simulation with 0-D turbine map - sections without connection (purple dotted line), simulation with 0-D turbine map - sections connected via orifice D = 10 mm (black dashed line), simulation with 0-D turbine map - sections connected via orifice D = 20 mm (red dashed line)

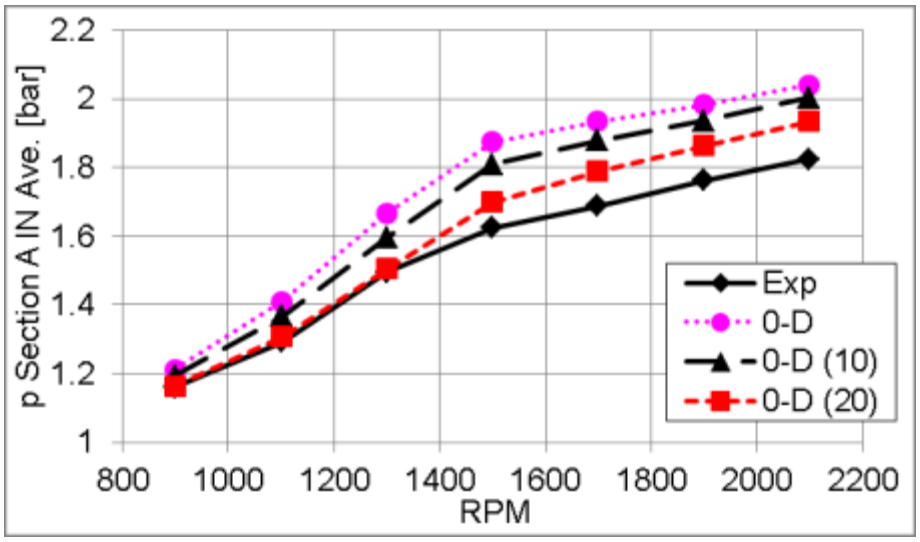

Figure 130 Pressure at inlet of turbine section A, experiment (black solid line), simulation with 0-D turbine map - sections without connection (purple dotted line), simulation with 0-D turbine map - sections connected via orifice D = 10 mm (black dashed line), simulation with 0-D turbine map - sections connected via orifice D = 20 mm (red dashed line)

The pressure courses downstream of the compressor (*Figure 128*) are consistent with the previous picture. The turbocharger speed (*Figure 129*) and pressure at inlet of turbine section A (*Figure 130*) are comparable with experimental data.

The simulation results with connection orifice are satisfactory. Further results are in Appendix 4. The 0-D turbine model with the connection orifice (diameter 20 mm) seems to be the best compromise from the 0-D turbine models, because the accordance with experiments is probably the best.

The unsteady results of engine simulation using the full 1-D turbine model and 0-D model with and without connection between exhaust branches upstream of the turbine are shown in sequent pictures. The physical values are plotted as functions of engine crank angle.

The pressure indicated at the intake port inlet and corresponding simulated traces are drawn in *Figure 131* and *Figure 132*. The results of the 1-D turbine model and 0-D model with the connection orifice are fully comparable with the indicated pressure. The pressure trace predicted by the 0-D turbine model without connection of exhaust branches has similar trend, but the achieved level of pressure is higher.

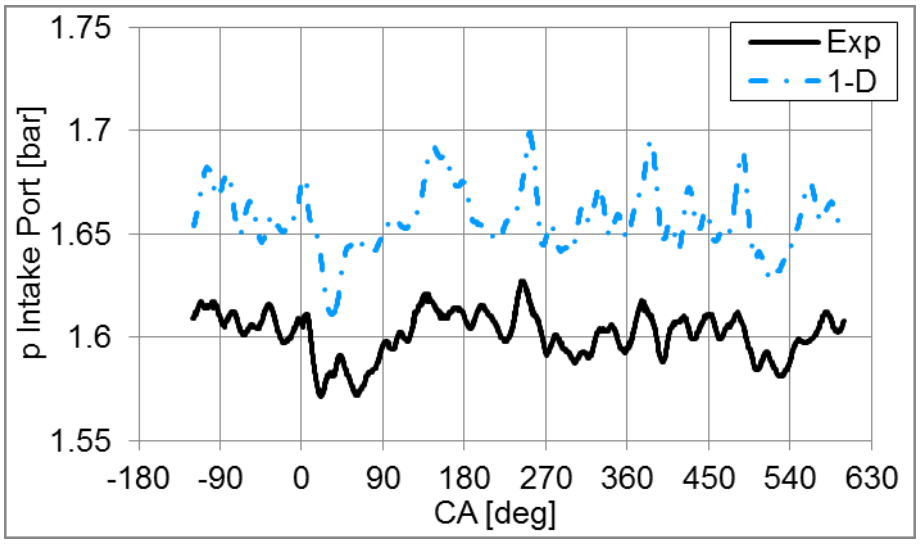

Figure 131 Pressure in intake port, experiment (black solid line), simulation with full 1-D unsteady turbine (blue dashed and dotted line); 1500 RPM, BMEP = 13 bar

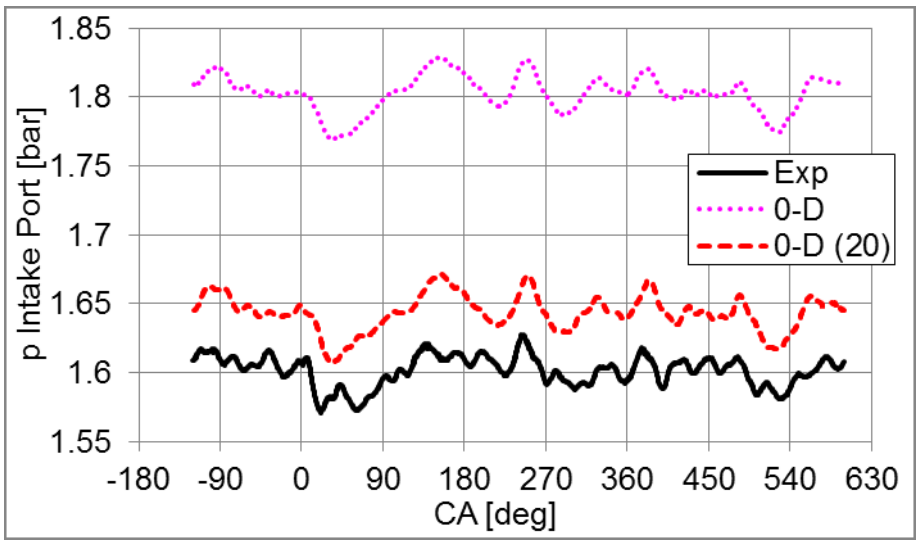

Figure 132 Pressure in intake port, experiment (black solid line), simulation with 0-D turbine map - sections without connection (purple dotted line), simulation with 0-D turbine map - sections connected via orifice D = 20 mm (red dashed line); 1500 RPM, BMEP = 13 bar

The pressure indicated in the cylinder is compared with simulation results in *Figure 133* and *Figure 134.*

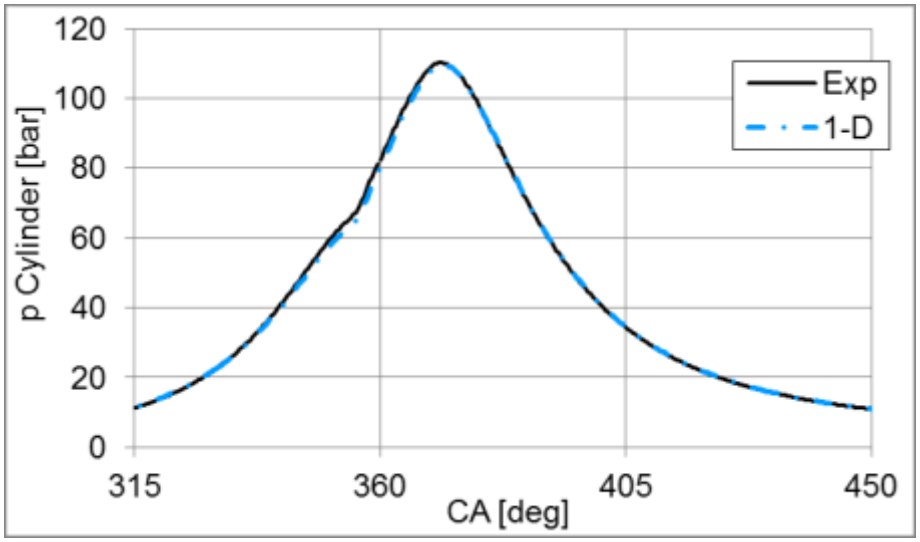

Figure 133 Pressure in cylinder, experiment (black solid line), simulation with full 1-D unsteady turbine (blue dashed and dotted line); 1500 RPM, BMEP = 13 bar

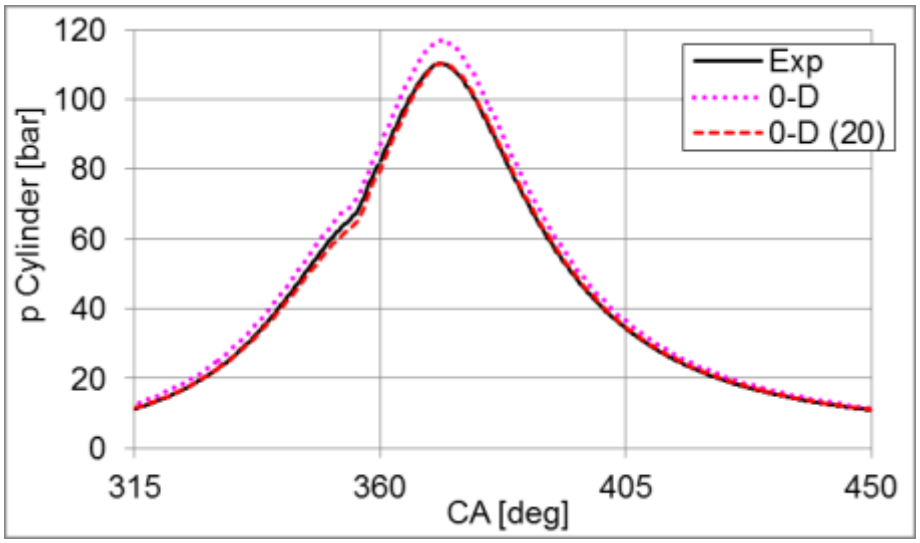

Figure 134 Pressure in cylinder, experiment (black solid line), simulation with 0-D turbine map - sections without connection (purple dotted line), simulation with 0-D turbine map - sections connected via orifice D = 20 mm (red dashed line); 1500 RPM, BMEP = 13 bar

The pressure traces at the exhaust port outlet are stated in *Figure 135.* The pressure indicated on the experimental engine is biased in the interval 450 - 630 degrees. The error occurred in all diagrams concerned the exhaust port. The engine simulation with the 1-D turbine predicts higher pressure amplitude compared with indicated pressure. The main pressure amplitude and phasing are satisfactory. The problems of the 0-D approach without the cross connection upstream of the turbine are obvious from *Figure 136.* The main pressure amplitude

is overestimated and the influence of the second turbine section is missing. The consistency of the pressure predicted by the 0-D model with the connection orifice and real pressure trace is slightly better than in the case of the full 1-D turbine model.

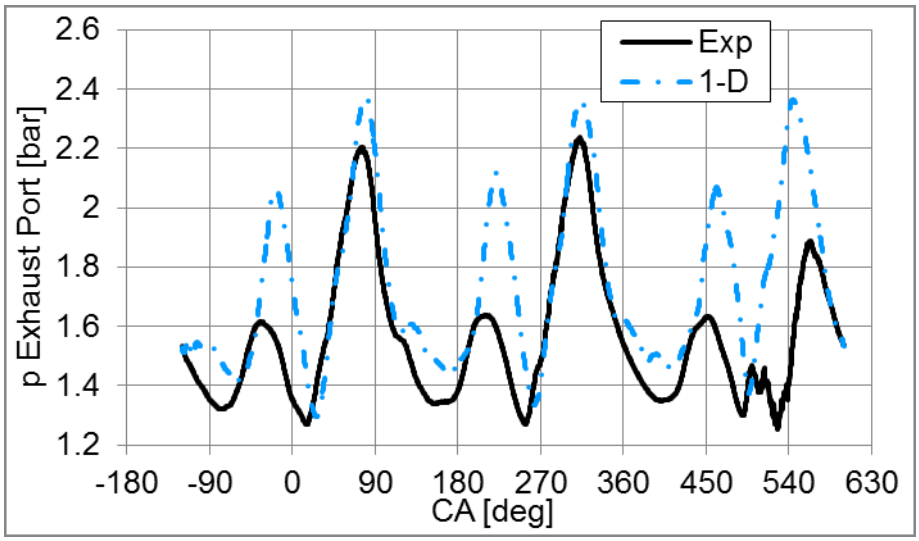

Figure 135 Pressure in exhaust port, experiment (black solid line), simulation with full 1-D unsteady turbine (blue dashed and dotted line); 1500 RPM, BMEP = 13 bar

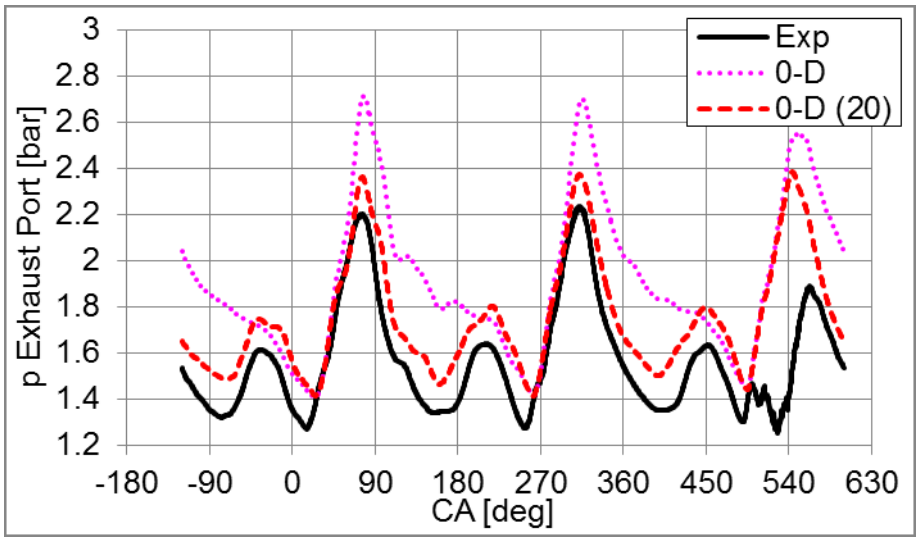

Figure 136 Pressure in exhaust port, experiment (black solid line), simulation with 0-D turbine map - sections without connection (purple dotted line), simulation with 0-D turbine map - sections connected via orifice D = 20 mm (red dashed line); 1500 RPM, BMEP = 13 bar

The pressures at the inlet of the turbine section A (*Figure 137* and *Figure 138*), predicted by the 1-D turbine model and 0-D model with the orifice upstream, are almost similar. The main pressure amplitude is like real one. The pressure trace calculated by the simple 0-D turbine model is the worst, because the interactions between turbine sections cannot be involved.

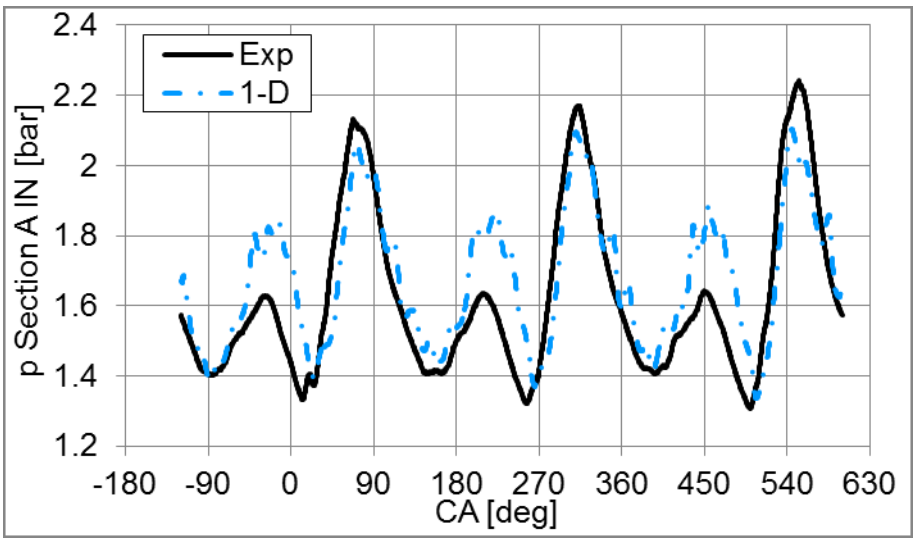

Figure 137 Pressure at inlet of turbine section A, experiment (black solid line), simulation with full 1-D unsteady turbine (blue dashed and dotted line); 1500 RPM, BMEP = 13 bar

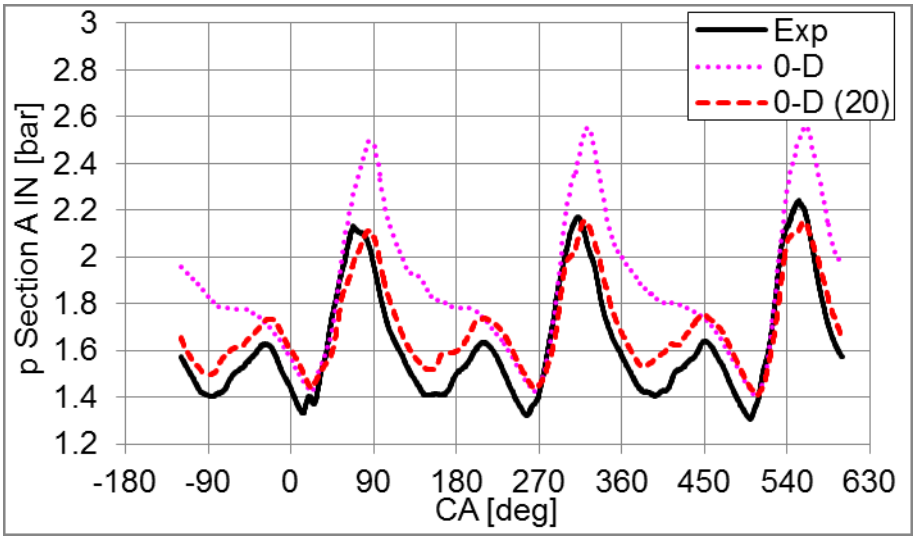

Figure 138 Pressure at inlet of turbine section A, experiment (black solid line), simulation with 0-D turbine map - sections without connection (purple dotted line), simulation with 0-D turbine map - sections connected via orifice D = 20 mm (red dashed line); 1500 RPM, BMEP = 13 bar

The inferior pressure amplitude in the turbine section B, performed by the full 1-D model (*Figure 139*) and 0-D model with the interconnection orifice (*Figure 140*), is not entirely accurate in both simulations. The influence of the nozzle placed downstream of the flow mixing zone (flowsplit template in function of flow joint), which may improve the behaviour of the 1-D turbine model under unsteady conditions, should be verified in the future. The features of the simple 0-D model with separated turbine sections mentioned above are naturally visible in *Figure 140* too.

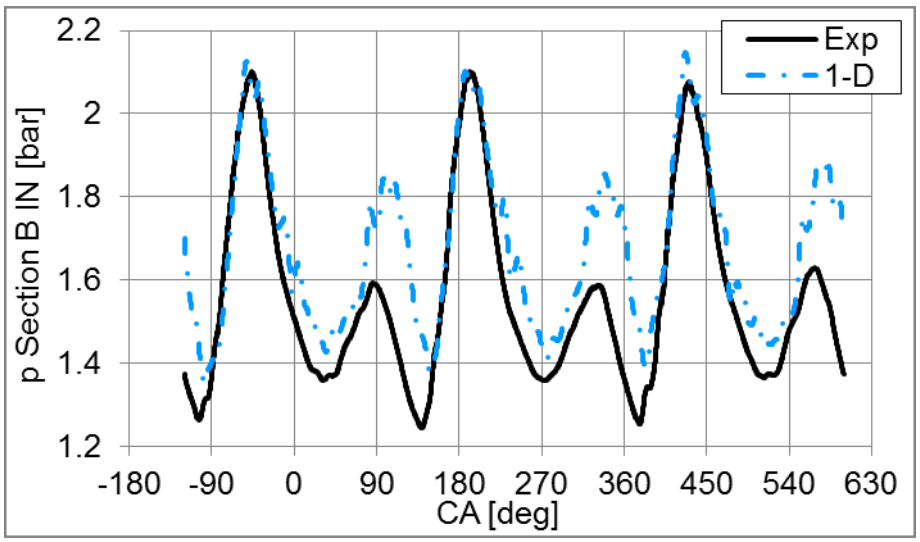

Figure 139 Pressure at inlet of turbine section B, experiment (black solid line), simulation with full 1-D unsteady turbine (blue dashed and dotted line); 1500 RPM, BMEP = 13 bar

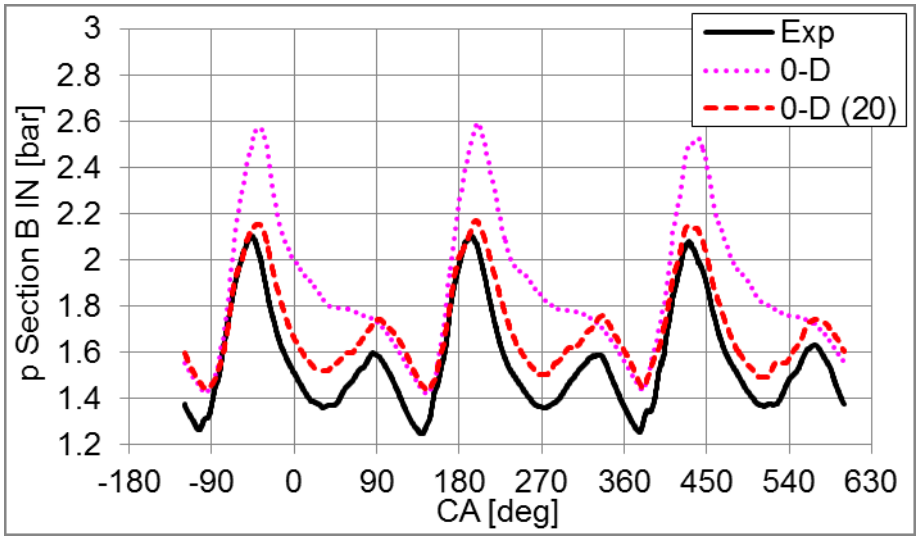

Figure 140 Pressure at inlet of turbine section B, experiment (black solid line), simulation with 0-D turbine map - sections without connection (purple dotted line), simulation with 0-D turbine map - sections connected via orifice D = 20 mm (red dashed line); 1500 RPM, BMEP = 13 bar

The simulated pressure traces downstream of the turbine (*Figure 141* and *Figure 142*) are comparable with indicated pressure. The phasing and level of amplitudes are sufficient.

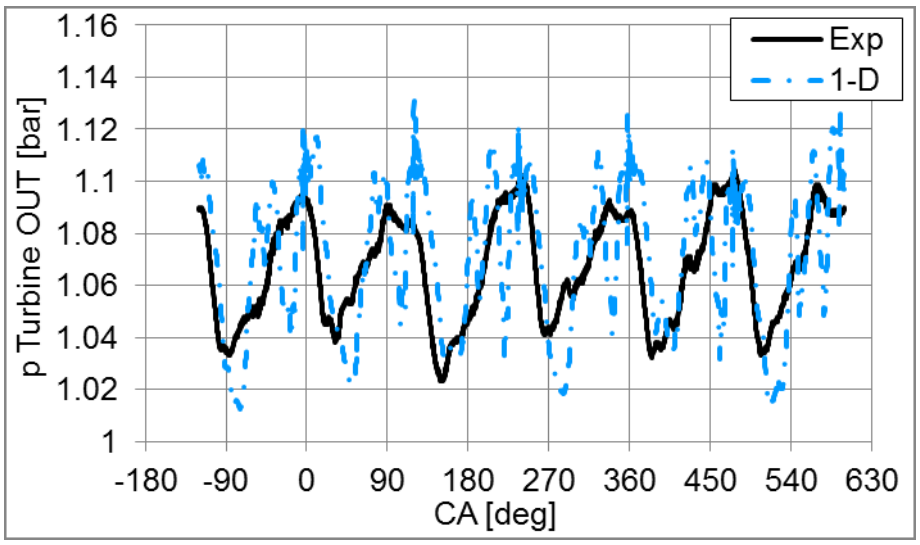

Figure 141 Pressure turbine downstream, experiment (black solid line), simulation with full 1-D unsteady turbine (blue dashed and dotted line); 1500 RPM, BMEP = 13 bar

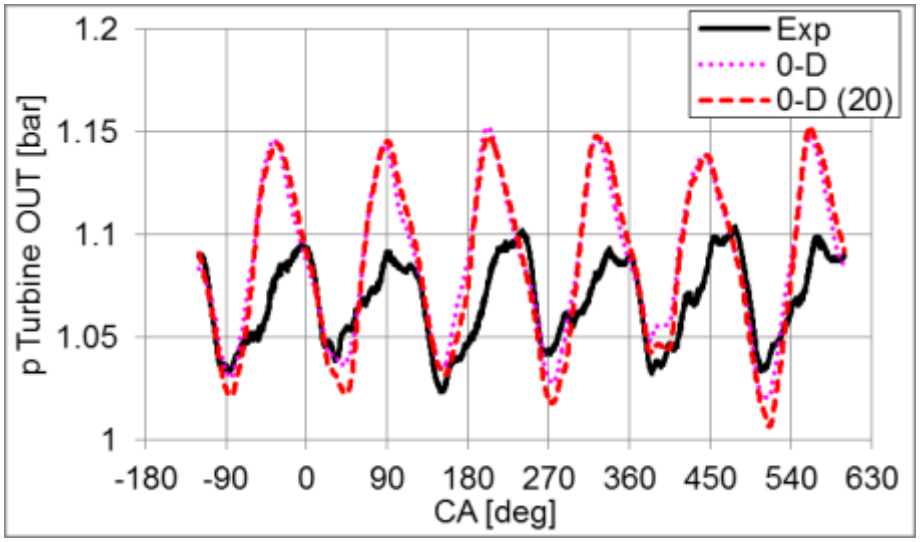

Figure 142 Pressure turbine downstream, experiment (black solid line), simulation with 0-D turbine map - sections without connection (purple dotted line), simulation with 0-D turbine map - sections connected via orifice D = 20 mm (red dashed line); 1500 RPM, BMEP = 13 bar

The full 1-D turbine model predicts the same turbocharger speed as measured speed. The 0-D model with orifice upstream predicts slightly lower speed. The turbocharger speed simulated by the simple 0-D turbine model is higher. The results in *Figure 143* and *Figure 144* are consistent with results shown above.

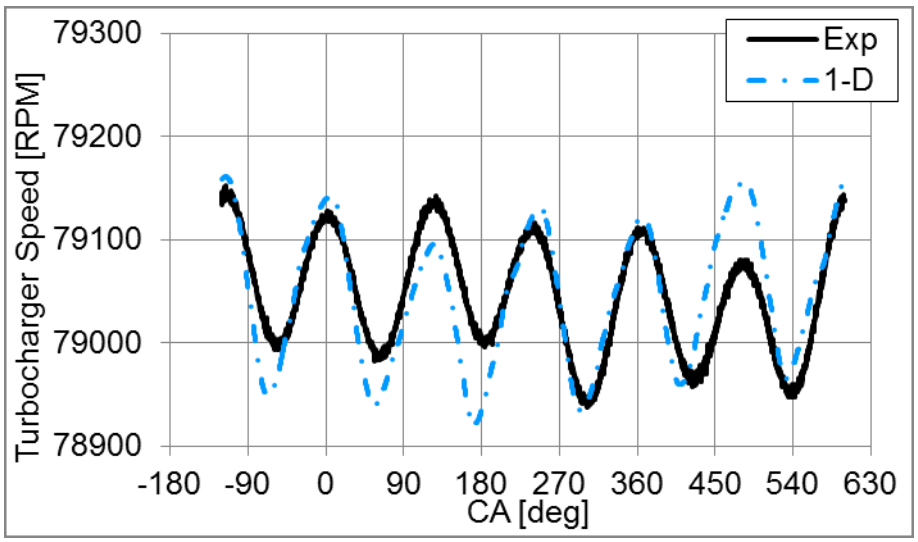

Figure 143 Turbocharger speed, experiment (black solid line), simulation with full 1-D unsteady turbine (blue dashed and dotted line); 1500 RPM, BMEP = 13 bar

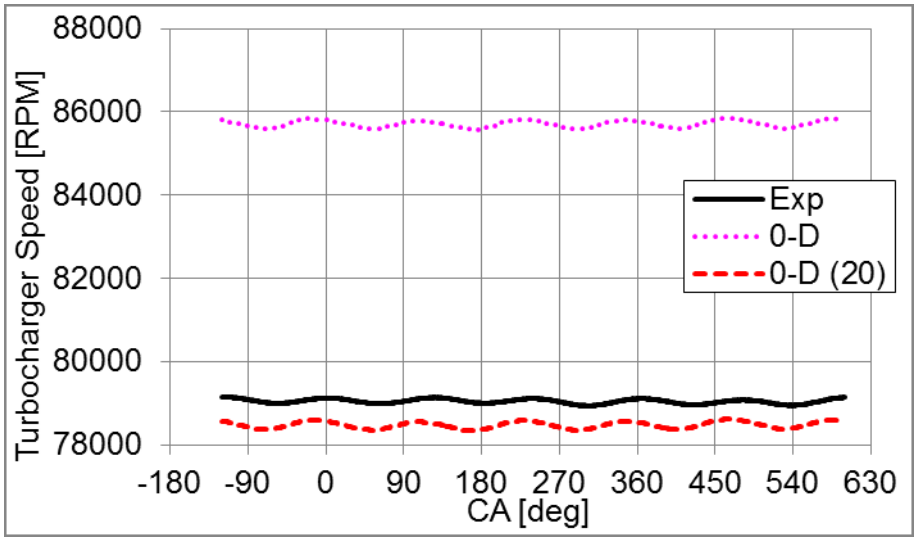

Figure 144 Turbocharger speed, experiment (black solid line), simulation with 0-D turbine map - sections without connection (purple dotted line), simulation with 0-D turbine map - sections connected via orifice D = 20 mm (red dashed line); 1500 RPM, BMEP = 13 bar

The results of only the full 1-D turbine model follow. The mass flow rates in turbine sections (*Figure 145* and *Figure 146*) demonstrate the extreme conditions of highly pulsating flow upstream of the turbine. The unsteady full 1-D turbine model predicts the backflow in both sections. The backflow in one section occurs, when the second section achieves the maximum positive mass flow rate.

The ability of the model to simulate the backflows is very important feature. The full 1-D turbine model is stable under extremely unsteady conditions with huge changes of mass flow rates in sections. It has to be stressed that the 1-D turbine model was not calibrated under conditions of backflows in sections. The developed steady flow turbocharger test bed for the twin scroll turbines is completely ready for the measurement of backflow in the section. The related experiments were not performed so far.

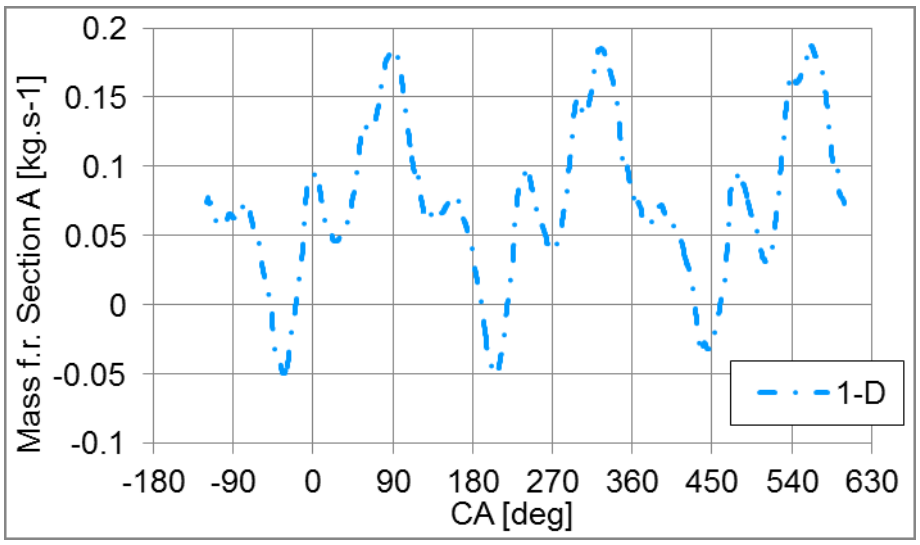

Figure 145 Mass flow rate via section A, simulation with full 1-D unsteady turbine (blue dashed and dotted line); 1500 RPM, BMEP = 13 bar

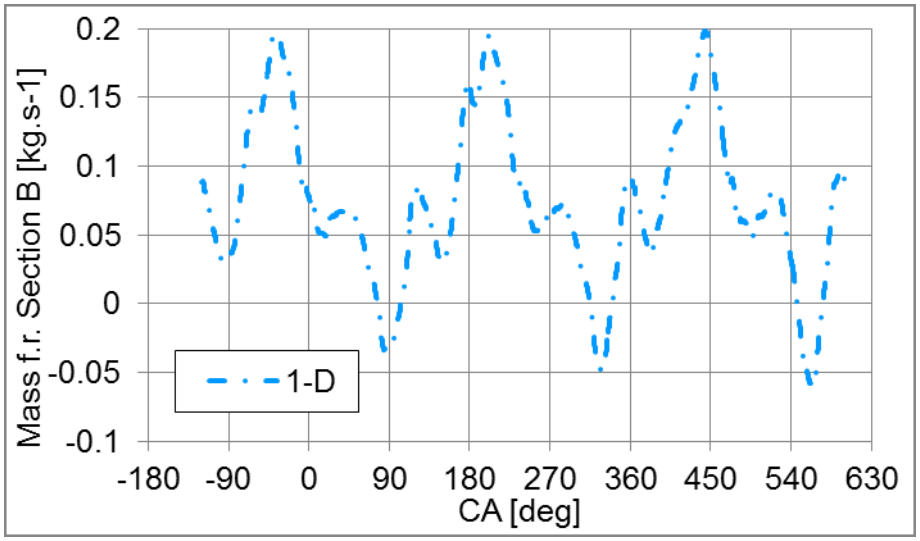

Figure 146 Mass flow rate via section B, simulation with full 1-D unsteady turbine (blue dashed and dotted line); 1500 RPM, BMEP = 13 bar

Turbine power calculated by the full 1-D model during the simulation of the six cylinder diesel engine is stated in *Figure 147*.

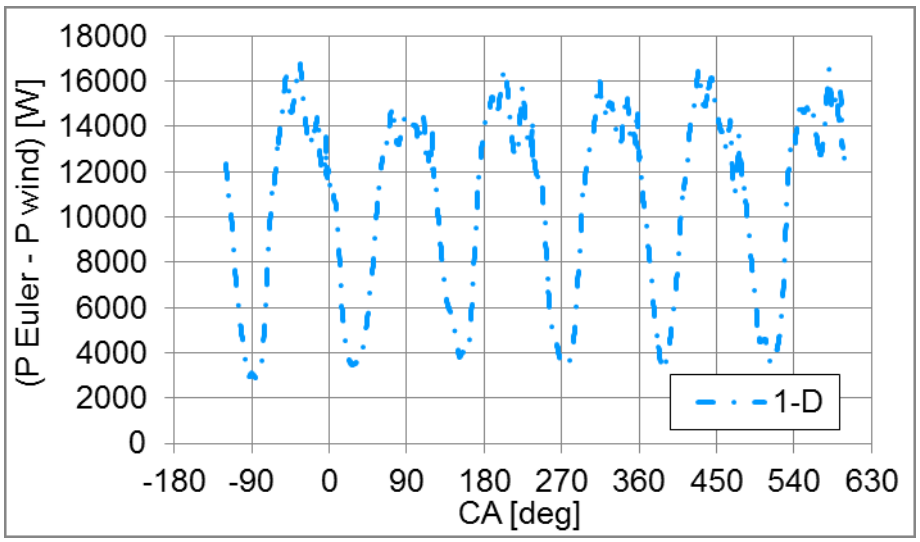

Figure 147 Turbine power, simulation with full 1-D unsteady turbine (blue dashed and dotted line); 1500 RPM, BMEP = 13 bar

The overall pressure ratio of the twin entry turbine in *Figure 148* determined by the 1-D model is consistent with traces of pressure in turbine sections (*Figure 137* and *Figure 139*) and downstream of the turbine (*Figure 141*).

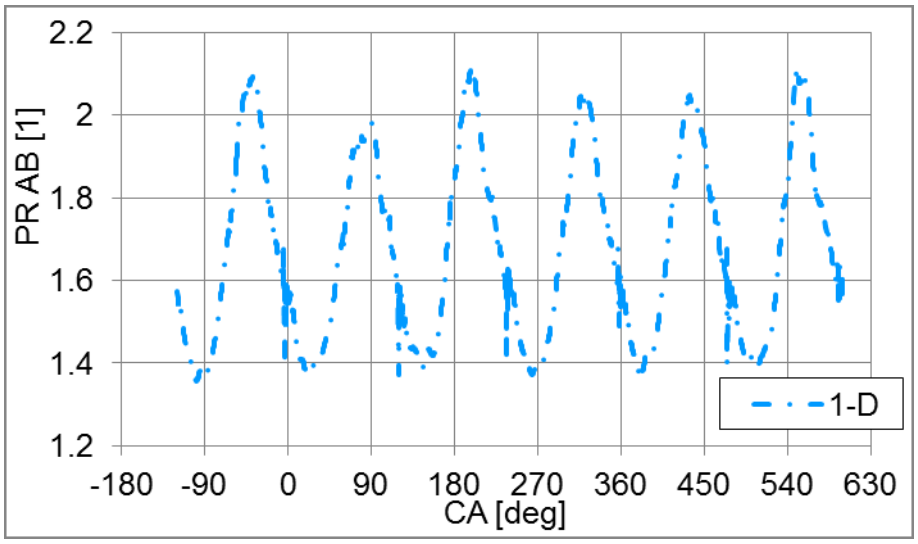

Figure 148 Overall pressure ratio AB, simulation with full 1-D unsteady turbine (blue dashed and dotted line); 1500 RPM, BMEP = 13 bar

Relatively broad range of the overall blade speed ratio of the turbine is visible in *Figure 149.*

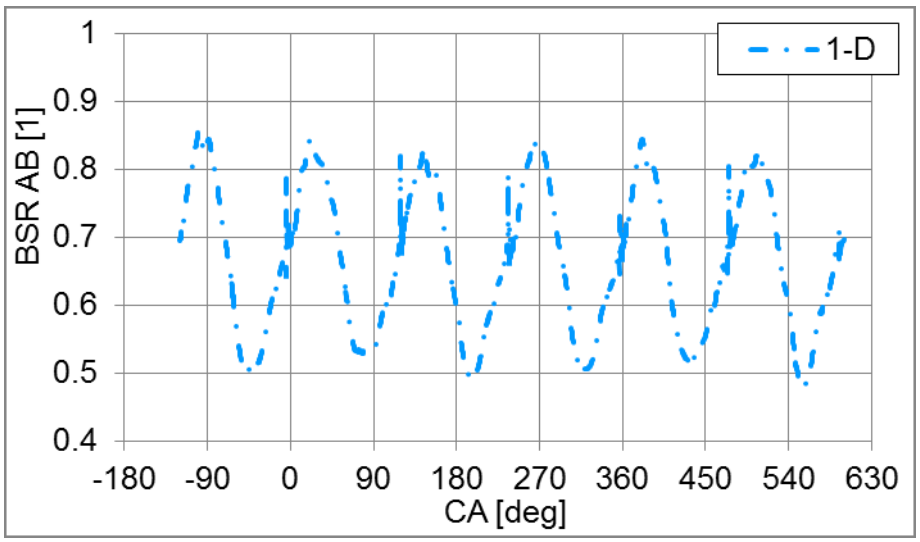

Figure 149 Blade speed ratio, simulation with full 1-D unsteady turbine (blue dashed and dotted line); 1500 RPM, BMEP = 13 bar

The governing calibration coefficients of the turbine, calibrated under steady flow, control the turbine performance under unsteady conditions as well. The actual value of each coefficient depends on the actual overall pressure ratio of a turbine and the level of impeller admission. All calibration coefficients at unsteady operation of a turbine keep within the bounds of the steady flow calibration. The angles alpha 2 and beta 3, the coefficients with the highest effect on the overall turbine parameters are drawn in *Figure 150* and *Figure 152.* The influence of nozzle exit angle deviation delta alpha 2 (*Figure 151*) is slight during unsteady operation.

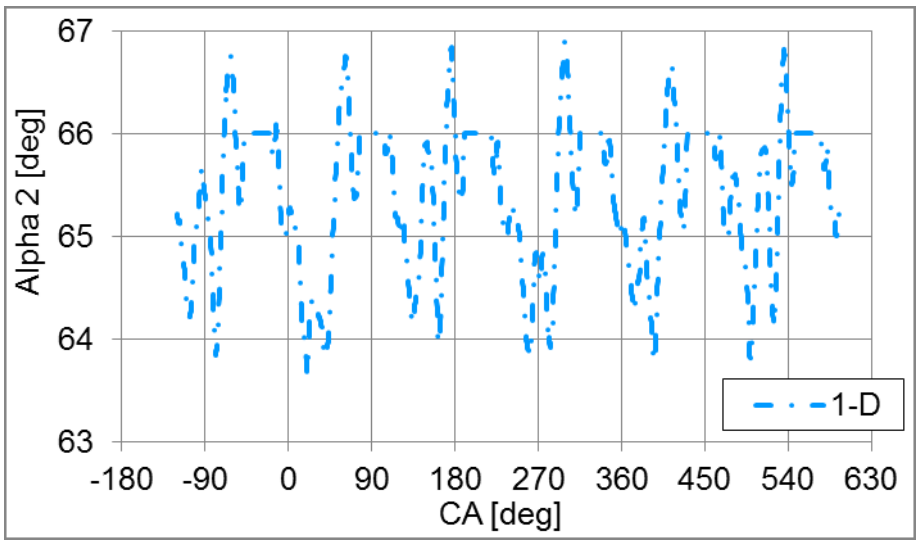

Figure 150 Alpha 2 - nozzle exit angle, simulation with full 1-D unsteady turbine (blue dashed and dotted line); 1500 RPM, BMEP = 13 bar

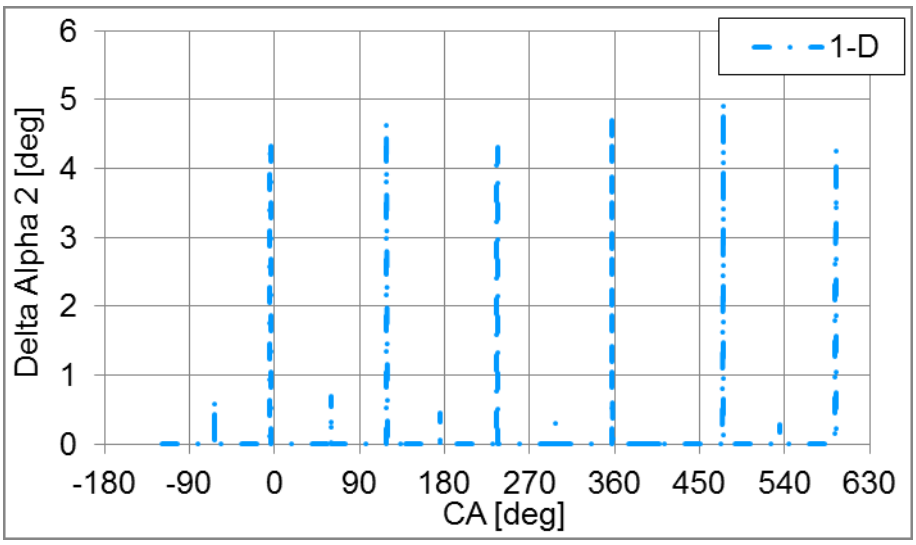

Figure 151 Delta Alpha 2 - deviation of nozzle exit angle, simulation with full 1-D unsteady turbine (blue dashed and dotted line); 1500 RPM, BMEP = 13 bar

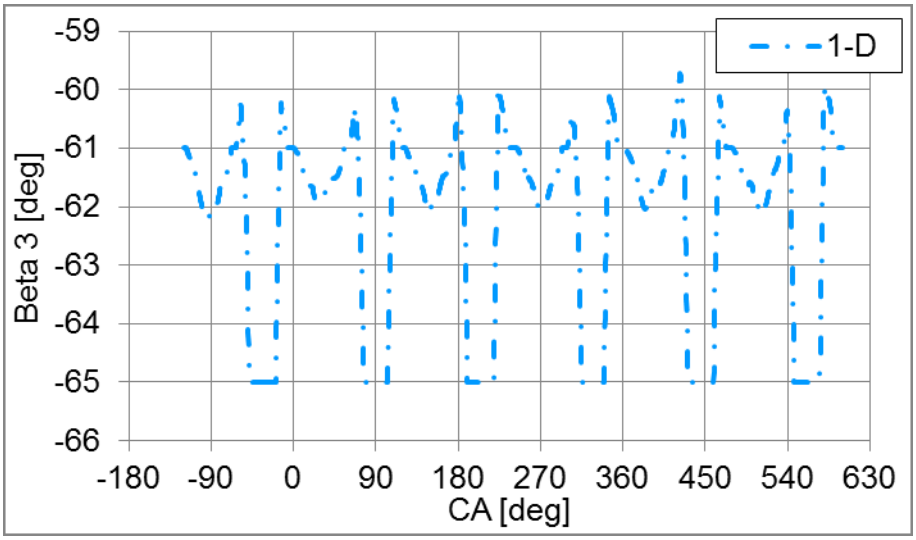

Figure 152 Beta 3 - impeller exit angle, simulation with full 1-D unsteady turbine (blue dashed and dotted line); 1500 RPM, BMEP = 13 bar

Flow separation coefficient K sep, which is independent on angle beta 3, is plotted in *Figure 153*. The unsteady trace of windage losses coefficient is stated in *Figure 154*.

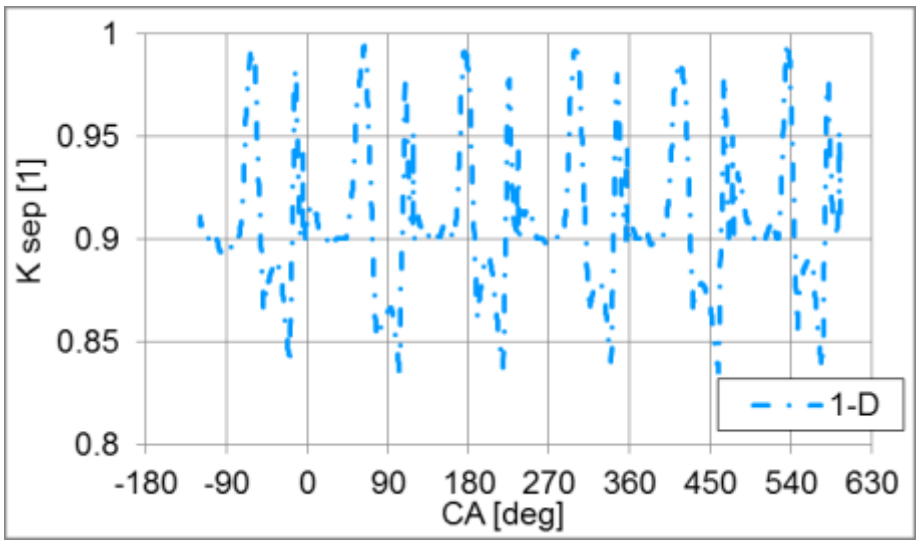

Figure 153 K sep - flow separation coefficient, simulation with full 1-D unsteady turbine (blue dashed and dotted line); 1500 RPM, BMEP = 13 bar

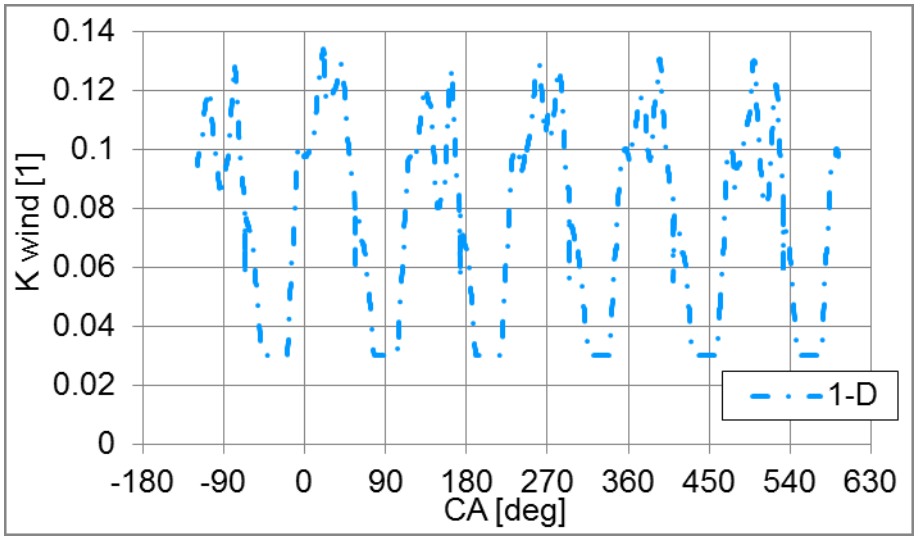

Figure 154 K wind - coefficient of windage losses, simulation with full 1-D unsteady turbine (blue dashed and dotted line); 1500 RPM, BMEP = 13 bar

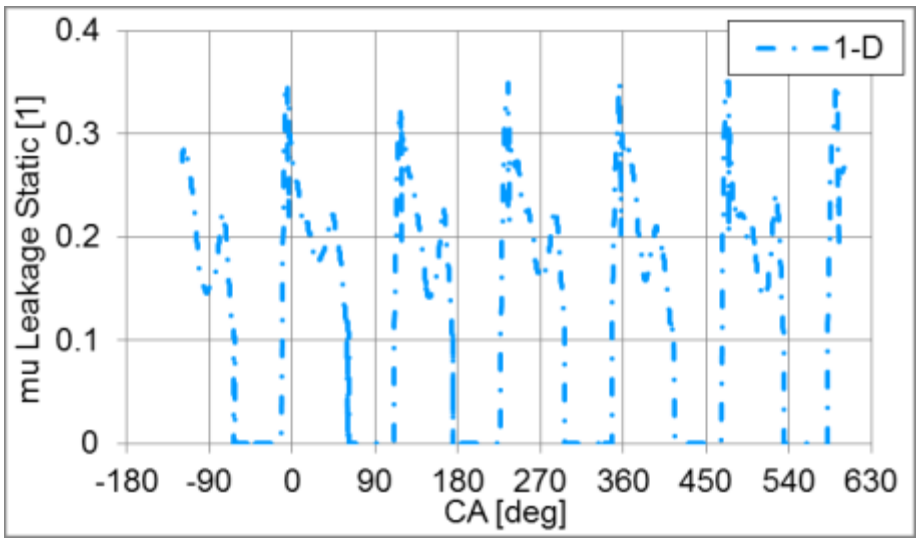

Figure 155 Discharge coefficient of static leakages, simulation with full 1-D unsteady turbine (blue dashed and dotted line); 1500 RPM, BMEP = 13 bar

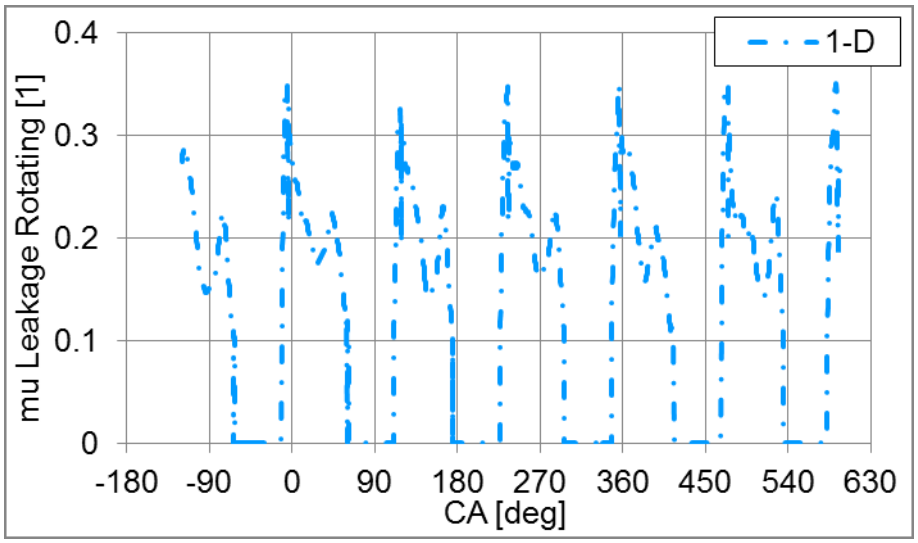

Figure 156 Discharge coefficient of rotating leakages, simulation with full 1-D unsteady turbine (blue dashed and dotted line); 1500 RPM, BMEP = 13 bar

Discharge coefficients of static and rotating leakages are presented in *Figure 155* and *Figure 156*. The pressure loss coefficient in the impeller pipe is in *Figure 157*.

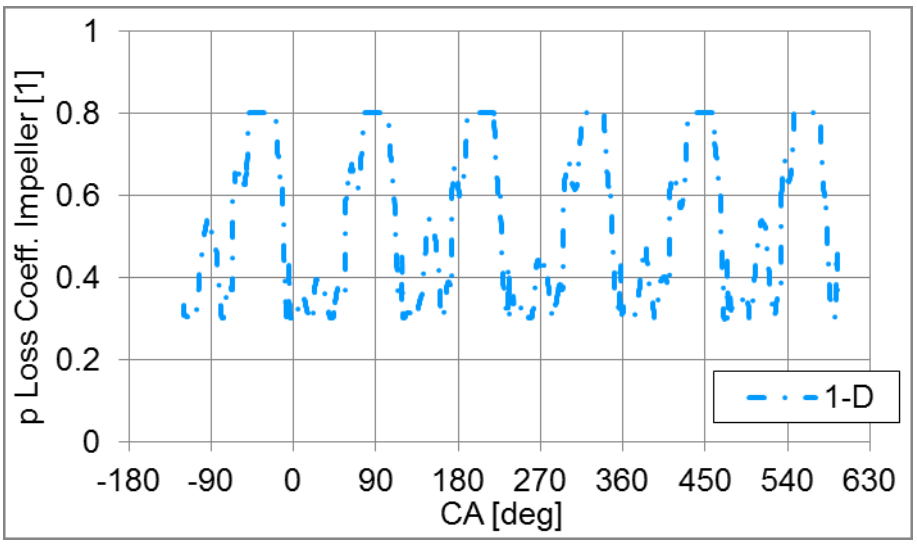

Figure 157 Pressure loss coefficient in impeller pipe, simulation with full 1-D unsteady turbine (blue dashed and dotted line); 1500 RPM, BMEP = 13 bar

The discharge coefficient at section A outlet CD A (*Figure 158*) in combination with pressure loss coefficient in section A (*Figure 160*) are dependent on the actual mass flow rate in section A and pressure ratio level. The coefficient CD B (*Figure 159*) and pressure loss coefficient in section B (*Figure 161*) depend, of course, on the mass flow rate in section B and also pressure ratio level.

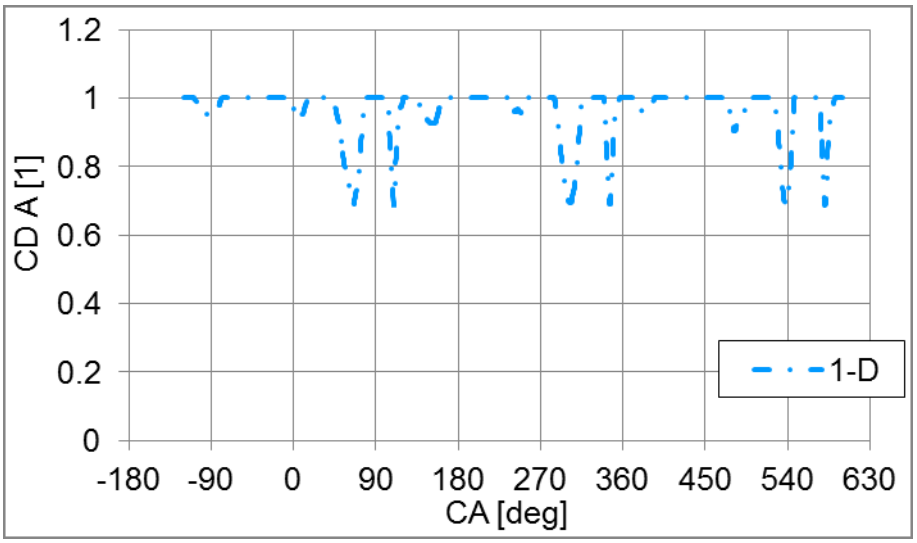

Figure 158 CD A - discharge coefficient at section A outlet {upstream of flow mixing}, simulation with full 1-D unsteady turbine (blue dashed and dotted line); 1500 RPM, BMEP = 13 bar

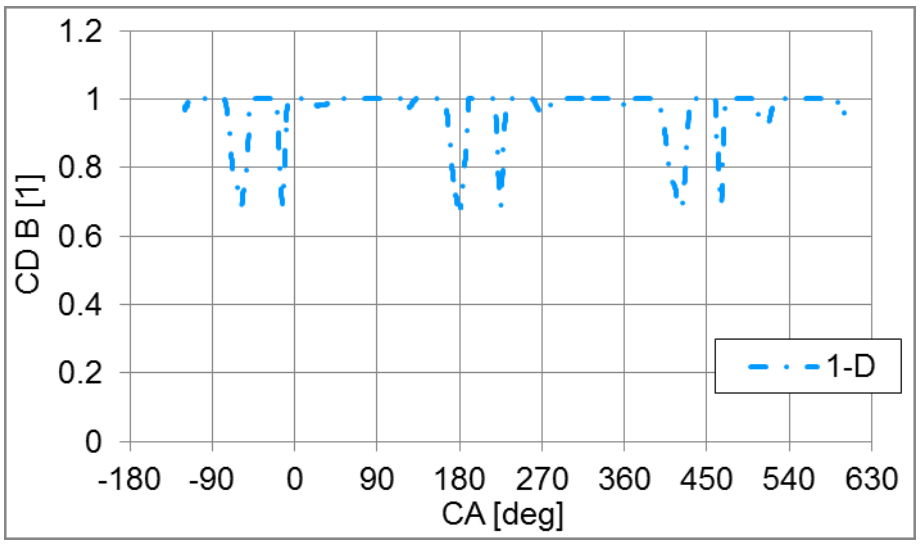

Figure 159 CD B - discharge coefficient at section B outlet {upstream of flow mixing}, simulation with full 1-D unsteady turbine (blue dashed and dotted line); 1500 RPM, BMEP = 13 bar

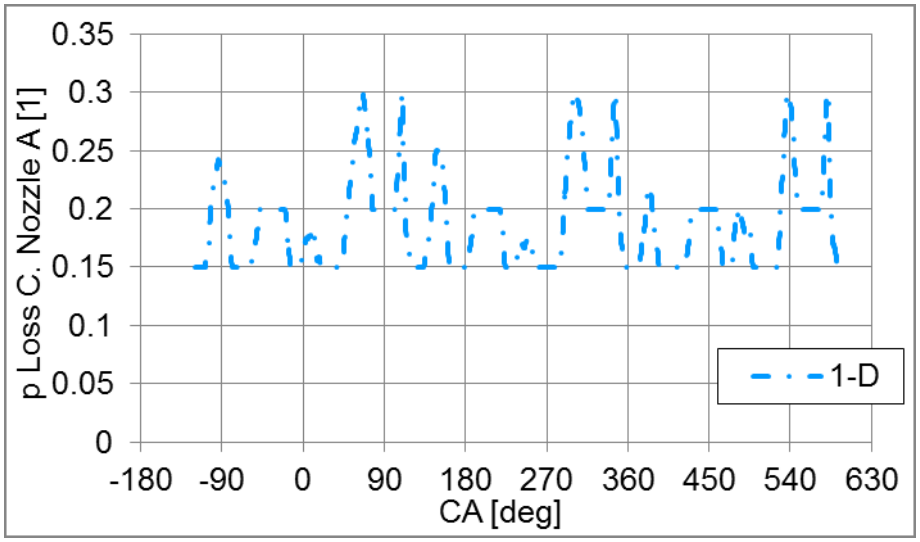

Figure 160 Pressure loss coefficient in section A, simulation with full 1-D unsteady turbine (blue dashed and dotted line); 1500 RPM, BMEP = 13 bar

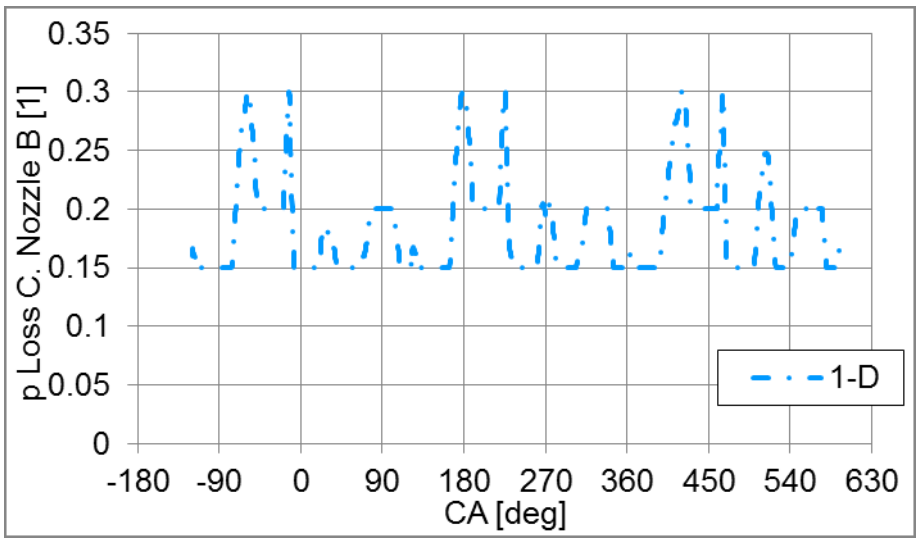

Figure 161 Pressure loss coefficient in section B, simulation with full 1-D unsteady turbine (blue dashed and dotted line); 1500 RPM, BMEP = 13 bar

The examples of engine simulation results (engine speed 900 and 2100 RPM) are stated below. The complete summary of results is in Appendix 5. The level of pulsations in our case, defined in [2] and [40], is highest at 900 RPM. The pressures in the turbine section A, predicted by the full 1-D turbine model (*Figure 162*) and 0-D model with the interconnection orifice upstream of the turbine (*Figure 163*) are fully comparable with indicated pressure on the real turbine. The pressure trace calculated by the simple 0-D turbine model with separated exhaust branches is not suitable.

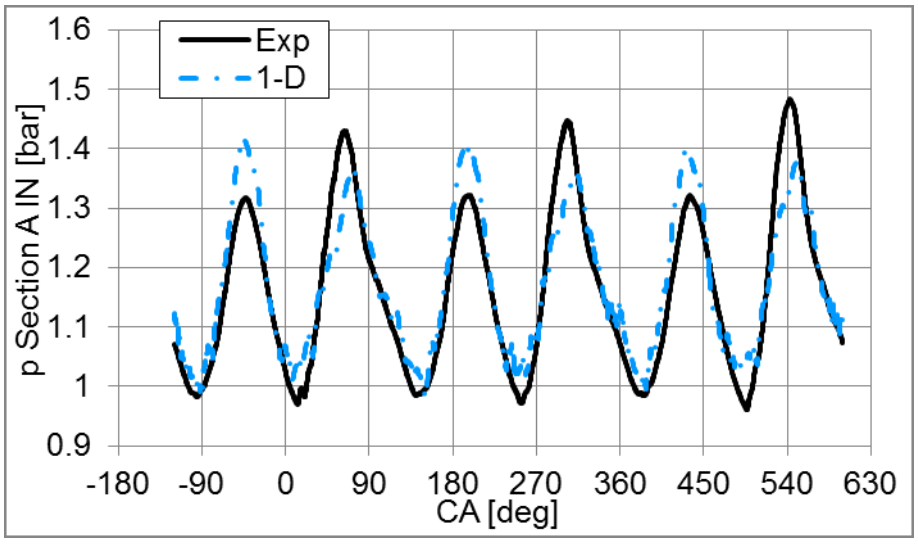

Figure 162 Pressure at inlet of turbine section A, experiment (black solid line), simulation with full 1-D unsteady turbine (blue dashed and dotted line); 900 RPM, BMEP = 8.9 bar

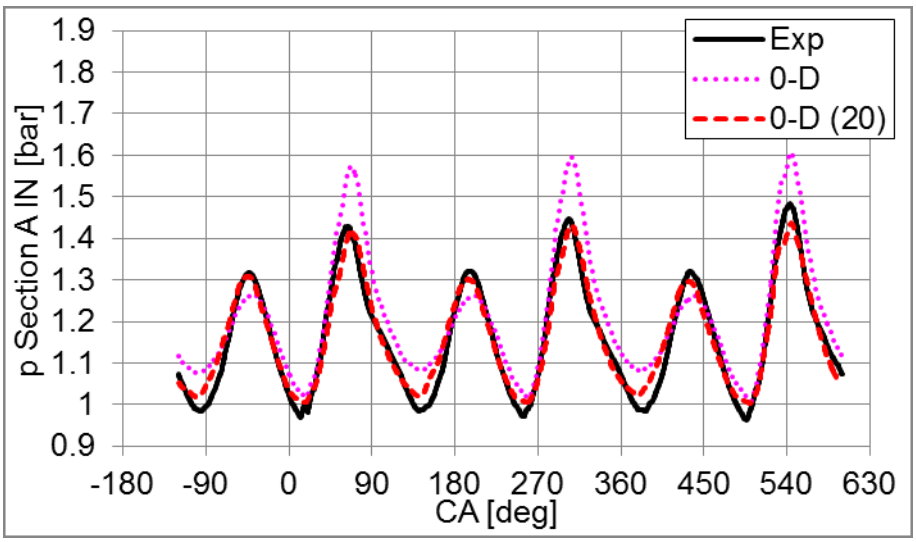

Figure 163 Pressure at inlet of turbine section A, experiment (black solid line), simulation with 0-D turbine map - sections without connection (purple dotted line), simulation with 0-D turbine map - sections connected via orifice D = 20 mm (red dashed line); 900 RPM, BMEP = 8.9 bar

The level of pulsations, from stated examples, is lowest at maximum engine speed of 2100 RPM. The comparison is introduced in *Figure 164* and *Figure 165.* The simple 0-D turbine model is able to predict the pressure amplitudes at least. The influence of flow interactions between turbine sections is clearly missing. The unsteady results of engine simulations are summarized in Appendix 5.

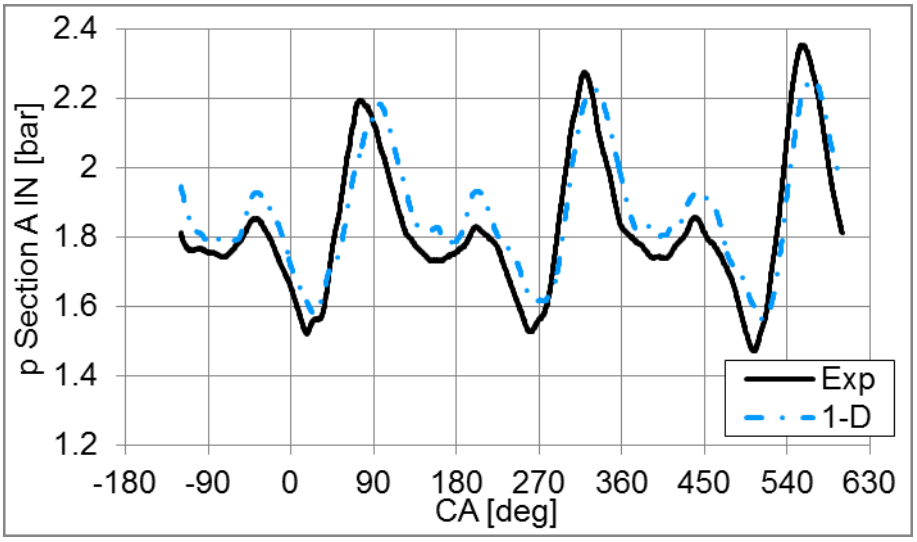

Figure 164 Pressure at inlet of turbine section A, experiment (black solid line), simulation with full 1-D unsteady turbine (blue dashed and dotted line); 2100 RPM, BMEP = 9.8 bar

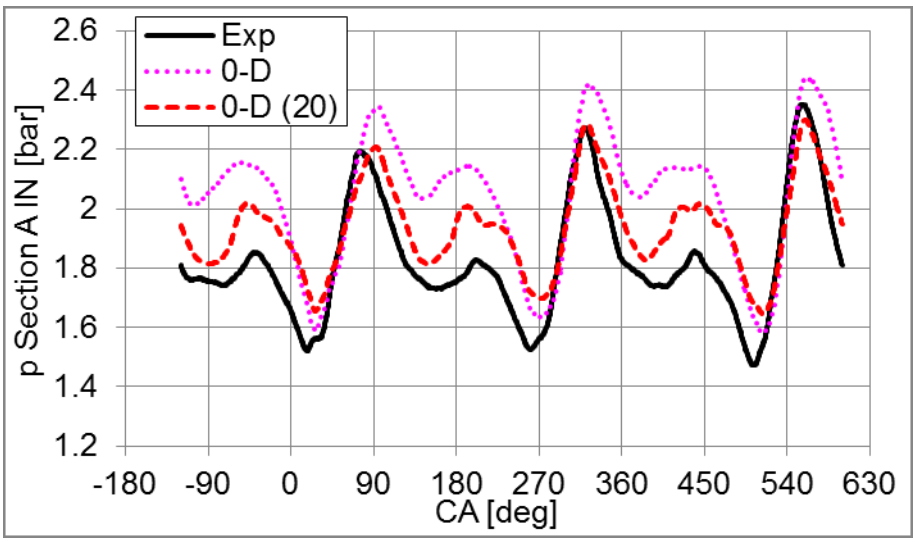

Figure 165 Pressure at inlet of turbine section A, experiment (black solid line), simulation with 0-D turbine map - sections without connection (purple dotted line), simulation with 0-D turbine map - sections connected via orifice D = 20 mm (red dashed line); 2100 RPM, BMEP = 9.8 bar

7.4 Transients

The goal of the transient simulation is to verify the stability, robustness and predictive capability of the full 1-D turbine model with the twin scroll. Rapidly changing conditions upstream of a turbine are the most demanding conditions for the developed turbine model.

The transient engine operation with changing engine load and speed would be useful for the mentioned purposes, but the dynamometer used for experiments is equipped only with the control of engine speed, therefore the engine transients at constant engine speed were measured.

The transients, at given constant engine speed, were defined by the fuel mass flow rate in time. The maximum amount of fuel corresponds with the steady state point at full engine load. The information about the injected fuel mass from the injector is not available. The actual value of the overall fuel mass flow rate is not absolutely correct due to delay of employed fuel mass flow meter.

The tested turbocharger used for measurements on the steady flow test bed and also for turbocharging of the experimental combustion engine has no regulation of the turbine.

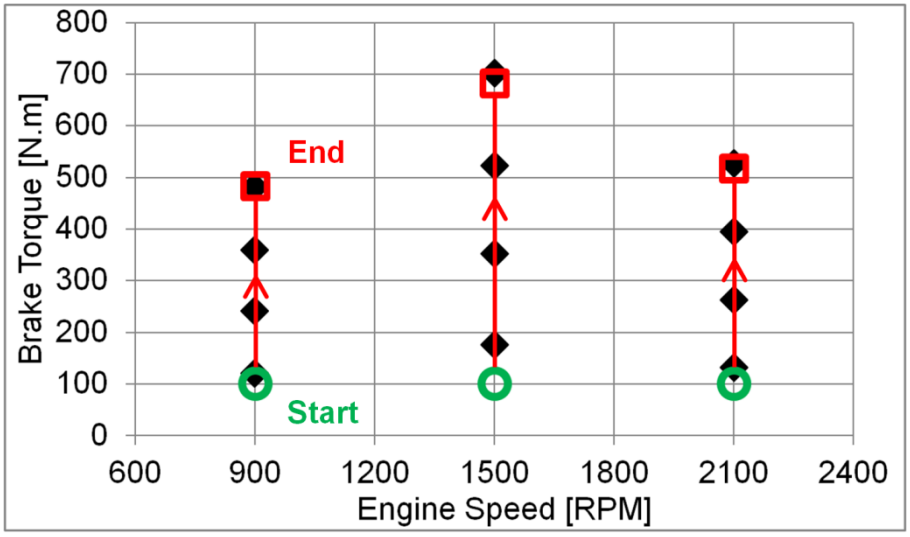

Figure 166 Draft of transients at constant engine speed (900; 1500; 2100 RPM), initial engine load level 100 N.m (green circles), end points (red squares); steady state points (black)

Draft of measured and simulated transient engine operation is stated in *Figure 166.* The initial level of engine load was given at brake torque of 100 N.m by the corresponding mass of fuel. The end of each transient was defined by appropriate full engine load.

The engine model was also calibrated in steady state points drawn in *Figure 166.* The full 1-D turbine model, 0-D model with the connection orifice upstream of the turbine and simple 0-D model without connection of exhaust branches, used for previous steady state engine simulation, were utilized in the simulation of engine transient operation without any modification.

The engine transient operation is defined by the fuel mass flow rate as a function of time (*Figure 167* and *Figure 168*). The course of the fuel flow rate step change was in reality limited by the original fuel injection pump. The engine control unit, based on NI compact RIO and equipped with in-house open source software, is naturally able to control the injected fuel mass, but only within the bounds which are governed by the control unit of a fuel pump. The original fuel pump belongs to tested combustion engine type.

It would be possible to adjust the fuel mass flow rate in simulation iteratively and slightly improve the traces of physical quantities, but it is not considerable for our purposes.

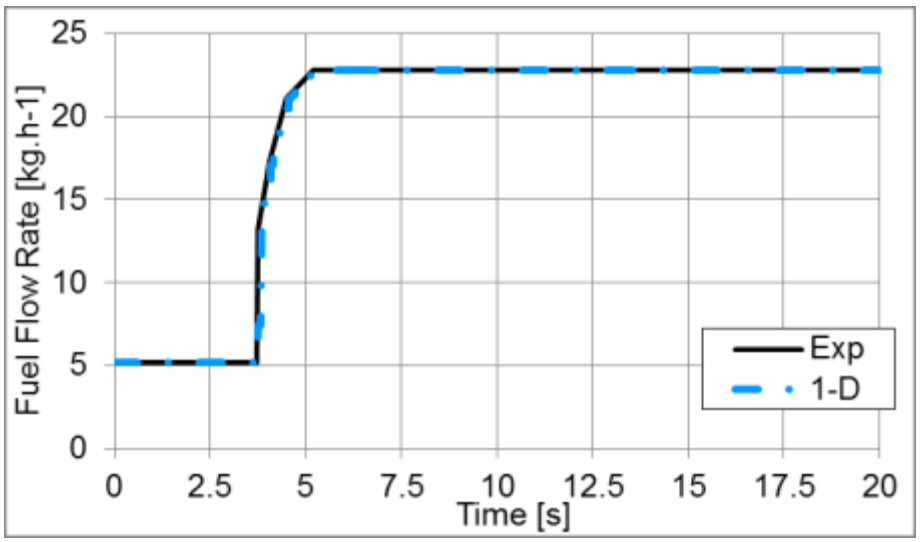

Figure 167 Fuel mass flow rate, experiment (black solid line), simulation with full 1-D unsteady turbine (blue dashed and dotted line); 1500 RPM

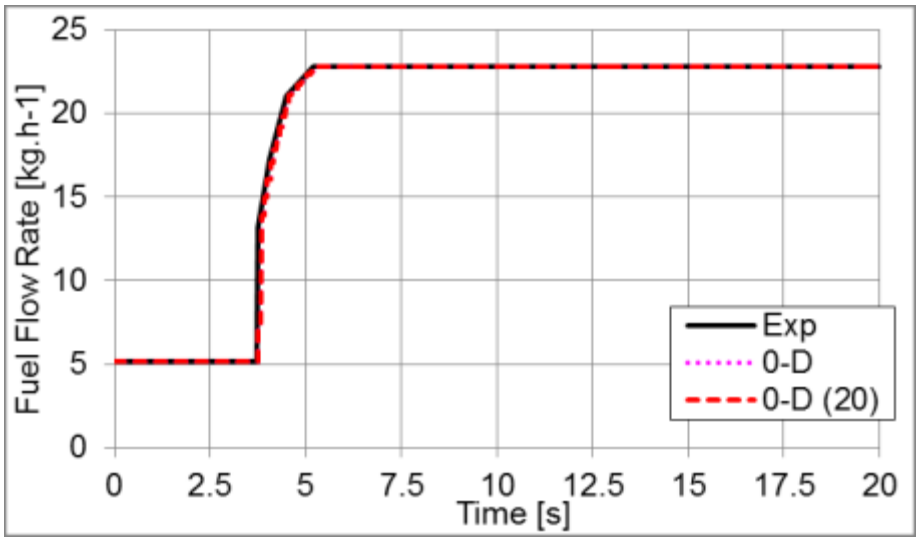

Figure 168 Fuel mass flow rate, experiment (black solid line), simulation with 0-D turbine map - sections without connection (purple dotted line), simulation with 0-D turbine map - sections connected via orifice D = 20 mm (red dashed line); 1500 RPM

The comparison of measured engine brake torque and simulation with full 1-D turbine model is in *Figure 169.* The difference between measured and simulated torque, before achievement of engine full load, is caused by the differences in fuel mass flow rates as mentioned above. The initial, final and main part of step change predicted by the engine simulation is correct. The results obtained by the simulation with 0-D turbine models are almost the same (*Figure 170*).

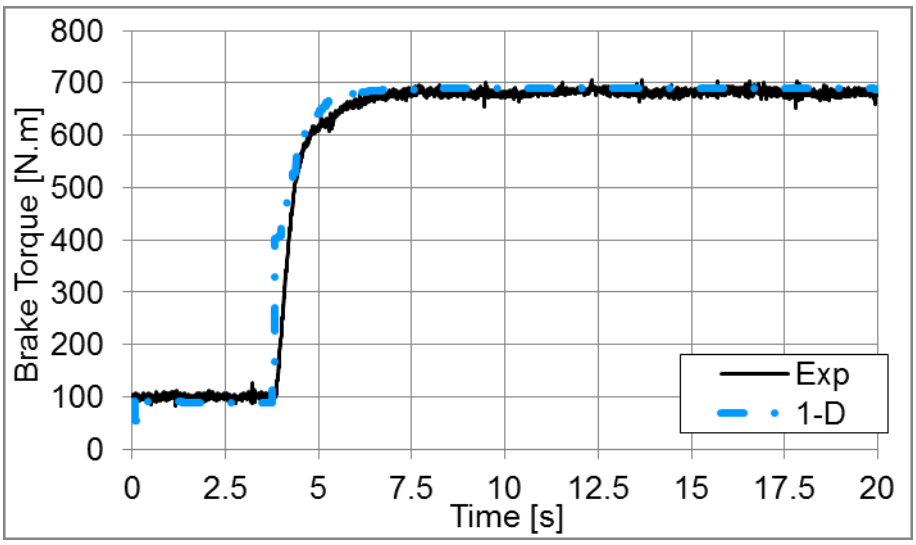

Figure 169 Brake torque, experiment (black solid line), simulation with full 1-D unsteady turbine (blue dashed and dotted line); 1500 RPM

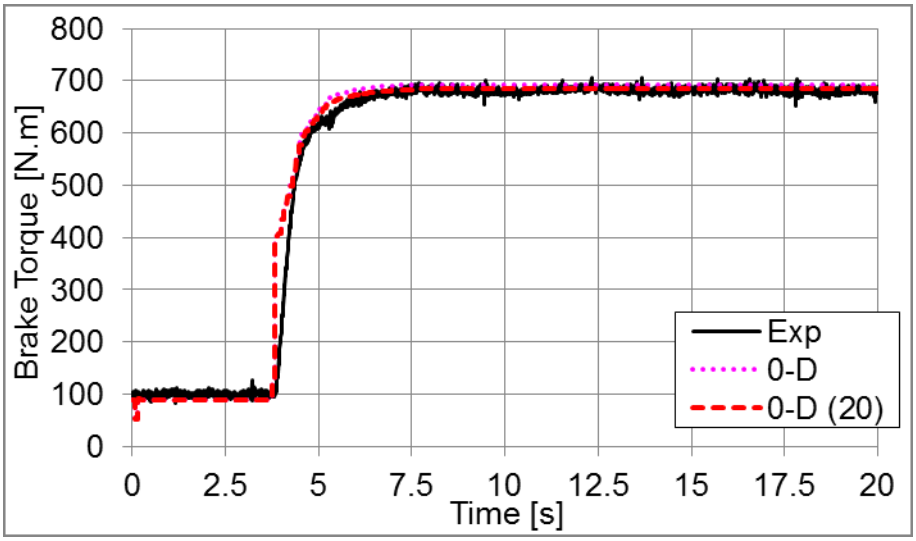

Figure 170 Brake torque, experiment (black solid line), simulation with 0-D turbine map - sections without connection (purple dotted line), simulation with 0-D turbine map - sections connected via orifice D = 20 mm (red dashed line); 1500 RPM

The turbocharger speeds predicted by the full 1-D model (*Figure 171*) and 0-D turbine model with the connection orifice (*Figure 172*) are similar. When we compare experimental values with simulation results at engine steady states (*Figure 112*), it is clear that the 1-D turbine model is consistent in prediction at transient. The turbocharger speed at the end of the transient (*Figure 171*) corresponds with the predicted value from steady state, but the speed measured during transient is lower than from experiment at steady state. The speed calculated by the simple 0-D turbine model without the interconnection of branches upstream of the turbine is overestimated (*Figure 172*).

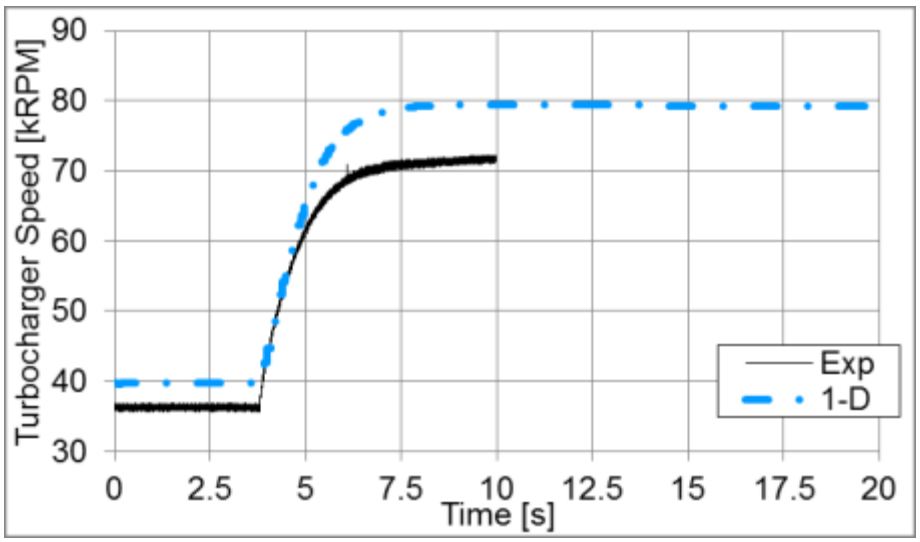

Figure 171 Turbocharger speed, experiment (black solid line), simulation with full 1-D unsteady turbine (blue dashed and dotted line); 1500 RPM

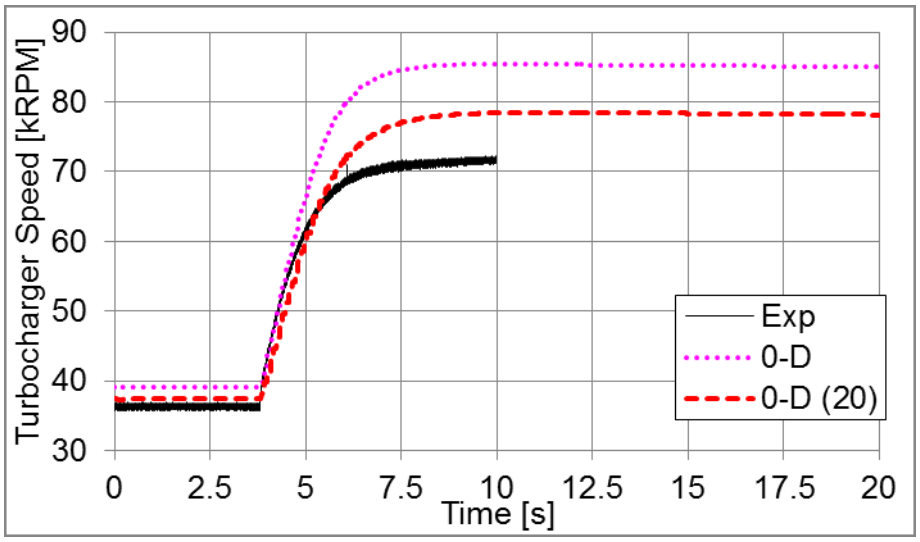

Figure 172 Turbocharger speed, experiment (black solid line), simulation with 0-D turbine map - sections without connection (purple dotted line), simulation with 0-D turbine map - sections connected via orifice D = 20 mm (red dashed line); 1500 RPM

The tendency of the pressure downstream of a compressor is similar to turbocharger speed. The pressure measured during transient is also lower than in the case of steady state (*Figure 113*). The results of 1-D simulation (*Figure 173*) and 0-D simulation with interconnected branches (*Figure 174*) are comparable. The pressure achieved during the engine simulation with the simple 0-D turbine model with separated sections is higher. The signal of static pressure, measured downstream of a compressor, is obviously delayed.

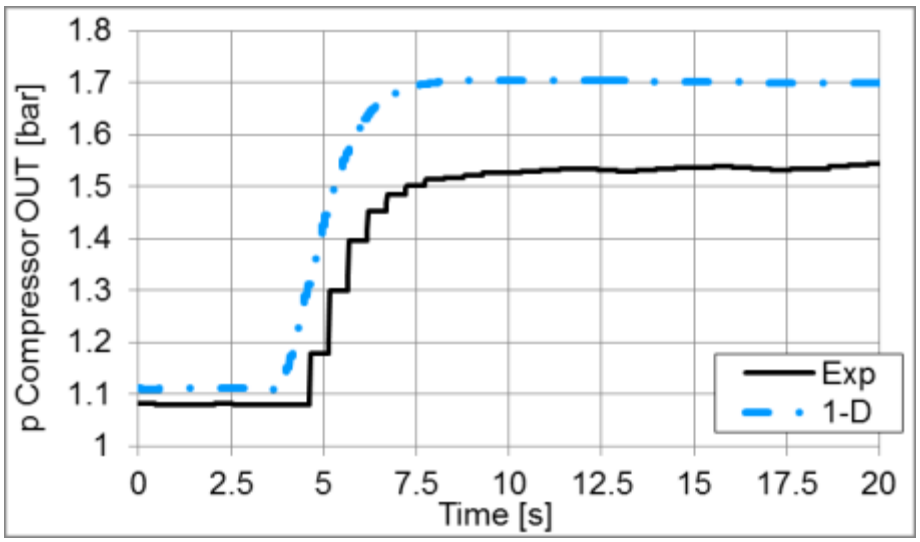

Figure 173 Pressure downstream of a compressor, experiment (black solid line), simulation with full 1-D unsteady turbine (blue dashed and dotted line); 1500 RPM

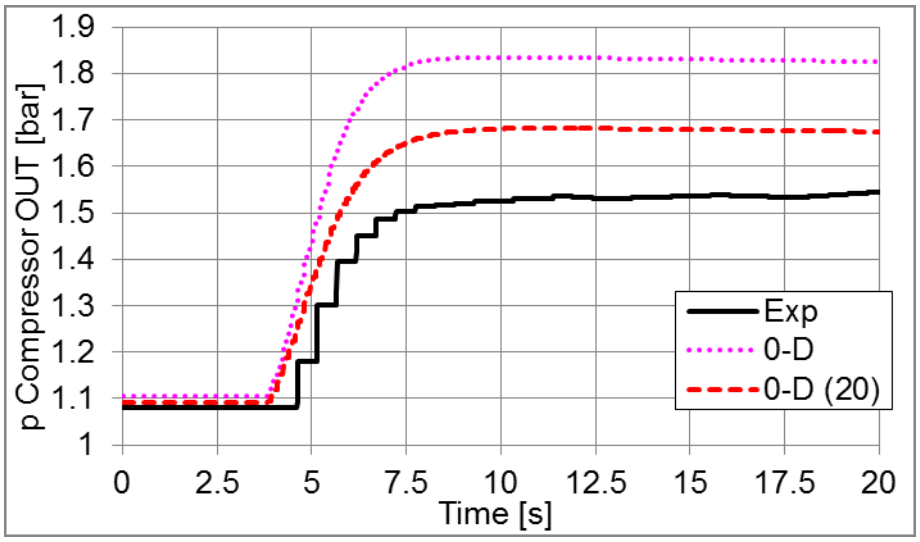

Figure 174 Pressure downstream of a compressor, experiment (black solid line), simulation with 0-D turbine map - sections without connection (purple dotted line), simulation with 0-D turbine map - sections connected via orifice D = 20 mm (red dashed line); 1500 RPM

The pressure at the inlet of turbine section A performed by the 1-D simulation is compared with the averaged indicated value in *Figure 175*. The pressure course predicted by the 0-D turbine model with interconnection is similar (*Figure 176*). The pressure calculated by the simple 0-D model is overestimated like the pressure downstream of a compressor above.

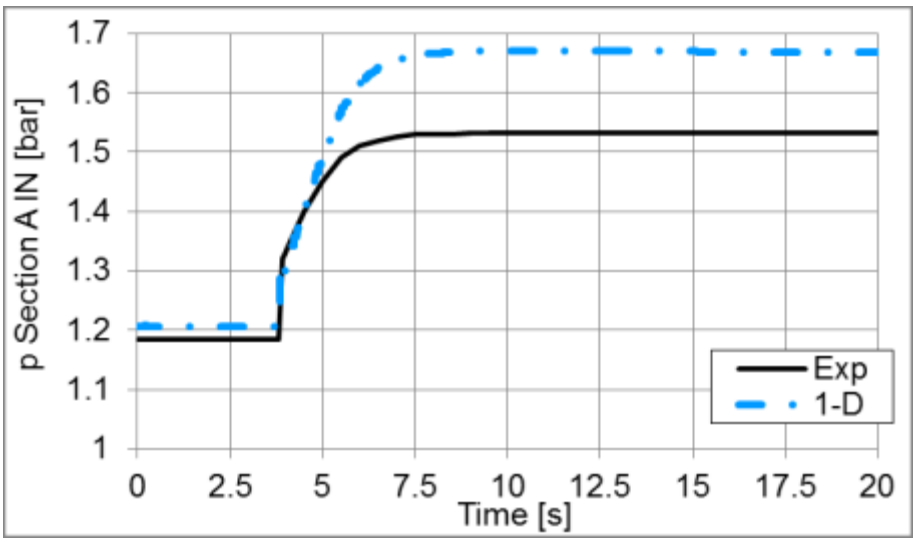

Figure 175 Pressure at inlet of turbine section A, experiment (black solid line), simulation with full 1-D unsteady turbine (blue dashed and dotted line); 1500 RPM

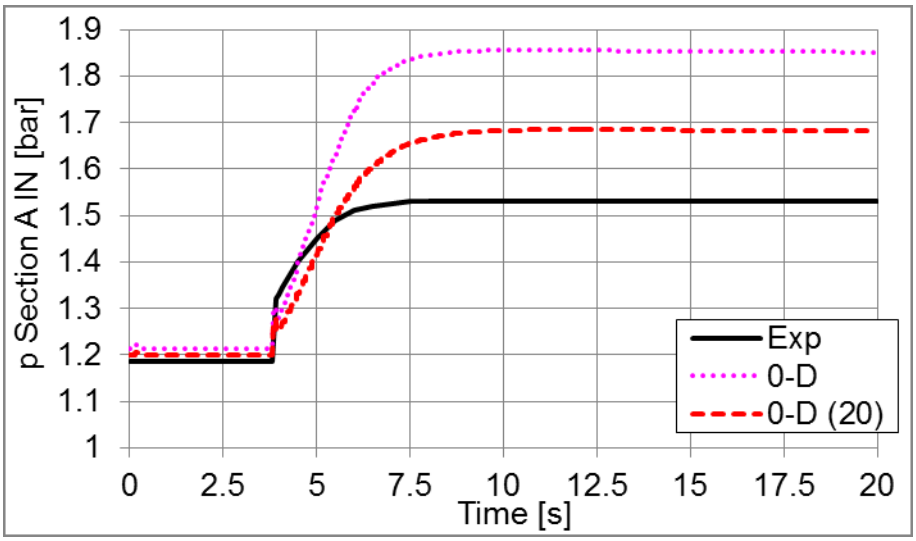

Figure 176 Pressure at inlet of turbine section A, experiment (black solid line), simulation with 0-D turbine map - sections without connection (purple dotted line), simulation with 0-D turbine map - sections connected via orifice D = 20 mm (red dashed line); 1500 RPM

The pressure measured at the inlet of turbine section B is slightly lower than in the section A due to asymmetric design of the exhaust runner as discussed in previous chapters. The pressures measured at the inlet of turbine sections are slightly lower in comparison with the steady state values, see *Figure 116* and *Figure 118*. The pressure courses predicted by simulation are almost the same in both turbine sections A and B (*Figure 175* and *Figure 177*). The pressure in the section B, calculated via the simple 0-D model, is higher as well (*Figure 178*).

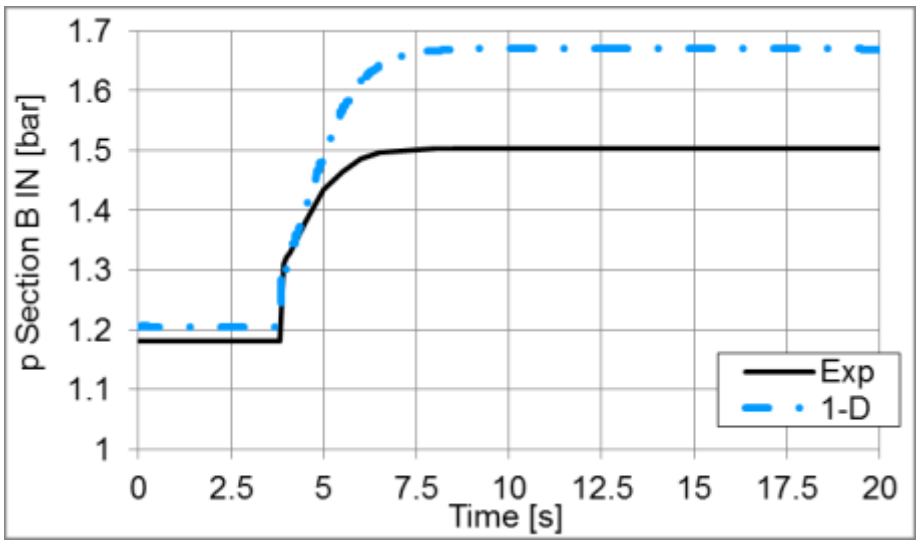

Figure 177 Pressure at inlet of turbine section B, experiment (black solid line), simulation with full 1-D unsteady turbine (blue dashed and dotted line); 1500 RPM

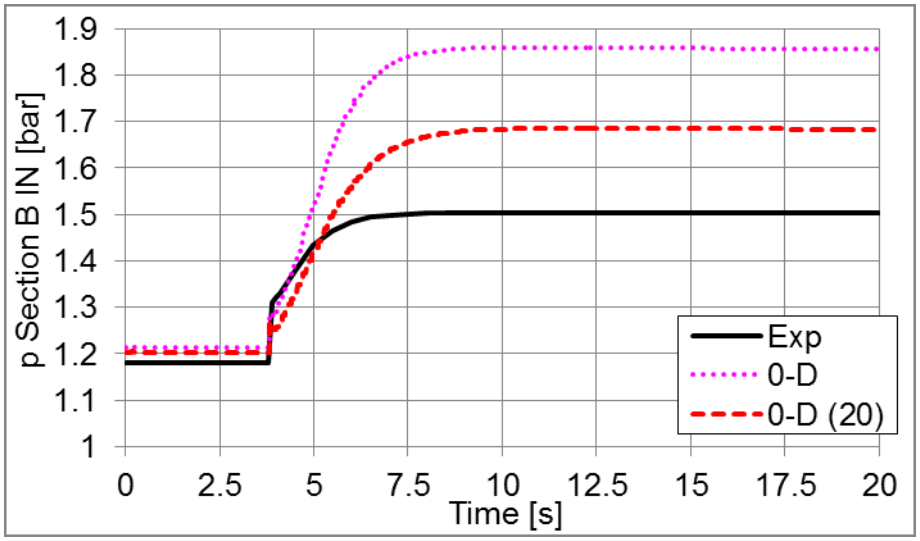

Figure 178 Pressure at inlet of turbine section B, experiment (black solid line), simulation with 0-D turbine map - sections without connection (purple dotted line), simulation with 0-D turbine map - sections connected via orifice D = 20 mm (red dashed line); 1500 RPM

The pressures downstream of the turbine are fully comparable in *Figure 179* and *Figure 180.*

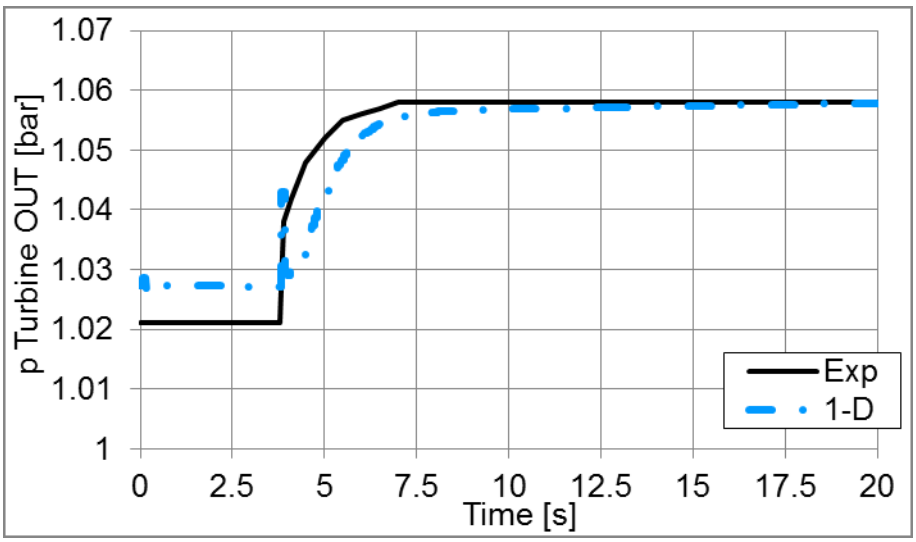

Figure 179 Pressure turbine downstream, experiment (black solid line), simulation with full 1-D unsteady turbine (blue dashed and dotted line); 1500 RPM

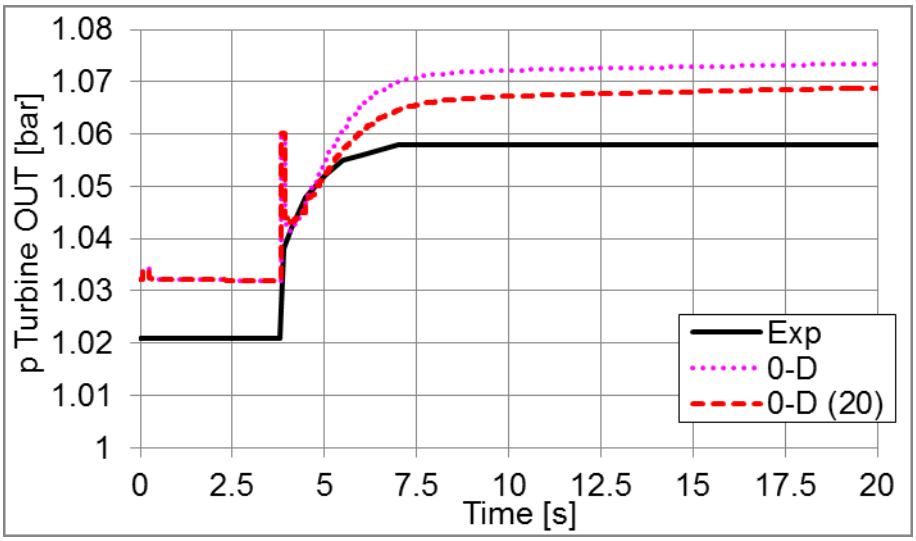

Figure 180 Pressure turbine downstream, experiment (black solid line), simulation with 0-D turbine map - sections without connection (purple dotted line), simulation with 0-D turbine map - sections connected via orifice D = 20 mm (red dashed line); 1500 RPM

The examples of the full 1-D turbine model results at the lowest and highest engine speed are in following pictures. The turbocharger speed during engine transient operation at constant engine speed of 900 RPM is in *Figure 181.*

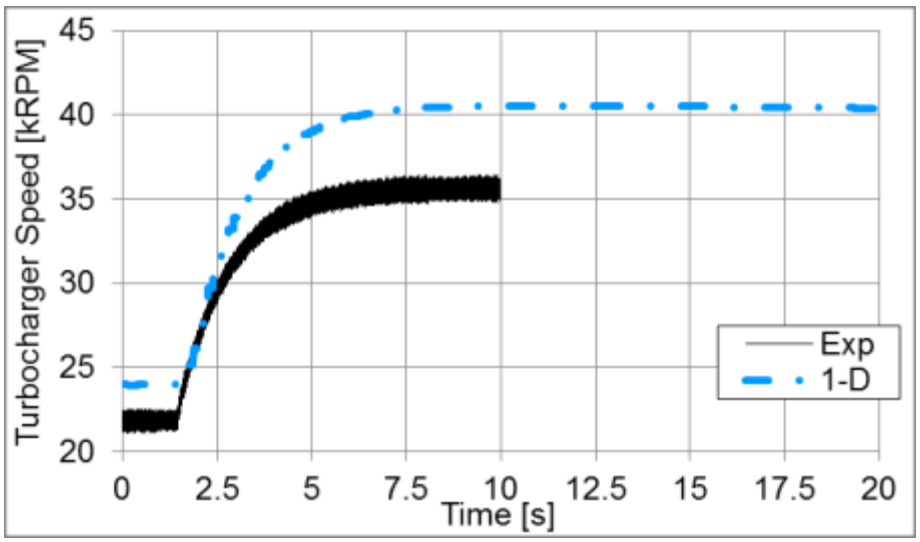

Figure 181 Turbocharger speed, experiment (black solid line), simulation with full 1-D unsteady turbine (blue dashed and dotted line); 900 RPM

The pressure downstream of the compressor predicted by the model with the full 1-D turbine is comparable with measurement in *Figure 182*. The measured signal is slightly delayed.

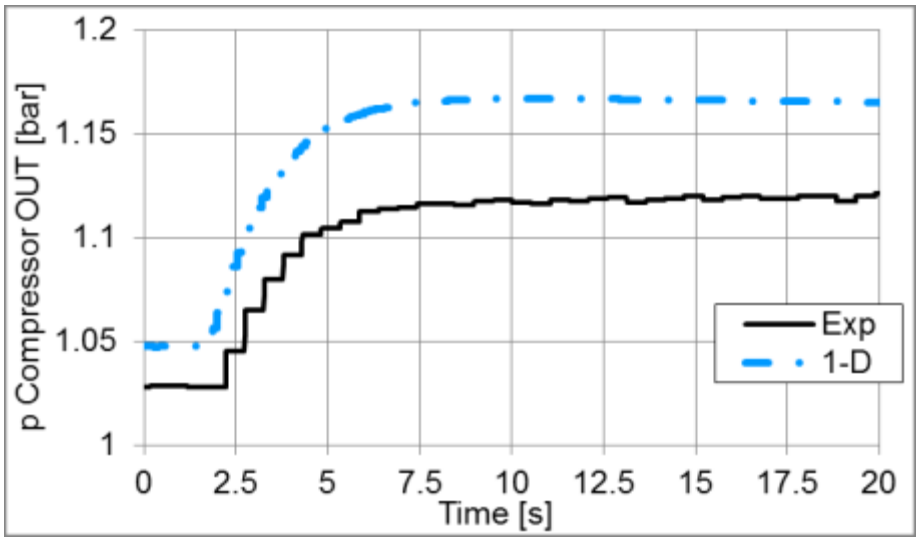

Figure 182 Pressure downstream of a compressor, experiment (black solid line), simulation with full 1-D unsteady turbine (blue dashed and dotted line); 900 RPM

The differences between simulated and measured pressures at inlet of turbine section A in *Figure 183* are insignificant.

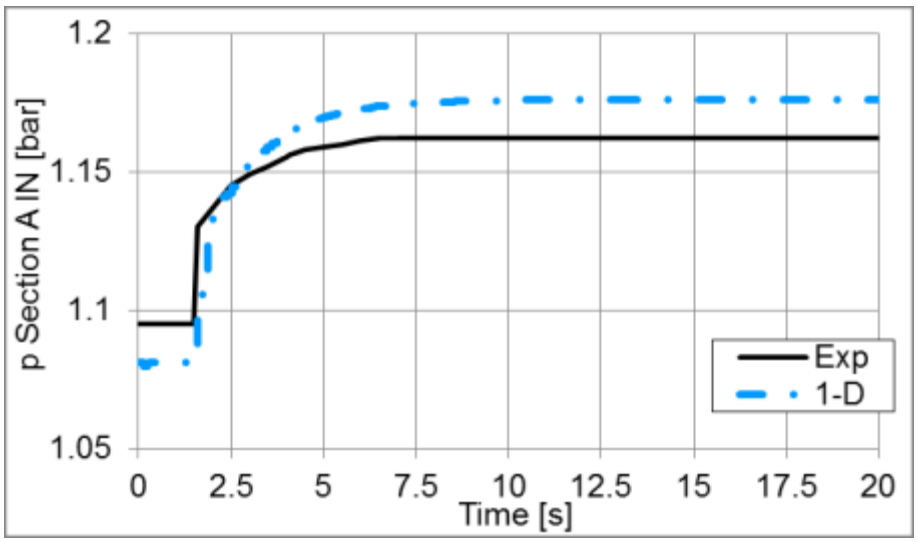

Figure 183 Pressure at inlet of turbine section A, experiment (black solid line), simulation with full 1-D unsteady turbine (blue dashed and dotted line); 900 RPM

The simulated turbocharger speed during the transient at highest engine speed of 2100 RPM is in *Figure 184*. The measured speed at the end of the transient is lower than the value from steady state experiment.

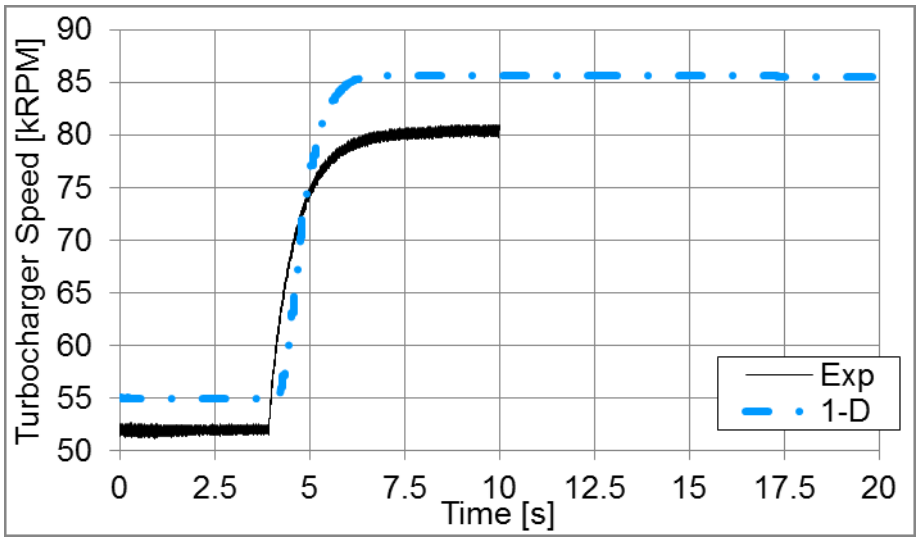

Figure 184 Turbocharger speed, experiment (black solid line), simulation with full 1-D unsteady turbine (blue dashed and dotted line); 2100 RPM

The pressure downstream of the compressor, predicted by the engine model with the full 1-D turbine, is in *Figure 185.*

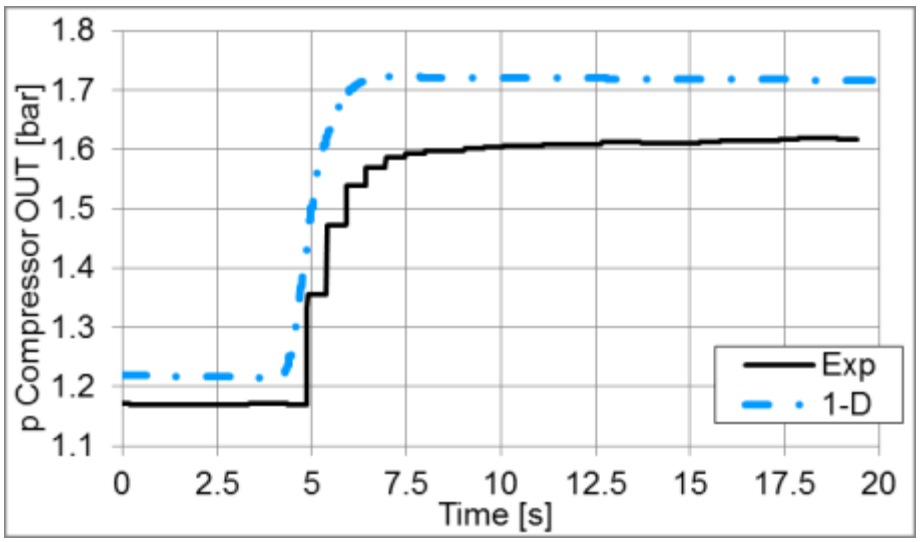

Figure 185 Pressure downstream of a compressor, experiment (black solid line), simulation with full 1-D unsteady turbine (blue dashed and dotted line); 2100 RPM

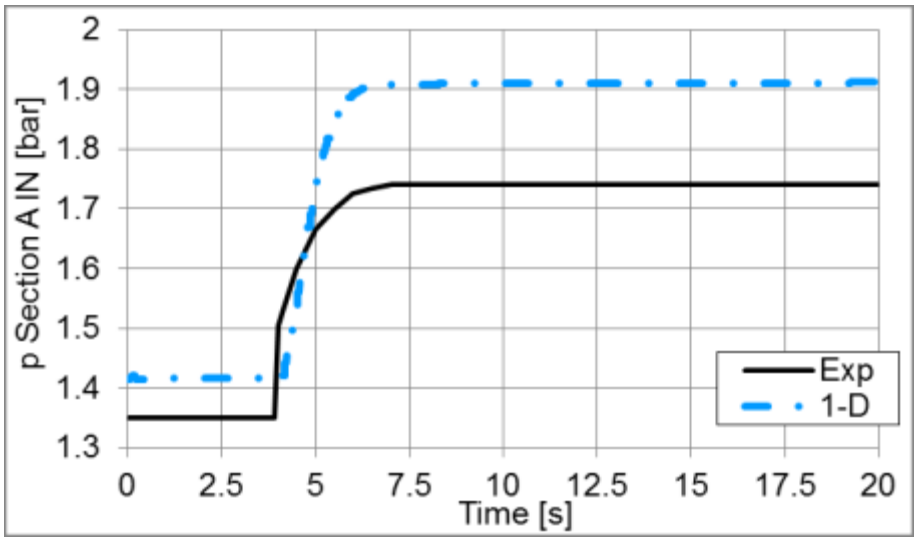

Figure 186 Pressure at inlet of turbine section A, experiment (black solid line), simulation with full 1-D unsteady turbine (blue dashed and dotted line); 2100 RPM

The pressure upstream of the turbine section A in *Figure 186*, performed by the full 1-D simulation, is consistent with previous results at engine speed of 2100 RPM, so the value at the end of transient corresponds with the value from steady state. The pressures measured downstream of a compressor and upstream of section A at the end of the transient are lower in comparison with the values from steady state. It has to be stressed that the 1-D model of a turbine is consistent in prediction of working conditions.

The summary of further results at engine transient operation, thus the simulations with 1-D and 0-D turbine models, is presented in Appendix 6.

8. Generalization of Results and Discussion

The developed unsteady 1-D model of a radial centripetal turbine with the twin scroll is modular. It is possible to adapt current version to specific design and dimensions of the required turbine and recalibrate the new model under steady flow conditions in compliance with experiments. The number of required measurements is relatively low, compared to classical map based approach, by virtue of the physical background of the model.

The model includes volute with two parallel sections. The design of each section is independent, thus the scrolls are generally asymmetrical. The number of turbine sections and their layout are practically unlimited. The model implicitly enables the single scroll turbine simulation. It is easy to close one section and the model then behaves like a single entry turbine. If required, the dimensions of the inlet volute and vaneless or bladed nozzle ring have to be tailored. The model is able to operate under adiabatic or diabatic conditions. The heat transfer in each part of the turbine model can be simulated, but it was not performed yet.

The current twin scroll turbine 1-D model, fully calibrated at steady flow conditions, enables to derive similar smaller and bigger size machines. The main dimensions would be tailored to a smaller and bigger turbine and steady flow calibration coefficients of the original measured and calibrated turbine would be utilized for the simulation purposes of virtual prototypes. The limits of the mentioned procedure should be identified in future.

The predictive capability of the physical based model, out of calibrated range, should be better in comparison with simplest multiplication of efficiency and mass flow rate in case of classical steady flow maps.

The turbine model presented in the thesis is completely prepared in GT-SUITE environment, but the model with the same features is possible to develop in any simulation software with similarly capable 1-D flow solver.

The steady flow calibration procedure may be carried out by independent optimization tool in conjunction with the primary simulation environment, where the turbine model was created.

The developed 1-D model of a twin scroll turbine proved its capability at steady and unsteady flow conditions. The unsteady conditions of highly pulsating flow of exhaust gases, typical of a turbocharged internal combustion engine, are generally demanding. The most important is the turbine model behaviour during fast transients. The fast response of the internal combustion engine during transient is as important as the overall engine parameters at full load, so the prediction of the turbocharger performance is essential.

The 1-D turbine model is able to simulate the backflow in each section. The current model was not calibrated for those conditions. The developed turbocharger test bed with separated sections upstream of a turbine is fully prepared for the measurement of backflow in turbine sections.

The specific turbocharger open-loop test bed for a twin scroll turbine is completely prepared and verified. The operation range of a turbine is limited by maximum mass flow rate via the test bed, maximum temperature downstream of the combustion chamber and employed compressor as a load. It enables to measure a twin scroll turbine under equal full admission and arbitrary unequal partial admission of an impeller.

The methodology of the measured steady flow data evaluation, including specific regression formulas for the compressor and turbine, and their utilization in the calibration process of the 1-D turbine model is also verified and ready to use for any turbocharger.

The full 1-D twin scroll turbine model is suitable for sensitivity analyses of main turbine features on overall parameters, because the phenomena inside the turbine are described by the model. In case of the 0-D model, which utilizes the turbine steady flow maps, the turbine itself is not modelled. The turbine model results may help at the beginning of the development process of a turbocharged internal combustion engine. The main features and parameters of the calibrated model are transferable to a similar turbine.

The map-less approach described in the thesis as a comprehensive methodology enables to create the physical based model of any turbocharger turbine. Relatively low number of measurements, compared with the map based approach, is required for the steady flow calibration process. The main dimensions of a turbine are also required. The experimental data from the steady flow turbocharger test bed are evaluated by the software developed for these purposes.

The physical based turbine model, full 1-D in our case, is calibrated at steady flow conditions in compliance with the measured values directly. The goal of the calibration procedure is to find out the proper combination of calibration coefficients, when the accordance of experimental and simulation results is the best. The fundamental values for simulation are mass flow rate via the turbine and corresponding turbine power.

The 1-D turbine model, fully calibrated at steady flow conditions, is then prepared for the unsteady and transient simulation connected with the model of the internal combustion engine. Neither the classical steady flow maps nor regressions are employed during the entire process for the appropriate turbine 1-D model development.

The map-less approach in relation to the 1-D turbine model provides useful information about the turbine as a machine, which is not known in case of the 0-D map based approach.

The advantage of the map-less approach will increase with the number of tested and calibrated turbines in relation to knowledge database, such as DASY, with the turbocharger library. The main features will be summarized and generalized.

The knowledge of turbine calibration coefficients tendencies in dependence on the turbine type, design and size, from the smallest to the biggest machine, would contribute to the increasing level of virtual prototypes.

8.1 Utilization of Developed Methodologies

The steady flow turbocharger test bed with open loop, complemented by the measuring section with separated branches upstream of a turbine, is completely ready for measurement of twin scroll turbines. The arbitrary level of the impeller admission is achievable via throttling in sections or section closure.

The requirements of map-less approach on the amount of experimental data are reasonable. The test bed can be of course utilized for the measurement of classical steady flow turbine maps. This method is relatively complicated by virtue of the huge number of required operating points under various admission levels, which are necessary for generation of sufficient maps describing the twin scroll turbine performance.

The appropriate software for measured data evaluation is fully capable to determine all physical quantities for the calibration procedure of the 1-D turbine model.

The twin scroll turbine 1-D model, after the steady flow calibration, is prepared for the simulation with the internal combustion engine at steady state and transients.

The steady flow simulation is suitable for sensitivity analyses of partial dimensions (scrolls, impeller, turbine outlet etc.) on overall turbine parameters, testing of new parts and solutions and also for scaling, thus for transformation of calibrated original to a similar virtual turbine.

The virtual turbine prototypes, based on the original calibrated physical 1-D model, may contribute to improvement of the entire turbine - compressor - internal combustion engine matching process. The obtained information may be helpful for higher level simulation such as 3-D CFD and also for the turbocharger manufacturer.

The regression formulas of the compressor, bearings and turbine can be tailored to tested machines. The regressions of turbine isentropic efficiency and discharge coefficient can be used for 0-D turbine maps with advantage.

The differences between the map-less approach with the physical based 1-D model of a turbine and the map based approach with the 0-D turbine model increase with the level of pulsating flow. The concept of a six cylinder engine equipped with a twin scroll turbine is almost ideal as discussed above. The situation is more complicated in case, when only two exhaust branches are connected in one turbine section, i.e. a four cylinder engine with a twin scroll turbine as presented in [52] and [51].

The full 1-D turbine model utilized in the engine simulation may be profitable at the beginning of the new turbocharged internal combustion engine development due to its predictive capability outside the original calibration range. The sensitivity analyses, based on physical models, would be advantageous during the decision-making process of turbocharger conception (single/twin scroll) and main dimensions (turbine housing and impeller) for a specific internal combustion engine and operating conditions with highest priority.

The comprehensive methodology that utilizes the map-less approach includes partial procedures, which are fundamental for the development of the relevant twin scroll turbine model. The number of required experiments on the steady flow turbocharger test bed is relatively low, but experiments are essential for the calibration procedure of the model. The turbine model, after calibration, is capable to predict the turbine performance under highly unsteady conditions including the phenomena inside the turbine. The simulation results are not perfect and never will be, but the level of current results is satisfactory.

Advantages of map-less approach:

The steady flow turbine maps are not required during the entire development process, but may be generated with advantage of the 1-D approach. It is not required to measure huge set of the steady flow maps for each level of the impeller admission. The number of measured operating points for the turbine description at different level of admission is relatively low in the case of map-less approach.

The map-less approach utilizes the entire turbine model, which involves the volumes inside a turbine and their natural accumulation of mass at unsteady operating conditions like a real machine. This feature is important at unsteady and transient conditions. The model is thus fully unsteady with mixing of flows at nozzle ring and proper conditions. It enables to achieve extreme partial admission including the backflow in sections.

The full 1-D turbine model also enables the sensitivity analyses of main dimensions on the overall parameters, which are important for the development of a similar virtual turbine. The virtual turbine may be beneficial at the beginning of the new internal combustion engine development.

The physical background of the turbine model enables extrapolation of the parameters outside the calibrated range. The physical approach should be generally more capable for the development of virtual prototypes, based on a calibrated similar turbine.

In case of the 0-D map based approach, the turbine is not modelled but only described by the steady flow maps, which are fitted by the simulation software.

Disadvantages of map-less approach:

The turbine 1-D model requires the knowledge of the geometric dimensions of main turbine parts such as scrolls, impeller and outlet part.

The current calibration process with many calibration coefficients is generally demanding and time-consuming.

The computational time requirement of the full 1-D turbine model at unsteady operation is notably higher, compared with the 0-D approach.

The usage of the steady flow turbine map in combination of the 0-D turbine model is simple, fast and operative.

8.2 Suggestions of Future Work

The future work suggestions from all areas of research presented in the thesis are briefly discussed below.

The power losses in bearings of the turbocharger shaft influence the overall turbine parameters. The measurement should be improved by increase of the oil mass flow rate via the turbocharger, increase of oil temperature and time duration of each test. The sophisticated model of specific bearings would improve the prediction of losses.

The procedure of measurement on the steady flow turbocharger test bed should be improved step by step. It would be beneficial to calculate the overall pressure ratio of a twin scroll turbine online and measure it at constant pressure ratio. It would be helpful to identify the problems of measurement under cold conditions, when the turbine is driven by cold air. The current results are not fully satisfactory. The measurement of a different turbine would help to analyse the known and unknown problems. The measurement of the backflow in sections is not essential, because the phenomenon is not so important, but it would be interesting to try it. It would be also helpful to test the partial admission of an impeller subsequently with throttling in both sections of a turbine.

The calibration procedure of the 1-D turbine model might be simpler and partially automatic in relation to independent optimization tool with sophisticated algorithms. The user has to enter specific turbine geometric dimensions, experimental data for comparison and limits of each calibration coefficient. After the initial learning phase, the optimization tool is able to decide about further progress and find the best fit of experimental and simulation results independently.

The next evolution of the turbine model might be simplified by removing of parts which are not essential, implementation of new templates with extended functions and reduction of the number of calibration coefficients. Lower number of calibration coefficients would be very helpful for the turbine calibration process.

The influence of the additional nozzle placed downstream of the zone of flow mixing should be also verified in the future. The nozzle located downstream of the flowsplit template may improve the results of the unsteady on-engine simulation.

The predictive capability of the twin scroll turbine model in case of overall pressure ratio and pressure differences between sections should be improved.

The sensitivity analysis of main turbine dimensions and their accuracy on the overall results of the turbine model would be useful for the estimation of virtual prototypes relevance.

Testing of new components such as waste gate (WG), exhaust gas recirculation valves (EGR) or turbine outlet diffuser should be performed in the future research.

The longtime goal is the extensive library of turbocharger models, as a part of appropriate knowledge database, based on the map-less approach, which can be also utilized for purposes of virtual prototypes.

9. Conclusions

The main goal of the thesis was to develop, validate and verify the comprehensive methodology, which utilizes the map-less approach for radial centripetal turbines equipped with the twin scroll. The map-less approach does not utilize the classical steady flow maps of a turbine during entire process of the full 1-D turbine model development.

The specific steady flow turbocharger test bed with separated turbine sections for measurement of the twin entry turbines was developed. The open loop hot gas stand is suitable for achievement of the arbitrary level of turbine impeller admission. The unequal partial level of admission is reached via the throttling in a turbine section and extreme partial admission by closure of one section.

The mentioned steady flow test bed was developed by means of the virtual turbocharger test bed models [SW 1]. The required set of twin scroll turbine measurements under arbitrary level of admission was also proposed and properly simulated on the created virtual test bed.

The selected type of a turbocharger with the twin scroll was properly measured under steady flow at the described real hot gas stand. The turbine was tested under different level of impeller admission and load.

All experimental data, measured on the steady flow turbocharger test bed, were evaluated by the in-house software developed for the purposes [SW 2]. The software includes the evaluation of the compressor power under adiabatic conditions, power losses in bearings and all relevant physical quantities, which describe the twin scroll turbine behaviour under steady flow conditions. The data are necessary for the calibration process of the full 1-D twin scroll turbine model. The results were presented in [49] and [48].

The same type of the turbocharger was measured under real conditions in conjunction with a diesel engine. The experimental internal combustion engine with six cylinder in-line design is ideal for the twin entry turbine. The high pulsating flow in separated exhaust branches and optimal firing between cylinders are proper operating conditions for the twin scroll turbine. The measurement chain of the internal combustion engine focused on the turbine behaviour. The important pressures at the engine and upstream/downstream of the turbine were indicated. The steady states and also transients at constant engine speeds were measured.

The aim of the experiments was to obtain relevant data, which are essential for the verification of the twin scroll turbine model predictive capability under highly pulsating flow of exhaust gases, thus the real operating conditions of a turbocharger turbine.

For the verification of the full 1-D twin scroll turbine model performance in engine simulation, a detailed model of the experimental internal combustion engine was created in GT-SUITE environment [SW 4]. The model of the six cylinder diesel engine equipped with a twin entry turbine was properly calibrated using the

experimental data. A single cylinder engine model was derived for the evaluation of the experimental data, especially for the three pressure analyses.

The developed modular unsteady full 1-D model of a radial centripetal turbine with twin scroll is a suitable tool for the description of the interactions between the internal combustion engine and a turbocharger [SW 3]. The model also describes the phenomena inside a turbine with mixing of flows upstream of the impeller at proper location under valid conditions in sections. The potential of the modular unsteady 1-D model of a radial centripetal turbine with the twin scroll consists in the physical description of the whole machine. The development process of the model was supported by the experience from previous turbine models presented in [56] and [53].

The physical approach respects conditions for mixing of flows inside the scroll, asymmetry of flow admission, turbine scroll design, dimensions of the impeller and interactions among the parts inside a radial turbine.

The twin scroll turbine model described in the thesis is built in the GT-SUITE simulation software, but the model might be created in any simulation environment with similarly capable 1-D flow solver.

The turbine model was properly calibrated at steady flow conditions using the experimental data measured on the turbocharger test bed. The best accordance of simulation and experimental results was achieved by proper combination of calibration coefficients. Both results, measured and simulated under steady flow, are not perfect and future improvement is desired. The 1-D model of a twin scroll turbine, after steady flow calibration process, is ready for highly unsteady simulation under pulsating flow conditions.

The predictive capability level of the turbine model during unsteady simulation with the internal combustion engine, especially at engine transient conditions, is the most important for the turbine model utilization in practice. The robustness of the developed twin scroll turbine model was proven under unsteady conditions of highly pulsating flow of exhaust gases on the engine. The results of unsteady engine simulation with the 1-D turbine model are satisfactory at engine steady states and also during transient operation at constant engine speed.

The comprehensive methodology utilizing the map-less approach was validated and verified on the tested radial turbine with the twin scroll. The results of entire process from measurement on the steady flow turbocharger test bed, evaluation of measured data and their employment along the calibration of a turbine model, were verified by the unsteady engine simulation with the full 1-D turbine model and comparison with corresponding data measured on the internal combustion engine. The map-less approach was presented in [51] and [46].

The developed, validated and verified methodology with the map-less approach is fully prepared for the employment in practice. The differences between the physical map-less approach and map based approach increase with the level of pulsating flow and under extreme conditions during the engine transient operation. The simulation study of a turbocharged four cylinder engine with comparison of both mentioned approaches was presented in [52].

The simulation support of experiments, higher simulation and design, based on the full 1-D turbine models, may contribute to the acceleration of turbocharger and internal combustion engine development process. The preliminary turbocharger design, i.e. main dimensions of the divided symmetrical or asymmetrical scroll, turbine impeller and outlet may be optimized using the developed unsteady 1-D model. The derived model is still based on the physical description of the machine.

References

[1] DIXON S. L.: Fluid Mechanics, Thermodynamics of Turbomachinery. Pergamon Press London 1975

[2] ZINNER, K., “Supercharging of Internal Combustion Engines”. Springer Heidelberg 1978

[3] HEYWOOD, J. B.: Internal Combustion Engine Fundamentals. McGraw-Hill series in mechanical engineering, printed in USA. McGraw-Hill, 1988. ISBN 0-07-028637-X.

[4] GT-SUITE Application Manuals, version 7.3, Gamma Technologies Inc., Westmont, IL, 2012.

[5] Romagnoli A, Martinez-Botas R, Performance prediction of a nozzled and nozzleless mixed-flow turbine in steady conditions, INTERNATIONAL JOURNAL OF MECHANICAL SCIENCES, Vol: 53, Pages: 557-574, ISSN: 0020-7403, 2011

[6] Romagnoli A, Martinez-Botas RF, Rajoo S., Steady state performance evaluation of variable geometry twin-entry turbine, INTERNATIONAL JOURNAL OF HEAT AND FLUID FLOW, Vol: 32, Pages: 477-489, ISSN: 0142-727X, 2011

[7] Serrano, J.R., Arnau F.J., Dolz V., Tiseira A., Cervelló C., A model of turbocharger radial turbines appropriate to be used in zero- and one-dimensional gas dynamics codes for internal combustion engines modelling, Energy Conversion and Management, Vol: 49, Pages: 3729–3745, ISSN: 0196-8904, 2008

[8] Payri F., Serrano J.R., Fajardo P., Reyes-Belmonte M.A., Gozalbo-Belles R., A physically based methodology to extrapolate performance maps of radial turbines, Energy Conversion and Management, Vol: 55, Pages: 149–163, ISSN: 0196-8904, 2012

[9] Chiong MS, Rajoo S, Martinez-Botas RF, Costall AWet al., Engine turbocharger performance prediction: One-dimensional modeling of a twin entry turbine, ENERGY CONVERSION AND MANAGEMENT, Vol: 57, Pages: 68-78, ISSN: 0196-8904, 2012

[10] Chiong MS, Rajoo S, Romagnoli A, Costall AW, Martinez-Botas RFet al., Integration of meanline and one-dimensional methods for prediction of pulsating performance of a turbocharger turbine, ENERGY CONVERSION AND MANAGEMENT, Vol: 81, Pages: 270-281, ISSN: 0196-8904, 2014

[11] Galindo J., Tiseira A., Fajardo P., García-Cuevas L.M.,Development and validation of a radial variable geometry turbine model for transient pulsating flow applications, ENERGY CONVERSION AND MANAGEMENT, Vol: 85, Pages: 190-203, ISSN: 0196-8904, 2014

[12] Chiong MS, Rajoo S, Romagnoli A, Costall AW, Martinez-Botas RFet al., Non-adiabatic pressure loss boundary condition for modelling turbocharger turbine pulsating flow, ENERGY CONVERSION AND MANAGEMENT, Vol: 93, Pages: 267-281, ISSN: 0196-8904, 2015

[13] De Bellis V., Marelli S., Bozza F., Capobianco M., 1D simulation and experimental analysis of a turbocharger turbine for automotive engines under steady and unsteady flow conditions, 68th Conference of the Italian Thermal Machines Engineering Association, ATI2013, Energy Procedia, Vol: 45, Pages: 909-918, ISSN: 1876-6102, 2014

[14] Hu, X. and Lawless, P., "Predictions of On-Engine Efficiency for the Radial Turbine of a Pulse Turbocharged Engine," SAE Technical Paper 2001-01-1238, 2001, doi:10.4271/2001-01-1238.

[15] Westin, F. and Ångström, H., "Calculation Accuracy of Pulsating Flow through the Turbine of SI-Engine Turbochargers - Part 1 Calculations for Choice of Turbines with Different Flow Characteristics," SAE Technical Paper 2005-01-0222, 2005, doi:10.4271/2005-01-0222.

[16] Westin, F. and Ångström, H., "Calculation Accuracy of Pulsating Flow through the Turbine of SI-engine Turbochargers - Part 2 Measurements, Simulation Correlations and Conclusions," SAE Technical Paper 2005-01-3812, 2005, doi:10.4271/2005-01-3812.

[17] Winkler, N., Ångström, H., and Olofsson, U., "Instantaneous On-Engine Twin-Entry Turbine Efficiency Calculations on a Diesel Engine," SAE Technical Paper 2005-01-3887, 2005, doi:10.4271/2005-01-3887.

[18] Winkler, N. and Ångström, H., "Study of Measured and Model Based Generated Turbine Performance Maps within a 1D Model of a Heavy-Duty Diesel Engine Operated During Transient Conditions," SAE Technical Paper 2007-01-0491, 2007, doi:10.4271/2007-01-0491.

[19] Hellstrom, F., Renberg, U., Westin, F., and Fuchs, L., "Predictions of the Performance of a Radial Turbine with Different Modeling Approaches: Comparison of the Results from 1-D and 3-D CFD," SAE Technical Paper 2010-01-1223, 2010, doi:10.4271/2010-01-1223.

[20] Serrano, J., Pla, B., Gozalbo, R., and Ospina, D., "Estimation of the Extended Turbine Maps for a Radial Inflow Turbine," SAE Technical Paper 2010-01-1234, 2010, doi:10.4271/2010-01-1234.

[21] Sakellaridis, N. and Hountalas, D., "Meanline Modeling of Radial Turbine Performance for Turbocharger Simulation and Diagnostic Applications," SAE Technical Paper 2013-01-0924, 2013, doi:10.4271/2013-01-0924.

[22] De Bellis, V., Bozza, F., Schernus, C., and Uhlmann, T., "Advanced Numerical and Experimental Techniques for the Extension of a Turbine Mapping," SAE Int. J. Engines 6(3):2013, doi:10.4271/2013-24-0119.

[23] De Bellis, V., Marelli, S., Bozza, F., and Capobianco, M., "Advanced Numerical/Experimental Methods for the Analysis of a Waste-Gated Turbocharger Turbine," SAE Int. J. Engines 7(1):2014, doi:10.4271/2014-01-1079.

[24] Serrano, J., Arnau, F., Novella, R., and Reyes-Belmonte, M., "A Procedure to Achieve 1D Predictive Modeling of Turbochargers under Hot and Pulsating Flow Conditions at the Turbine Inlet," SAE Technical Paper 2014-01-1080, 2014, doi:10.4271/2014-01-1080.

[25] Schorn, N., "The Radial Turbine for Small Turbocharger Applications: Evolution and Analytical Methods for Twin-Entry Turbine Turbochargers," SAE Int. J. Engines 7(3):2014, doi:10.4271/2014-01-1647.

[26] Cavina, N., Borelli, A., Calogero, L., Cevolani, R. et al., "Turbocharger Control-Oriented Modeling: Twin-Entry Turbine Issues and Possible Solutions," SAE Int. J. Engines 8(5):2015, doi:10.4271/2015-24-2427.

[27] Hribernik, A., Dobovišek, Z., and Černej, A., "Determination of Twin-Turbine Discharge Coefficients Under Partial Admission Conditions," SAE Technical Paper 930192, 1993, doi:10.4271/930192.

[28] Brinkert N., Sumser S., Schulz A., Weber S., Fieweger K. and Bauer H.-J., Understanding the twin-scroll turbine-flow similarity. ASME Turbo Expo, GT2011-46820, 49:2207–2218, 2011.

[29] Fredriksson C. F., Xuwen Qiu, Baines N. C., Müller M., Brinkert N. and Gutmann C., Meanline Modeling of Radial Inflow Turbine With Twin-Entry Scroll. ASME Turbo Expo 2012,doi:10.1115/GT2012-69018

[30] Aymanns R., Scharf J., Uhlmann T., Pischinger S.,Turbocharger Efficiencies in Pulsating Exhaust Gas Flow, MTZ, Vol. 73, 07-08/2012.

[31] Lückmann D., Uhlmann T., Kindl H., Pischinger S., Separation in Double Entry Turbine Housings at Boosted Gasoline Engines. MTZ, Vol. 74, 10/2013

[32] Uhlmann, T., et al. "Development and Matching of Double Entry Turbines for the Next Generation of Highly Boosted Gasoline Engines." 34th International Vienna Motor Symposium. 2013.

[33] Macek, J. and Vitek, O., "Determination and Representation of Turbocharger Thermodynamic Efficiencies," SAE Technical Paper 2016-01-1042, 2016, doi:10.4271/2016-01-1042.

[34] Macek, J., Vítek, O., Burič, J., and Doleček, V., "Comparison of Lumped and Unsteady 1-D Models for Simulation of a Radial Turbine," SAE Int. J. Engines 2(1):173-188, 2009, doi:10.4271/2009-01-0303.

[35] Vítek, O., Macek, J., and Polášek, M., "New Approach to Turbocharger Optimization using 1-D Simulation Tools," SAE Technical Paper 2006-01-0438, 2006, doi:10.4271/2006-01-0438.

[36] Macek, J. and Vítek, O., "Simulation of Pulsating Flow Unsteady Operation of a Turbocharger Radial Turbine," SAE Technical Paper 2008-01-0295, 2008, doi:10.4271/2008-01-0295.

[37] Macek, J., Vávra, J., and Vítek, O., "1-D Model of Radial Turbocharger Turbine Calibrated by Experiments," SAE Technical Paper 2002-01-0377, 2002, doi:10.4271/2002-01-0377.

[38] Vávra, J., Macek, J., Vítek, O., and Takáts, M., "Investigation of Radial Turbocharger Turbine Characteristics under Real Conditions," SAE Technical Paper 2009-01-0311, 2009, doi:10.4271/2009-01-0311.

[39] MACEK, J.: Spalovací motory I., (in Czech), Nakladatelství ČVUT, vydání první, 2007, Praha, ISBN 978-80-01-03618-1

[40] MACEK, J. - KLIMENT, V.: Spalovací turbiny, turbodmychadla a ventilátory (Přeplňování spalovacích motorů). (in Czech) Nakladatelství ČVUT, vydání čtvrté, 2006, Praha, ISBN 80-01-03529-8

[41] BAUMRUK, P.: Problematika náplně válce spalovacích motorů. (in Czech) Vydavatelství ČVUT, vydání druhé, 1999, Praha, ISBN 80-01-02010-X

[42] STREDA I.: Dynamika plynu, (in Czech) Edicni stredisko CVUT, Praha, 1984

[43] WOSCHNI, G., A universally applicable equation for the instantaneous heat transfer coefficient in the internal combustion engine. SAE paper 670931. 1967.

[44] WOSCHNI, G., Prediction of thermal loading of supercharged diesel engines. SAE paper 790821. 1979.

[45] Bogomolov, S., Macek, J., Mikulec, A., and Valasek, M., "Design Assistance System and Its Application," SAE Technical Paper 2012-01-0916, 2012, doi:10.4271/2012-01-0916.

[46] Vitek O., Macek J., Zak Z. (2017). Chap. 9, The Physical Model of a Radial Turbine with Unsteady Flow Used for the Optimization of Turbine Matching. In E. G. Giakoumis, Turbochargers and Turbocharging: Advancements, Applications and Research. NY USA: Nova Science Publishers, Inc. ISBN: 978-1-53612-239-8

[47] ZAK, Z., EMRICH, M., TAKATS M., MACEK, J.: In-Cylinder Heat Transfer Modelling. In: MECCA Journal of Middle European Construction and Design of Cars. 2016, vol.14, no.3, p.2-10. ISSN (Online) 1804-9338, DOI: https://doi.org/10.1515/mecdc-2016-0009

[48] ZAK, Z., MACEK, J., HATSCHBACH, P.: Evaluation of Experiments on a Twin Scroll Turbocharger Turbine for Calibration of a Complex 1-D Model. In: MECCA Journal of Middle European Construction and Design of Cars. 2016, vol.14, no.3, p.11-18. ISSN (Online) 1804-9338, DOI: https://doi.org/10.1515/mecdc-2016-0010.

[49] ZAK, Z., MACEK, J., HATSCHBACH, P.: Measurement of Twin Scroll Turbine Performance Under Steady Flow. In: Proceedings of XLVII. Conference of ICE Research Depts. of Czech and Slovak Universities. KOKA 2016. Brno: Brno University of technology, Faculty of mechanical engineering, Institute of automotive engineering. 2016.

[50] ZAK, Z., HVEZDA, J., MACEK, J., EMRICH, M., TAKATS M..: User Model in GT-SUITE. In: Proceedings of XLVII. Conference of ICE Research Depts. of Czech and Slovak Universities. KOKA 2016. Brno: Brno University of technology, Faculty of mechanical engineering, Institute of automotive engineering. 2016.

[51] Zak Z., Macek J., Vitek O., Emrich M., Takats M., Hatschbach P., Vavra J.: Physical Model of a Twin Scroll Turbine in GT-SUITE. 2015 European GT Conference. Frankfurt am Main. 2015

[52] MACEK, J., ZAK, Z., VITEK, O.: "Physical Model of a Twin-scroll Turbine with Unsteady Flow," SAE Technical Paper 2015-01-1718, 2015, doi:10.4271/2015-01-1718.

[53] ZAK, Z., VITEK, O., MACEK, J.: Application of a Radial Turbine 1-D Model. In: MECCA Journal of Middle European Construction and Design of Cars. 2013, vol. 11, no. 1, p. 1-8. ISSN 1214-0821, ISSN 1804-9338 (Online)

[54] ZAK, Z., HVEZDA, J., EMRICH, M., MACEK, J., CERVENKA, L.: Utilization of Multi-zone Model Results in SI Engine Modeling. In: MECCA Journal of Middle European Construction and Design of Cars. 2012, vol. 10, no. 2, p. 23-30. ISSN 1214-0821.

[55] POHORELSKY, L., ZAK, Z., MACEK, J., and VITEK, O., "Study of Pressure Wave Supercharger Potential using a 1-D and a 0-D Approach," SAE Int. J. Engines 4(1):1331-1353, 2011, doi:10.4271/2011-01-1143.

[56] MACEK, J., VITEK, O., ZAK, Z.: "Calibration and Results of a Radial Turbine 1-D Model with Distributed Parameters," SAE Technical Paper 2011-01-1146, 2011, doi:10.4271/2011-01-1146.

[57] MACEK, J., VITEK, O., POHORELSKY, L., ZAK, Z.,: Pressure Wave Supercharger 0-D Model. In: MECCA Journal of Middle European Construction and Design of Cars. 2011, vol. 9, no. 1, p. 32-39. ISSN 1214- 0821.

[58] MACEK, J., VITEK, O., POHORELSKY, L., ZAK, Z.,: Simulating Boost Pressure System by Differential or Algebraic Equations Model. In: MECCA Journal of Middle European Construction and Design of Cars. 2010, vol. 8, no. 3 and 4, p. 26-34. ISSN 1214-0821.

[59] POHORELSKY, L., ZAK, Z., MACEK, J., VITEK, O.: Study of Pressure Wave Supercharger Potential using a 1-D Approach. In: MECCA Journal of Middle European Construction and Design of Cars. 2010, vol. 8, no. 2, p. 5-13. ISSN 1214-0821.

[60] ZAK, Z.: The Influence of Turbocharger System on Compression Ignition Engine Efficiency. Diploma Thesis (Master degree) D2008 - M 12, Faculty of Mechanical Engineering, Czech Technical University in Prague, Prague 2008.

Software References

[SW 1] ZAK, Z.: Models of turbocharger test beds in GT-SUITE [Software], CTU in Prague, Faculty of Mechanical Engineering, Library of software 12201, 2017

[SW 2] ZAK, Z.: Software for evaluation of the experimental data measured on the turbocharger test bed [Software], CTU in Prague, Faculty of Mechanical Engineering, Library of software 12201, 2017

[SW 3] ZAK, Z.: Full 1-D unsteady model of a radial centripetal turbine with twin scroll in GT-SUITE [Software], CTU in Prague, Faculty of Mechanical Engineering, Library of software 12201, 2017

[SW 4] ZAK, Z.: Models of the experimental diesel engine John Deere 6068 in GT-SUITE (single cylinder model for TPA included) [Software], CTU in Prague, Faculty of Mechanical Engineering, Library of software 12201, 2017

Appendices

Appendix 1 - Compressor with Larger Wheel

The measured data and regression results of compressor with larger wheel are presented in following pictures.

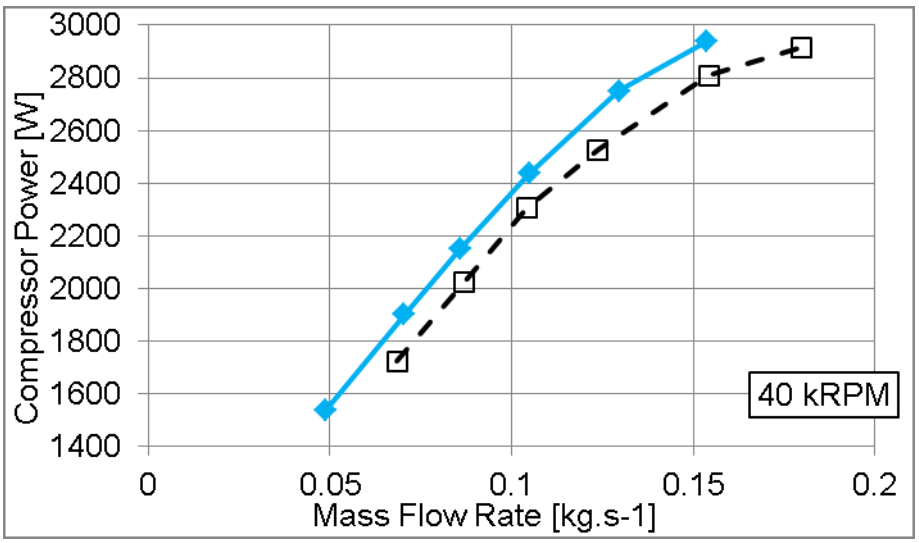

Figure 187 Compressor power evaluated from measured temperature difference (compressor with larger wheel); turbine driven by exhaust gases (blue); turbine driven by cold air (black dashed line); turbocharger speed 40 kRPM

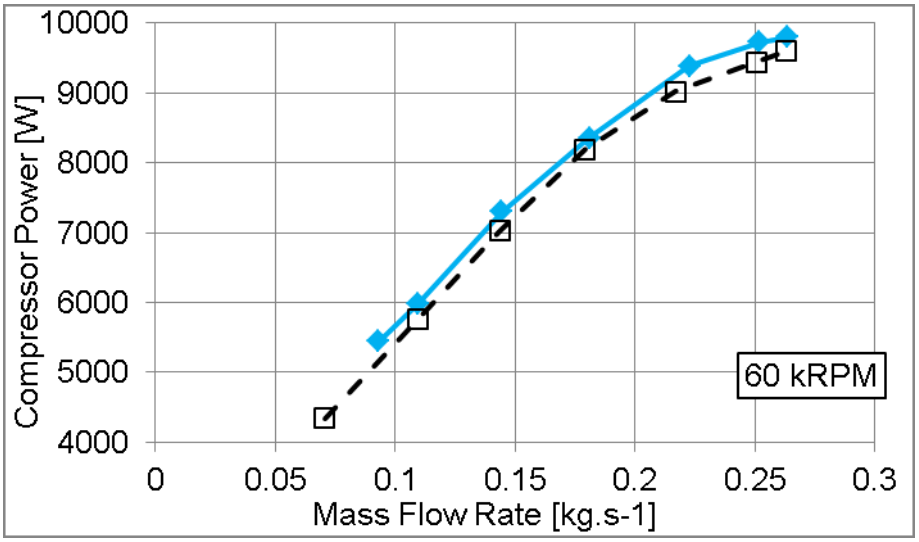

Figure 188 Compressor power evaluated from measured temperature difference (compressor with larger wheel); turbine driven by exhaust gases (blue); turbine driven by cold air (black dashed line); turbocharger speed 60 kRPM

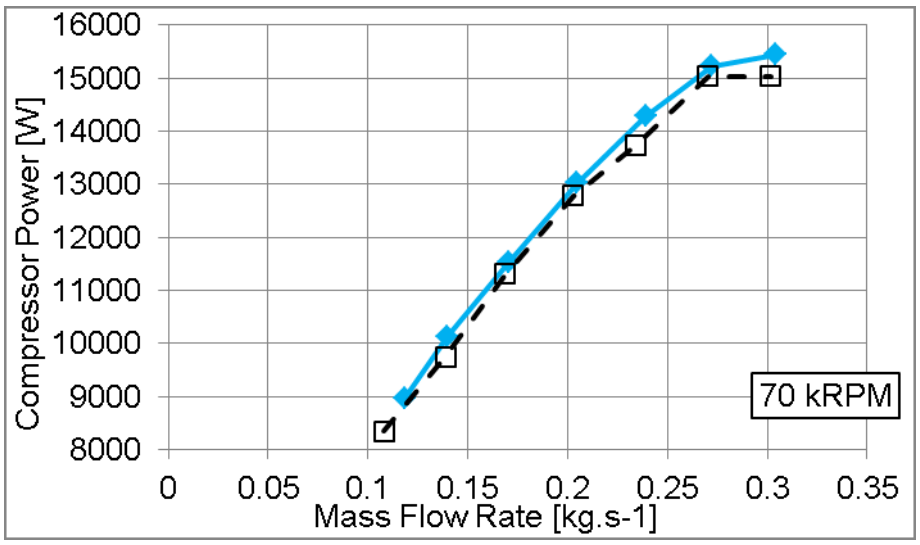

Figure 189 Compressor power evaluated from measured temperature difference (compressor with larger wheel); turbine driven by exhaust gases (blue); turbine driven by cold air (black dashed line); turbocharger speed 70 kRPM

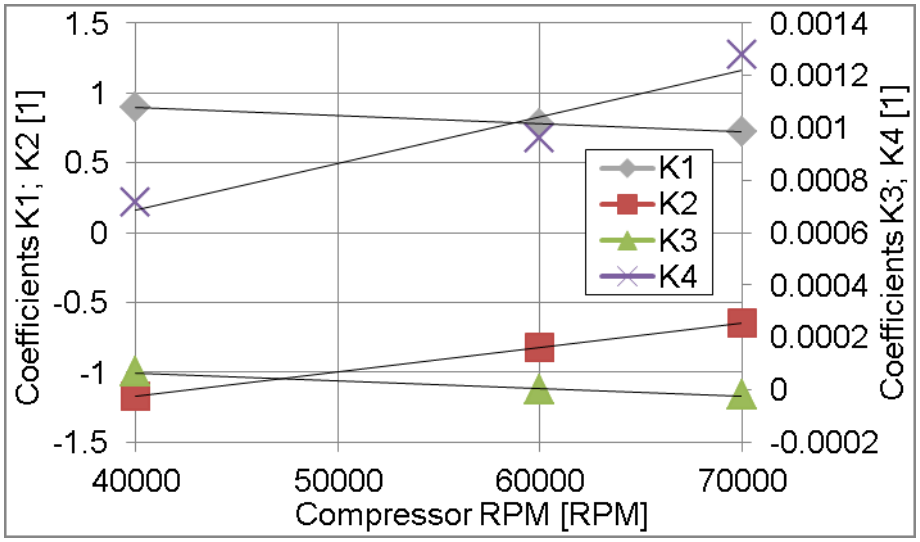

Figure 190 Courses of regression coefficients K1 - K4 used in formula for calculation of compressor power (type with larger wheel)

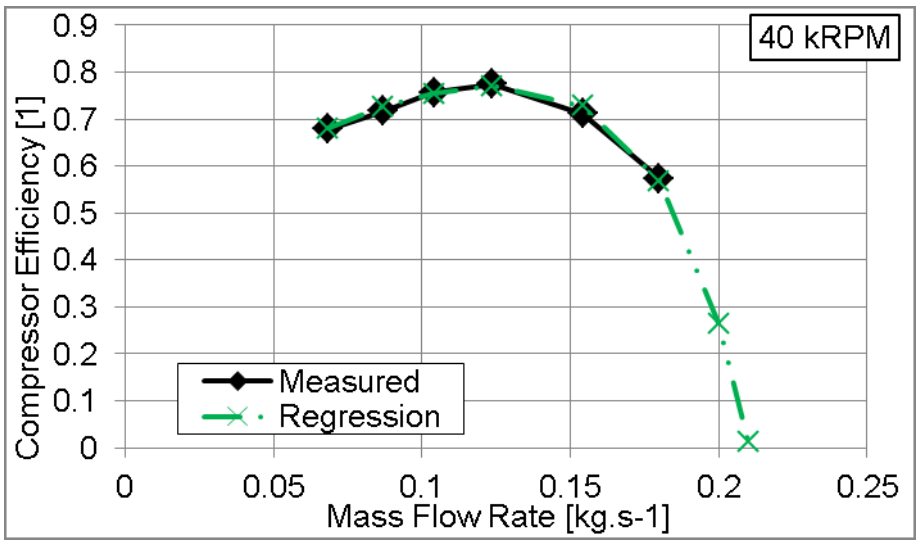

Figure 191 Comparison of measured compressor efficiency (turbine driven by cold air) with results of regression formula; larger compressor wheel; turbocharger speed 40 kRPM

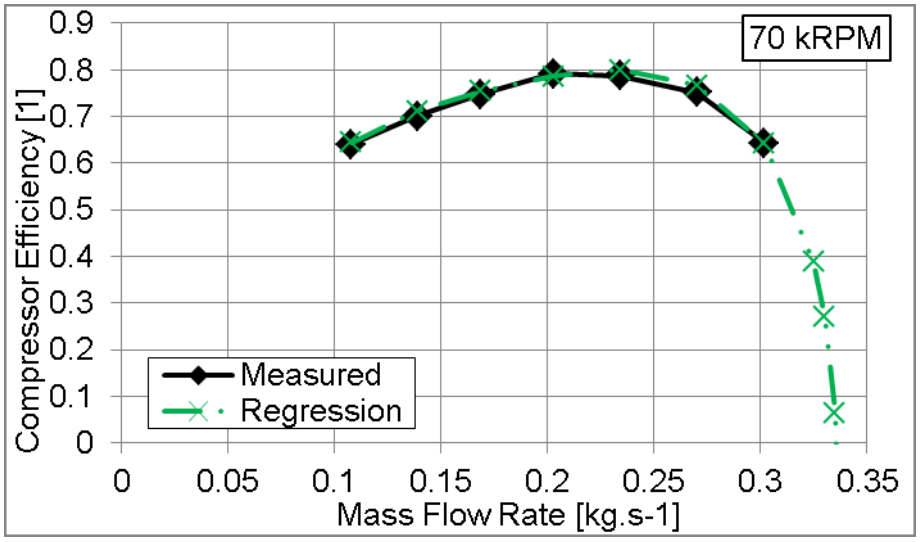

Figure 192 Comparison of measured compressor efficiency (turbine driven by cold air) with results of regression formula; larger compressor wheel; turbocharger speed 70 kRPM

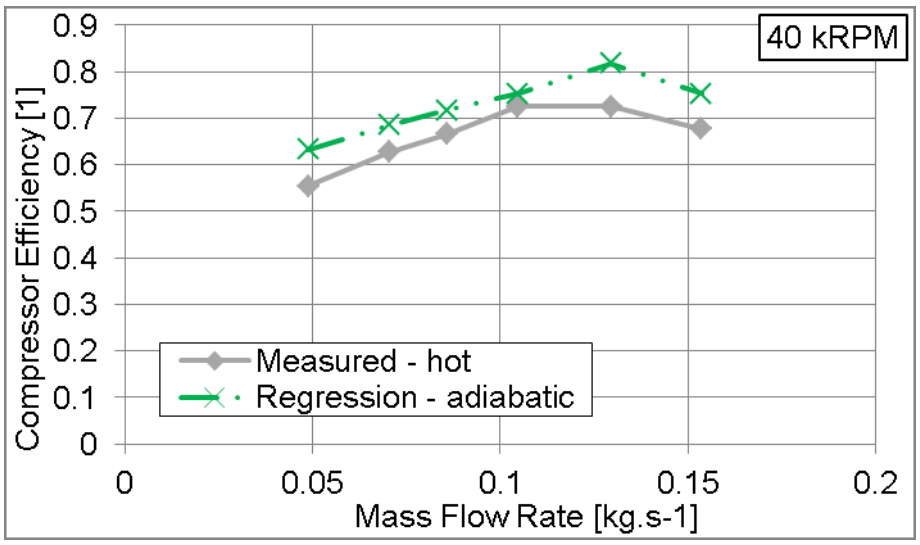

Figure 193 Comparison of measured compressor efficiency (turbine driven by exhaust gases) and efficiency of the adiabatic machine based on regression formula; compressor with larger wheel; turbocharger speed 40 kRPM

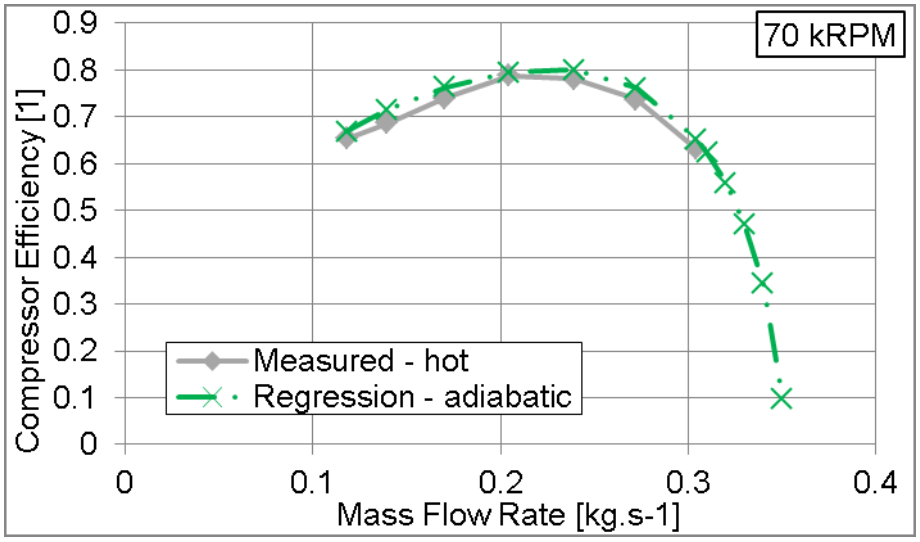

Figure 194 Comparison of measured compressor efficiency (turbine driven by exhaust gases) and efficiency of the adiabatic machine based on regression formula; compressor with larger wheel; turbocharger speed 70 kRPM

Appendix 2 - Experimental Results - Turbocharger

Evaluated data measured on the steady flow turbocharger test bed are stated below.

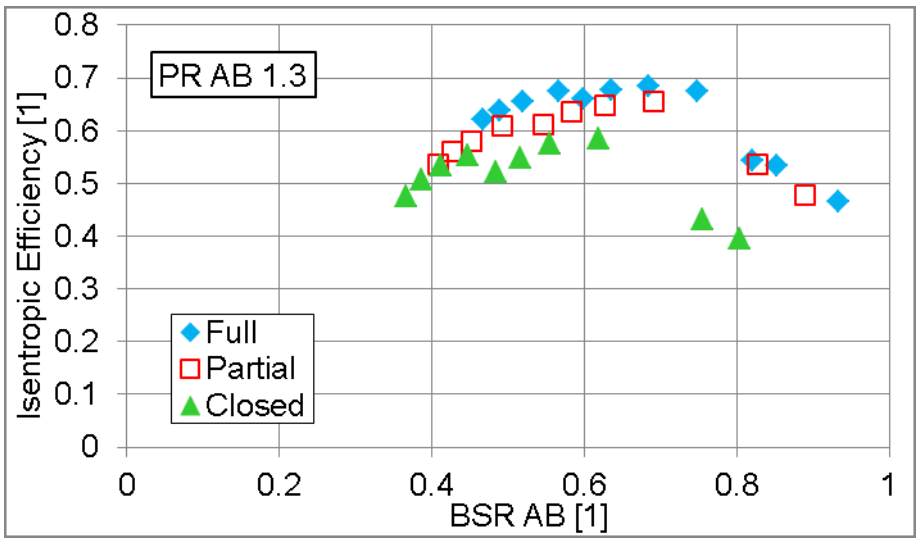

Figure 195 Comparison of turbine isentropic efficiency courses - overall pressure ratio PR AB = 1.3; full admission - blue; partial admission level A approx. 0.87 - red squares; closed section - green triangles

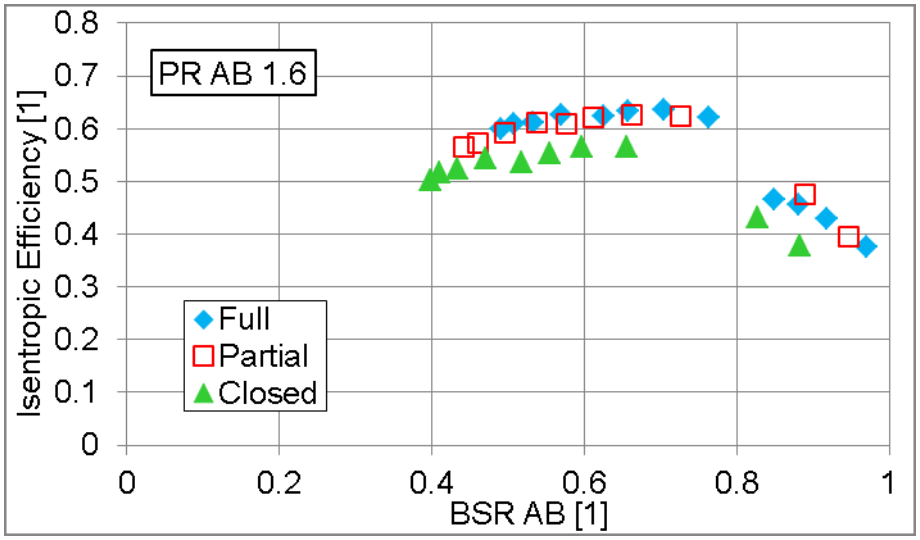

Figure 196 Comparison of turbine isentropic efficiency courses - overall pressure ratio PR AB = 1.6; full admission - blue; partial admission level A approx. 0.87 - red squares; closed section - green triangles

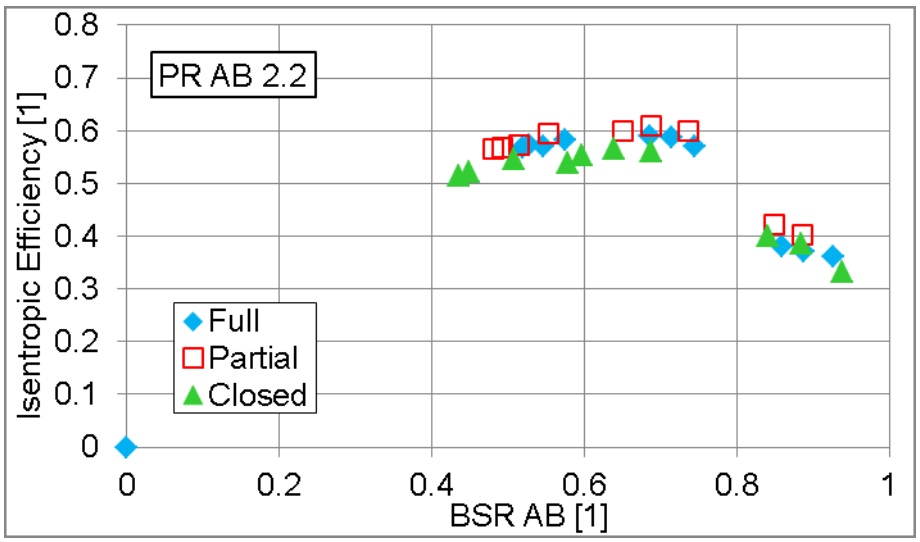

Figure 197 Comparison of turbine isentropic efficiency courses - overall pressure ratio PR AB = 2.2; full admission - blue (zero point measured at BSR = 0); partial admission level A approx. 0.87 - red squares; closed section - green triangles

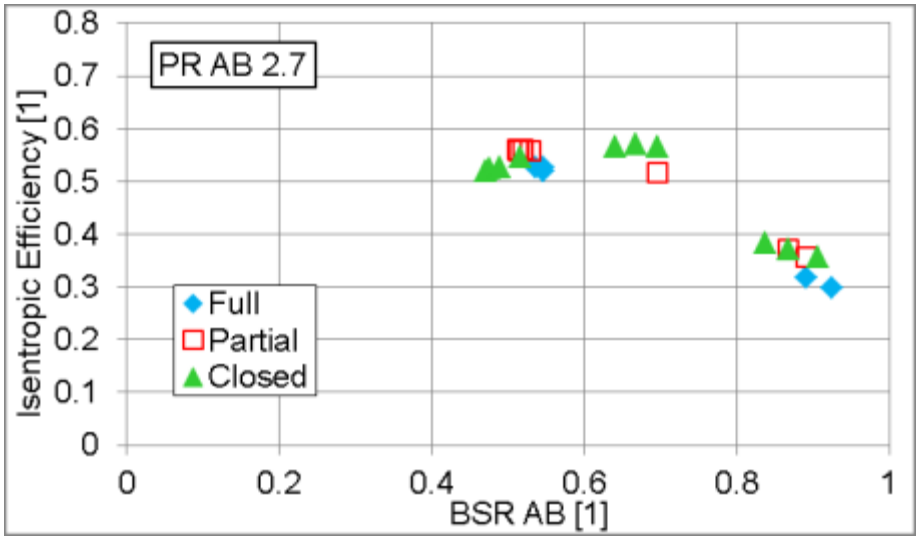

Figure 198 Comparison of turbine isentropic efficiency courses - overall pressure ratio PR AB = 2.7; full admission - blue; partial admission level A approx. 0.87 - red squares; closed section - green triangles

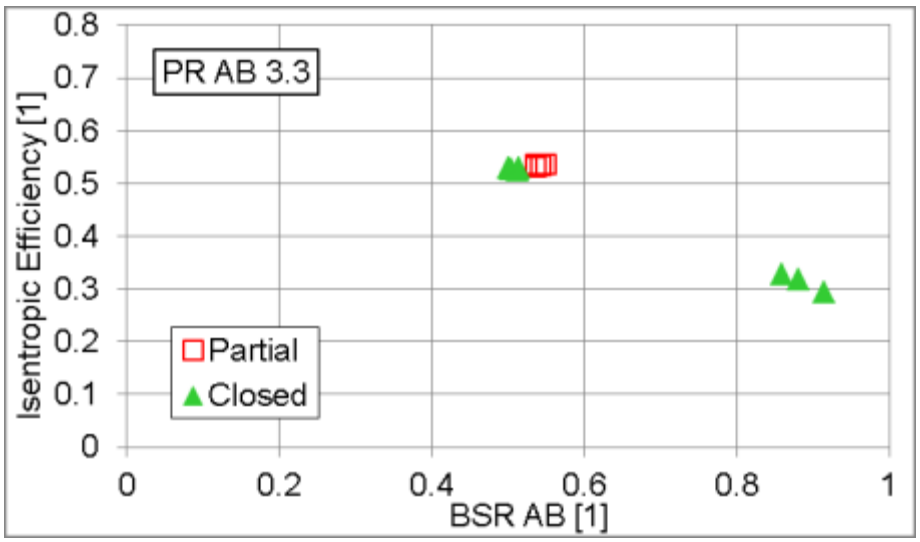

Figure 199 Comparison of turbine isentropic efficiency courses - overall pressure ratio PR AB = 3.3; partial admission level A approx. 0.87 - red squares; closed section - green triangles

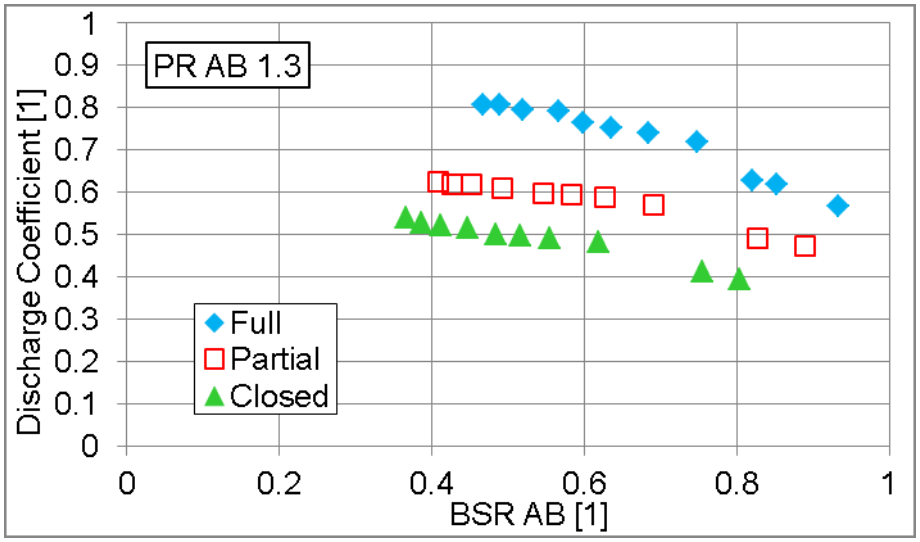

Figure 200 Discharge coefficient of a turbine - overall pressure ratio PR AB = 1.3; full admission - blue; partial admission level A approx. 0.87 - red squares; closed section - green triangles

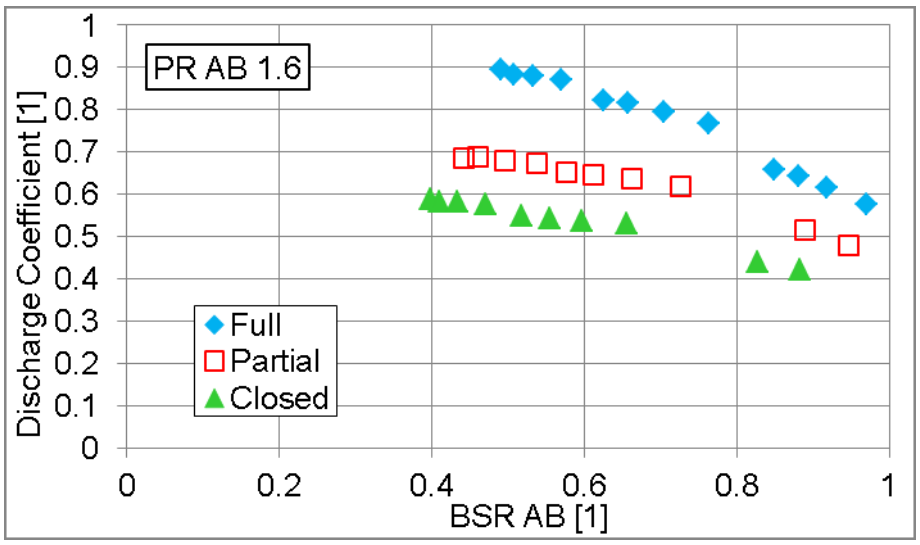

Figure 201 Discharge coefficient of a turbine - overall pressure ratio PR AB = 1.6; full admission - blue; partial admission level A approx. 0.87 - red squares; closed section - green triangles

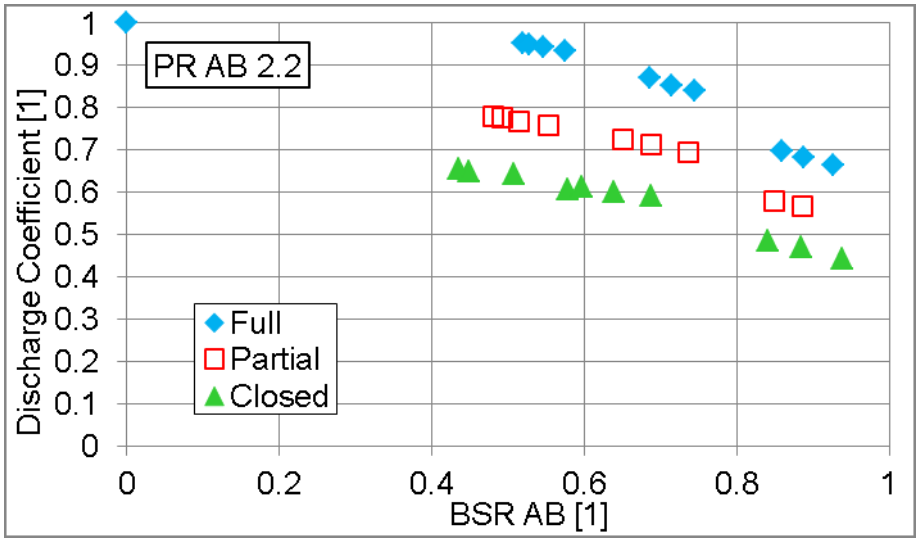

Figure 202 Discharge coefficient of a turbine - overall pressure ratio PR AB = 2.2; full admission - blue (zero point measured at BSR = 0); partial admission level A approx. 0.87 - red squares; closed section - green triangles

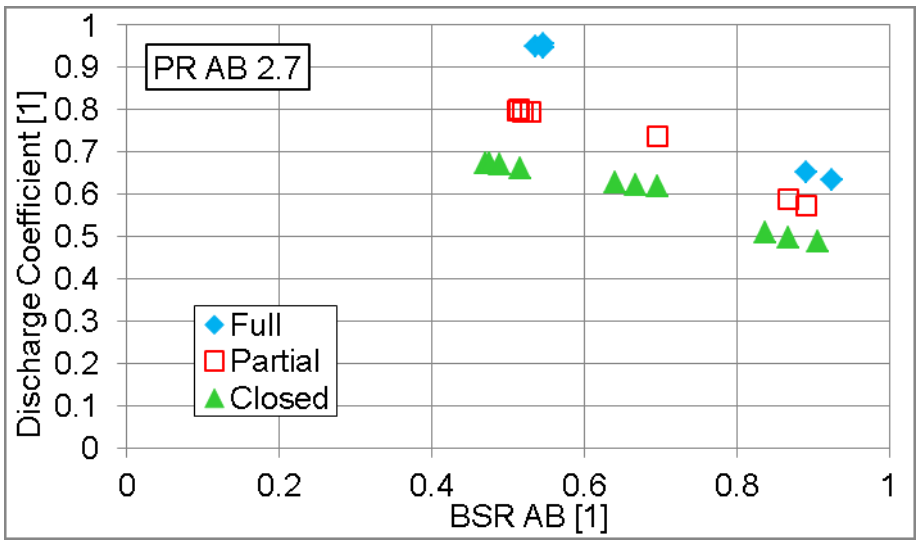

Figure 203 Discharge coefficient of a turbine - overall pressure ratio PR AB = 2.7; full admission - blue; partial admission level A approx. 0.87 - red squares; closed section - green triangles

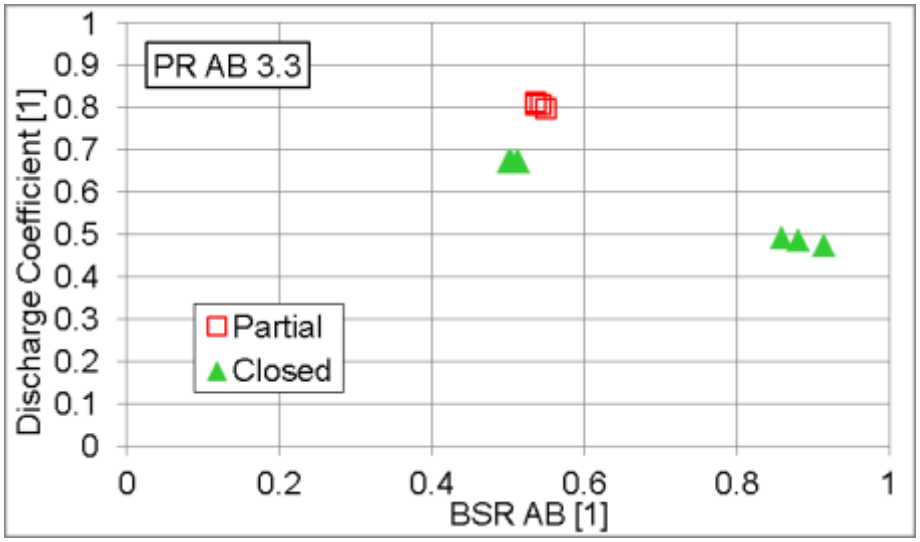

Figure 204 Discharge coefficient of a turbine - overall pressure ratio PR AB = 3.3; partial admission level A approx. 0.87 - red squares; closed section - green triangles

Appendix 3 - Simulation Results - Steady Flow Calibration of the 1-D Twin Scroll Turbine Model

The steady flow results of calibrated twin scroll turbine model are summarized in sequent pictures.

Calibration coefficients - approximate pressure ratio level PR AB = 1.3

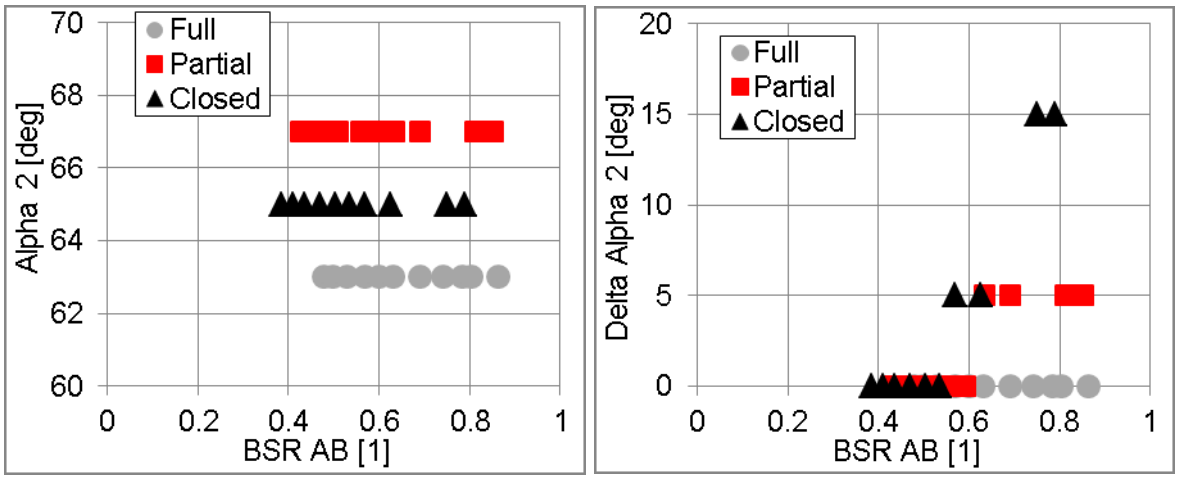

Figure 205 Calibration coefficients plotted vs. blade speed ratio BSR AB (approximate pressure ratio level PR AB = 1.3), Alpha 2 - nozzle exit angle (left), Delta Alpha 2 - deviation of nozzle exit angle (right); full admission of an impeller (gray circle), partial admission level A = 0.87 (red square), one section closed (black triangle)

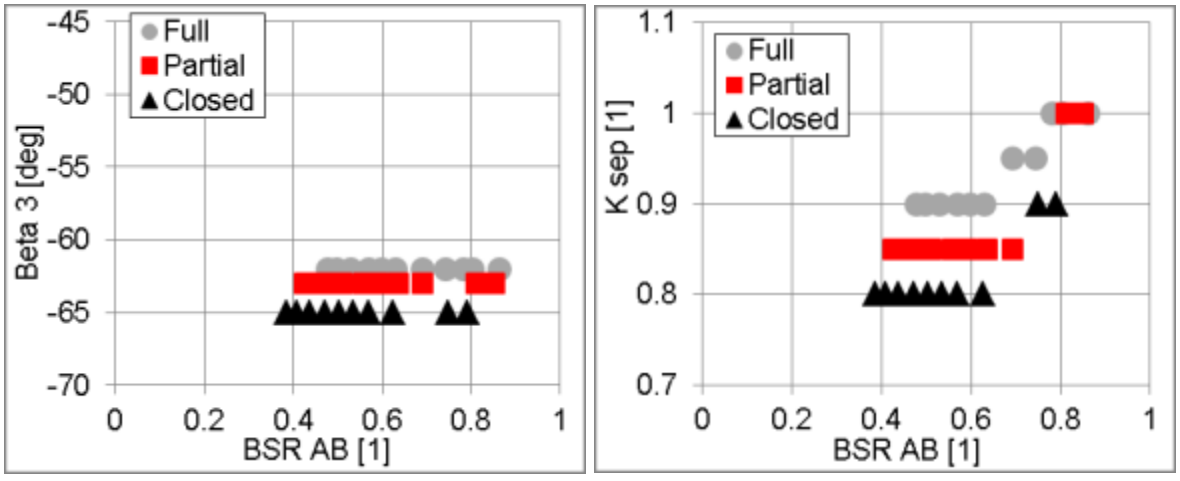

Figure 206 Calibration coefficients plotted vs. blade speed ratio BSR AB (approximate pressure ratio level PR AB = 1.3), Beta 3 - impeller exit angle (left), K sep - flow separation coefficient (right); full admission of an impeller (gray circle), partial admission level A = 0.87 (red square), one section closed (black triangle)

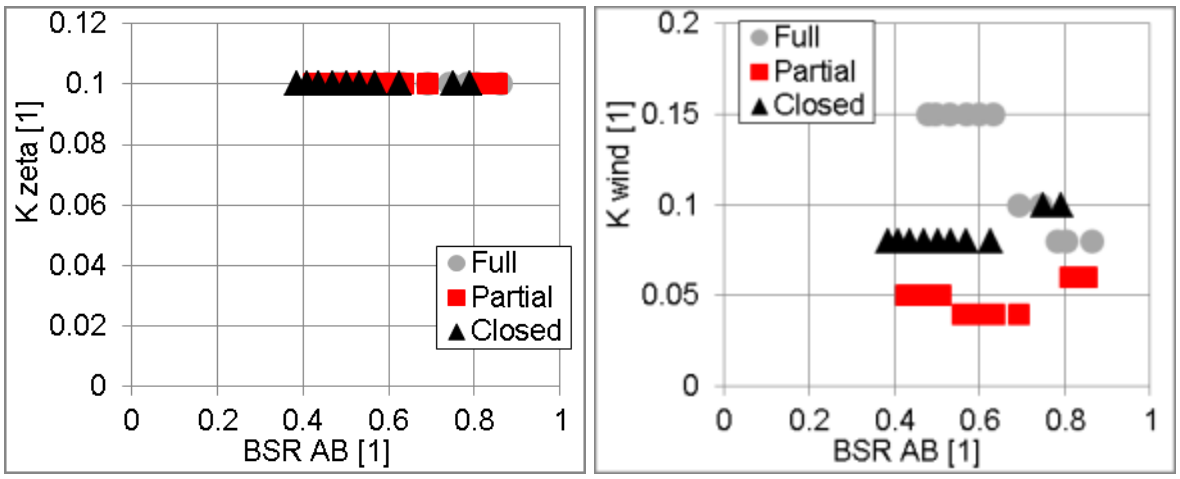

Figure 207 Calibration coefficients plotted vs. blade speed ratio BSR AB (approximate pressure ratio level PR AB = 1.3), K zeta - correction of impeller incidence loss (left), K wind - coefficient of windage losses (right); full admission of an impeller (gray circle), partial admission level A = 0.87 (red square), one section closed (black triangle)

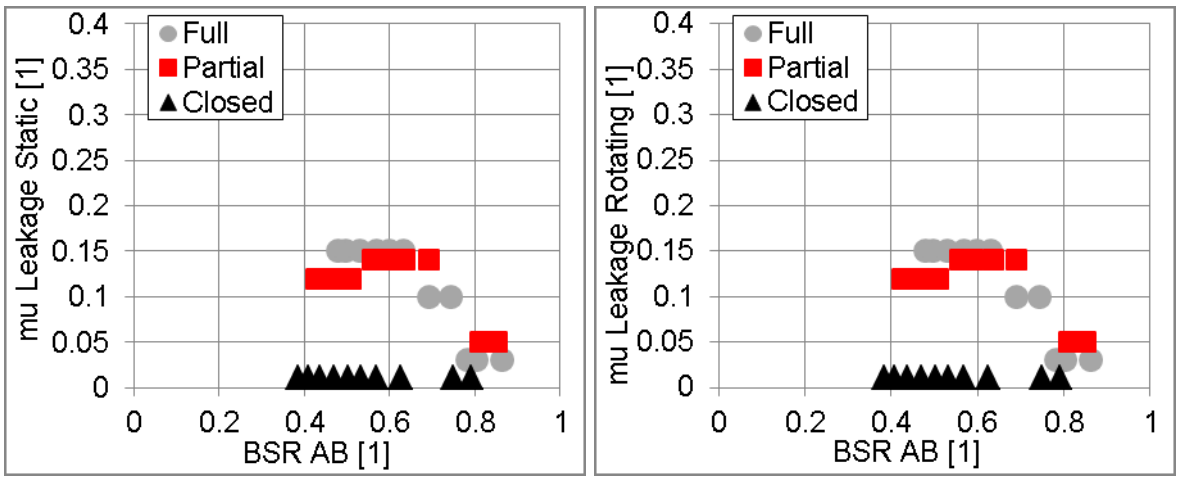

Figure 208 Calibration coefficients plotted vs. blade speed ratio BSR AB (approximate pressure ratio level PR AB = 1.3), mu Leakage Static - discharge coefficient of static leakages (left), mu Leakage Rotating - discharge coefficient of rotating leakages (right); full admission of an impeller (gray circle), partial admission level A = 0.87 (red square), one section closed (black triangle)

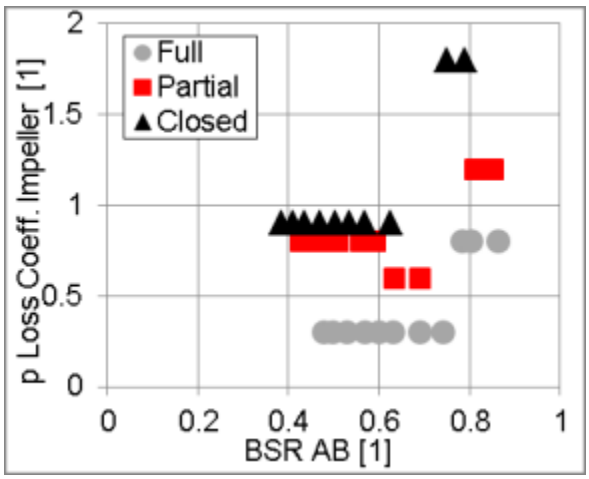

Figure 209 Calibration coefficient plotted vs. blade speed ratio BSR AB (approximate pressure ratio level PR AB = 1.3), pressure loss coefficient in impeller pipe; full admission of an impeller (gray circle), partial admission level A = 0.87 (red square), one section closed (black triangle)

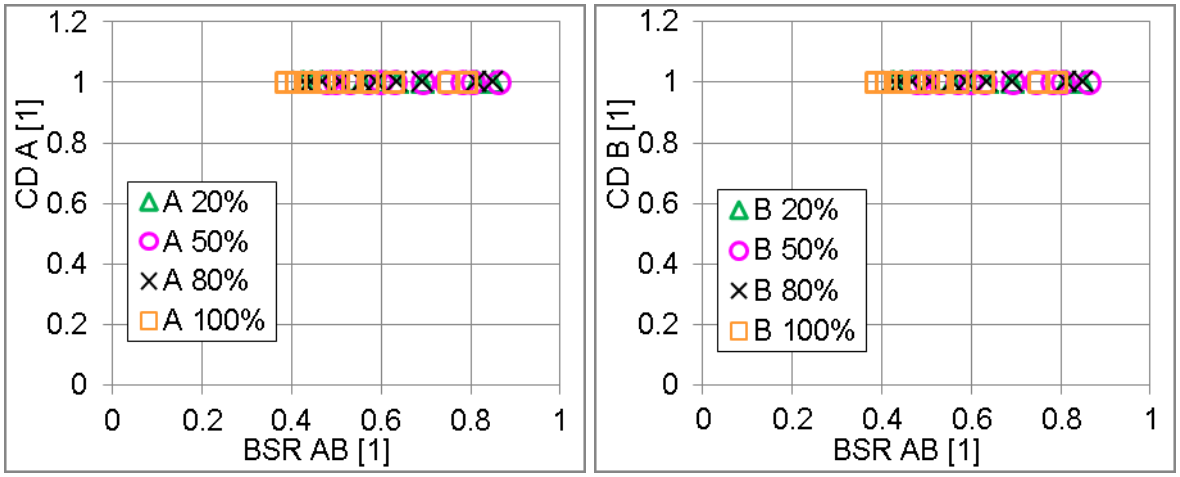

Figure 210 Calibration coefficients plotted vs. blade speed ratio BSR AB (approximate pressure ratio level PR AB = 1.3), CD A - discharge coefficient at section A outlet {upstream of flow mixing} (left) and CD B - discharge coefficient at section B outlet {upstream of flow mixing} (right) according to mass flow rate level in each section

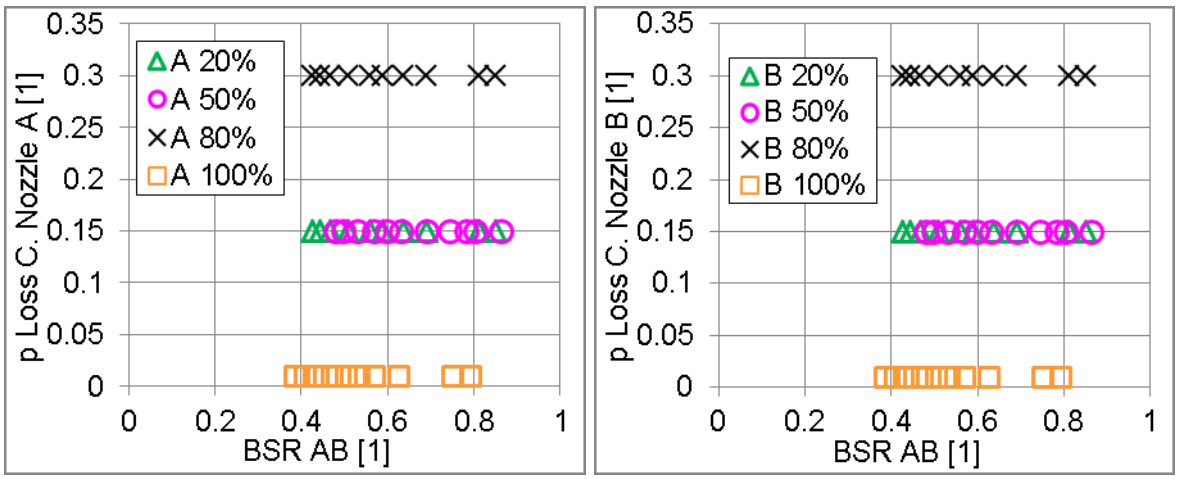

Figure 211 Calibration coefficients plotted vs. blade speed ratio BSR AB (approximate pressure ratio level PR AB = 1.3), pressure loss coefficient in section A (left) and pressure loss coefficient in section B (right) according to mass flow rate level in each section

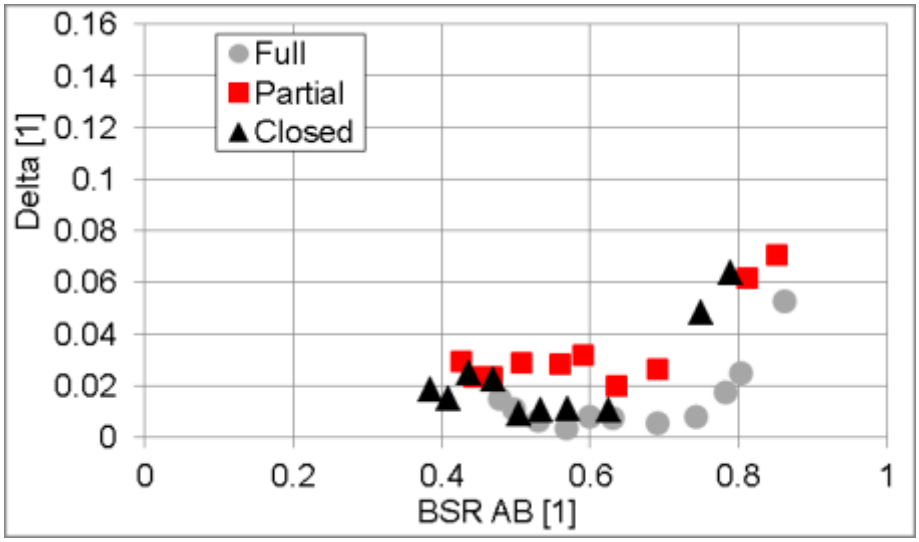

Figure 212 Overall error - Delta plotted vs. blade speed ratio BSR AB (approximate pressure ratio level PR AB = 1.3); full admission of an impeller (gray circle), partial admission level A = 0.87 (red square), one section closed (black triangle)

Calibration coefficients - approximate pressure ratio level PR AB = 1.6

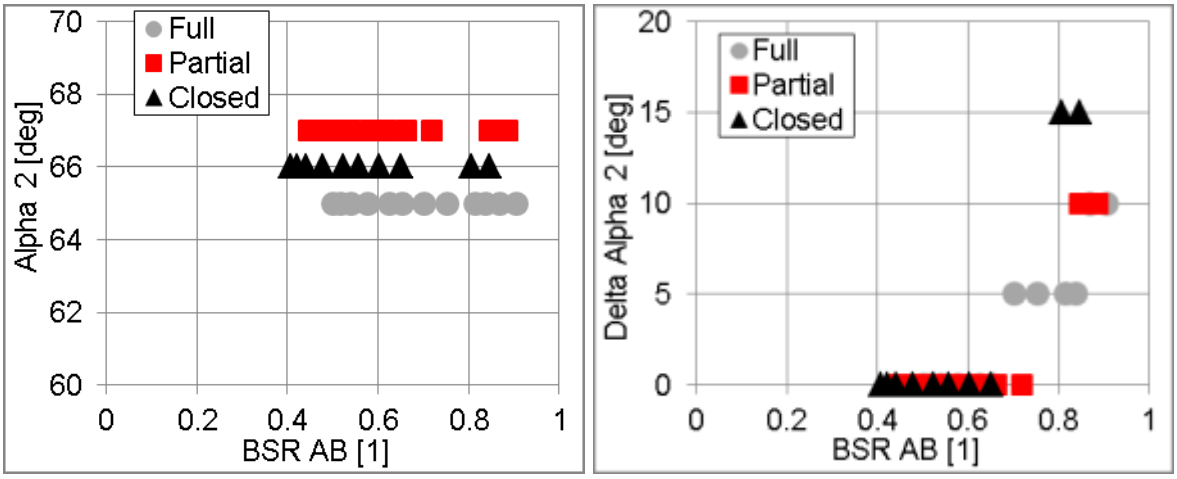

Figure 213 Calibration coefficients plotted vs. blade speed ratio BSR AB (approximate pressure ratio level PR AB = 1.6), Alpha 2 - nozzle exit angle (left), Delta Alpha 2 - deviation of nozzle exit angle (right); full admission of an impeller (gray circle), partial admission level A = 0.87 (red square), one section closed (black triangle)

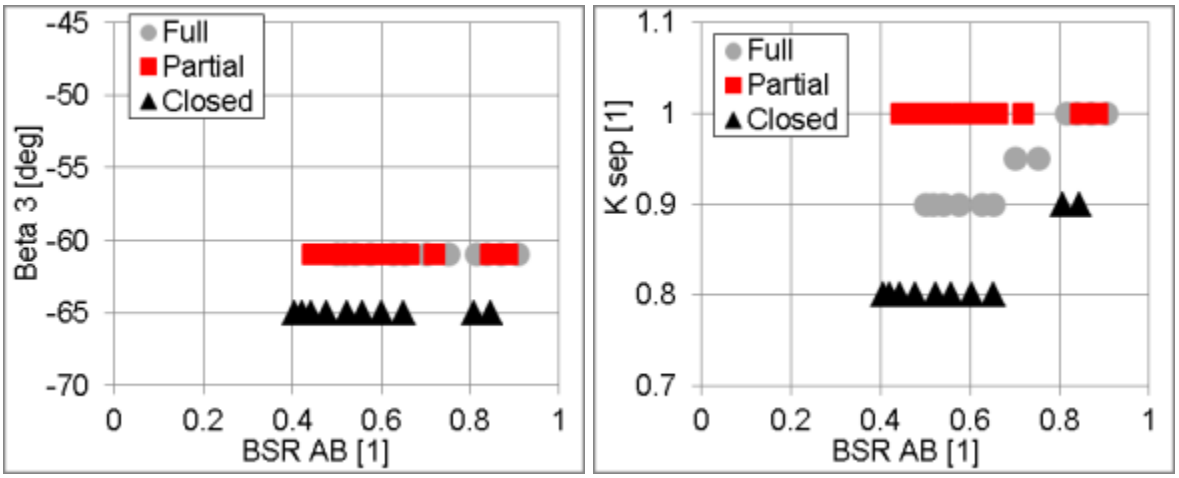

Figure 214 Calibration coefficients plotted vs. blade speed ratio BSR AB (approximate pressure ratio level PR AB = 1.6), Beta 3 - impeller exit angle (left), K sep - flow separation coefficient (right); full admission of an impeller (gray circle), partial admission level A = 0.87 (red square), one section closed (black triangle)

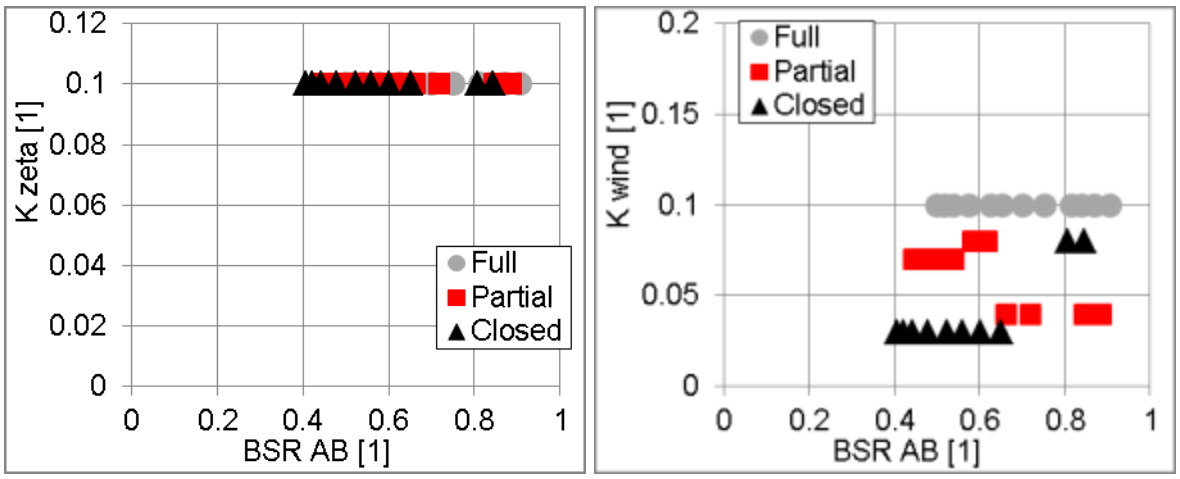

Figure 215 Calibration coefficients plotted vs. blade speed ratio BSR AB (approximate pressure ratio level PR AB = 1.6), K zeta - correction of impeller incidence loss (left), K wind - coefficient of windage losses (right); full admission of an impeller (gray circle), partial admission level A = 0.87 (red square), one section closed (black triangle)

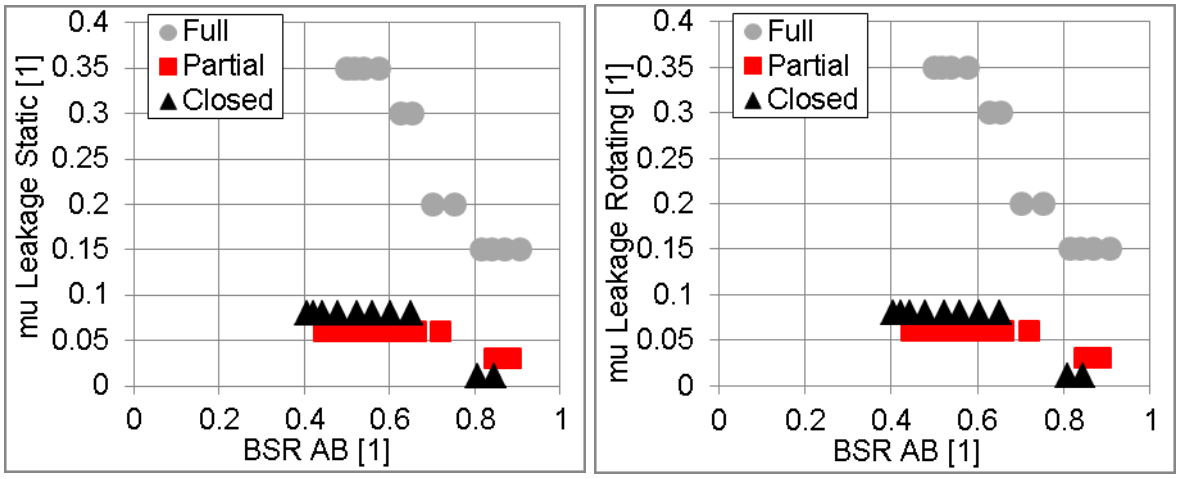

Figure 216 Calibration coefficients plotted vs. blade speed ratio BSR AB (approximate pressure ratio level PR AB = 1.6), mu Leakage Static - discharge coefficient of static leakages (left), mu Leakage Rotating - discharge coefficient of rotating leakages (right); full admission of an impeller (gray circle), partial admission level A = 0.87 (red square), one section closed (black triangle)

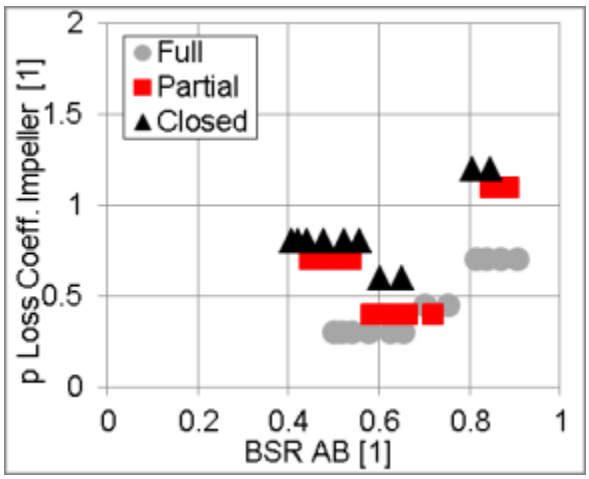

Figure 217 Calibration coefficient plotted vs. blade speed ratio BSR AB (approximate pressure ratio level PR AB = 1.6), pressure loss coefficient in impeller pipe; full admission of an impeller (gray circle), partial admission level A = 0.87 (red square), one section closed (black triangle)

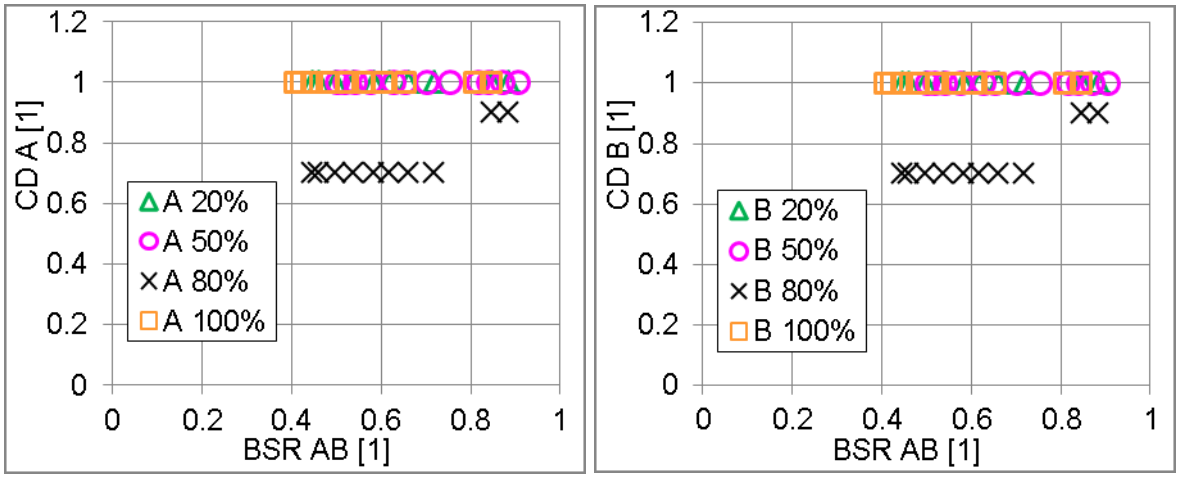

Figure 218 Calibration coefficients plotted vs. blade speed ratio BSR AB (approximate pressure ratio level PR AB = 1.6), CD A - discharge coefficient at section A outlet {upstream of flow mixing} (left) and CD B - discharge coefficient at section B outlet {upstream of flow mixing} (right) according to mass flow rate level in each section

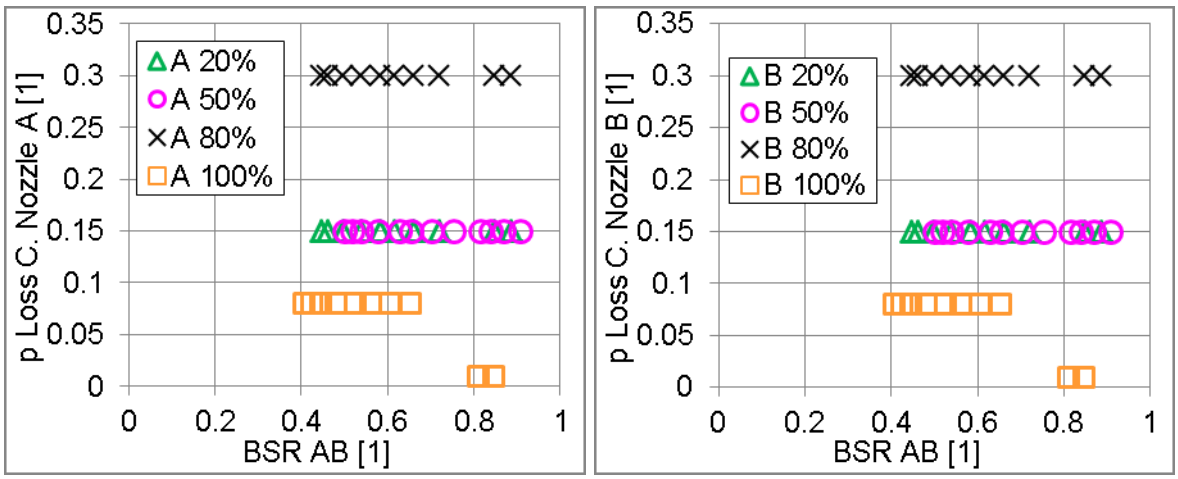

Figure 219 Calibration coefficients plotted vs. blade speed ratio BSR AB (approximate pressure ratio level PR AB = 1.6), pressure loss coefficient in section A (left) and pressure loss coefficient in section B (right) according to mass flow rate level in each section

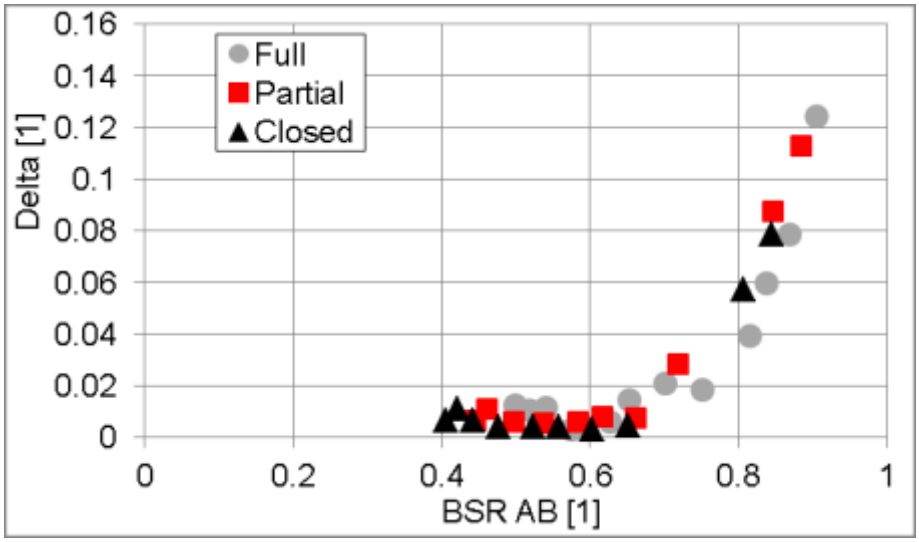

Figure 220 Overall error - Delta plotted vs. blade speed ratio BSR AB (approximate pressure ratio level PR AB = 1.6); full admission of an impeller (gray circle), partial admission level A = 0.87 (red square), one section closed (black triangle)

Calibration coefficients - approximate pressure ratio level PR AB = 2.7

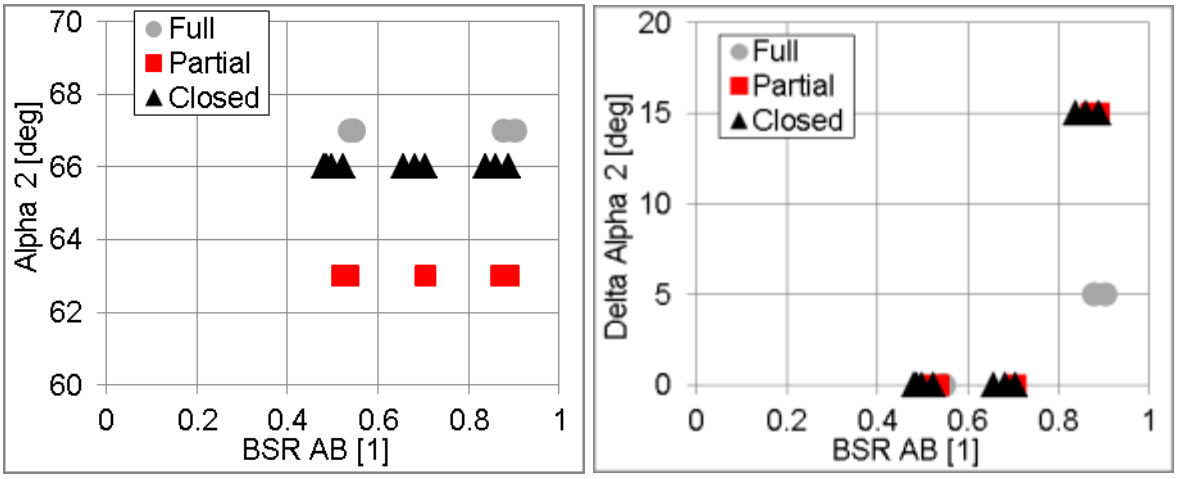

Figure 221 Calibration coefficients plotted vs. blade speed ratio BSR AB (approximate pressure ratio level PR AB = 2.7), Alpha 2 - nozzle exit angle (left), Delta Alpha 2 - deviation of nozzle exit angle (right); full admission of an impeller (gray circle), partial admission level A = 0.87 (red square), one section closed (black triangle)

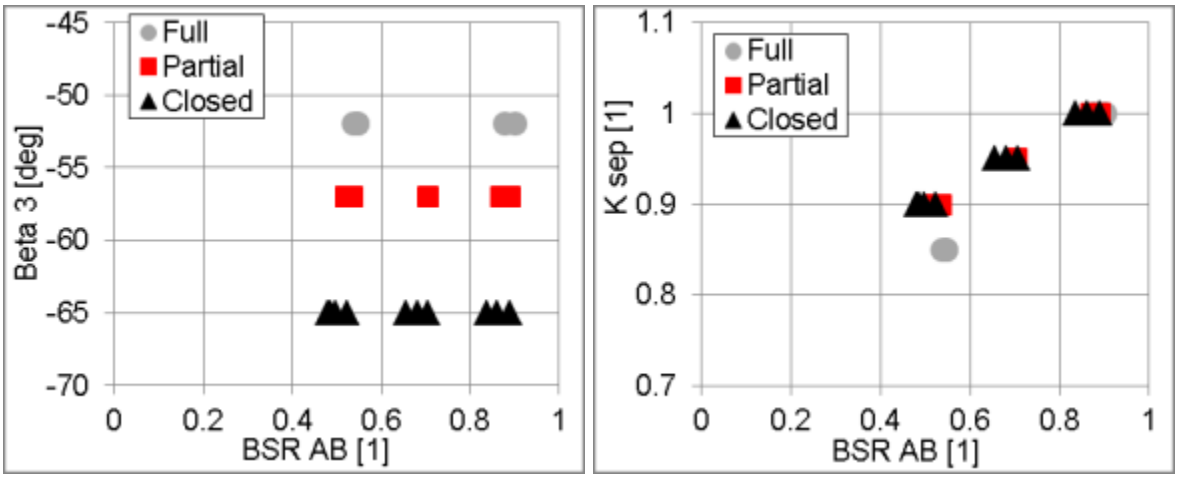

Figure 222 Calibration coefficients plotted vs. blade speed ratio BSR AB (approximate pressure ratio level PR AB = 2.7), Beta 3 - impeller exit angle (left), K sep - flow separation coefficient (right); full admission of an impeller (gray circle), partial admission level A = 0.87 (red square), one section closed (black triangle)

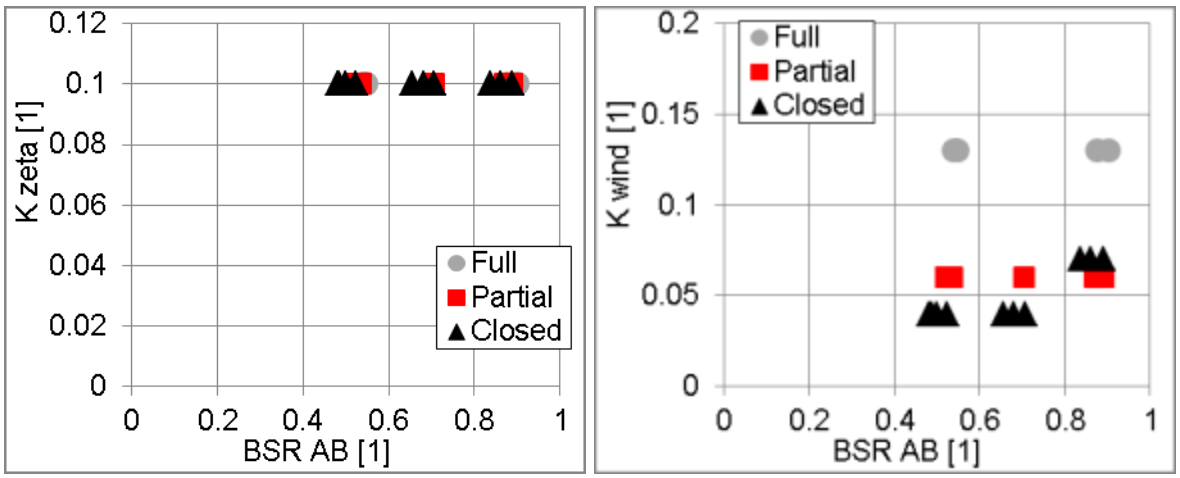

Figure 223 Calibration coefficients plotted vs. blade speed ratio BSR AB (approximate pressure ratio level PR AB = 2.7), K zeta - correction of impeller incidence loss (left), K wind - coefficient of windage losses (right); full admission of an impeller (gray circle), partial admission level A = 0.87 (red square), one section closed (black triangle)

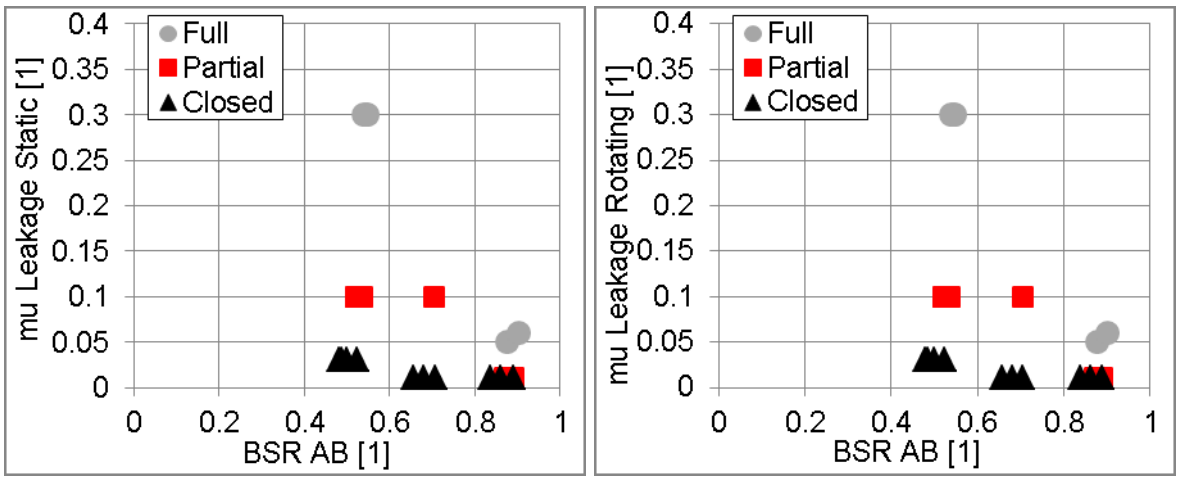

Figure 224 Calibration coefficients plotted vs. blade speed ratio BSR AB (approximate pressure ratio level PR AB = 2.7), mu Leakage Static - discharge coefficient of static leakages (left), mu Leakage Rotating - discharge coefficient of rotating leakages (right); full admission of an impeller (gray circle), partial admission level A = 0.87 (red square), one section closed (black triangle)

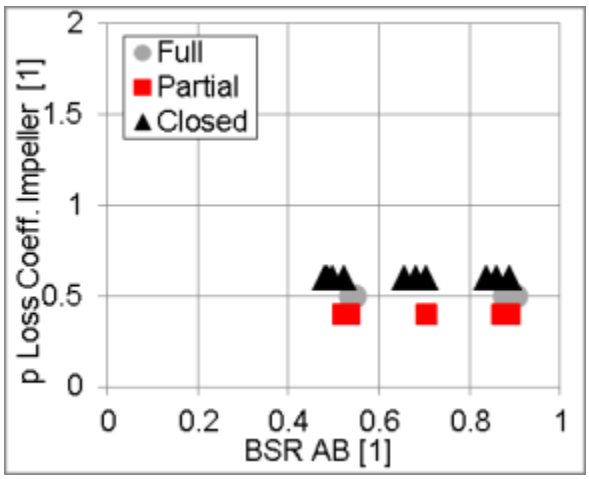

Figure 225 Calibration coefficient plotted vs. blade speed ratio BSR AB (approximate pressure ratio level PR AB = 2.7), pressure loss coefficient in impeller pipe; full admission of an impeller (gray circle), partial admission level A = 0.87 (red square), one section closed (black triangle)

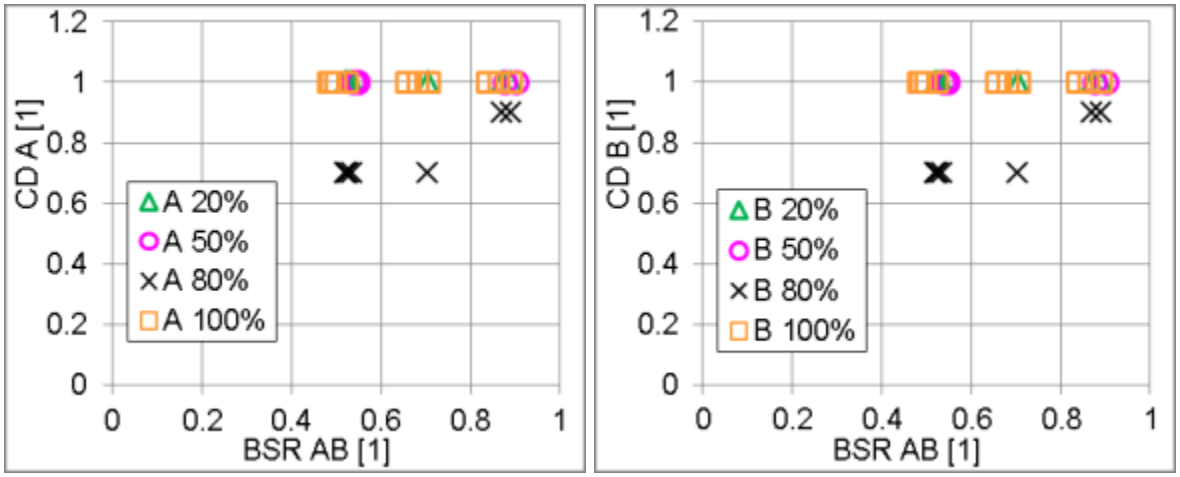

Figure 226 Calibration coefficients plotted vs. blade speed ratio BSR AB (approximate pressure ratio level PR AB = 2.7), CD A - discharge coefficient at section A outlet {upstream of flow mixing} (left) and CD B - discharge coefficient at section B outlet {upstream of flow mixing} (right) according to mass flow rate level in each section

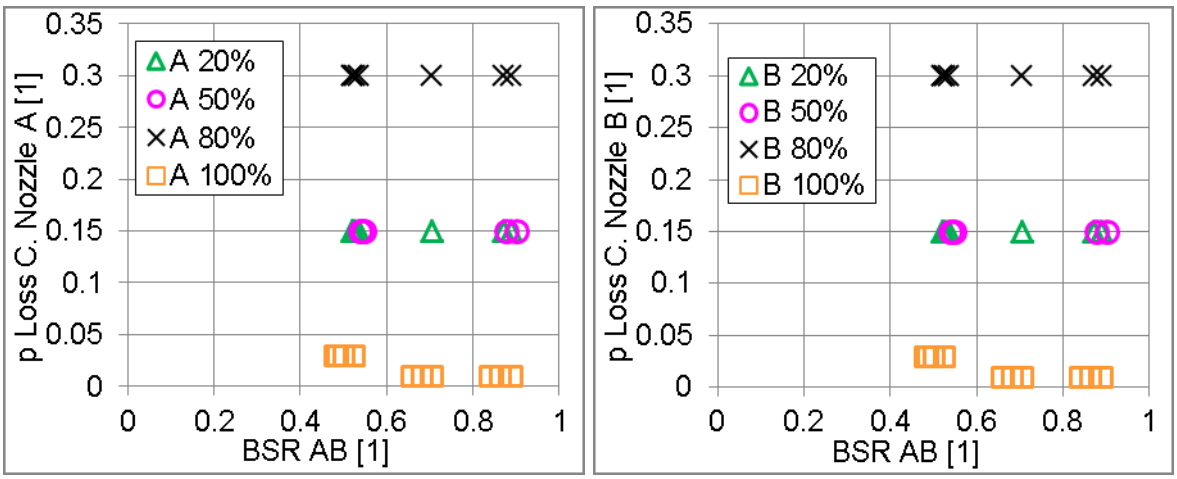

Figure 227 Calibration coefficients plotted vs. blade speed ratio BSR AB (approximate pressure ratio level PR AB = 2.7), pressure loss coefficient in section A (left) and pressure loss coefficient in section B (right) according to mass flow rate level in each section

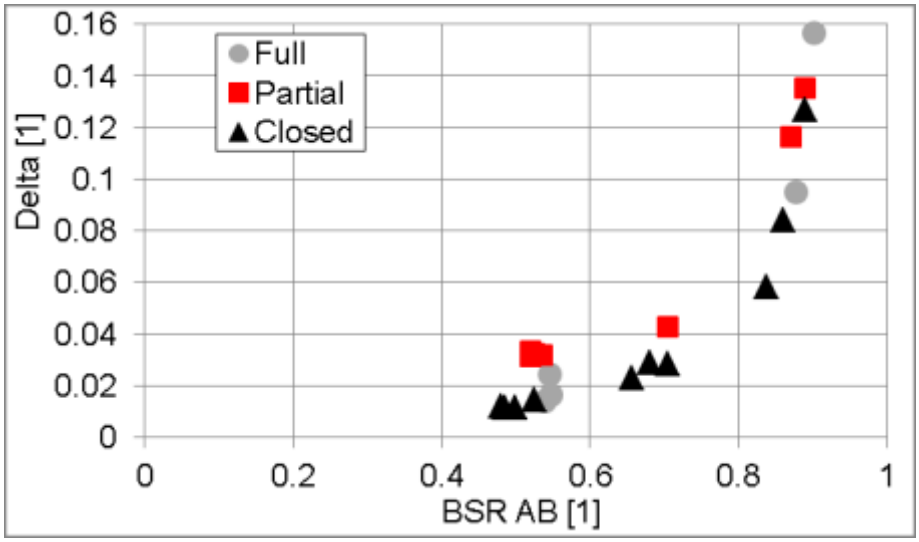

Figure 228 Overall error - Delta plotted vs. blade speed ratio BSR AB (approximate pressure ratio level PR AB = 2.7); full admission of an impeller (gray circle), partial admission level A = 0.87 (red square), one section closed (black triangle)

Calibration coefficients - approximate pressure ratio level PR AB = 3.3

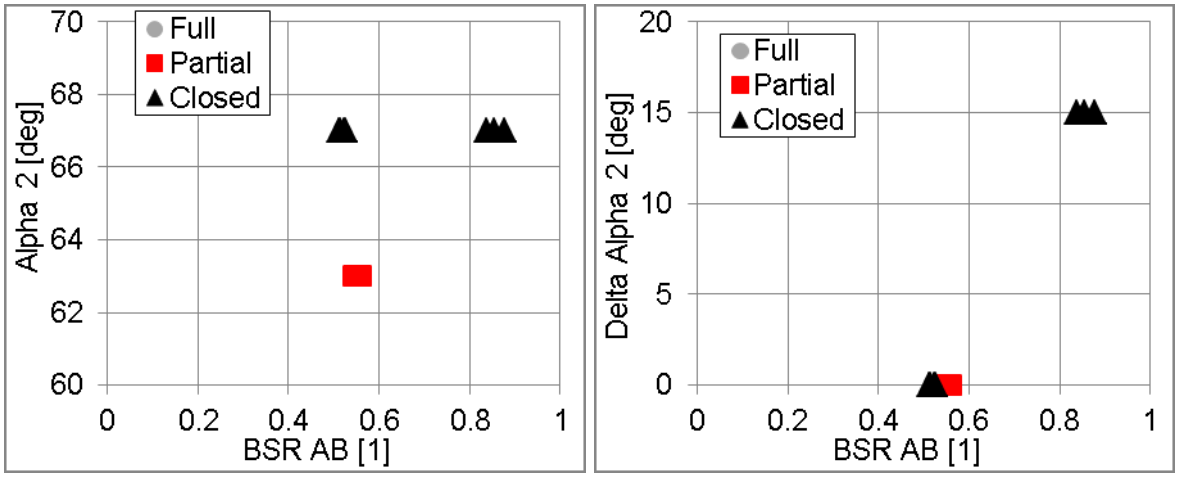

Figure 229 Calibration coefficients plotted vs. blade speed ratio BSR AB (approximate pressure ratio level PR AB = 3.3), Alpha 2 - nozzle exit angle (left), Delta Alpha 2 - deviation of nozzle exit angle (right); full admission of an impeller (gray circle), partial admission level A = 0.87 (red square), one section closed (black triangle)

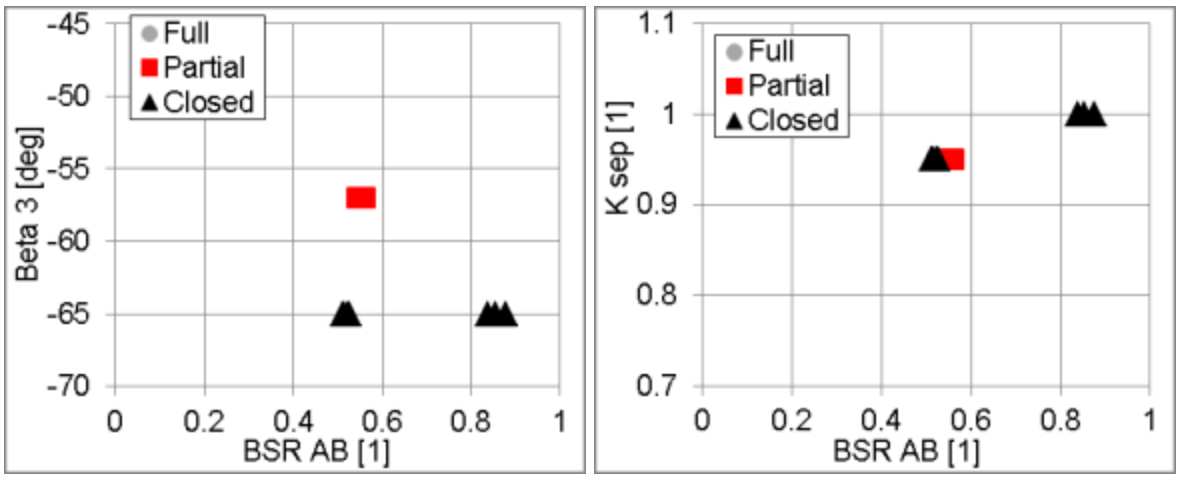

Figure 230 Calibration coefficients plotted vs. blade speed ratio BSR AB (approximate pressure ratio level PR AB = 3.3), Beta 3 - impeller exit angle (left), K sep - flow separation coefficient (right); full admission of an impeller (gray circle), partial admission level A = 0.87 (red square), one section closed (black triangle)

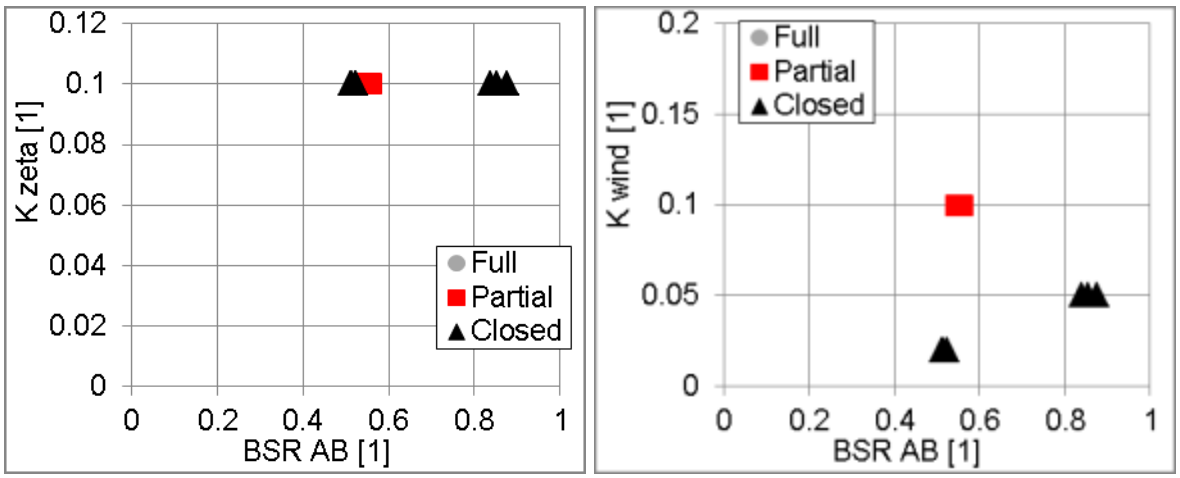

Figure 231 Calibration coefficients plotted vs. blade speed ratio BSR AB (approximate pressure ratio level PR AB = 3.3), K zeta - correction of impeller incidence loss (left), K wind - coefficient of windage losses (right); full admission of an impeller (gray circle), partial admission level A = 0.87 (red square), one section closed (black triangle)

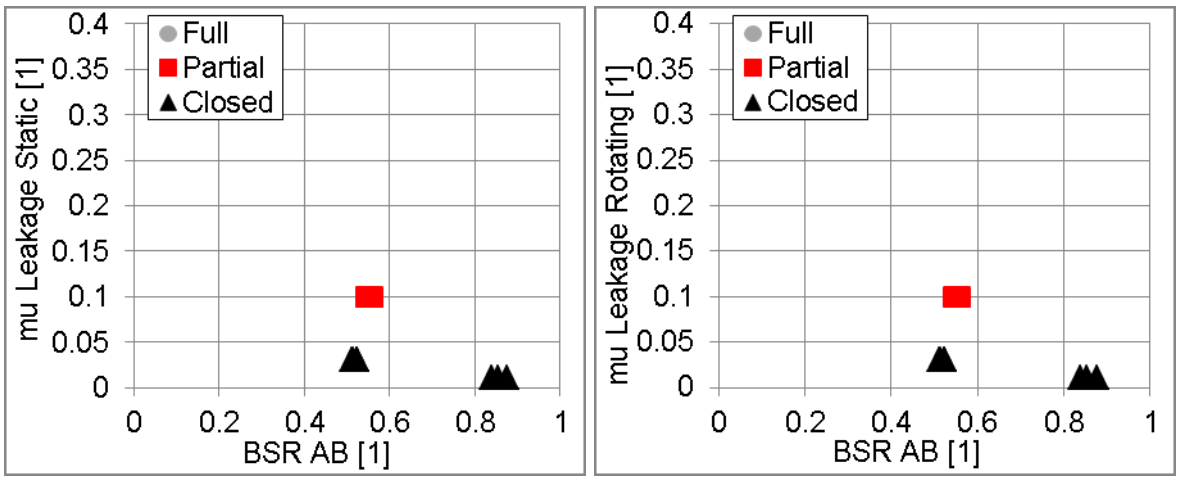

Figure 232 Calibration coefficients plotted vs. blade speed ratio BSR AB (approximate pressure ratio level PR AB = 3.3), mu Leakage Static - discharge coefficient of static leakages (left), mu Leakage Rotating - discharge coefficient of rotating leakages (right); full admission of an impeller (gray circle), partial admission level A = 0.87 (red square), one section closed (black triangle)

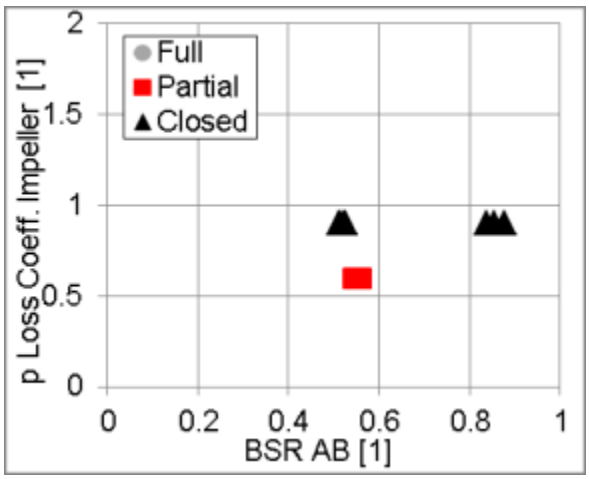

Figure 233 Calibration coefficient plotted vs. blade speed ratio BSR AB (approximate pressure ratio level PR AB = 3.3), pressure loss coefficient in impeller pipe; full admission of an impeller (gray circle), partial admission level A = 0.87 (red square), one section closed (black triangle)

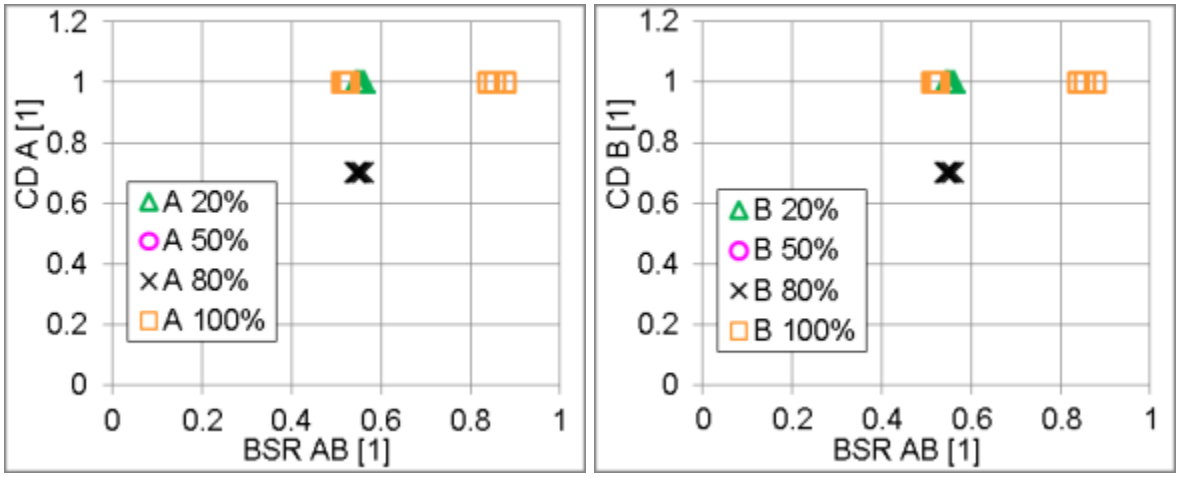

Figure 234 Calibration coefficients plotted vs. blade speed ratio BSR AB (approximate pressure ratio level PR AB = 3.3), CD A - discharge coefficient at section A outlet {upstream of flow mixing} (left) and CD B - discharge coefficient at section B outlet {upstream of flow mixing} (right) according to mass flow rate level in each section

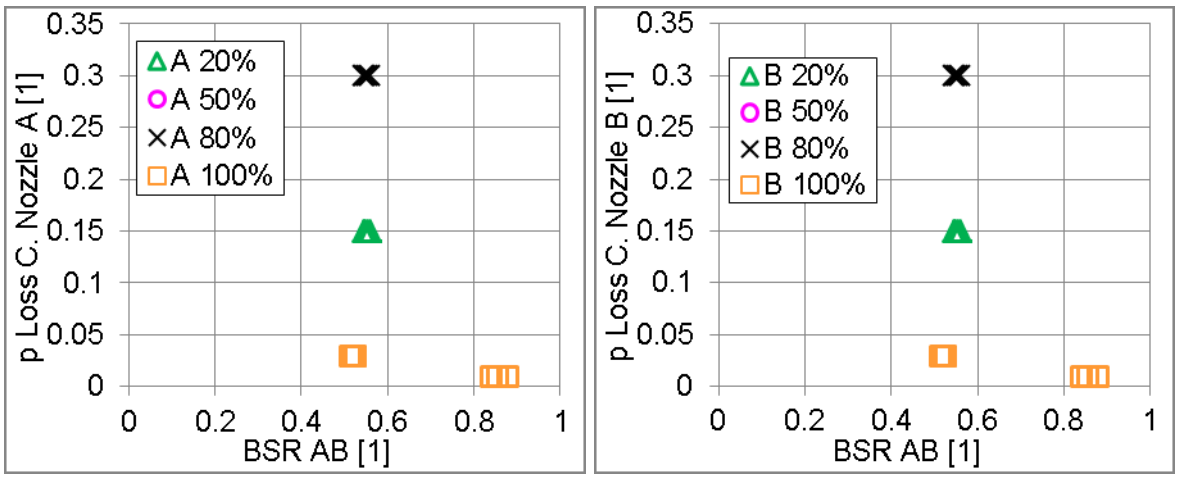

Figure 235 Calibration coefficients plotted vs. blade speed ratio BSR AB (approximate pressure ratio level PR AB = 3.3), pressure loss coefficient in section A (left) and pressure loss coefficient in section B (right) according to mass flow rate level in each section

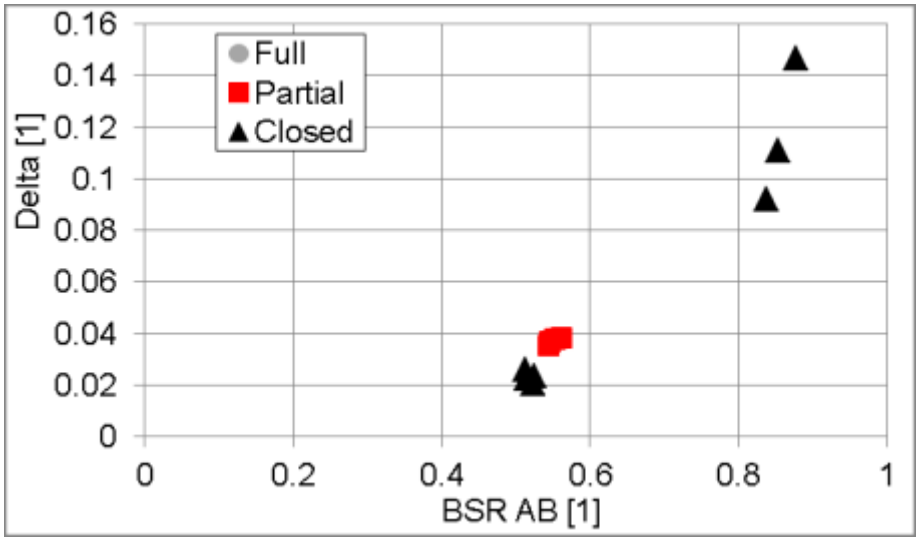

Figure 236 Overall error - Delta plotted vs. blade speed ratio BSR AB (approximate pressure ratio level PR AB = 3.3); full admission of an impeller (gray circle), partial admission level A = 0.87 (red square), one section closed (black triangle)

Results of steady flow calibration follow in more practical format, plotted versus blade speed ratio. The isentropic efficiency of a turbine was not a goal of the calibration procedure, but it is included for completeness.

Full admission, PR AB = 1.3

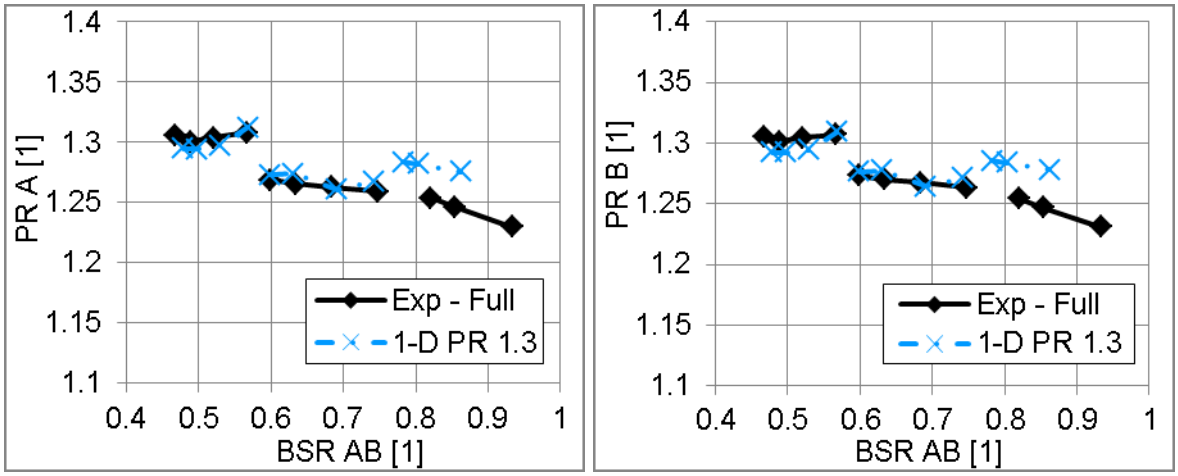

Figure 237 Pressure ratio A (left) and B (right) vs. BSR (approximate pressure ratio level PR AB = 1.3), full admission of an impeller; experiments (black); simulation 1-D turbine (blue crosses)

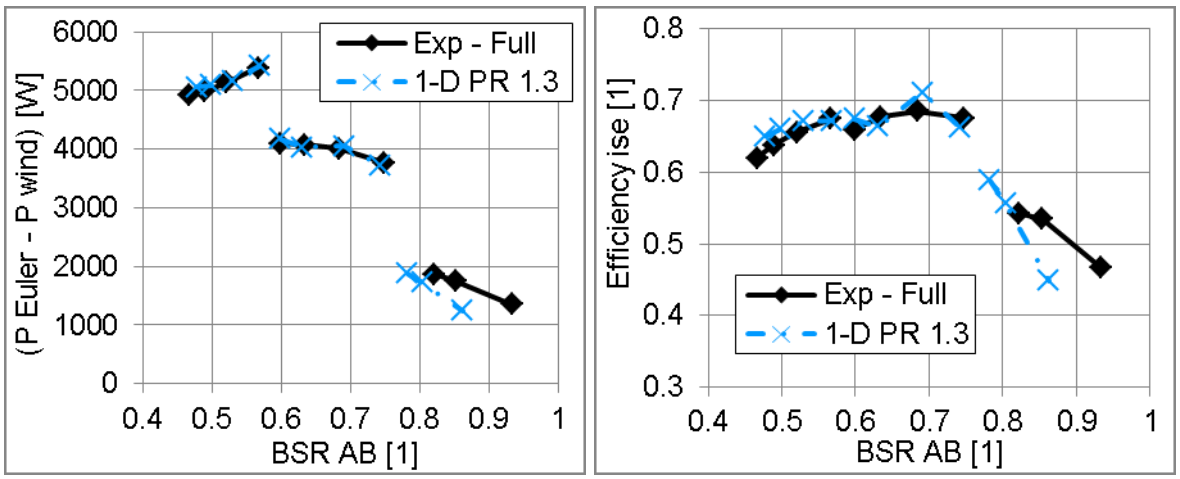

Figure 238 Turbine power (left) and isentropic efficiency (right) vs. BSR (approximate pressure ratio level PR AB = 1.3), full admission of an impeller; experiments (black); simulation 1-D turbine (blue crosses)

Full admission, PR AB = 1.6

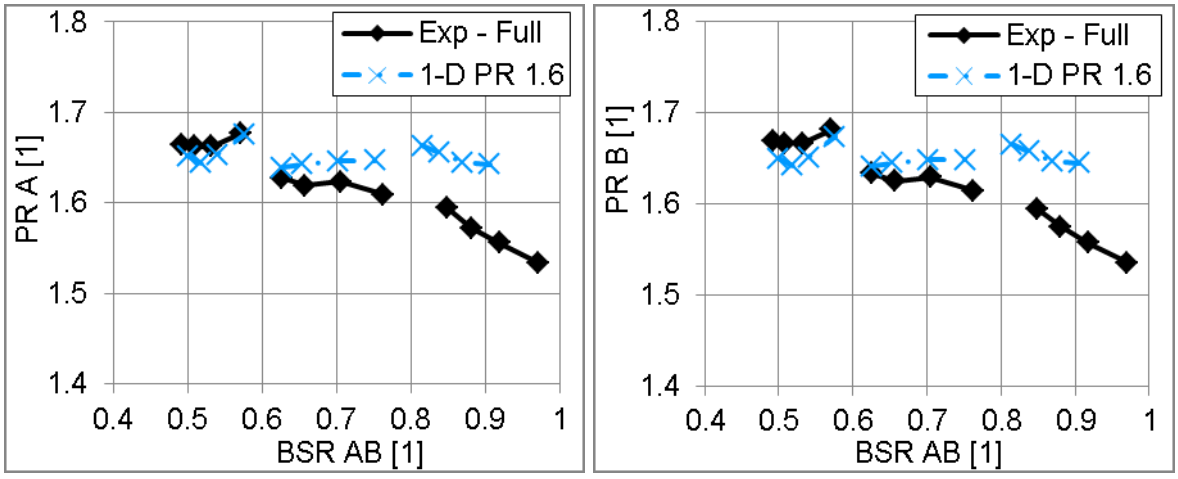

Figure 239 Pressure ratio A (left) and B (right) vs. BSR (approximate pressure ratio level PR AB = 1.6), full admission of an impeller; experiments (black); simulation 1-D turbine (blue crosses)

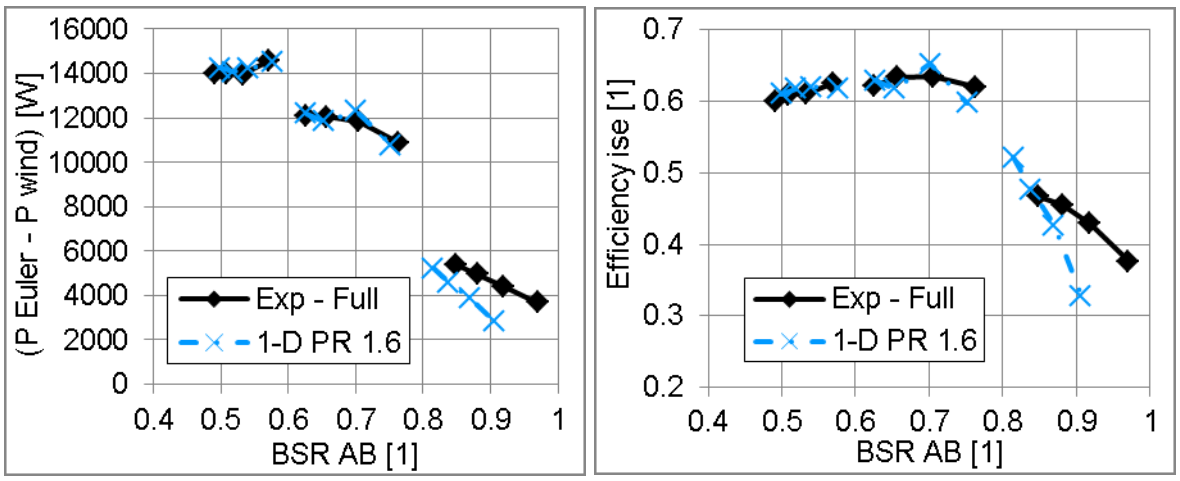

Figure 240 Turbine power (left) and isentropic efficiency (right) vs. BSR (approximate pressure ratio level PR AB = 1.6), full admission of an impeller; experiments (black); simulation 1-D turbine (blue crosses)

Full admission, PR AB = 2.2

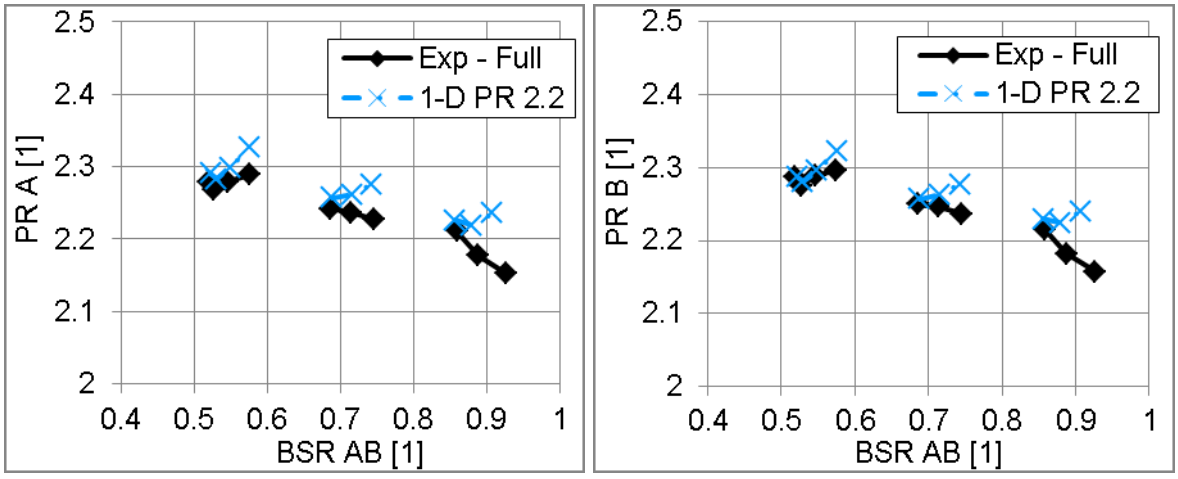

Figure 241 Pressure ratio A (left) and B (right) vs. BSR (approximate pressure ratio level PR AB = 2.2), full admission of an impeller; experiments (black); simulation 1-D turbine (blue crosses)

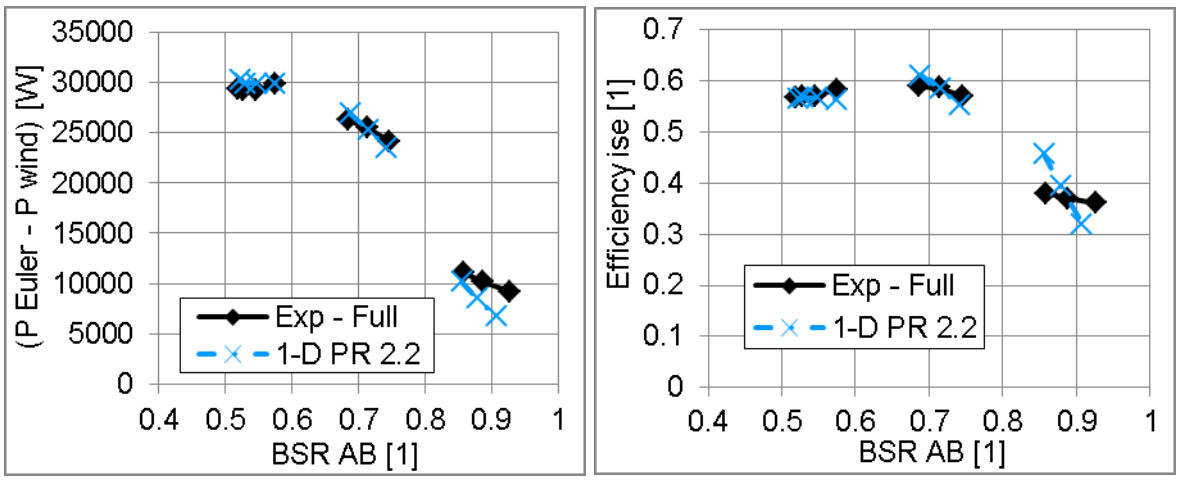

Figure 242 Turbine power (left) and isentropic efficiency (right) vs. BSR (approximate pressure ratio level PR AB = 2.2), full admission of an impeller; experiments (black); simulation 1-D turbine (blue crosses)

Full admission, PR AB = 2.7

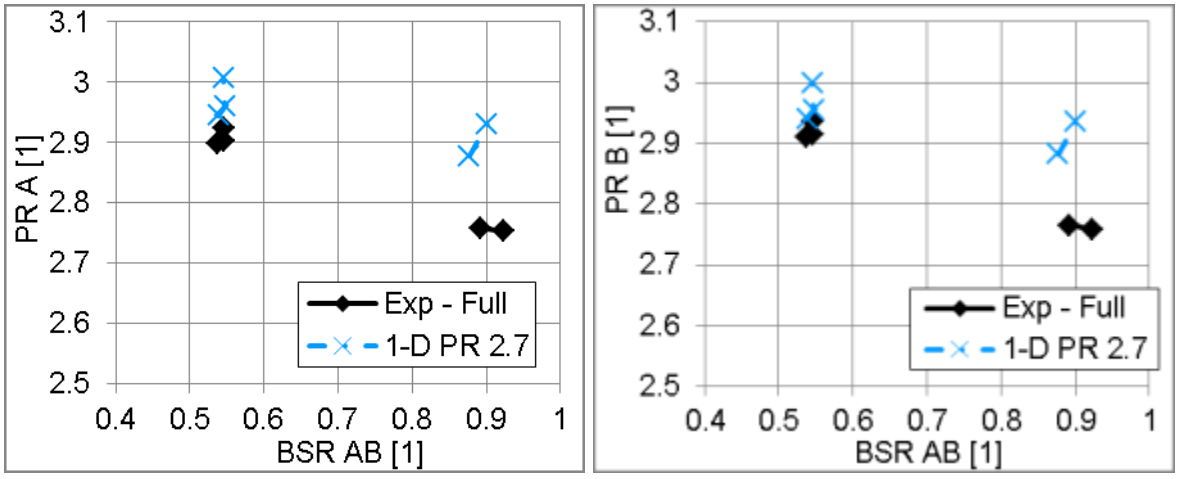

Figure 243 Pressure ratio A (left) and B (right) vs. BSR (approximate pressure ratio level PR AB = 2.7), full admission of an impeller; experiments (black); simulation 1-D turbine (blue crosses)

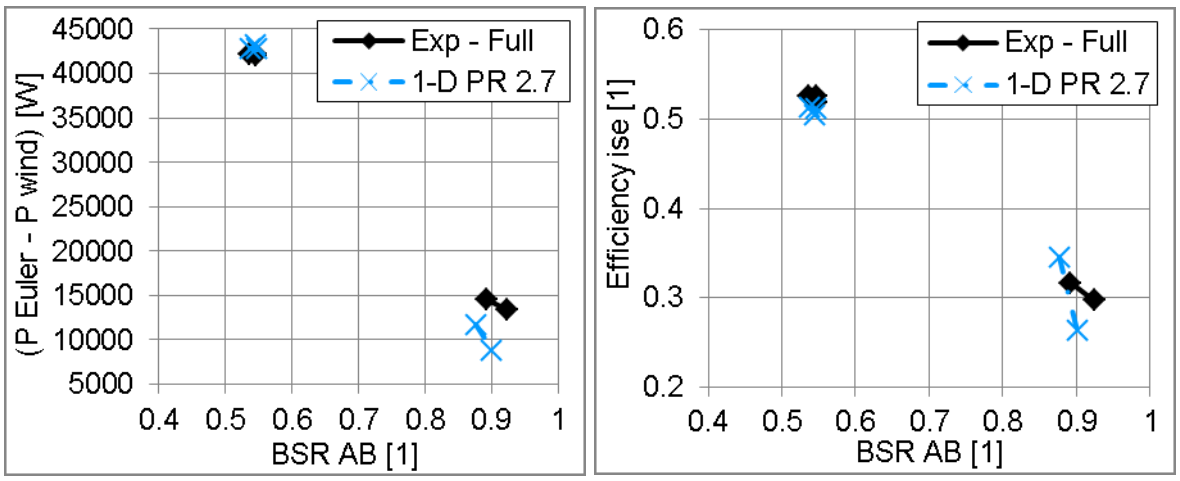

Figure 244 Turbine power (left) and isentropic efficiency (right) vs. BSR (approximate pressure ratio level PR AB = 2.7), full admission of an impeller; experiments (black); simulation 1-D turbine (blue crosses)

The partial level of the impeller admission was achieved by throttling in section B of a turbine. Utilization of the isentropic efficiency, under partial admission, for the description of the twin entry turbine is limited due to irreversible mixing of flows inside.

Partial admission, PR AB = 1.3

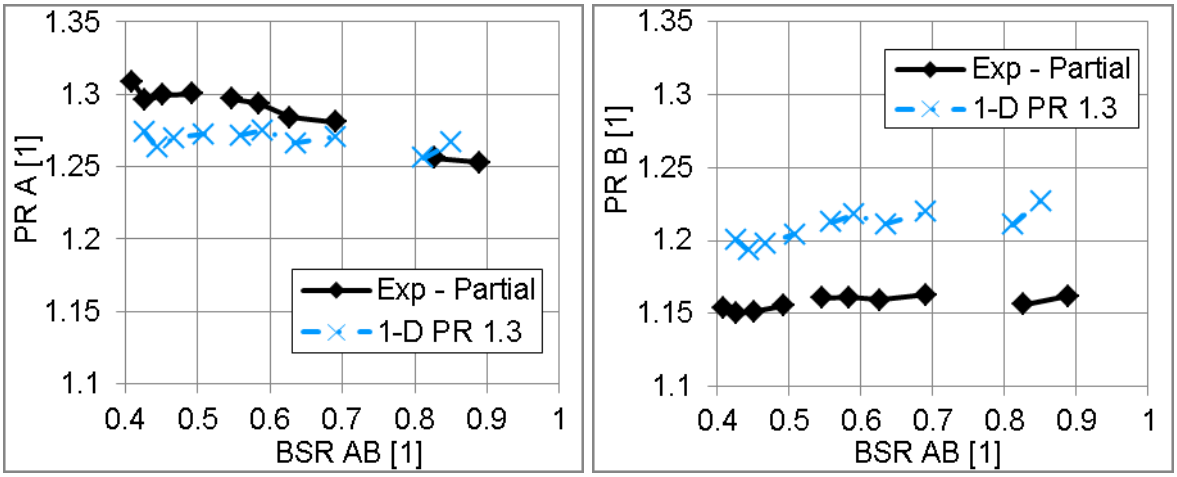

Figure 245 Pressure ratio A (left) and B (right) vs. BSR (approximate pressure ratio level PR AB = 1.3), partial admission level A = 0.87; experiments (black); simulation 1-D turbine (blue crosses)

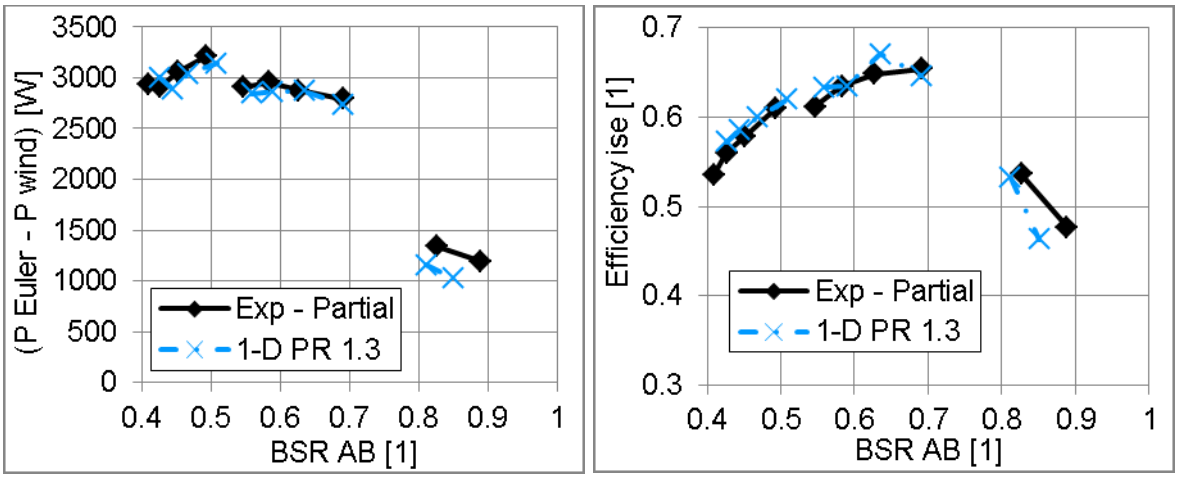

Figure 246 Turbine power (left) and isentropic efficiency (right) vs. BSR (approximate pressure ratio level PR AB = 1.3), partial admission level A = 0.87; experiments (black); simulation 1-D turbine (blue crosses)

Partial admission, PR AB = 1.6

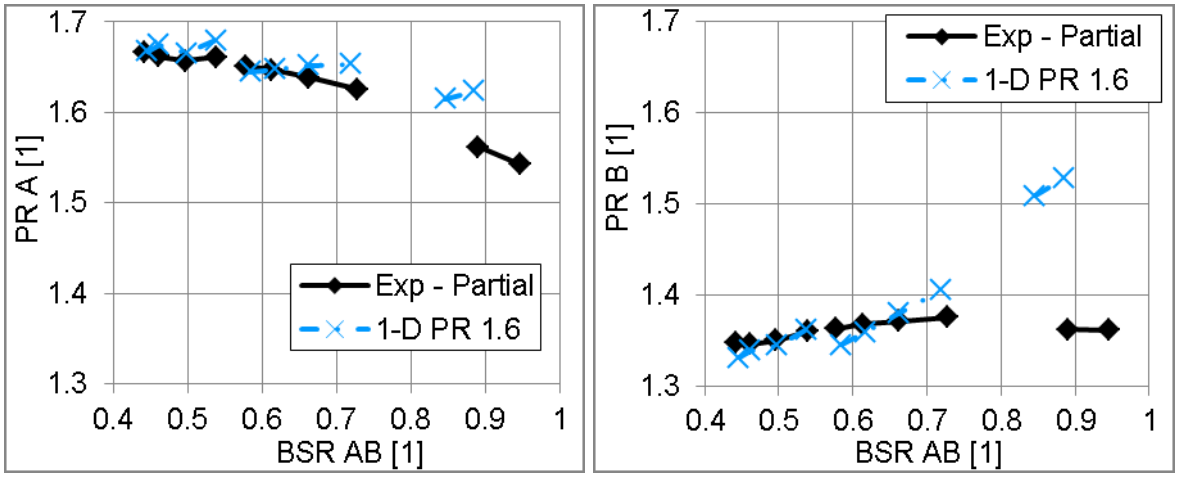

Figure 247 Pressure ratio A (left) and B (right) vs. BSR (approximate pressure ratio level PR AB = 1.6), partial admission level A = 0.87; experiments (black); simulation 1-D turbine (blue crosses)

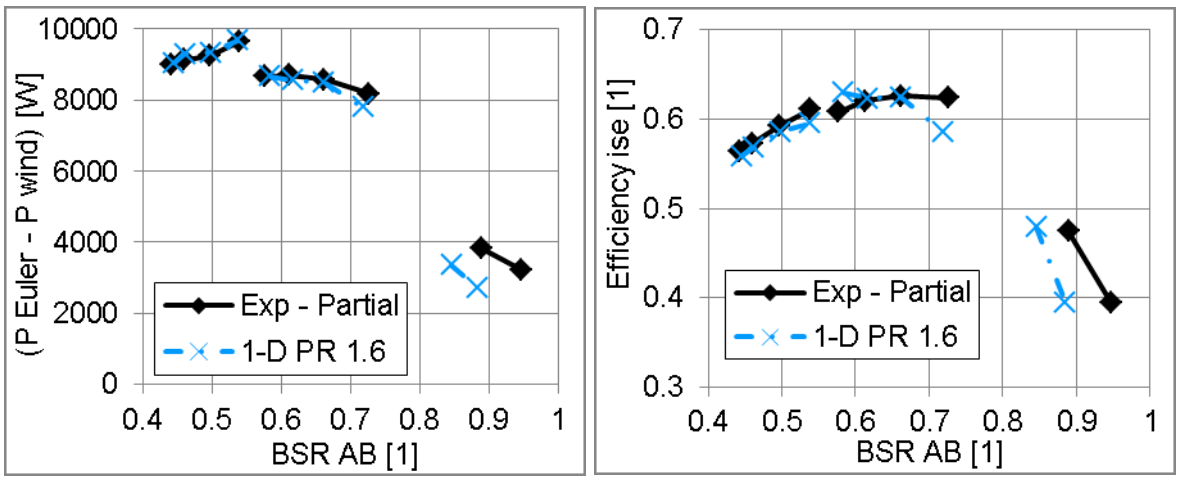

Figure 248 Turbine power (left) and isentropic efficiency (right) vs. BSR (approximate pressure ratio level PR AB = 1.6), partial admission level A = 0.87; experiments (black); simulation 1-D turbine (blue crosses)

Partial admission, PR AB = 2.2

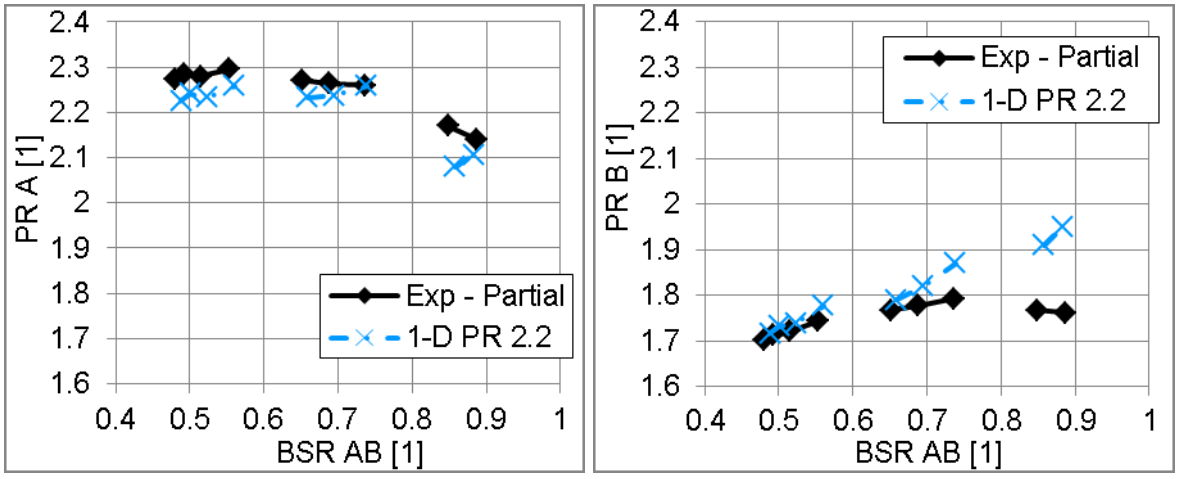

Figure 249 Pressure ratio A (left) and B (right) vs. BSR (approximate pressure ratio level PR AB = 2.2), partial admission level A = 0.87; experiments (black); simulation 1-D turbine (blue crosses)

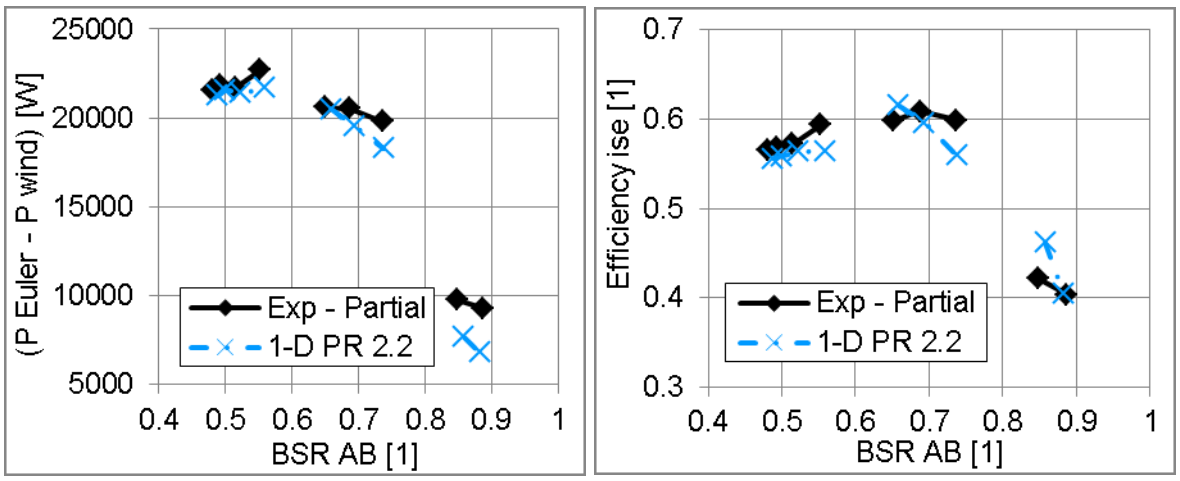

Figure 250 Turbine power (left) and isentropic efficiency (right) vs. BSR (approximate pressure ratio level PR AB = 2.2), partial admission level A = 0.87; experiments (black); simulation 1-D turbine (blue crosses)

Partial admission, PR AB = 2.7

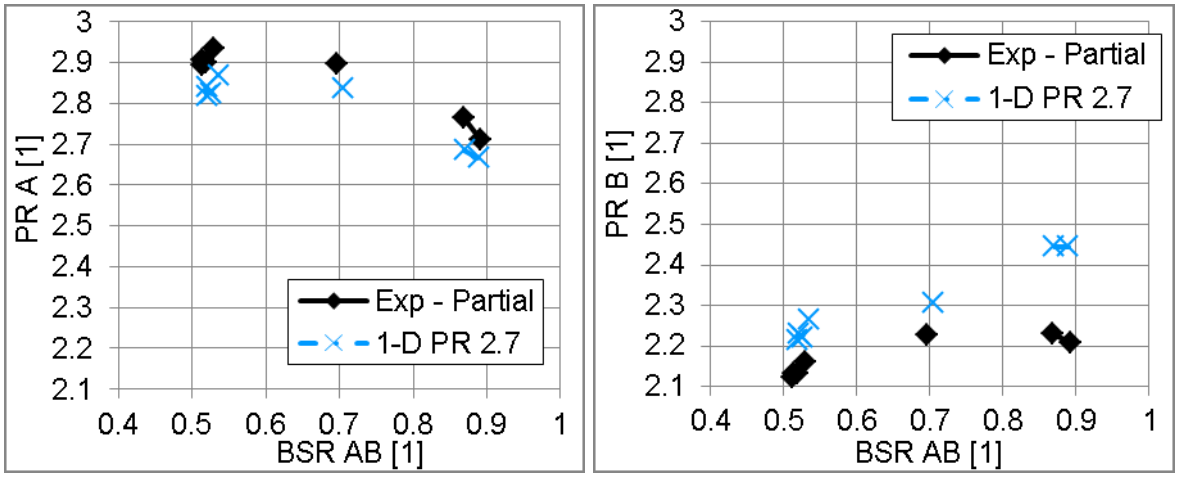

Figure 251 Pressure ratio A (left) and B (right) vs. BSR (approximate pressure ratio level PR AB = 2.7), partial admission level A = 0.87; experiments (black); simulation 1-D turbine (blue crosses)

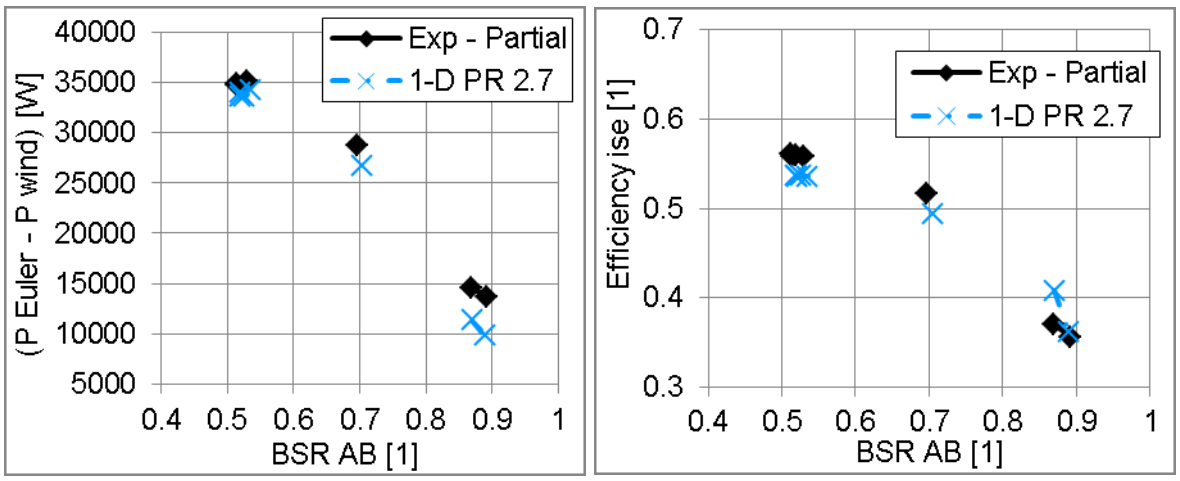

Figure 252 Turbine power (left) and isentropic efficiency (right) vs. BSR (approximate pressure ratio level PR AB = 2.7), partial admission level A = 0.87; experiments (black); simulation 1-D turbine (blue crosses)

Partial admission, PR AB = 3.3

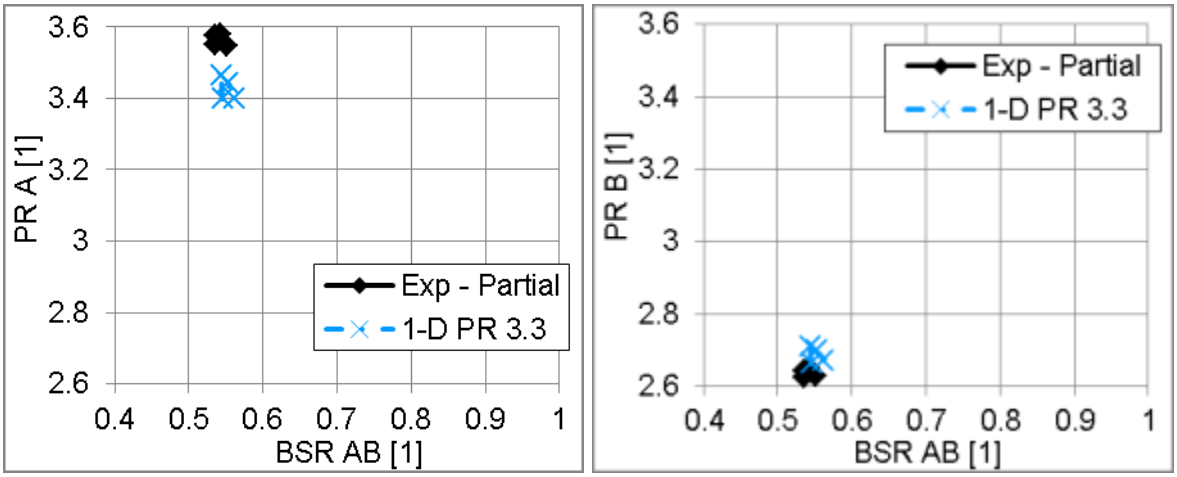

Figure 253 Pressure ratio A (left) and B (right) vs. BSR (approximate pressure ratio level PR AB = 3.3), partial admission level A = 0.87; experiments (black); simulation 1-D turbine (blue crosses)

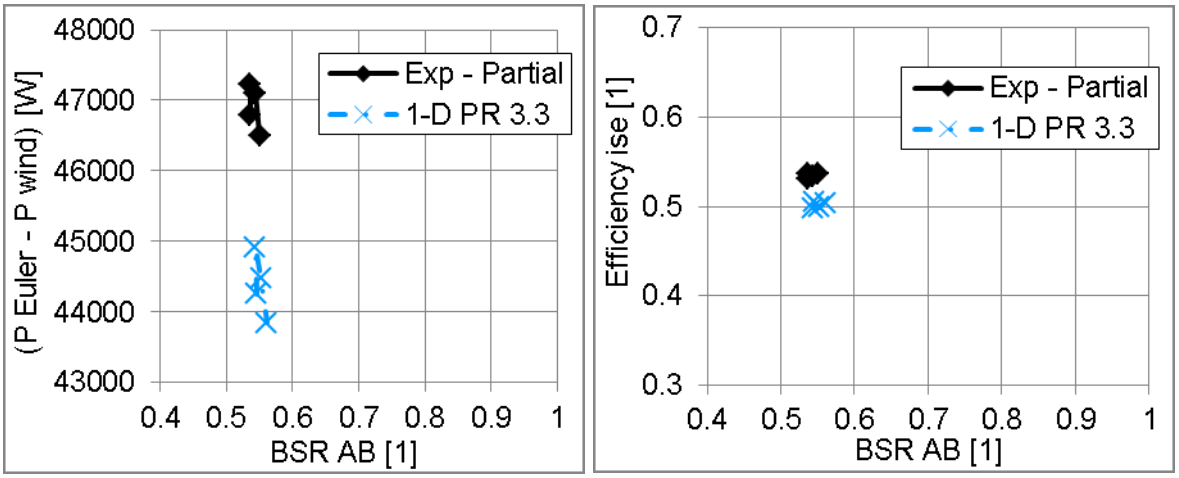

Figure 254 Turbine power (left) and isentropic efficiency (right) vs. BSR (approximate pressure ratio level PR AB = 3.3), partial admission level A = 0.87; experiments (black); simulation 1-D turbine (blue crosses)

Extreme partial admission with closed section B

Closed section - PR = 1.3

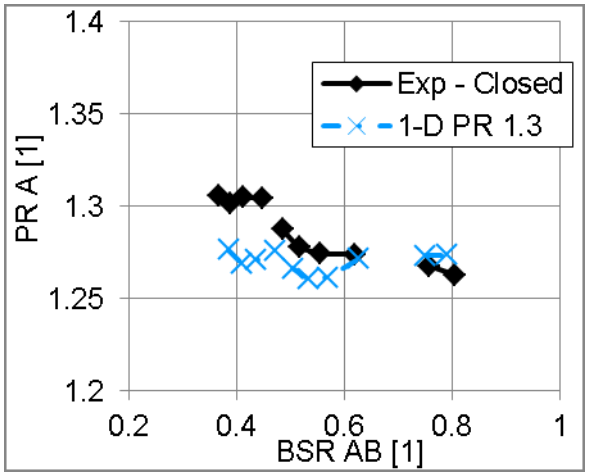

Figure 255 Pressure ratio A vs. BSR (approximate pressure ratio level PR AB = 1.3), section B closed; experiments (black); simulation 1-D turbine (blue crosses)

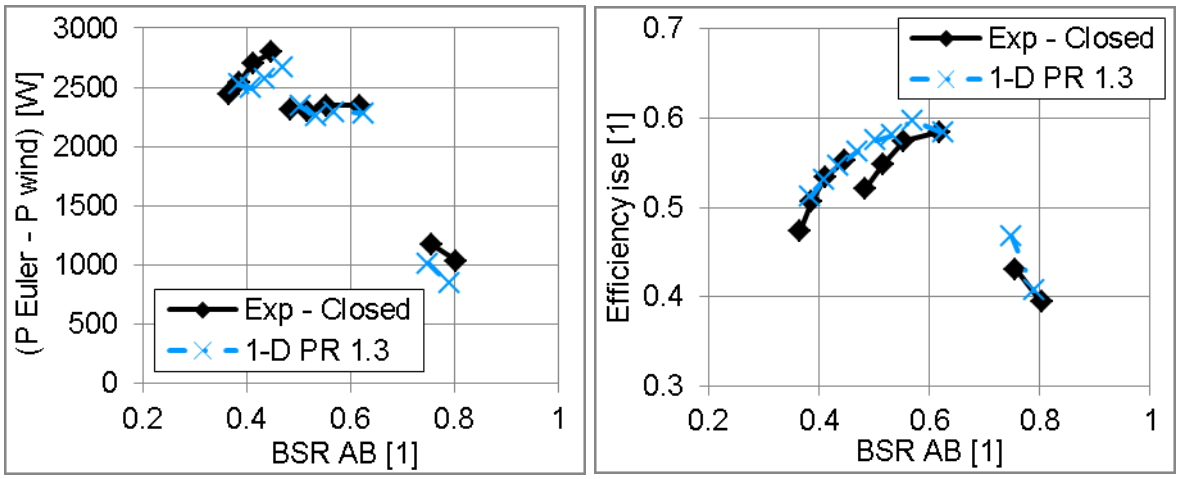

Figure 256 Turbine power (left) and isentropic efficiency (right) vs. BSR (approximate pressure ratio level PR AB = 1.3), section B closed; experiments (black); simulation 1-D turbine (blue crosses)

Closed section - PR = 1.6

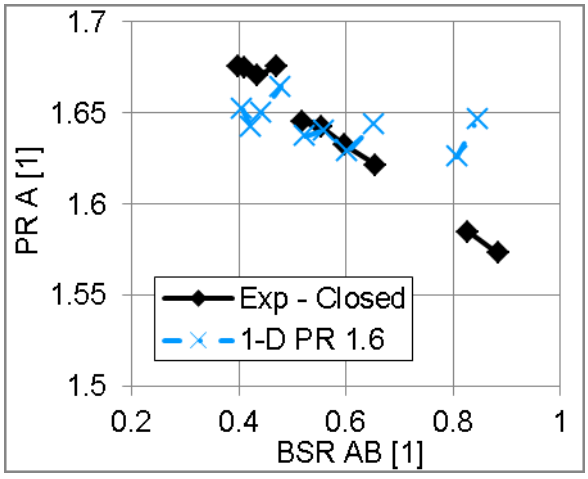

Figure 257 Pressure ratio A vs. BSR (approximate pressure ratio level PR AB = 1.6), section B closed; experiments (black); simulation 1-D turbine (blue crosses)

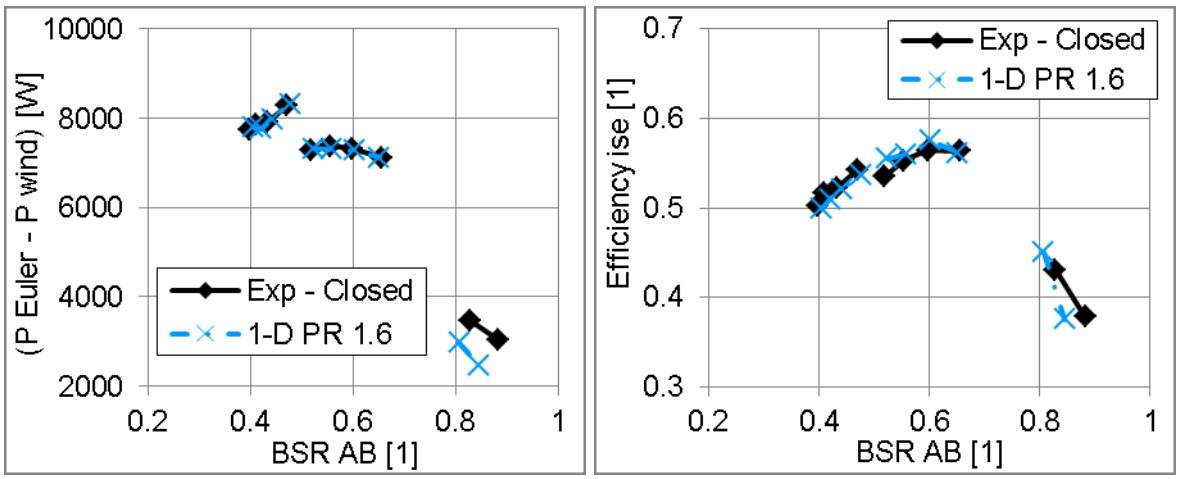

Figure 258 Turbine power (left) and isentropic efficiency (right) vs. BSR (approximate pressure ratio level PR AB = 1.6), section B closed; experiments (black); simulation 1-D turbine (blue crosses)

Closed section - PR = 2.2

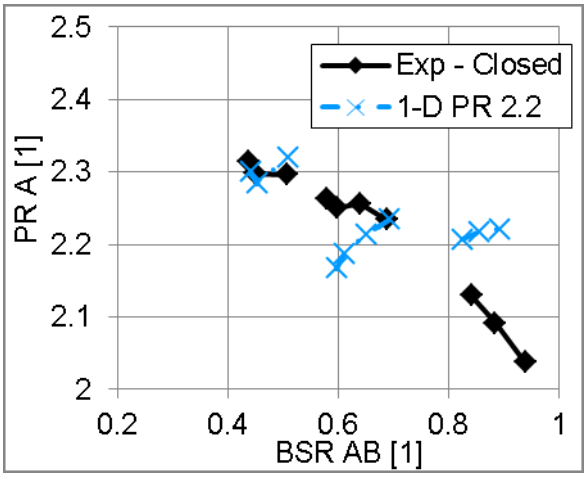

Figure 259 Pressure ratio A vs. BSR (approximate pressure ratio level PR AB = 2.2), section B closed; experiments (black); simulation 1-D turbine (blue crosses)

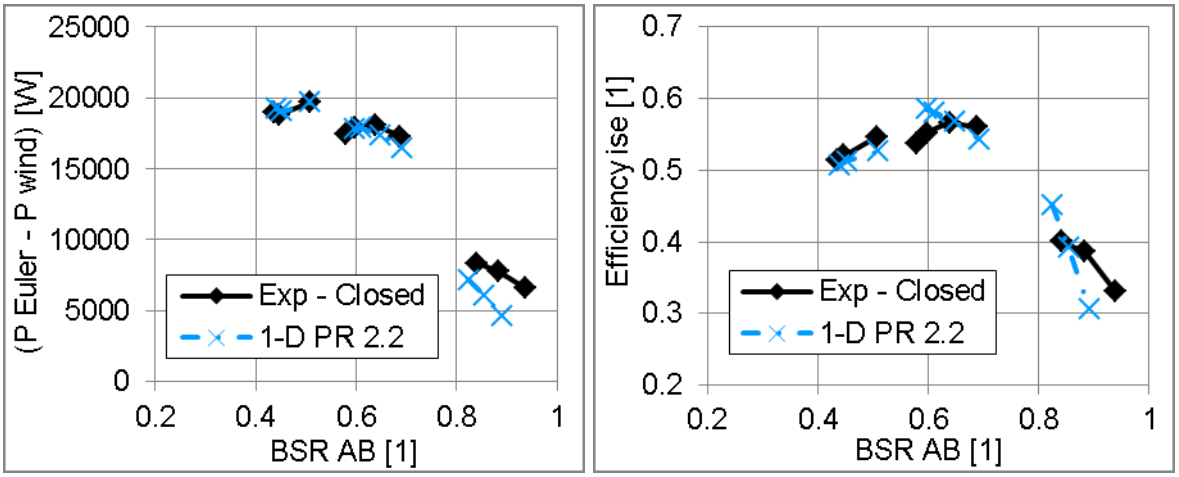

Figure 260 Turbine power (left) and isentropic efficiency (right) vs. BSR (approximate pressure ratio level PR AB = 2.2), section B closed; experiments (black); simulation 1-D turbine (blue crosses)

Closed section - PR = 2.7

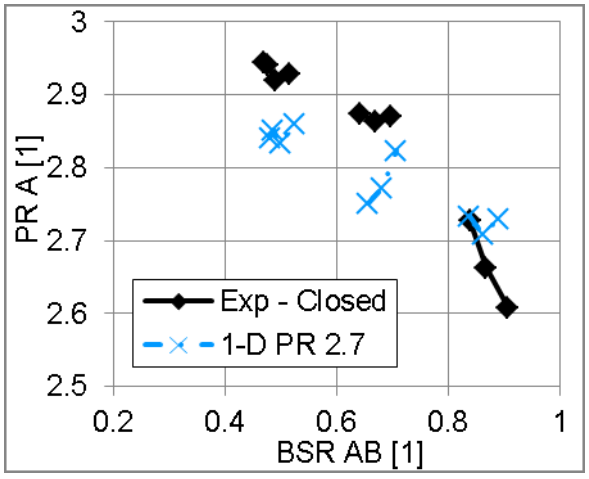

Figure 261 Pressure ratio A vs. BSR (approximate pressure ratio level PR AB = 2.7), section B closed; experiments (black); simulation 1-D turbine (blue crosses)

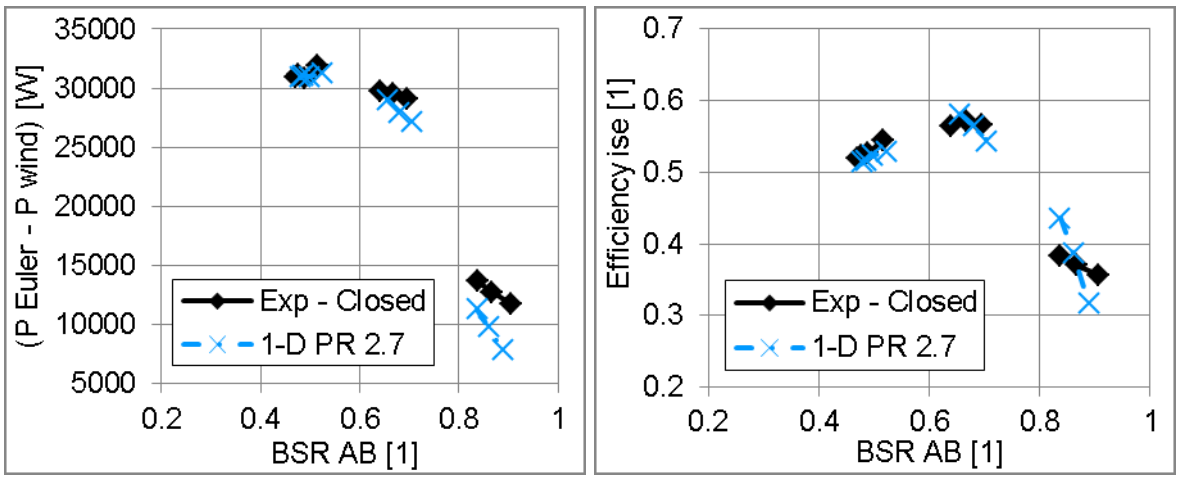

Figure 262 Turbine power (left) and isentropic efficiency (right) vs. BSR (approximate pressure ratio level PR AB = 2.7), section B closed; experiments (black); simulation 1-D turbine (blue crosses)

Closed section - PR = 3.3

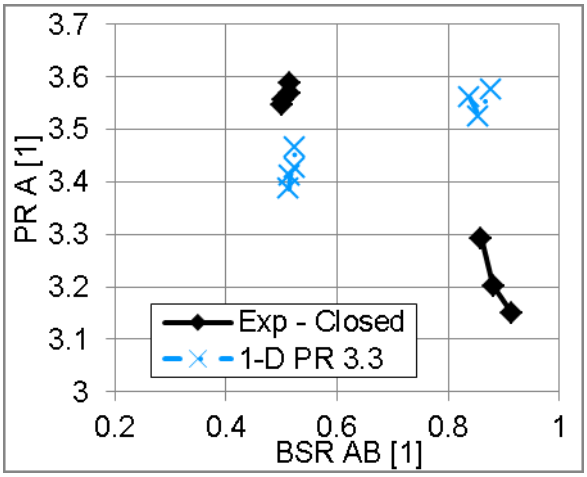

Figure 263 Pressure ratio A vs. BSR (approximate pressure ratio level PR AB = 3.3), section B closed; experiments (black); simulation 1-D turbine (blue crosses)

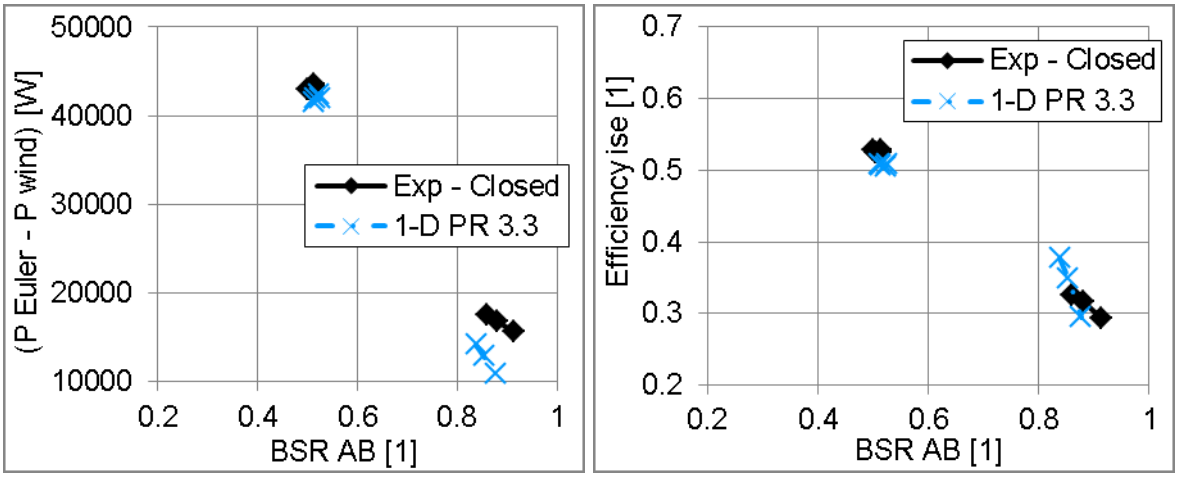

Figure 264 Turbine power (left) and isentropic efficiency (right) vs. BSR (approximate pressure ratio level PR AB = 3.3), section B closed; experiments (black); simulation 1-D turbine (blue crosses)

Appendix 4 - Simulation Results - Six Cylinder Diesel Engine

The results of engine simulation at steady states are compared with appropriate experimental data in pictures below.

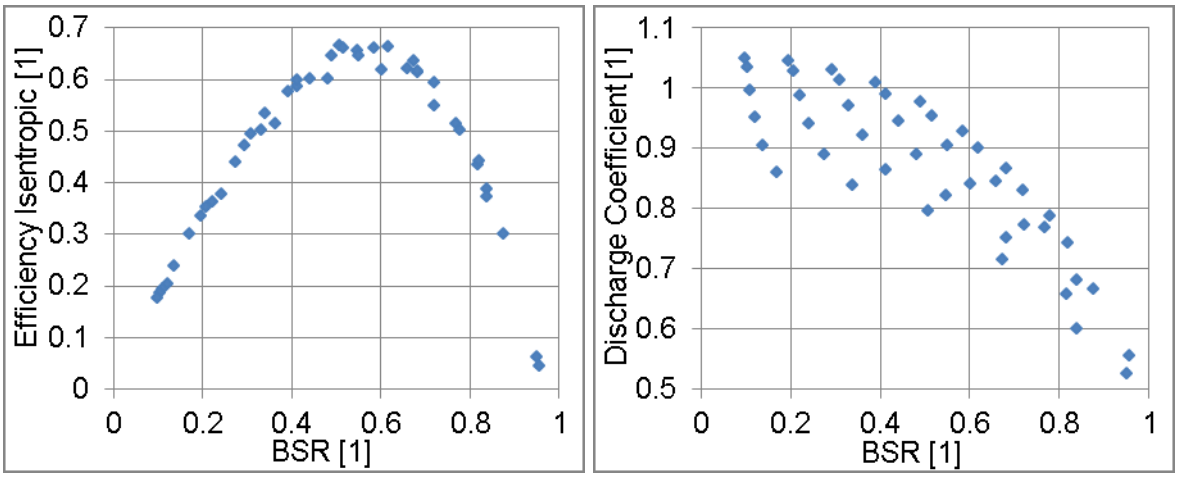

Figure 265 Turbine map used for 0-D simulation - based on results of calibrated 1-D turbine model (full admission of an impeller); turbine isentropic efficiency (left); discharge coefficient (right)

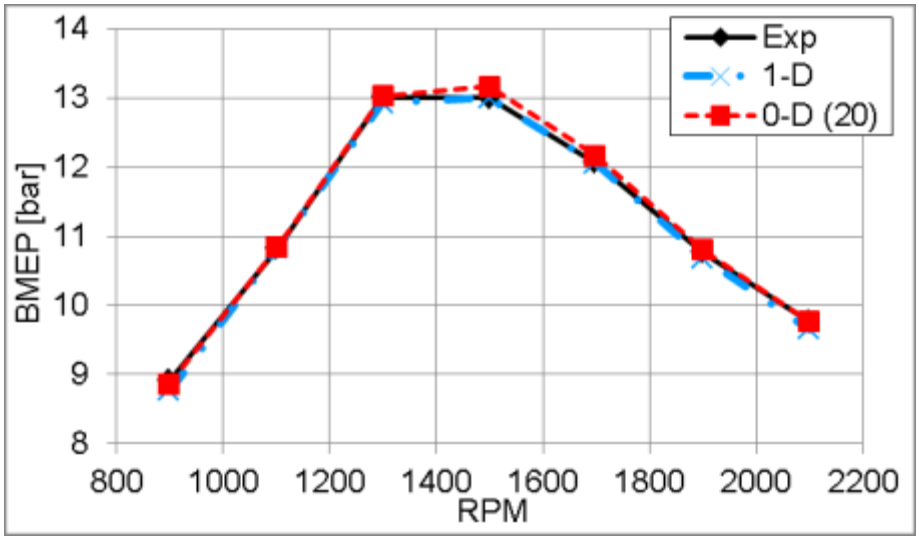

Figure 266 Brake mean effective pressure, experiment (black solid line), simulation with full 1-D unsteady turbine (blue dashed and dotted line), simulation with 0-D turbine map - sections connected via orifice D = 20 mm (red dashed line)

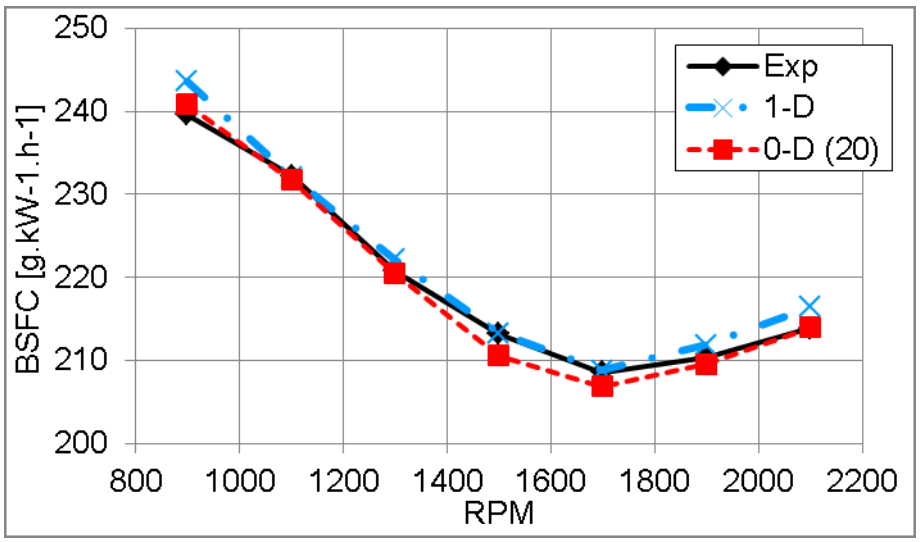

Figure 267 Brake specific fuel consumption, experiment (black solid line), simulation with full 1-D unsteady turbine (blue dashed and dotted line), simulation with 0-D turbine map - sections connected via orifice D = 20 mm (red dashed line)

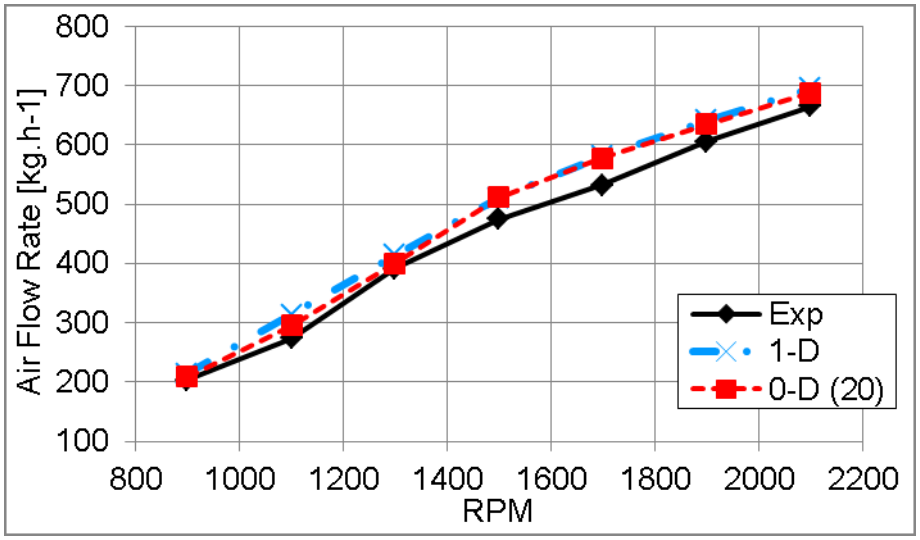

Figure 268 Air mass flow rate, experiment (black solid line), simulation with full 1-D unsteady turbine (blue dashed and dotted line), simulation with 0-D turbine map - sections connected via orifice D = 20 mm (red dashed line)

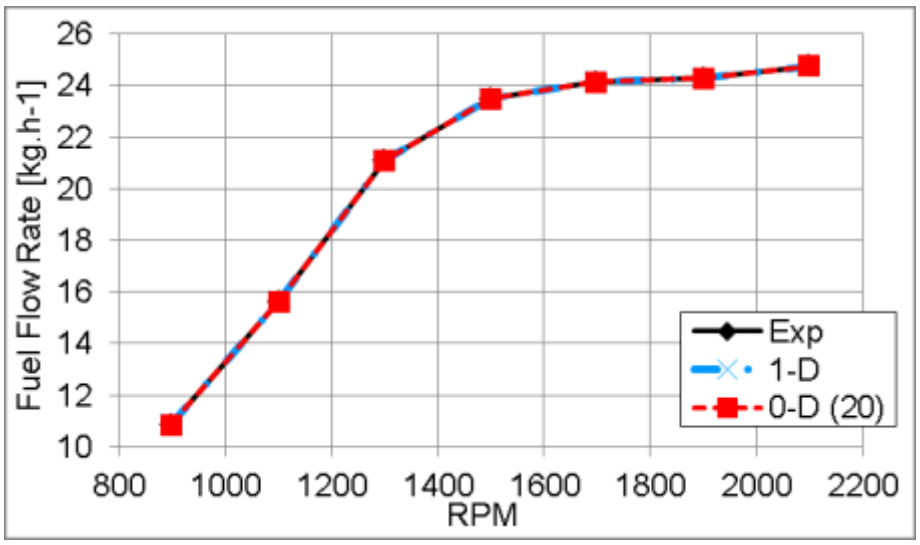

Figure 269 Fuel mass flow rate, experiment (black solid line), simulation with full 1-D unsteady turbine (blue dashed and dotted line), simulation with 0-D turbine map - sections connected via orifice D = 20 mm (red dashed line)

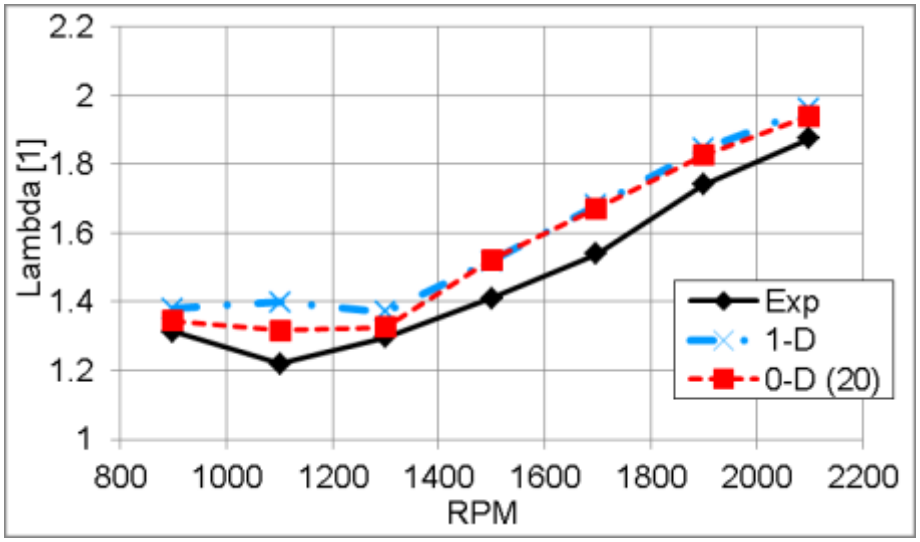

Figure 270 Lambda, experiment (black solid line), simulation with full 1-D unsteady turbine (blue dashed and dotted line), simulation with 0-D turbine map - sections connected via orifice D = 20 mm (red dashed line)

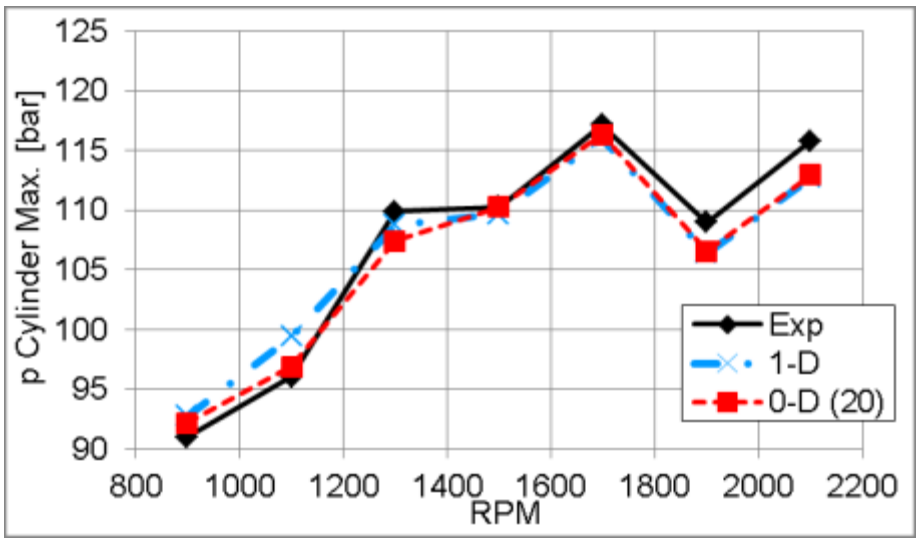

Figure 271 Maximum pressure in cylinder, experiment (black solid line), simulation with full 1-D unsteady turbine (blue dashed and dotted line), simulation with 0-D turbine map - sections connected via orifice D = 20 mm (red dashed line)

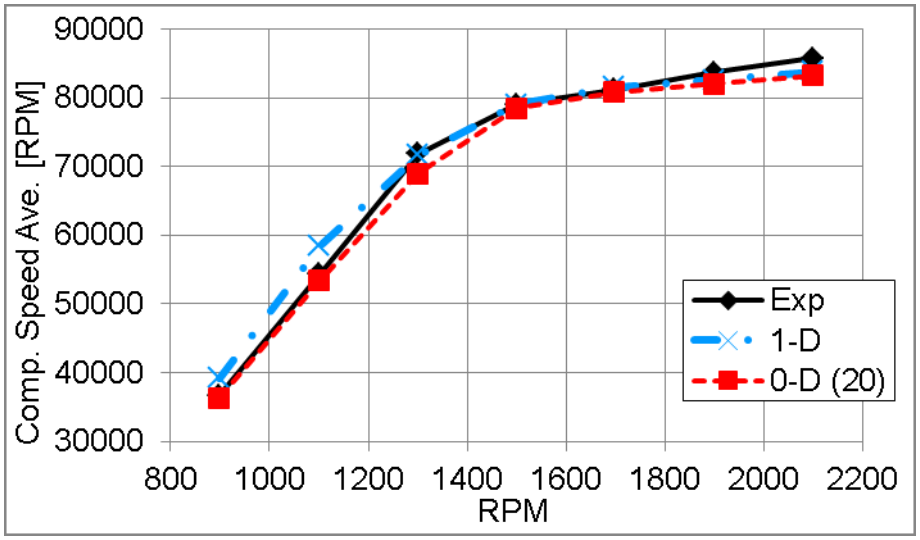

Figure 272 Compressor speed, experiment (black solid line), simulation with full 1-D unsteady turbine (blue dashed and dotted line), simulation with 0-D turbine map - sections connected via orifice D = 20 mm (red dashed line)

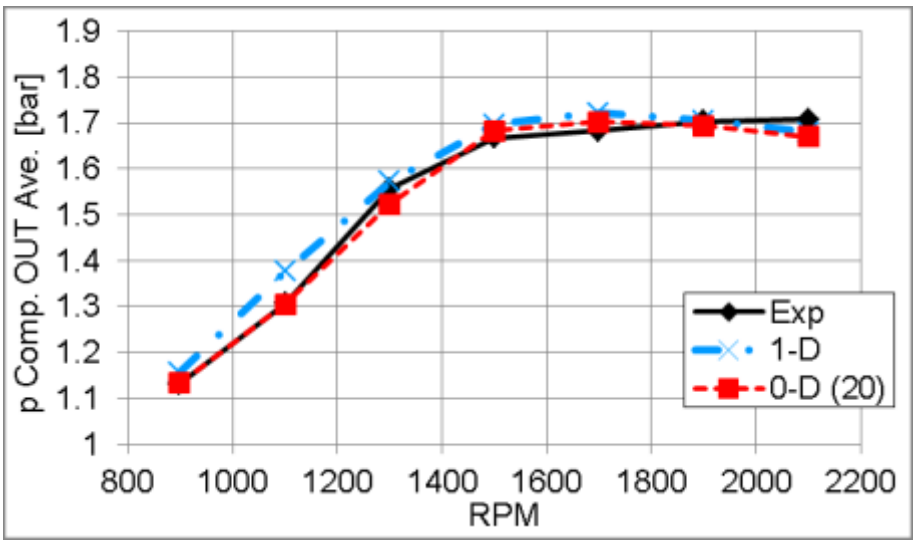

Figure 273 Pressure downstream of a compressor, experiment (black solid line), simulation with full 1-D unsteady turbine (blue dashed and dotted line), simulation with 0-D turbine map - sections connected via orifice D = 20 mm (red dashed line)

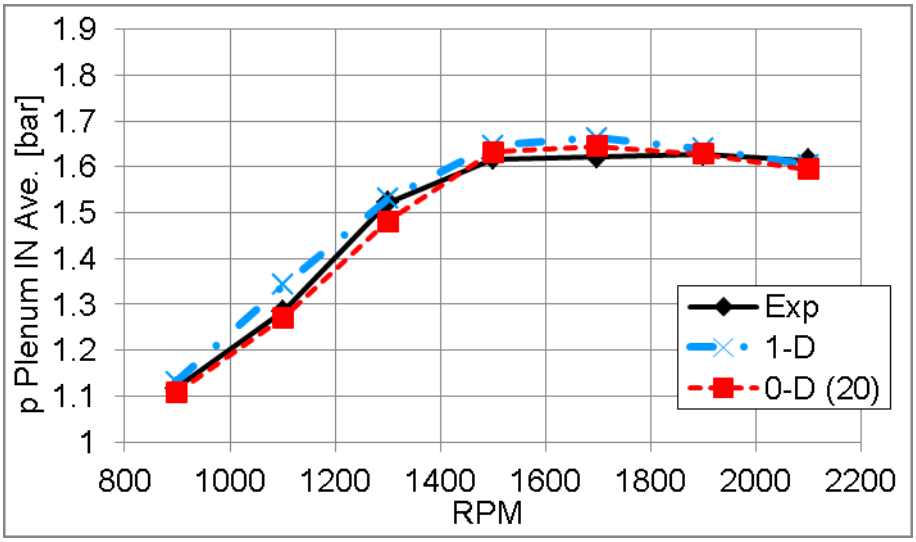

Figure 274 Pressure in intake plenum, experiment (black solid line), simulation with full 1-D unsteady turbine (blue dashed and dotted line), simulation with 0-D turbine map - sections connected via orifice D = 20 mm (red dashed line)

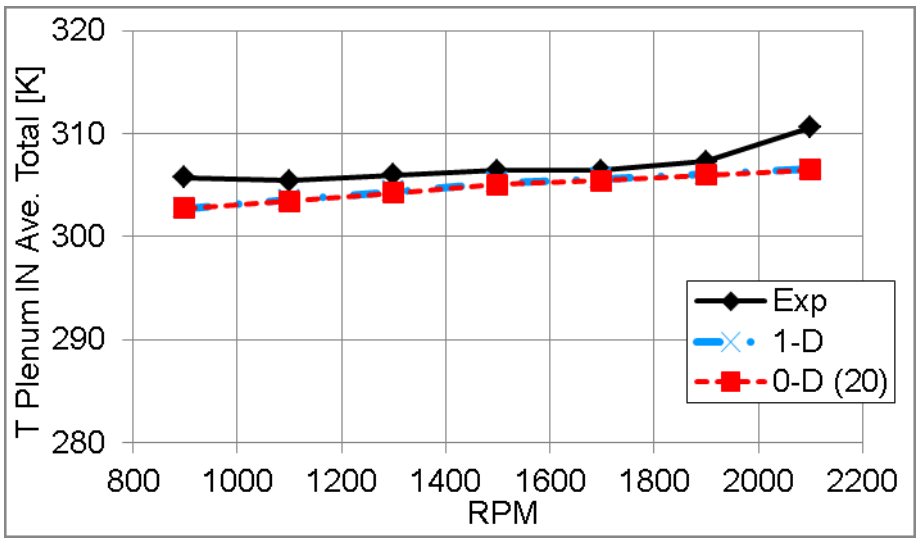

Figure 275 Total temperature in intake plenum, experiment (black solid line), simulation with full 1-D unsteady turbine (blue dashed and dotted line), simulation with 0-D turbine map - sections connected via orifice D = 20 mm (red dashed line)

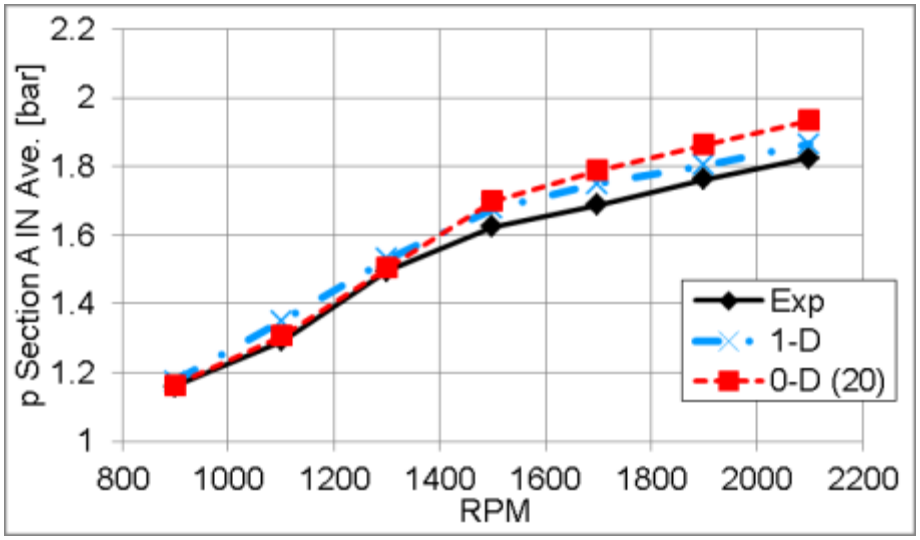

Figure 276 Pressure at inlet of turbine section A, experiment (black solid line), simulation with full 1-D unsteady turbine (blue dashed and dotted line), simulation with 0-D turbine map - sections connected via orifice D = 20 mm (red dashed line)

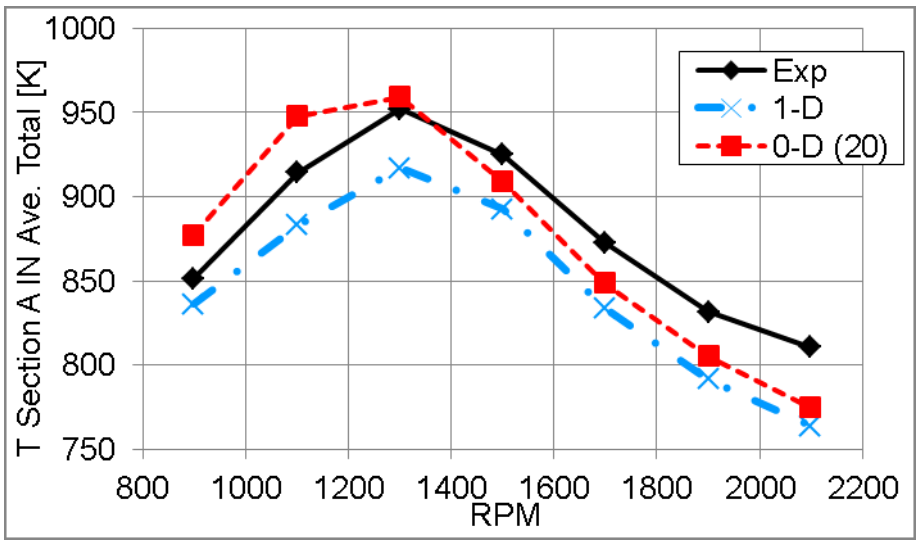

Figure 277 Total temperature at inlet of turbine section A, experiment (black solid line), simulation with full 1-D unsteady turbine (blue dashed and dotted line), simulation with 0-D turbine map - sections connected via orifice D = 20 mm (red dashed line)

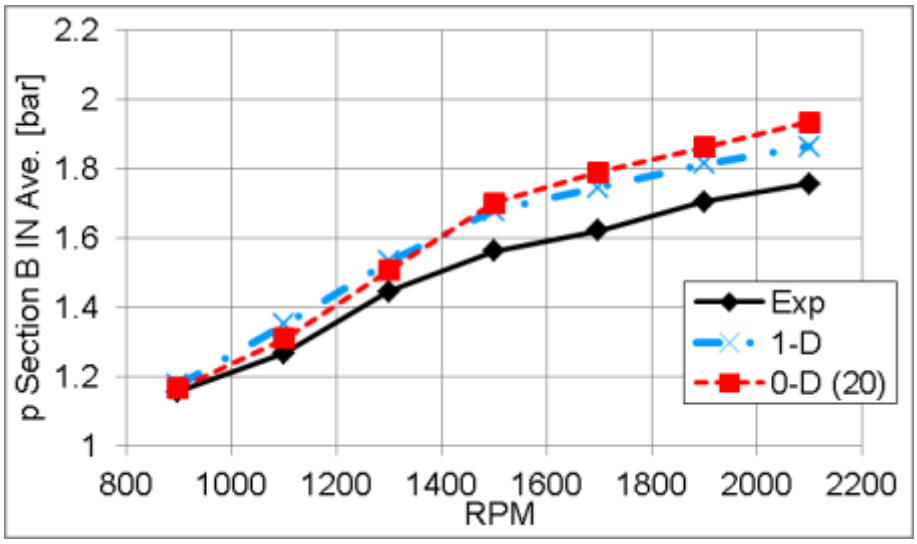

Figure 278 Pressure at inlet of turbine section B, experiment (black solid line), simulation with full 1-D unsteady turbine (blue dashed and dotted line), simulation with 0-D turbine map - sections connected via orifice D = 20 mm (red dashed line)

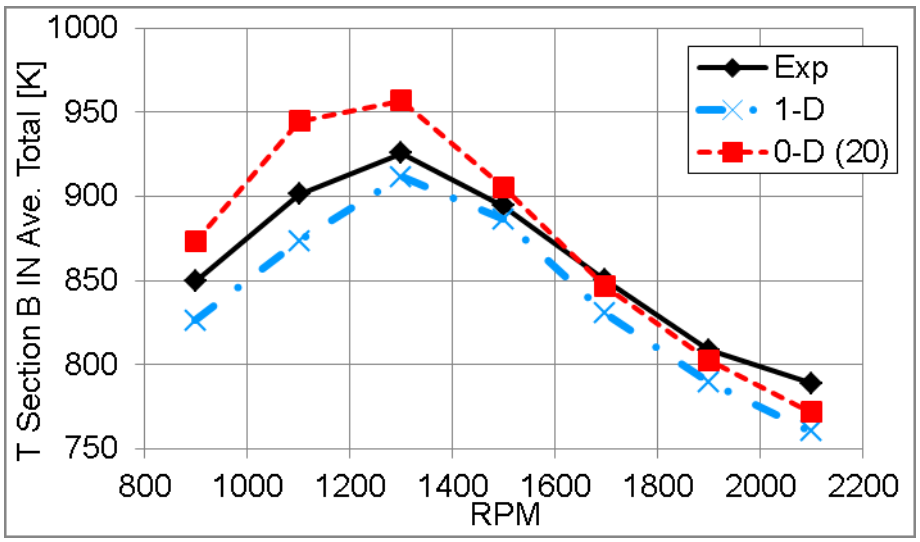

Figure 279 Total temperature at inlet of turbine section B, experiment (black solid line), simulation with full 1-D unsteady turbine (blue dashed and dotted line), simulation with 0-D turbine map - sections connected via orifice D = 20 mm (red dashed line)

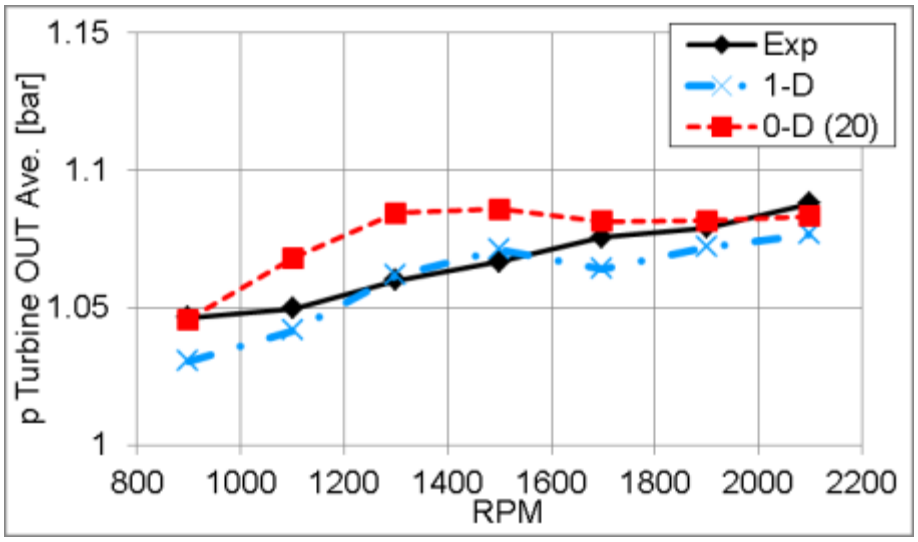

Figure 280 Pressure turbine downstream, experiment (black solid line), simulation with full 1-D unsteady turbine (blue dashed and dotted line), simulation with 0-D turbine map - sections connected via orifice D = 20 mm (red dashed line)

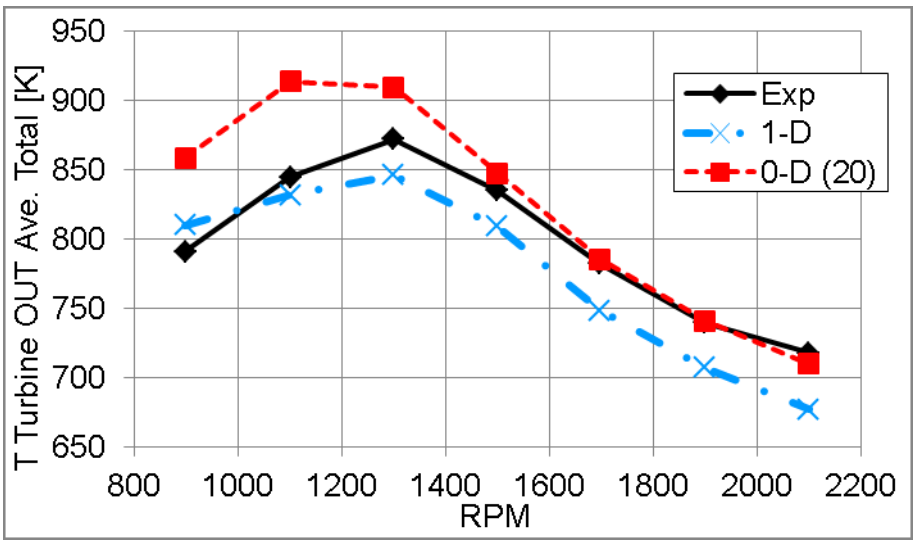

Figure 281 Total temperature turbine downstream, experiment (black solid line), simulation with full 1-D unsteady turbine (blue dashed and dotted line), simulation with 0-D turbine map - sections connected via orifice D = 20 mm (red dashed line)

The comparison of experiments and results of engine simulation with several 0-D turbine models follows.

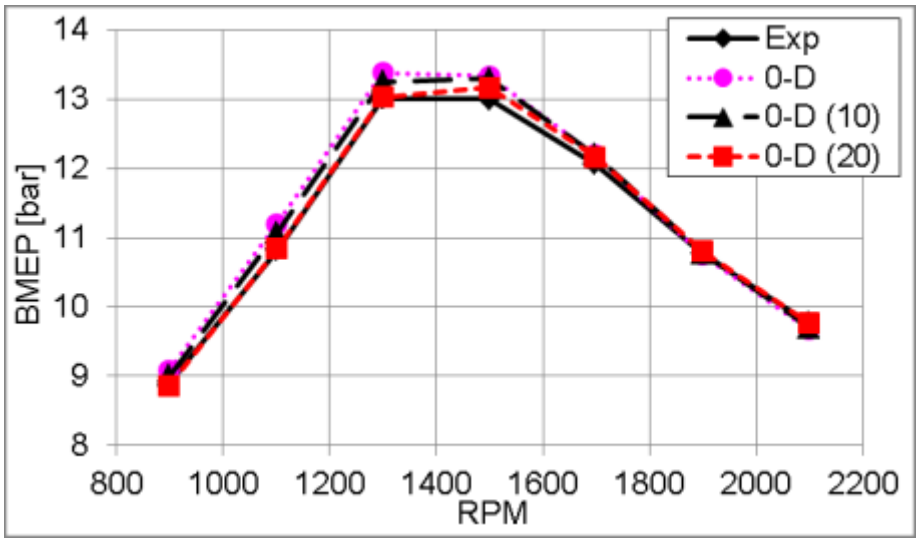

Figure 282 Brake mean effective pressure, experiment (black solid line), simulation with 0-D turbine map - sections without connection (purple dotted line), simulation with 0-D turbine map - sections connected via orifice D = 10 mm (black dashed line), simulation with 0-D turbine map - sections connected via orifice D = 20 mm (red dashed line)

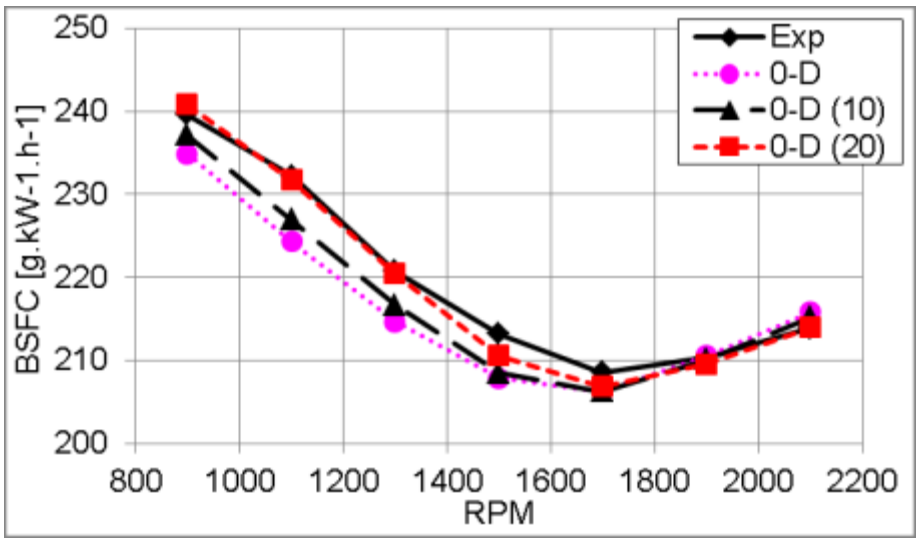

Figure 283 Brake specific fuel consumption, experiment (black solid line), simulation with 0-D turbine map - sections without connection (purple dotted line), simulation with 0-D turbine map - sections connected via orifice D = 10 mm (black dashed line), simulation with 0-D turbine map - sections connected via orifice D = 20 mm (red dashed line)

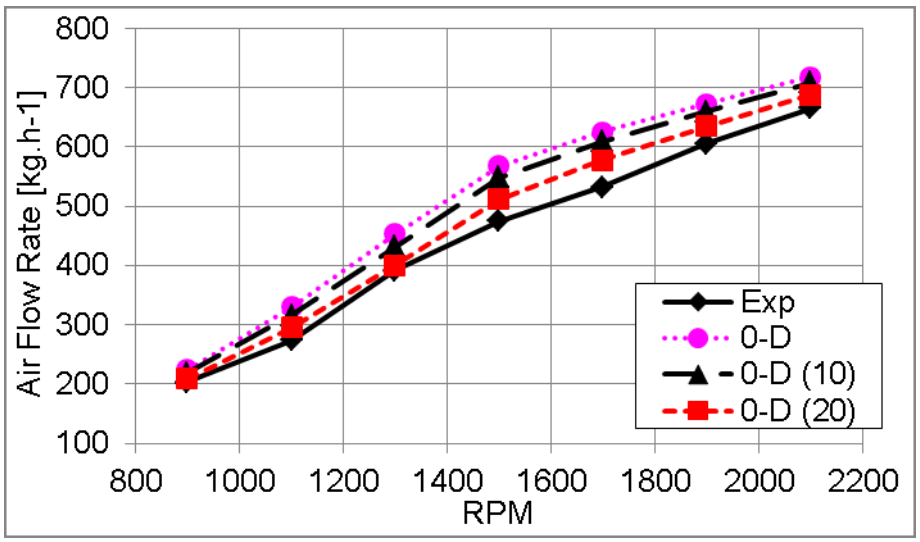

Figure 284 Air mass flow rate, experiment (black solid line), simulation with 0-D turbine map - sections without connection (purple dotted line), simulation with 0-D turbine map - sections connected via orifice D = 10 mm (black dashed line), simulation with 0-D turbine map - sections connected via orifice D = 20 mm (red dashed line)

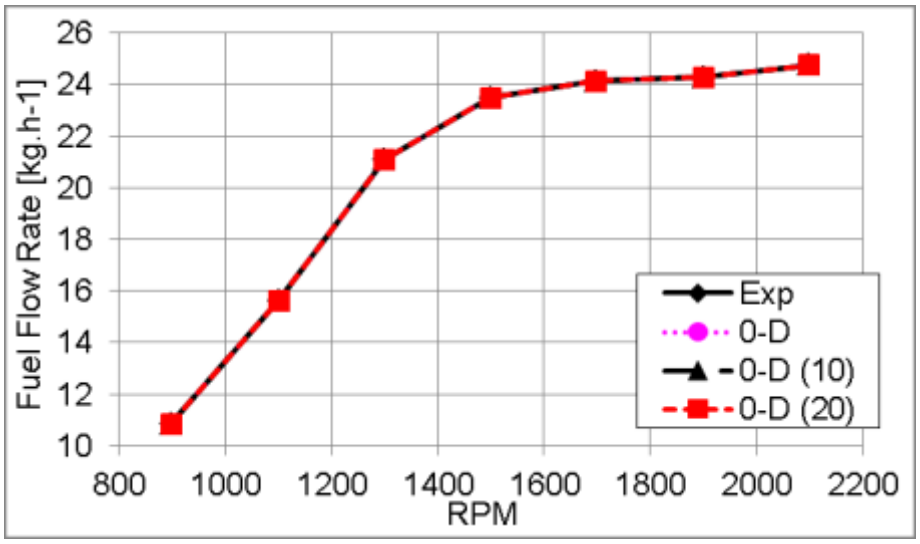

Figure 285 Fuel mass flow rate, experiment (black solid line), simulation with 0-D turbine map - sections without connection (purple dotted line), simulation with 0-D turbine map - sections connected via orifice D = 10 mm (black dashed line), simulation with 0-D turbine map - sections connected via orifice D = 20 mm (red dashed line)

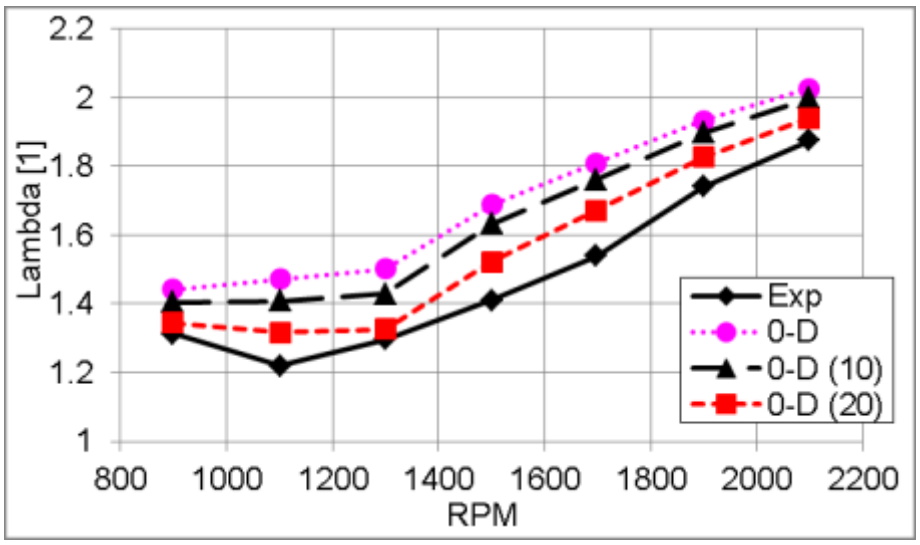

Figure 286 Lambda, experiment (black solid line), simulation with 0-D turbine map - sections without connection (purple dotted line), simulation with 0-D turbine map - sections connected via orifice D = 10 mm (black dashed line), simulation with 0-D turbine map - sections connected via orifice D = 20 mm (red dashed line)

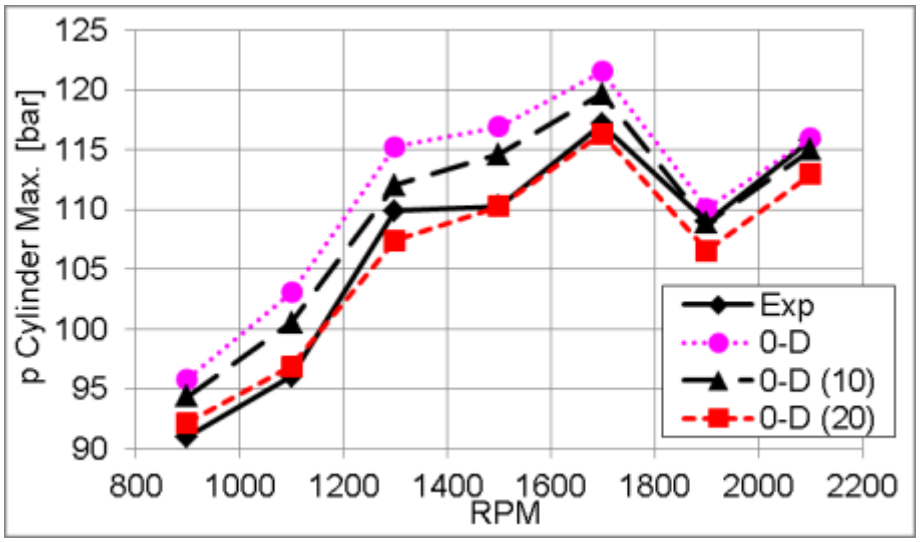

Figure 287 Maximum pressure in cylinder, experiment (black solid line), simulation with 0-D turbine map - sections without connection (purple dotted line), simulation with 0-D turbine map - sections connected via orifice D = 10 mm (black dashed line), simulation with 0-D turbine map - sections connected via orifice D = 20 mm (red dashed line)

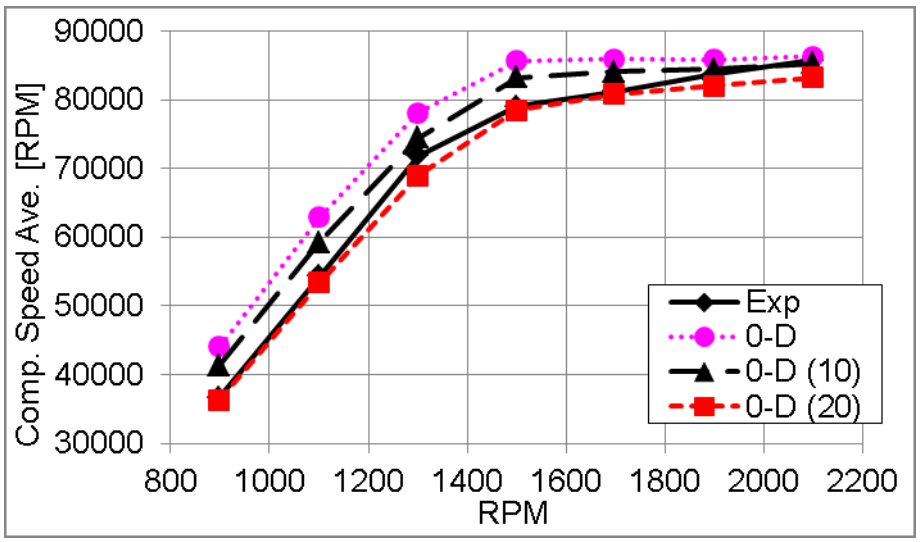

Figure 288 Compressor speed, experiment (black solid line), simulation with 0-D turbine map - sections without connection (purple dotted line), simulation with 0-D turbine map - sections connected via orifice D = 10 mm (black dashed line), simulation with 0-D turbine map - sections connected via orifice D = 20 mm (red dashed line)

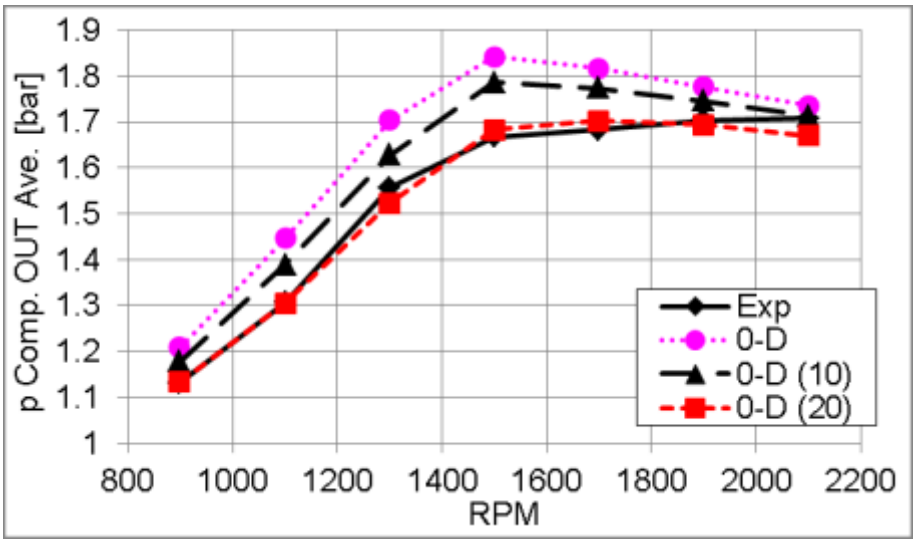

Figure 289 Pressure downstream of a compressor, experiment (black solid line), simulation with 0-D turbine map - sections without connection (purple dotted line), simulation with 0-D turbine map - sections connected via orifice D = 10 mm (black dashed line), simulation with 0-D turbine map - sections connected via orifice D = 20 mm (red dashed line)

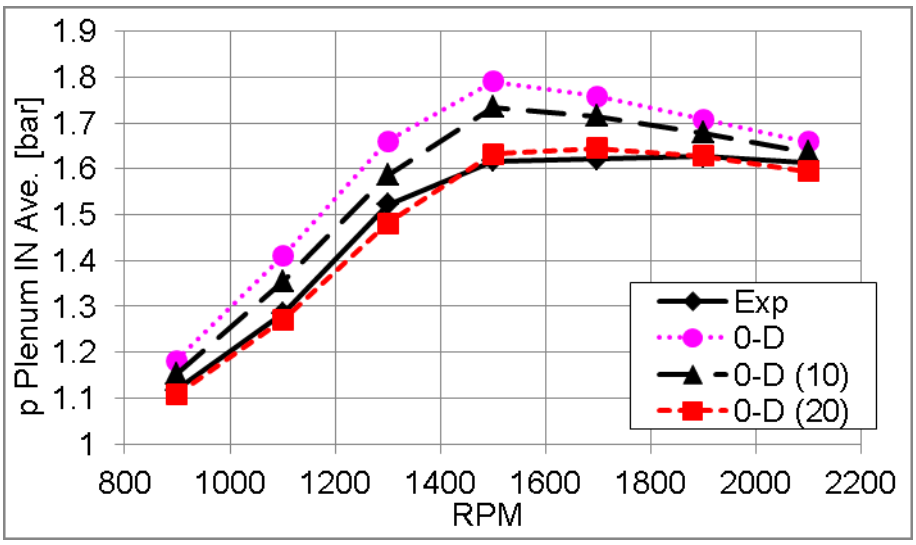

Figure 290 Pressure in intake plenum, experiment (black solid line), simulation with 0-D turbine map - sections without connection (purple dotted line), simulation with 0-D turbine map - sections connected via orifice D = 10 mm (black dashed line), simulation with 0-D turbine map - sections connected via orifice D = 20 mm (red dashed line)

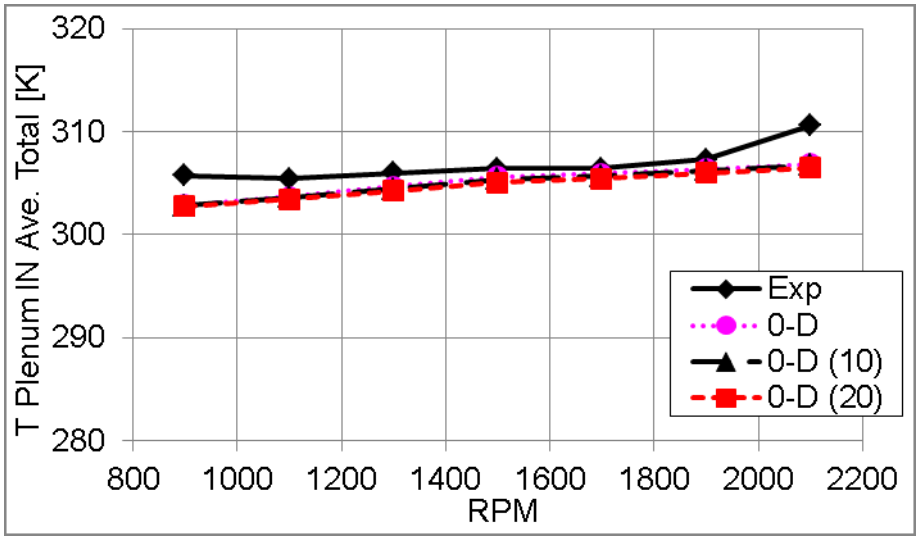

Figure 291 Total temperature in intake plenum, experiment (black solid line), simulation with 0-D turbine map - sections without connection (purple dotted line), simulation with 0-D turbine map - sections connected via orifice D = 10 mm (black dashed line), simulation with 0-D turbine map - sections connected via orifice D = 20 mm (red dashed line)

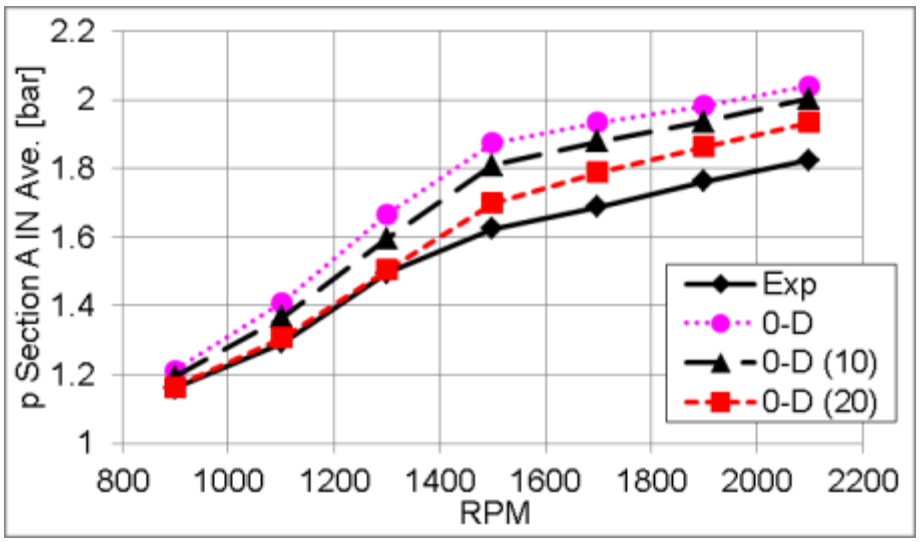

Figure 292 Pressure at inlet of turbine section A, experiment (black solid line), simulation with 0-D turbine map - sections without connection (purple dotted line), simulation with 0-D turbine map - sections connected via orifice D = 10 mm (black dashed line), simulation with 0-D turbine map - sections connected via orifice D = 20 mm (red dashed line)

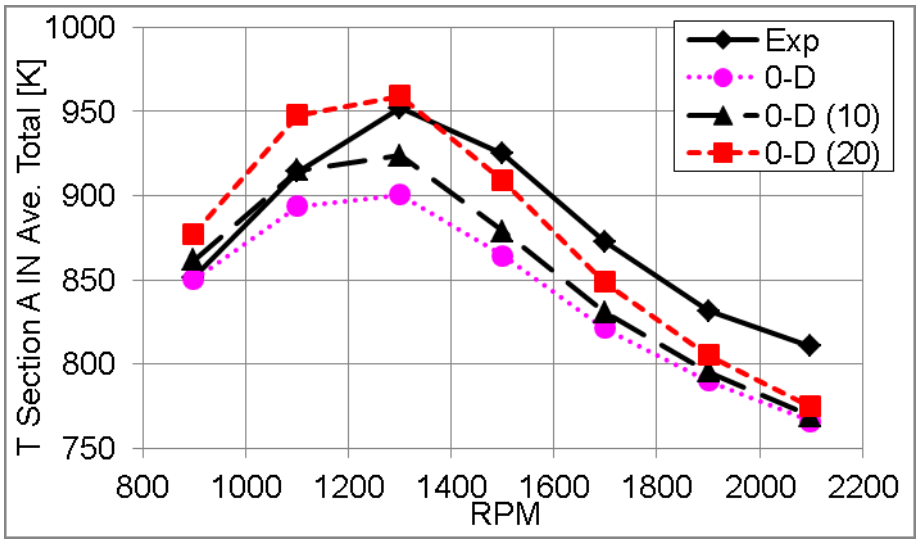

Figure 293 Total temperature at inlet of turbine section A, experiment (black solid line), simulation with 0-D turbine map - sections without connection (purple dotted line), simulation with 0-D turbine map - sections connected via orifice D = 10 mm (black dashed line), simulation with 0-D turbine map - sections connected via orifice D = 20 mm (red dashed line)

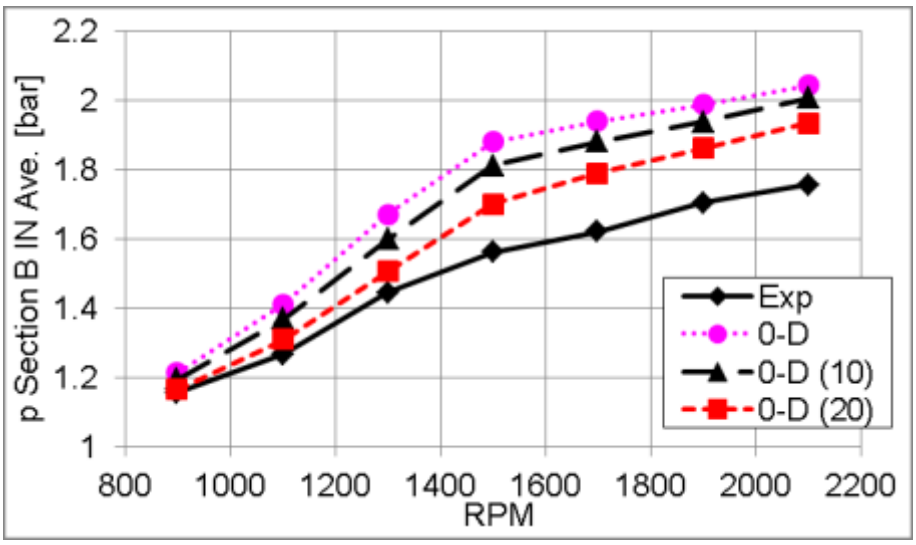

Figure 294 Pressure at inlet of turbine section B, experiment (black solid line), simulation with 0-D turbine map - sections without connection (purple dotted line), simulation with 0-D turbine map - sections connected via orifice D = 10 mm (black dashed line), simulation with 0-D turbine map - sections connected via orifice D = 20 mm (red dashed line)

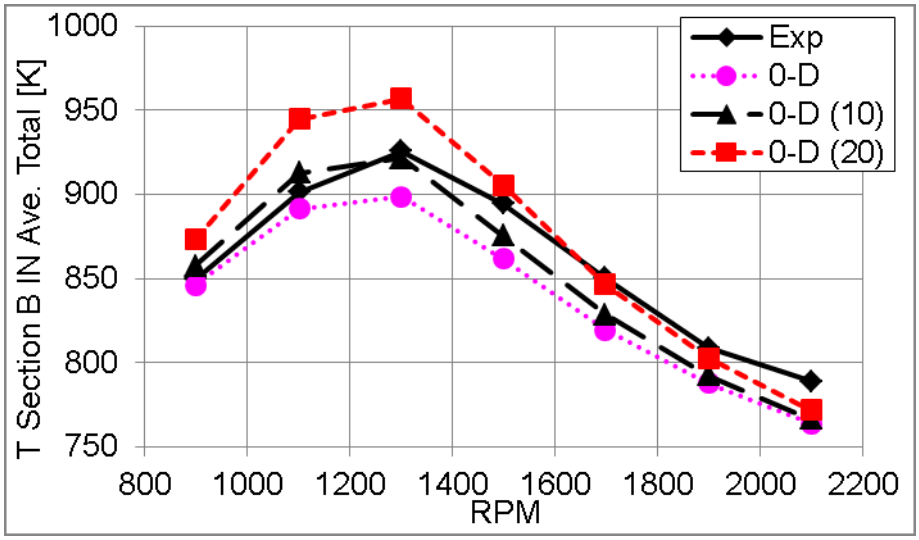

Figure 295 Total temperature at inlet of turbine section B, experiment (black solid line), simulation with 0-D turbine map - sections without connection (purple dotted line), simulation with 0-D turbine map - sections connected via orifice D = 10 mm (black dashed line), simulation with 0-D turbine map - sections connected via orifice D = 20 mm (red dashed line)

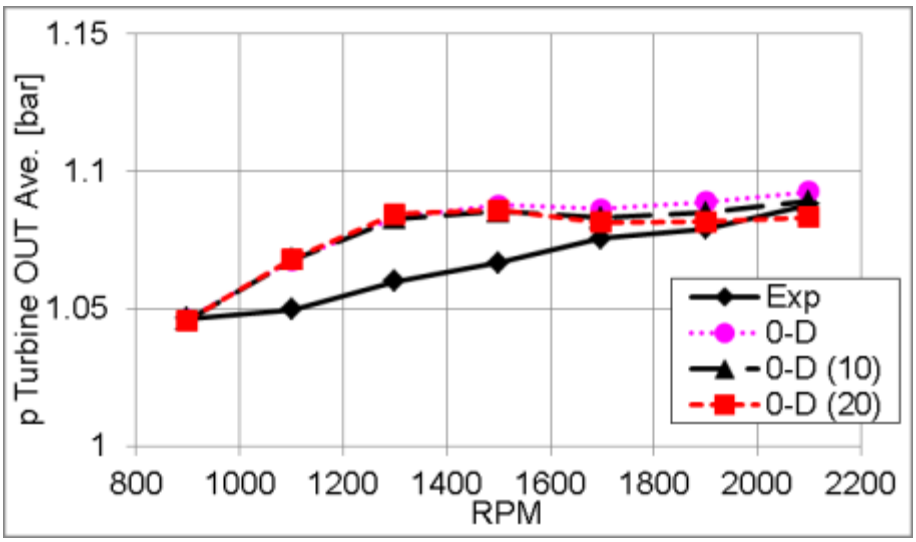

Figure 296 Pressure turbine downstream, experiment (black solid line), simulation with 0-D turbine map - sections without connection (purple dotted line), simulation with 0-D turbine map - sections connected via orifice D = 10 mm (black dashed line), simulation with 0-D turbine map - sections connected via orifice D = 20 mm (red dashed line)

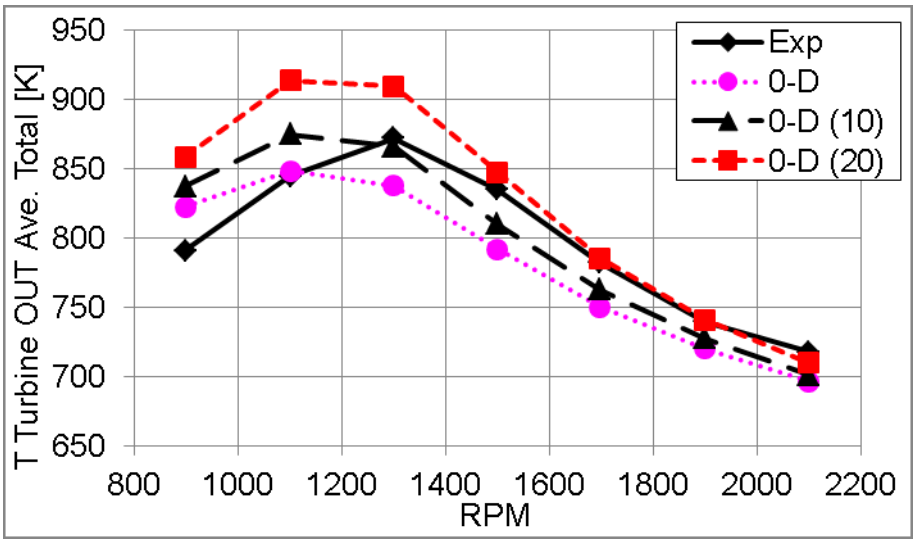

Figure 297 Total temperature turbine downstream, experiment (black solid line), simulation with 0-D turbine map - sections without connection (purple dotted line), simulation with 0-D turbine map - sections connected via orifice D = 10 mm (black dashed line), simulation with 0-D turbine map - sections connected via orifice D = 20 mm (red dashed line)

Appendix 5 - Simulation Results - Six Cylinder Diesel Engine - Unsteady Results

The unsteady results of engine simulation, compared with experimental data, are summarized in the pictures.

Engine speed: 900 RPM

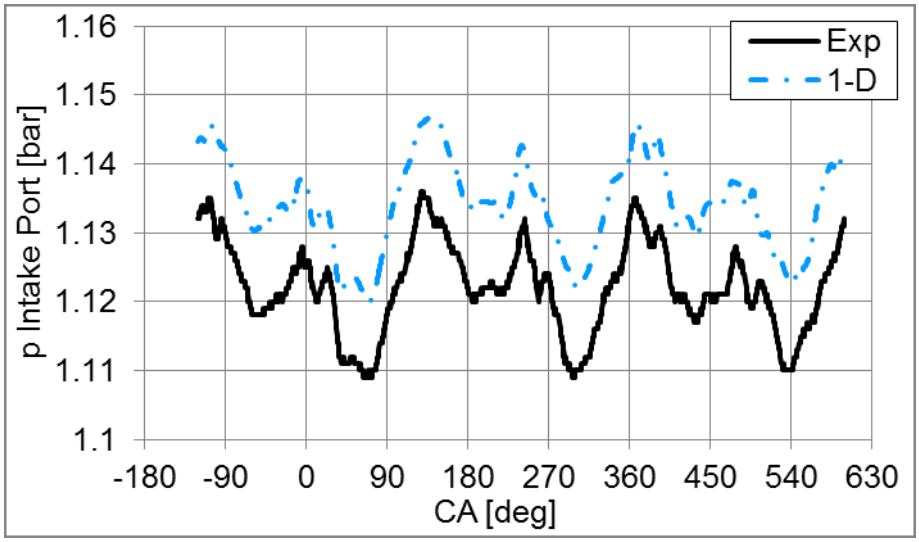

Figure 298 Pressure in intake port, experiment (black solid line), simulation with full 1-D unsteady turbine (blue dashed and dotted line); 900 RPM, BMEP = 8.9 bar

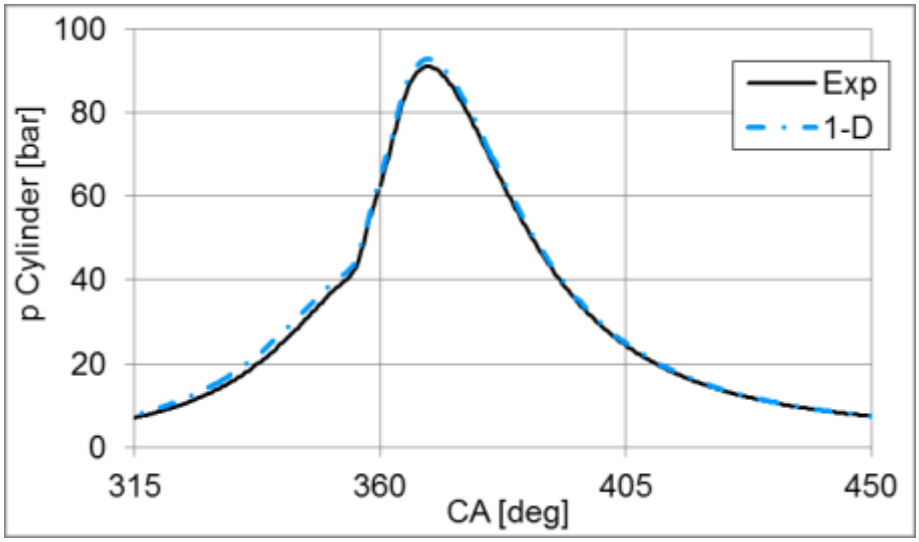

Figure 299 Pressure in cylinder, experiment (black solid line), simulation with full 1-D unsteady turbine (blue dashed and dotted line); 900 RPM, BMEP = 8.9 bar

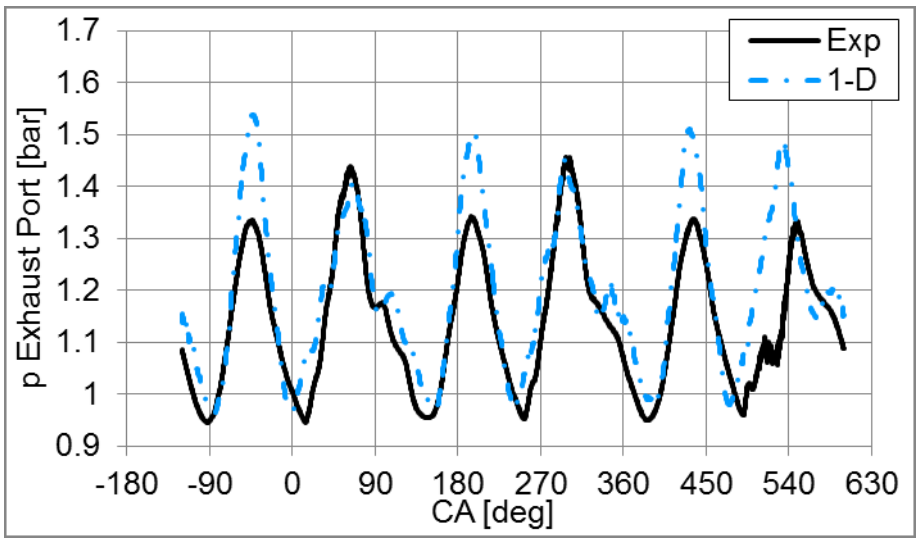

Figure 300 Pressure in exhaust port, experiment (black solid line), simulation with full 1-D unsteady turbine (blue dashed and dotted line); 900 RPM, BMEP = 8.9 bar

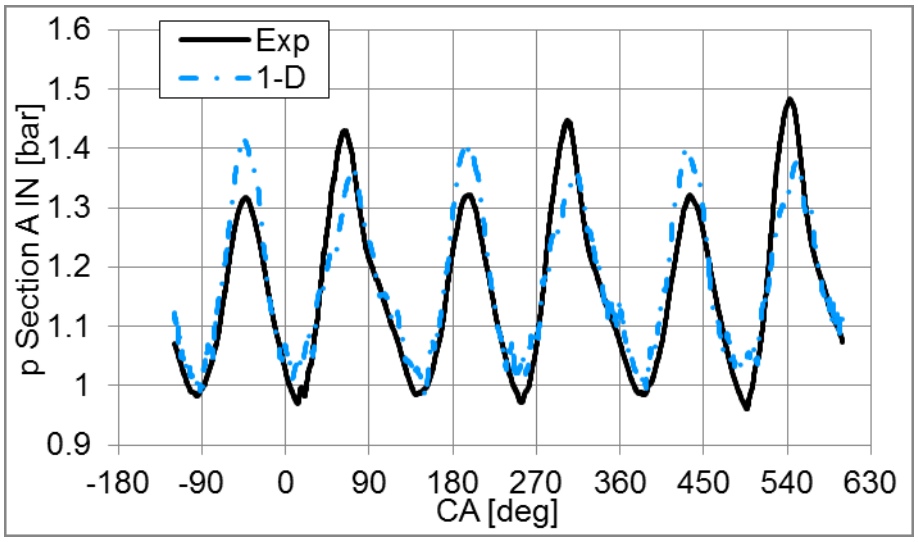

Figure 301 Pressure at inlet of turbine section A, experiment (black solid line), simulation with full 1-D unsteady turbine (blue dashed and dotted line); 900 RPM, BMEP = 8.9 bar

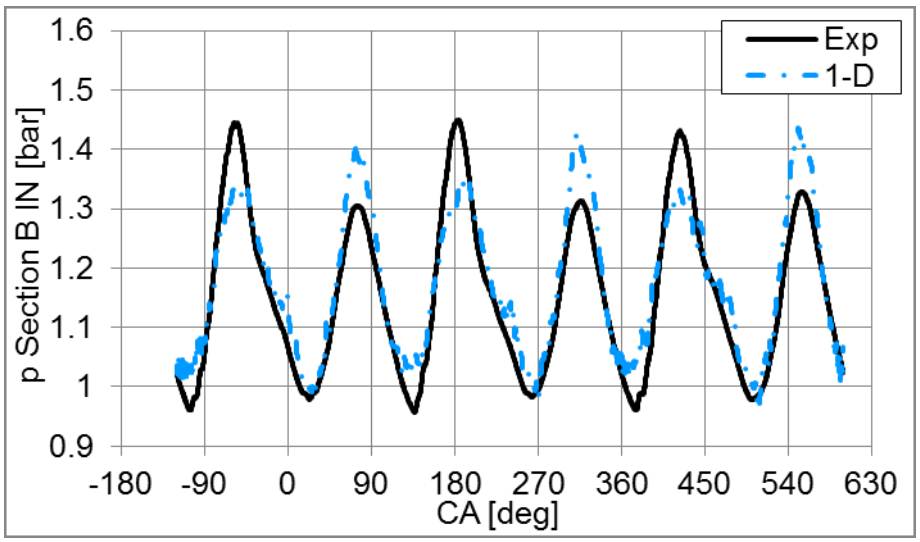

Figure 302 Pressure at inlet of turbine section B, experiment (black solid line), simulation with full 1-D unsteady turbine (blue dashed and dotted line); 900 RPM, BMEP = 8.9 bar

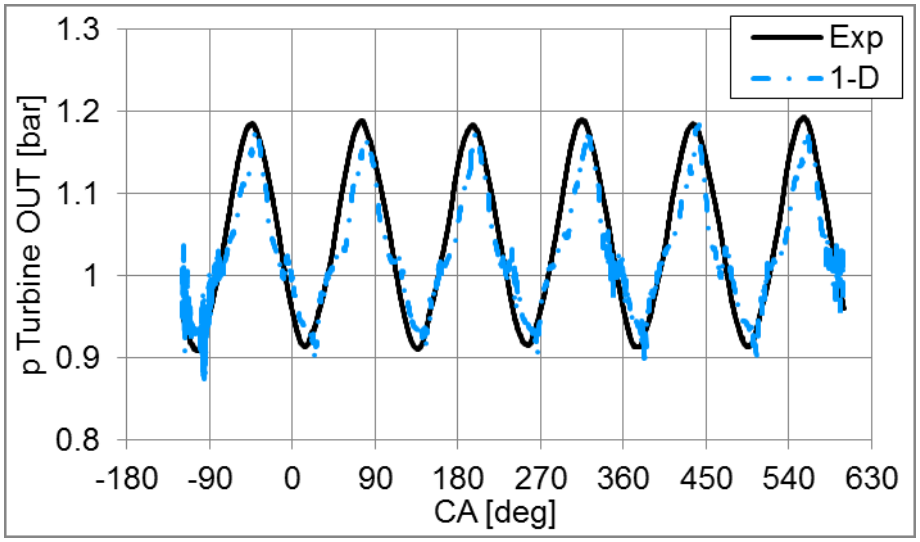

Figure 303 Pressure turbine downstream, experiment (black solid line), simulation with full 1-D unsteady turbine (blue dashed and dotted line); 900 RPM, BMEP = 8.9 bar

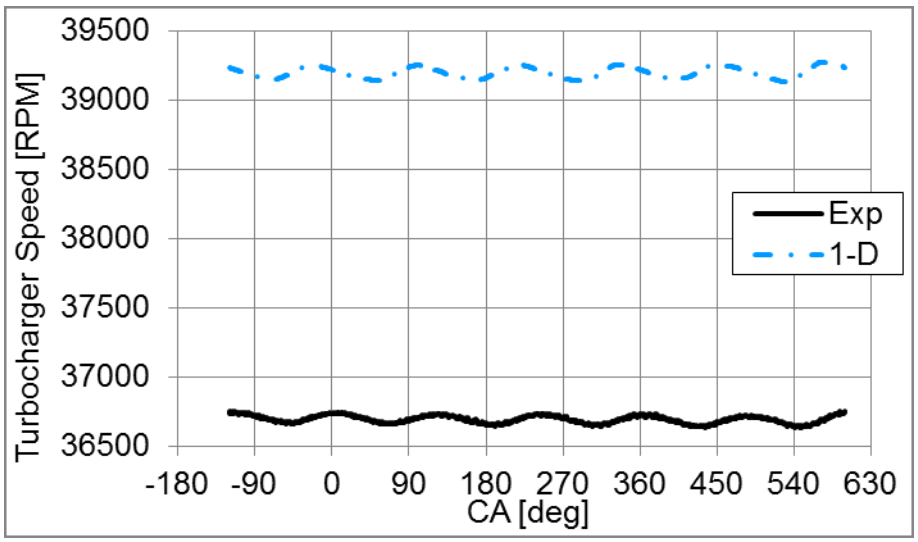

Figure 304 Turbocharger speed, experiment (black solid line), simulation with full 1-D unsteady turbine (blue dashed and dotted line); 900 RPM, BMEP = 8.9 bar

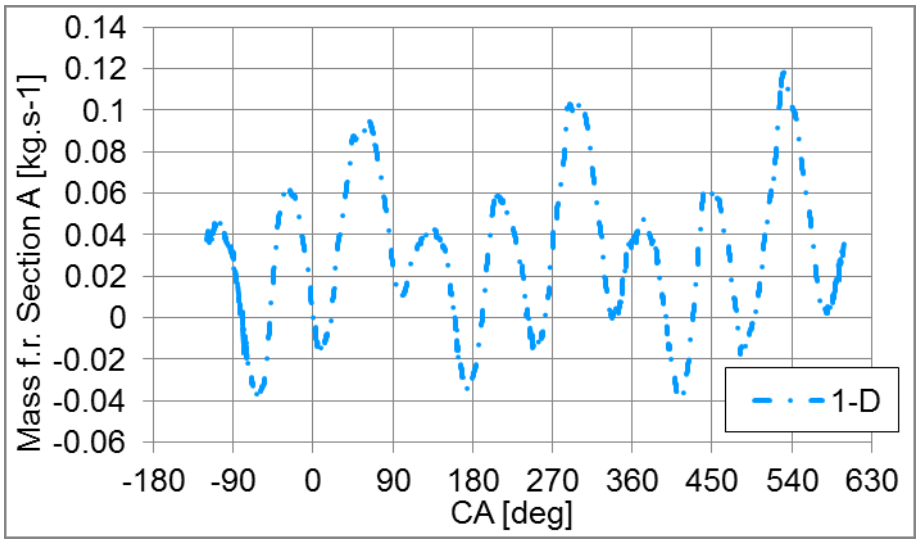

Figure 305 Mass flow rate via section A, simulation with full 1-D unsteady turbine (blue dashed and dotted line); 900 RPM, BMEP = 8.9 bar

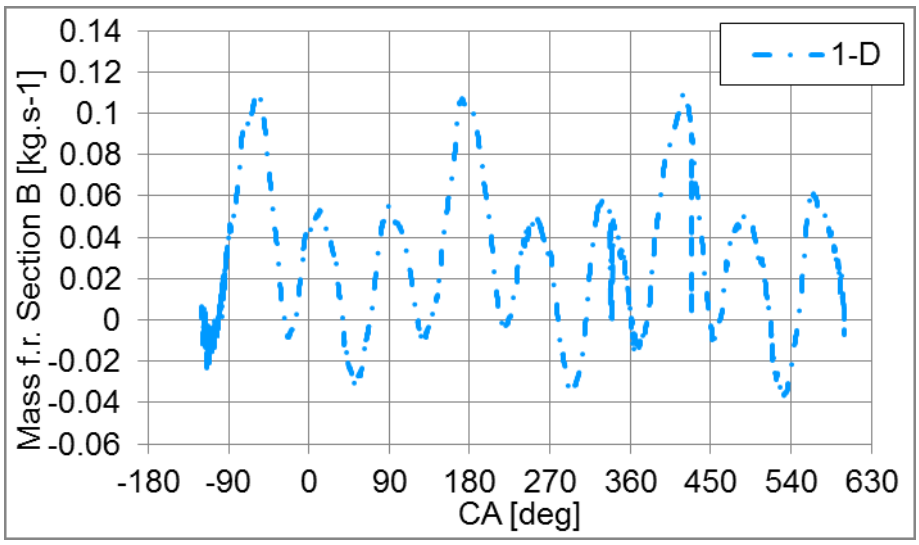

Figure 306 Mass flow rate via section B, simulation with full 1-D unsteady turbine (blue dashed and dotted line); 900 RPM, BMEP = 8.9 bar

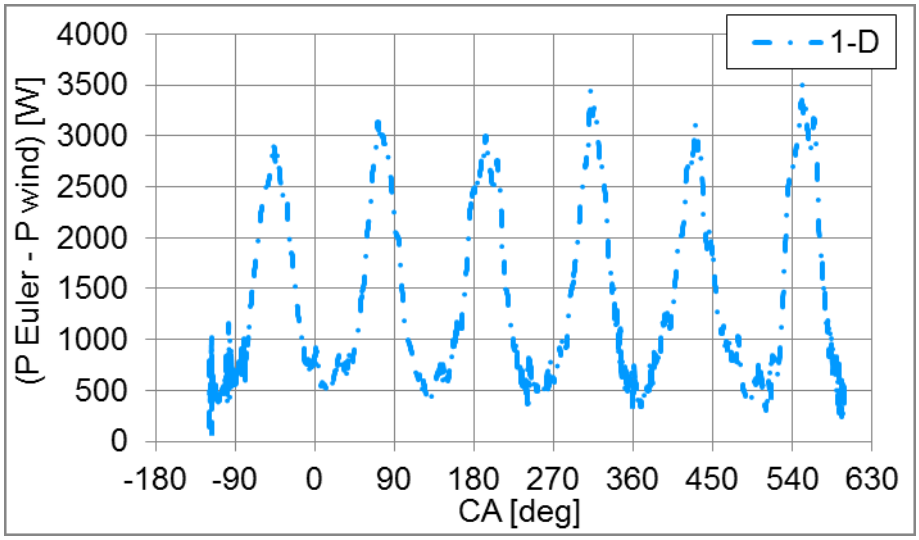

Figure 307 Turbine power, simulation with full 1-D unsteady turbine (blue dashed and dotted line); 900 RPM, BMEP = 8.9 bar

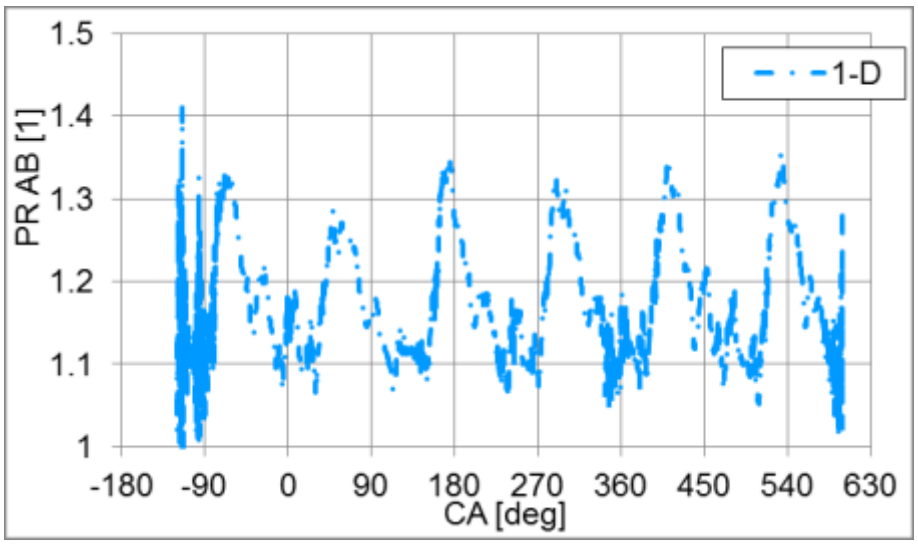

Figure 308 Overall pressure ratio AB, simulation with full 1-D unsteady turbine (blue dashed and dotted line); 900 RPM, BMEP = 8.9 bar

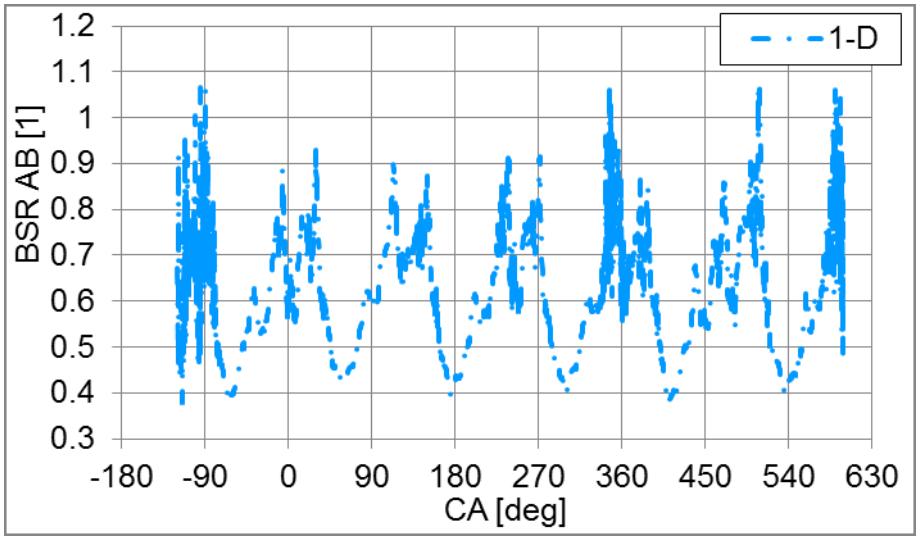

Figure 309 Blade speed ratio, simulation with full 1-D unsteady turbine (blue dashed and dotted line); 900 RPM, BMEP = 8.9 bar

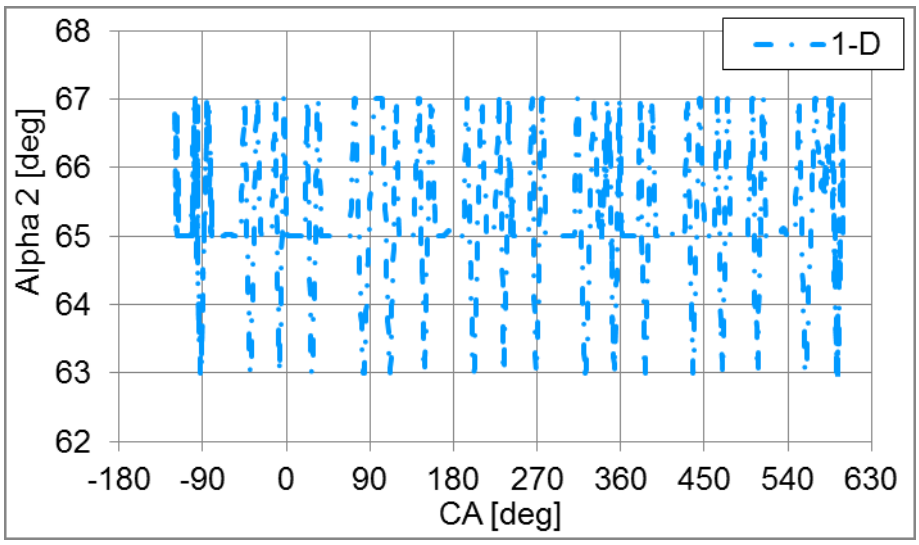

Figure 310 Alpha 2 - nozzle exit angle, simulation with full 1-D unsteady turbine (blue dashed and dotted line); 900 RPM, BMEP = 8.9 bar

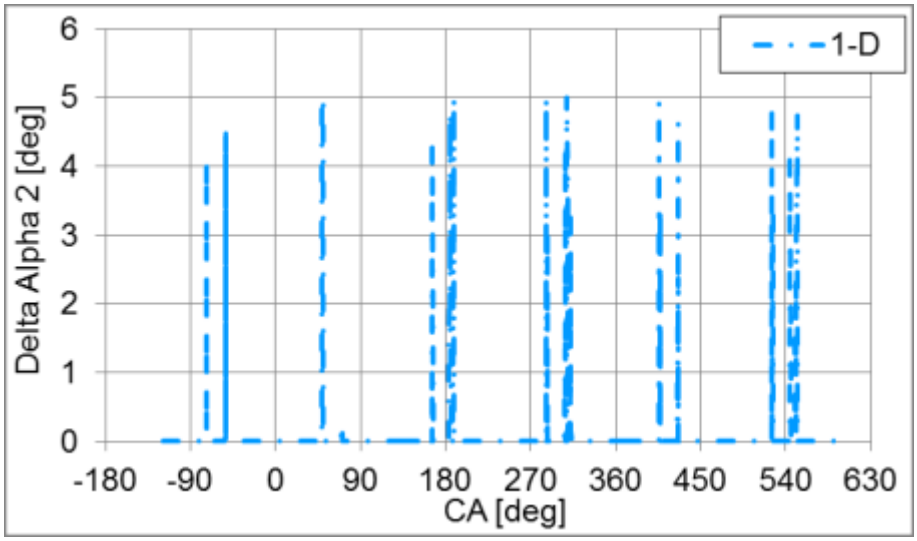

Figure 311 Delta Alpha 2 - deviation of nozzle exit angle, simulation with full 1-D unsteady turbine (blue dashed and dotted line); 900 RPM, BMEP = 8.9 bar

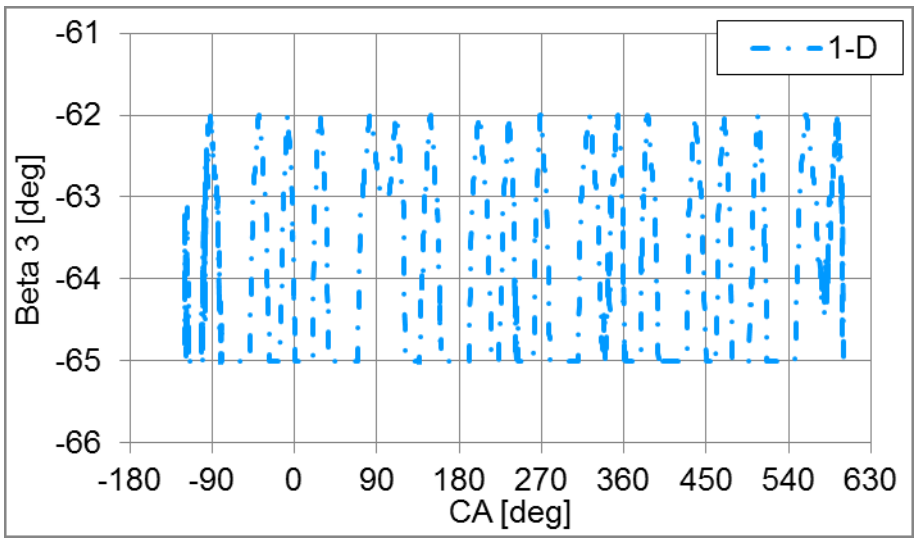

Figure 312 Beta 3 - impeller exit angle, simulation with full 1-D unsteady turbine (blue dashed and dotted line); 900 RPM, BMEP = 8.9 bar

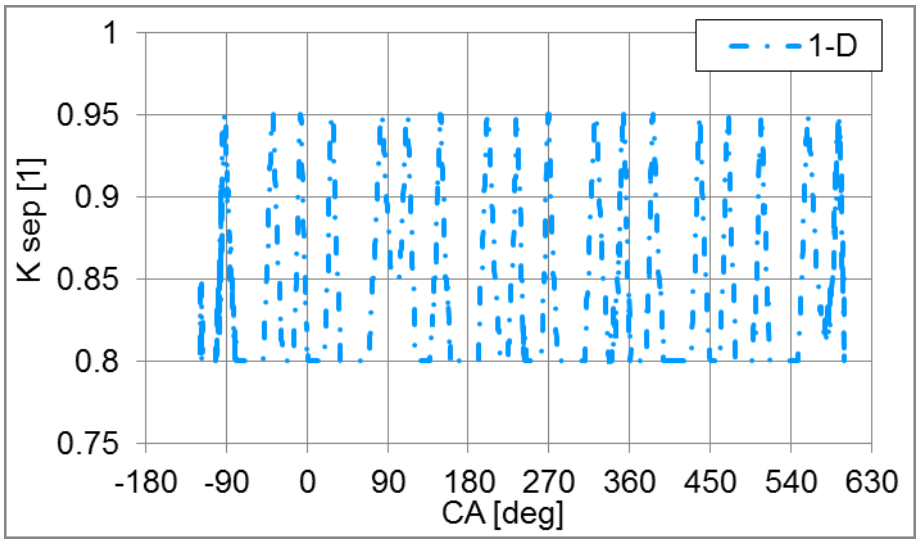

Figure 313 K sep - flow separation coefficient, simulation with full 1-D unsteady turbine (blue dashed and dotted line); 900 RPM, BMEP = 8.9 bar

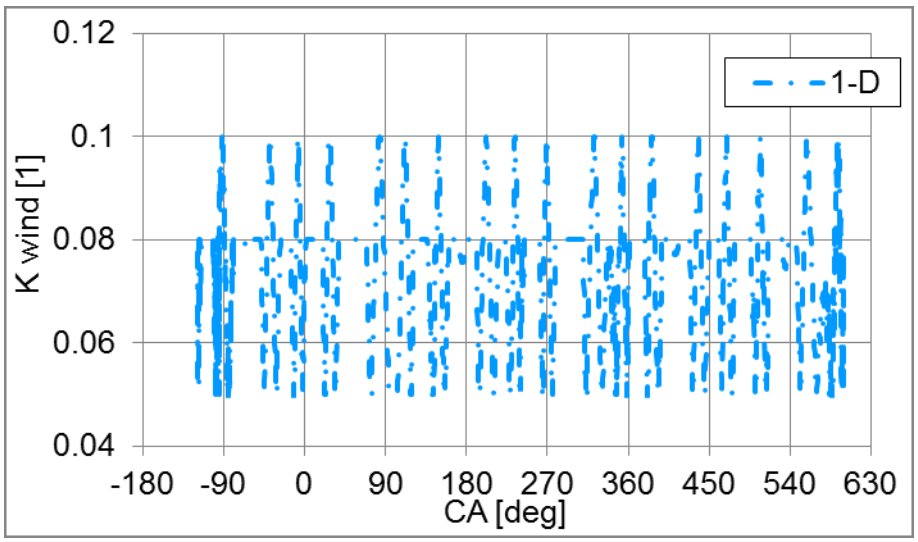

Figure 314 K wind - coefficient of windage losses, simulation with full 1-D unsteady turbine (blue dashed and dotted line); 900 RPM, BMEP = 8.9 bar

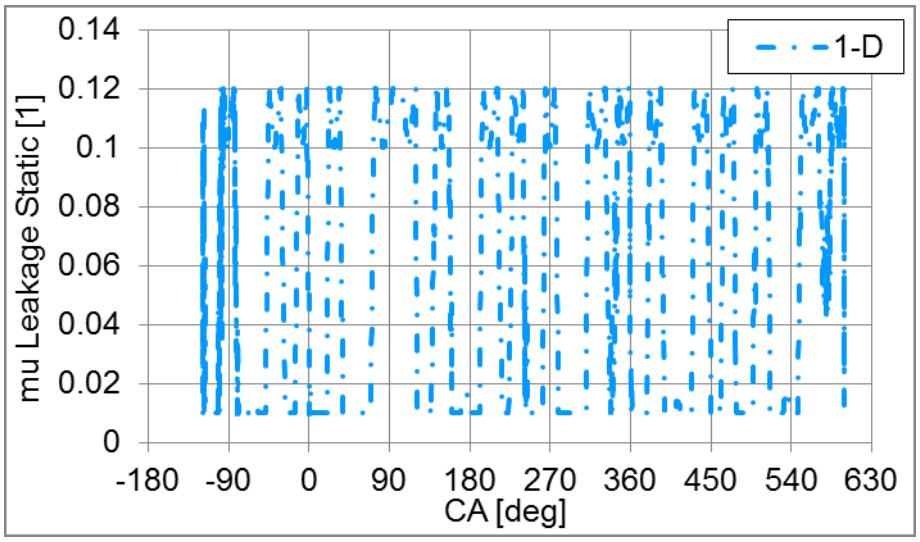

Figure 315 Discharge coefficient of static leakages, simulation with full 1-D unsteady turbine (blue dashed and dotted line); 900 RPM, BMEP = 8.9 bar

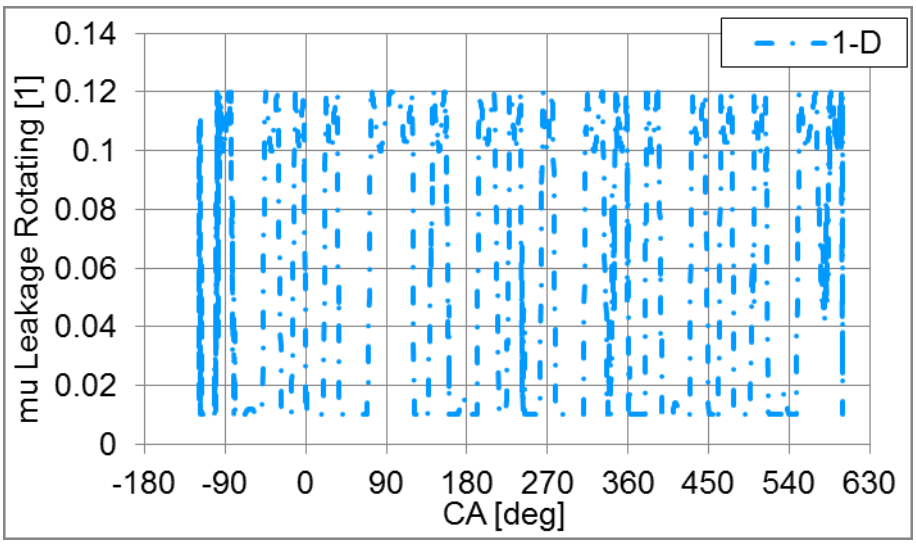

Figure 316 Discharge coefficient of rotating leakages, simulation with full 1-D unsteady turbine (blue dashed and dotted line); 900 RPM, BMEP = 8.9 bar

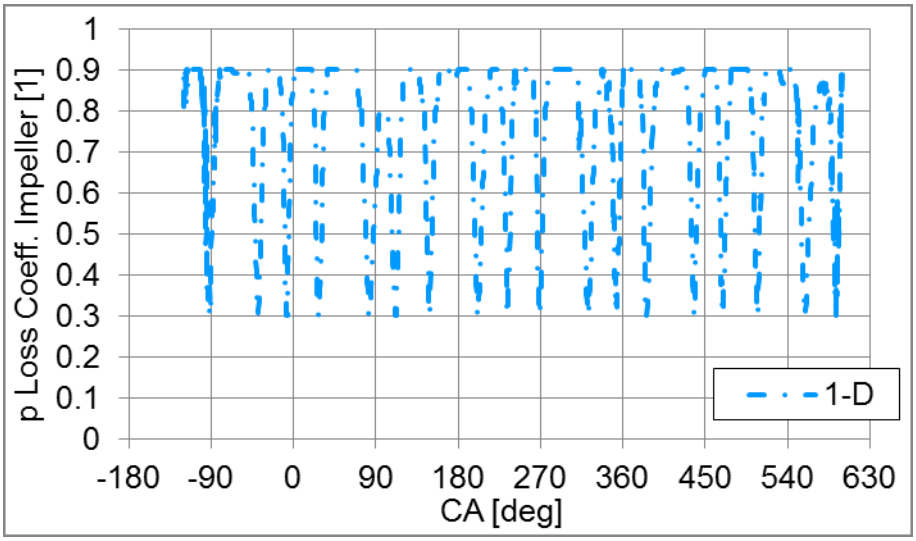

Figure 317 Pressure loss coefficient in impeller pipe, simulation with full 1-D unsteady turbine (blue dashed and dotted line); 900 RPM, BMEP = 8.9 bar

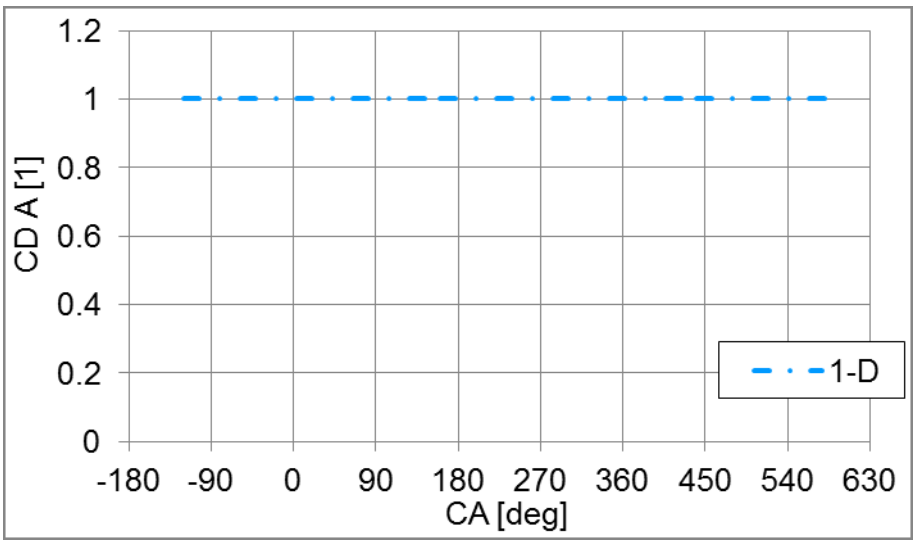

Figure 318 CD A - discharge coefficient at section A outlet {upstream of flow mixing}, simulation with full 1-D unsteady turbine (blue dashed and dotted line); 900 RPM, BMEP = 8.9 bar

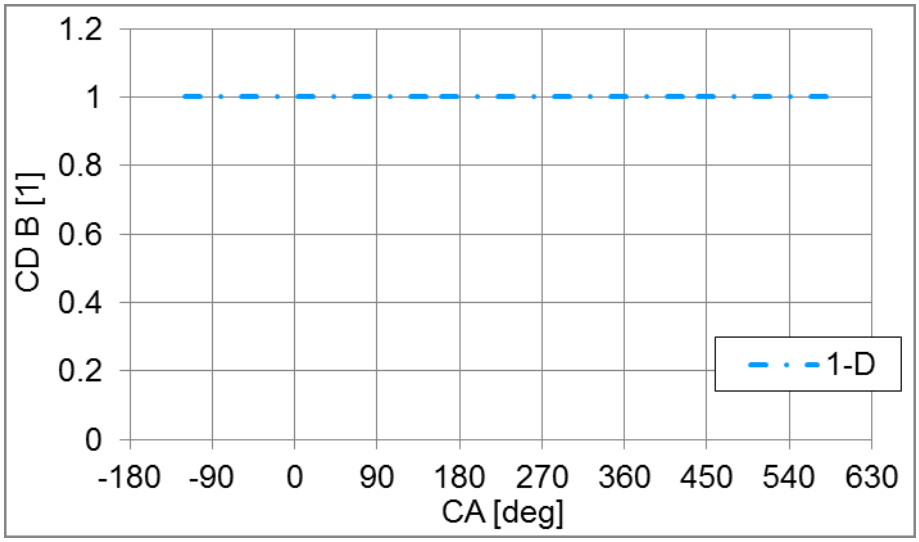

Figure 319 CD B - discharge coefficient at section B outlet {upstream of flow mixing}, simulation with full 1-D unsteady turbine (blue dashed and dotted line); 900 RPM, BMEP = 8.9 bar

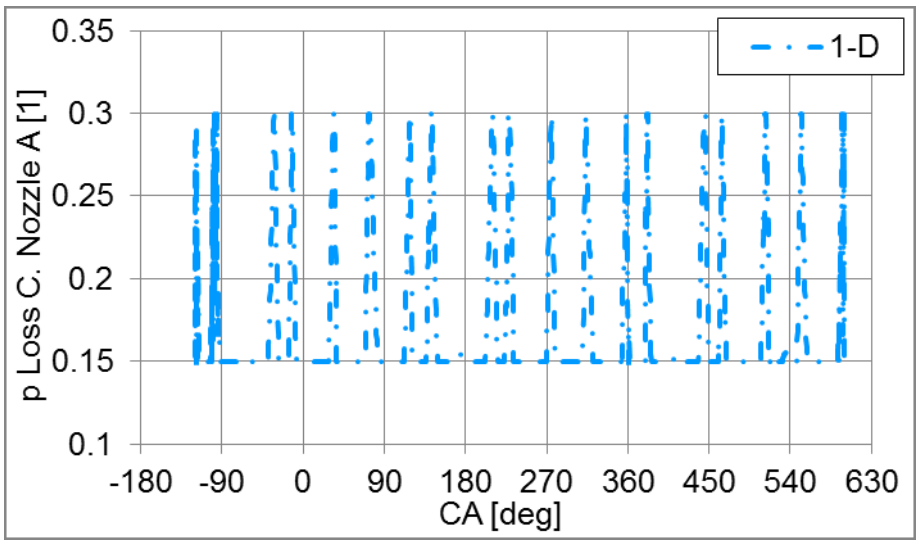

Figure 320 Pressure loss coefficient in section A, simulation with full 1-D unsteady turbine (blue dashed and dotted line); 900 RPM, BMEP = 8.9 bar

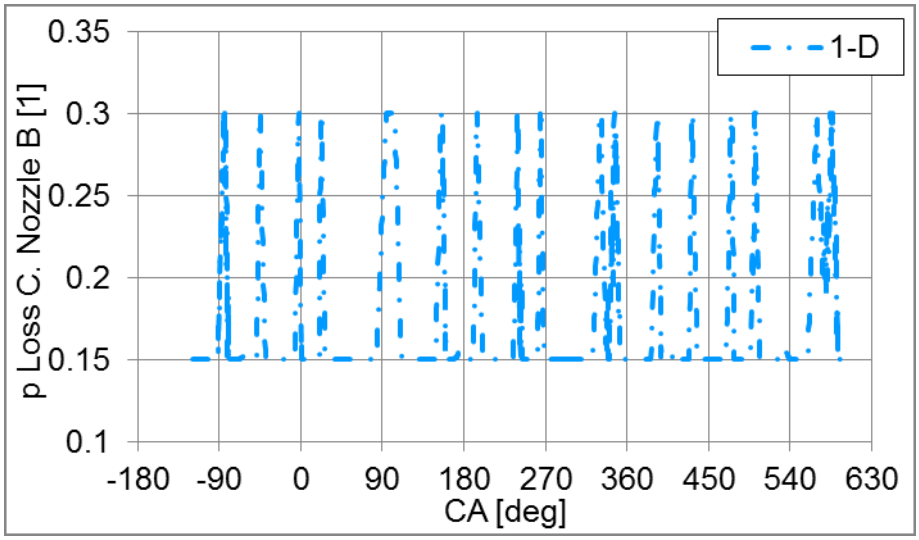

Figure 321 Pressure loss coefficient in section B, simulation with full 1-D unsteady turbine (blue dashed and dotted line); 900 RPM, BMEP = 8.9 bar

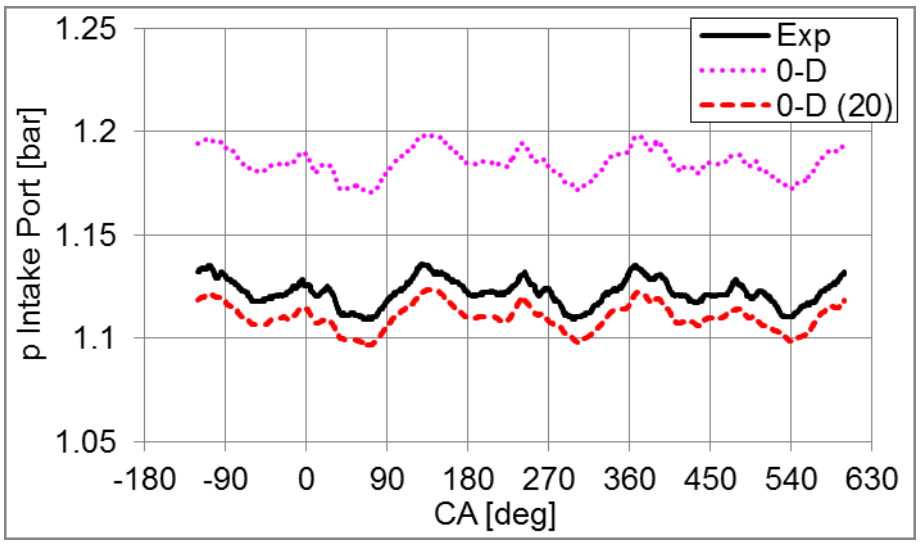

Figure 322 Pressure in intake port, experiment (black solid line), simulation with 0-D turbine map - sections without connection (purple dotted line), simulation with 0-D turbine map - sections connected via orifice D = 20 mm (red dashed line); 900 RPM, BMEP = 8.9 bar

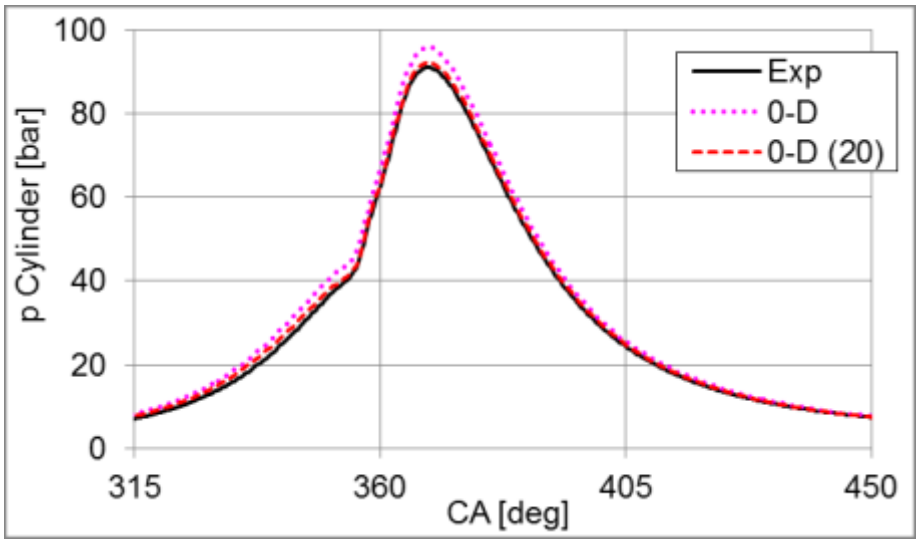

Figure 323 Pressure in cylinder, experiment (black solid line), simulation with 0-D turbine map - sections without connection (purple dotted line), simulation with 0-D turbine map - sections connected via orifice D = 20 mm (red dashed line); 900 RPM, BMEP = 8.9 bar

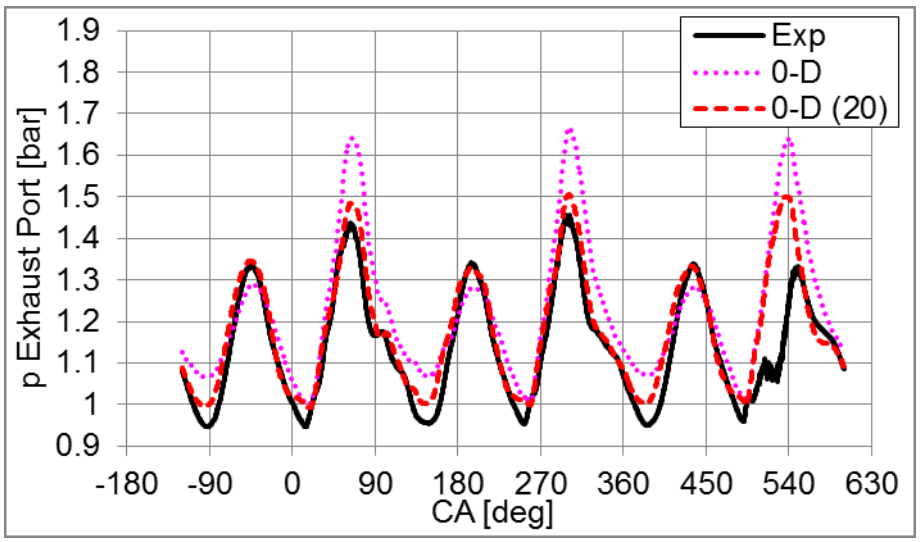

Figure 324 Pressure in exhaust port, experiment (black solid line), simulation with 0-D turbine map - sections without connection (purple dotted line), simulation with 0-D turbine map - sections connected via orifice D = 20 mm (red dashed line); 900 RPM, BMEP = 8.9 bar

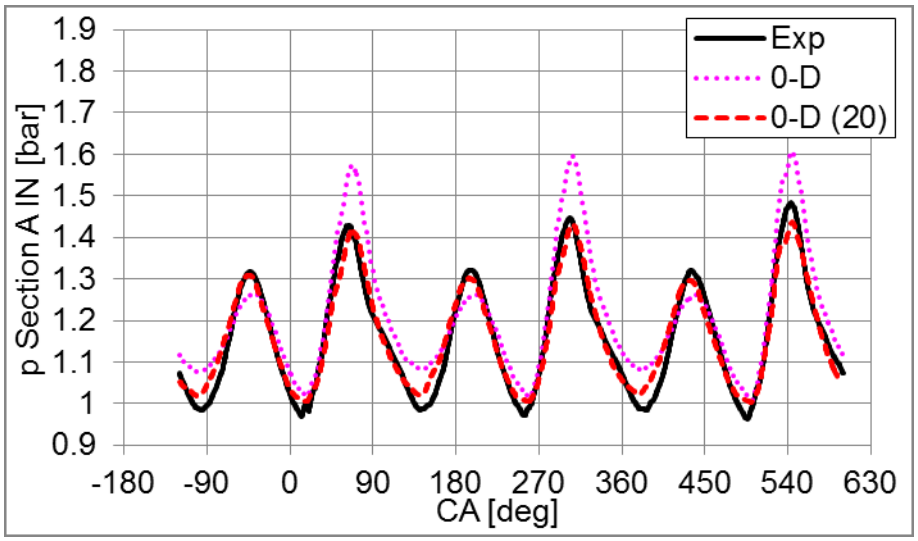

Figure 325 Pressure at inlet of turbine section A, experiment (black solid line), simulation with 0-D turbine map - sections without connection (purple dotted line), simulation with 0-D turbine map - sections connected via orifice D = 20 mm (red dashed line); 900 RPM, BMEP = 8.9 bar

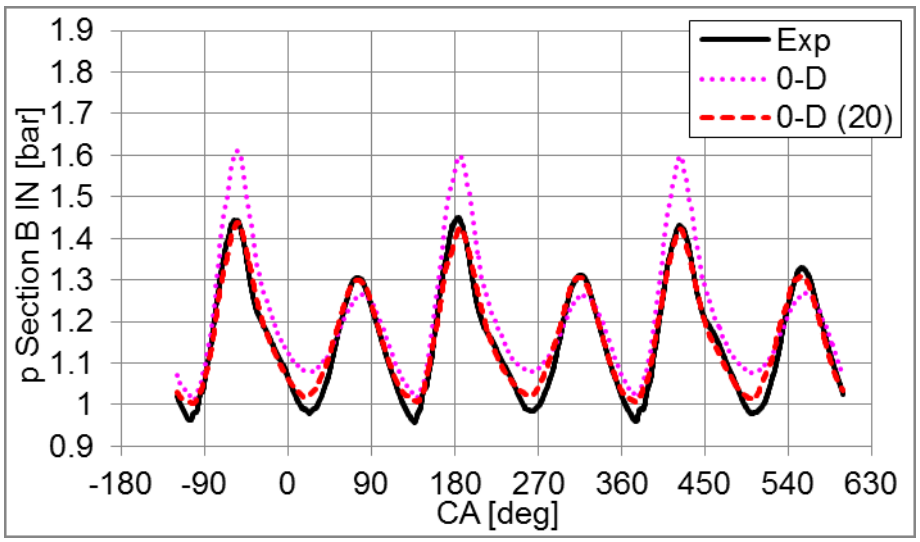

Figure 326 Pressure at inlet of turbine section B, experiment (black solid line), simulation with 0-D turbine map - sections without connection (purple dotted line), simulation with 0-D turbine map - sections connected via orifice D = 20 mm (red dashed line); 900 RPM, BMEP = 8.9 bar

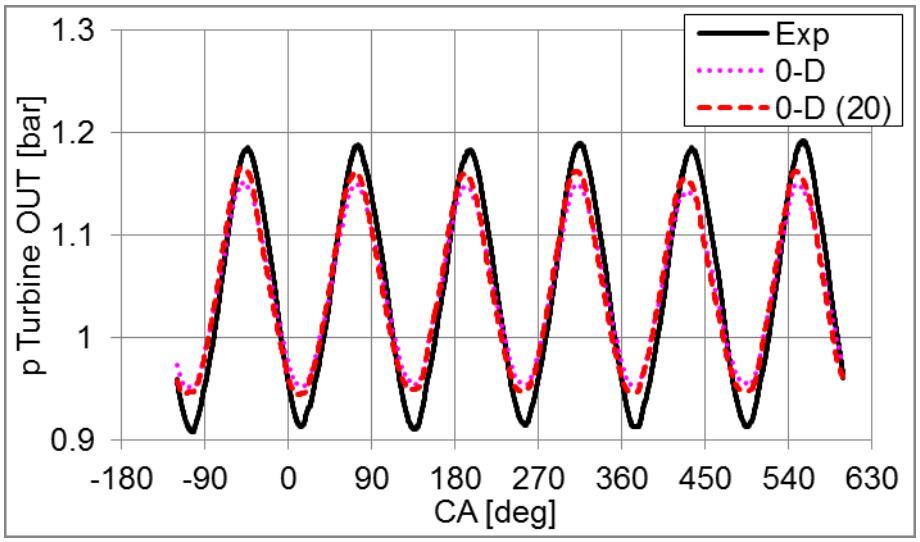

Figure 327 Pressure turbine downstream, experiment (black solid line), simulation with 0-D turbine map - sections without connection (purple dotted line), simulation with 0-D turbine map - sections connected via orifice D = 20 mm (red dashed line); 900 RPM, BMEP = 8.9 bar

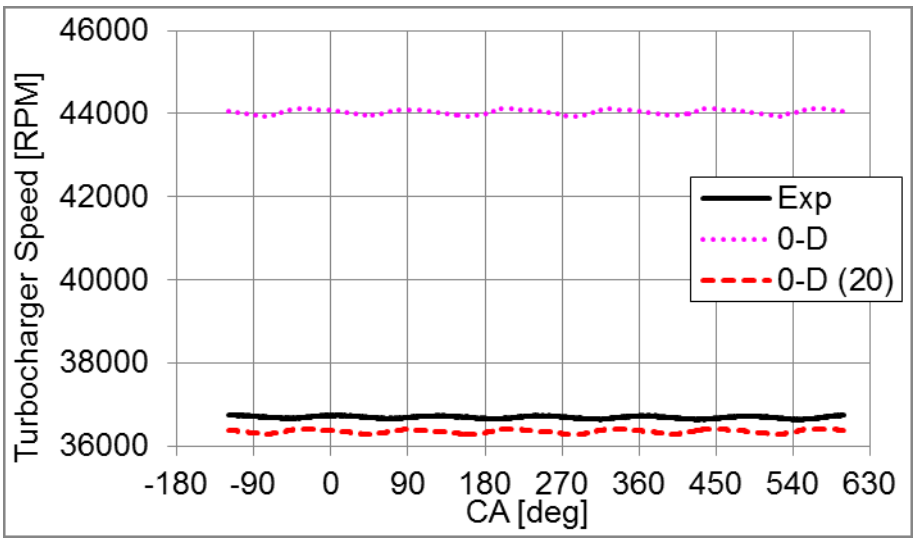

Figure 328 Turbocharger speed, experiment (black solid line), simulation with 0-D turbine map - sections without connection (purple dotted line), simulation with 0-D turbine map - sections connected via orifice D = 20 mm (red dashed line); 900 RPM, BMEP = 8.9 bar

Engine speed: 2100 RPM

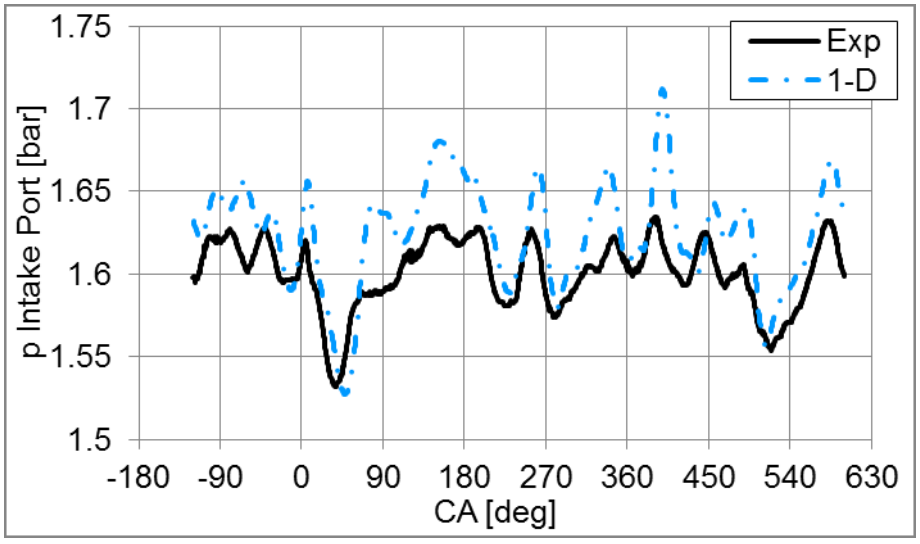

Figure 329 Pressure in intake port, experiment (black solid line), simulation with full 1-D unsteady turbine (blue dashed and dotted line); 2100 RPM, BMEP = 9.8 bar

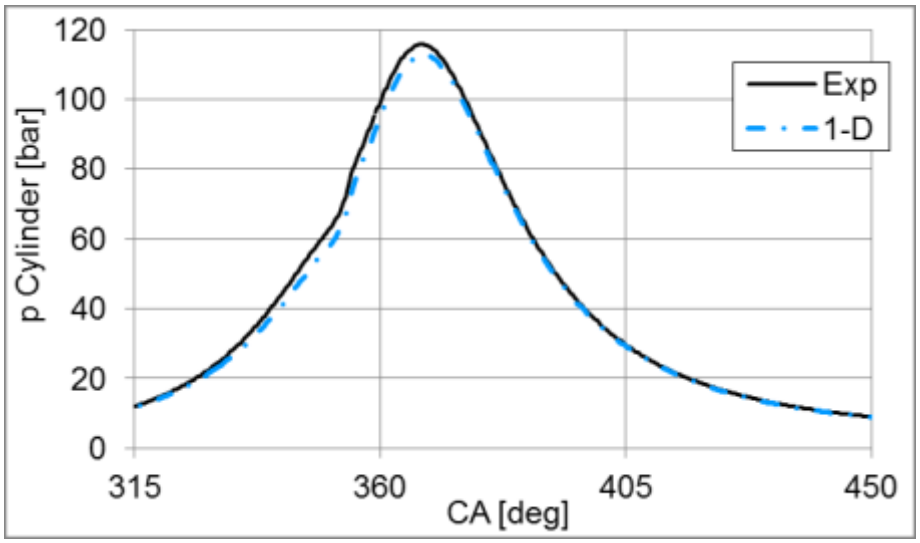

Figure 330 Pressure in cylinder, experiment (black solid line), simulation with full 1-D unsteady turbine (blue dashed and dotted line); 2100 RPM, BMEP = 9.8 bar

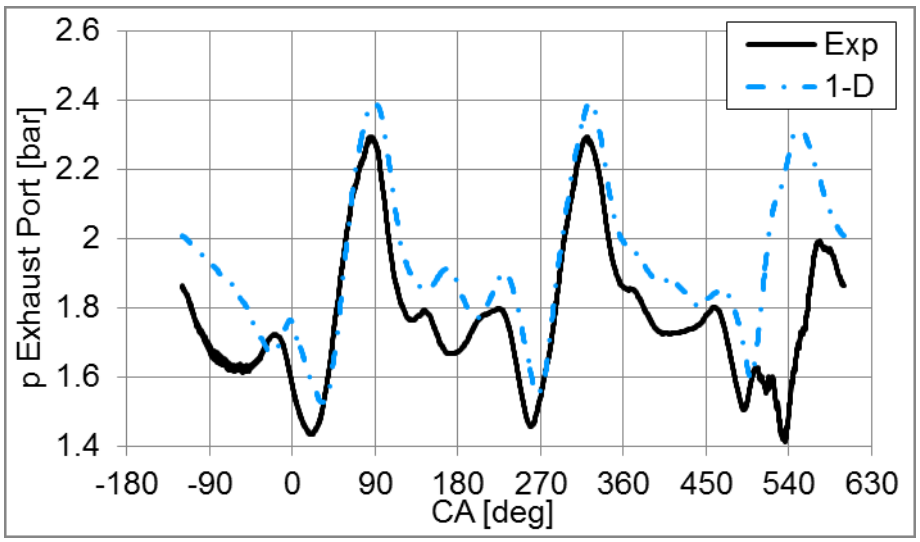

Figure 331 Pressure in exhaust port, experiment (black solid line), simulation with full 1-D unsteady turbine (blue dashed and dotted line); 2100 RPM, BMEP = 9.8 bar

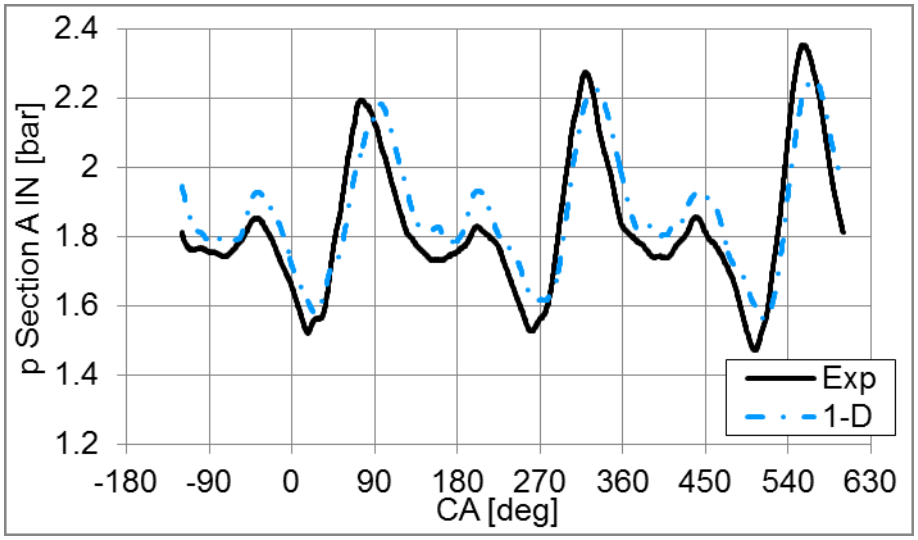

Figure 332 Pressure at inlet of turbine section A, experiment (black solid line), simulation with full 1-D unsteady turbine (blue dashed and dotted line); 2100 RPM, BMEP = 9.8 bar

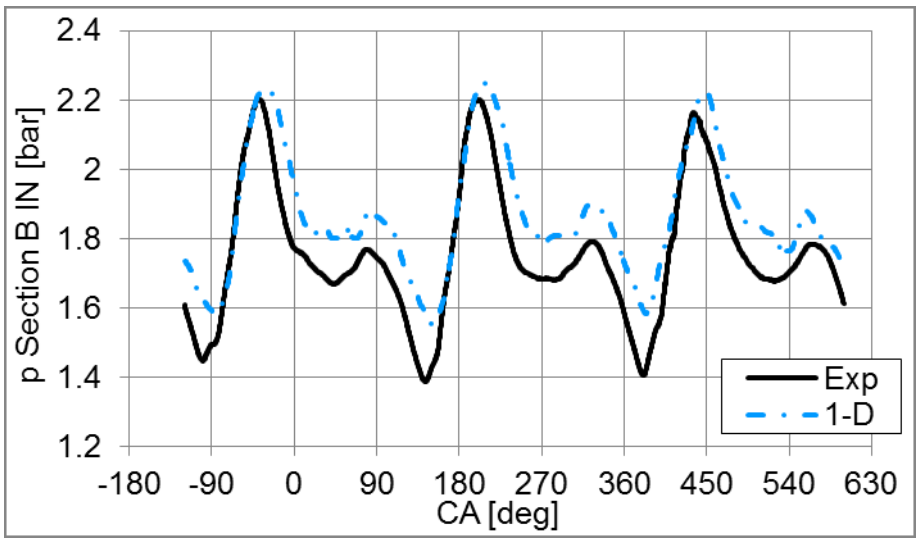

Figure 333 Pressure at inlet of turbine section B, experiment (black solid line), simulation with full 1-D unsteady turbine (blue dashed and dotted line); 2100 RPM, BMEP = 9.8 bar

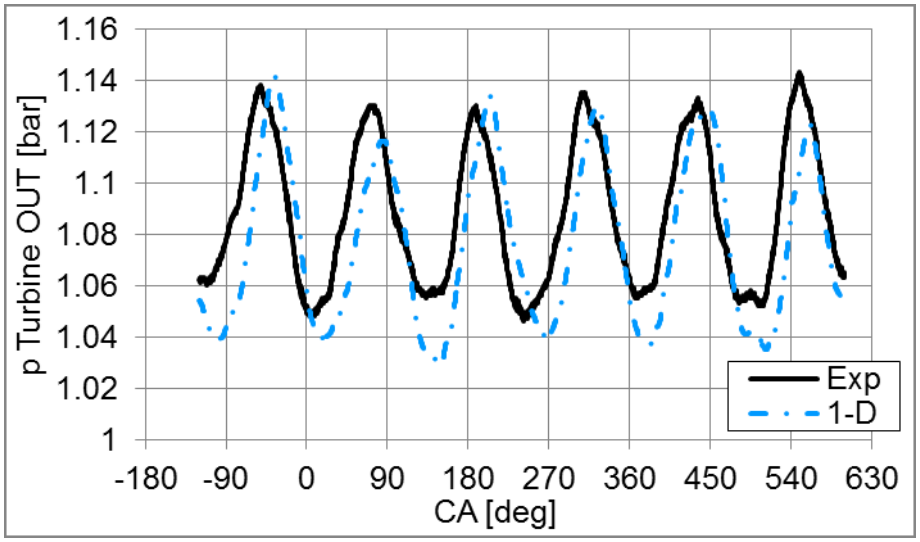

Figure 334 Pressure turbine downstream, experiment (black solid line), simulation with full 1-D unsteady turbine (blue dashed and dotted line); 2100 RPM, BMEP = 9.8 bar

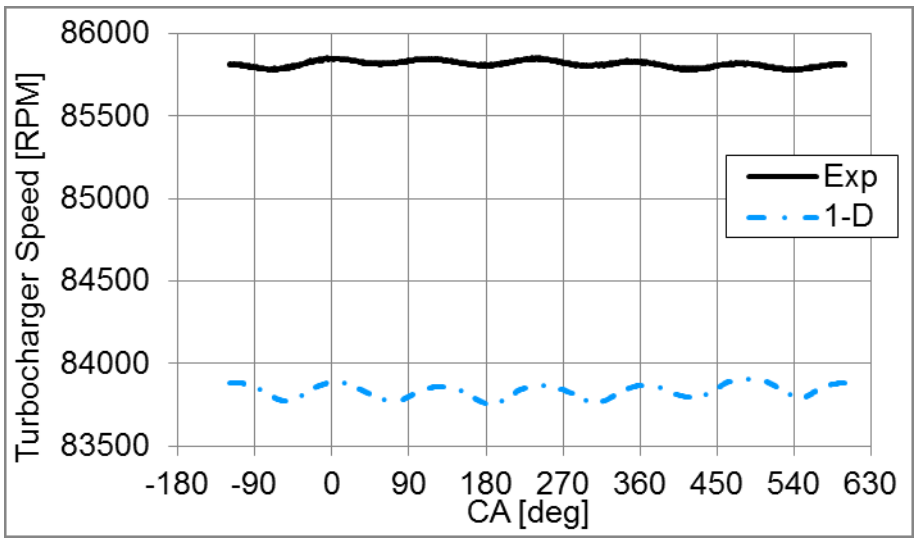

Figure 335 Turbocharger speed, experiment (black solid line), simulation with full 1-D unsteady turbine (blue dashed and dotted line); 2100 RPM, BMEP = 9.8 bar

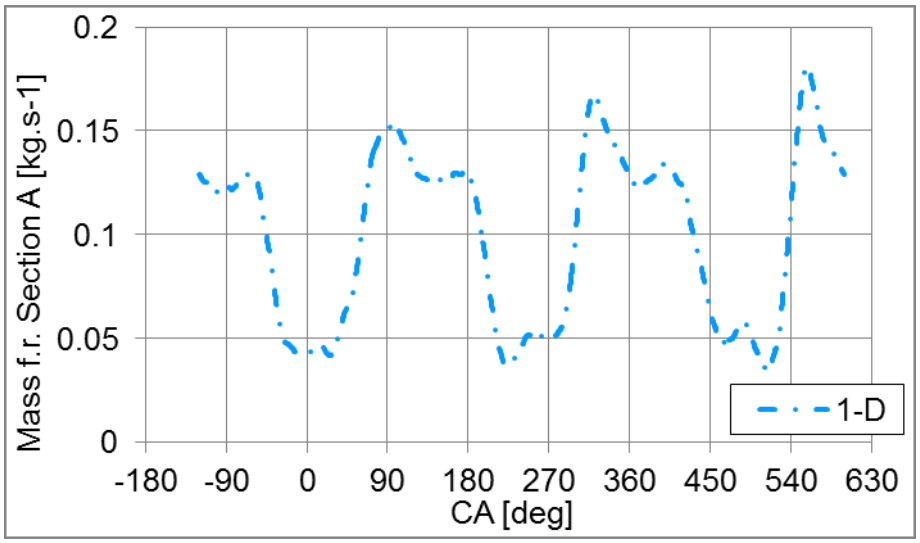

Figure 336 Mass flow rate via section A, simulation with full 1-D unsteady turbine (blue dashed and dotted line); 2100 RPM, BMEP = 9.8 bar

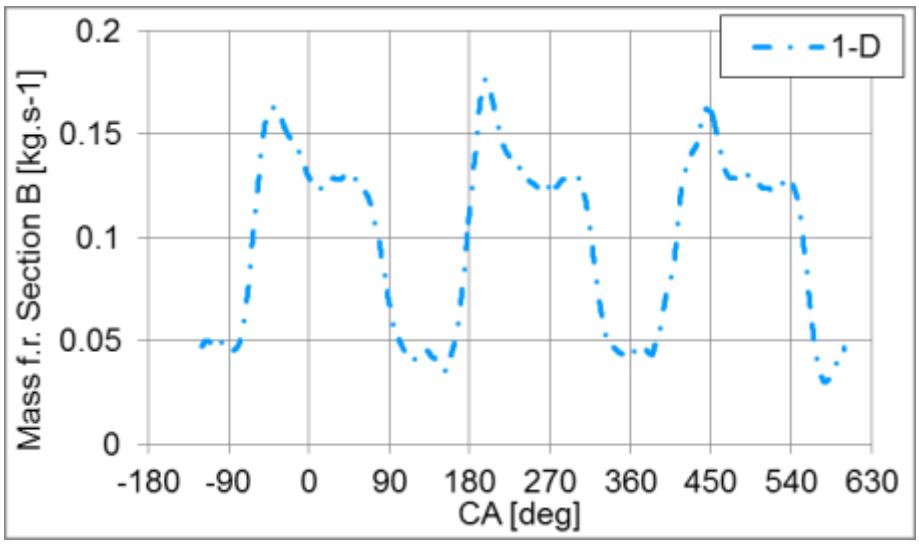

Figure 337 Mass flow rate via section B, simulation with full 1-D unsteady turbine (blue dashed and dotted line); 2100 RPM, BMEP = 9.8 bar

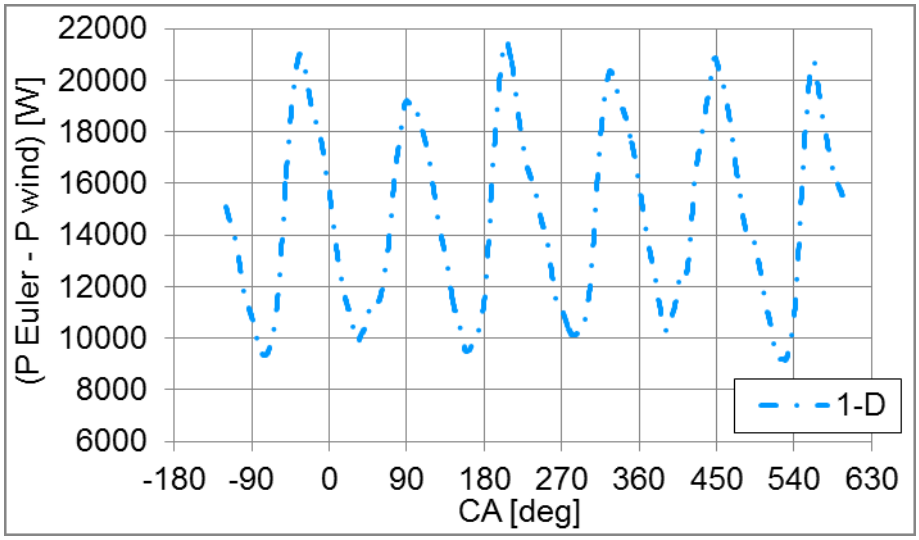

Figure 338 Turbine power, simulation with full 1-D unsteady turbine (blue dashed and dotted line); 2100 RPM, BMEP = 9.8 bar

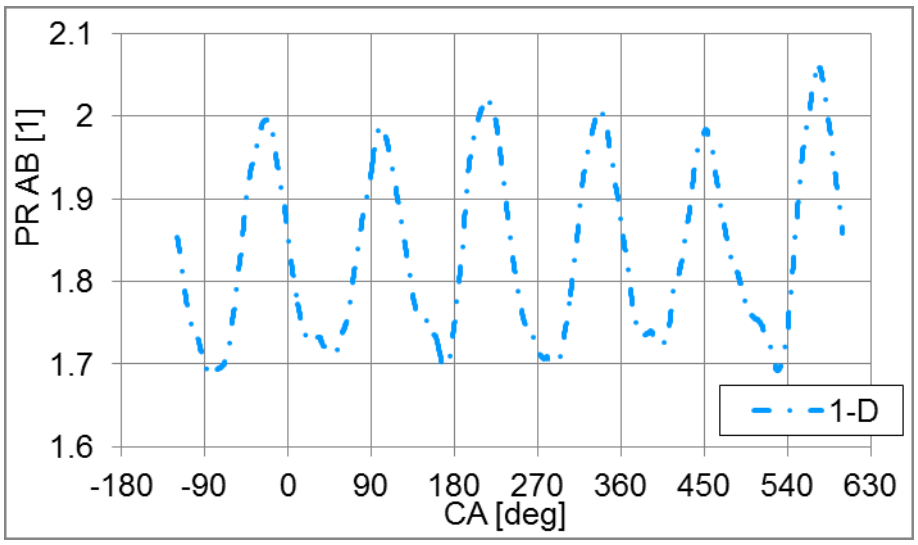

Figure 339 Overall pressure ratio AB, simulation with full 1-D unsteady turbine (blue dashed and dotted line); 2100 RPM, BMEP = 9.8 bar

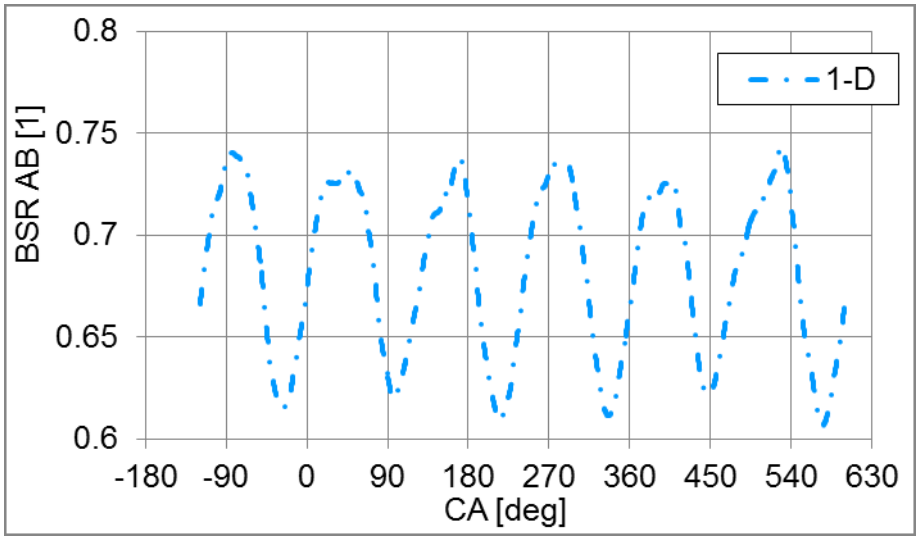

Figure 340 Blade speed ratio, simulation with full 1-D unsteady turbine (blue dashed and dotted line); 2100 RPM, BMEP = 9.8 bar

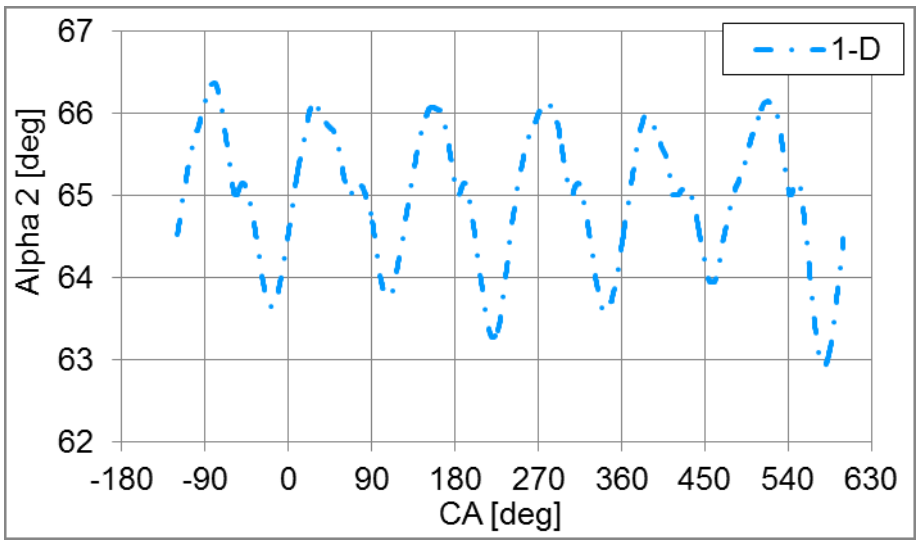

Figure 341 Alpha 2 - nozzle exit angle, simulation with full 1-D unsteady turbine (blue dashed and dotted line); 2100 RPM, BMEP = 9.8 bar

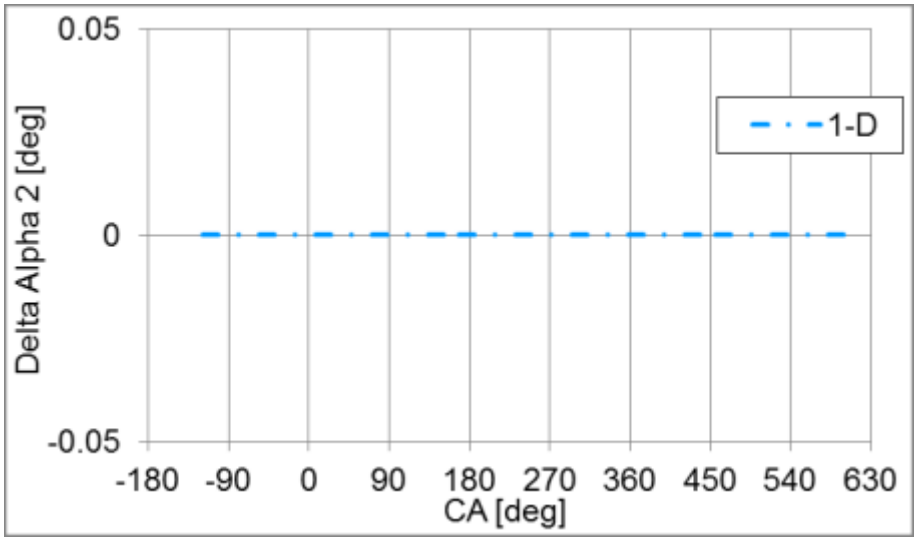

Figure 342 Delta Alpha 2 - deviation of nozzle exit angle, simulation with full 1-D unsteady turbine (blue dashed and dotted line); 2100 RPM, BMEP = 9.8 bar

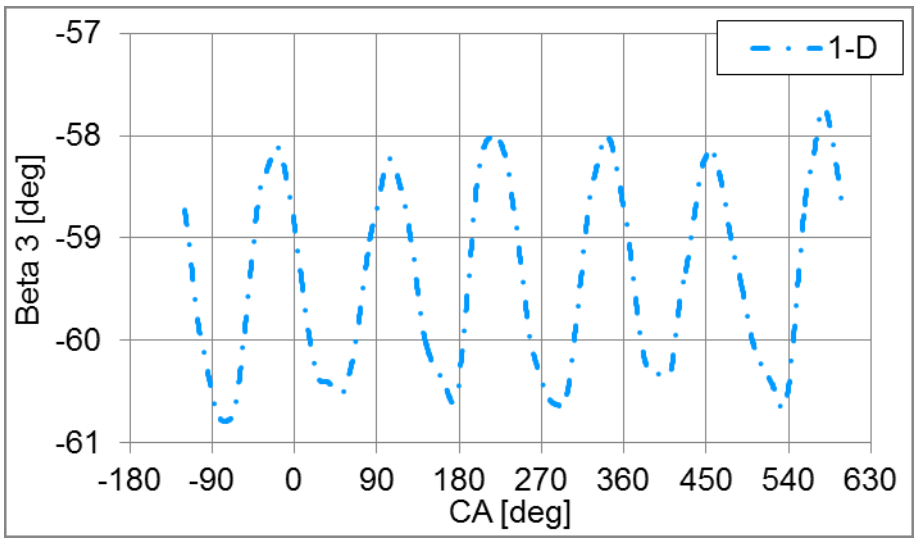

Figure 343 Beta 3 - impeller exit angle, simulation with full 1-D unsteady turbine (blue dashed and dotted line); 2100 RPM, BMEP = 9.8 bar

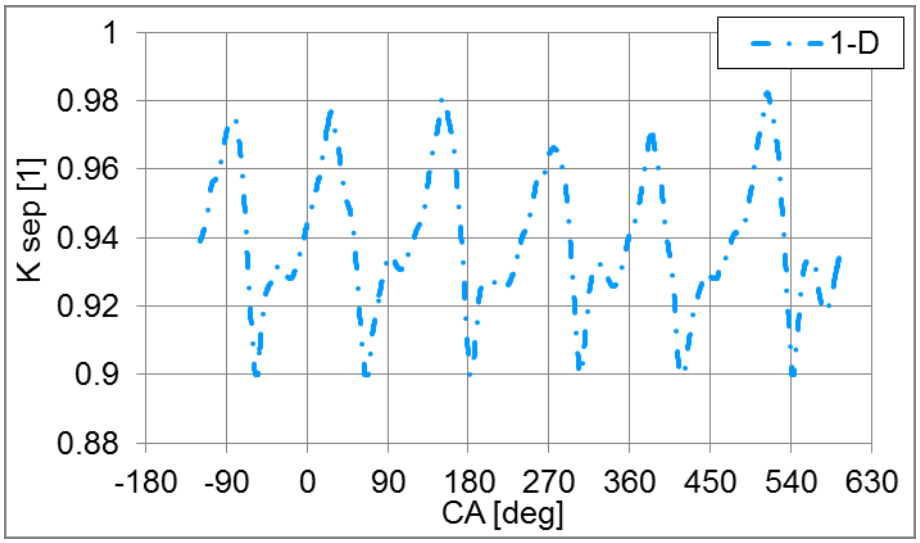

Figure 344 K sep - flow separation coefficient, simulation with full 1-D unsteady turbine (blue dashed and dotted line); 2100 RPM, BMEP = 9.8 bar

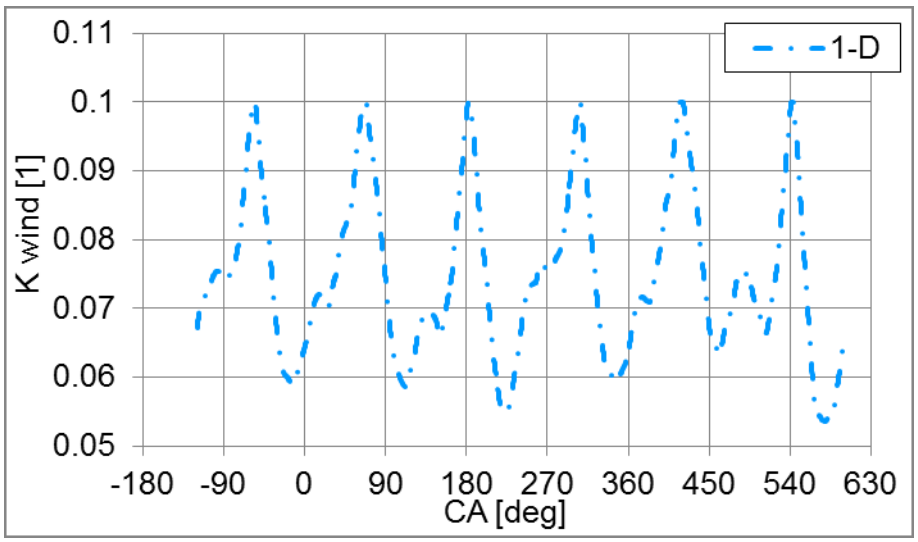

Figure 345 K wind - coefficient of windage losses, simulation with full 1-D unsteady turbine (blue dashed and dotted line); 2100 RPM, BMEP = 9.8 bar

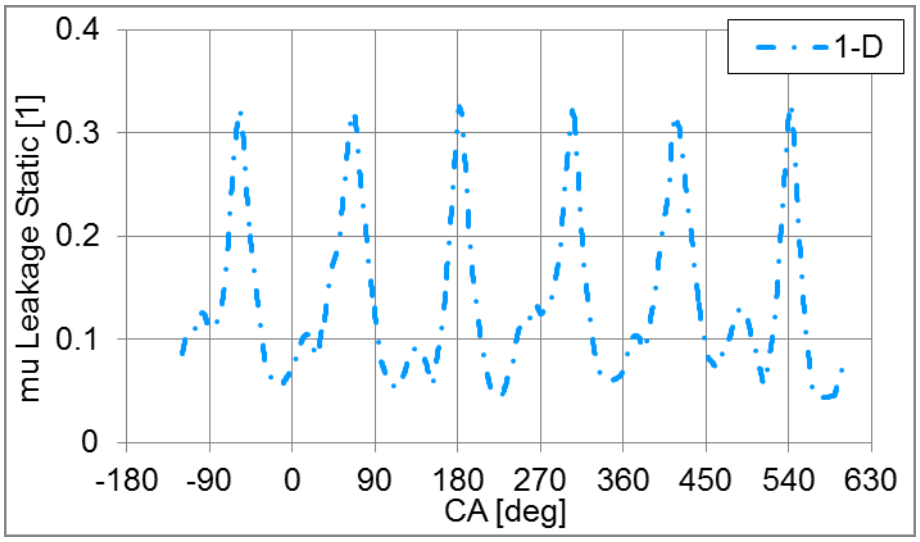

Figure 346 Discharge coefficient of static leakages, simulation with full 1-D unsteady turbine (blue dashed and dotted line); 2100 RPM, BMEP = 9.8 bar

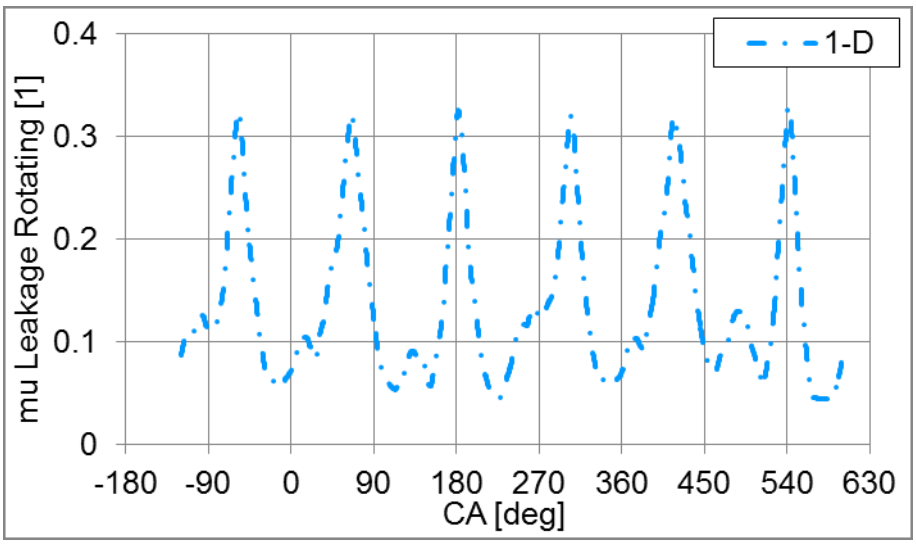

Figure 347 Discharge coefficient of rotating leakages, simulation with full 1-D unsteady turbine (blue dashed and dotted line); 2100 RPM, BMEP = 9.8 bar

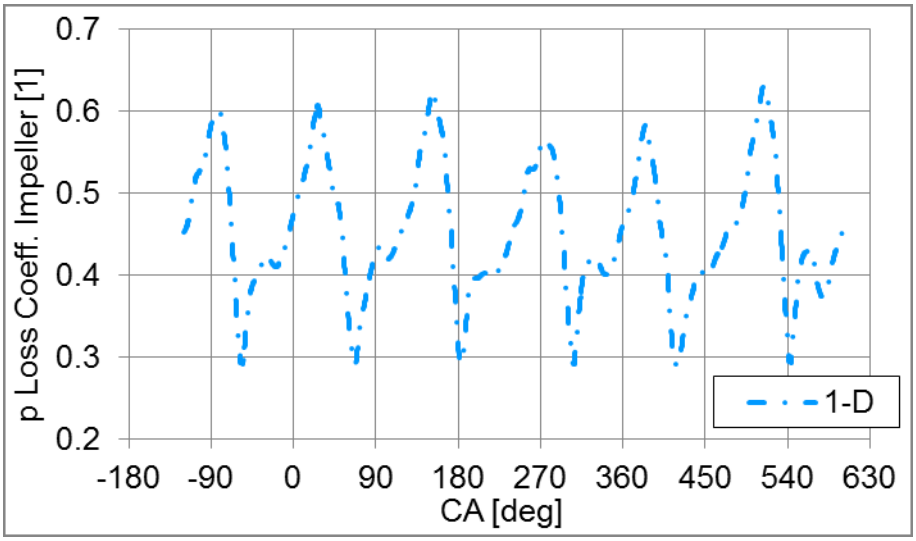

Figure 348 Pressure loss coefficient in impeller pipe, simulation with full 1-D unsteady turbine (blue dashed and dotted line); 2100 RPM, BMEP = 9.8 bar

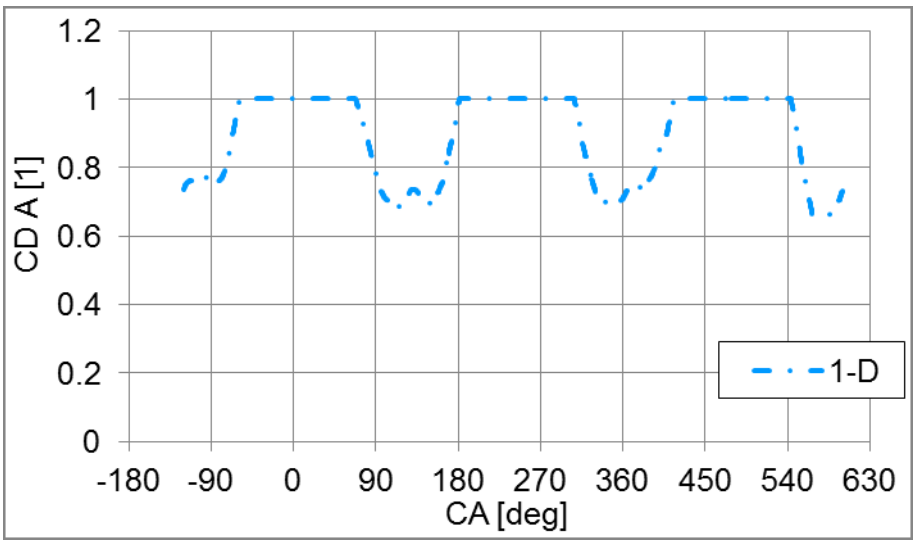

Figure 349 CD A - discharge coefficient at section A outlet {upstream of flow mixing}, simulation with full 1-D unsteady turbine (blue dashed and dotted line); 2100 RPM, BMEP = 9.8 bar

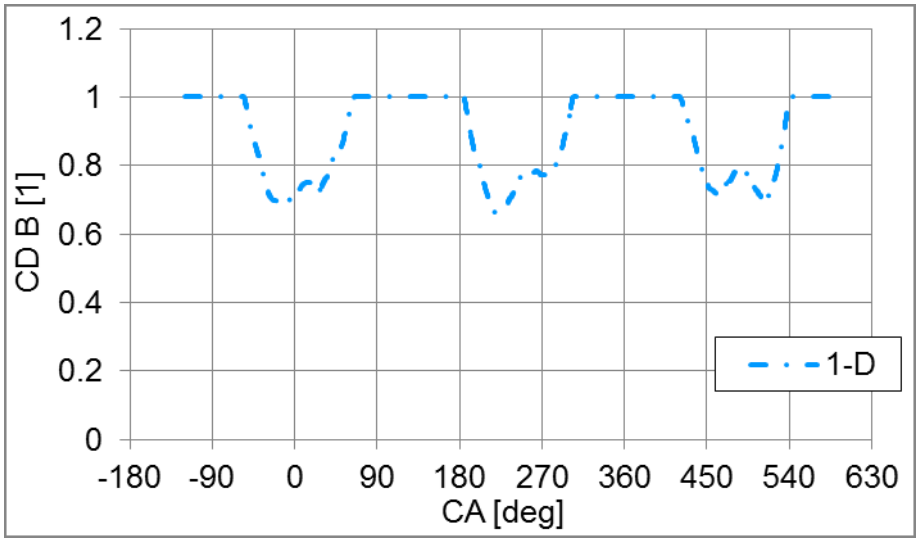

Figure 350 CD B - discharge coefficient at section B outlet {upstream of flow mixing}, simulation with full 1-D unsteady turbine (blue dashed and dotted line); 2100 RPM, BMEP = 9.8 bar

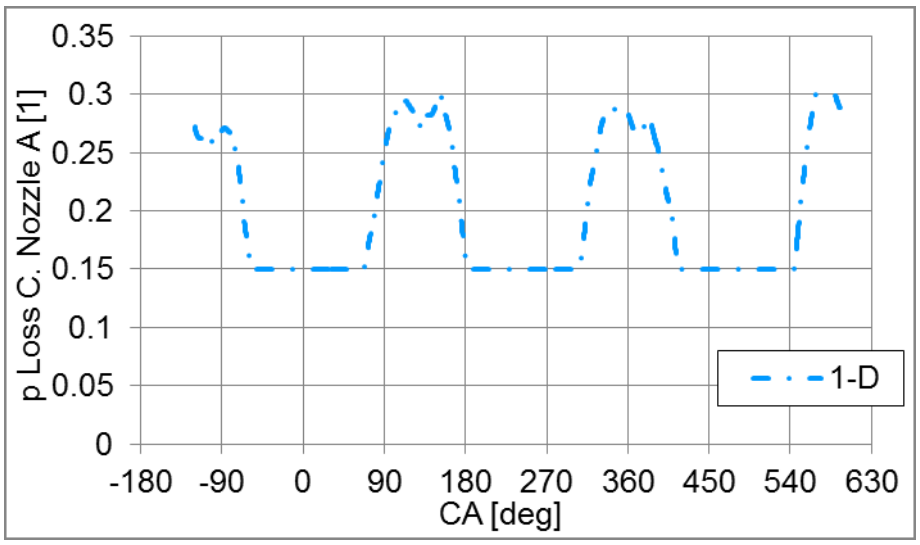

Figure 351 Pressure loss coefficient in section A, simulation with full 1-D unsteady turbine (blue dashed and dotted line); 2100 RPM, BMEP = 9.8 bar

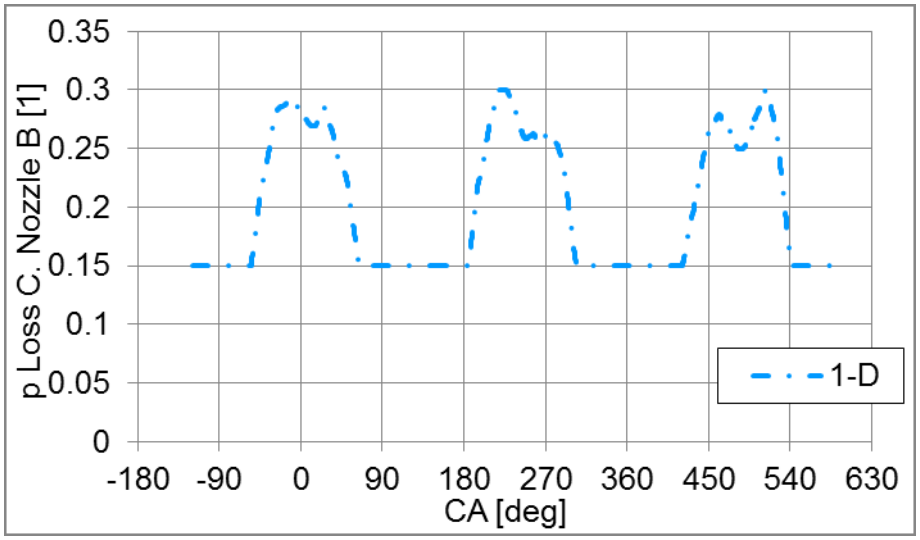

Figure 352 Pressure loss coefficient in section B, simulation with full 1-D unsteady turbine (blue dashed and dotted line); 2100 RPM, BMEP = 9.8 bar

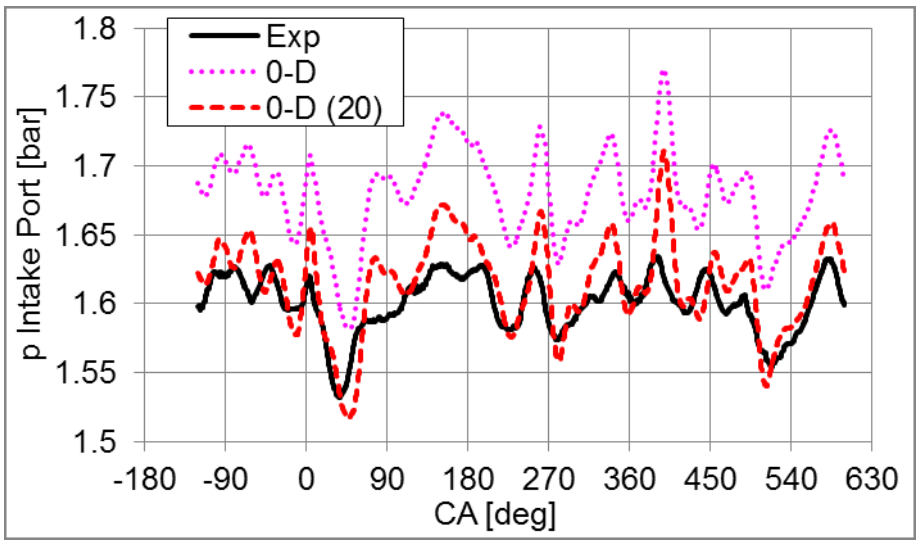

Figure 353 Pressure in intake port, experiment (black solid line), simulation with 0-D turbine map - sections without connection (purple dotted line), simulation with 0-D turbine map - sections connected via orifice D = 20 mm (red dashed line); 2100 RPM, BMEP = 9.8 bar

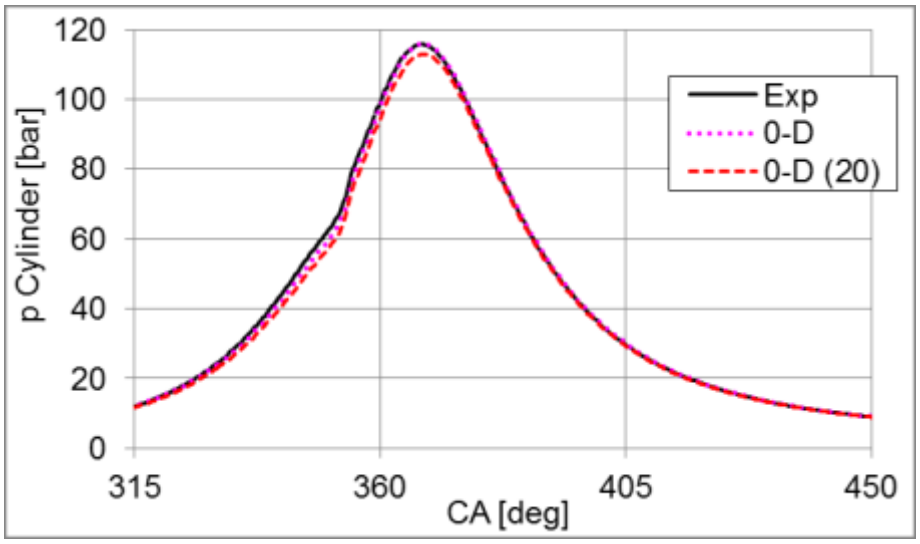

Figure 354 Pressure in cylinder, experiment (black solid line), simulation with 0-D turbine map - sections without connection (purple dotted line), simulation with 0-D turbine map - sections connected via orifice D = 20 mm (red dashed line); 2100 RPM, BMEP = 9.8 bar

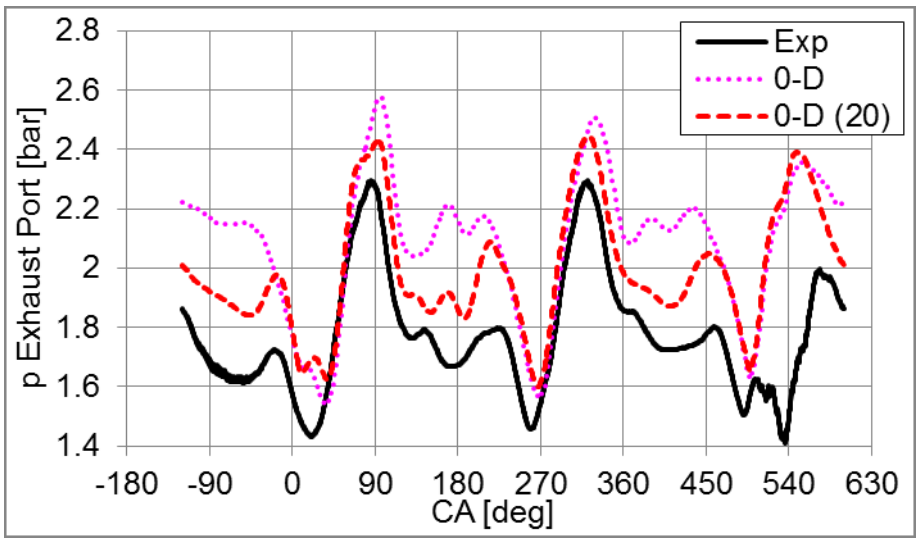

Figure 355 Pressure in exhaust port, experiment (black solid line), simulation with 0-D turbine map - sections without connection (purple dotted line), simulation with 0-D turbine map - sections connected via orifice D = 20 mm (red dashed line); 2100 RPM, BMEP = 9.8 bar

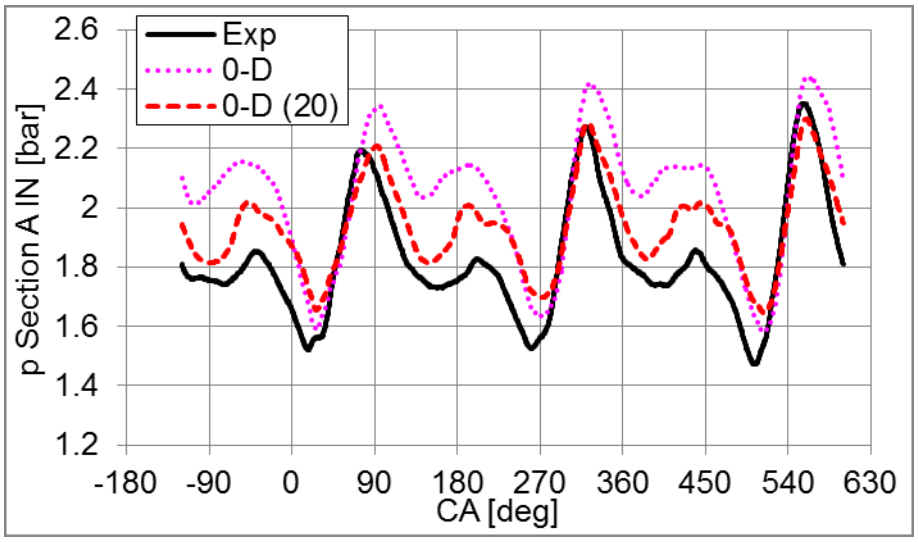

Figure 356 Pressure at inlet of turbine section A, experiment (black solid line), simulation with 0-D turbine map - sections without connection (purple dotted line), simulation with 0-D turbine map - sections connected via orifice D = 20 mm (red dashed line); 2100 RPM, BMEP = 9.8 bar

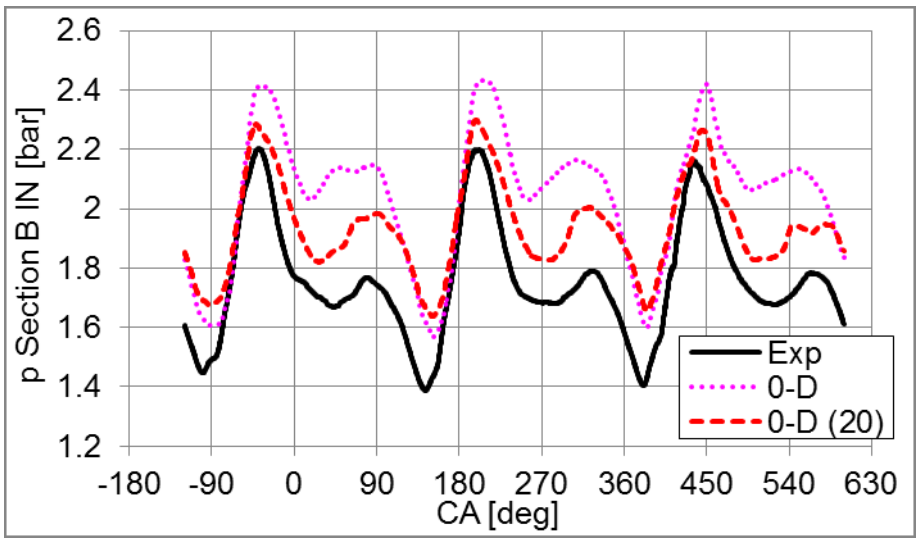

Figure 357 Pressure at inlet of turbine section B, experiment (black solid line), simulation with 0-D turbine map - sections without connection (purple dotted line), simulation with 0-D turbine map - sections connected via orifice D = 20 mm (red dashed line); 2100 RPM, BMEP = 9.8 bar

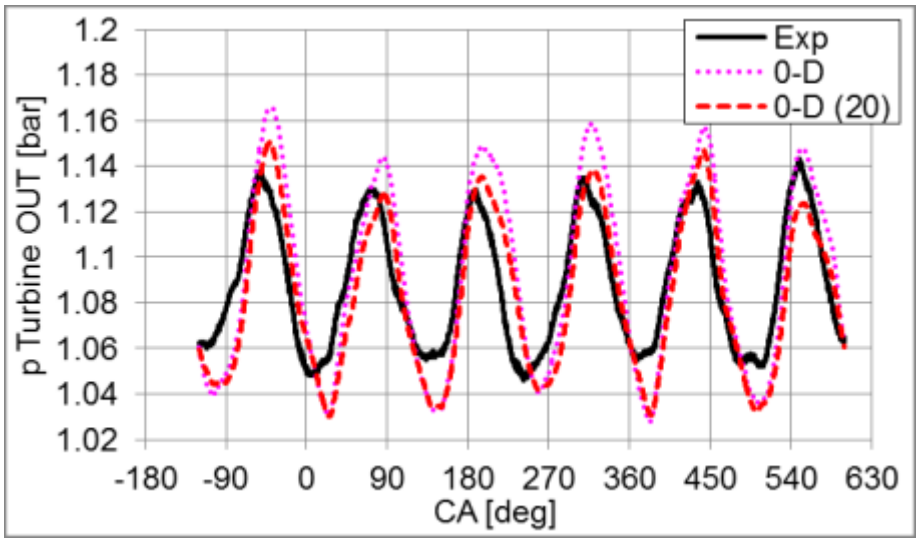

Figure 358 Pressure turbine downstream, experiment (black solid line), simulation with 0-D turbine map - sections without connection (purple dotted line), simulation with 0-D turbine map - sections connected via orifice D = 20 mm (red dashed line); 2100 RPM, BMEP = 9.8 bar

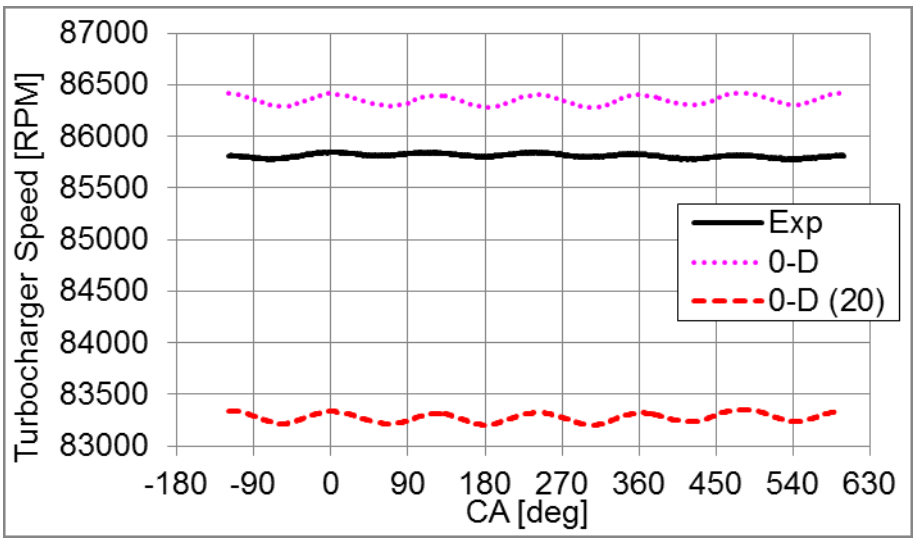

Figure 359 Turbocharger speed, experiment (black solid line), simulation with 0-D turbine map - sections without connection (purple dotted line), simulation with 0-D turbine map - sections connected via orifice D = 20 mm (red dashed line); 2100 RPM, BMEP = 9.8 bar

Appendix 6 - Simulation Results - Six Cylinder Diesel Engine - Transients

The measured values and results of engine simulation during transients at constant engine speed are summarized in stated pictures.

Engine speed: 900 RPM

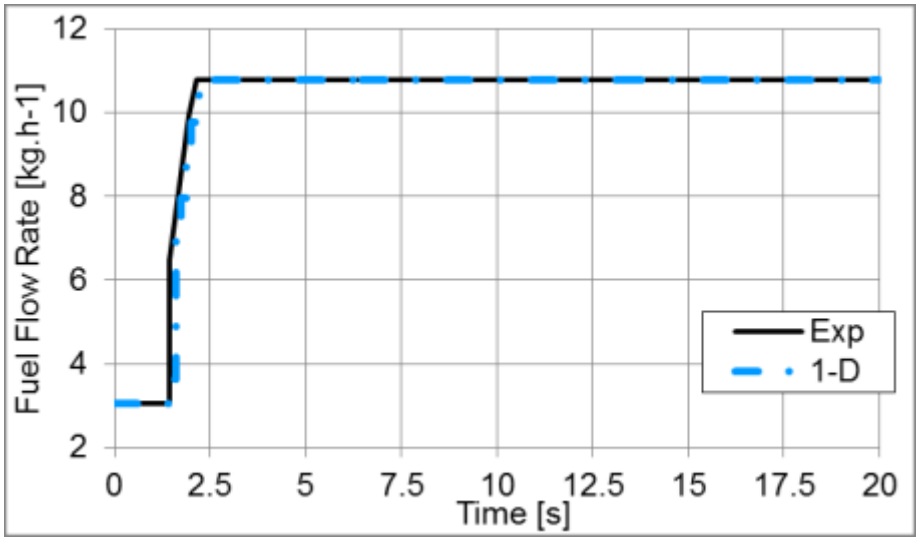

Figure 360 Fuel mass flow rate, experiment (black solid line), simulation with full 1-D unsteady turbine (blue dashed and dotted line); 900 RPM

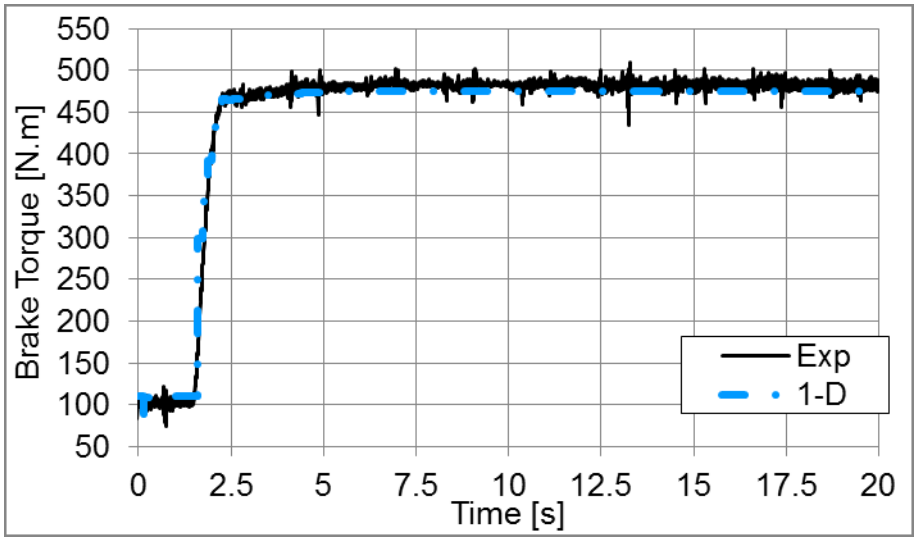

Figure 361 Brake torque, experiment (black solid line), simulation with full 1-D unsteady turbine (blue dashed and dotted line); 900 RPM

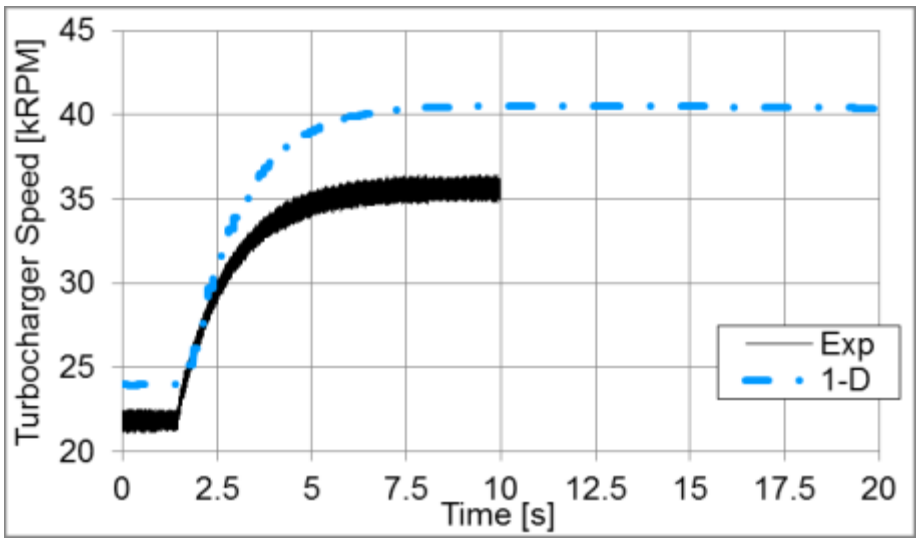

Figure 362 Turbocharger speed, experiment (black solid line), simulation with full 1-D unsteady turbine (blue dashed and dotted line); 900 RPM

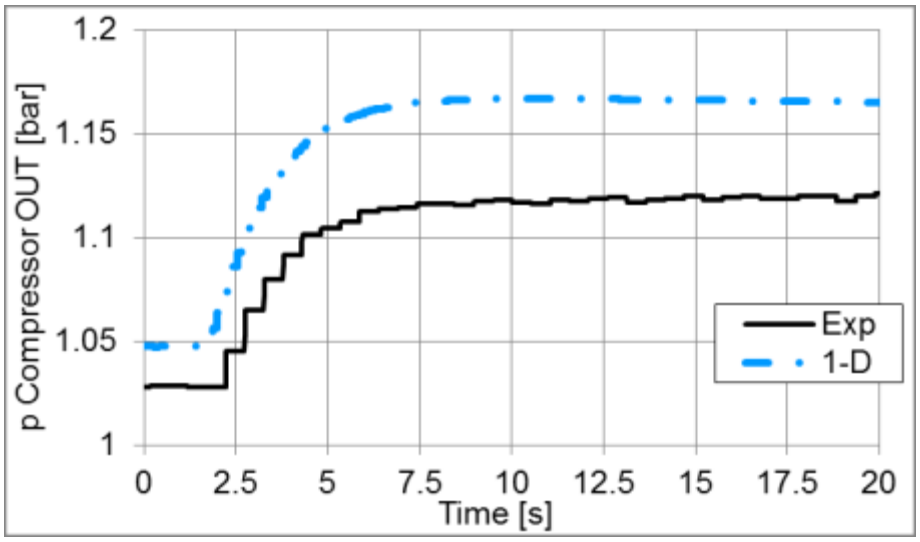

Figure 363 Pressure downstream of a compressor, experiment (black solid line), simulation with full 1-D unsteady turbine (blue dashed and dotted line); 900 RPM

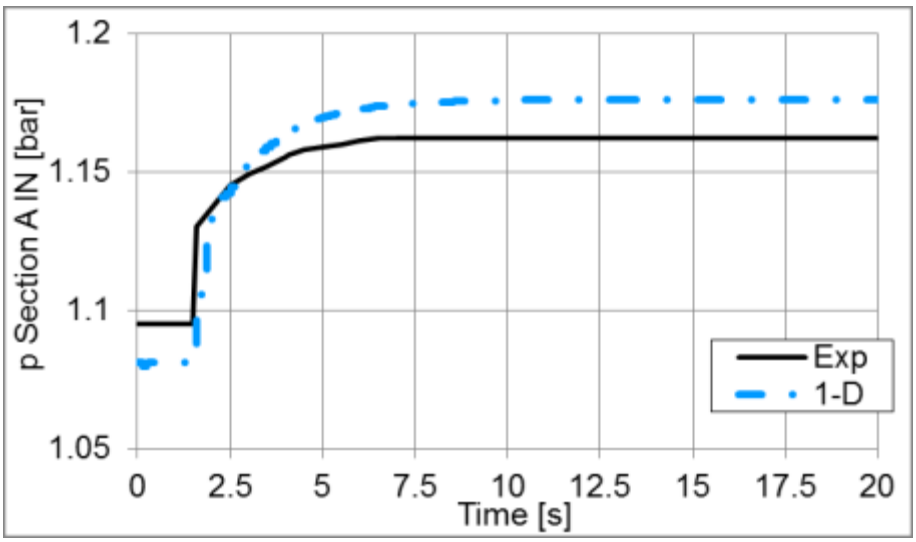

Figure 364 Pressure at inlet of turbine section A, experiment (black solid line), simulation with full 1-D unsteady turbine (blue dashed and dotted line); 900 RPM

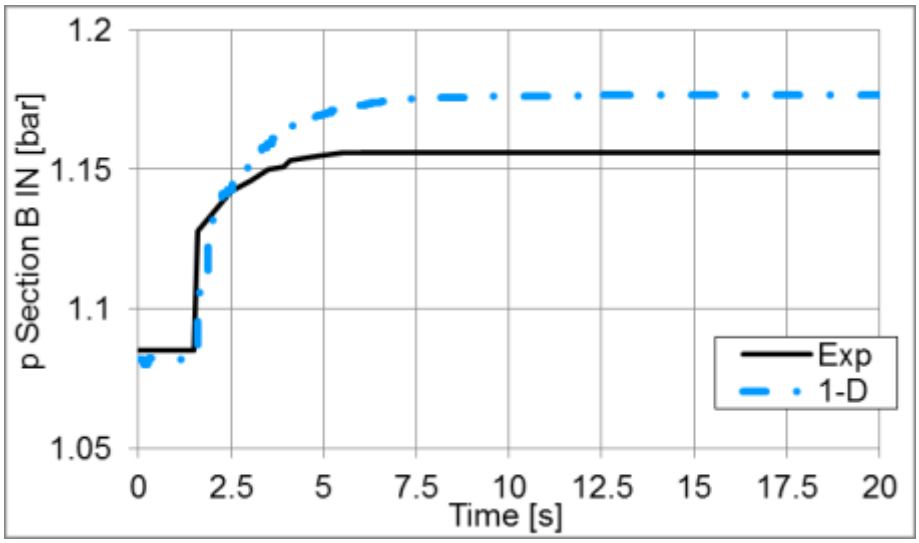

Figure 365 Pressure at inlet of turbine section B, experiment (black solid line), simulation with full 1-D unsteady turbine (blue dashed and dotted line); 900 RPM

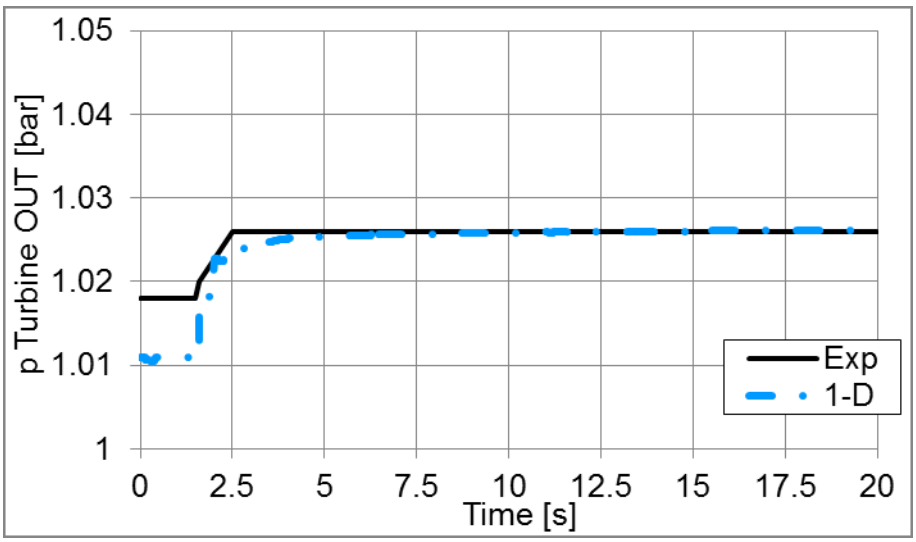

Figure 366 Pressure turbine downstream, experiment (black solid line), simulation with full 1-D unsteady turbine (blue dashed and dotted line); 900 RPM

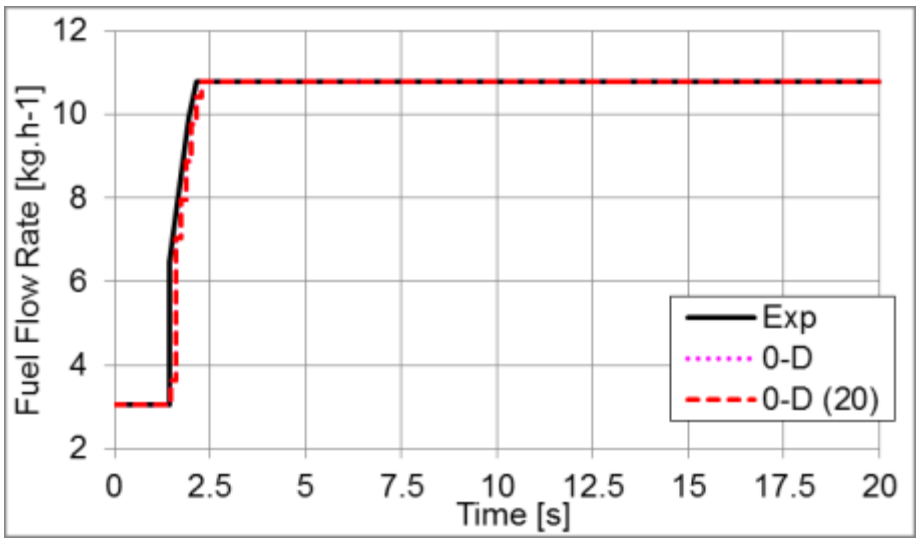

Figure 367 Fuel mass flow rate, experiment (black solid line), simulation with 0-D turbine map - sections without connection (purple dotted line), simulation with 0-D turbine map - sections connected via orifice D = 20 mm (red dashed line); 900 RPM

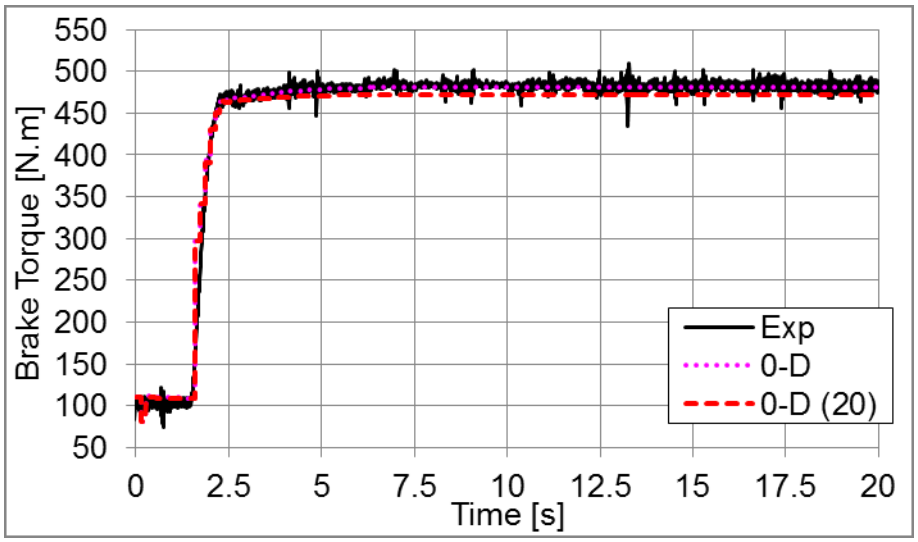

Figure 368 Brake torque, experiment (black solid line), simulation with 0-D turbine map - sections without connection (purple dotted line), simulation with 0-D turbine map - sections connected via orifice D = 20 mm (red dashed line); 900 RPM

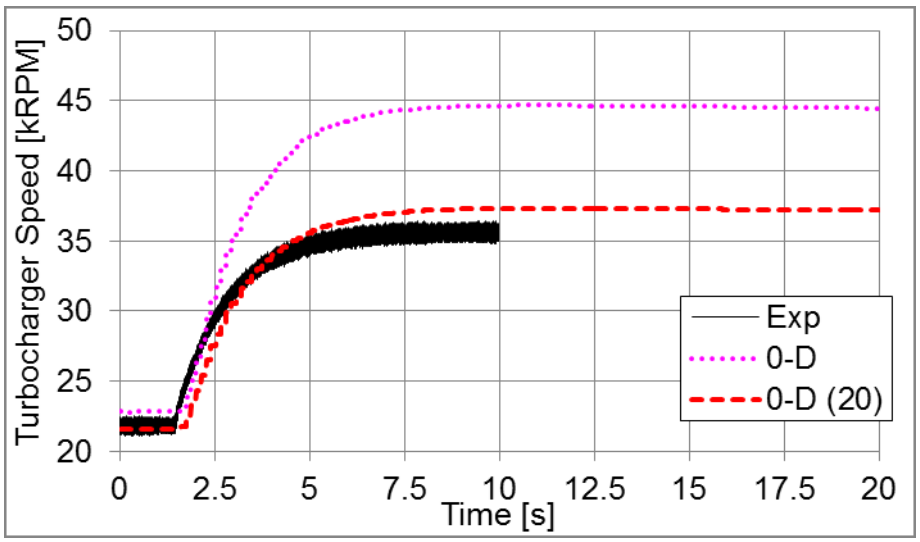

Figure 369 Turbocharger speed, experiment (black solid line), simulation with 0-D turbine map - sections without connection (purple dotted line), simulation with 0-D turbine map - sections connected via orifice D = 20 mm (red dashed line); 900 RPM

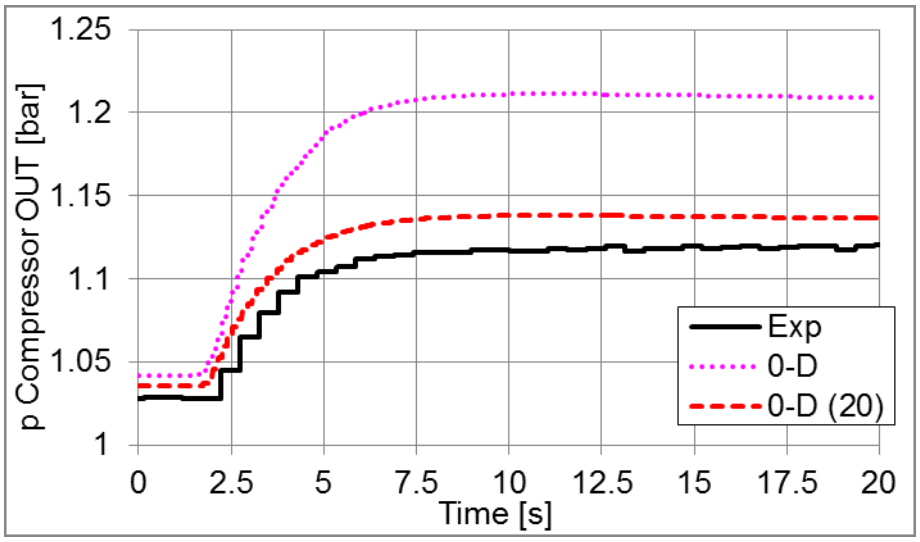

Figure 370 Pressure downstream of a compressor, experiment (black solid line), simulation with 0-D turbine map - sections without connection (purple dotted line), simulation with 0-D turbine map - sections connected via orifice D = 20 mm (red dashed line); 900 RPM

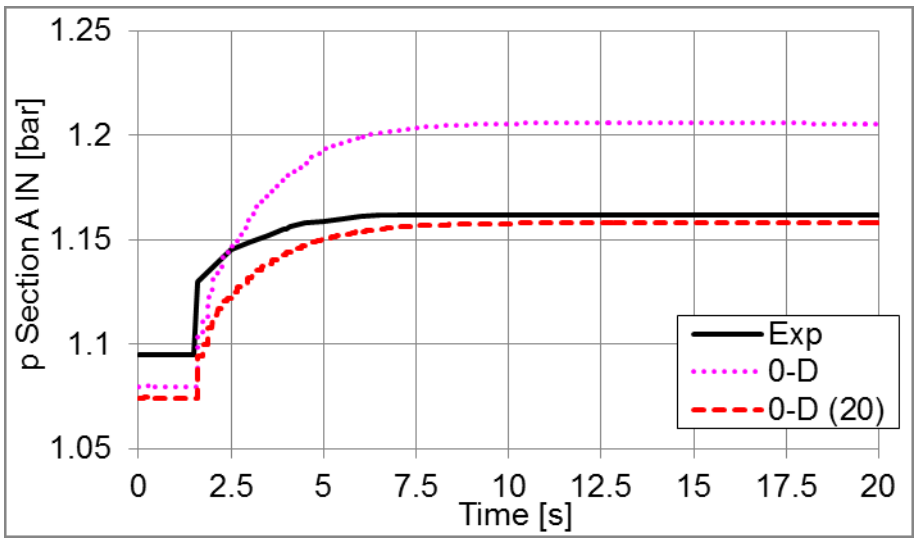

Figure 371 Pressure at inlet of turbine section A, experiment (black solid line), simulation with 0-D turbine map - sections without connection (purple dotted line), simulation with 0-D turbine map - sections connected via orifice D = 20 mm (red dashed line); 900 RPM

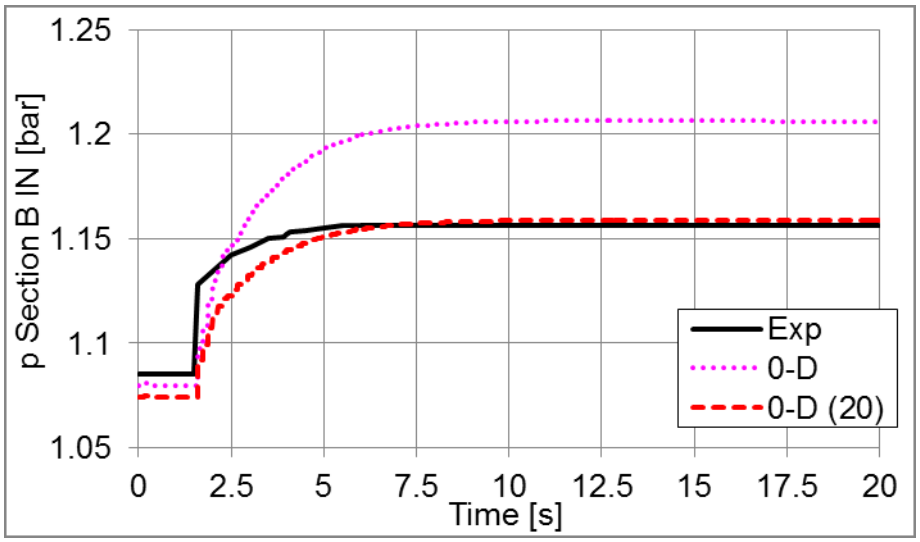

Figure 372 Pressure at inlet of turbine section B, experiment (black solid line), simulation with 0-D turbine map - sections without connection (purple dotted line), simulation with 0-D turbine map - sections connected via orifice D = 20 mm (red dashed line); 900 RPM

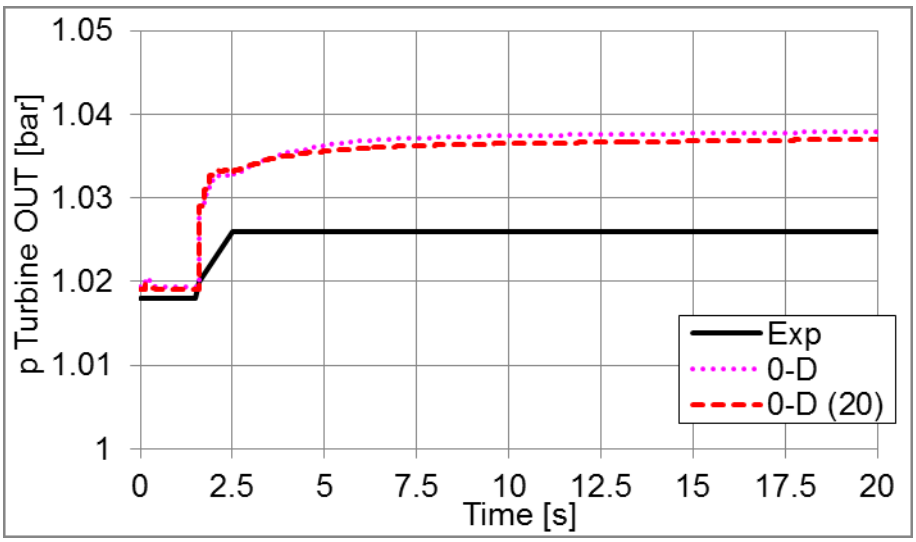

Figure 373 Pressure turbine downstream, experiment (black solid line), simulation with 0-D turbine map - sections without connection (purple dotted line), simulation with 0-D turbine map - sections connected via orifice D = 20 mm (red dashed line); 900 RPM

Engine speed: 2100 RPM

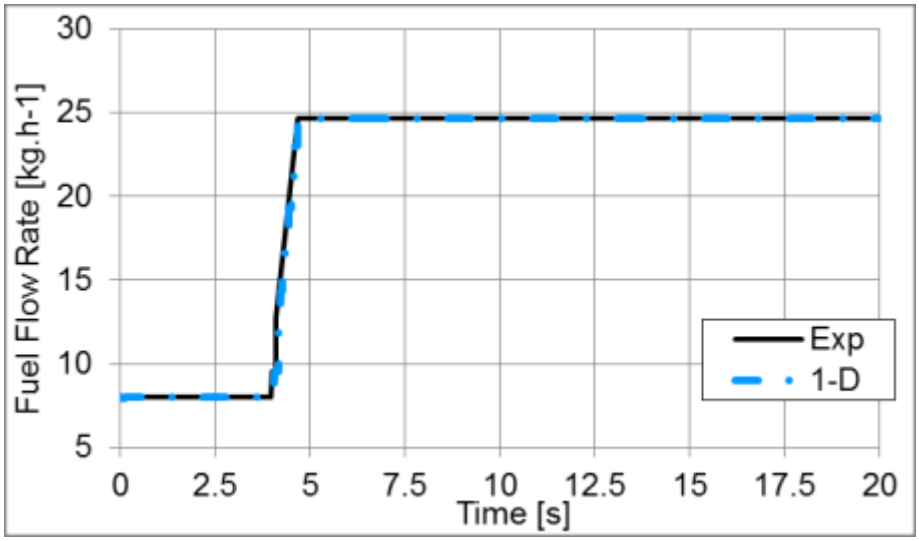

Figure 374 Fuel mass flow rate, experiment (black solid line), simulation with full 1-D unsteady turbine (blue dashed and dotted line); 2100 RPM

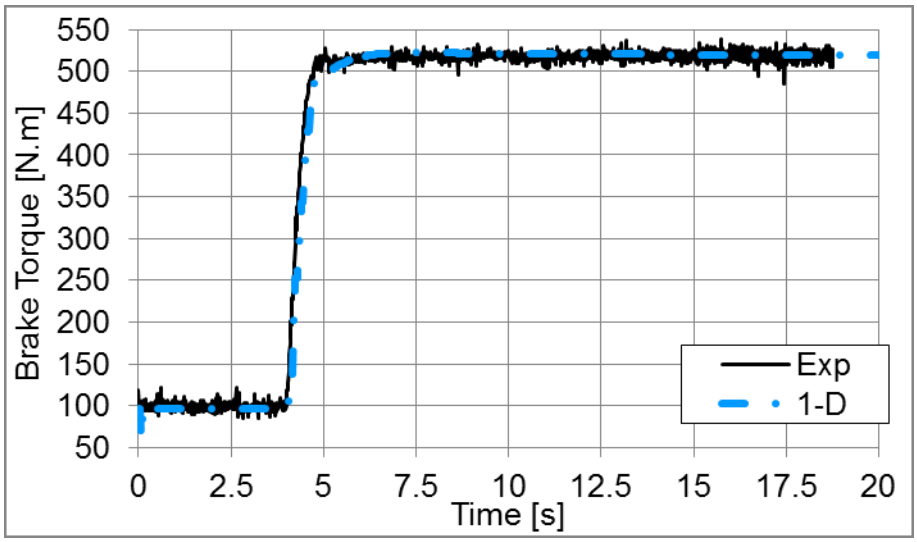

Figure 375 Brake torque, experiment (black solid line), simulation with full 1-D unsteady turbine (blue dashed and dotted line); 2100 RPM

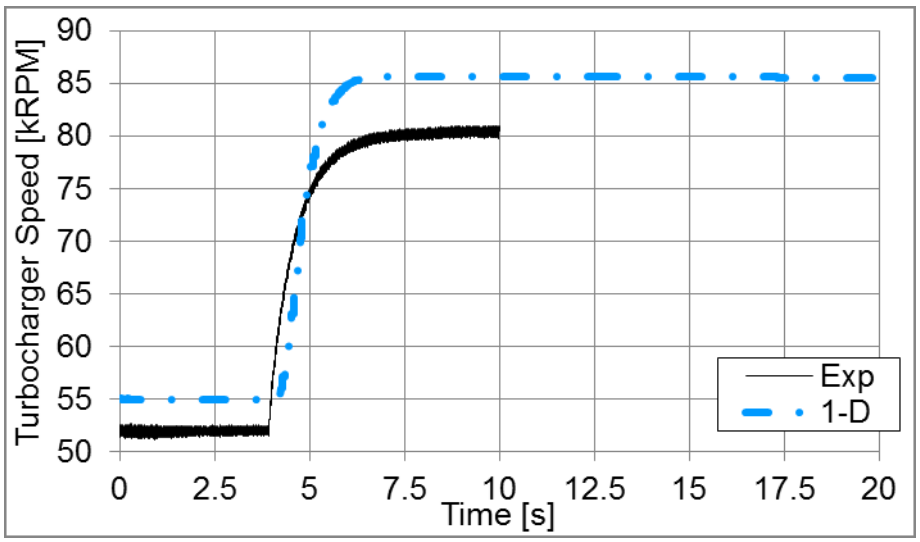

Figure 376 Turbocharger speed, experiment (black solid line), simulation with full 1-D unsteady turbine (blue dashed and dotted line); 2100 RPM

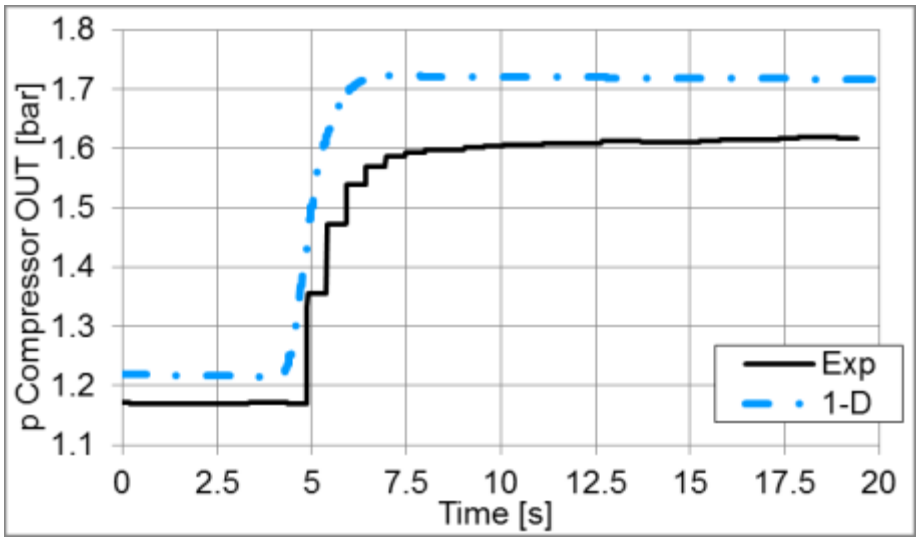

Figure 377 Pressure downstream of a compressor, experiment (black solid line), simulation with full 1-D unsteady turbine (blue dashed and dotted line); 2100 RPM

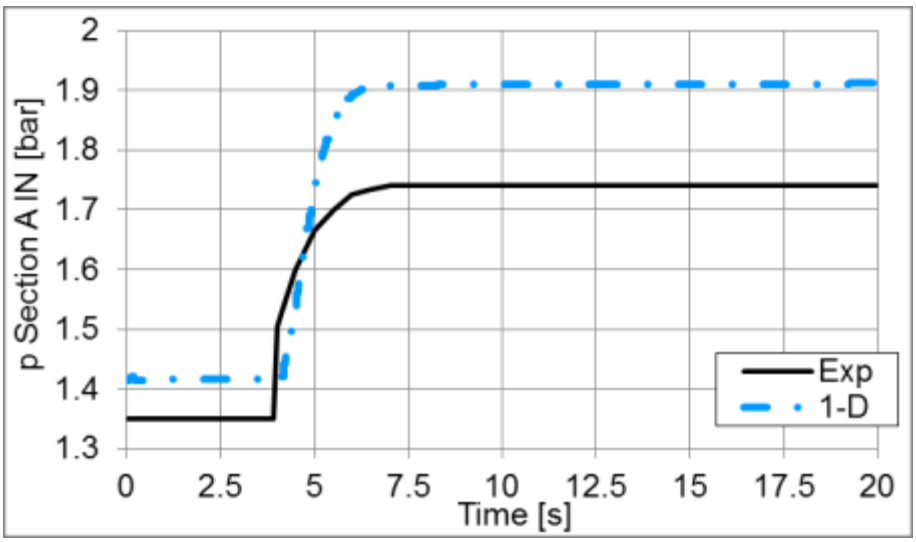

Figure 378 Pressure at inlet of turbine section A, experiment (black solid line), simulation with full 1-D unsteady turbine (blue dashed and dotted line); 2100 RPM

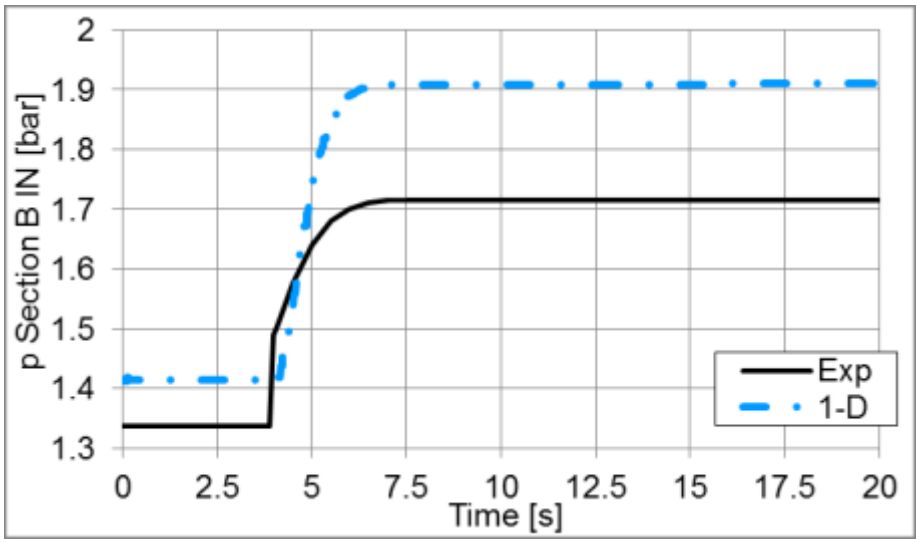

Figure 379 Pressure at inlet of turbine section B, experiment (black solid line), simulation with full 1-D unsteady turbine (blue dashed and dotted line); 2100 RPM

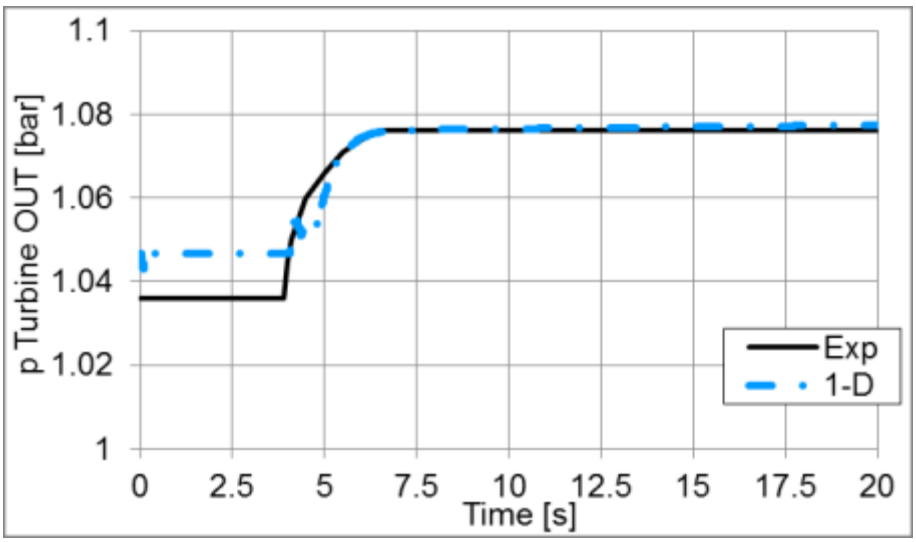

Figure 380 Pressure turbine downstream, experiment (black solid line), simulation with full 1-D unsteady turbine (blue dashed and dotted line); 2100 RPM

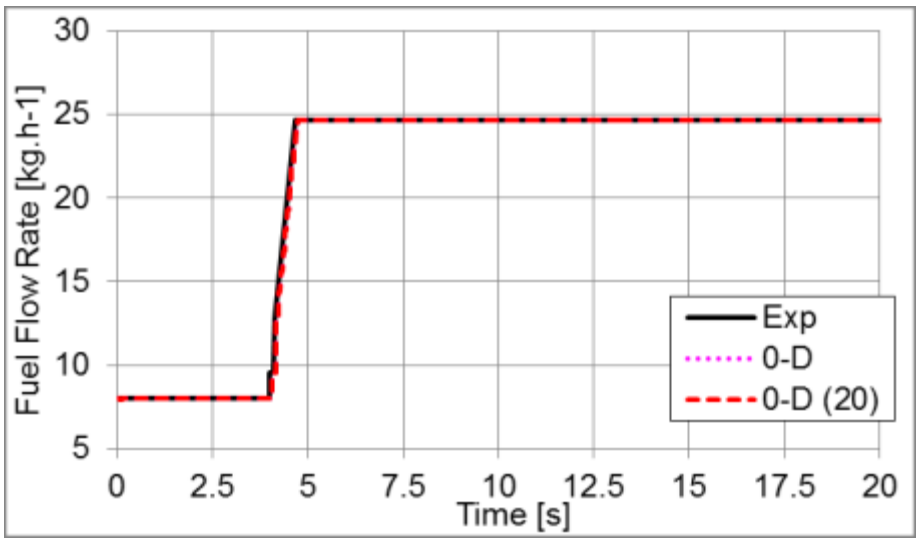

Figure 381 Fuel mass flow rate, experiment (black solid line), simulation with 0-D turbine map - sections without connection (purple dotted line), simulation with 0-D turbine map - sections connected via orifice D = 20 mm (red dashed line); 2100 RPM

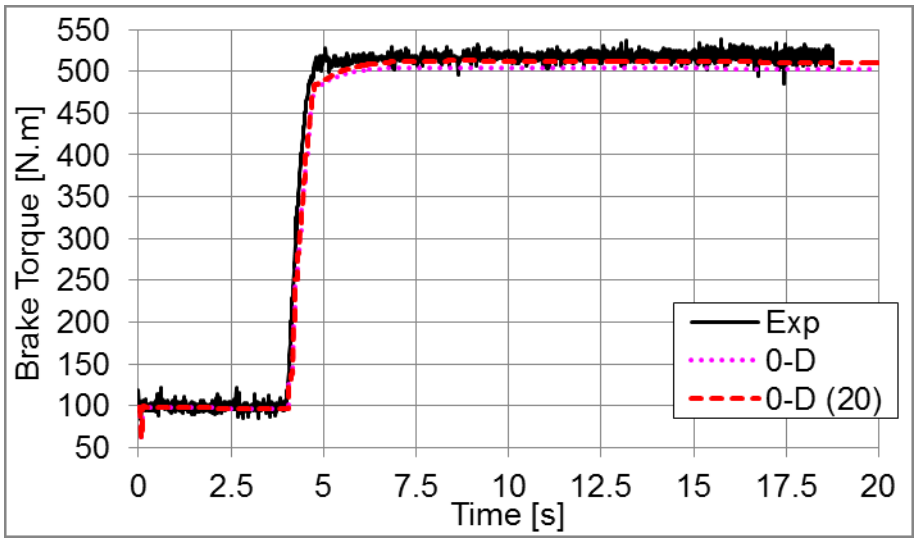

Figure 382 Brake torque, experiment (black solid line), simulation with 0-D turbine map - sections without connection (purple dotted line), simulation with 0-D turbine map - sections connected via orifice D = 20 mm (red dashed line); 2100 RPM

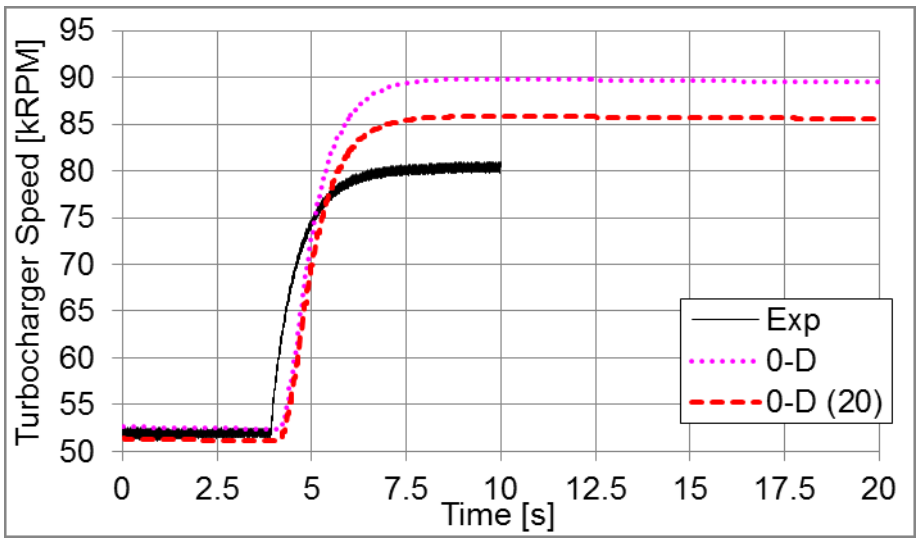

Figure 383 Turbocharger speed, experiment (black solid line), simulation with 0-D turbine map - sections without connection (purple dotted line), simulation with 0-D turbine map - sections connected via orifice D = 20 mm (red dashed line); 2100 RPM

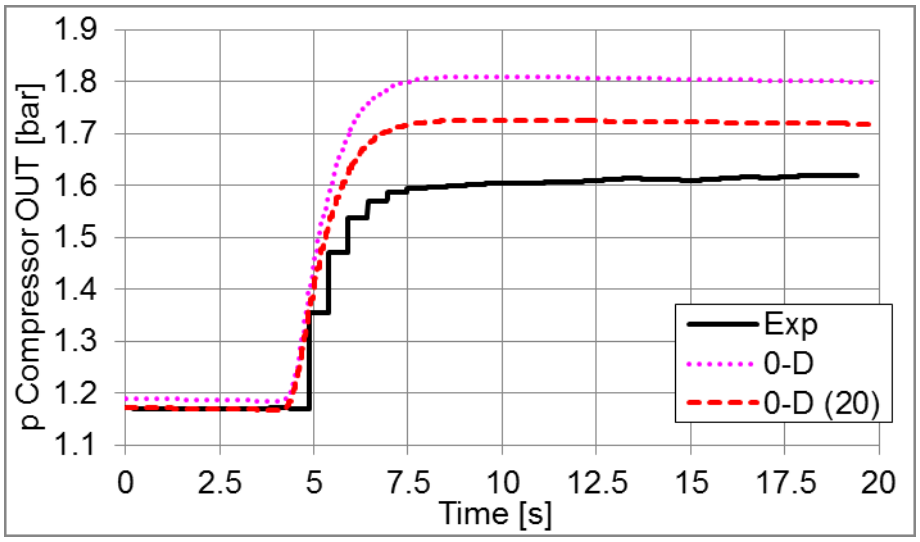

Figure 384 Pressure downstream of a compressor, experiment (black solid line), simulation with 0-D turbine map - sections without connection (purple dotted line), simulation with 0-D turbine map - sections connected via orifice D = 20 mm (red dashed line); 2100 RPM

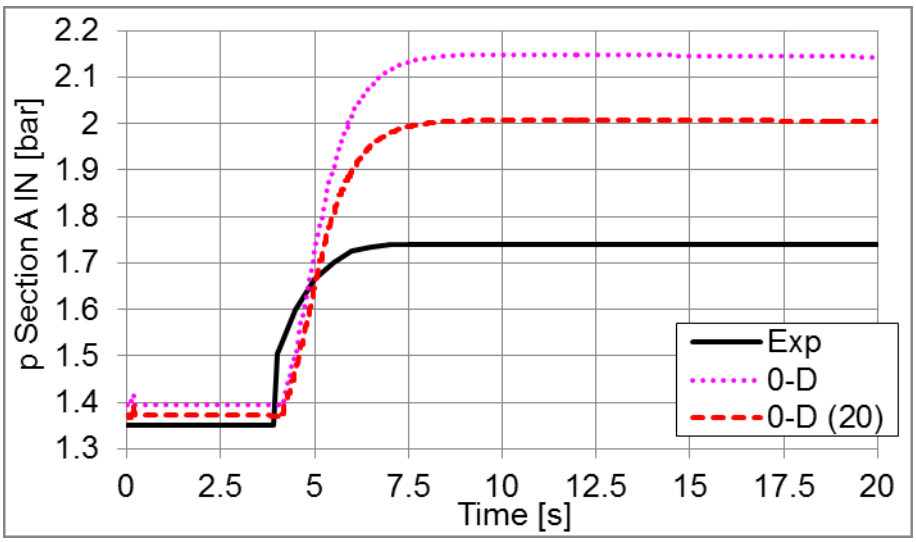

Figure 385 Pressure at inlet of turbine section A, experiment (black solid line), simulation with 0-D turbine map - sections without connection (purple dotted line), simulation with 0-D turbine map - sections connected via orifice D = 20 mm (red dashed line); 2100 RPM

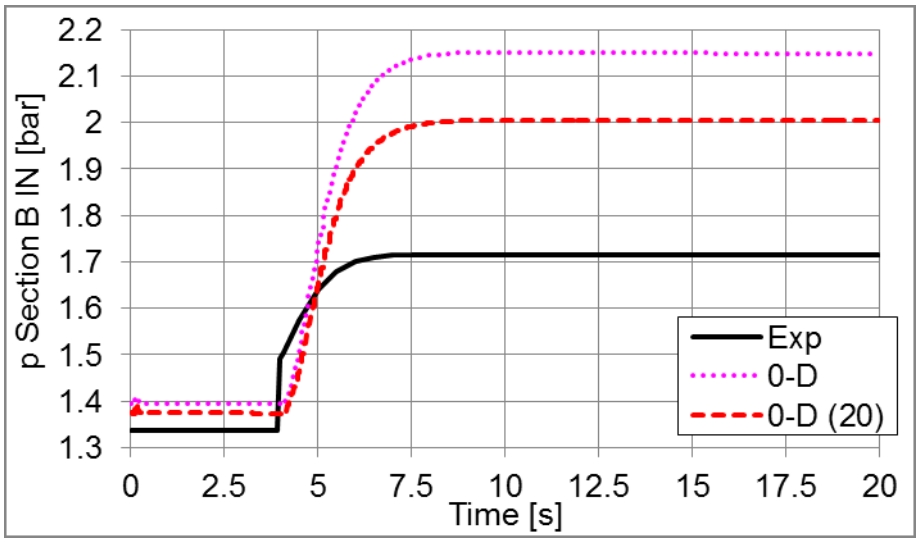

Figure 386 Pressure at inlet of turbine section B, experiment (black solid line), simulation with 0-D turbine map - sections without connection (purple dotted line), simulation with 0-D turbine map - sections connected via orifice D = 20 mm (red dashed line); 2100 RPM

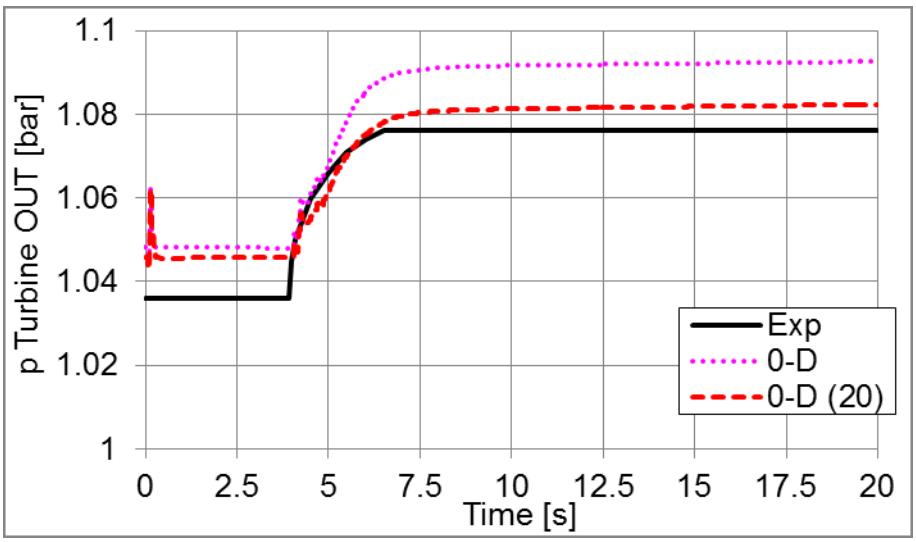

Figure 387 Pressure turbine downstream, experiment (black solid line), simulation with 0-D turbine map - sections without connection (purple dotted line), simulation with 0-D turbine map - sections connected via orifice D = 20 mm (red dashed line); 2100 RPM

Appendix 7 - Turbine Model Scheme in GT-SUITE

The scheme of the developed twin scroll turbine 1-D model is shown in the picture.

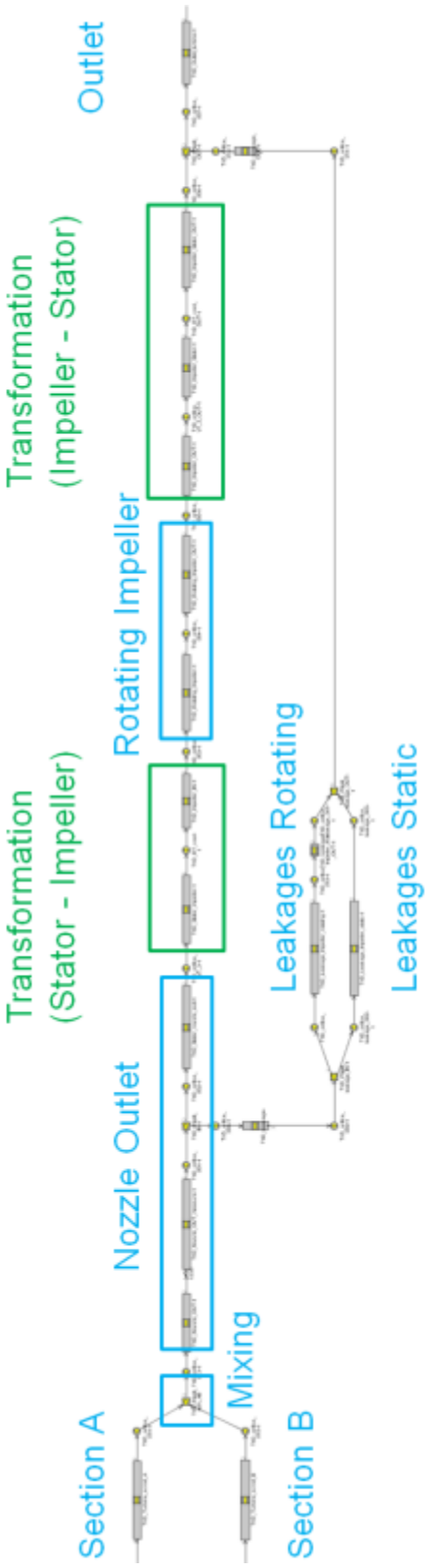

Figure 388 Scheme of the 1-D unsteady model of a twin scroll radial centripetal turbine in GT-SUITE